Alaska Department of Transportation & Public Facilities

Research & Technology Transfer

**ALASKA DEPARTMENT OF TRANSPORTATION**

# Single Lane Live Load Distribution Factor for Decked Precast/Prestressed Concrete Girder Bridges


Prepared by: Zhongguo (John) Ma, Ph.D., P.E.
J. Leroy Hulsey, Ph.D., P.E.
Department of Civil and Environmental Engineering
Institute of Northern Engineering
University of Alaska Fairbanks
Fairbanks, Alaska 99775



**December 2004**

**Prepared for:**
Alaska Department of Transportation
Statewide Research Office
3132 Channel Drive
Juneau, AK 99801-7898

FHWA-AK-RD-04-03

# REPORT DOCUMENTATION PAGE

Form approved OMB No.

Public reporting for this collection of information is estimated to average 1 hour per response, including the time for reviewing instructions, searching existing data sources, gathering and maintaining the data needed, and completing and reviewing the collection of information. Send comments regarding this burden estimate or any other aspect of this collection of information, including suggestion for reducing this burden to Washington Headquarters Services, Directorate for Information Operations and Reports, 1215 Jefferson Davis Highway, Suite 1204, Arlington, VA 22202-4302, and to the Office of Management and Budget, Paperwork Reduction Project (0704-1833), Washington, DC 20503

| 1. AGENCY USE ONLY (LEAVE BLANK) | 2. REPORT DATE | 3. REPORT TYPE AND DATES COVERED |
|---|---|---|
| FHWA-AK-RD-04-03 | December 2004 | Final |

4. TITLE AND SUBTITLE

Single Lane Live Load Distribution Factor for Decked Precast/Prestressed Concrete Girder Bridges

5. FUNDING NUMBERS

T2-01-01
RES-01-018

6. AUTHOR(S)

Zhongguo (John) Ma, Ph.D., P.E.
J. Leroy Hulsey, Ph.D., P.E.

7. PERFORMING ORGANIZATION NAME(S) AND ADDRESS(ES)
Department of Civil and Environmental Engineering
University of Alaska Fairbanks
Fairbanks, Alaska 99775

8. PERFORMING ORGANIZATION REPORT NUMBER

9. SPONSORING/MONITORING AGENCY NAME(S) AND ADDRESS(ES)

State of Alaska, Alaska Dept. of Transportation and Public Facilities
Research and Technology Transfer
2301 Peger Rd
Fairbanks, AK 99709-5399

10. SPONSORING/MONITORING AGENCY REPORT NUMBER

FHWA-AK-RD-04-03

11. SUPPLENMENTARY NOTES

Performed in cooperation with the U.S. Department of Transportation, Federal Highway Administration.
Research Project Title: "Evaluation of Single Lane Live Load Distribution Factor (DF) for the Alaska Style Decked Bulb-Tee Girder Bridge"

12a. DISTRIBUTION / AVAILABILITY STATEMENT

No restrictions.
This document is available to the public through the National Technical Information Service, Springfield, VA 22161

12b. DISTRIBUTION CODE

13. ABSTRACT (Maximum 200 words)

The live load distribution factor (DF) equations provided by AASHTO-LRFD for the decked precast/prestressed concrete (DPPC) girder bridge system do not differentiate between a single or multilane loaded condition. This practice results in a single lane load rating penalty for DPPC girder bridges. The objective of this project is to determine DF equations which accurately predict the distribution factor of the DPPC girder bridge system when it is only subjected to single lane loading. Eight DPPC girder bridges were instrumented. Each bridge was loaded with a single load vehicle to simulate the single lane loaded condition. The experimental data was used to calibrate 3D FE models and 2D grillage models of the DPPC girder bridge system. The calibrated models were used to conduct a parametric study of the DPPC girder bridge system subjected to a single lane loaded condition. Two sets of new equations that describe the single lane loaded distribution factor for both shear and moment forces of these bridges are proposed and compared with AASHTO-LRFD DF equations.

14. KEYWORDS : Girder bridges, Prefabricated bridges, Prestressed concrete bridges, Load Transfer, Load factor, Investigation of structure, Computer models, Mathematical models

15. NUMBER OF PAGES
445

16. PRICE CODE
N/A

| 17. SECURITY CLASSIFICATION OF REPORT | 18. SECURITY CLASSIFICATION OF THIS PAGE | 19. SECURITY CLASSIFICATION OF ABSTRACT | 20. LIMITATION OF ABSTRACT |
|---|---|---|---|
| Unclassified | Unclassified | Unclassified | N/A |

# SI* (MODERN METRIC) CONVERSION FACTORS

## APPROXIMATE CONVERSIONS TO SI UNITS

| Symbol | When You Know | Multiply By | To Find | Symbol |
|---|---|---|---|---|
| | | **LENGTH** | | |
| in | inches | 25.4 | millimeters | mm |
| ft | feet | 0.305 | meters | m |
| yd | yards | 0.914 | meters | m |
| mi | miles | 1.61 | kilometers | km |
| | | **AREA** | | |
| $in^2$ | square inches | 645.2 | square millimeters | $mm^2$ |
| $ft^2$ | square feet | 0.093 | square meters | $m^2$ |
| $yd^2$ | square yard | 0.836 | square meters | $m^2$ |
| ac | acres | 0.405 | hectares | ha |
| $mi^2$ | square miles | 2.59 | square kilometers | $km^2$ |
| | | **VOLUME** | | |
| fl oz | fluid ounces | 29.57 | milliliters | mL |
| gal | gallons | 3.785 | liters | L |
| $ft^3$ | cubic feet | 0.028 | cubic meters | $m^3$ |
| $yd^3$ | cubic yards | 0.765 | cubic meters | $m^3$ |
| | NOTE: volumes greater than 1000 L shall be shown in $m^3$ | | | |
| | | **MASS** | | |
| oz | ounces | 28.35 | grams | g |
| lb | pounds | 0.454 | kilograms | kg |
| T | short tons (2000 lb) | 0.907 | megagrams (or "metric ton") | Mg (or "t") |
| | | **TEMPERATURE (exact degrees)** | | |
| $^oF$ | Fahrenheit | 5 (F-32)/9 or (F-32)/1.8 | Celsius | $^oC$ |
| | | **ILLUMINATION** | | |
| fc | foot-candles | 10.76 | lux | lx |
| fl | foot-Lamberts | 3.426 | candela/$m^2$ | cd/$m^2$ |
| | | **FORCE and PRESSURE or STRESS** | | |
| lbf | poundforce | 4.45 | newtons | N |
| lbf/$in^2$ | poundforce per square inch | 6.89 | kilopascals | kPa |

## APPROXIMATE CONVERSIONS FROM SI UNITS

| Symbol | When You Know | Multiply By | To Find | Symbol |
|---|---|---|---|---|
| | | **LENGTH** | | |
| mm | millimeters | 0.039 | inches | in |
| m | meters | 3.28 | feet | ft |
| m | meters | 1.09 | yards | yd |
| km | kilometers | 0.621 | miles | mi |
| | | **AREA** | | |
| $mm^2$ | square millimeters | 0.0016 | square inches | $in^2$ |
| $m^2$ | square meters | 10.764 | square feet | $ft^2$ |
| $m^2$ | square meters | 1.195 | square yards | $yd^2$ |
| ha | hectares | 2.47 | acres | ac |
| $km^2$ | square kilometers | 0.386 | square miles | $mi^2$ |
| | | **VOLUME** | | |
| mL | milliliters | 0.034 | fluid ounces | fl oz |
| L | liters | 0.264 | gallons | gal |
| $m^3$ | cubic meters | 35.314 | cubic feet | $ft^3$ |
| $m^3$ | cubic meters | 1.307 | cubic yards | $yd^3$ |
| | | **MASS** | | |
| g | grams | 0.035 | ounces | oz |
| kg | kilograms | 2.202 | pounds | lb |
| Mg (or "t") | megagrams (or "metric ton") | 1.103 | short tons (2000 lb) | T |
| | | **TEMPERATURE (exact degrees)** | | |
| $^oC$ | Celsius | 1.8C+32 | Fahrenheit | $^oF$ |
| | | **ILLUMINATION** | | |
| lx | lux | 0.0929 | foot-candles | fc |
| cd/$m^2$ | candela/$m^2$ | 0.2919 | foot-Lamberts | fl |
| | | **FORCE and PRESSURE or STRESS** | | |
| N | newtons | 0.225 | poundforce | lbf |
| kPa | kilopascals | 0.145 | poundforce per square inch | lbf/$in^2$ |

*SI is the symbol for the International System of Units. Appropriate rounding should be made to comply with Section 4 of ASTM E380.
(Revised March 2003)

# SINGLE LANE LIVE LOAD DISTRIBUTION FACTOR FOR DECKED PRECAST/PRESTRESSED CONCRETE GIRDER BRIDGES

FINAL REPORT

Prepared for

Alaska Department of Transportation & Public Facilities

by

Zhongguo (John) Ma, Ph.D., P.E.
J. Leroy Hulsey, Ph.D., P.E.
Department of Civil and Environmental Engineering
Institute of Northern Engineering
University of Alaska Fairbanks
Fairbanks, AK 99775

Report # FHWA-AK-RD-04-03
Research Project #: RES – 01 – 018
Research Project Title: "Evaluation of Single Lane Live Load Distribution Factor (DF) for the Alaska Style Decked Bulb-Tee Girder Bridge"

Sponsored by the
Alaska Department of Transportation and Public Facilities
In Cooperation with the
U.S. Department of Transportation
Federal Highway Administration

December 2004

## DISCLAIMER

The contents of this report reflect the views of the authors, who are responsible for the facts and the accuracy of the data presented herein. The contents do not necessarily reflect the official views of policies of neither the Alaska Department of Transportation and Public Facilities (AKDOT&PF), the Federal Highway Administration nor the University of Alaska Fairbanks. This report does not constitute a standard, specification, or regulation. Trade or manufactures' names, which may appear in this report, are cited only because they are considered essential to the objectives of the report. The U.S. government and the State of Alaska do not endorse products or manufactures.

## ACKNOWLEDGMENTS

This project was sponsored by the Alaska Department of Transportation and Public Facilities (AKDOT&PF), the Federal Highway Administration (FHWA) and the University of Alaska Fairbanks (UAF). Support of Clint Adler, Research Engineer and Elmer Marx, Bridge Engineer of AKDOT&PF is gratefully acknowledged. They spent many hours to coordinate this project, discuss its technical direction and inspire the University researchers. We also want to thank AKDOT&PF's field personnel who helped with the testing. We especially want to thank Gary Scarborough and John Orbistondo of AKDOT&PF for their assistance during testing. The University team consisted of authors of this final report and the first author's graduate research assistants Jason Millam and Sanjay Chaudhury.

# EXECUTIVE SUMMARY

## Project Objectives

This 2.5-year project was intended to provide an accurate method of analysis for the calculation of a single lane DF for the Alaska Bulb-Tee Bridge. Safety assessment or load rating bridge structures depends on the amount of load that is expected to be taken by a member. The amount of load transferred to the member is dependent on live load distribution factor for single lane loading condition. The live load distribution factor for load rating purpose can be different from the distribution factor for bridge design. For bridge design purpose, the governing distribution factor is a function of girder location. The scope of this study, however, is limited to determining the appropriate distribution factors for load rating purposes. The idea is to find an equation that describes a distribution factor for an interior girder subjected to the maximum single load that can cross the bridge. Subsequent bridge load ratings will incorporate the new single lane DF.

## Background

For the Alaska decked bulb-tee bridges, the AASHTO Specifications provide for one live load distribution factor (DF) equation regardless of number of loaded lanes. As a result, it is the practice of AKDOT&PF to use AASHTO multiple lane live load DFs for load rating. It seems that this practice results in a load rating penalty for Alaska Bulb-Tee girder bridges. A 2.5-year research project has been initiated and completed in Alaska.

## Findings

During the research period, the research team successfully completed the following tasks: (1) reviewed all relevant literature on this subject, especially the historical development of AASHTO Specifications on load distribution of this bridge system; (2) tested eight (4 Sets of Twin Bridges) decked bulb-tee bridges in Anchorage, Alaska using one truck to simulate the single lane loading condition; (3) developed three-dimensional finite element models using ABAQUS software available on Arctic Region Supercomputer at UAF to simulate tested bridges and to study the impact of intermediate diaphragms. The number of degrees of freedom of the 3D models varies from 150,000 for Set 1 bridges to 900,000 for Set 2 bridges; (4) calibrated a two-dimensional grillage model based on field testing and 3D FE model results; (5) built a total of 1248 computer models using the developed 2D Grillage modeling technique to study the impact of parameters such as girder spacing, girder stiffness, bridge span, deck thickness, stiffness of the longitudinal joint, and number of girders on the load distribution characteristics; and (6) developed two sets of load distribution factor equations and compared the proposed equations with the LRFD equations.

Based on this 2.5-year research, the research team concluded the following findings for single lane loaded decked bulb-tee bridges:

(1) The following two sets of single-lane live load DF equations are proposed:

Moment over Interior Girder (MI):

$$DF(S) = \frac{S}{13}$$

$$DF(S,L,I) = \frac{S}{12.5} + \frac{I}{300} - \frac{L}{10} \cdot \left( \frac{S-3}{200} \right)$$

Moment over Exterior Girder (ME):

$$DF(S) = \frac{S}{11}$$

$$DF(S,L,I) = \frac{S}{10} + \frac{I}{300} - \frac{L}{10} \cdot \left( \frac{S-1}{300} \right)$$

Shear over Interior Girder (SI):

$$DF(S) = \frac{S}{11}$$

$$DF(S,L,I) = \frac{S}{12.5} + \frac{I}{250} - \frac{L}{100} \cdot \left( \frac{S}{100} \right)$$

Shear over Exterior Girder (SE):

$$DF(S) = \frac{S}{10}$$

$$DF(S,L,I) = \frac{S}{12} + \frac{I}{400} - \frac{L}{100} \cdot \left( \frac{S-3}{100} \right) + 0.07$$

where,

S = Girder Spacing, the distance between the centerlines of two consecutive girders in units of ft.

L = Span Length of the bridge measured from the centers of each support in units of ft.

I = The area moment of inertia about the horizontal axis of one girder in the bridge system. The moment of inertia used should be calculated from the whole girder including the whole width of the top flange deck portion. The units of this term are in $ft^4$.

(2) The proposed two sets of DF equations are easy to use and are still more accurate for the single lane loaded condition than the existing LRFD equations provided for this bridge system, as shown in the Tables below.

**Moment Distribution Factors Based on Different Methods**

a) Interior Girders

| Tested Bridges | Data | LRFD | DF(S) | DF(S,L,I) |
|---|---|---|---|---|
| 100th | 0.35 | 0.66 | 0.57 | 0.40 |
| Huffman | 0.31 | 0.55 | 0.46 | 0.34 |
| Campbell | 0.34 | 0.66 | 0.57 | 0.39 |
| Diamond/Dowling | 0.32 | 1.48 | 0.58 | 0.40 |

b) Exterior Girders

| Tested Bridges | Data | LRFD | DF(S) | DF(S,L,I) |
|---|---|---|---|---|
| 100th | 0.45 | 0.76 | 0.67 | 0.55 |
| Huffman | 0.49 | 0.61 | 0.61* | 0.48* |
| Campbell | 0.53 | 0.76 | 0.67 | 0.54 |
| Diamond/Dowling | 0.46 | 0.77 | 0.69 | 0.56 |

* Skew adjustment factor was included.

**Shear Distribution Factors Based on Different Methods**

a) Interior Girders

| Tested Bridges | Data | LRFD | DF(S) | DF(S,L,I) |
|---|---|---|---|---|
| 100th | 0.43 | 0.60 | 0.67 | 0.58 |
| Huffman | 0.46 | 0.57* | 0.61* | 0.52* |
| Campbell | 0.50 | 0.60 | 0.67 | 0.61 |
| Diamond/Dowling | 0.55† | 0.60 | 0.69 | 0.57 |

b) Exterior Girders

| Tested Bridges | Data | LRFD | DF(S) | DF(S,L,I) |
|---|---|---|---|---|
| 100th | 0.66 | 0.76 | 0.74 | 0.68 |
| Huffman | 0.58 | 0.67* | 0.66* | 0.63* |
| Campbell | 0.71 | 0.76 | 0.74 | 0.70 |
| Diamond/Dowling | 0.60† | 0.77 | 0.76 | 0.68 |

* Skew adjustment factor was included.
† Indicates value not found directly from testing data but from a FE model that closely approximates the testing data.

(3) The current LRFD equation for the distribution factor of moment on interior girders includes the aspect ratio as one of its parameters. According to this study, the number of girders and overall width of the bridge has little effect on the load distribution. On the other hand, parameters such as girder spacing, girder stiffness and span length are the most factors which should be considered in the DF equations.

(4) The LRFD equation for distribution of moment on interior girders for bridges with girders only connected enough to prevent relative vertical translation, is an average of 44% to 96% conservative depending on the aspect ratio of the bridge.

(5) For the moment DF of both interior and exterior girders, spacing has the greatest effect followed by span length, and then by girder stiffness. For the shear DF, spacing has the greatest effect followed by girder stiffness and then by span length.

(6) For shear distributions on exterior and interior girders, the LRFD equations are an average of 32% conservative for both the flexural transverse continuous and discontinuous cases.

(7) The research team investigated the effects of the longitudinal joint on the load distribution of decked bulb-tee bridges. Based on field testing and modeling results, it appears that the bridges, although they did not have any transverse post-tensioning, behaved as if they had full transverse flexural continuity. The 3D finite element modeling of these bridges shows that this behavior could be caused by the intermediate steel diaphragms. By varying the stiffness of the hinge joint in the grillage model, these models show that this behavior could also be caused by the stiffness of the grouted joint and shear keys. Further study in this area is needed and recommended.

(8) The skew adjustment factor specified in the LRFD Specs is recommended to be used at this time pending further parametric studies on this topic.

## TABLE OF CONTENTS

Page No.

**DISCLAIMER** ..... ii
**ACKNOWLEDGMENT** ..... iii
**EXECUTIVE SUMMARY** ..... iv
**TABLE OF CONTENTS** ..... viii
**LIST OF FIGURES** ..... xi
**LIST OF TABLES** ..... xvi
**CHAPTER 1 INTRODUCTION** ..... 1
**1.1 Review of Distribution Factor Equations** ..... 1
1.1.1 AASHTO Standard Specifications, 12th Edition, 1977 ..... 2
1.1.2 University of Washington Study ..... 3
1.1.3 AASHTO Standard Specifications, 16th Edition, 1996 ..... 3
1.1.4 AASHTO LRFD Specifications, Second Edition with 2001 Interim .. 4
**1.2 Applicable Theories** ..... 6
**1.3 Impact of Single Lane Loading** ..... 8
1.3.1 AASHTO Specifications ..... 8
1.3.2 Discussions ..... 11
1.3.3 Multibeam (e.g. Decked Bulb Tee) Bridges ..... 13
**CHAPTER 2 FIELD TESTING PROGRAM** ..... 15
**2.1 Summary of Bridges Tested** ..... 15
**2.2 Equipment and Personnel** ..... 17
2.2.1 Testing Personnel ..... 17
2.2.2 Equipment ..... 17
2.2.3 Load Vehicle Description ..... 17
**2.3 Load Positions** ..... 20
2.3.1 Longitudinal Positioning of Load Vehicle ..... 20
2.3.2 Transverse Positioning of Load Vehicle ..... 22
2.3.3 Loading Key ..... 24
**2.4 Strain Gauge Positioning** ..... 25
**2.5 Field Testing Results** ..... 28
2.5.1 Collection of Testing Data Figures ..... 29
**CHAPTER 3 DEVELOPMENT OF 3D FE MODELS** ..... 286
**3.1 Three-Dimensional (3D) FE Model Development** ..... 286
3.1.1 Elements and Mesh ..... 286
3.1.2 Scheme Used ..... 287
3.1.3 Shear Connectors ..... 288
3.1.4 Intermediate Steel Diaphragms ..... 291
3.1.5 Boundary Conditions ..... 291
3.1.6 Modeling Constants ..... 292
**3.2 3D FE Model Verification** ..... 293
3.2.1 Comparisons with Set 1 Bridges ..... 294
3.2.2 Comparisons with Set 2 Bridges ..... 302
3.2.3 Comparisons with Set 3 Bridges ..... 309
3.2.4 Comparisons with Set 4 Bridges ..... 317

**3.3 Discussions** ..... 327
**CHAPTER 4 DISTRIBUTION FACTORS BASED ON FIELD TESTING** ..... 328
**4.1 DF Analysis of Bridges at 100th Ave and Minnesota (Set 1)** ..... 328
4.1.1 Description of the Bridges ..... 328
4.1.2 Load Distribution Factors for Moment ..... 329
4.1.3 Load Distribution Factors for Shear ..... 334
**4.2 DF Analysis of Bridges at Huffman Intersection (Set 2)** ..... 339
4.2.1 Description of the Bridges ..... 339
4.2.2 Load Distribution Factors for Moment ..... 339
4.2.3 Load Distribution Factors for Shear ..... 345
**4.3 DF Analysis of Bridges at Campbell Creek (Set 3)** ..... 351
4.3.1 Description of the Bridges ..... 351
4.3.2 Load Distribution Factors for Moment ..... 351
4.3.3 Load Distribution Factors for Shear ..... 356
**4.4 DF Analysis of Bridges at Diamond and Dowling (Set 4)** ..... 360
4.4.1 Description of the Bridges ..... 360
4.4.2 Load Distribution Factors for Moment ..... 360
4.4.3 Load Distribution Factors for Shear ..... 365
**4.5 Summary of Findings from Field Testing** ..... 366
**CHAPTER 5 DEVELOPMENT OF 2D GRILLAGE MODELS** ..... 368
**5.1 2D Grillage Model Development** ..... 368
5.1.1 Longitudinal Joint ..... 368
5.1.2 Torsional Constant ..... 370
5.1.3 Mesh Density ..... 371
5.1.4 Effect of the Intermediate Steel Diaphragms (ISD) ..... 373
5.1.5 Boundary Conditions ..... 379
**5.2 2D Grillage Model Verification** ..... 381
5.2.1 Comparisons with Set 1 Bridges ..... 381
5.2.2 Comparisons with Set 3 Bridges and 3D FE Models ..... 382
5.2.3 Comparisons with Set 2 Bridges and 3D FE Models ..... 385
5.2.4 Comparisons with Set 4 Bridges and 3D FE Models ..... 388
**5.3 Summary** ..... 393
**CHAPTER 6 PARAMETRIC STUDY** ..... 394
**6.1 Selection of Bridge Parameters** ..... 394
6.1.1 Two Sets of Bridges ..... 394
6.1.2 Loadings ..... 396
6.1.3 Practical Bridge Database ..... 397
**6.2 Comparison with LRFD Equations** ..... 398
**6.3 Sensitivity Study of Parameters** ..... 402
**6.4 Summary of Findings** ..... 406
**CHAPTER 7 SINGLE LANE LIVE LOAD DF EQUATIONS** ..... 407
**7.1 Understanding the Behavior of Load Distribution** ..... 407
**7.2 Distribution Factor Equations** ..... 412
**7.3 Evaluation of Proposed DF Equations** ..... 414

**CHAPTER 8 CONCLUSIONS** ..... 424
**REFERENCES** ..... 426

## LIST OF FIGURES


| | | Page No. |
|---|---|---|
| Fig.1.1 | Impact of Loaded Lanes on "D" Values (AASHTO Standard) | 8 |
| Fig.1.2 | Impact of Loaded Lanes on "D" Values (AASHTO LRFD) | 9 |
| Fig. 1.3 | Comparison between $D_{single\text{-}lane}$ and $D_{two\text{-}lane}$ according to AASHTO | 10 |
| Fig. 1.4 | Free Body Diagram – Lever Rule Method | 11 |
| Fig. 1.5 | Impact of Bridge Geometry on $D_{single\text{-}lane}/D_{two\text{-}lane1}$ | 12 |
| Fig. 1.6 | Cross-sections of Multi-Beam / Precast Systems | 13 |
| Fig. 1.7 | Parameter Studies Considering Number of Loaded Lanes | 14 |
| Fig. 2.1 | Underside of Campbell Creek Bridge | 16 |
| Fig. 2.2 | Strain Transducer | 17 |
| Fig. 2.3 | Mobile Lab with Data Acquisition Equipment | 18 |
| Fig. 2.4 | Load Vehicle | 18 |
| Fig. 2.5 | Load Vehicle Wheel Load Diagram | 19 |
| Fig. 2.6 | Load Vehicle at Third Stop Position at Midspan | 21 |
| Fig. 2.7 | Longitudinal Stop Positions | 21 |
| Fig. 2.8 | Transverse Vehicle Positions (General) | 22 |
| Fig. 2.9 | Transverse Vehicle Positions (Huffman) | 23 |
| Fig. 2.10 | Transverse Vehicle Positions (Diamond / Dowling) | 23 |
| Fig. 2.11 | Gauge Positions (Elevation) | 25 |
| Fig. 2.12 | Shear Strain Gauges in Place | 26 |
| Fig. 2.13 | Placement of Moment Strain | 26 |
| Fig. 2.14 | Gauge Location on Steel Diaphragm | 27 |
| Fig. 2.15 | Picture of Strain Gauge on Steel Diaphragm | 27 |
| Fig. 3.1 | The 20-node Solid Element | 287 |
| Fig. 3.2 | Refined Mesh Example | 287 |
| Fig. 3.3 | Cross Section of the Shear Connection | 289 |
| Fig. 3.4 | Plan View of the Shear Connectors | 289 |
| Fig. 3.5 | Model of Shear Connectors | 290 |
| Fig. 3.6 | Girders connected by Intermediate Steel Diaphragms | 291 |
| Fig. 3.7 | Modeling Intermediate Steel Diaphragms | 291 |
| Fig. 3.8 | 3D FE Model of the West $100^{th}$ Avenue Bridge | 293 |
| Fig. 3.9 | 3D FE Model of the Dimond & Dowling Bridge | 293 |
| Fig. 3.10 | Comparison of Flexural Strains ($100^{th}$ NB and SB-3-G1/G5) | 295 |
| Fig. 3.11 | Comparison of Flexural Strains ($100^{th}$ NB and SB-3-G2/G4) | 296 |
| Fig. 3.12 | Comparison of Flexural Strains ($100^{th}$ NB and SB-3-G3) | 296 |
| Fig. 3.13 | Comparison of Shear Strains ($100^{th}$ NB and SB-1-G1_Left) | 297 |
| Fig. 3.14 | Comparison of Shear Strains ($100^{th}$ NB and SB-1-G1_Right) | 297 |
| Fig. 3.15 | Comparison of Shear Strains ($100^{th}$ NB and SB-1-G2_Left) | 298 |
| Fig. 3.16 | Comparison of Shear Strains ($100^{th}$ NB and SB-1-G2_Right) | 298 |
| Fig. 3.17 | Comparison of Shear Strains ($100^{th}$ NB and SB-1-G3_Left) | 299 |
| Fig. 3.18 | Comparison of Shear Strains ($100^{th}$ NB and SB-1-G3_Right) | 299 |
| Fig. 3.19 | Comparison of Shear Strains ($100^{th}$ NB and SB-1-G4_Left) | 300 |
| Fig. 3.20 | Comparison of Shear Strains ($100^{th}$ NB and SB-1-G4_Right) | 300 |
| Fig. 3.21 | Comparison of Shear Strains ($100^{th}$ NB and SB-1-G5_Left) | 301 |

| | | |
|---|---|---|
| Fig. 3.22 | Comparison of Shear Strains (100th NB and SB-1-G5_Right) | 301 |
| Fig. 3.23 | Comparison of Flexural Strains (Huffman NB and SB-3-G1) | 302 |
| Fig. 3.24 | Comparison of Flexural Strains (Huffman NB and SB-3-G6) | 303 |
| Fig. 3.25 | Comparison of Flexural Strains (Huffman NB and SB-3-Center Line) | 303 |
| Fig. 3.26 | Comparison of Flexural Strains (Huffman NB and SB-3-Right of Joint) | 304 |
| Fig. 3.27 | Comparison of Shear Strains (Huffman NB and SB-1-G1_Left) | 305 |
| Fig. 3.28 | Comparison of Shear Strains (Huffman NB and SB-1-G1_Right) | 305 |
| Fig. 3.29 | Comparison of Shear Strains (Huffman NB and SB-1-G6_Left) | 306 |
| Fig. 3.30 | Comparison of Shear Strains (Huffman NB and SB-1-G6_Right) | 306 |
| Fig. 3.31 | Comparison of Shear Strains (Huffman NB and SB-1-Center_Left) | 307 |
| Fig. 3.32 | Comparison of Shear Strains (Huffman NB and SB-1-Center_Right) | 307 |
| Fig. 3.33 | Comparison of Shear Strains (Huffman NB & SB-1-RightofJoint_Left) | 308 |
| Fig. 3.34 | Comparison of Shear Strains (Huffman NB & SB-1-RightofJoint_Right) | 308 |
| Fig. 3.35 | Comparison of Flexural Strains (Campbell NB and SB-3-G1) | 309 |
| Fig. 3.36 | Comparison of Flexural Strains (Campbell SB-3-G5) | 309 |
| Fig. 3.37 | Comparison of Flexural Strains (Campbell NB & SB-3-G2) | 310 |
| Fig. 3.38 | Comparison of Flexural Strains (Campbell NB & SB-3-G4) | 310 |
| Fig. 3.39 | Comparison of Flexural Strains (Campbell NB & SB-3-G3) | 311 |
| Fig. 3.40 | Comparison of Shear Strains (Campbell SB-1-G1_Left) | 312 |
| Fig. 3.41 | Comparison of Shear Strains (Campbell SB-1-G1_Right) | 312 |
| Fig. 3.42 | Comparison of Shear Strains (Campbell SB-1-G2_Left) | 313 |
| Fig. 3.43 | Comparison of Shear Strains (Campbell SB-1-G2_Right) | 313 |
| Fig. 3.44 | Comparison of Shear Strains (Campbell SB-1-G3_Left) | 314 |
| Fig. 3.45 | Comparison of Shear Strains (Campbell SB-1-G3_Right) | 314 |
| Fig. 3.46 | Comparison of Shear Strains (Campbell SB-1-G4_Left) | 315 |
| Fig. 3.47 | Comparison of Shear Strains (Campbell SB-1-G4_Right) | 315 |
| Fig. 3.48 | Comparison of Shear Strains (Campbell SB-1-G5_Left) | 316 |
| Fig. 3.49 | Comparison of Shear Strains (Campbell SB-1-G5_Right) | 316 |
| Fig. 3.50 | Comparison of Flexural Strains (Diamond & Dowling-3-G1) | 317 |
| Fig. 3.51 | Comparison of Flexural Strains (Diamond & Dowling-3-G2) | 318 |
| Fig. 3.52 | Comparison of Flexural Strains (Diamond & Dowling-3-G3) | 318 |
| Fig. 3.53 | Comparison of Flexural Strains (Diamond & Dowling-3-G4) | 319 |
| Fig. 3.54 | Comparison of Flexural Strains (Diamond & Dowling-3-G6) | 319 |
| Fig. 3.55 | Comparison of Flexural Strains (Diamond & Dowling-3-G7) | 320 |
| Fig. 3.56 | Comparison of Shear Strains (Diamond & Dowling-1-G1_Left) | 321 |
| Fig. 3.57 | Comparison of Shear Strains (Diamond & Dowling-1-G1_Right) | 321 |
| Fig. 3.58 | Comparison of Shear Strains (Diamond & Dowling-1-G2_Left) | 322 |
| Fig. 3.59 | Comparison of Shear Strains (Diamond & Dowling-1-G2_Right) | 322 |
| Fig. 3.60 | Comparison of Shear Strains (Diamond & Dowling-1-G3_Left) | 323 |
| Fig. 3.61 | Comparison of Shear Strains (Diamond & Dowling-1-G3_Right) | 323 |
| Fig. 3.62 | Comparison of Shear Strains (Diamond & Dowling-1-G4_Left) | 324 |
| Fig. 3.63 | Comparison of Shear Strains (Diamond & Dowling-1-G4_Right) | 324 |
| Fig. 3.64 | Comparison of Shear Strains (Diamond & Dowling-1-G6_Left) | 325 |
| Fig. 3.65 | Comparison of Shear Strains (Diamond & Dowling-1-G6_Right) | 325 |
| Fig. 3.66 | Comparison of Shear Strains (Diamond & Dowling-1-G7_Left) | 326 |
| Fig. 3.67 | Comparison of Shear Strains (Diamond & Dowling-1-G7_Right) | 326 |

| | | |
|---|---|---|
| Fig. 4.1 | Cross Section of Set 1 Bridges | 328 |
| Fig. 4.2 | Model for Applying Lever Rule | 330 |
| Fig. 4.3 | Moment Distribution Factors ($100^{th}$ NB – 3 – G1&G2) | 331 |
| Fig. 4.4 | Moment Distribution Factors ($100^{th}$ NB – 3 – G4&G5) | 331 |
| Fig. 4.5 | Load Distribution Factors for Moment ($100^{th}$ NB Bridge) | 332 |
| Fig. 4.6 | Load Distribution Factors for Moment ($100^{th}$ SB Bridge) | 333 |
| Fig. 4.7 | Model for Applying Lever Rule | 334 |
| Fig. 4.8 | Shear Distribution Factor ($100^{th}$ NB – 1 – G1&G2) | 335 |
| Fig. 4.9 | Shear Distribution Factor ($100^{th}$ NB – 1 – G4&G5) | 335 |
| Fig. 4.10 | Shear Distribution Factor ($100^{th}$ SB – 1 – G1&G2) | 336 |
| Fig. 4.11 | Shear Distribution Factor ($100^{th}$ SB – 1 – G4&G5) | 336 |
| Fig. 4.12 | Load Distribution Factors for Shear ($100^{th}$ NB Bridge) | 337 |
| Fig. 4.13 | Load Distribution Factors for Shear ($100^{th}$ SB Bridge) | 338 |
| Fig. 4.14 | Cross Section of the Bridge | 339 |
| Fig. 4.15 | Moment Distribution Factor (Huffman NB – 3 – G1&G3) | 341 |
| Fig. 4.16 | Moment Distribution Factor (Huffman NB – 3 – G6) | 341 |
| Fig. 4.17 | Moment Distribution Factor (Huffman SB – 3 – G1&G3) | 342 |
| Fig. 4.18 | Moment Distribution Factor (Huffman SB – 3 – G4&G6) | 342 |
| Fig. 4.19 | Moment Distribution Factors (Huffman NB Bridge) | 343 |
| Fig. 4.20 | Moment Distribution Factors (HuffmanSB Bridge) | 344 |
| Fig. 4.21 | Shear Distribution Factor (Huffman NB – 1 – G1&G3) | 347 |
| Fig. 4.22 | Shear Distribution Factor (Huffman NB – 1 – G6) | 347 |
| Fig. 4.23 | Shear Distribution Factor (Huffman SB – 1 – G1&G3) | 348 |
| Fig. 4.24 | Shear Distribution Factor (Huffman SB – 1 – G4&G6) | 348 |
| Fig. 4.25 | Shear Distribution Factors (Huffman NB Bridge) | 349 |
| Fig. 4.26 | Shear Distribution Factors (Huffman SB Bridge) | 350 |
| Fig. 4.27 | Cross section of the bridge | 351 |
| Fig. 4.28 | Moment Distribution Factor (Campbell NB – 3 – G1&G2) | 352 |
| Fig. 4.29 | Moment Distribution Factor (Campbell NB – 3 – G4&G5) | 352 |
| Fig. 4.30 | Moment Distribution Factor (Campbell SB – 3 – G1&G2) | 353 |
| Fig. 4.31 | Moment Distribution Factor (Campbell SB – 3 – G4&G5) | 353 |
| Fig. 4.32 | Moment Distribution Factors (Campbell NB Bridge) | 354 |
| Fig. 4.33 | Moment Distribution Factors (Campbell SB Bridge) | 355 |
| Fig. 4.34 | Shear Distribution Factor (Campbell NB – 1 – G1&G2) | 356 |
| Fig. 4.35 | Shear Distribution Factor (Campbell NB – 1 – G4&G5) | 357 |
| Fig. 4.36 | Shear Distribution Factor (Campbell SB – 1 – G1&G2) | 357 |
| Fig. 4.37 | Shear Distribution Factor (Campbell SB – 1 – G4&G5) | 358 |
| Fig. 4.38 | Shear Distribution Factors (Campbell NB Bridge) | 359 |
| Fig. 4.39 | Shear Distribution Factors (Campbell SB Bridge) | 359 |
| Fig. 4.40 | Cross section of the bridge | 360 |
| Fig. 4.41 | Moment Distribution Factor (Dowling – 3 – G1, G2, G3) | 361 |
| Fig. 4.42 | Moment Distribution Factor (Dowling – 3 – G4, G6, G7) | 362 |
| Fig. 4.43 | Moment Distribution Factor (Diamond – 3 – G1, G2, G3) | 362 |
| Fig. 4.44 | Moment Distribution Factor (Diamond – 3 – G4, G6, G7) | 363 |
| Fig. 4.45 | Moment Distribution Factors (Diamond Bridge) | 364 |
| Fig. 4.46 | Moment Distribution Factors (Dowling Bridge) | 364 |

| | | |
|---|---|---|
| Fig. 5.1 | Cross-section of 100th Ave Bridge | 368 |
| Fig. 5.2 | Impact of the Longitudinal Joint on Moment DF | 369 |
| Fig. 5.3 | Evaluation of Torsional Constant in Hinged Grillage Models | 370 |
| Fig. 5.4 | Evaluation of Torsional Constant in Rigid Grillage Models | 371 |
| Fig. 5.5 | Evaluation of Mesh Density in Grillage Models | 372 |
| Fig. 5.6 | Exaggerated Deflection of the Hinged Model | 373 |
| Fig. 5.7 | Intermediate Steel Diaphragms help to resist rotation | 373 |
| Fig. 5.8 | Moment DF comparison With/Without ISD | 374 |
| Fig. 5.9 | Shear DF comparison With/Without ISD | 375 |
| Fig. 5.10 | Midspan Moments from Different Models (100th – 3 – G3) | 376 |
| Fig. 5.11 | Midspan Moments from Different Models (100th – 3 – G2) | 377 |
| Fig. 5.12 | Midspan Moments from Different Models (100th – 3 – G1) | 378 |
| Fig. 5.13 | Schematic of Diagram of Grillage Model | 379 |
| Fig. 5.14 | Impact of Model Support Conditions | 380 |
| Fig. 5.15 | Moment Distribution Factor Comparison (100th NB&SB Bridge) | 381 |
| Fig. 5.16 | Shear Distribution Factor Comparison (100th NB&SB Bridge) | 382 |
| Fig. 5.17 | Midspan Moment from Different Models (Campbell NB&SB) | 383 |
| Fig. 5.18 | Moment Distribution Factor Comparisons (Campbell NB&SB Bridge) | 384 |
| Fig. 5.19 | Shear Distribution Factor Comparisons (Campbell NB&SB Bridge) | 384 |
| Fig. 5.20 | Midspan Moment from Different Models (Huffman NB&SB) | 385 |
| Fig. 5.21 | Moment Distribution Factor Comparisons (Huffman NB&SB Bridge) | 386 |
| Fig. 5.22 | Shear Distribution Factor Comparisons (Huffman NB&SB Bridge) | 387 |
| Fig. 5.23 | Moment Distribution Factor Comparisons (Diamond & Dowling Bridges) | 388 |
| Fig. 5.24 | Shear Distribution Factor Comparisons (Diamond & Dowling – 1 – G1) | 389 |
| Fig. 5.25 | Shear Distribution Factor Comparisons (Diamond & Dowling – 1 – G2) | 389 |
| Fig. 5.26 | Shear Distribution Factor Comparisons (Diamond & Dowling – 1 – G3) | 390 |
| Fig. 5.27 | Shear Distribution Factor Comparisons (Diamond & Dowling – 1 – G4) | 390 |
| Fig. 5.28 | Shear Distribution Factor Comparisons (Diamond & Dowling – 1 – G6) | 391 |
| Fig. 5.29 | Shear Distribution Factor Comparisons (Diamond & Dowling – 1 – G7) | 391 |
| Fig. 5.30 | Shear Distribution Factor Comparisons (Diamond and Dowling Bridges) | 392 |
| Fig. 6.1 | Typical Cross-sections of the girders in Set I | 395 |
| Fig. 6.2 | Typical Cross-section used in Set II | 396 |
| Fig. 6.3 | Typical Transverse Loading used in Parametric Study | 396 |
| Fig. 6.4 | Comparison of LRFD DF Equations to Rigid-Grillage Models from Set I | 398 |
| Fig. 6.5 | Comparison of LRFD DF Equations to Rigid-Grillage Models from Set I | 399 |
| Fig. 6.6 | LRFD DF Equations vs. Rigid-Grillage Models from Set II | 400 |
| Fig. 6.7 | LRFD DF Equations vs. Hinged-Grillage Models from Set II | 400 |
| Fig. 6.8 | Sensitivity Study (Models from Set I) | 402 |
| Fig. 6.9 | Sensitivity Study of Hinged Models from Set II | 403 |
| Fig. 6.10 | Sensitivity Study of Rigid Models from Set II | 404 |
| Fig. 7.1 | Simple Beam on Elastic Foundation Model (BEFM) | 407 |
| Fig. 7.2 | Simply Supported Beam | 407 |
| Fig. 7.3 | Rigid Supported Beam With Induced Deflection at One Support | 408 |
| Fig. 7.4 | Moment DF for Interior Girders [Set of DF(S)] | 414 |
| Fig. 7.5 | Moment DF for Interior Girders [Set of DF(S,L,I)] | 415 |
| Fig. 7.6 | Moment DF for Exterior Girders [Set of DF(S)] | 415 |

| | | |
|---|---|---|
| Fig. 7.7 | Moment DF for Exterior Girders [Set of DF(S,L,I)] | 416 |
| Fig. 7.8 | Shear DF for Interior Girders [Set of DF(S)] | 416 |
| Fig. 7.9 | Shear DF for Interior Girders [Set of DF(S,L,I)] | 417 |
| Fig. 7.10 | Shear DF for Exterior Girders [Set of DF(S)] | 417 |
| Fig. 7.11 | Shear DF for Exterior Girders [Set of DF(S,L,I)] | 418 |
| Fig. 7.12 | Evaluation of **Moment** Distribution Factors on **Interior** Girders | 419 |
| Fig. 7.13 | Evaluation of **Moment** Distribution Factors on **Exterior** Girders | 420 |
| Fig. 7.14 | Evaluation of **Shear** Distribution Factors on **Interior** Girders | 421 |
| Fig. 7.15 | Evaluation of **Shear** Distribution Factors on **Exterior** Girders | 422 |

## LIST OF TABLES


| | | Page No. |
|---|---|---|
| Table 2.1 | Field Tested Bridges (From May 6 to May 19, 2003) | 15 |
| Table 4.1 | Distribution Factor for Moment for Set 1 Bridges | 333 |
| Table 4.2 | Distribution Factor for Shear for Set 1 Bridges | 337 |
| Table 4.3 | Distribution Factor for Moment for Set 2 Bridges | 343 |
| Table 4.4 | Distribution Factor for Shear for Set 2 Bridges | 349 |
| Table 4.5 | Distribution Factor for Moment for Set 3 Bridges | 354 |
| Table 4.6 | Distribution Factor for Shear for Set 3 Bridges | 358 |
| Table 4.7 | Distribution Factor for Moment for Diamond and Dowling | 363 |
| Table 4.8 | Distribution Factor for Moment | 366 |
| Table 4.9 | Distribution Factor for Shear | 366 |
| Table 6.1 | Span Lengths (in feet) of Realistic Bridges in Set I | 397 |
| Table 6.2 | Span Lengths (in feet) of Realistic Bridges in Set II | 397 |
| Table 6.3 | Example of Sensitivity Study Calculations | 402 |
| Table 7.1 | Moment Distribution Factors Based on Different Methods | 423 |
| Table 7.2 | Shear Distribution Factors Based on Different Methods | 423 |

# CHAPTER 1 - INTRODUCTION

The State of Alaska is unique in that its construction season is much shorter than other states. Due to this shortened construction season, Alaska Department of Transportation and Public Facilities (AKDOT& PF) uses the decked bulb-tee bridge girder system to construct most of the new highway bridges in the state. The decked bulb-tee girder is a precast, prestressed concrete girder with a top flange wide and deep enough to act as the bridge deck. The construction of these bridge systems only requires placing the girders then connecting the girders with a shear key and grout. There is no requirement for form work or cast in place concrete. This type of system allows for very rapid bridge construction and is ideal for the short construction season in Alaska. While this bridge system is very prevalent in Alaska it is not used much in other states and therefore the system has not been thoroughly researched.

The AKDOT uses the AASHTO Load Resistance Factor Design (LRFD) Bridge Design Specifications for design and evaluation of Alaska's highway bridges [AASHTO LRFD 1998]. For most bridge systems, the LRFD Specifications has two distinct groups of simplified equations to determine the live load distribution factor (DF) of a bridge girder. One set of equations provides the DF under general or multilane loaded conditions. The other set of equations provides the DF when the bridge is subjected to a single lane loaded condition. Typically, the DF equations for the single lane loaded condition provide a lower distribution factor than the equations for the multi lane loaded condition. However, the simplified equations for the decked bulb-tee bridge girder system, where the girders are only connected enough to prevent relative vertical translation, do not distinguish between the single lane and multi lane loaded condition. Typically designers use the DF equations for the single lane loaded condition to rate bridges for permit loads or overload conditions where the bridge will be subjected to only one truck. Because the LRFD design does not distinguish between the multilane loaded and single lane loaded condition, there is a load rating penalty for the decked bulb-tee bridge girder system. Due to this load rating penalty, the AKDOT has funded research aimed at determining an accurate set of DF equations that describe the behavior of the decked bulb-tee bridge system under a single lane-loaded condition.

## 1.1 Review of Distribution Factor Equations

Based on Newmark's research [Newmark 1948], the lateral wheel load distribution factors were determined by the expression:

$$g = \frac{S}{D} \tag{1.1}$$

where **g** = the wheel load distribution factor (DF); **S** = the center-to-center girder spacing (ft); and **D** = different constants for different bridge systems (ft). Please note that the "D" value is used to determine the portion of live load carried by a girder line, and incorporates bridge type, loading configuration as well as number of loaded lanes.

Simple "S-over" live-load distribution factors have been used for bridge design since the American Association of State Highway Officials (AASHO) published its first edition of Standard Specifications for Highway Bridges in 1931. These factors allow the designer to uncouple transverse behavior from longitudinal behavior. However, live-load distribution provisions for multibeam precast concrete bridges (such as Alaska style decked bulb tee bridges) were not included in the specifications until 1965, when AASHTO published its ninth edition of Standard Specifications. In its ninth edition, the distribution criteria for multibeam bridges were only limited to a brief reference in the slab design section. Specifically, the distribution width per wheel is equal to 4.0+0.06L (L = Span ) (ft) with a maximum of 7.0 ft.

### 1.1.1 AASHTO Standard Specifications, 12th Edition, 1977

In 1977, the distribution criteria for multibeam bridges was incorporated into the "Distribution of Loads" section with other bridge systems. The DF formula for multibeam bridges took the same format (of Eq. (1.1)) as other bridge systems, but included the following refinements:

$$S = \text{effective girder spacing} = \frac{12N_L + 9}{N_g} \tag{1.2}$$

$$\begin{aligned} D &= 5 + \frac{N_L}{10} + (3 - \frac{2N_L}{7})(1 - \frac{C}{3})^2 \qquad C \le 3 \\ &= 5 + \frac{N_L}{10} \qquad C > 3 \end{aligned} \tag{1.3}$$

where $N_L$ = total number of design traffic lanes; $N_g$ = number of longitudinal beams; and C = a stiffness parameter that depends on the type of bridge, bridge and beam geometry, and material properties, calculated based on the following:

$$C = K\frac{W}{L} \tag{1.4}$$

$$K = \sqrt{\frac{E}{2G}\frac{I_1}{J_1 + J_t}} \tag{1.5}$$

where W = the overall width of the bridge (ft); L = span length (ft); $EI_1$ = flexural stiffness of the transformed beam section per unit width; $GJ_1$ = torsional stiffness of the transformed beam section per unit width; and $GJ_t$ = torsional stiffness of a unit width of bridge deck slab.

These DF formulas for multibeam bridges were proposed by Sanders and Elleby in NCHRP Report 83 [Sanders and Elleby 1970]. The multibeam criteria were, as most criteria, based on no reduction in load intensity (i.e., without considering the multiple presence factor).

### 1.1.2 University of Washington Study

The only stemmed members addressed in NCHRP Report 83 were channels. Considering sections such as double tees, bulb tees, single tees, as well as decked bulb tees have come into common use for bridges, the University of Washington conducted the NCHRP 12-24 study on load distribution for precast stemmed multibeam bridges [Stanton and Mattock 1986]. The specific objectives of that research were to investigate the distribution of truck wheel loads in the decks of bridges made from single-stem and multi-stemmed precast concrete tee-shaped members. It was also an objective to make recommendations for their design in a form suitable for inclusion in the AASHTO Standard Specifications. The following DF formulas were proposed in the final report [Stanton and Mattock 1986] of the NCHRP Project 12-24:

S = width of precast member (1.6)

$$\begin{aligned} D &= (5.75 - 0.5N_L) + 0.7N_L(1 - 0.2C)^2 \qquad C \le 5 \\ &= (5.75 - 0.5N_L) \qquad C > 5 \end{aligned} \tag{1.7}$$

$$C = K\frac{W}{L} \tag{1.8}$$

$$K = \sqrt{\frac{EI}{2GJ}} \tag{1.9}$$

where EI = flexural stiffness of each girder; GJ = torsional stiffness of each girder; and others are the same as before.

Comparing Eqs (1.6)-(1.9) with Eqs (1.2)-(1.5), the following changes are noted:

* The former use the effective girder spacing while the later use the actual girder spacing.
* There is a difference in calculating the stiffness parameter K.
* The wheel load fractions from both sets of formulas give nearly identical results for small C values (i.e., long narrow bridges made from torsionally stiff members). D increases when C decreases. This is because torsionally stiff members deflect under load but twist little, thereby causing adjacent members to deflect and spread the load. However, for large C values (i.e., short wide bridges made from stemmed members), the 1977 AASHTO relationships (Eqs (1.2)-(1.5)) predict significantly larger D values.
* Eqs (1.6)-(1.9) consider bridges with skew angles up to 45 degrees while Eqs (1.2)-(1.5) do not take skew into account. For skewed bridges, bridge width W is measured perpendicular to the longitudinal girders and bridge span L is measured parallel to longitudinal girders in Eqs (1.6) – (1.9).

### 1.1.3 AASHTO Standard Specifications, 16th Edition, 1996

The current edition of Standard Specifications [AASHTO STD 1996] has the same DF formulas as Eqs (1.6) – (1.9). The current specifications state that if the value of $\sqrt{\frac{I}{J}}$

exceeds 5.0, the live load distribution should be determined using a more precise method, such as the Articulated Plate Theory or Grillage Analysis.

It also states that for non-voided rectangular beams, channels, and tee beams, Saint-Venant torsion constant "J" may be estimated using the following equation:

$$J = \sum \{ \frac{bt^3}{3} (1 - 0.630 \frac{t}{b}) \} \qquad (1.10)$$

where b = the length of each rectangular component within the section; t = the thickness of each rectangular component within the section. The flanges and stems of stemmed or channel sections are considered as separate rectangular components whose values are summed together to calculate "J".

The current Standard Specifications also require full-depth rigid end diaphragms to ensure proper load distribution for channel, single- and multi-stemmed tee beams.

### 1.1.4 AASHTO LRFD Specifications, Second Edition with 2001 Interim

The provisions for load distribution for "multi-beam decks which are not sufficiently interconnected to act as a unit" are the same in the LRFD Specification [AASHTO LRFD 1998] as the provisions that appear in recent editions of the Standard Specifications.

Some of the changes are as follows:

* Instead of using wheel load fraction, as in Standard Specifications, LRFD Specs use lane load fraction. Thus, "D" value from LRFD is twice as much as the one in Standard Specs.
* There is no range of applicability specified in LRFD Specs other than that the number of beams is not less than four, beams are parallel and have approximately the same stiffness, and the stem spacing of stemmed beams is more than 4 ft or less than 10 ft.
* The multiple presence factors in LRFD Specs are different from those in Standard Specs.
* The St. Venant torsional inertia, J, may be determined as:

$$J = \frac{1}{3} \sum bt^3 \qquad \text{For thin-walled open beam} \qquad (1.11)$$

$$J = \frac{A^4}{40.0 I_p} \qquad \text{For stoky open sections (such as T-beams)} \qquad (1.12)$$

where A = area of cross-section; and $I_p$ = polar moment of inertia.

* The load fraction formulas for the interior and exterior beams are the same in Standard Specifications, while the lane load fraction for exterior beams is based on "Lever Rule" in LRFD Specifications.
* Similar to Standard Specs, there is no correction factor available for skewed bridges in LRFD Specs.
* The "Lever Rule" is recommended as the method to be used to calculate the load distribution factor for shear.

* There are no correction factors for load distribution factors for support shear of obtuse corners of skewed bridges.

The AASHTO LRFD Specifications recommend using the “Lever Rule” – a method of determining the live-load shear carried by a single girder assuming that the deck acts as a simply supported span between girders.

Using the “Lever Rule” results in two perceived problems:

* The “Lever Rule” is invalid for Alaska Decked Bulb-Tee Girders. The deck formed by these girders has a longitudinal joint midway between adjacent girders. This longitudinal joint acts in a manner similar to a hinge. The assumption of hinges over the girders would result in an instability in the system using the “Lever Rule”.
* The “Lever Rule” method may be overly conservative for analyzing Alaska Decked Bulb-Tee Girders.

## 1.2 Applicable Theories

The behavior of multi-beam bridges is in many respects similar to that of the beam and slab bridges. The major difference is the elimination of the moment restraint between the individual beam units, which leads to some modifications in the applicable theories. The methods of analyses can be divided into three major categories. The first category is normally called the methods of compatible deformation based on the flexibility methods. The second category can be classified as a plate theory. The third category is the grillage analysis.

Plate theory is often used to approximate bridge decks. This technique allows for closed form solutions. Plate theory may be divided into several subsets. For example, one approach might be to assume no flexural rigidity exists in the transverse direction. It might be argued that this approximation is a reasonable approach to model discontinuities resulting from the longitudinal shear key between bridge beams. It may also be argued that some flexural rigidity is available. This is due to the effects of transverse prestress forces and some continuity that exists in the shear key. A second method, discussed below, would account for these affects. The first method is usually known as articulated plate theory [Watanabe 1968]; the latter is termed orthotropic plate theory.

The orthotropic plate theory was first studied by Guyon. It was later modified by Massonnet to account for torsional stiffness. Rowe than modified the method to account for Possion's ratio [Rowe 1955]. It appears that Spindel was the first to set the transverse stiffness to zero and use the orthotropic plate theory to analyze the hinged joint multi-beam bridges [Spindel 1961]. The method is now commonly called the "articulated-plate" method. Later, Watanabe added a restraint-of-warping torsion term [Watanabe 1968]. Local stiffening by edge beams may also be accounted for [Pama and Cusens 1967]. Given bridge geometry and stiffness, this method may be used to analyze many types of bridges. It is convenient for developing dimensionless design charts.

The orthotropic-plate method, or rather the special case called the articulated-plate theory, is unable to distinguish between a bridge made from many narrow beams and one of the same width, but made from a few wide beams, if both have the same total flexural and torsion stiffness. Difficulties also exist over the interpretation of the value to be used for warping torsion stiffness per unit width, since this cross-sectional property varies as length to the fifth power, whereas the flexural and torsional parameters vary only as length to the third power. So, if the size of their members is halved and their number is doubled, it is possible to keep the same values for flexural and torsional stiffness, but the value for restraint-of-warping torsional stiffness will be different. Thus, the simplicity of the nondimensional results usually obtainable with orthotropic-plate theory is lost. Further disadvantages are presented by skew supports and diaphragms, so the method was rejected in favor of the beam-grillage approach in the UW study [Stanton and Mattock 1986].

The grillage analysis is appealing because beam behavior is better understood by more engineers than is orthotropic-plate theory. The primary advantage is that virtually any special conditions, such as skew, hinges between members, diaphragms at discrete points,

asymmetric edge stiffening beams, etc., can be modeled without difficulty. The main drawback is that diagonal beams are required in the grillage in order to model precisely the torsional properties of a plate and, if this is done, interpretation of results becomes somewhat complex [Yettram and Husain 1965]. The diagonals can be omitted for simplicity and the primary penalty is the loss of coupling effects, whereby imposed curvature in one direction in a plate causes bending moments in the other. However, ignoring the coupling effects seldom gives rise to serious errors. This method has been widely used, particularly in England. In most applications only three degrees of freedom per node are retained (vertical and two rotations), leading to a reasonably economical solution. That is, provided the number of girders and cross beams is not excessive. Reilly included restraint-of-warping torsion in grillage analyses requiring an extra degree of freedom per node [Reilly 1972].

A three dimensional finite element model offers an improvement over the other techniques discussed in that simplifications to approximate the behavior as a two-dimensional system are not required. The finite element method has become a popular method for calculating the load distribution factors for bridges of various types [Barr et al 2000, Hays et al 1986, Imbsen and Nutt 1978]. It provides excellent results and it requires the fewest assumptions and it can be used to account for the greatest number of variables that affect structural response.

Hays et al. (1986) idealized the bridge superstructure using plate elements and plane or space frame members with the centroid of the girders coinciding with the centroid of the concrete slab. Imbsen and Nutt (1978) imposed rigid links between the idealized concrete slab, which was modeled as plate elements, and steel beams, which were modeled as space frame members, to accommodate the eccentricity of the beams. However, Bishara (1984) modeled the bridge superstructure using plate elements for the concrete slab, space frame members for the girder flanges, and plate elements for the girder web.

The finite element method is an important tool for use in conducting a detailed and accurate analysis of bridge decks. Stiffness and loads affect results. So, accuracy is depends on having representative model. Besides geometry, material properties, density, and the boundary conditions may dramatically affect results. Truckloads should be placed at positions that produce the maximum response in the components being investigated. It is essential that independent checks are conducted to detect gross errors that may be introduced through incorrect input data.

## 1.3 Impact of Single Loading

Consider a single load lane distribution factor for the Alaska Bulb Tee Bridge. The live load distribution factor for load rating purpose can be different from the distribution factor for bridge design. For example, a multiple lane distribution factor will over estimate the live load carried by a girder due to single lane loading. These results in a reduction in the allowable live load carried by the bridge, and the "operating" or maximum bridge live load capacity is reduced. At present, research data is available for finding a realistic value for these structures.

### 1.3.1 AASHTO Specifications

According to the current AASHTO Specifications, there are two different live load DF equations for most bridges. One equation is for single lane loaded, and the other is for two or more lane loaded. Regardless of number of loaded lanes, however, the same D value is used for precast concrete beams as that used in multibeam decks which includes the Alaska style decked bulb-tees.

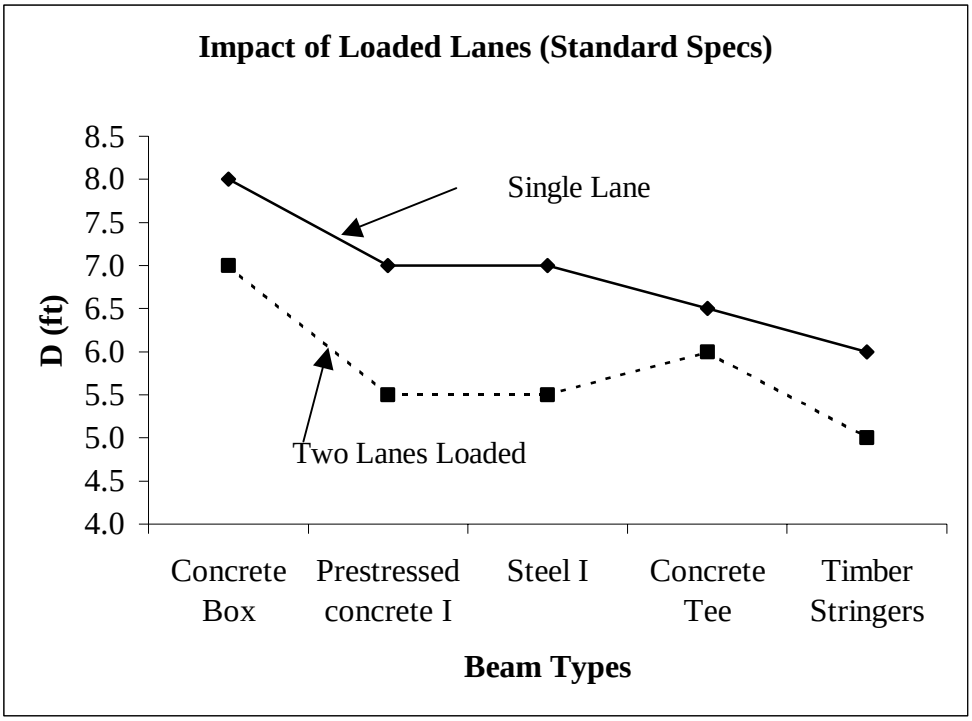


Fig.1.1 Impact of Loaded Lanes on "D" Values (AASHTO Standard)

Figure 1.1 shows the impact of the number of loaded lanes on "D" values in the "S-over" live-load distribution factor for different bridge systems based on AASHTO Standard Specifications. Several observations can be drawn from Figure 1.1. First, D increases for all five bridge systems considered when the same bridge is changed from two lanes loaded into single lane loaded. A larger D value suggests better live-load distribution. The degree of increase in D values for different bridge systems is different. The D value of single lane

loaded prestressed concrete and steel I-beams is about the 127% of D value of the two lanes loaded counterpart. For a concrete tee beam system, the D value is only increased by 8%.

The second observation is that for both single lane loaded and two lanes loaded bridge systems, the multi-cell concrete box system has the highest D values and the timber stringer system, the lowest.

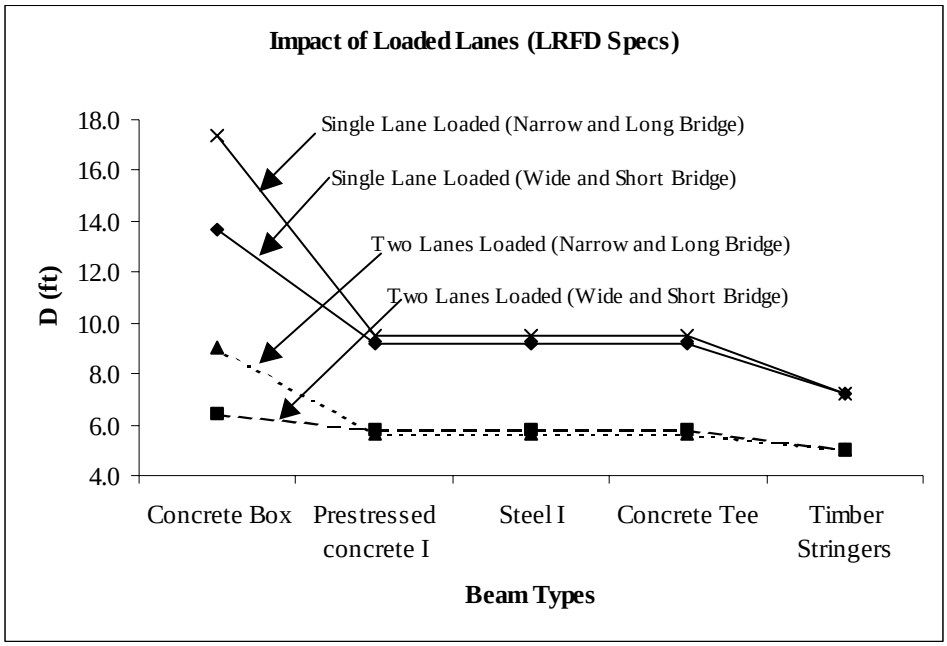


Fig.1.2 Impact of Loaded Lanes on "D" Values (AASHTO LRFD)

Figure 1.2 shows the impact for a number of loaded lanes according to AASHTO LRFD Specifications. Based on NCHRP Project 12 – 26, new, more accurate, and more complex live-load distribution factor equations were developed and proposed to AASHTO as replacements for the simple "S-over" factors in AASHTO Standard Specifications [Zokaie et al 1991]. These equations are included in the LRFD Specifications.

Other changes in LRFD Specifications include:

* The multiple presence factor of "1.2" is applied to single lane loaded bridges.
* The lane distribution factor is used in LRFD instead of the wheel load distribution factor.
* The lane distribution factor in LRFD depends on stiffness parameters, and width and span of bridges, as well as the girder spacing parameter, as in Standard Specifications.

In order to facilitate comparisons, the lane load distribution factor has been converted to a common basis in the format of "S-over" formula. In calculating the equivalent "D" values shown in Figure 1.2, bridges are grouped into "wide and short" and "narrow and long" categories according to the range of applicability specified in LRFD Specs. In the first category, the high range of girder spacing and the low range of span are used. And the low range of girder spacing and the high range of span are applied in the second category. Other

assumptions used are: The number of cells is 6 for concrete box girder bridges. And $\frac{K_g}{12Lt_s^3}$ is assumed to be equal to 1.0 for deck-and-slab bridges. In order to convert to a value free of multiple presence factors, the D values are multiplied by 1.2 for the single lane loaded bridges.

Comparing Figure 1.2 with Figure 1.1, some similar observations can be found. However, the following conclusions can be also drawn from Figure 1.2:

* Except for concrete box bridge systems, differences in D values between "wide and short" and "narrow and long" bridges are not significant.
* Improvement in load distribution for single lane loaded bridges is even better according to LRFD Specs (i.e., $D_{single\text{-}lane}$ value is much larger than $D_{two\text{-}lane}$ value), as shown in Figure 1.3.

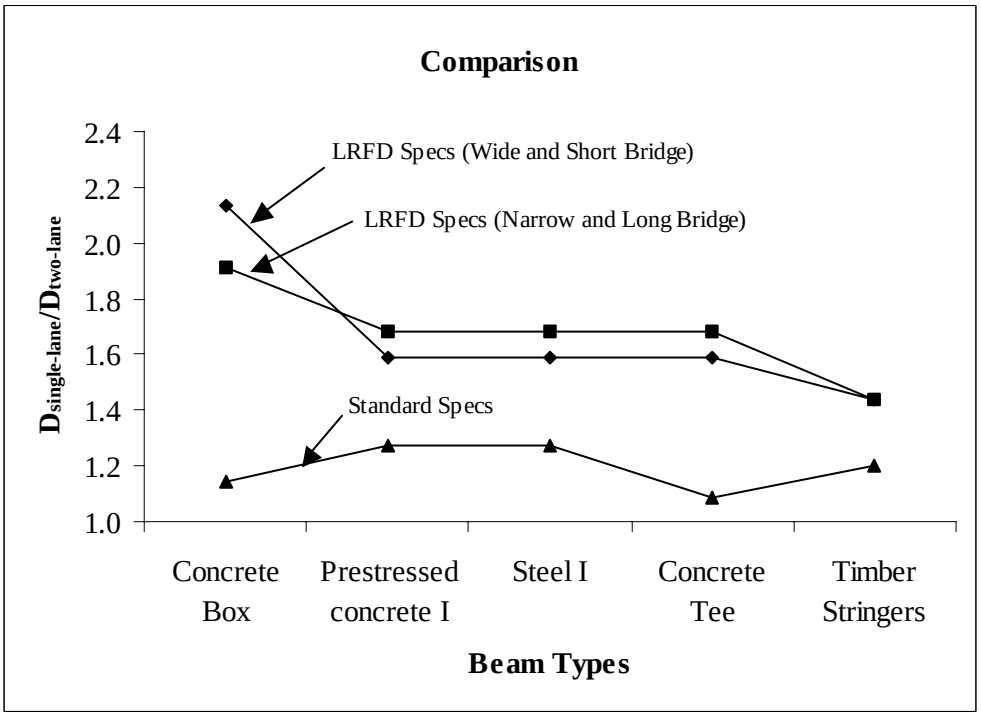


Fig. 1.3 Comparison between $D_{single\text{-}lane}$ and $D_{two\text{-}lane}$ according to AASHTO

Obviously, there exists a difference between AASHTO Standard Specs and AASHTO LRFD Specs as shown in Figure 1.3. In general, LRFD Specs predict a higher ratio of D values, especially for the concrete box bridge system, than Standard Specs. It also appears that the bridge geometry plays a very important role in calculating the live-load distribution factor for single lane loaded bridges according to LRFD Specs.

### 1.3.2 Discussions

As shown in Figure 1.3, the single lane DF will be about 78% of the multiple lane DF factor based on AASHTO Standard Specifications, and even lower DF for single lane based on AASHTO LRFD Specifications. This seems reasonable from the perspective of the "Level Rule," as shown in Figure 1.4.

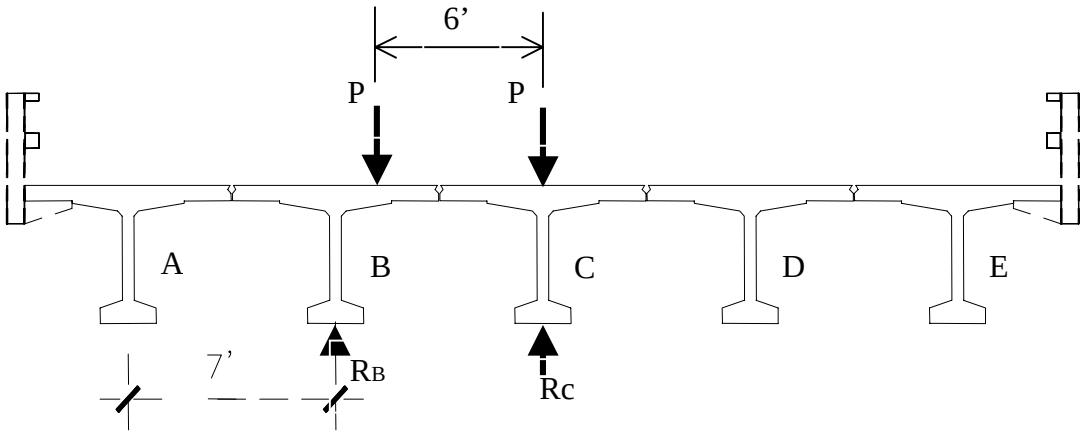


(a) Single Lane Loaded

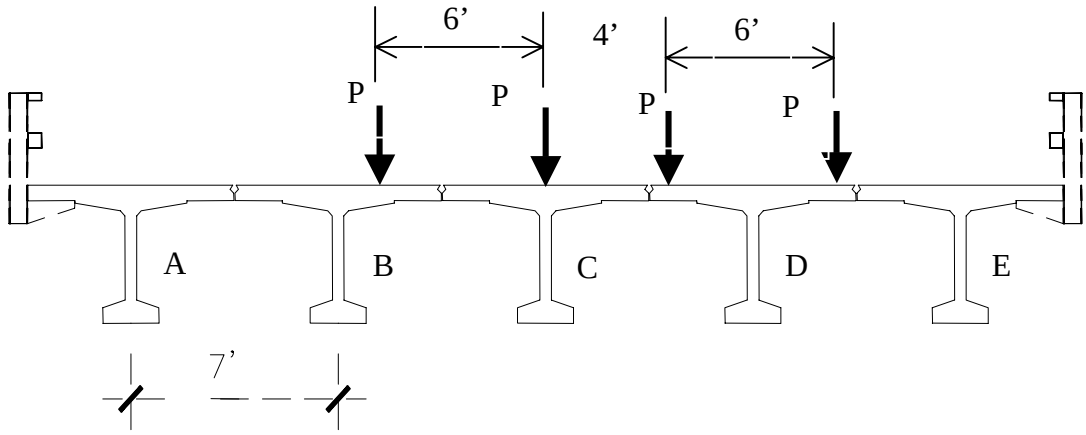


(b) Two Lanes Loaded

Fig. 1.4 Free Body Diagram – Lever Rule Method

Consider Figure 1.4 (a). The deck is assumed to be simply supported by each girder except over the exterior girders A and E where the cantilever is continuous. If we consider one lane loaded, the reaction at C (Rc) is established by balancing the moment about B.

Rc (7) = P (7) + P (7-6)

which reduces to

Rc = P + P/7 = 1.143 P

The fraction of the single lane that is carried by the Girder C is 1.143P/(2P) = 0.572. Thus, the girder distribution factor is 0.572 (without the multiple presence factor).

The distribution factor for the same Girder C subjected to two loaded lanes is established by considering trucks positioned with axles on deck panels BC, CD, and DE, as shown in Figure 1.4 (b). Equilibrium requires that the reaction at C is

Rc = (P + P/7) + [(7-4)/7]P = 1.572P

And the distribution factor (without considering the multiple presence factor) is 1.572P/(2P) = 0.786, which is larger than the distribution factor for single lane loaded.

The above discussion is based on the "Level Rule" assumption, which may or may not apply to all bridge systems. The possible load distribution mechanisms between single loaded lane and multiple loaded lanes still need to be studied. In the traditional "S-over" approach, it is assumed that for consideration of longitudinal bending, the slab can be thought of as a series of strips, each forming a top flange of a T-beam. No check has been made to confirm that after notionally cutting up the deck the displacements of the parts are compatible, i.e. that the parts can in fact be joined together without additional forces and distortion hitherto not considered.

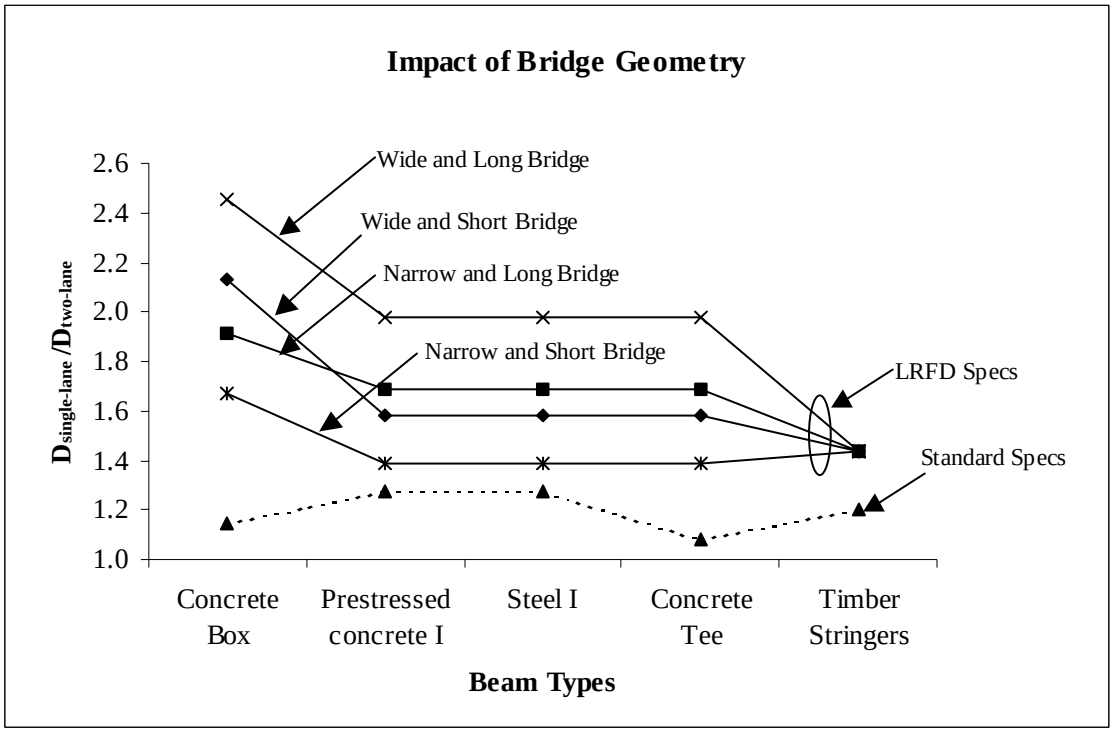


Fig. 1.5 Impact of Bridge Geometry on $D_{single\text{-}lane}/D_{two\text{-}lane}$

If all separated “T-beams” flex about a neutral axis passing through their centroids, the ends of the slab flanges are displaced relative to each other. In reality this step displacement cannot happen, and the relative movement of the tops of the “T-beams” is resisted and reduced by longitudinal shear forces in the connecting slab. This is also referred to as “slab membrane action” [Hambly 1991]. These shear forces are in equilibrium with axial tension/compression forces in beams near midspan. The forces have two effects on deck behavior. First, the axial tension forces in the beams with the largest deflections (i.e. under the load) cause the neutral axis to rise locally while compression forces elsewhere cause the neutral axis to move down. Secondly, the load distribution characteristics of the deck are improved. The longitudinal interbeam shear forces and axial forces are at different levels and thus form couples which reduce the moment in the loaded beams and increase moments elsewhere. This explains why single lane loaded bridges have better live-load distribution characteristics than multi-lane loaded ones. Single lane loads cause larger deflection differences between “separated T-beams” than multi-lane loads. Also, wider slabs have larger in-plane bending resistance, and thus larger interbeam shear forces. Longer span bridges tend to have larger deflection differences than short span bridges. Figure 1.5 shows the impact of bridge geometry on the ratio of D values based on LRFD Specs. It appears to support the above discussion.

### 1.3.3 Multibeam (e.g. Decked Bulb Tee) Bridges

As stated earlier, the multi-beam precast concrete bridge system was not addressed in the design specifications until 1965. This category of bridges includes all precast concrete bridges that are made up of precast sections that span the whole length of the bridge. These sections are then placed side by side with a longitudinal joint between each precast section. The precast sections are then connected to one another across this longitudinal joint with shear keys and grout. The cross-section of these multi-beam precast concrete bridges encompasses a wide variety of shapes ranging from solid slab sections, box girder sections, channel sections, double Tee section, to decked bulb-tee sections, as shown in Figure 1.6.

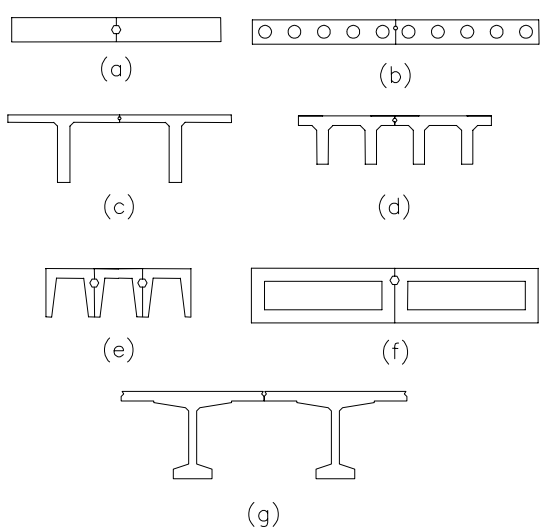


(a) Solid Slab

(b) Voided Slab

(c) Single Tee

(d) Double Tee

(e) Channel

(f) Box Girder

(g) Decked Bulb-Tee

Fig. 1.6 Cross-sections of Multi-Beam / Precast Systems

For the Alaska decked bulb-tee bridges (Fig.1.6 g), the AASHTO Specifications do not consider the impact of a single lane loaded case, AASHTO provides for one live load DF equation, regardless of the number of loaded lanes. As a result, it is the practice of AKDOT&PF to use AASHTO multiple lane live load distribution factors for load rating. It seems that this practice results in a load rating penalty for Alaska Bulb-Tee girder bridges. So a method for finding single lane distribution factors is needed for Alaska Bulb-Tee girder bridges.

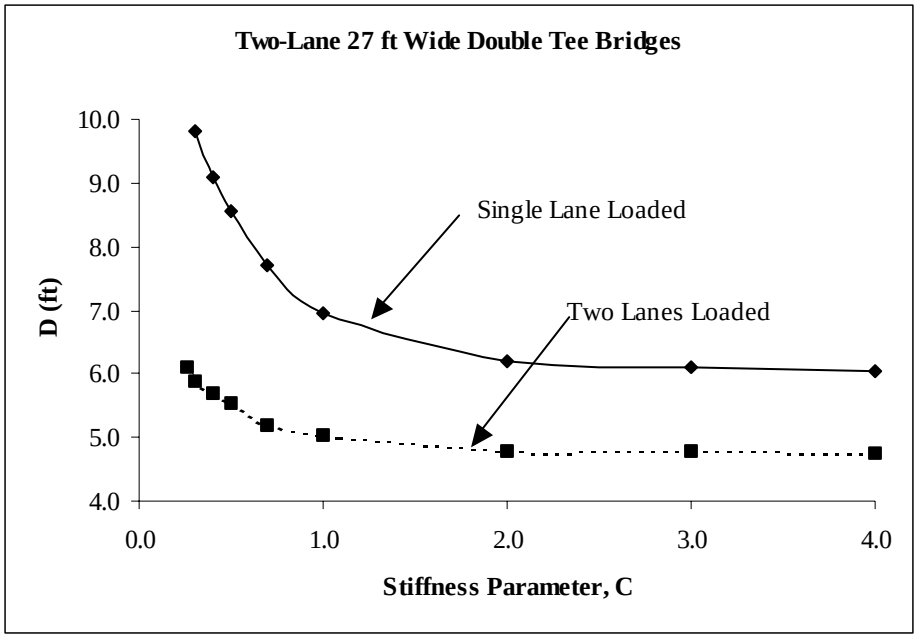


Fig. 1.7 Parameter Studies Considering Number of Loaded Lanes

As discussed before, the live-load distribution factor equations for multibeam bridges in AASHTO Specifications were based on study performed at the University of Washington (UW) [Stanton and Mattock 1986]. In the UW study, six bridge widths were considered (27, 36, 39, 48, 51, and 60-ft). The final equations were based on the lowest D values from the multi-lane loaded cases.

By re-assembling the parameter studies performed in the original UW study, we have found that the D value for a single lane loaded 27 ft wide double tee bridge is about 1.28 times the D value of the same bridge with two lanes loaded, as shown in Figure 1.7.

# CHAPTER 2 – FIELD TESTING PROGRAM

During the research period, the research team successfully tested the selected 8 bridges in Anchorage from May 6 to May 19, 2003. Field testing results are summarized in this chapter. The purpose of this bridge testing is to verify the accuracy of the rigorous mathematical models used to analyze the Alaskan style decked bulb T bridge girder system. The gauges were placed in areas that experience the largest stresses in the bridge and tend to control the design of the bridge. These are the same areas that the researchers will analyze in the math models to determine a simplified expression describing the distribution factor for the bulb T bridge system.

## 2.1 Summary of Bridges Tested

Table 2.1 shows the tested eight bridges in Anchorage, Alaska. Figure 2.1 shows the underside of a typical tested bridge. In selecting the bridges to instrument, UAF researchers considered the following factors.

* They are all located in or near Anchorage, Alaska.
* Traffic can be closed during late night hours for all these bridges.
* They are all accessible to instrument.
* They represent different geometry of the bridges in Alaska in terms of skew angles and aspect ratio (length/width).

The research team has also decided to test paired structures to provide verification of the instrumentation and modeling procedures.

Table 2.1 Field Tested Bridges (From May 6 to May 19, 2003)

| Name | | Bridge Geometry | | | Girder | |
|---|---|---|---|---|---|---|
| | | **Span(ft)** | **Width(ft)** | **Skew($^o$)** | **Spacing(in.)** | **Depth(in.)** |
| Set 1 | W100th NB<br>W100th SB | 115.0 | 37.0 | 0 | 88.8 | 54.0 |
| Set 2 | Huffman NB<br>Huffman SB | 125.0 | 37.0 | 27.5 | 74.0 | 54.5 |
| Set 3 | Campbell NB<br>Campbell SB | 137.0 | 37.0 | 4.3 | 88.8 | 66.0 |
| Set 4* | Diamond Rd<br>Dowling Rd | 109.0 | 106.0 | 0 | 90.8 | 54.0 |

* Note: Tee shape girder in Set 4 instead of decked Bulb-Tee shape used in Sets 1, 2, and 3.

Fig. 2.1 Underside of Campbell Creek Bridge

## 2.2 Equipment and Personnel

### 2.2.1 Testing Personnel

The research team consisted of a joint operation between the University of Alaska Fairbanks (UAF) and the Alaska Department of Transportation (AKDOT). From UAF the principal researchers were Dr. John Ma, and Dr. Leroy Hulsey with research assistants Jason Millam and Sanjay Chaudhury. From AKDOT Bridge Section, Gary Scarborough, and John Orbistondo assisted in the testing. Load vehicle drivers and traffic control personnel also assisted as required.

### 2.2.2 Equipment

Strain Transducers – Full-bridge reusable strain transducers fabricated by Bridge Diagnostics, Inc. (BDI) were used. Transducers shown in Figure 2.2 were attached to the concrete using Loctite Brand instant adhesive. Data Acquisition System – MEGADAC 5414 Series by OPTIM Electronics was used in the testing. This system was connected to a laptop computer utilizing TCS for Windows Version 3.4 Software. Figure 2.3 shows a setup of the mobile lab assembled by the UAF team.

Fig. 2.2 Strain Transducer

### 2.2.3 Load Vehicle Description

The Load vehicle used in the testing was a loaded DOT End Dump Truck. See Figures 2.4 and 2.5 for a picture of the load vehicle approximate vehicle foot print location and wheel loads. Wheel loads were measured on 5/8/03 and have a measured error of ± 1%. These values changed over the course of the testing period due to rain and different fuel levels.

Fig. 2.3 Mobile Lab with Data Acquisition Equipment

Fig. 2.4 Load Vehicle

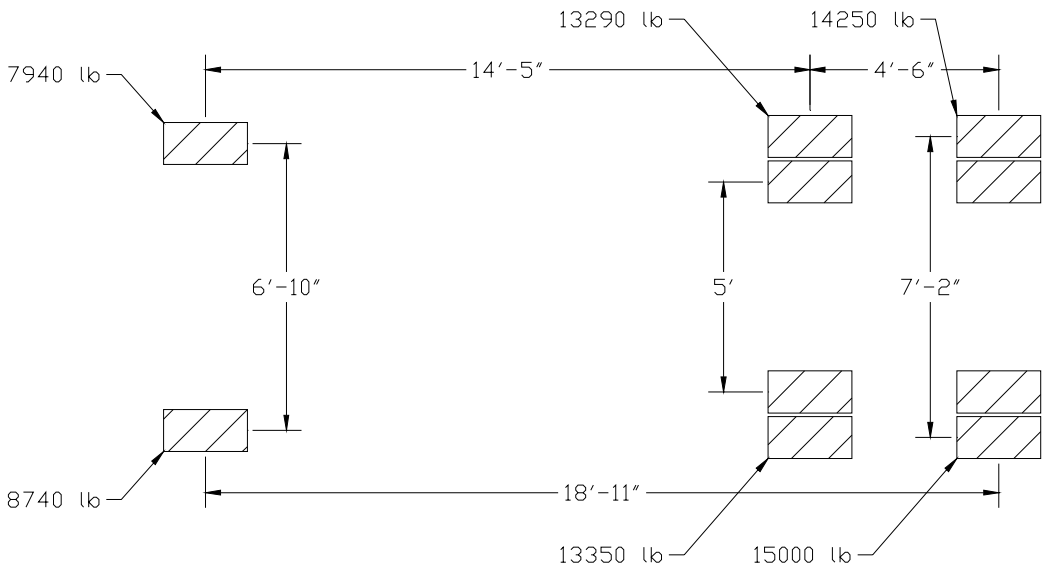


Fig. 2.5 Load Vehicle Wheel Load Diagram

## 2.3 Load Positions

### 2.3.1 Longitudinal Positioning of Load Vehicle

During loading, the load vehicle would travel across the bridge in the same direction for each transverse load position, and for each loading condition. The direction of loading for each bridge is as follows: For Campbell SB and NB, Huffman NB, 100$^{th}$ NB, the direction of loading was the same direction as the direction of normal traffic crossing the bridge (ie. direction of loading was north on Huffman NB); For Huffman SB, and 100$^{th}$ SB the direction of loading was opposite the direction of traffic (ie. direction of loading was north on Huffman SB). The Diamond and Dowling Bridges each had both North and South bound traffic crossing the bridge. Diamond bridge was loaded only on the eastern side of the bridge which typically has North Bound Traffic, however, the direction of loading on this bridge was South, Opposite the direction of traffic. Dowling bridge was loaded only on the western side of the bridge which typically has South Bound Traffic, and the direction of loading on this bridge was South in the same direction as traffic. During the testing period, there were two main methods of loading the bridge: Continuous Loading, and Static Loading.

During Continuous Loading, the load vehicle drove at a constant speed of two miles per hour along a straight longitudinal girder line across the bridge. Data during this loading condition recorded continuously before the load vehicle moved onto the bridge, while the vehicle moved across the bridge, and as the vehicle moved off the bridge. During this loading condition the transverse position of the vehicle is known, there is no method of relating the measured strain values to the vehicle's longitudinal position on the bridge. Normally, this loading condition was conducted to verify the accuracy of the data and determine whether or not any strain gauges might be malfunctioning.

During the Static Loading, the load vehicle drove to three known longitudinal stop positions along a given girder line. The first set of data was recorded as the vehicle drove onto the bridge to its first stop position. The next set of data was recorded as the vehicle drove from its first stop position to its second stop position. The third set of data was recorded as the vehicle drove from its second stop position to its third stop position located roughly halfway along the length of the bridge. Figure 2.6 shows the load vehicle in the third stop position. Three data sets were recorded for each girder line or transverse positioning which the vehicle drove along. A minimum of 30 seconds of data was recorded as the vehicle remained stationary in the stop position. Figure 2.7 depicts the three longitudinal stop positions which the load vehicle moved to during the static loading condition. The first stop position places the vehicle with its driver's side rear wheel centered at a distance H (representing the girder depth) away from the abutment. The second stop positions locates the vehicle with its second axle (driver's side wheel) ¼ of the span length of the bridge. The third stop position locates the vehicle's second axle (driver's side wheel) at the center line of the bridge span. For non skew bridges, both the driver's side and passenger's side wheels will be located at the same relative longitudinal position. There is an error of ± 12" in the placement of vehicle on its longitudinal position.

Fig. 2.6 Load Vehicle at Third Stop Position at Midspan

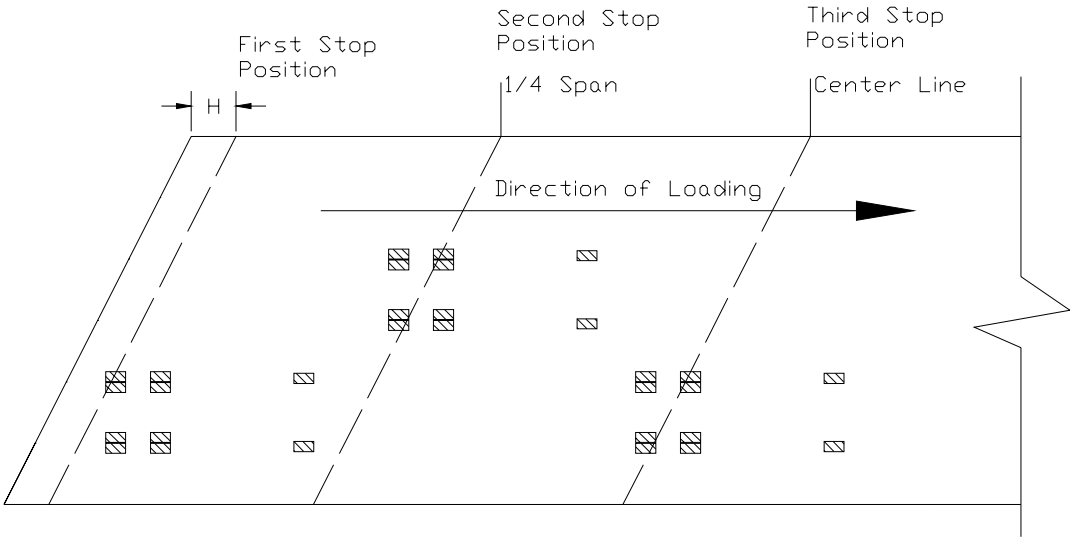


Fig. 2.7 Longitudinal Stop Positions

*Note: The diagram depicts the vehicle at different transverse positions for clarity. During actual loading the vehicle stayed in the same transverse position as it moved to its three longitudinal stop positions.*

### 2.3.2 Transverse Positioning of Load Vehicle

Most of the transverse loading positions are located directly over a girder. These loading positions are defined by the girder number over which they drive. The girder numbering system is as follows: Girder number one is always the furthest girder to the right of the bridge based off the direction of traffic, not the direction of loading, girders are then numbered consecutively from right to left. Girder number one on the Diamond Bridge is the easternmost girder. Girder number one on the Dowling Bridge is the westernmost girder. From the perspective of the loading direction, Girder number one is the girder furthest to the right for Campbell NB & SB, Huffman NB, 100$^{th}$ NB, and Dowling. From the perspective of the loading direction, Girder number one is the girder furthest to the left for Huffman SB, 100$^{th}$ SB, and Diamond. For each interior girder loaded, the load vehicle is positioned so that its wheels are centered over the centerline of the girder. For each exterior girder loaded, the vehicle is positioned with the centerline of its outside wheel line to be approximately 2 ft from the edge of the bridge. Figure 2.8 shows the wheel loads relative to the girders.

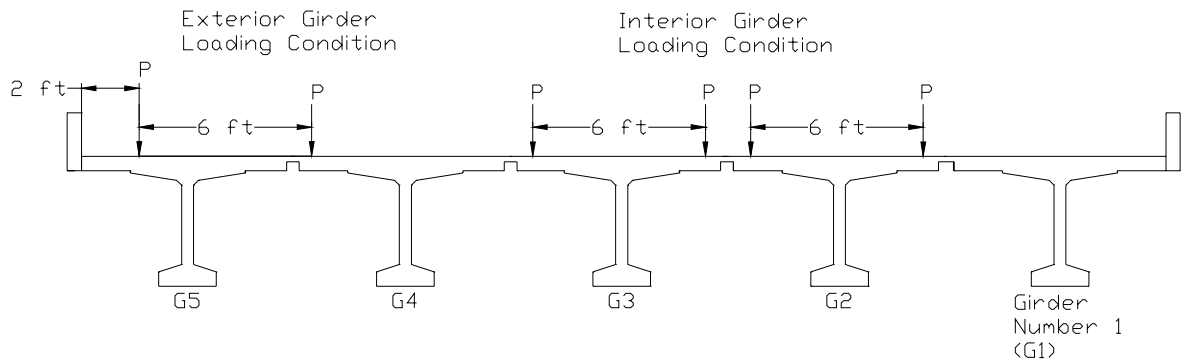


Fig. 2.8 Transverse Vehicle Positions (General)

The Huffman St. Bridge had a unique transverse loading positioning because it was an even numbered girder bridge. The exterior girders for the Huffman St. Bridge (G1, G6) were each loaded in the same manner as the exterior girders of the other bridges. Instead of positioning the vehicle directly over each interior girder, the vehicle was positioned with its driver side wheels on the center line of the bridge (Joint Right), with its wheels centered over the center line of the bridge (Center), and with its passenger side wheels on the center line of the bridge (Joint Left). This can be seen in figure 2.9.

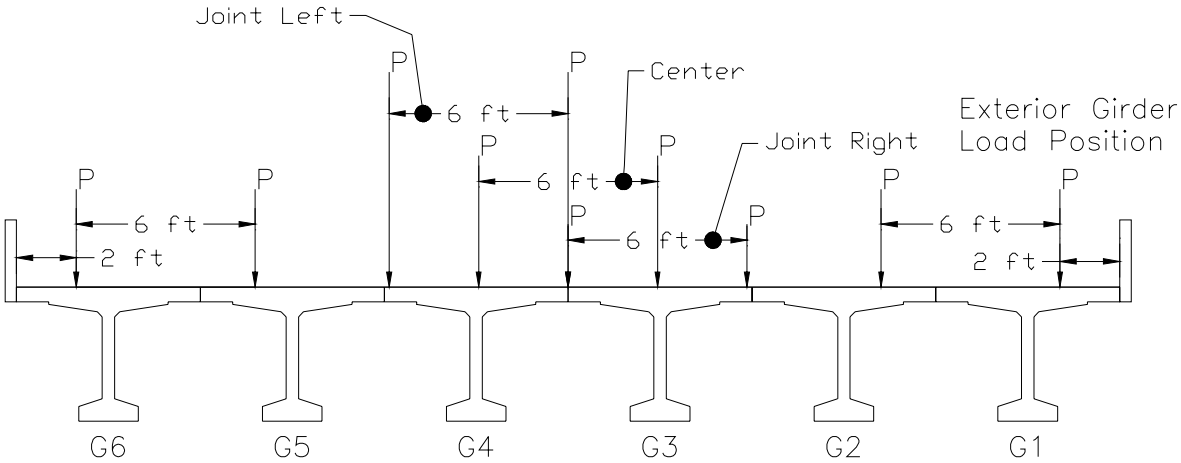


Fig. 2.9 Transverse Vehicle Positions (Huffman)

*Note: The diagram depicts the girder numbering system as it would appear for Huffman NB. For Huffman SB the girders would be numbered with G1 on the left and G6 on the right because the direction of loading is opposite the direction of traffic.*

The Bridges at Diamond and Dowling intersections also had a unique loading positioning referred to as Joint Loading. For each of these bridges, the Joint Loading conditions refers to one wheel line positioned directly on the joint between girder's 3 and 4 while the other wheel line is placed over the top of girder 3. Figure 2.10 shows the joint loading condition. The remainder of the girder line loading conditions on Diamond and Dowling are Similar to the General Position noted in Figure 2.8.

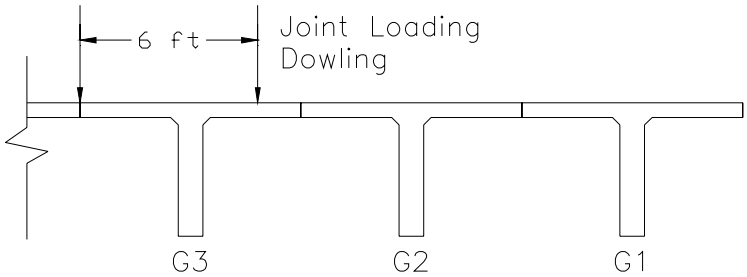


Fig. 2.10 Transverse Vehicle Positions (Diamond / Dowling)

*Note: The diagram depicts the girder numbering system as it would appear for Dowling. For Diamond the diagram would be a mirror image of this diagram.*

### 2.3.3 Loading Key

We used the following labeling system to define the experimental load position:

Name – N – Gi

The first term (Name) indicates name of the bridge being loaded, the second term (N) represents the longitudinal location of the load (N = 1, 2, or 3), and the final term indicates the transverse position of the load by labeling the girder (Gi) over which the majority of the load is positioned. The Bridge names are as following: 100th NB, 100th SB, Huffman NB, Huffman SB, Campbell NB, Campbell SB, Diamond and Dowling. Three labels were used to define the longitudinal position of the load: "1" represents the shear loading position located a distance of "H" (height of the girder) away from the abutment, i.e. the "First Stop Position" in Figure 2.7; "2" represents the vehicle loading at ¼ span ("Second Stop Position in Figure 2.7); and "3" represents the vehicle loading at midspan ("Third Stop Position" in Figure 2.7).

The transverse loading is labeled according to the girder over which most of the load is positioned. For most cases the load is centered over the girder, however for the edge girders the load is positioned as close the edge of the bridge as was possible which is not necessarily centered over the edge girder. Girders are numbered consecutively with the first girder G1 representing the girder on the right side of the bridge based off the direction of traffic (not necessarily the direction of loading).

For example, let's say we are about to test the 100$^{th}$ Street North Bound bridge. We will start the test at the bridge end as a shear test (N = 1), and we have the truck on the outside right position near the railing (Gi = G1). The label used to record data will be "100$^{th}$ NB – 1 – G1".

## 2.4 Strain Gauge Positioning

During field testing 24 gauges were placed to measure strain on each bridge except Campbell South Bound and Huffman North Bound. These two bridges only had 22 gauges. There were three main categories of gauge placement: one set of gauges would be used to measure shear response; the second set of gauges would be used to measure flexural stresses due to midspan moment; and the third set of gauges would be used to measure axial stress in the intermediate steel diaphragms.

For each girder, there were a potential of six different locations which where shear gauges were placed and two different locations where moment gauges were placed. The shear gauges would always be placed a distance H (H = depth of the girder) away from the face of the end diaphragm and vertically on the approximate location of the neutral axis (N. A.). The shear gauges could either be oriented 45deg towards (S1) or away (S3) from the end diaphragm or vertically (S2). They could also be positioned either on the right (S1R) or left (S1L) side of the girder. Note that the right and left hand side of a girder is distinguished by the direction in which the girder is loaded. The moment gauges were always positioned at midspan and located either centered on the bottom flange (M1) or on the left hand side of the web (M2). The moment gauges positioned on the web were located vertically at the highest position on the web just below the top flange. The positions of the gauges are shown in Figure 2.11. Figure 2.12 shows shear gauges in place and Figure 2.13 shows the placement of moment gauges. The right or left side of the girder is always based off of the direction the load vehicle moves across the bridge.

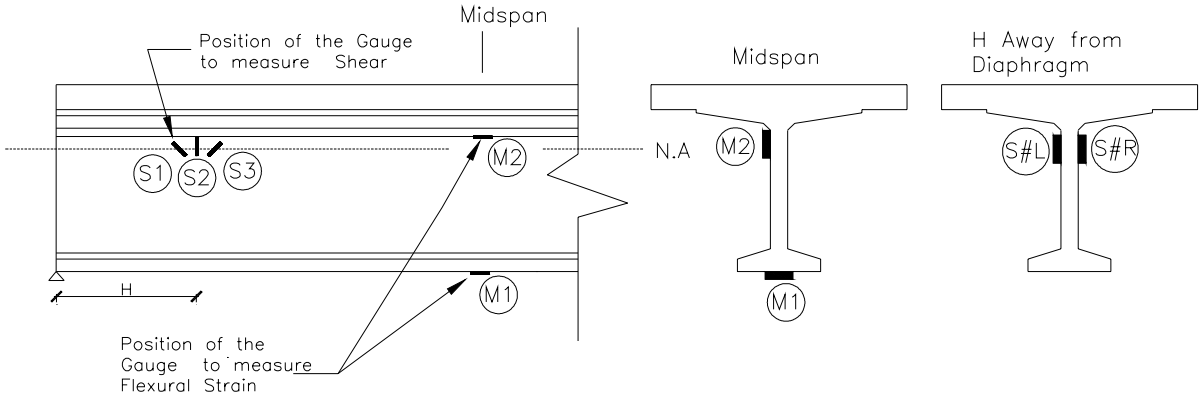


Fig. 2.11 Gauge Positions (Elevation)

Fig. 2.12 Shear Strain Gauges in Place

Fig. 2.13 Placement of Moment Strain

The Diaphragm gauges are located at either quarter span or midspan. The gauges were placed halfway between the midpoint of the K brace and the edge of the girder. The gauges are identified by the two girder between which they reside. Figures 2.14 and 2.15 show the general location of the gauges on the steel diaphragms.

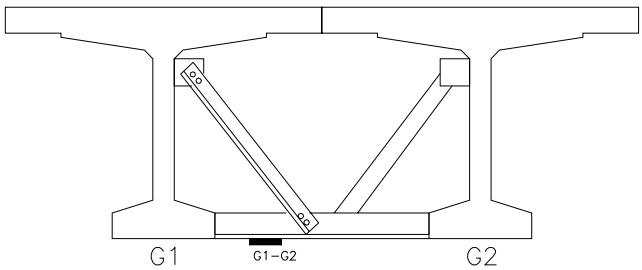


Fig.2.14 Gauge Location on Steel Diaphragm

Fig. 2.15 Picture of Strain Gauge on Steel Diaphragm

## 2.5 Field Testing Results

The following **"Collection of Testing Data Figures** (please note that they are not numbered)**"** section shows graphs of all the data collected for the eight bridges. The data for the bridges are in the following order:

100th NB
100th SB
Campbell NB
Campbell SB
Huffman NB
Huffman SB
Diamond
Dowling

This is not the chronological order in which we tested the bridges. Each bridge will have between two and four graphs per loading condition. Each graph will present the data of a group of strain gauges (Shear, Moment).

For example, the 100th NB Bridge has 4 graphs per loading condition. The title of each of the graphs describes the loading condition. 100th NB has either continuous or static loading over each of the different girders (G1-G5). All of these loading conditions are depicted in Figure 2.8. The graphs of the static loading conditions show all three stop positions for a given girder line in one graph. To distinguish between the different static loading conditions there is a 10 second separation period where the graph is flat and has the same value for 10 seconds between the different static loading conditions.

The first graph shows all of the gauges that are in the S2 and S3 position (Figure 2.11). For this bridge only the Girder number 1 had gauges in the S2 Position and Girder 1 & 3 had gauges in the S3 position. The gauges are distinguished by the girder number they are on, whether it is in the S2 position (denoted by V) or the S3 Position (denoted by C), and whether it is on the left (L) or right (R) side of the girder. The series entitled G1CR represents the gauge located on girder 1 in the S3 position on the right hand side of the girder.

The second graph shows all of the shear gauges in S1 Position (angled 45deg into the end diaphragm) from Figure 2.11. Since all of the gauges are in the same position, they are only distinguished by the girder number they are on and whether they are on the left or right side of that girder. For example, series G3R represents the shear gauge located on girder number 3 which is the middle girder of the 100th avenue bridge, it is angled into the diaphragm and is on the right side of the girder.

The third graph shows the strains in the steel diaphragm of which only three gauges were placed on the steel diaphragms. Each series is labeled by the two girders between which the diaphragm resides. Series G1-G2 M represents the strain gauge located on the steel

diaphragm between girder's 1 and 2, and the M show that its location is at midspan instead of quarter span.

The fourth (final) graph for 100$^{th}$ NB's first loading position (over Girder 1) is a graph which shows all of the midspan moment gauges. Each gauge is located at the bottom flange at the M1 position from Figure 2.11. For 100$^{th}$ NB there were no gauges placed in the M2 Position. Each of the different series represents the midspan gauge for a certain girder. For example, the series entitled G1 represents the gauge located at the M1 position on Girder number 1 which is an edge girder located on the right hand side of the 100$^{th}$ NB Bridge. This data is used to determine the distribution factor of each of the bridges as will be shown later.

For the rest of the bridge, the same groups of gauges will be presented on the same graphs the only difference is the different loading conditions under which the gauges are subjected.

All subsequent data for the seven other bridges is presented in the same manner as 100$^{th}$ NB. The Diamond and Dowling bridges had numerous girders and only had gauges positioned in the M1 and S1 locations, and no gauges were placed on steel diaphragms. Therefore, these two bridges only have two graphs per loading condition.

### 2.5.1 Collection of Testing Data Figures

(shown in the next 256 pages)

# $100^{TH}$ NB

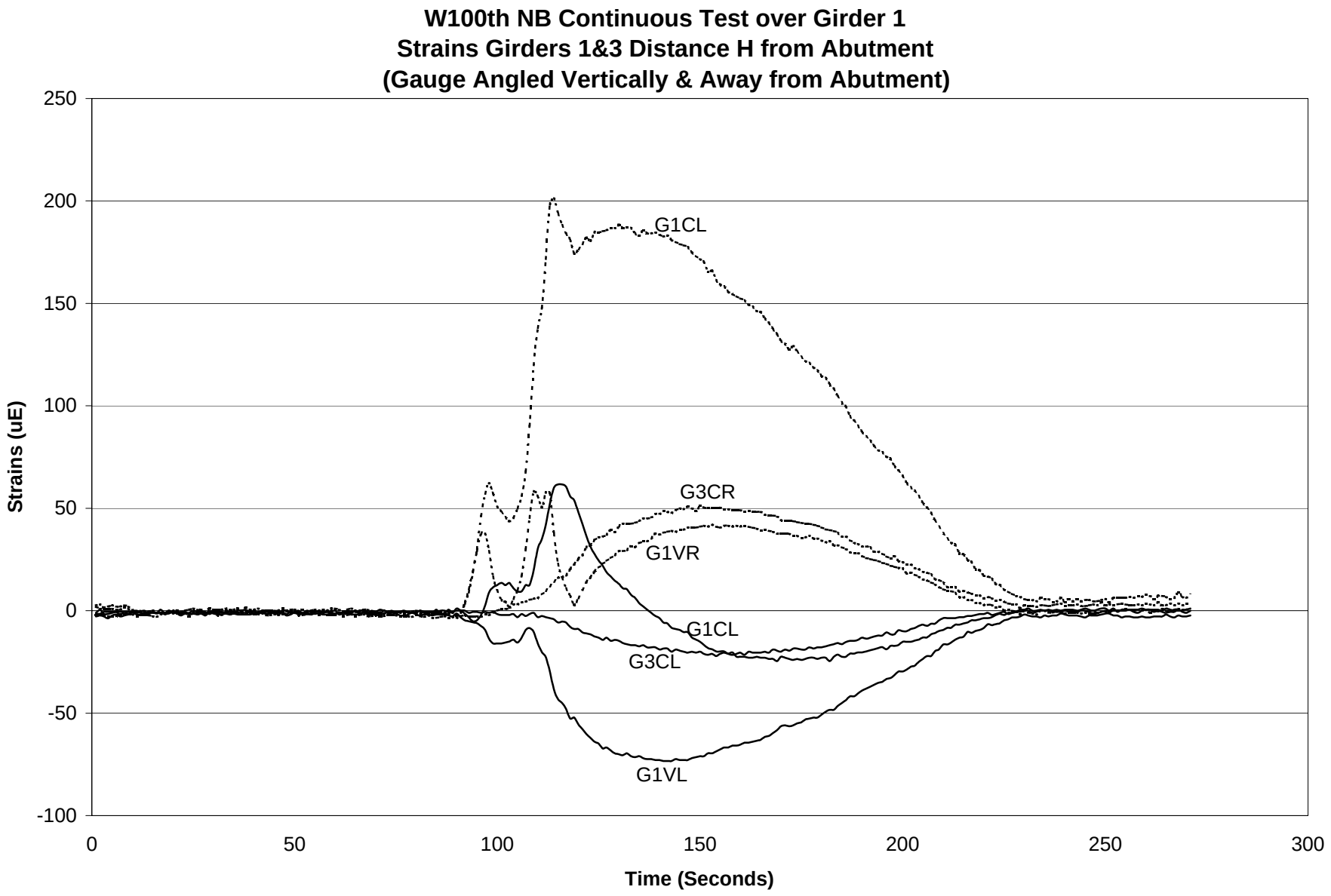
W100th NB Continuous Test over Girder 1
Strains Girders 1&3 Distance H from Abutment
(Gauge Angled Vertically & Away from Abutment)
Strains (uE)
Time (Seconds)
250
200
150
100
50
0
-50
-100
0
50
100
150
200
250
300
G1CL
G3CR
G1VR
G1CL
G3CL
G1VL

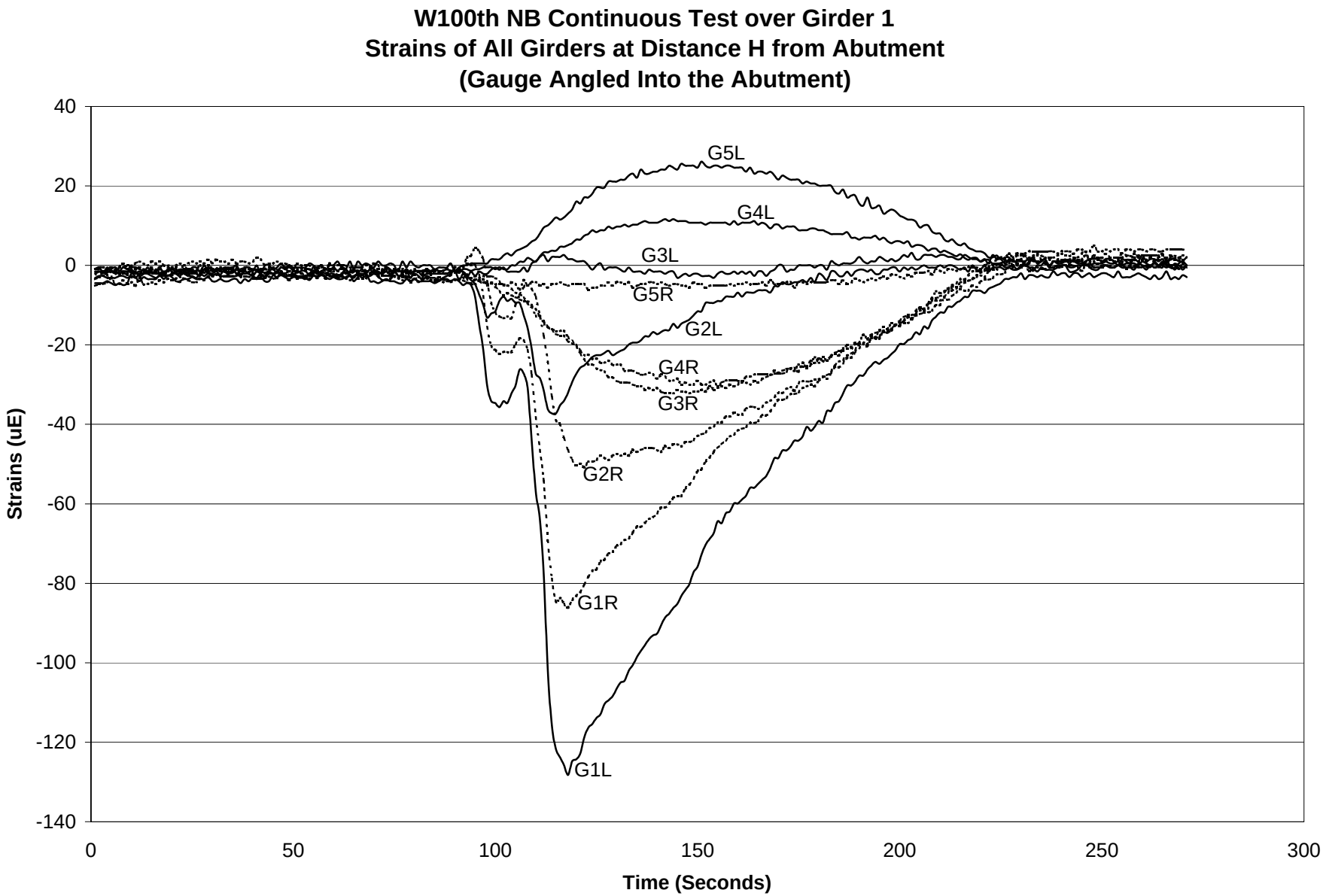
W100th NB Continuous Test over Girder 1
Strains of All Girders at Distance H from Abutment
(Gauge Angled Into the Abutment)
Strains (uE)
Time (Seconds)
40
20
0
-20
-40
-60
-80
-100
-120
-140
0
50
100
150
200
250
300
G5L
G4L
G3L
G5R
G2L
G4R
G3R
G2R
G1R
G1L

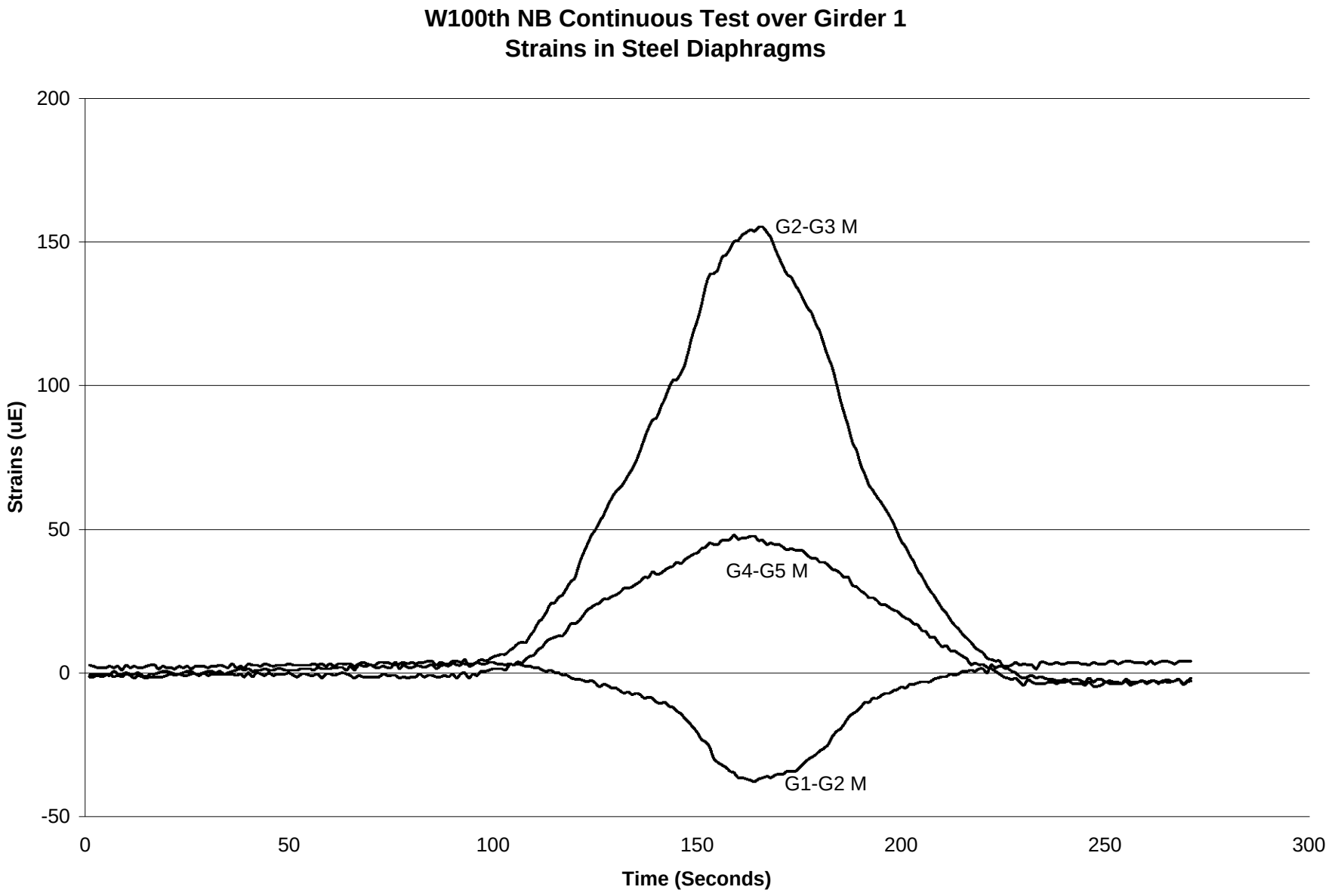
W100th NB Continuous Test over Girder 1
Strains in Steel Diaphragms
200
150
100
50
0
-50
Strains (uE)
0
50
100
150
200
250
300
Time (Seconds)
G2-G3 M
G4-G5 M
G1-G2 M

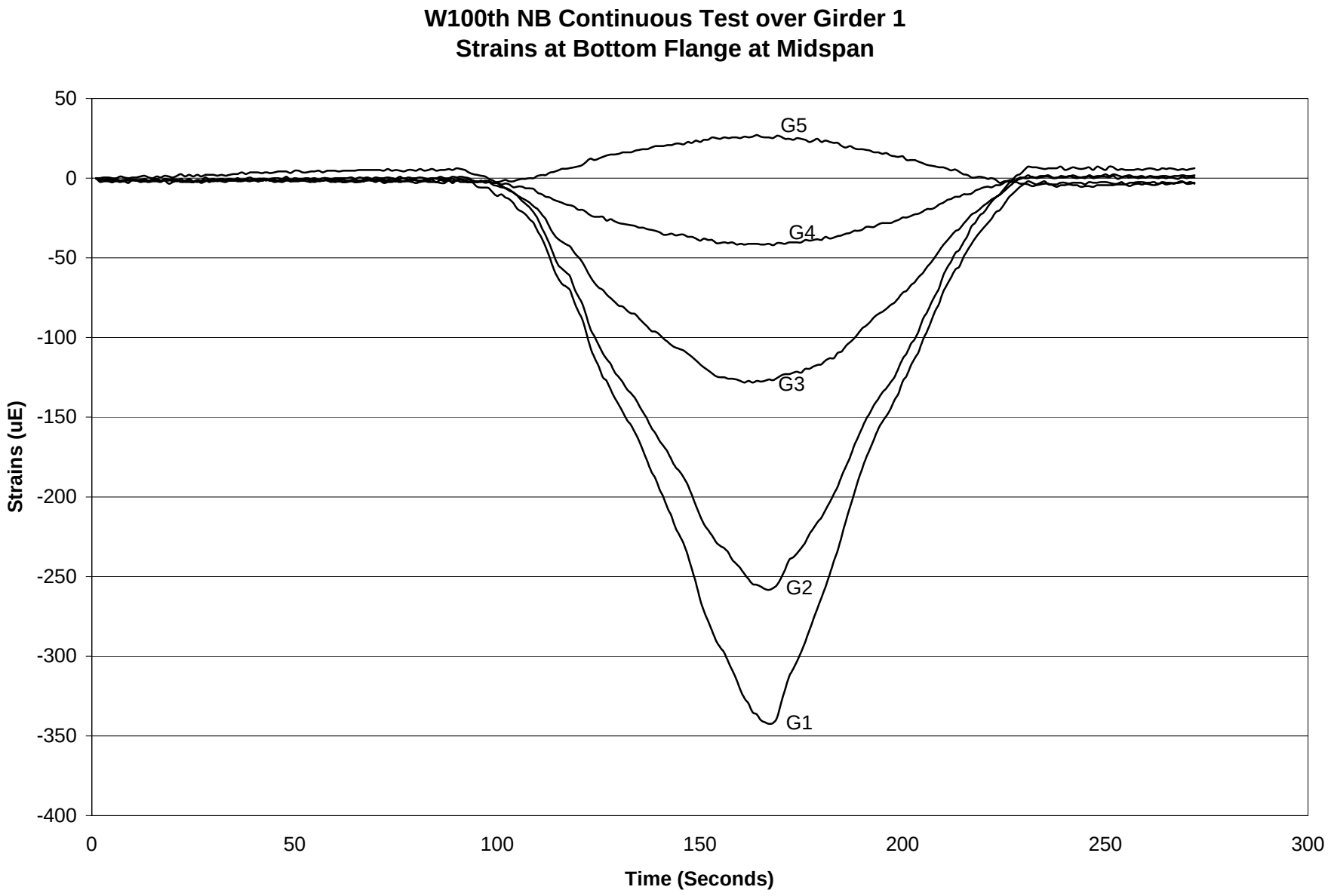
W100th NB Continuous Test over Girder 1
Strains at Bottom Flange at Midspan
Strains (uE)
Time (Seconds)
50
0
-50
-100
-150
-200
-250
-300
-350
-400
0
50
100
150
200
250
300
G5
G4
G3
G2
G1

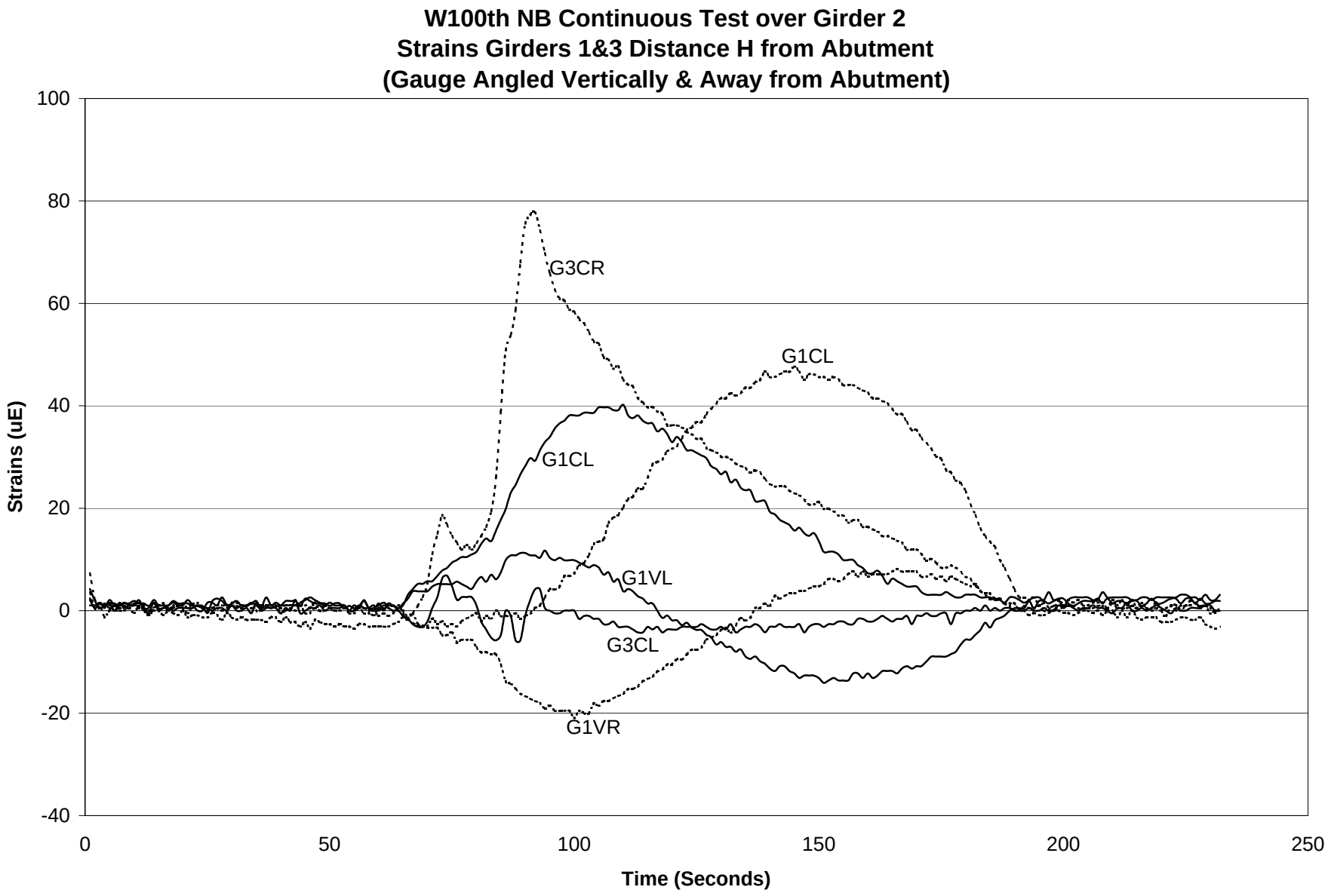
W100th NB Continuous Test over Girder 2
Strains Girders 1&3 Distance H from Abutment
(Gauge Angled Vertically & Away from Abutment)
Strains (uE)
Time (Seconds)
100
80
60
40
20
0
-20
-40
0
50
100
150
200
250
G3CR
G1CL
G1CL
G1VL
G3CL
G1VR

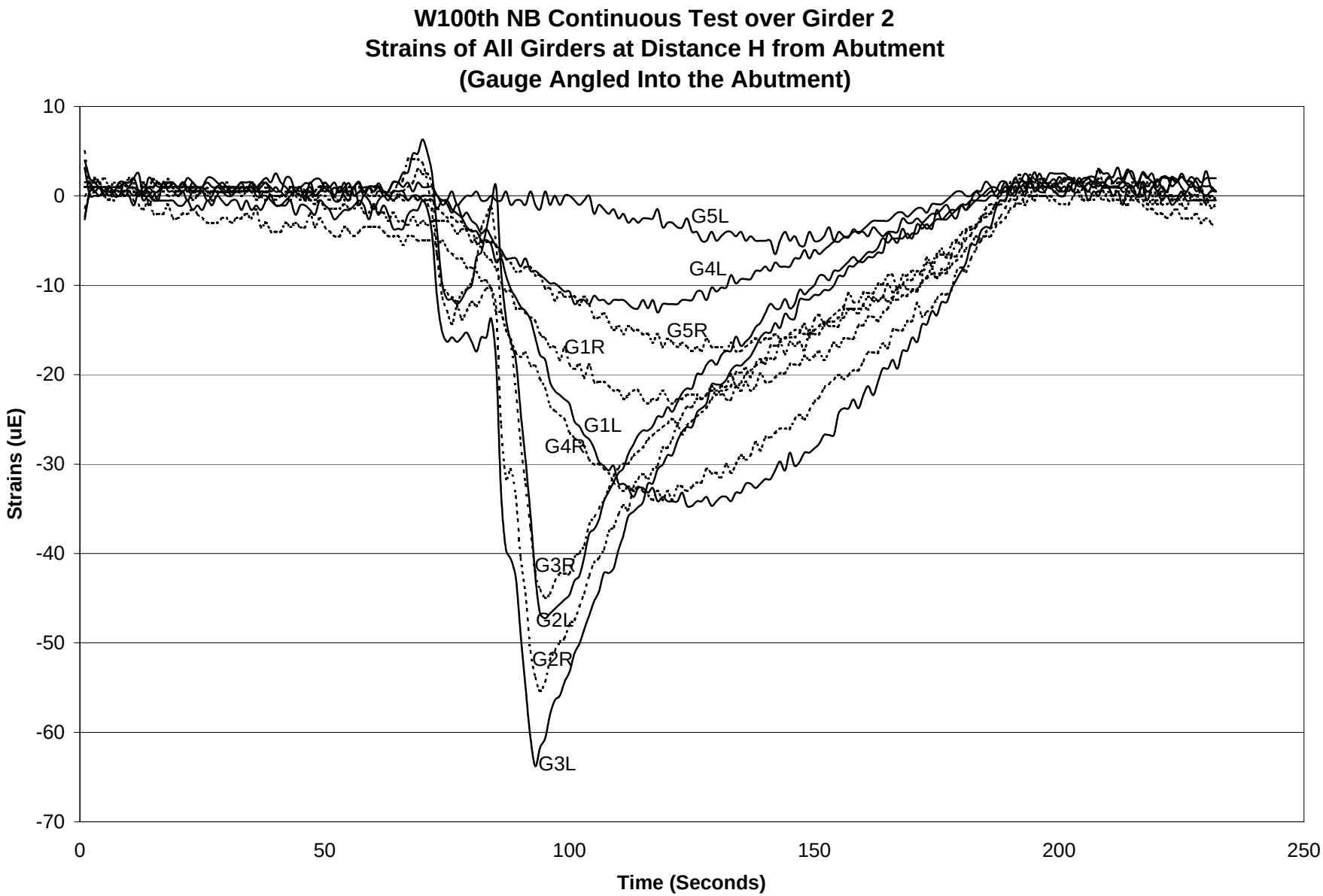
W100th NB Continuous Test over Girder 2
Strains of All Girders at Distance H from Abutment
(Gauge Angled Into the Abutment)
Strains (uE)
Time (Seconds)
10
0
-10
-20
-30
-40
-50
-60
-70
0
50
100
150
200
250
G5L
G4L
G5R
G1R
G1L
G4R
G3R
G2L
G2R
G3L

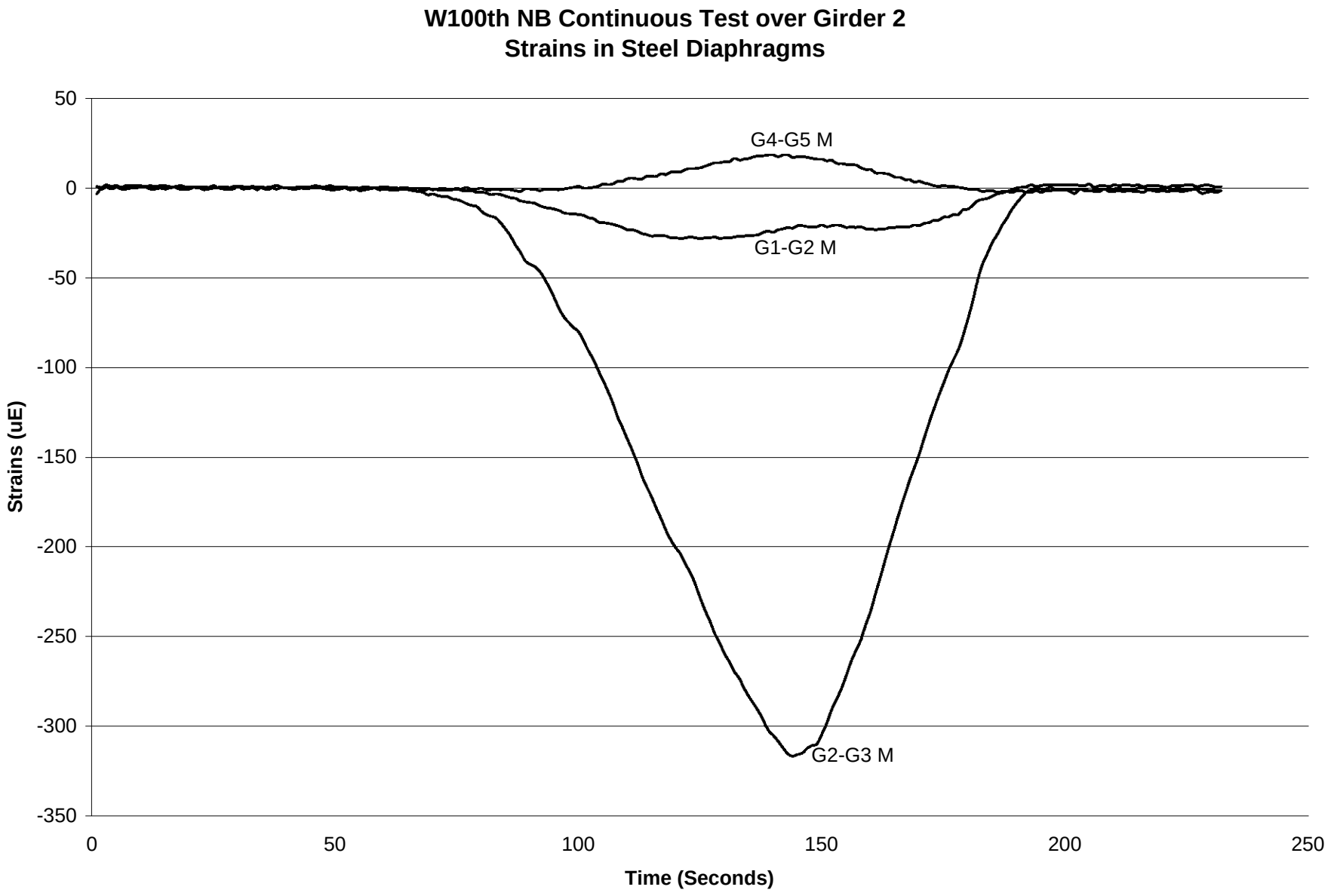
W100th NB Continuous Test over Girder 2
Strains in Steel Diaphragms
G4-G5 M
G1-G2 M
G2-G3 M
Strains (uE)
Time (Seconds)
50
0
-50
-100
-150
-200
-250
-300
-350
0
50
100
150
200
250

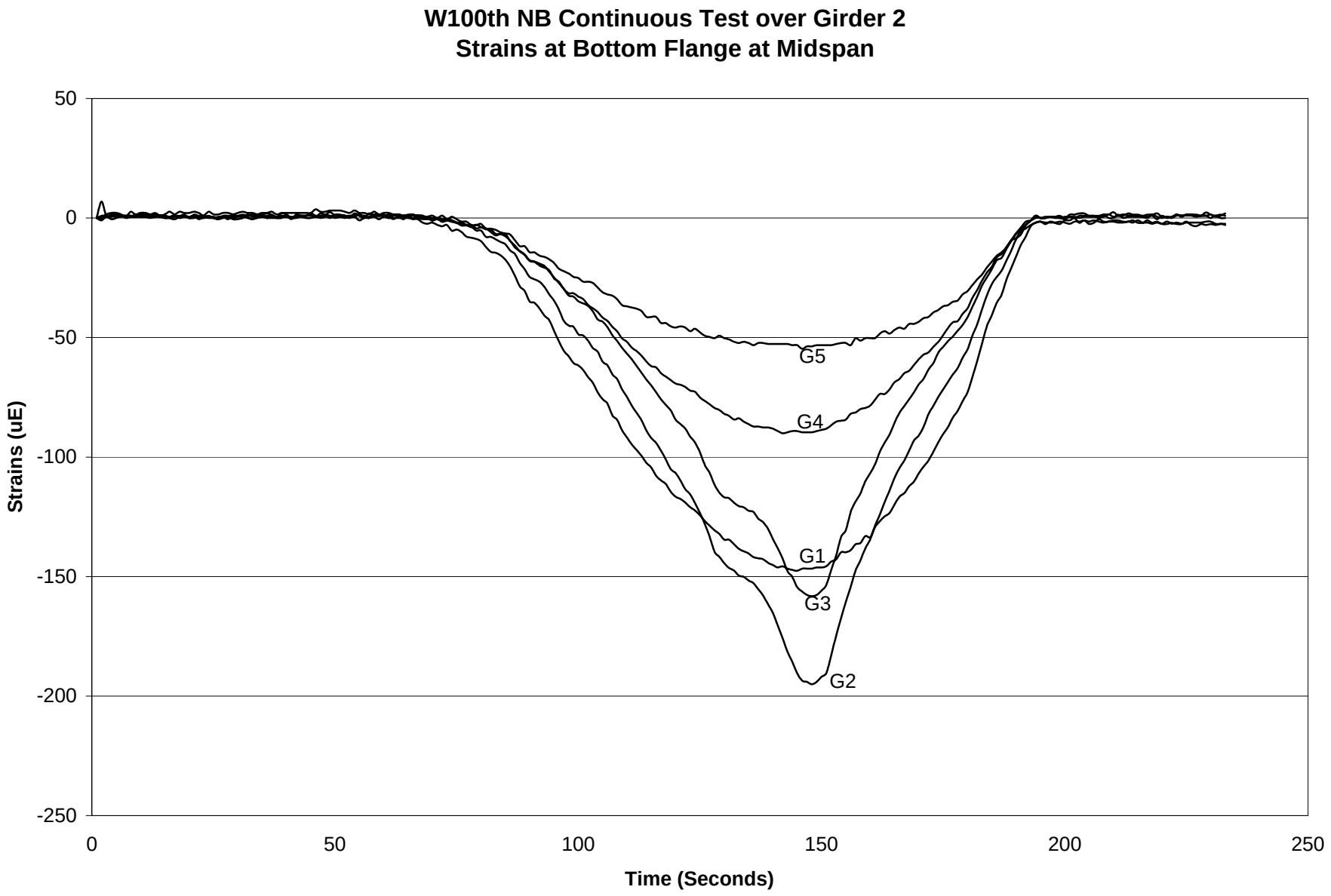
W100th NB Continuous Test over Girder 2
Strains at Bottom Flange at Midspan
50
0
-50
-100
-150
-200
-250
Strains (uE)
0
50
100
150
200
250
Time (Seconds)
G5
G4
G1
G3
G2

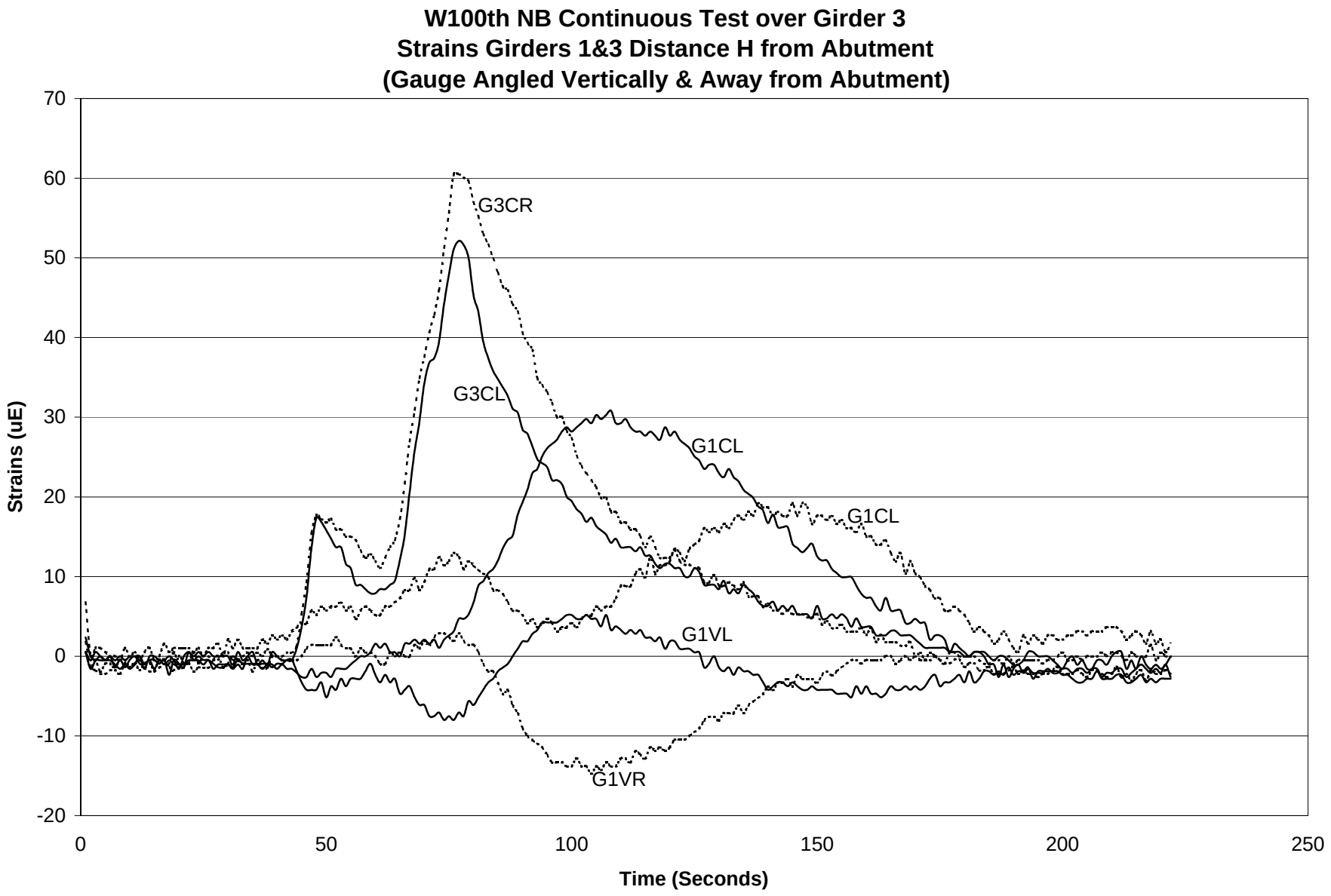
W100th NB Continuous Test over Girder 3
Strains Girders 1&3 Distance H from Abutment
(Gauge Angled Vertically & Away from Abutment)
Strains (uE)
Time (Seconds)
70
60
50
40
30
20
10
0
-10
-20
0
50
100
150
200
250
G3CR
G3CL
G1CL
G1CL
G1VL
G1VR

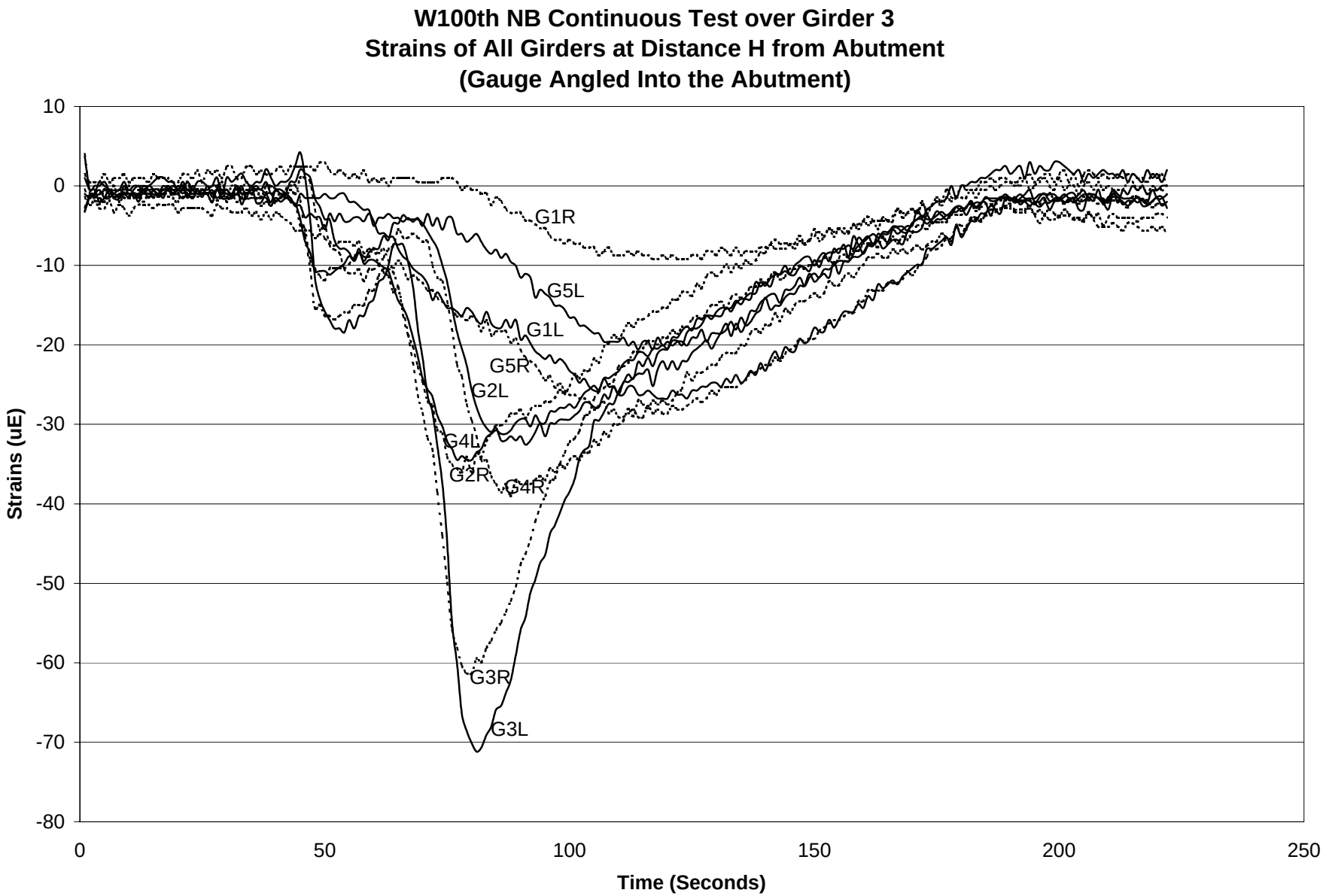
W100th NB Continuous Test over Girder 3
Strains of All Girders at Distance H from Abutment
(Gauge Angled Into the Abutment)
Strains (uE)
Time (Seconds)
10
0
-10
-20
-30
-40
-50
-60
-70
-80
0
50
100
150
200
250
G1R
G5L
G1L
G5R
G2L
G4L
G2R
G4R
G3R
G3L

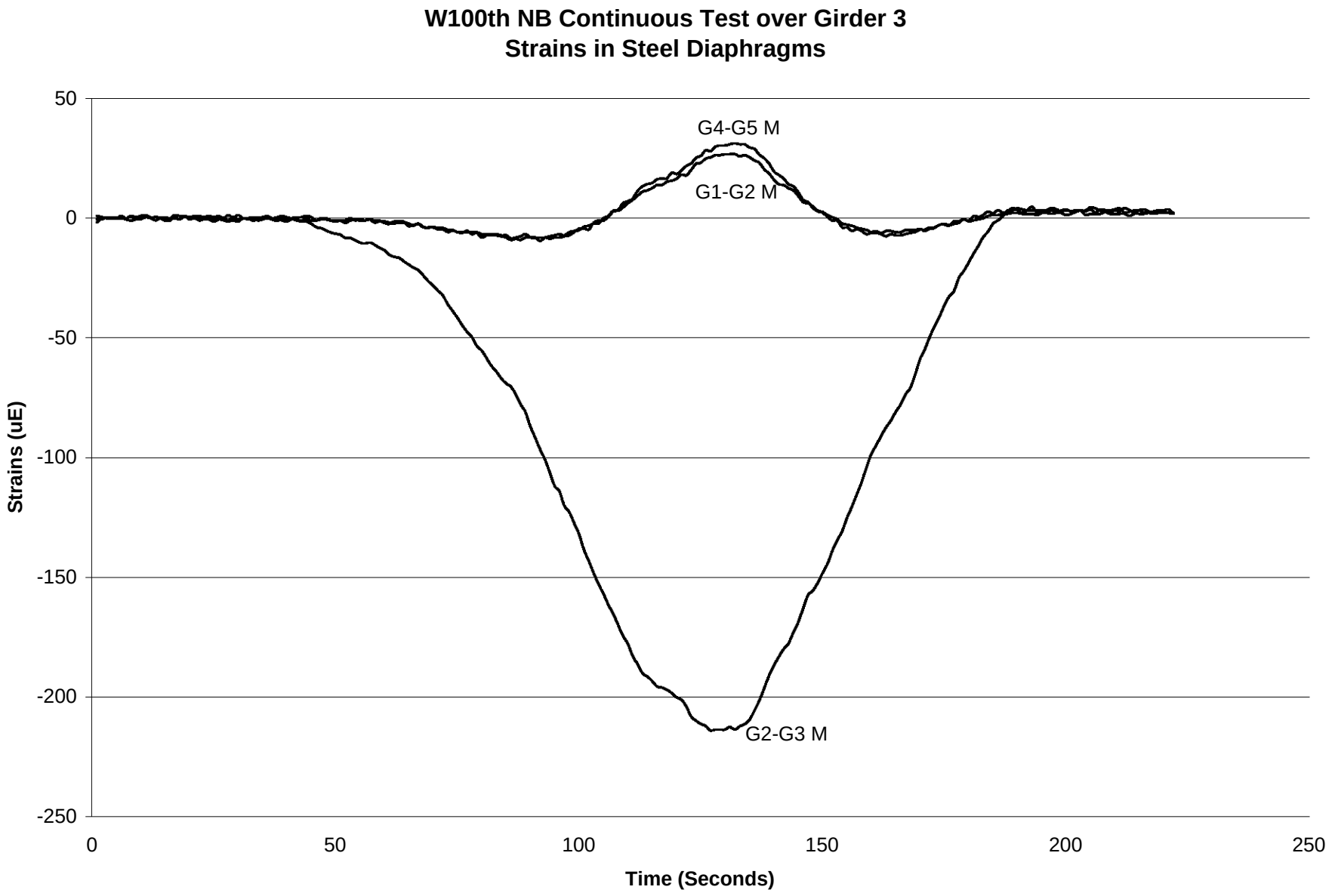
W100th NB Continuous Test over Girder 3
Strains in Steel Diaphragms
G4-G5 M
G1-G2 M
G2-G3 M
Strains (uE)
Time (Seconds)
50
0
-50
-100
-150
-200
-250
0
50
100
150
200
250

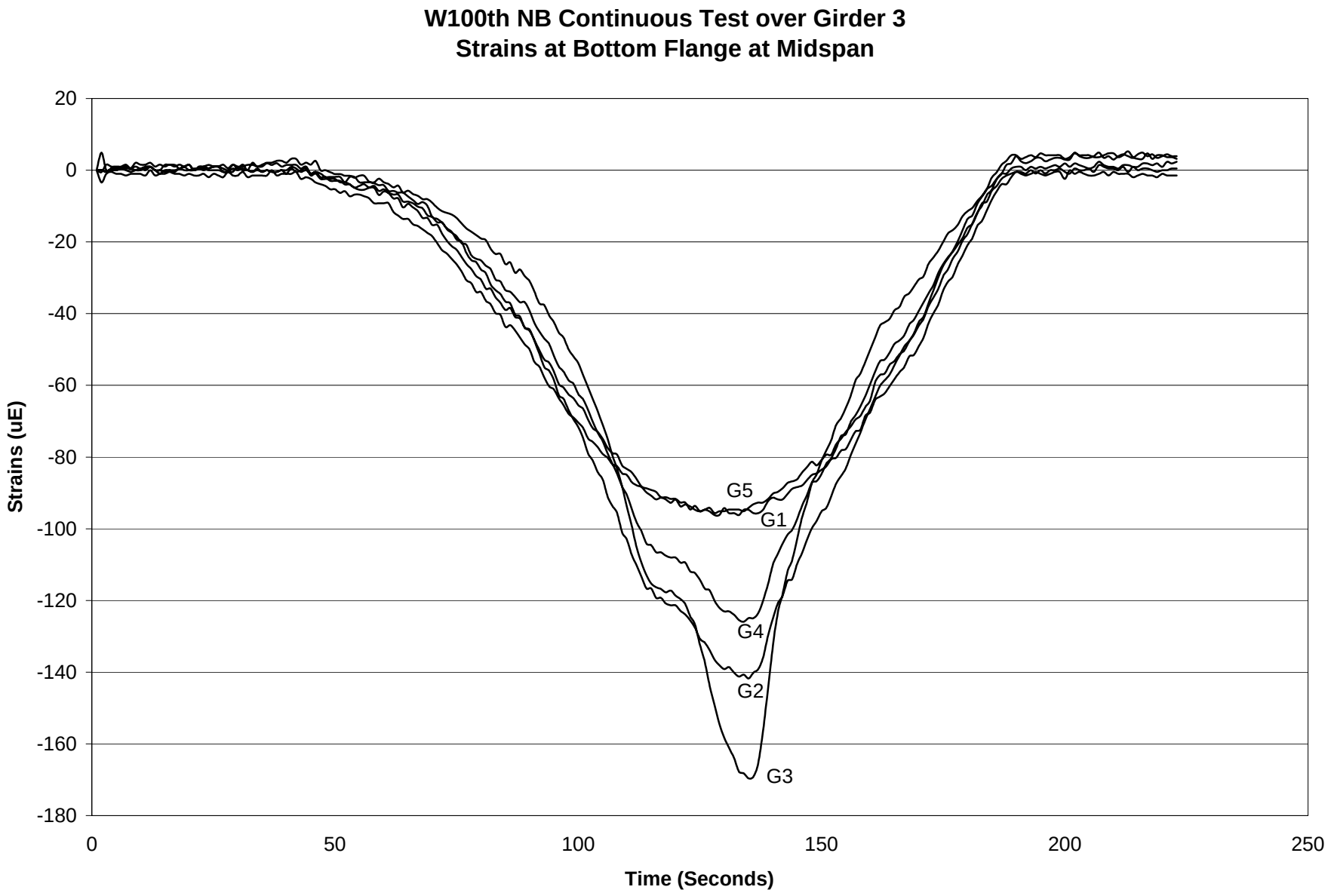
W100th NB Continuous Test over Girder 3
Strains at Bottom Flange at Midspan
Strains (uE)
Time (Seconds)
20
0
-20
-40
-60
-80
-100
-120
-140
-160
-180
0
50
100
150
200
250
G5
G1
G4
G2
G3

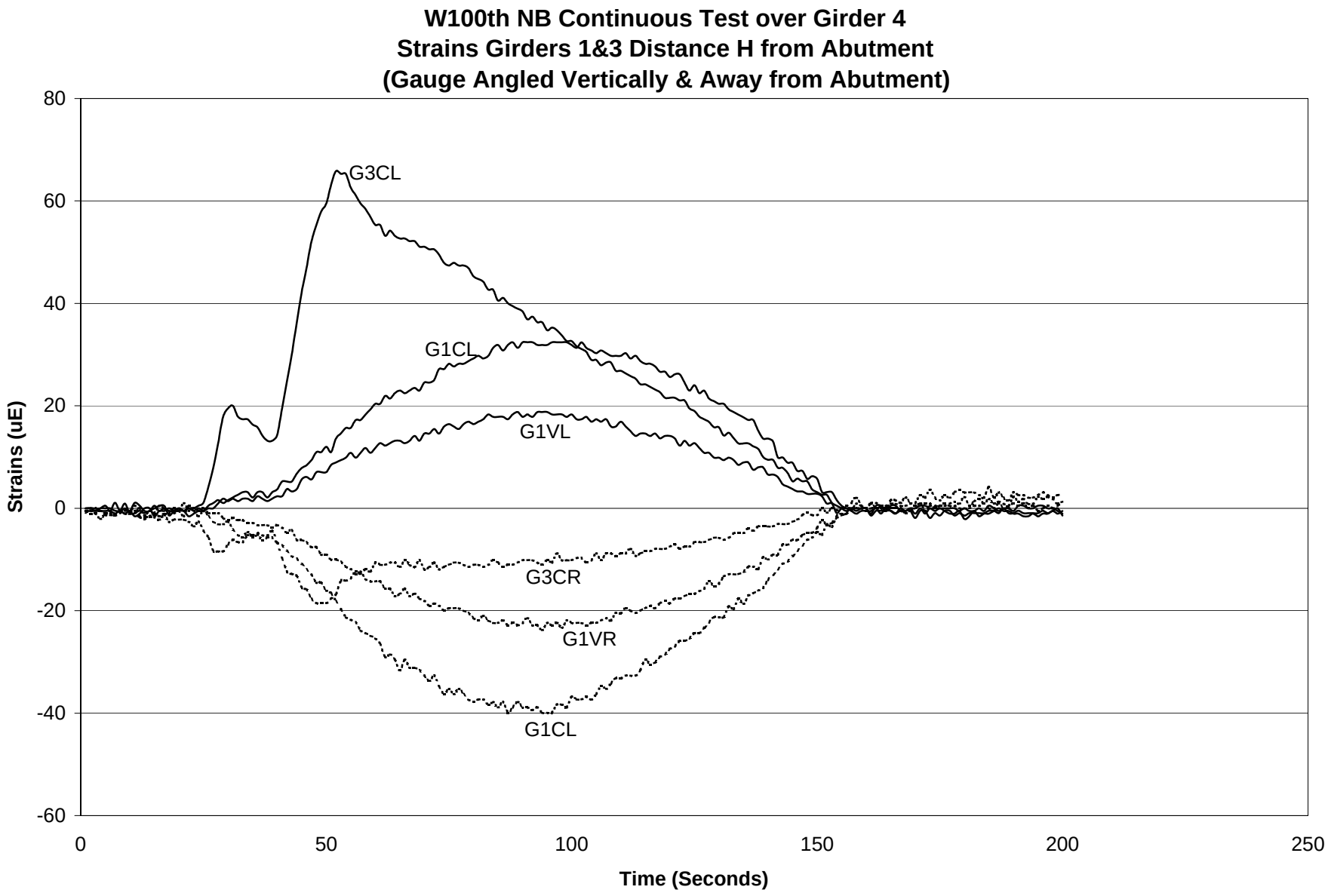
W100th NB Continuous Test over Girder 4
Strains Girders 1&3 Distance H from Abutment
(Gauge Angled Vertically & Away from Abutment)
Strains (uE)
Time (Seconds)
80
60
40
20
0
-20
-40
-60
0
50
100
150
200
250
G3CL
G1CL
G1VL
G3CR
G1VR
G1CL

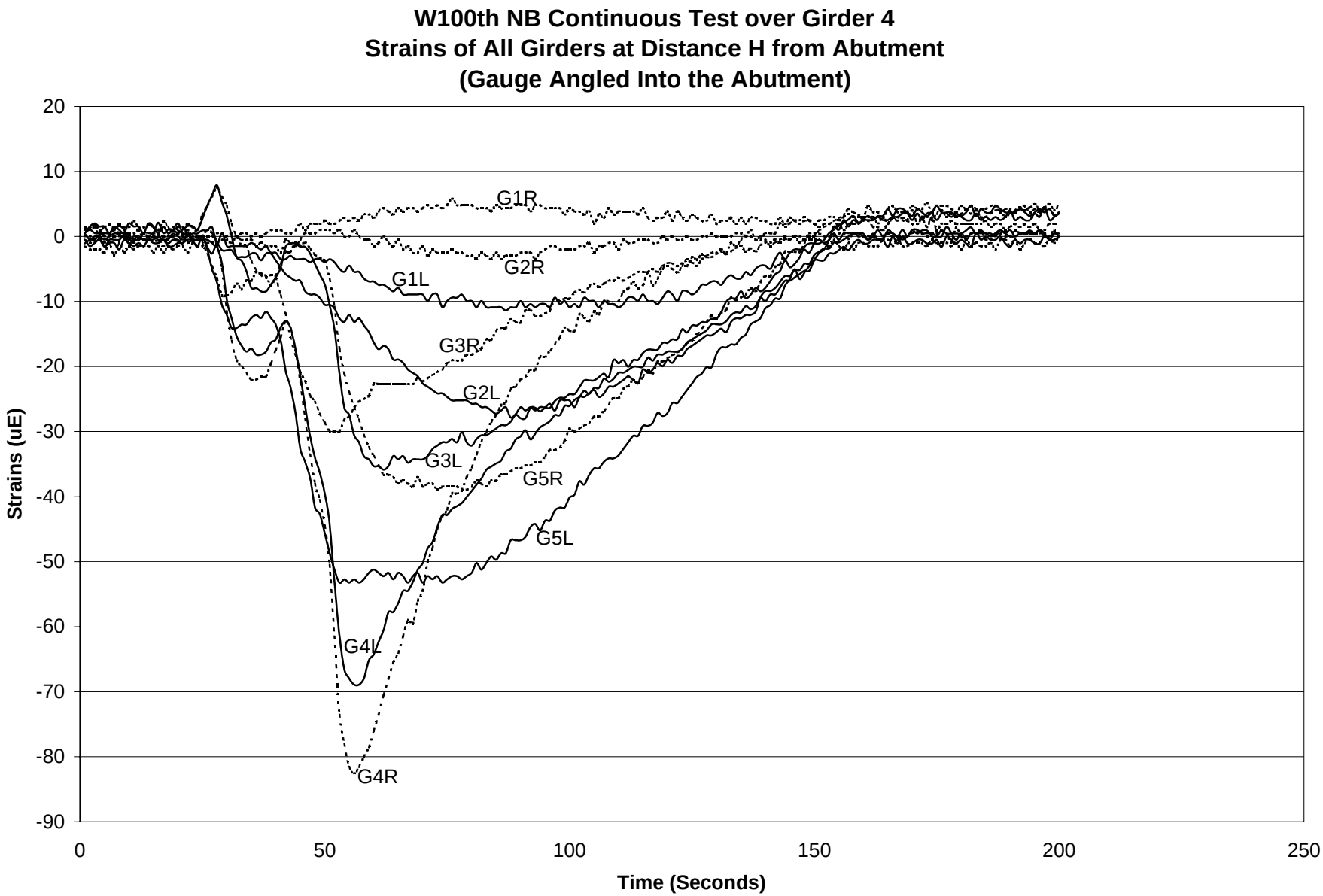
W100th NB Continuous Test over Girder 4
Strains of All Girders at Distance H from Abutment
(Gauge Angled Into the Abutment)
Strains (uE)
Time (Seconds)
20
10
0
-10
-20
-30
-40
-50
-60
-70
-80
-90
0
50
100
150
200
250
G1R
G2R
G1L
G3R
G2L
G3L
G5R
G5L
G4L
G4R

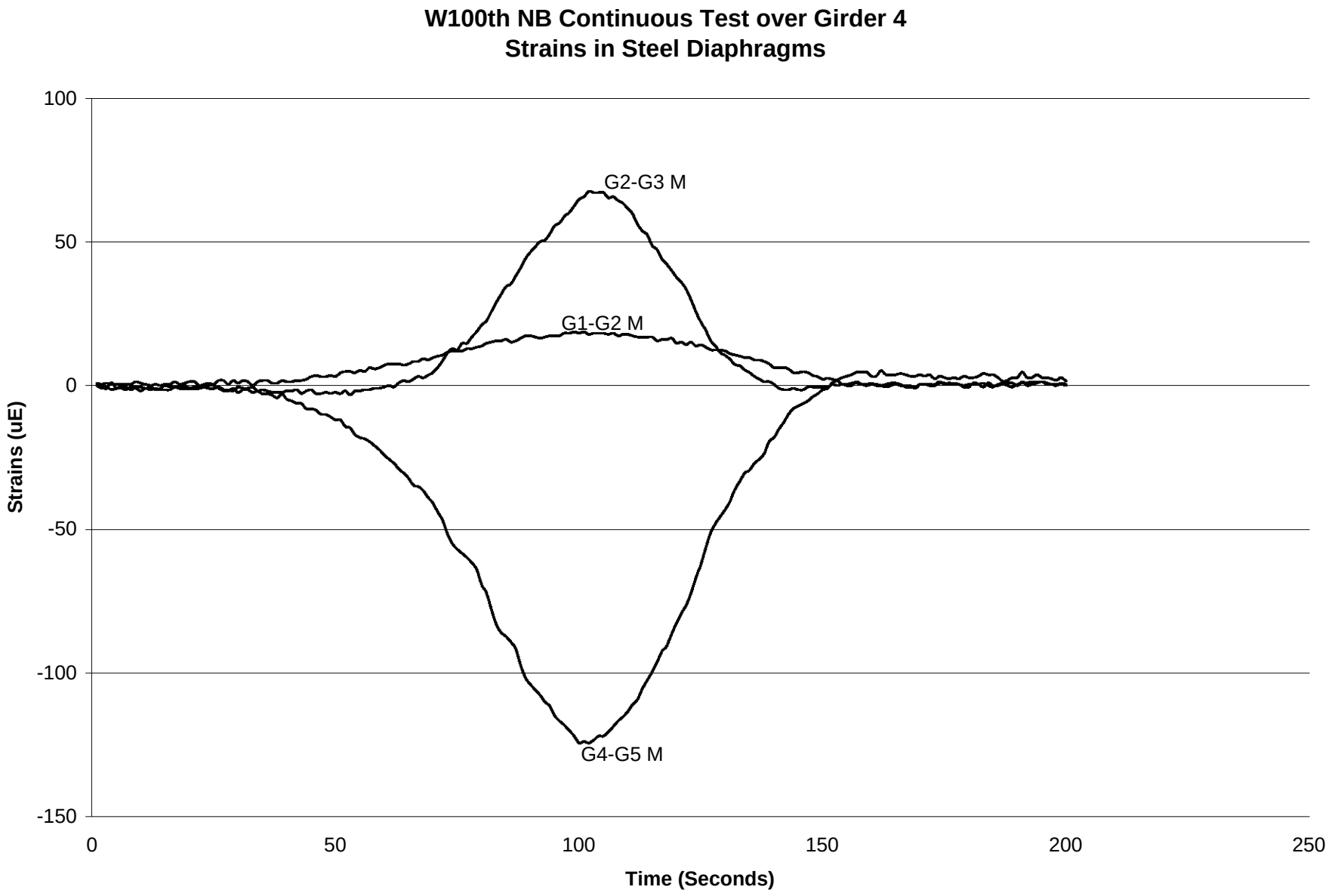
W100th NB Continuous Test over Girder 4
Strains in Steel Diaphragms
100
50
0
-50
-100
-150
Strains (uE)
0
50
100
150
200
250
Time (Seconds)
G2-G3 M
G1-G2 M
G4-G5 M

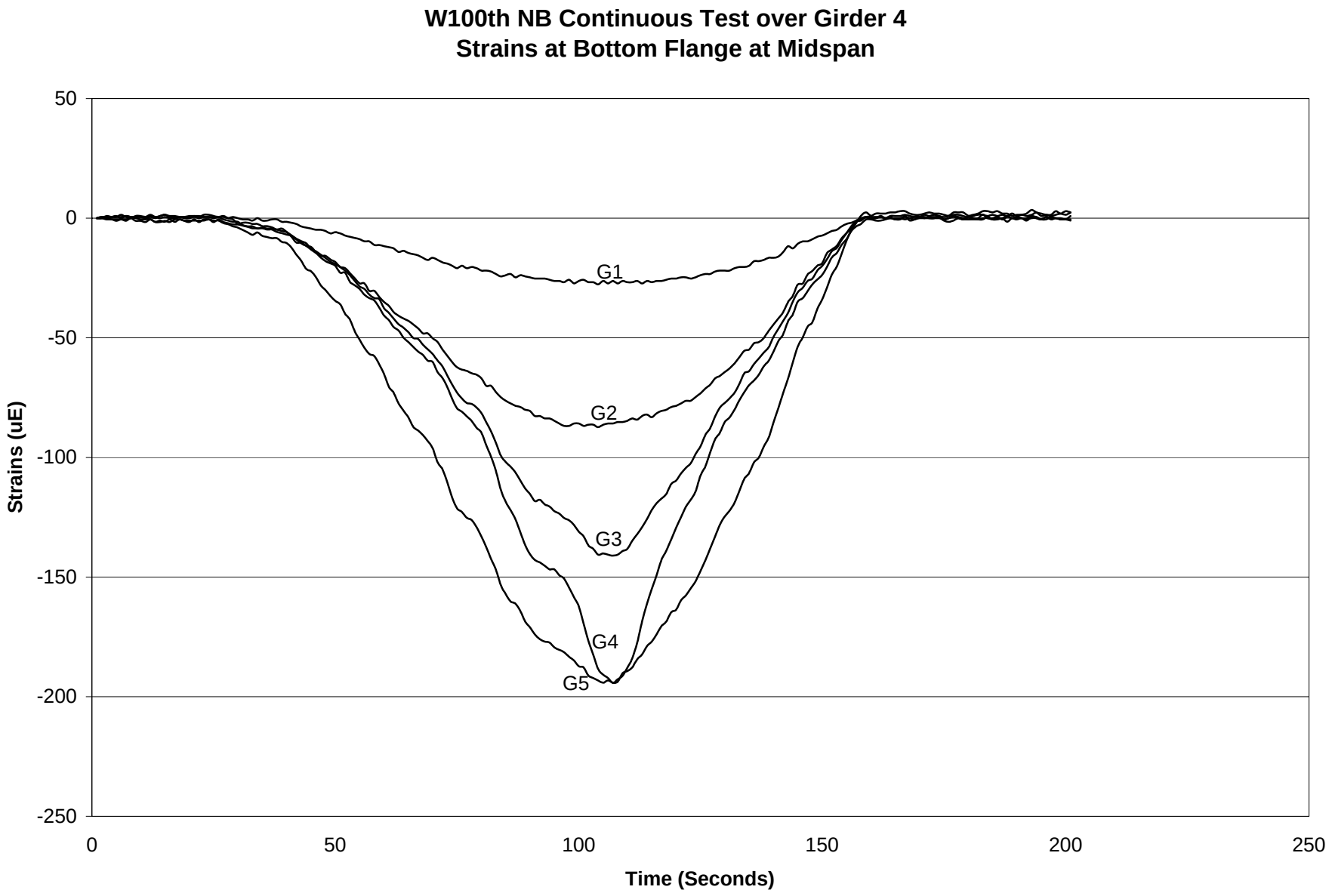
W100th NB Continuous Test over Girder 4
Strains at Bottom Flange at Midspan
50
0
-50
-100
-150
-200
-250
Strains (uE)
0
50
100
150
200
250
Time (Seconds)
G1
G2
G3
G4
G5

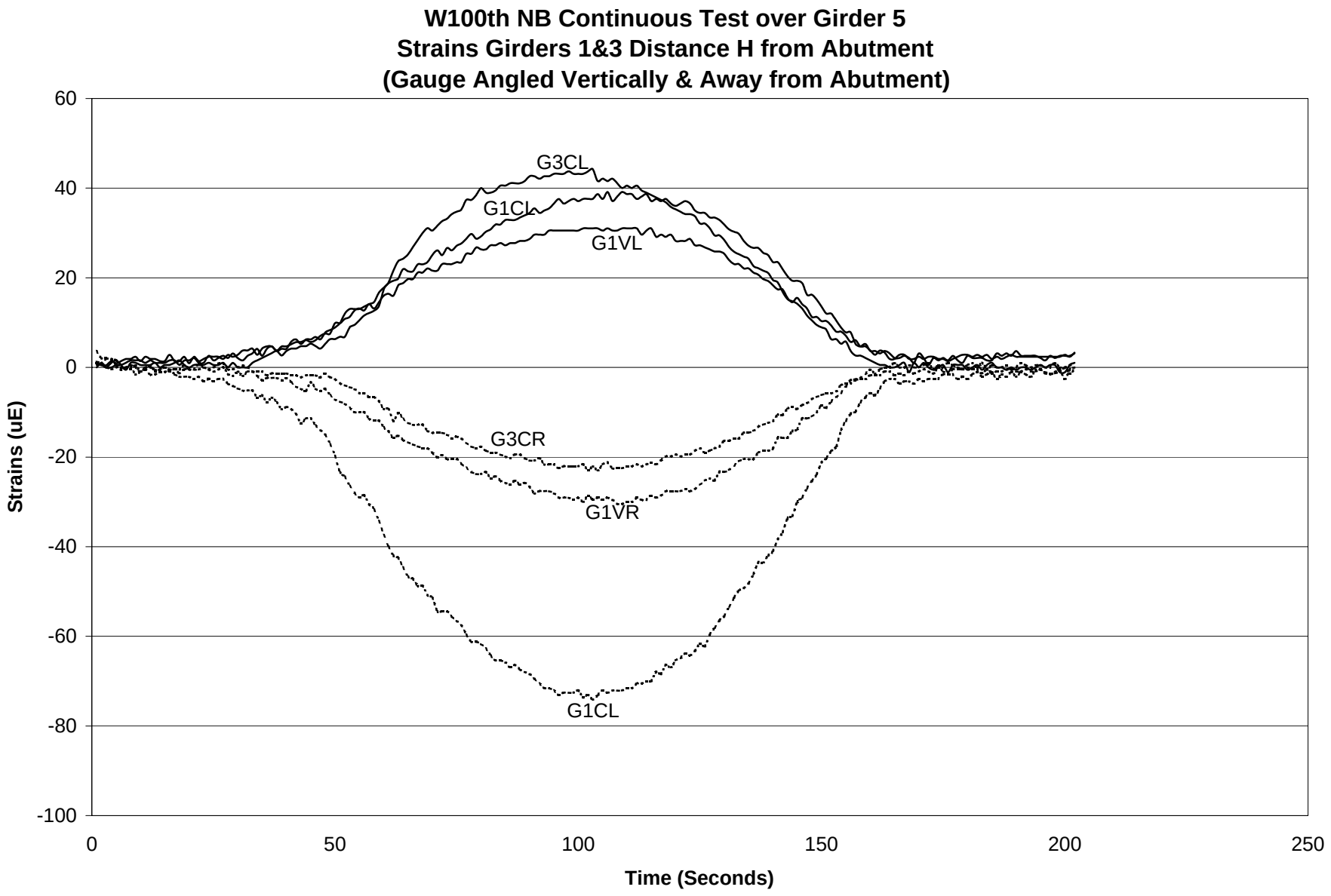
W100th NB Continuous Test over Girder 5
Strains Girders 1&3 Distance H from Abutment
(Gauge Angled Vertically & Away from Abutment)
Strains (uE)
Time (Seconds)
60
40
20
0
-20
-40
-60
-80
-100
0
50
100
150
200
250
G3CL
G1CL
G1VL
G3CR
G1VR
G1CL

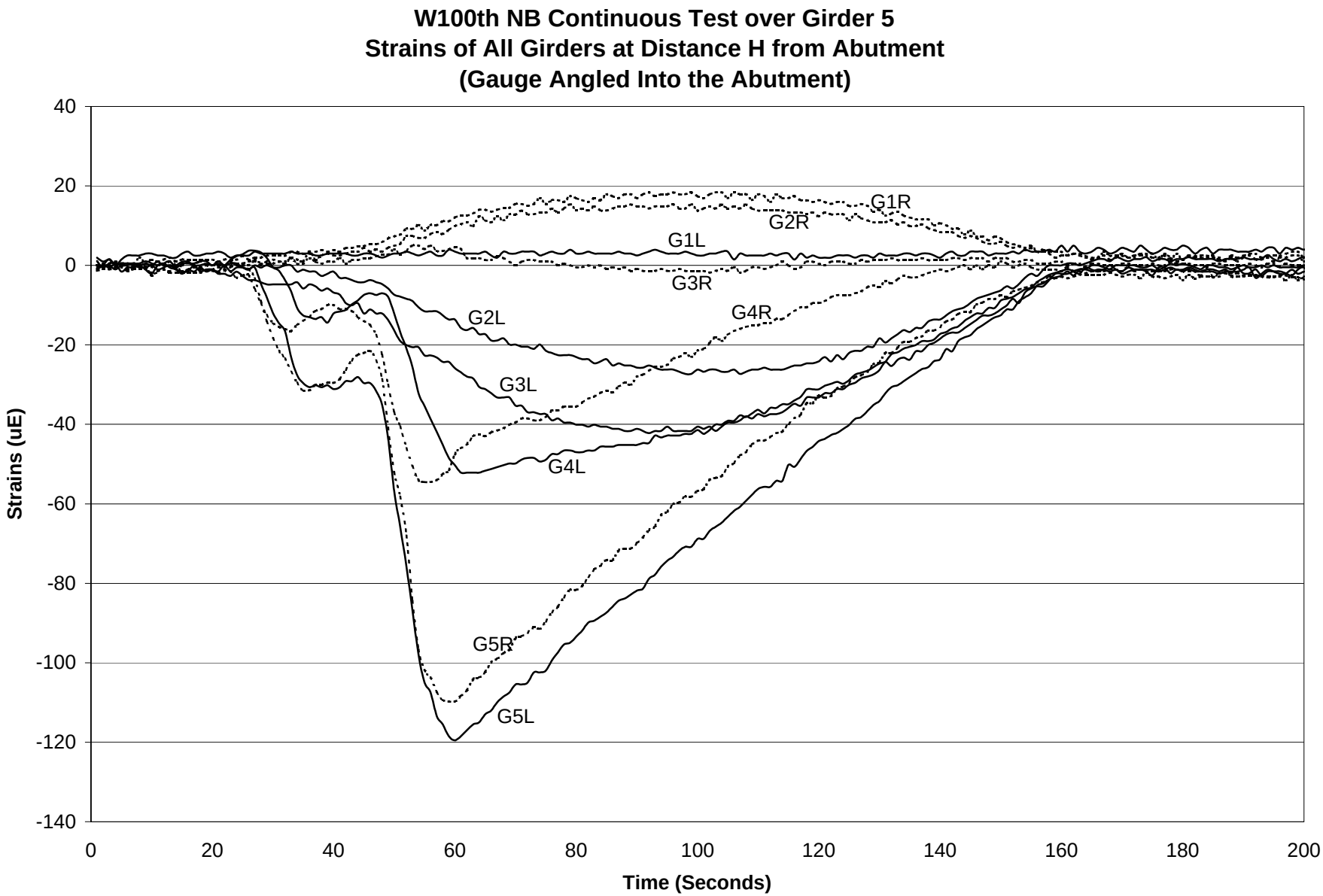
W100th NB Continuous Test over Girder 5
Strains of All Girders at Distance H from Abutment
(Gauge Angled Into the Abutment)
Strains (uE)
Time (Seconds)
40
20
0
-20
-40
-60
-80
-100
-120
-140
0
20
40
60
80
100
120
140
160
180
200
G1R
G2R
G1L
G3R
G4R
G2L
G3L
G4L
G5R
G5L

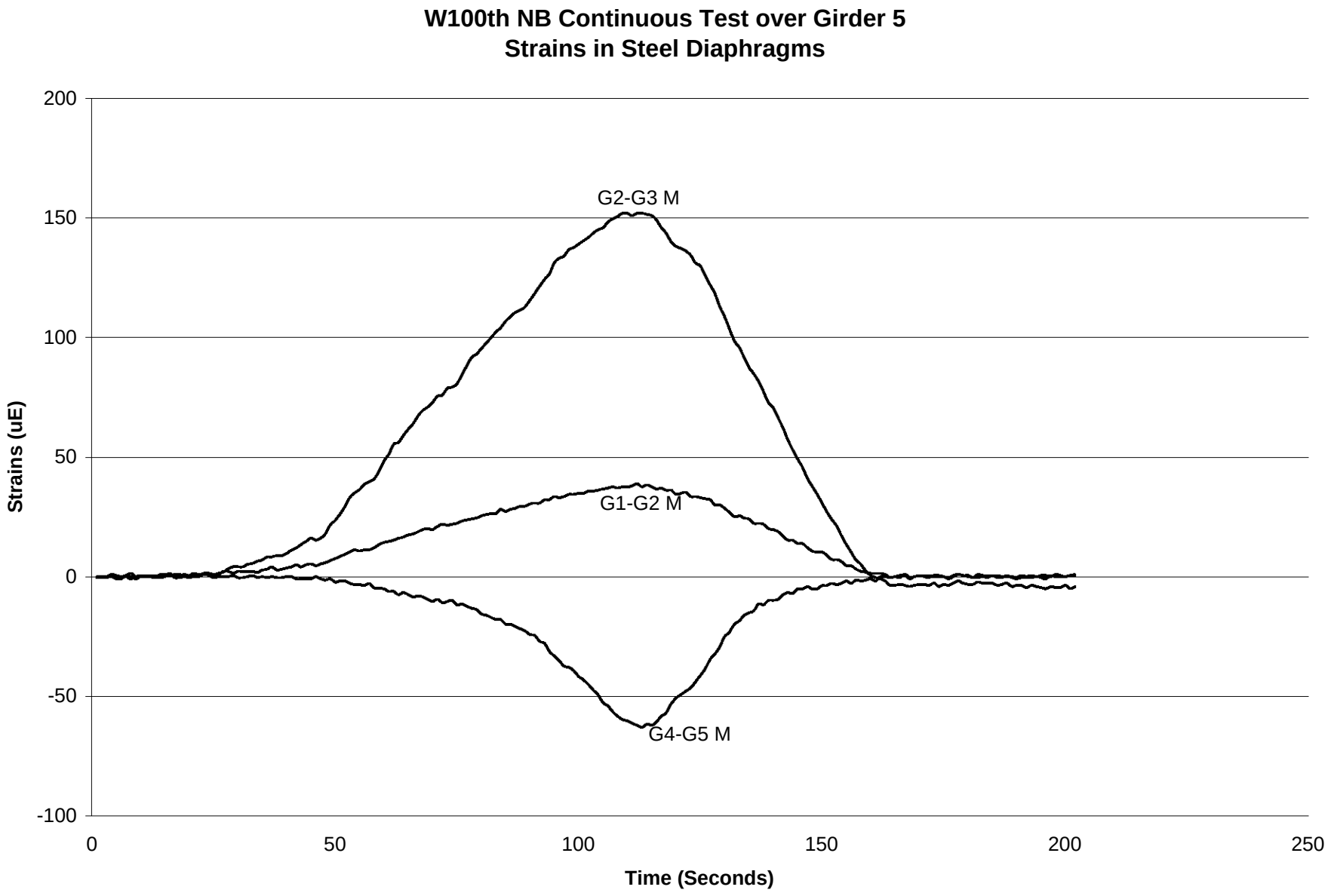
W100th NB Continuous Test over Girder 5
Strains in Steel Diaphragms
200
150
100
50
0
-50
-100
Strains (uE)
G2-G3 M
G1-G2 M
G4-G5 M
0
50
100
150
200
250
Time (Seconds)

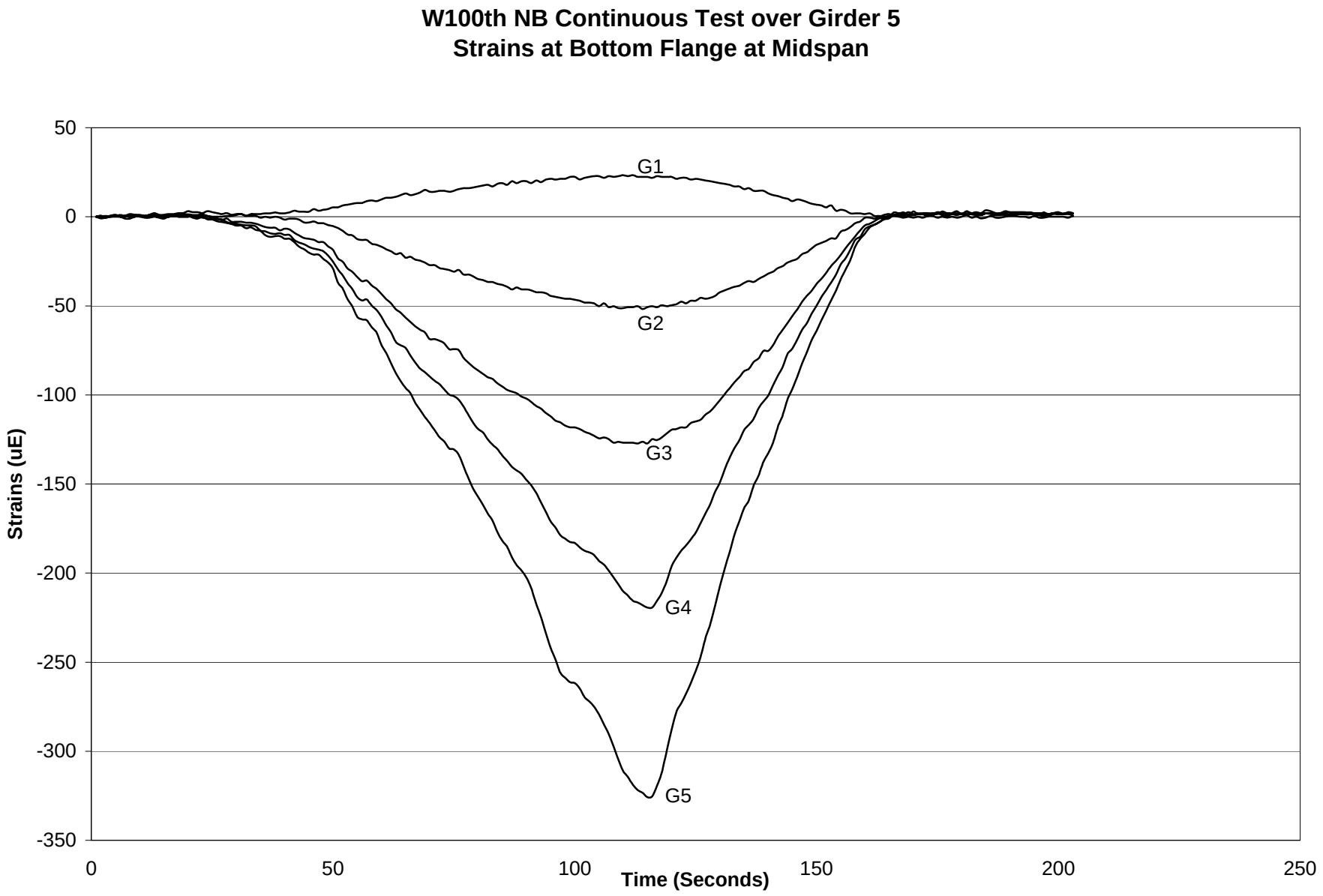
W100th NB Continuous Test over Girder 5
Strains at Bottom Flange at Midspan
Strains (uE)
Time (Seconds)
50
0
-50
-100
-150
-200
-250
-300
-350
0
50
100
150
200
250
G1
G2
G3
G4
G5

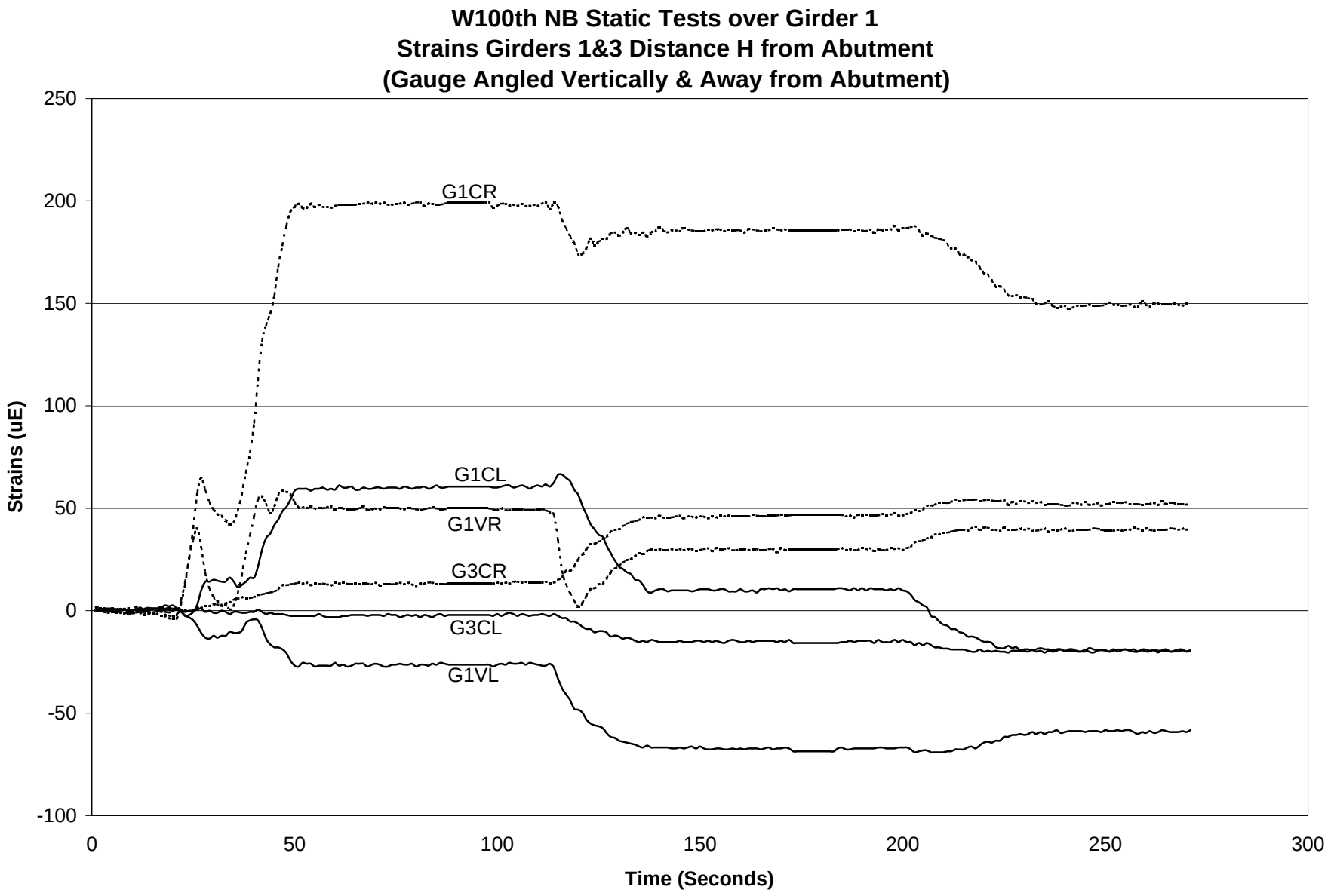
W100th NB Static Tests over Girder 1
Strains Girders 1&3 Distance H from Abutment
(Gauge Angled Vertically & Away from Abutment)
Strains (uE)
Time (Seconds)
250
200
150
100
50
0
-50
-100
0
50
100
150
200
250
300
G1CR
G1CL
G1VR
G3CR
G3CL
G1VL

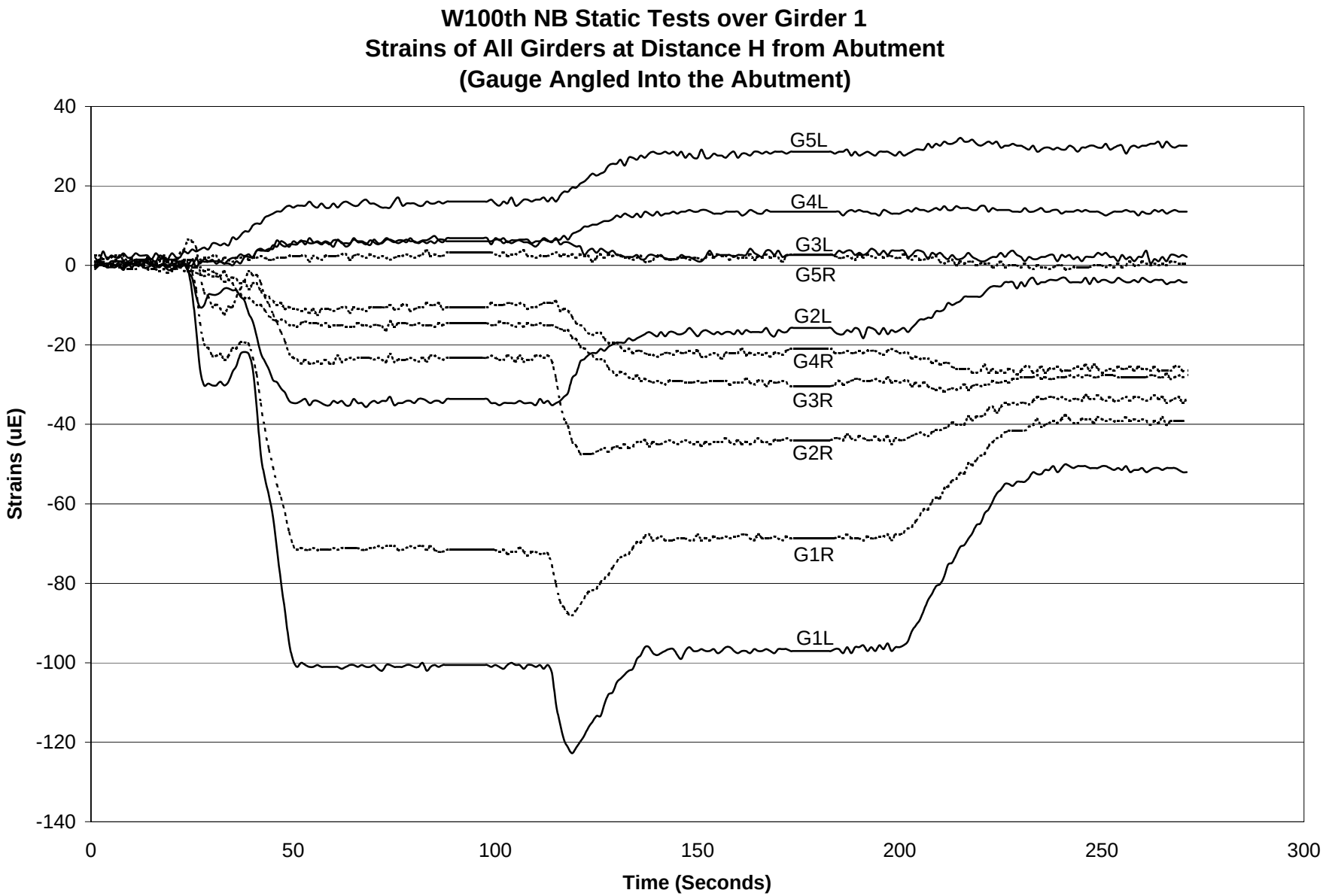
W100th NB Static Tests over Girder 1
Strains of All Girders at Distance H from Abutment
(Gauge Angled Into the Abutment)
Strains (uE)
Time (Seconds)
40
20
0
-20
-40
-60
-80
-100
-120
-140
0
50
100
150
200
250
300
G5L
G4L
G3L
G5R
G2L
G4R
G3R
G2R
G1R
G1L

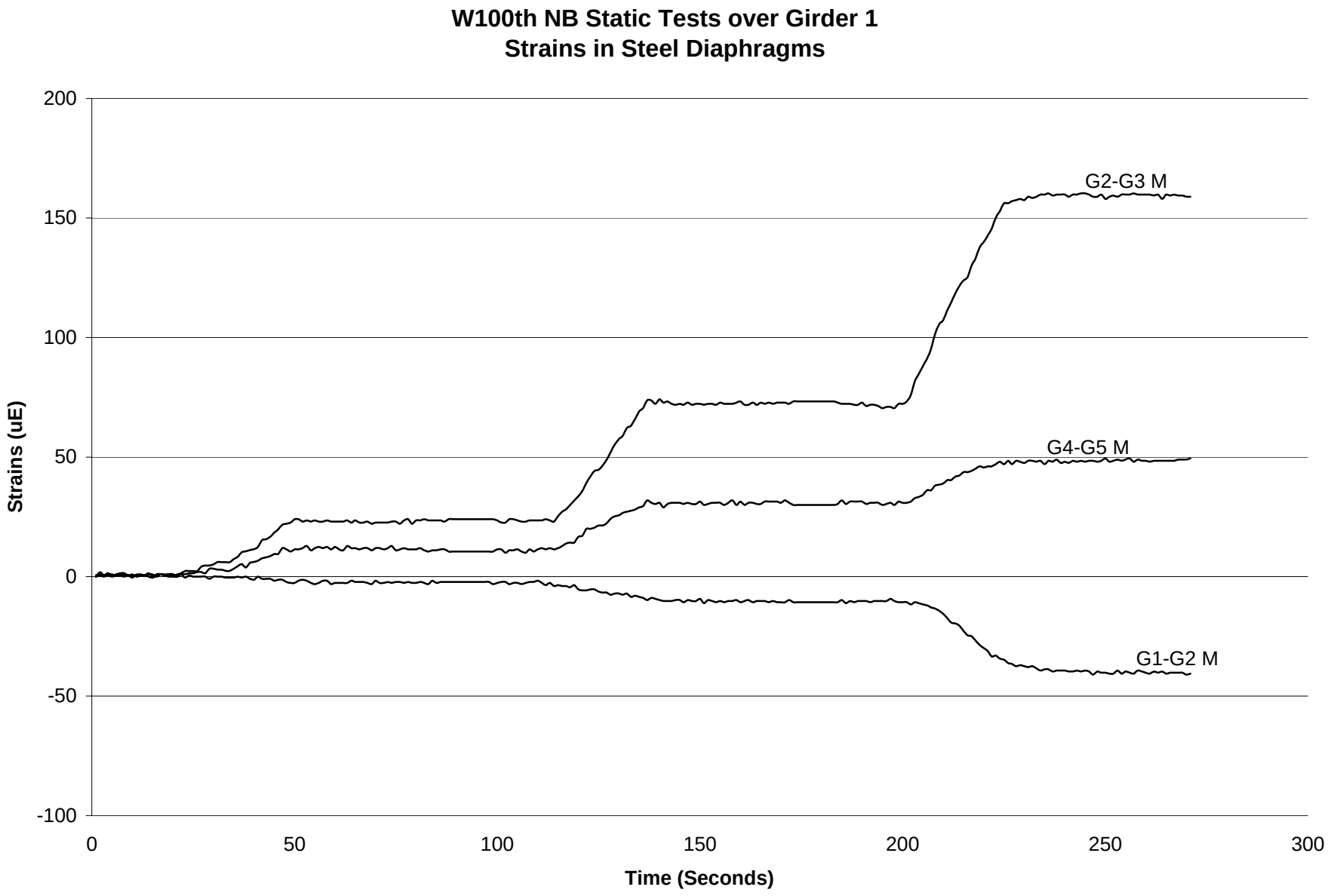
W100th NB Static Tests over Girder 1
Strains in Steel Diaphragms
Strains (uE)
200
150
100
50
0
-50
-100
0
50
100
150
200
250
300
Time (Seconds)
G2-G3 M
G4-G5 M
G1-G2 M

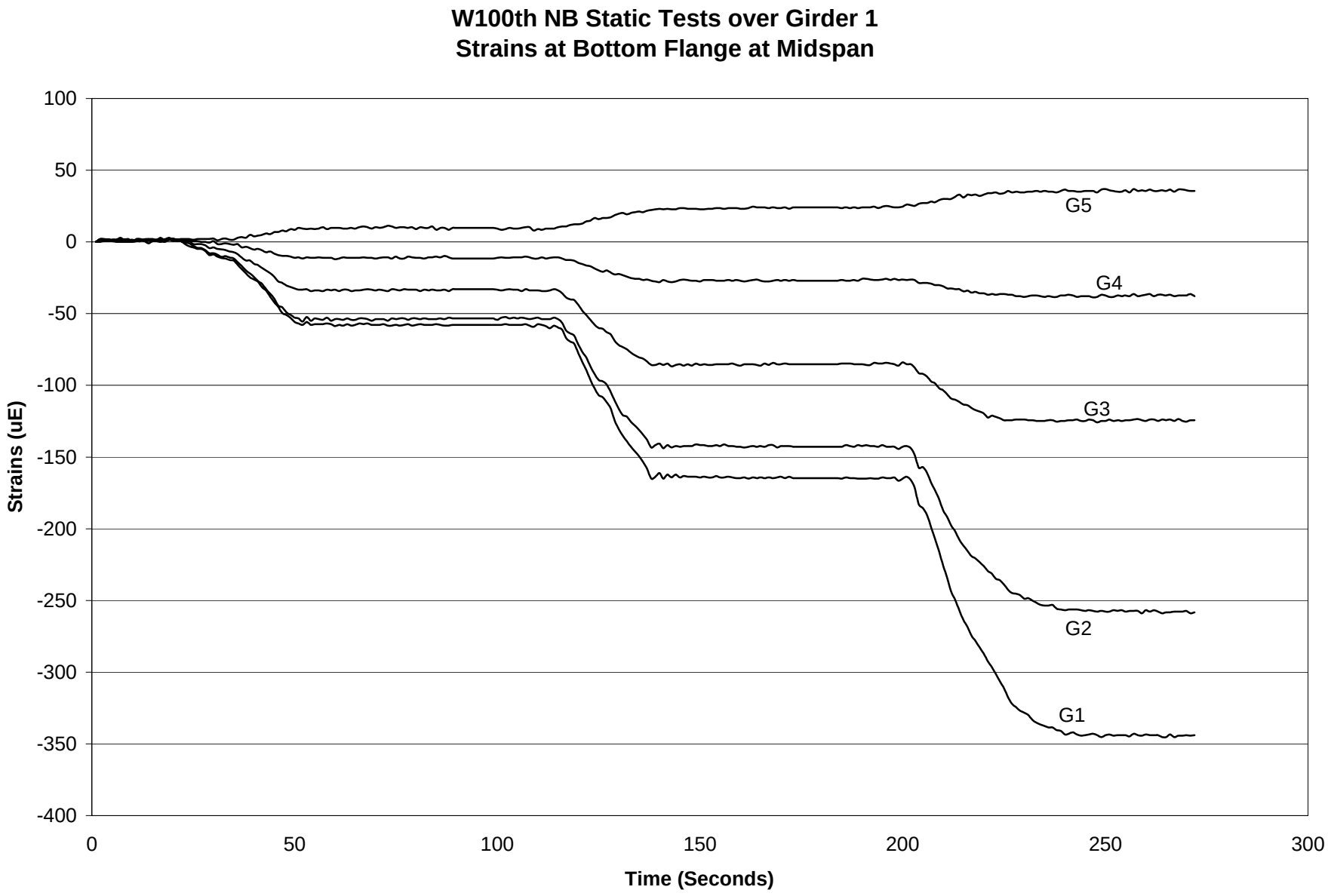
W100th NB Static Tests over Girder 1
Strains at Bottom Flange at Midspan
Strains (uE)
100
50
0
-50
-100
-150
-200
-250
-300
-350
-400
0
50
100
150
200
250
300
Time (Seconds)
G5
G4
G3
G2
G1

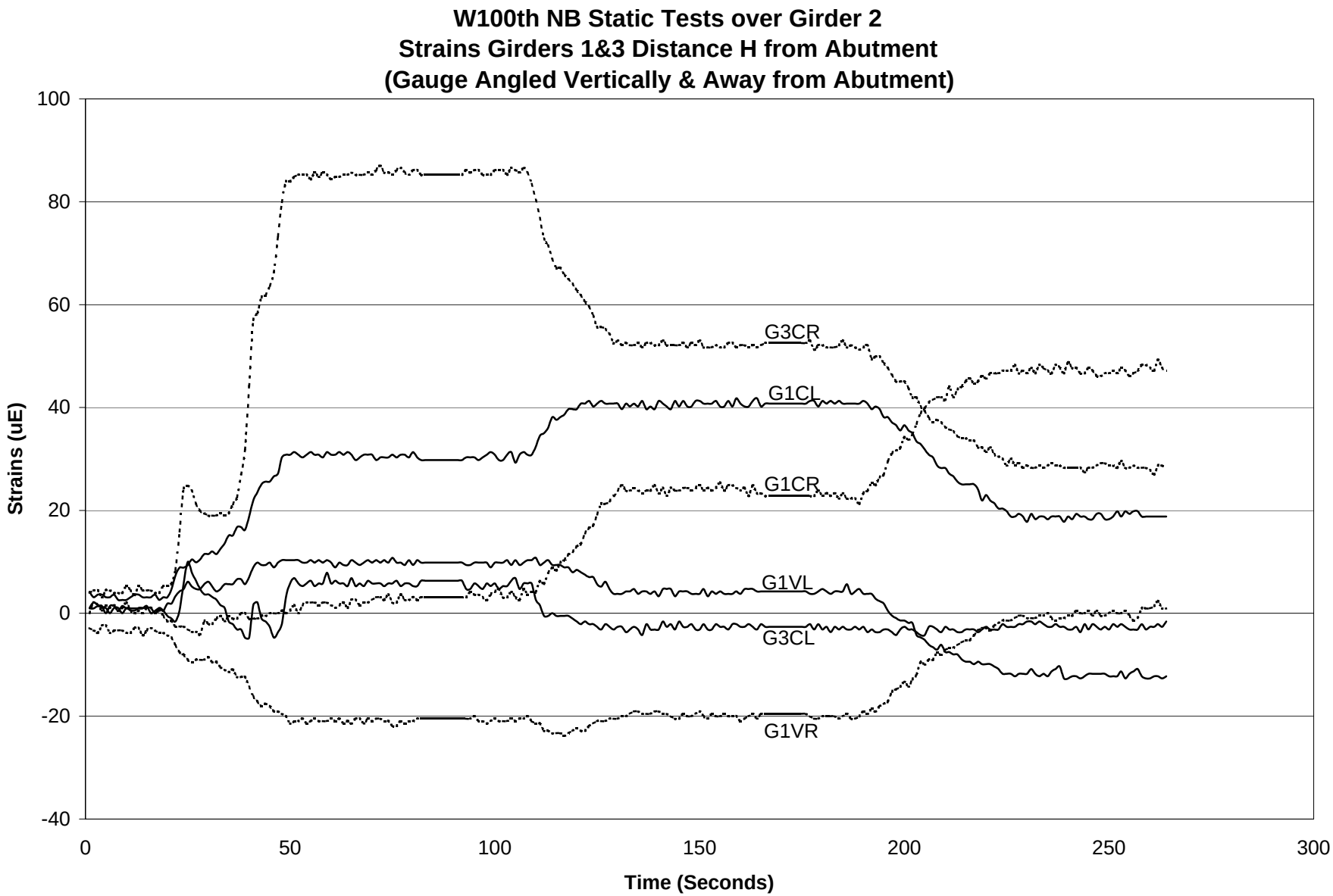
W100th NB Static Tests over Girder 2
Strains Girders 1&3 Distance H from Abutment
(Gauge Angled Vertically & Away from Abutment)
Strains (uE)
Time (Seconds)
100
80
60
40
20
0
-20
-40
0
50
100
150
200
250
300
G3CR
G1CL
G1CR
G1VL
G3CL
G1VR

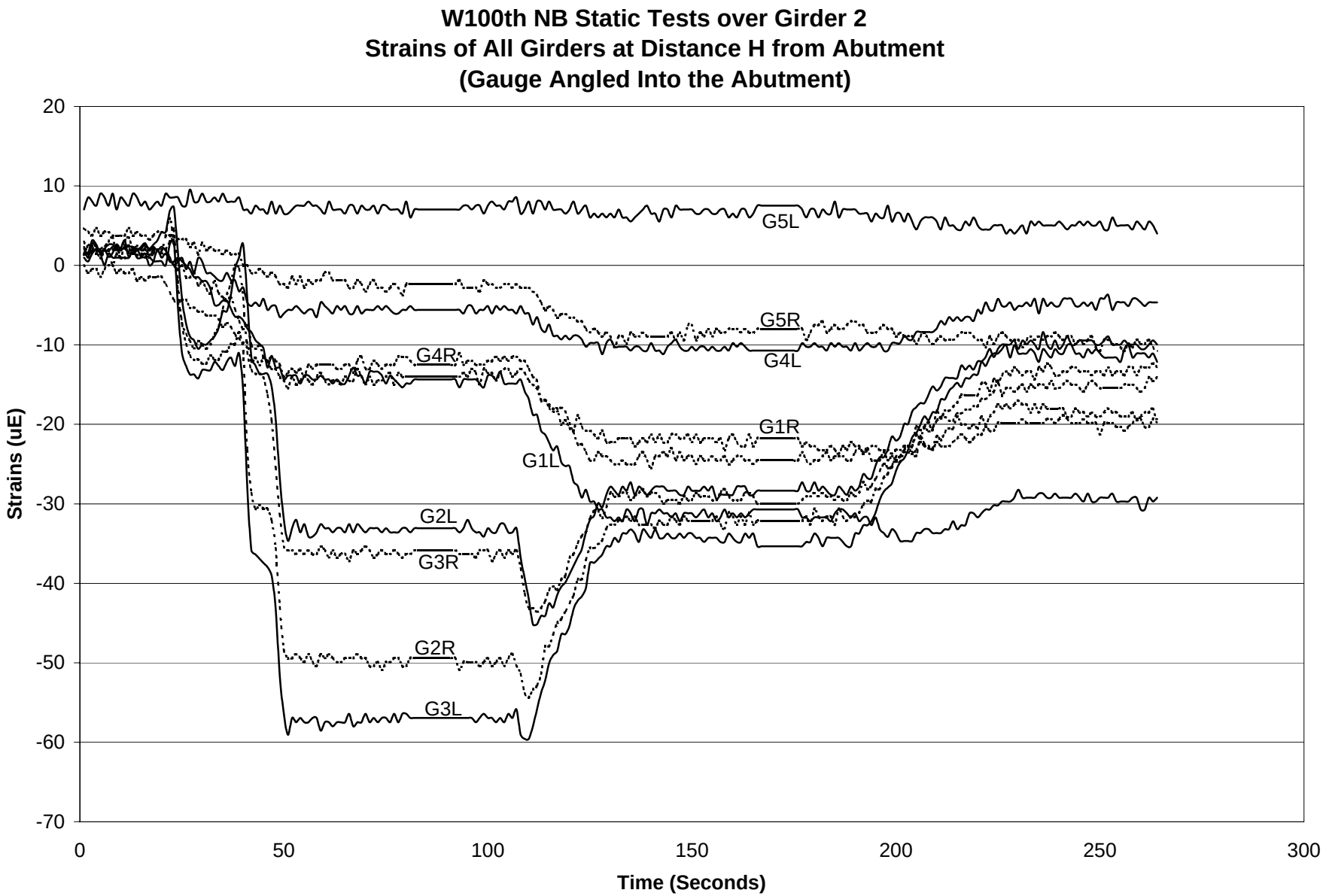
W100th NB Static Tests over Girder 2
Strains of All Girders at Distance H from Abutment
(Gauge Angled Into the Abutment)
Strains (uE)
Time (Seconds)
20
10
0
-10
-20
-30
-40
-50
-60
-70
0
50
100
150
200
250
300
G5L
G5R
G4L
G4R
G1R
G1L
G2L
G3R
G2R
G3L

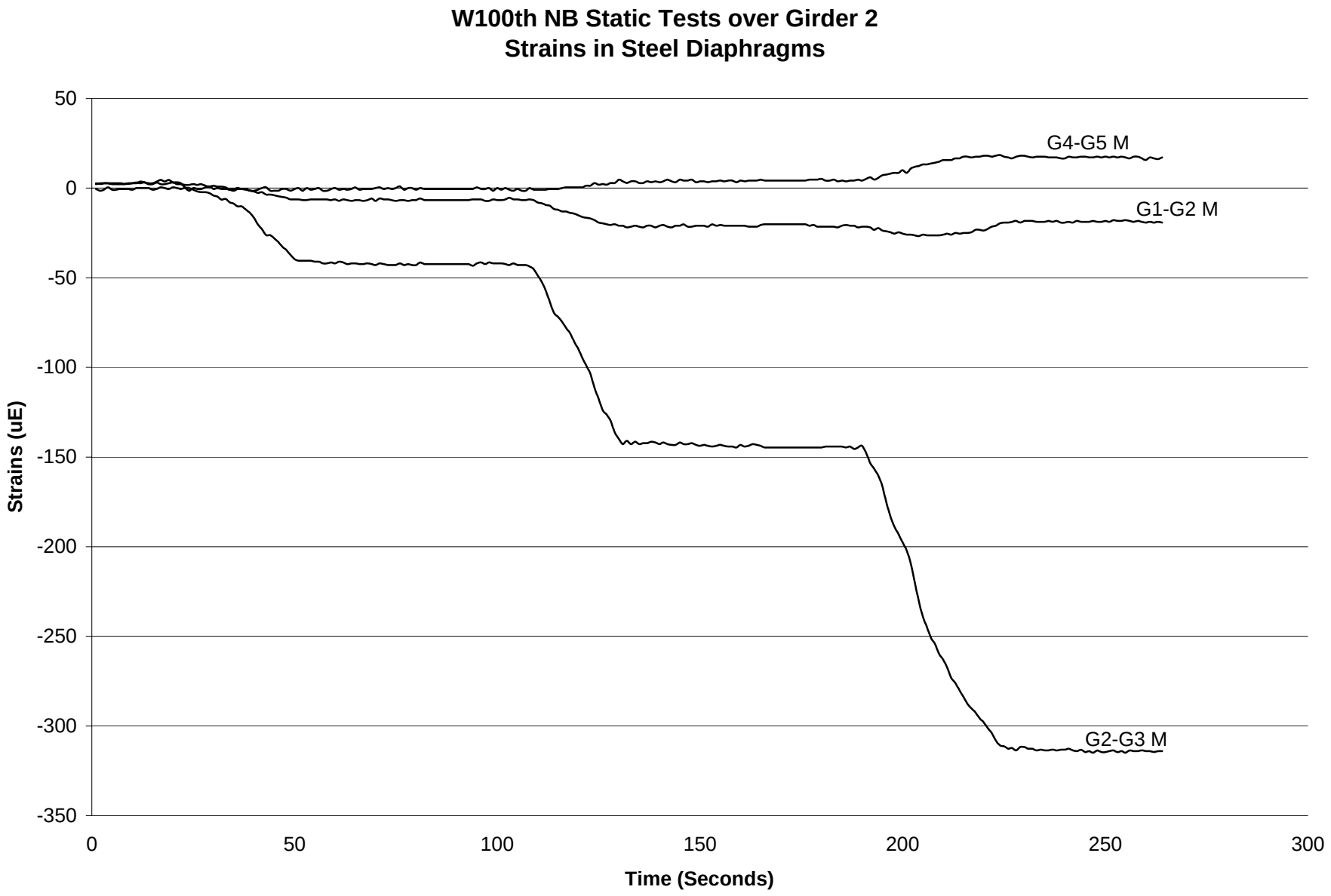
W100th NB Static Tests over Girder 2
Strains in Steel Diaphragms
50
0
-50
-100
-150
-200
-250
-300
-350
Strains (uE)
0
50
100
150
200
250
300
Time (Seconds)
G4-G5 M
G1-G2 M
G2-G3 M

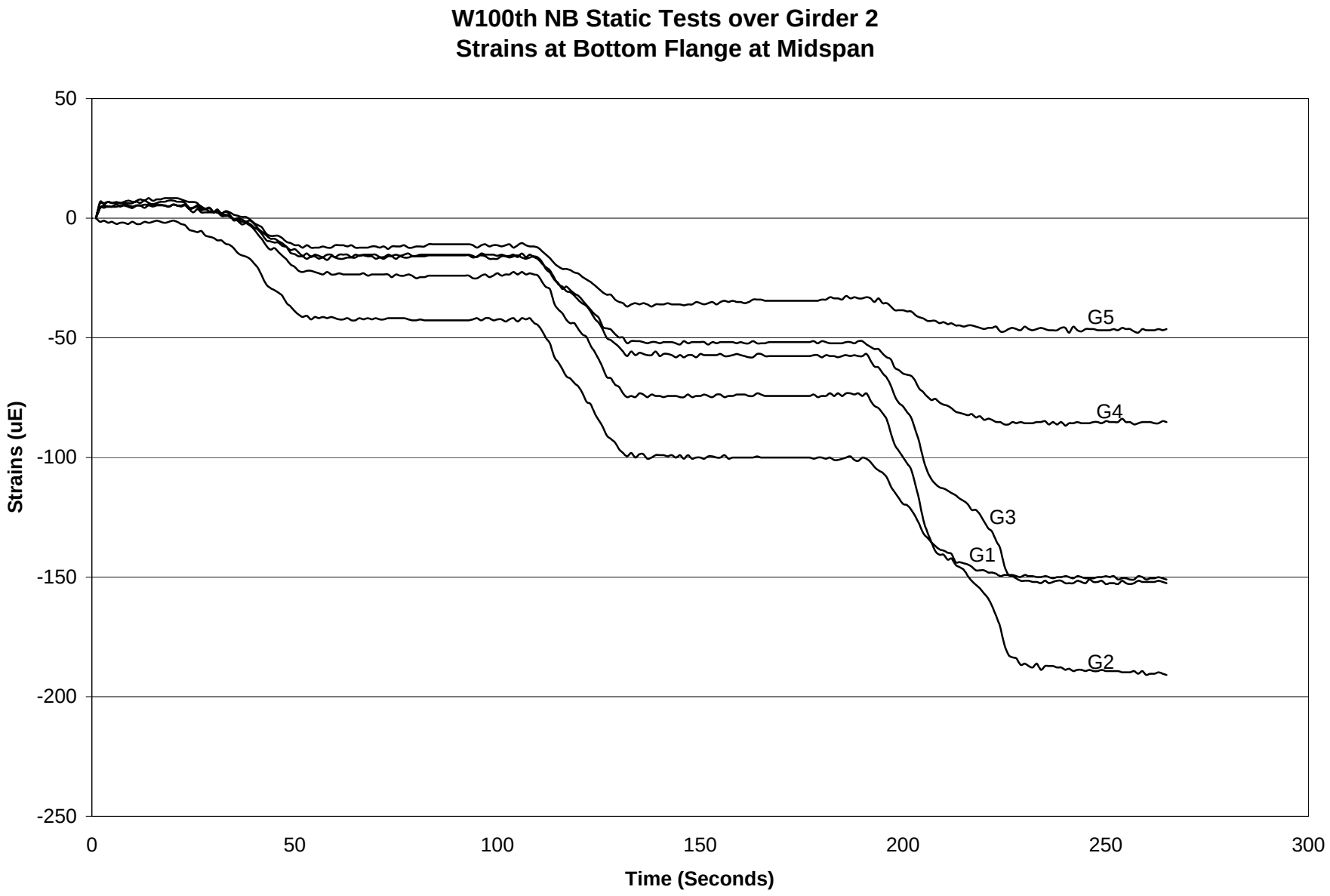
W100th NB Static Tests over Girder 2
Strains at Bottom Flange at Midspan
Strains (uE)
50
0
-50
-100
-150
-200
-250
0
50
100
150
200
250
300
Time (Seconds)
G5
G4
G3
G1
G2

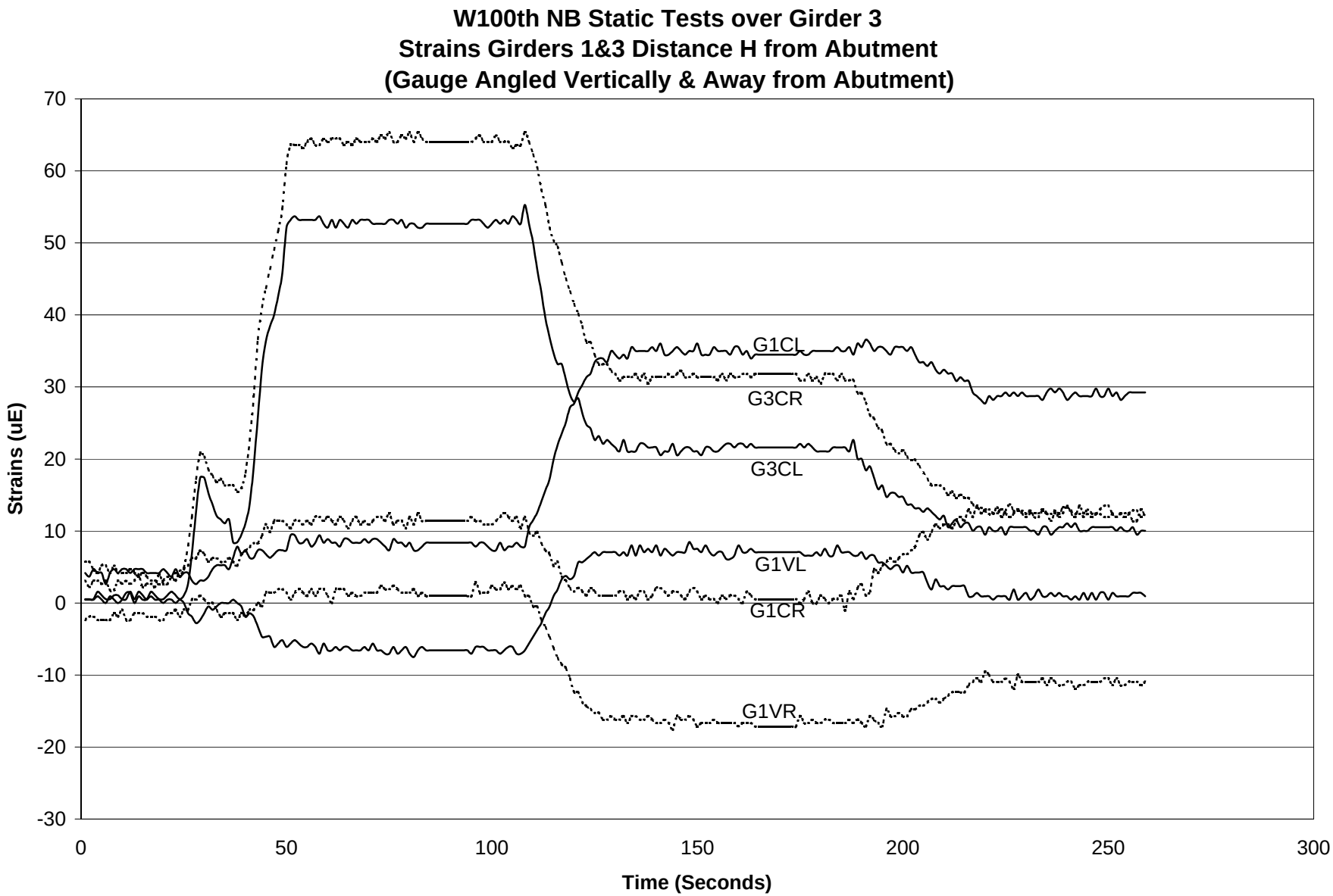
W100th NB Static Tests over Girder 3
Strains Girders 1&3 Distance H from Abutment
(Gauge Angled Vertically & Away from Abutment)
Strains (uE)
Time (Seconds)
70
60
50
40
30
20
10
0
-10
-20
-30
0
50
100
150
200
250
300
G1CL
G3CR
G3CL
G1VL
G1CR
G1VR

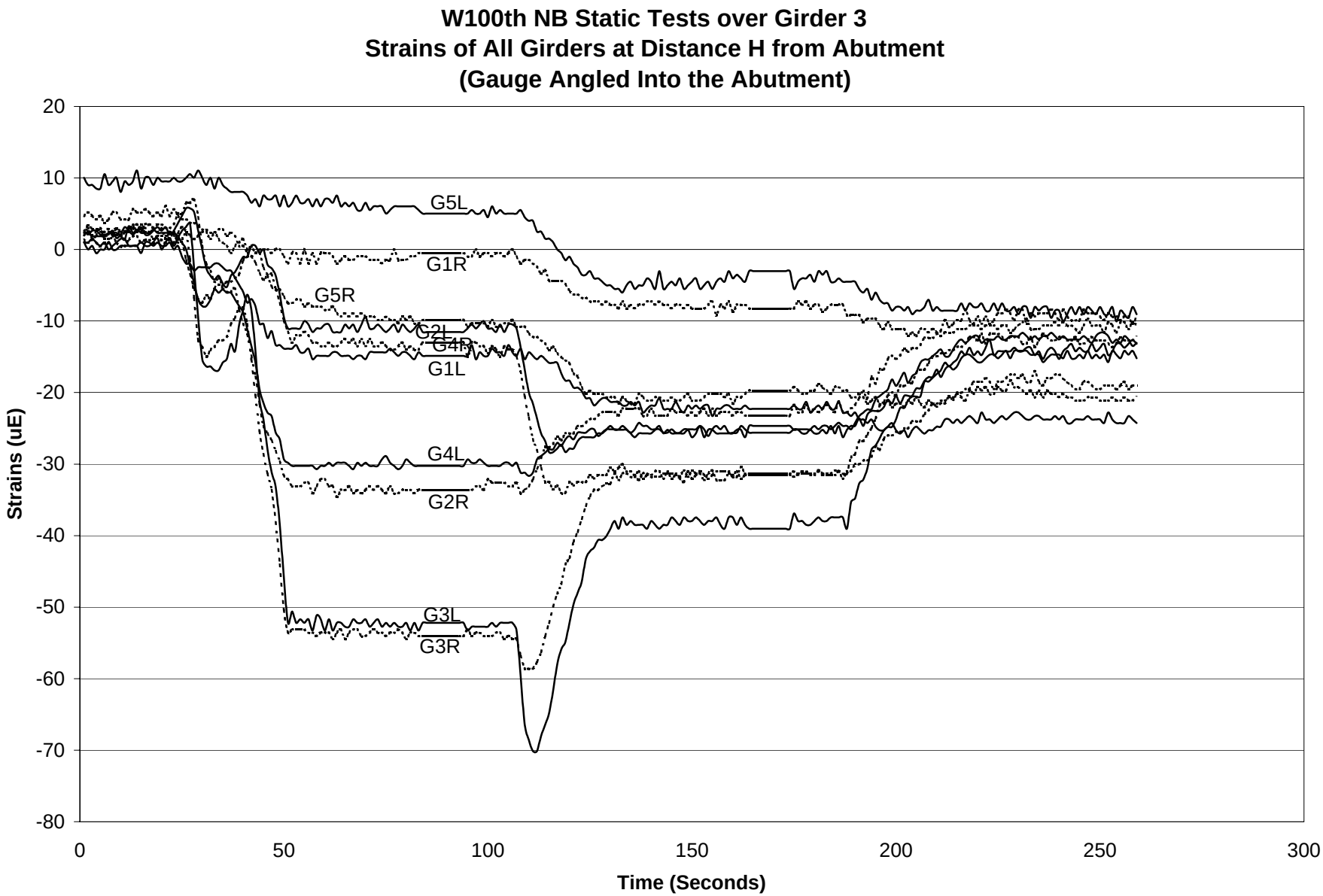
W100th NB Static Tests over Girder 3
Strains of All Girders at Distance H from Abutment
(Gauge Angled Into the Abutment)
Strains (uE)
Time (Seconds)
20
10
0
-10
-20
-30
-40
-50
-60
-70
-80
0
50
100
150
200
250
300
G5L
G1R
G5R
G2L
G4R
G1L
G4L
G2R
G3L
G3R

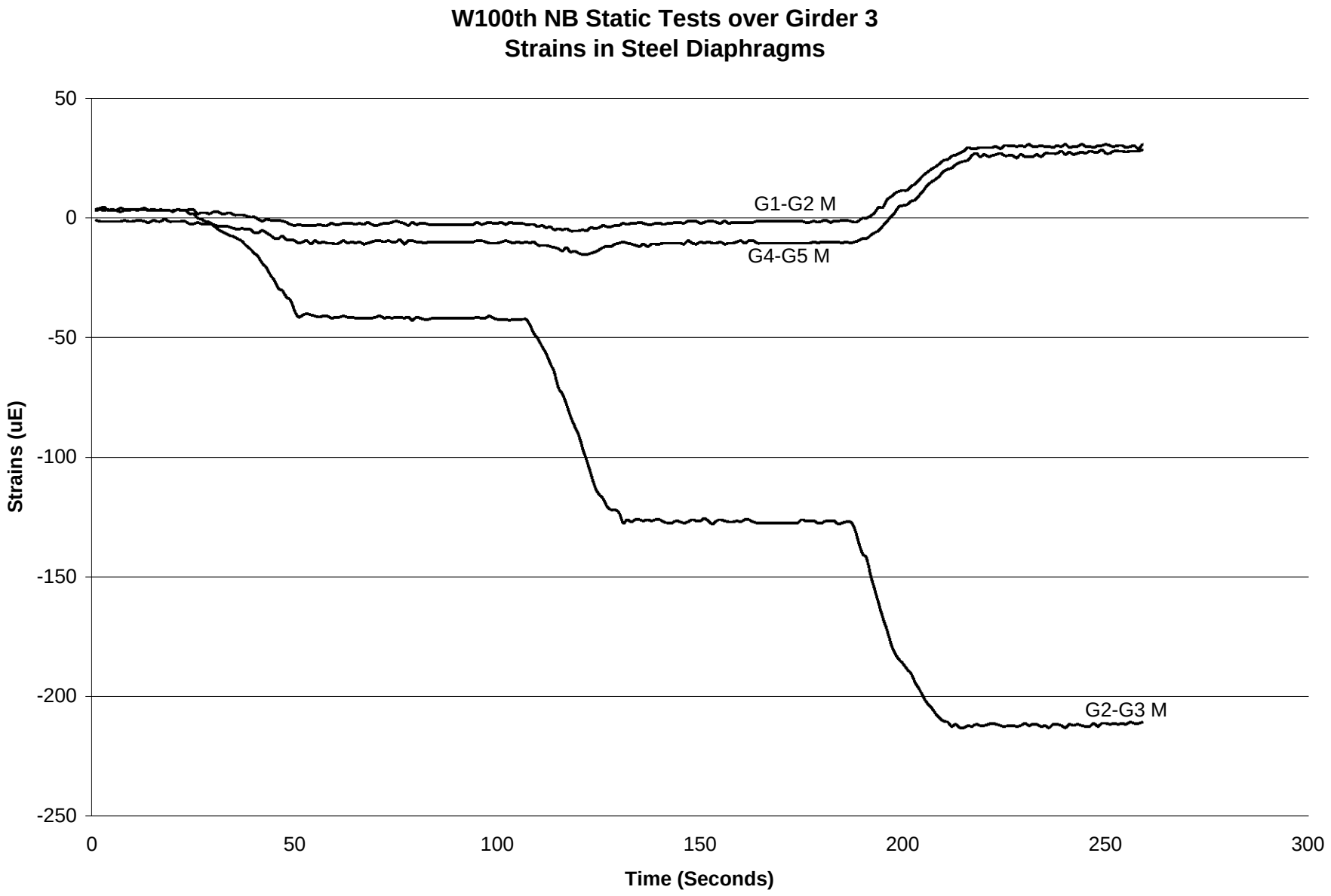
W100th NB Static Tests over Girder 3
Strains in Steel Diaphragms
50
0
-50
-100
-150
-200
-250
Strains (uE)
0
50
100
150
200
250
300
Time (Seconds)
G1-G2 M
G4-G5 M
G2-G3 M

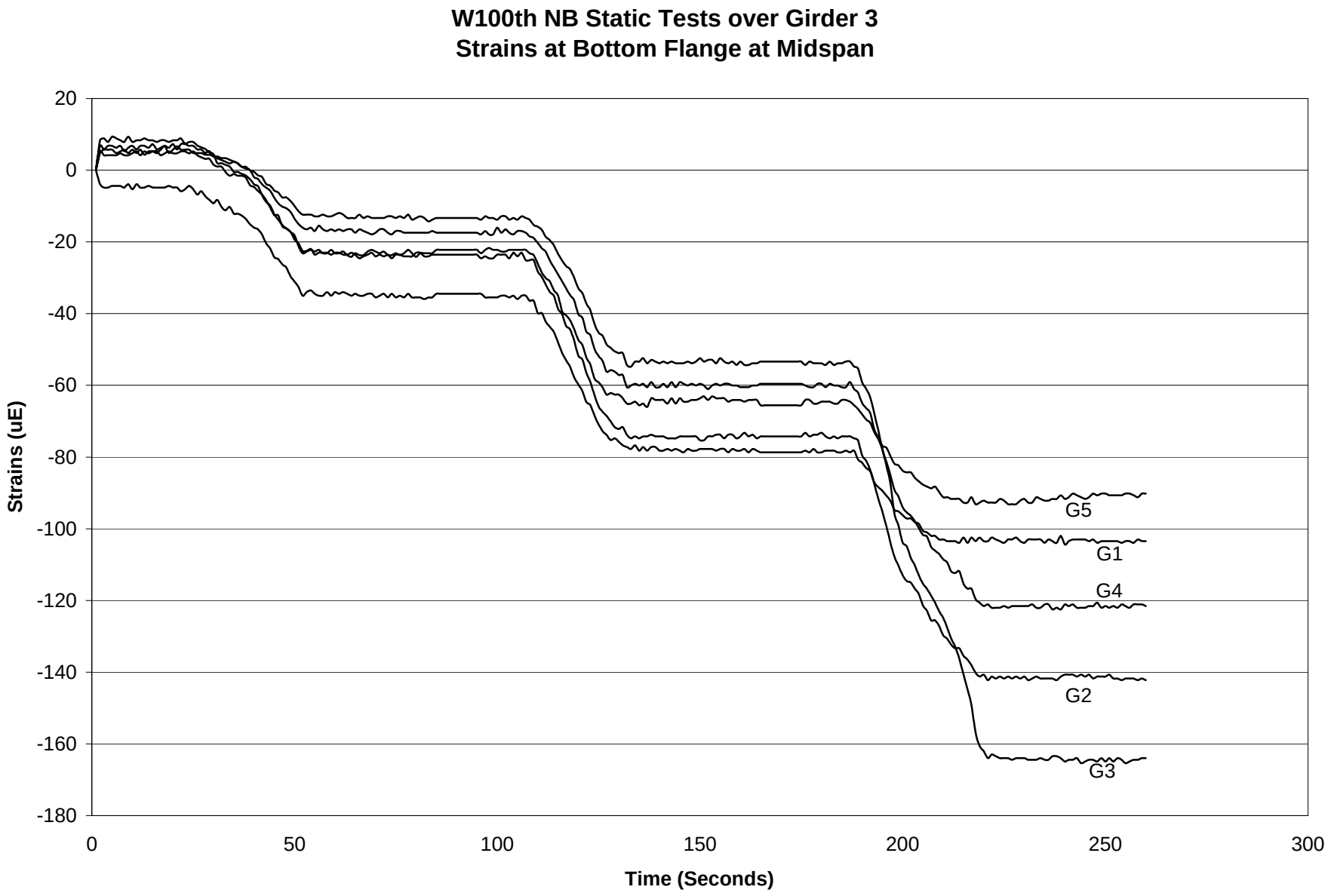
W100th NB Static Tests over Girder 3
Strains at Bottom Flange at Midspan
Strains (uE)
20
0
-20
-40
-60
-80
-100
-120
-140
-160
-180
0
50
100
150
200
250
300
Time (Seconds)
G5
G1
G4
G2
G3

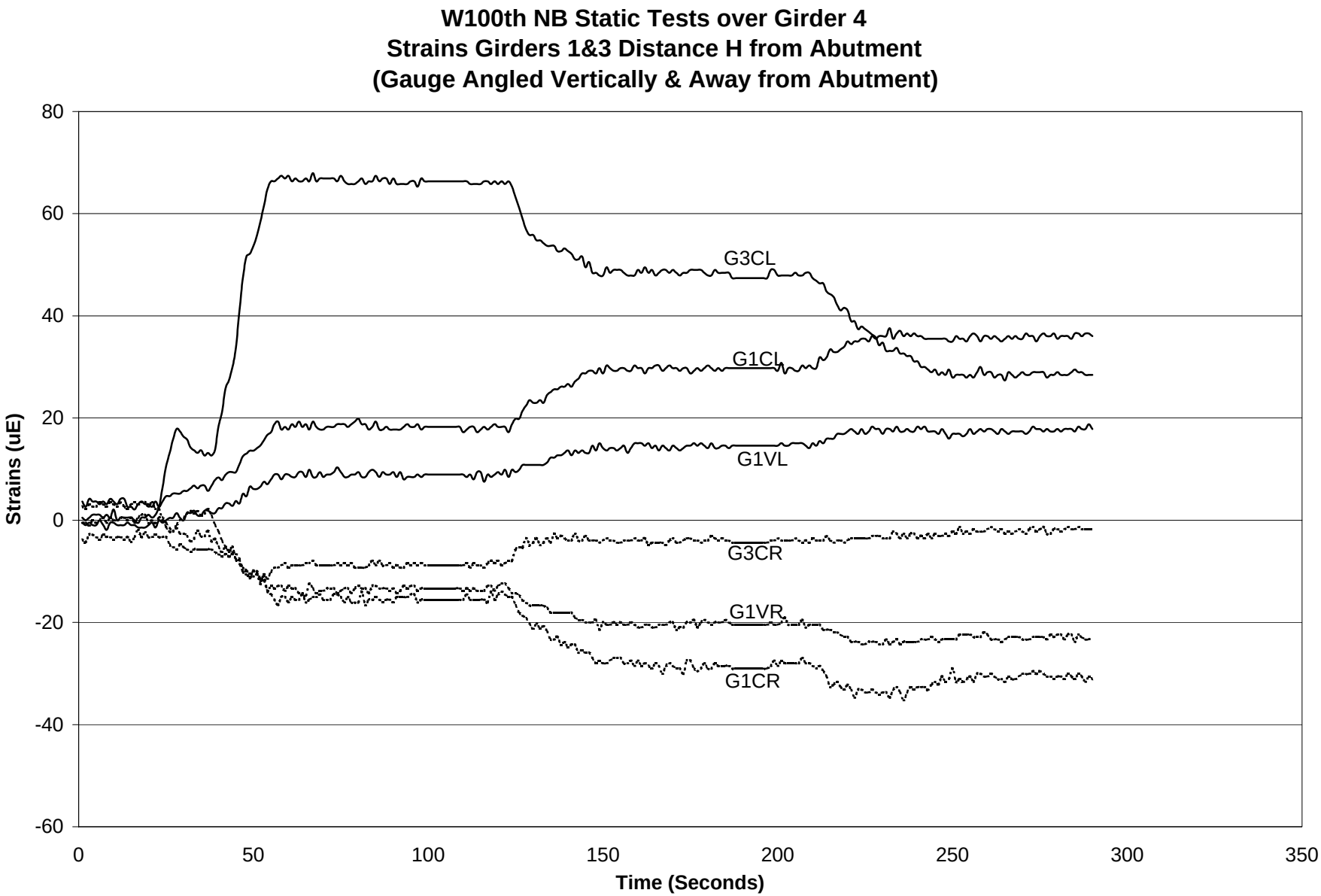
W100th NB Static Tests over Girder 4
Strains Girders 1&3 Distance H from Abutment
(Gauge Angled Vertically & Away from Abutment)
Strains (uE)
Time (Seconds)
80
60
40
20
0
-20
-40
-60
0
50
100
150
200
250
300
350
G3CL
G1CL
G1VL
G3CR
G1VR
G1CR

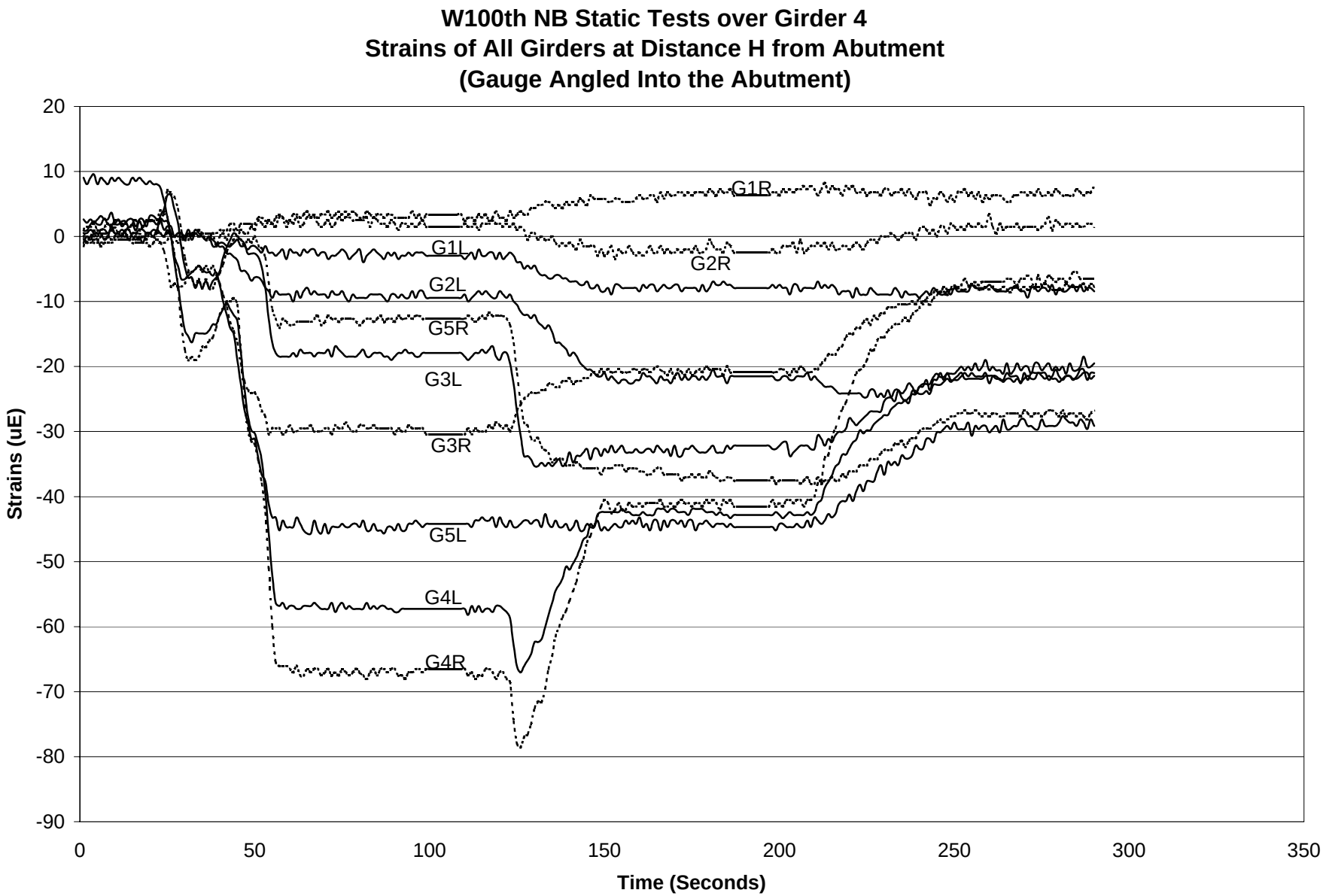
W100th NB Static Tests over Girder 4
Strains of All Girders at Distance H from Abutment
(Gauge Angled Into the Abutment)
Strains (uE)
Time (Seconds)
20
10
0
-10
-20
-30
-40
-50
-60
-70
-80
-90
0
50
100
150
200
250
300
350
G1R
G1L
G2R
G2L
G5R
G3L
G3R
G5L
G4L
G4R

W100th NB Static Tests over Girder 4
Strains in Steel Diaphragms
100
50
0
-50
-100
-150
Strains (uE)
0
50
100
150
200
250
300
350
Time (Seconds)
G2-G3 M
G1-G2 M
G4-G5 M

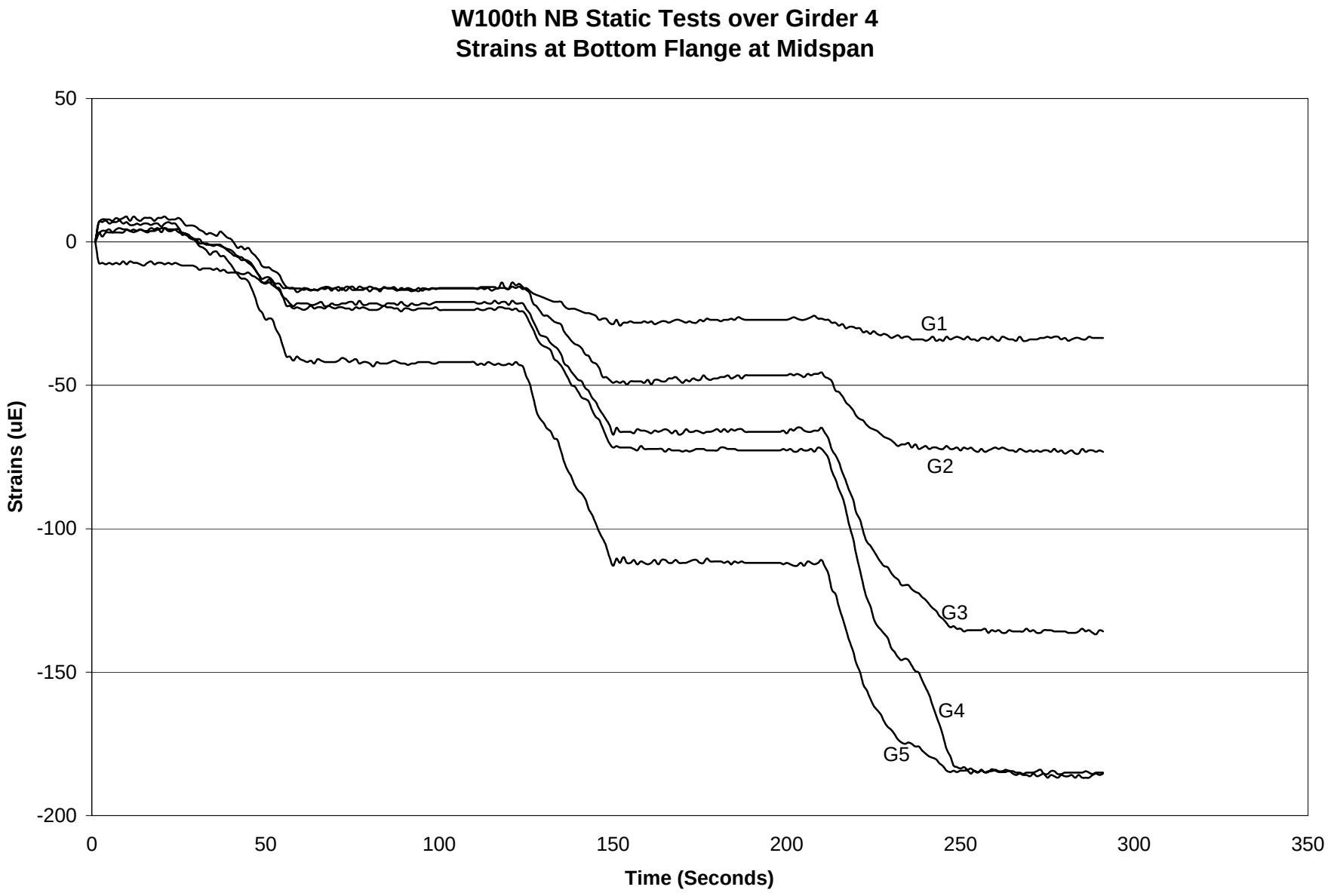
W100th NB Static Tests over Girder 4
Strains at Bottom Flange at Midspan
Strains (uE)
Time (Seconds)
50
0
-50
-100
-150
-200
0
50
100
150
200
250
300
350
G1
G2
G3
G4
G5

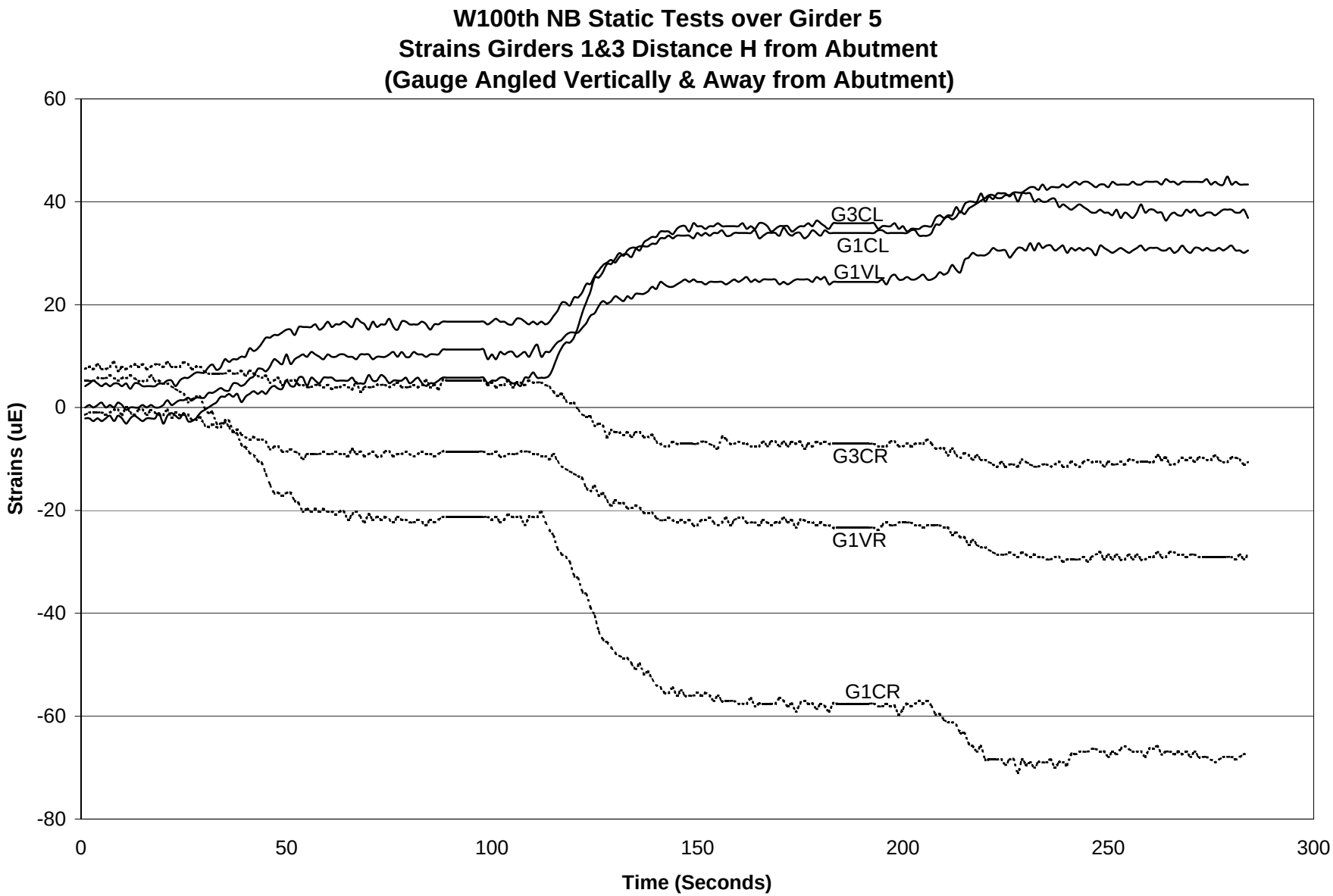
W100th NB Static Tests over Girder 5
Strains Girders 1&3 Distance H from Abutment
(Gauge Angled Vertically & Away from Abutment)
Strains (uE)
Time (Seconds)
60
40
20
0
-20
-40
-60
-80
0
50
100
150
200
250
300
G3CL
G1CL
G1VL
G3CR
G1VR
G1CR

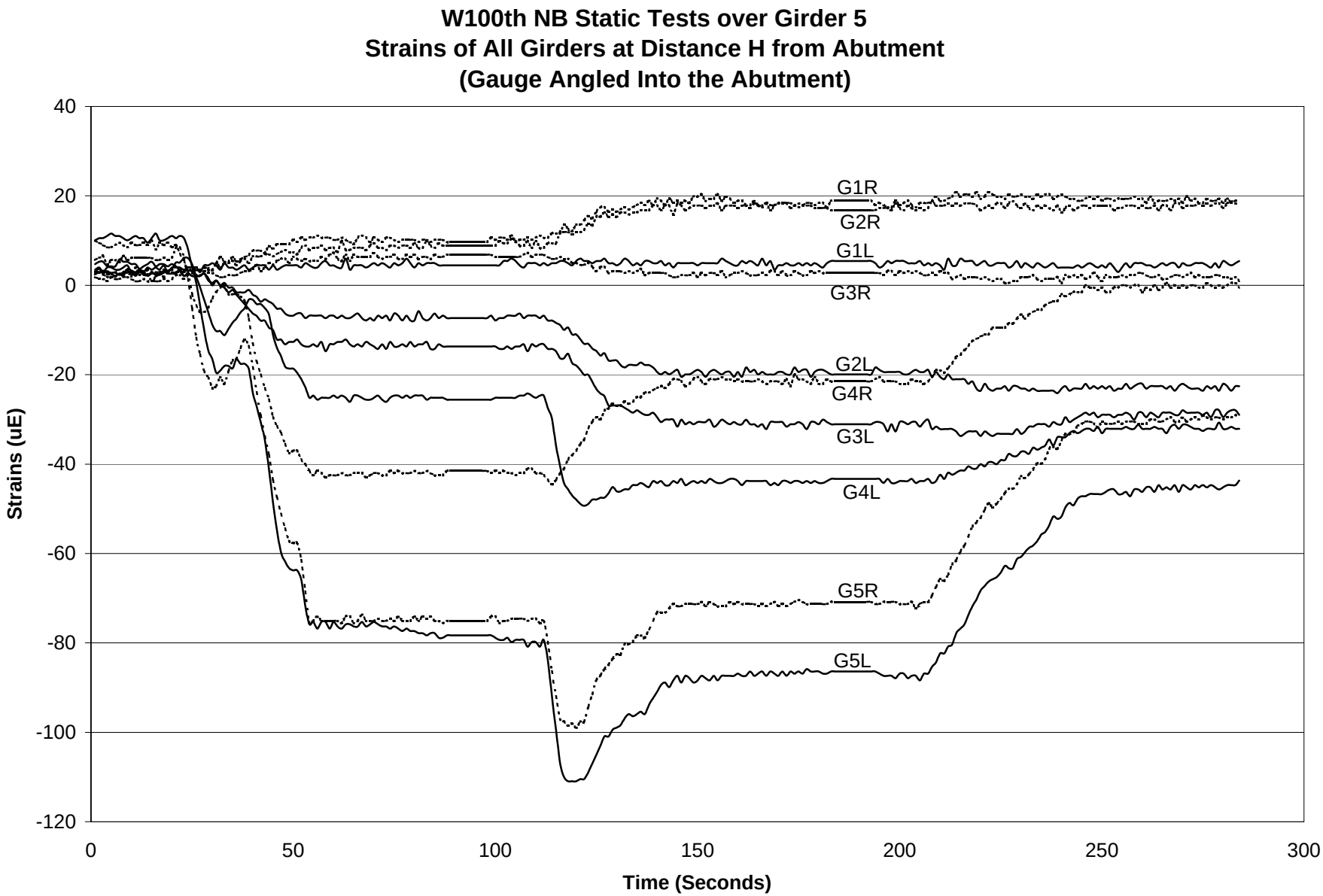
W100th NB Static Tests over Girder 5
Strains of All Girders at Distance H from Abutment
(Gauge Angled Into the Abutment)
Strains (uE)
Time (Seconds)
40
20
0
-20
-40
-60
-80
-100
-120
0
50
100
150
200
250
300
G1R
G2R
G1L
G3R
G2L
G4R
G3L
G4L
G5R
G5L

W100th NB Static Tests over Girder 5
Strains in Steel Diaphragms
Strains (uE)
200
150
100
50
0
-50
-100
0
50
100
150
200
250
300
Time (Seconds)
G2-G3 M
G1-G2 M
G4-G5 M

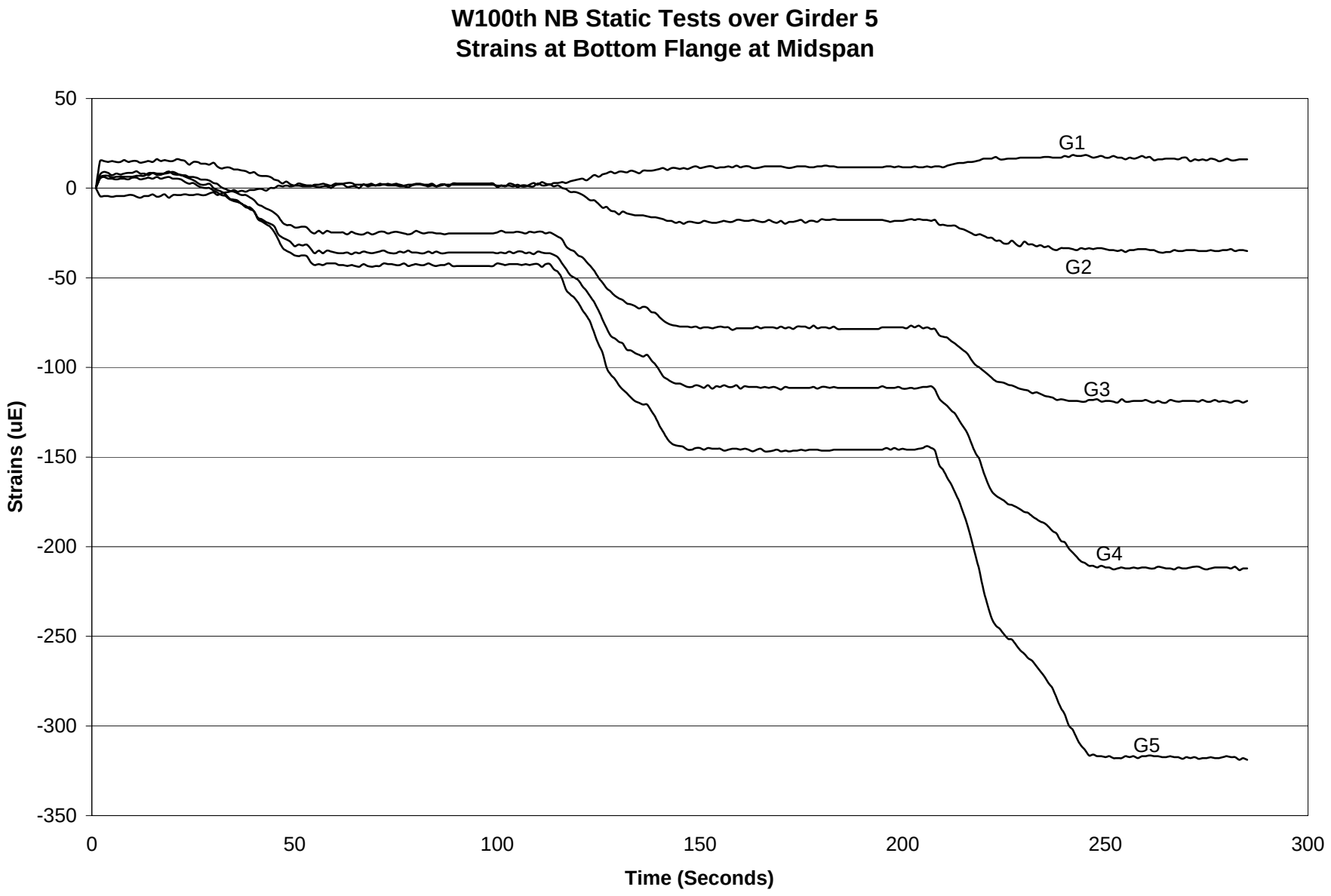
W100th NB Static Tests over Girder 5
Strains at Bottom Flange at Midspan
Strains (uE)
Time (Seconds)
50
0
-50
-100
-150
-200
-250
-300
-350
0
50
100
150
200
250
300
G1
G2
G3
G4
G5

# 100TH SB

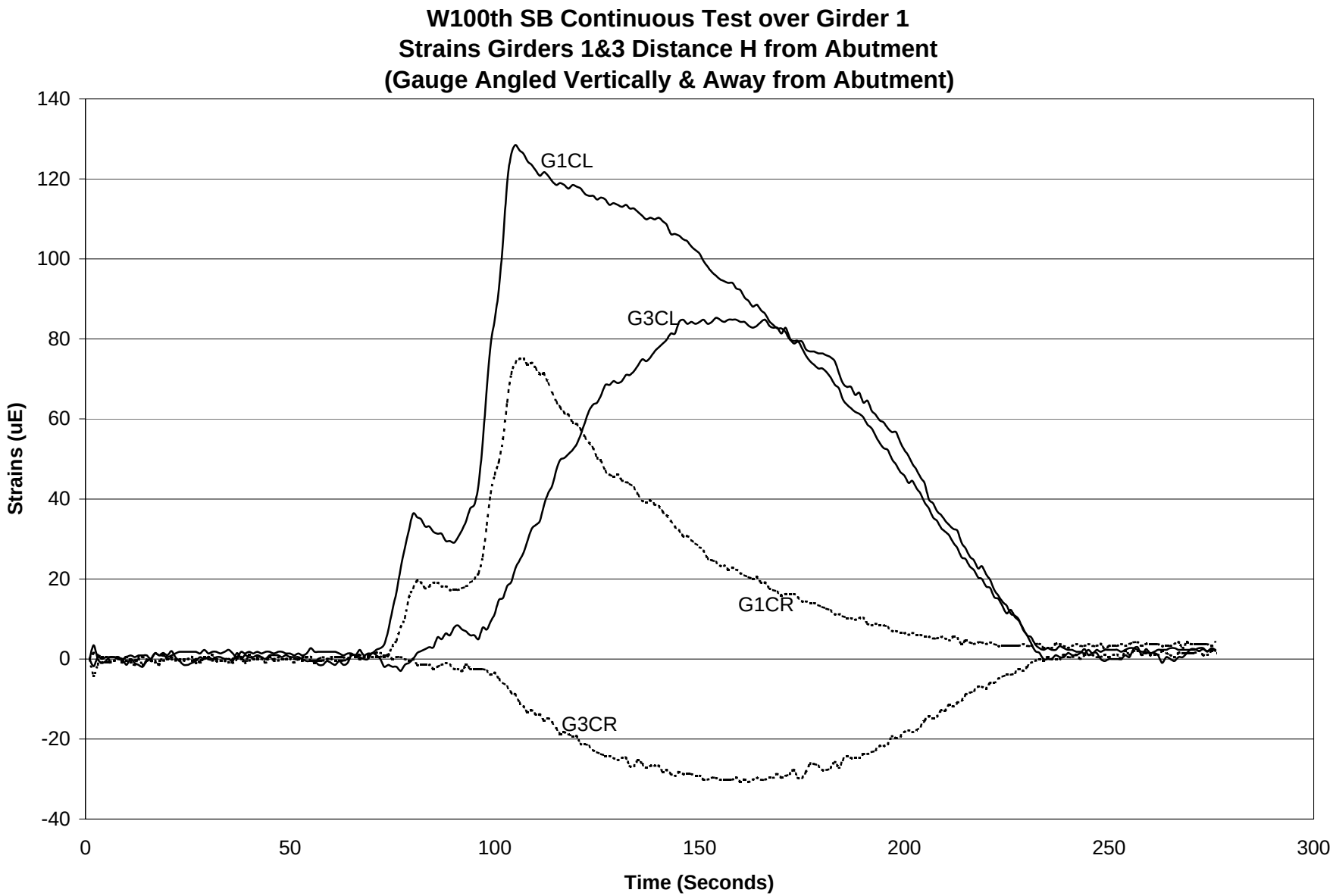
W100th SB Continuous Test over Girder 1
Strains Girders 1&3 Distance H from Abutment
(Gauge Angled Vertically & Away from Abutment)
Strains (uE)
Time (Seconds)
140
120
100
80
60
40
20
0
-20
-40
0
50
100
150
200
250
300
G1CL
G3CL
G1CR
G3CR

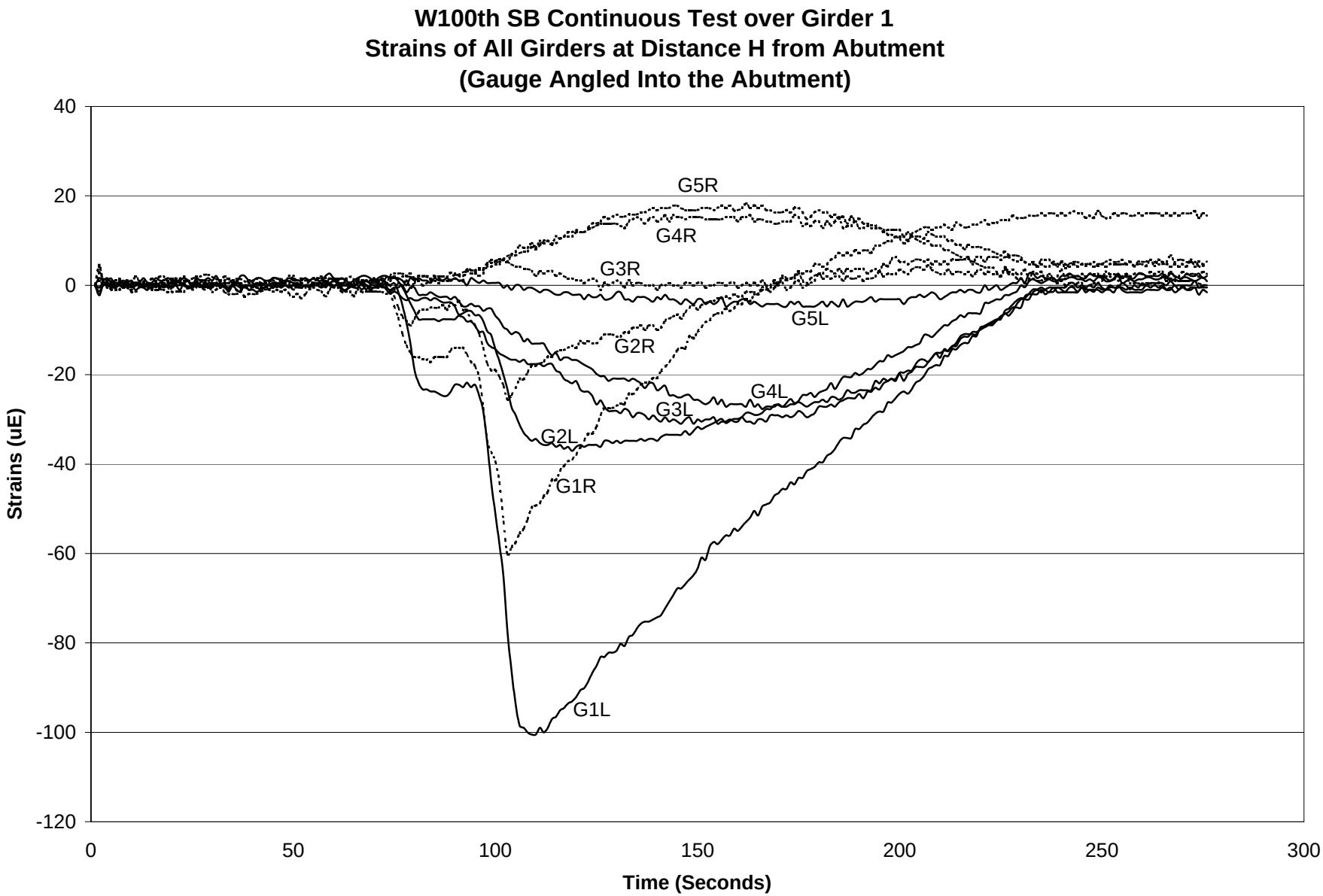
W100th SB Continuous Test over Girder 1
Strains of All Girders at Distance H from Abutment
(Gauge Angled Into the Abutment)
Strains (uE)
Time (Seconds)
40
20
0
-20
-40
-60
-80
-100
-120
0
50
100
150
200
250
300
G5R
G4R
G3R
G5L
G2R
G4L
G3L
G2L
G1R
G1L

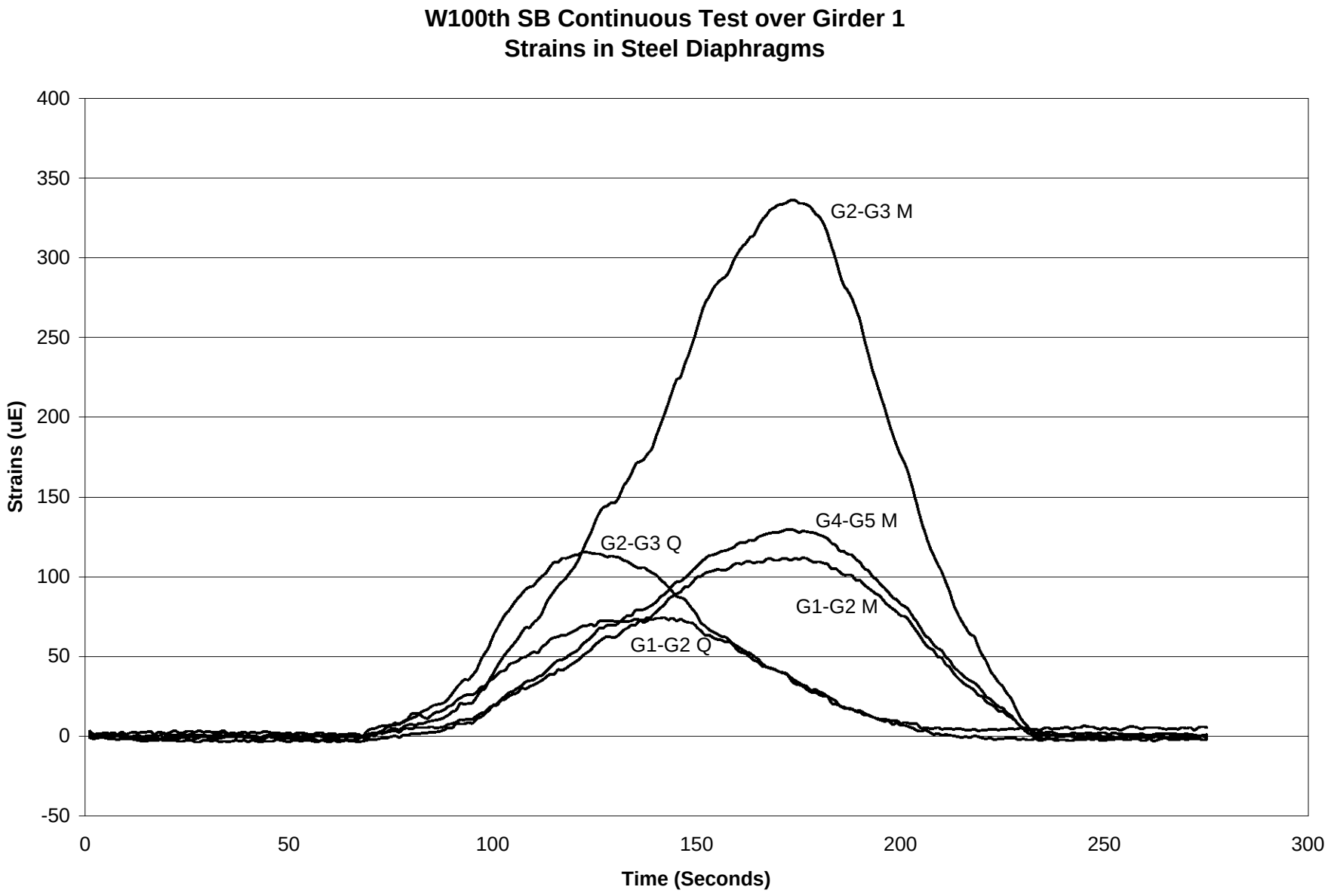
W100th SB Continuous Test over Girder 1
Strains in Steel Diaphragms
Strains (uE)
Time (Seconds)
400
350
300
250
200
150
100
50
0
-50
0
50
100
150
200
250
300
G2-G3 M
G4-G5 M
G2-G3 Q
G1-G2 M
G1-G2 Q

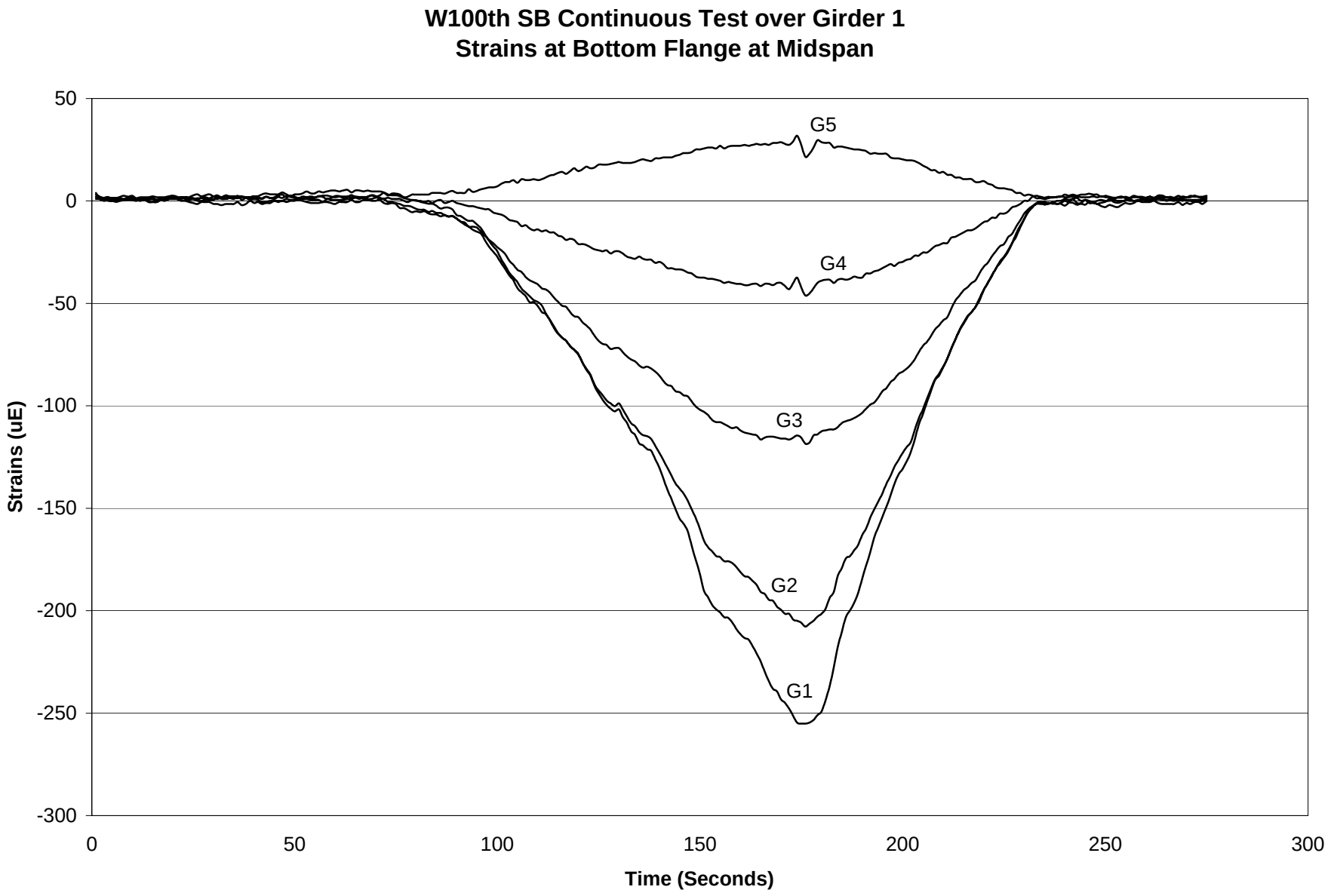
W100th SB Continuous Test over Girder 1
Strains at Bottom Flange at Midspan
Strains (uE)
Time (Seconds)
50
0
-50
-100
-150
-200
-250
-300
0
50
100
150
200
250
300
G5
G4
G3
G2
G1

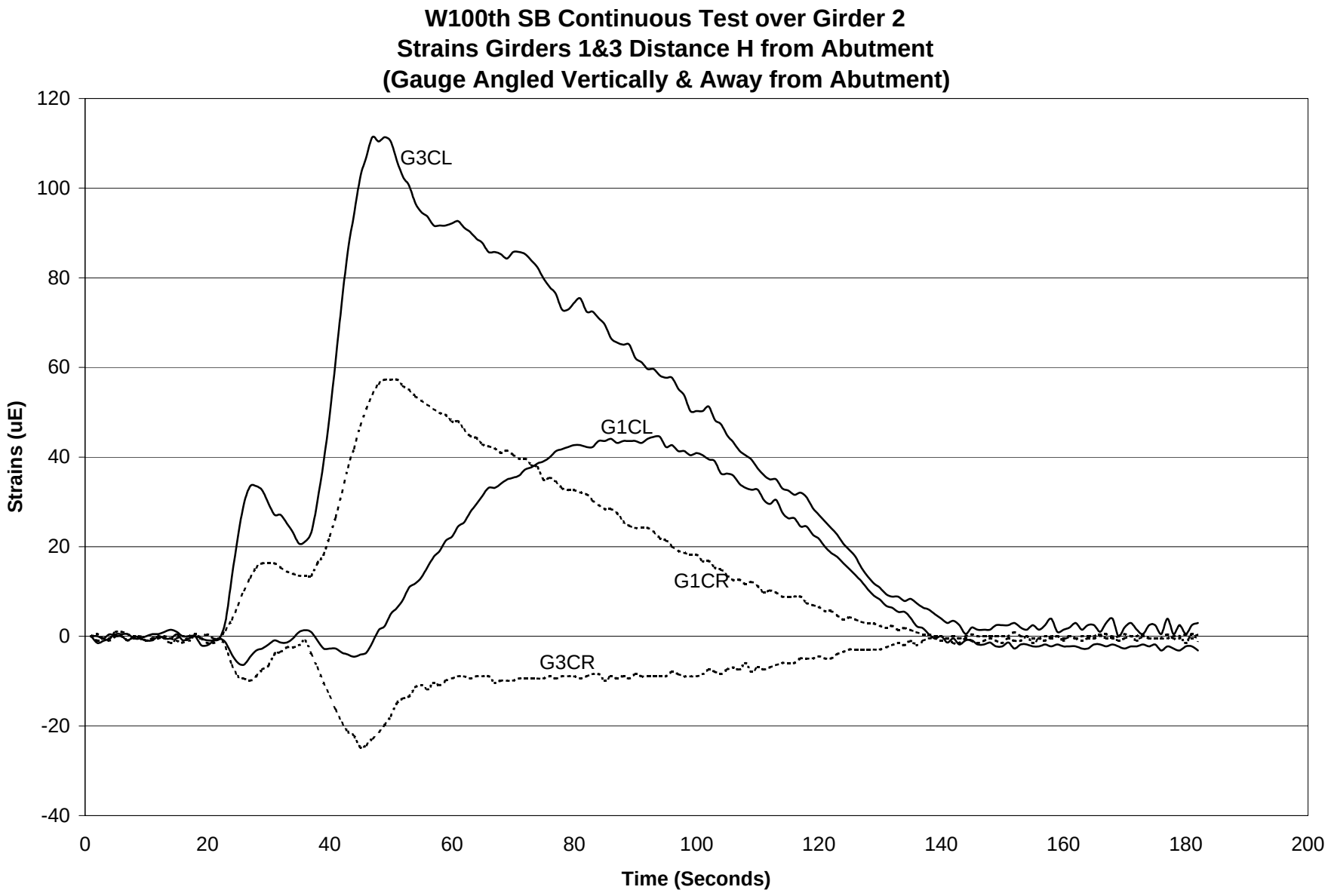
W100th SB Continuous Test over Girder 2
Strains Girders 1&3 Distance H from Abutment
(Gauge Angled Vertically & Away from Abutment)
Strains (uE)
Time (Seconds)
120
100
80
60
40
20
0
-20
-40
0
20
40
60
80
100
120
140
160
180
200
G3CL
G1CL
G1CR
G3CR

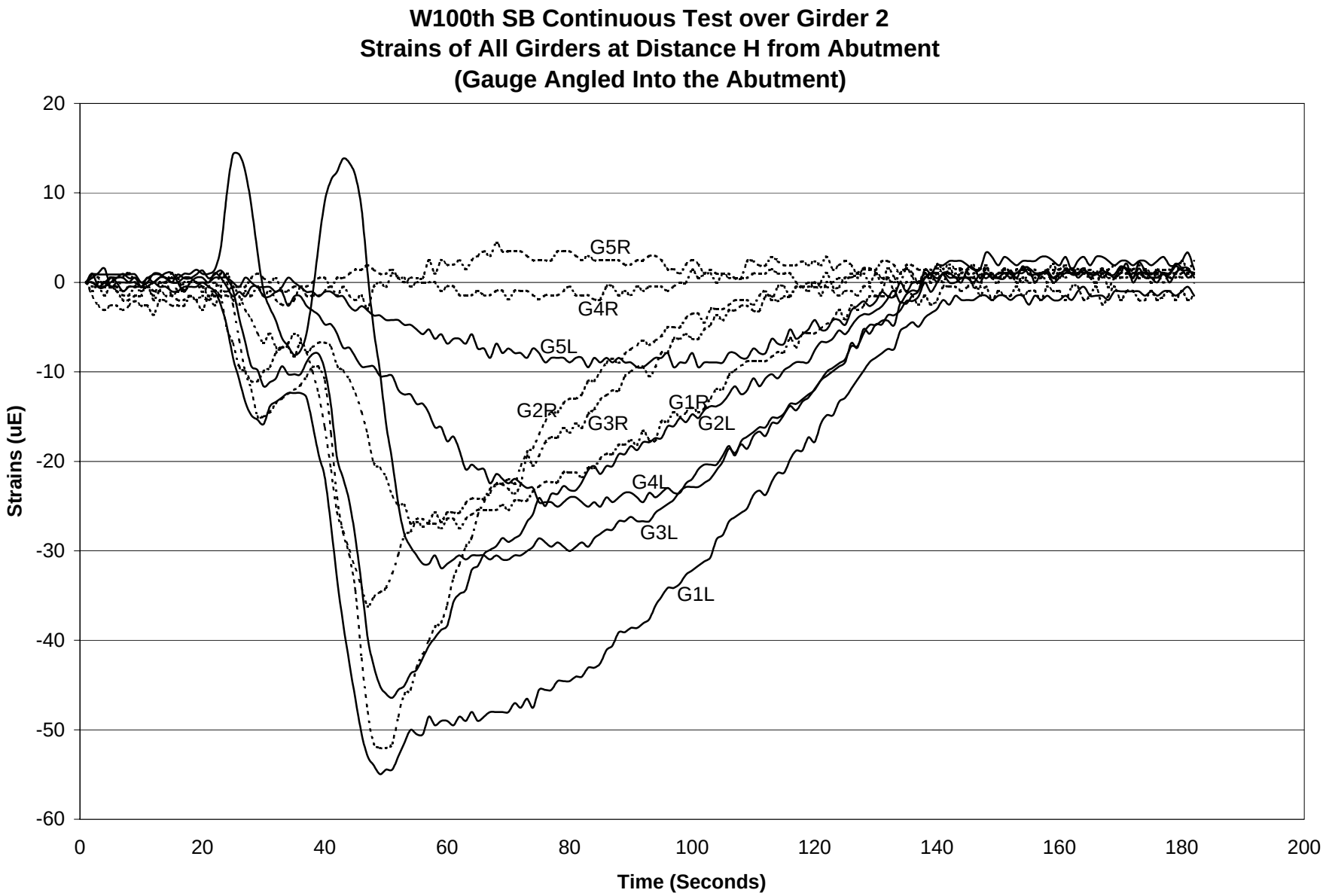
W100th SB Continuous Test over Girder 2
Strains of All Girders at Distance H from Abutment
(Gauge Angled Into the Abutment)
Strains (uE)
Time (Seconds)
20
10
0
-10
-20
-30
-40
-50
-60
0
20
40
60
80
100
120
140
160
180
200
G5R
G4R
G5L
G2R
G3R
G1R
G2L
G4L
G3L
G1L

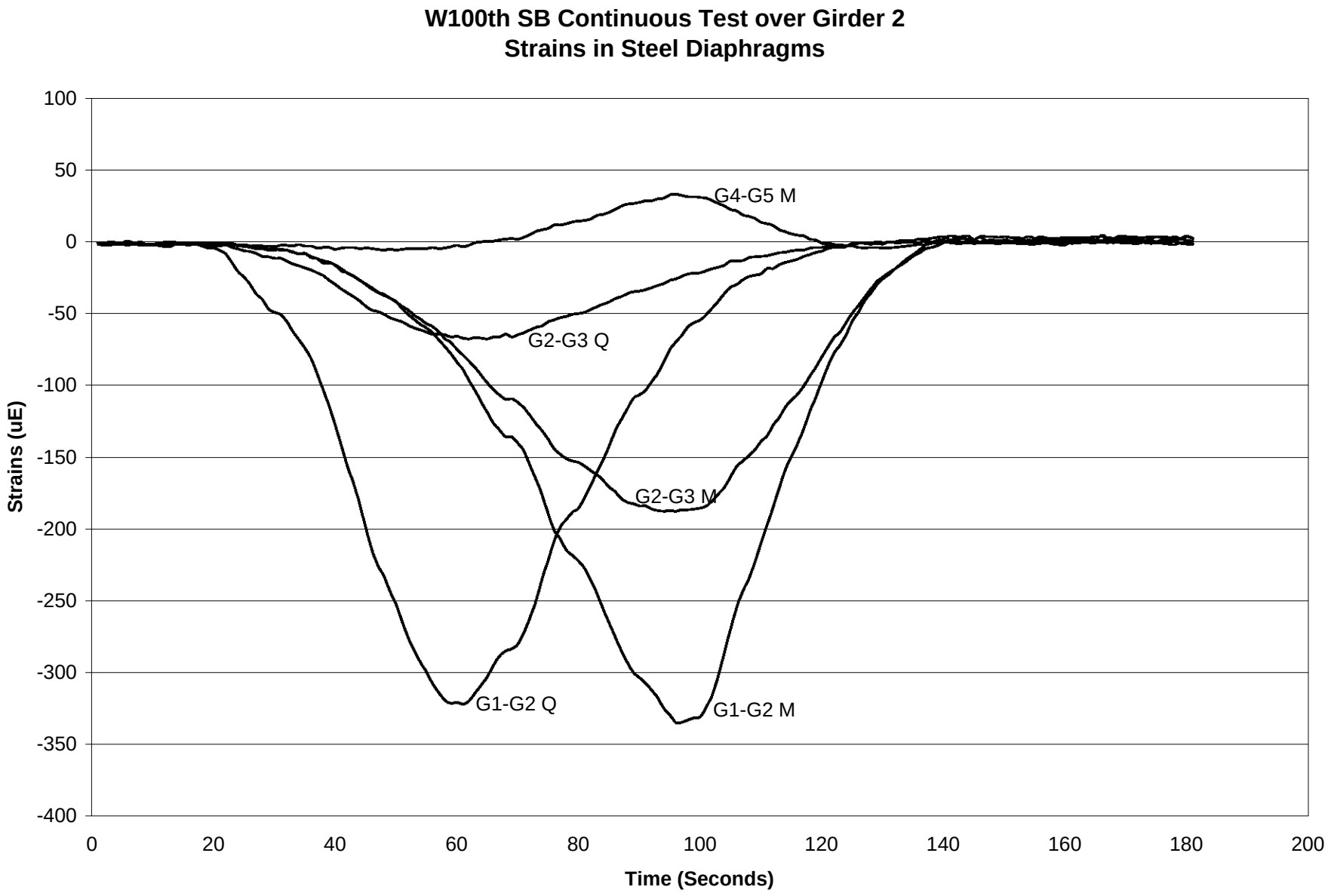
W100th SB Continuous Test over Girder 2
Strains in Steel Diaphragms
Strains (uE)
Time (Seconds)
100
50
0
-50
-100
-150
-200
-250
-300
-350
-400
0
20
40
60
80
100
120
140
160
180
200
G4-G5 M
G2-G3 Q
G2-G3 M
G1-G2 Q
G1-G2 M

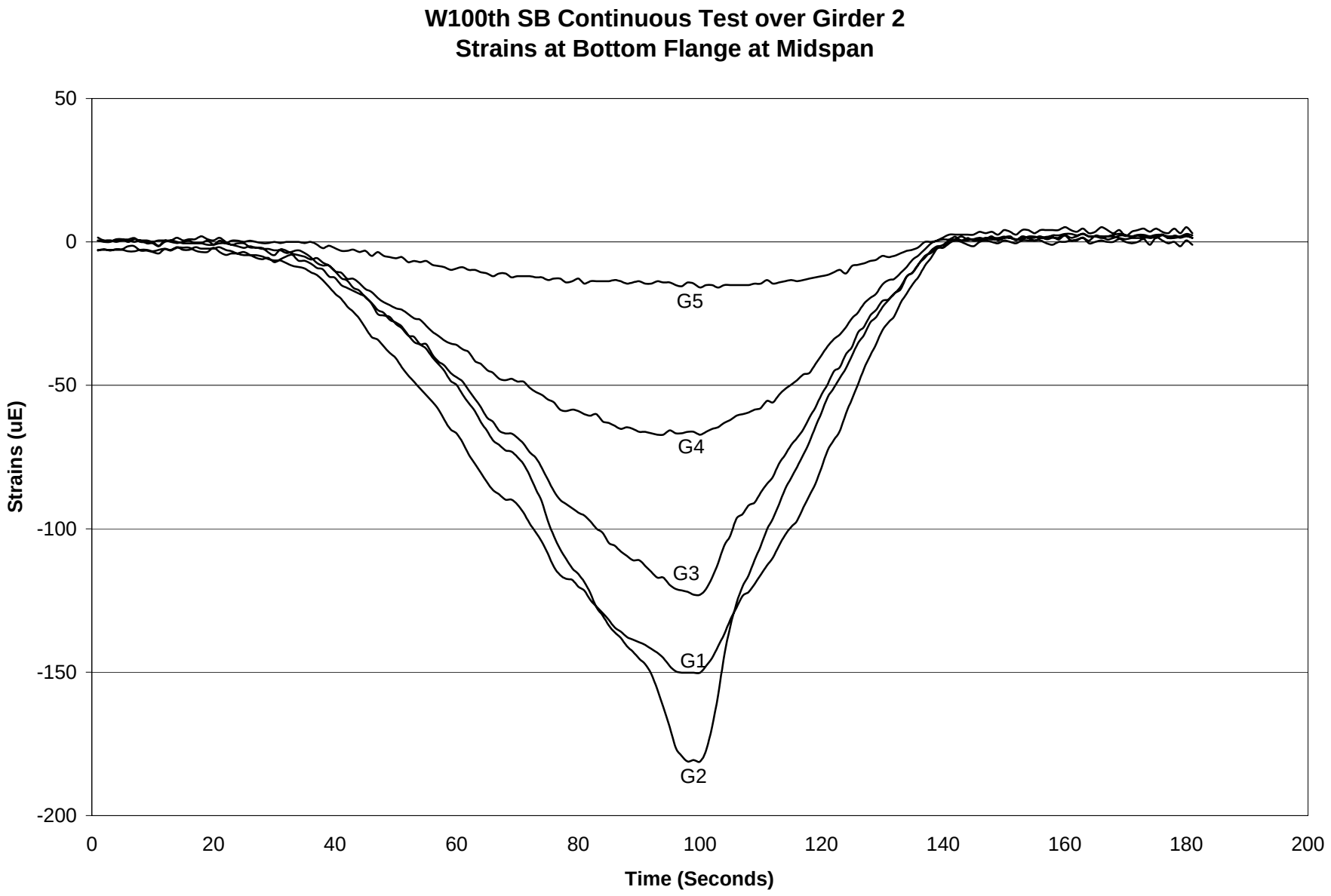
W100th SB Continuous Test over Girder 2
Strains at Bottom Flange at Midspan
Strains (uE)
Time (Seconds)
50
0
-50
-100
-150
-200
0
20
40
60
80
100
120
140
160
180
200
G5
G4
G3
G1
G2

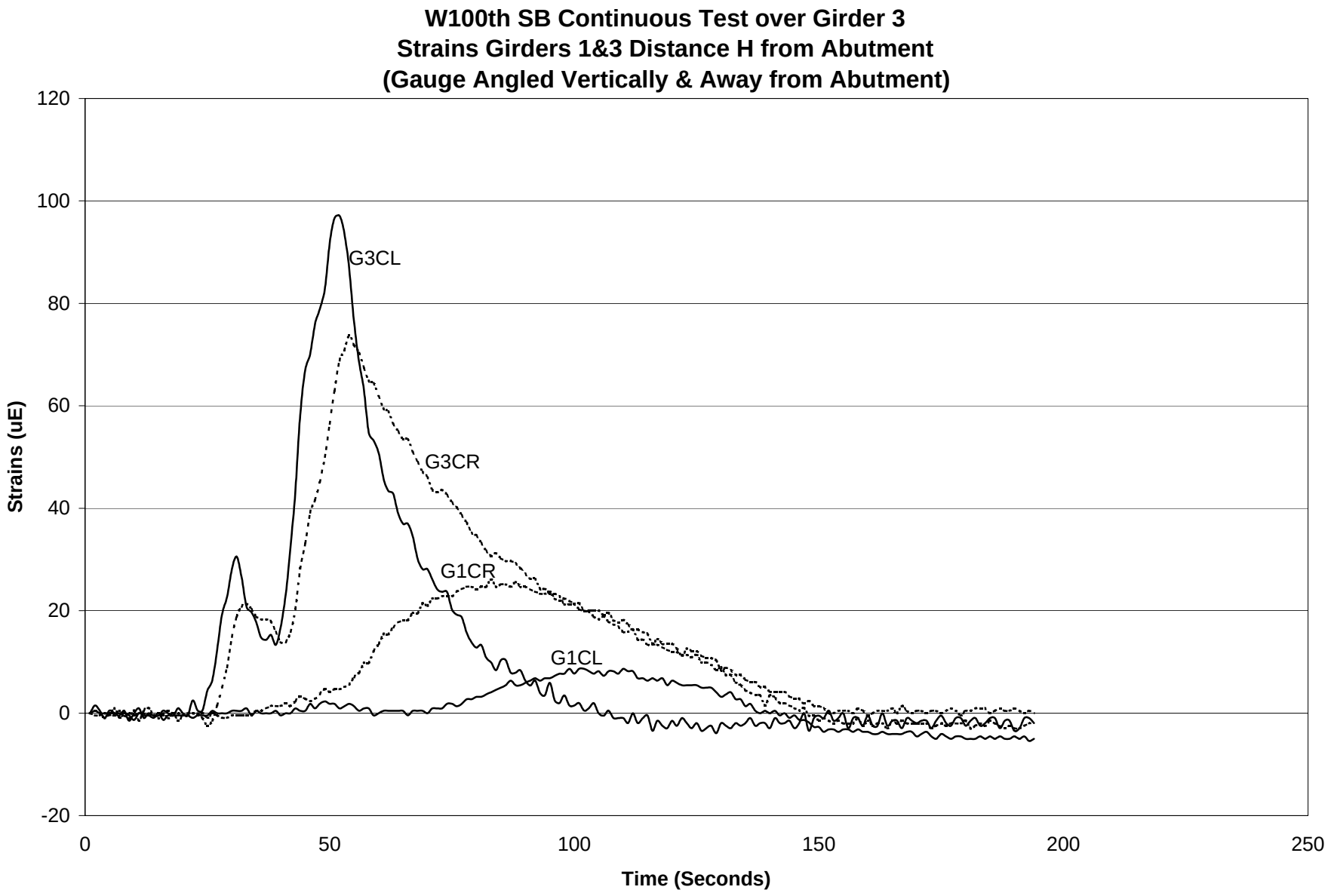
W100th SB Continuous Test over Girder 3
Strains Girders 1&3 Distance H from Abutment
(Gauge Angled Vertically & Away from Abutment)
Strains (uE)
Time (Seconds)
120
100
80
60
40
20
0
-20
0
50
100
150
200
250
G3CL
G3CR
G1CR
G1CL

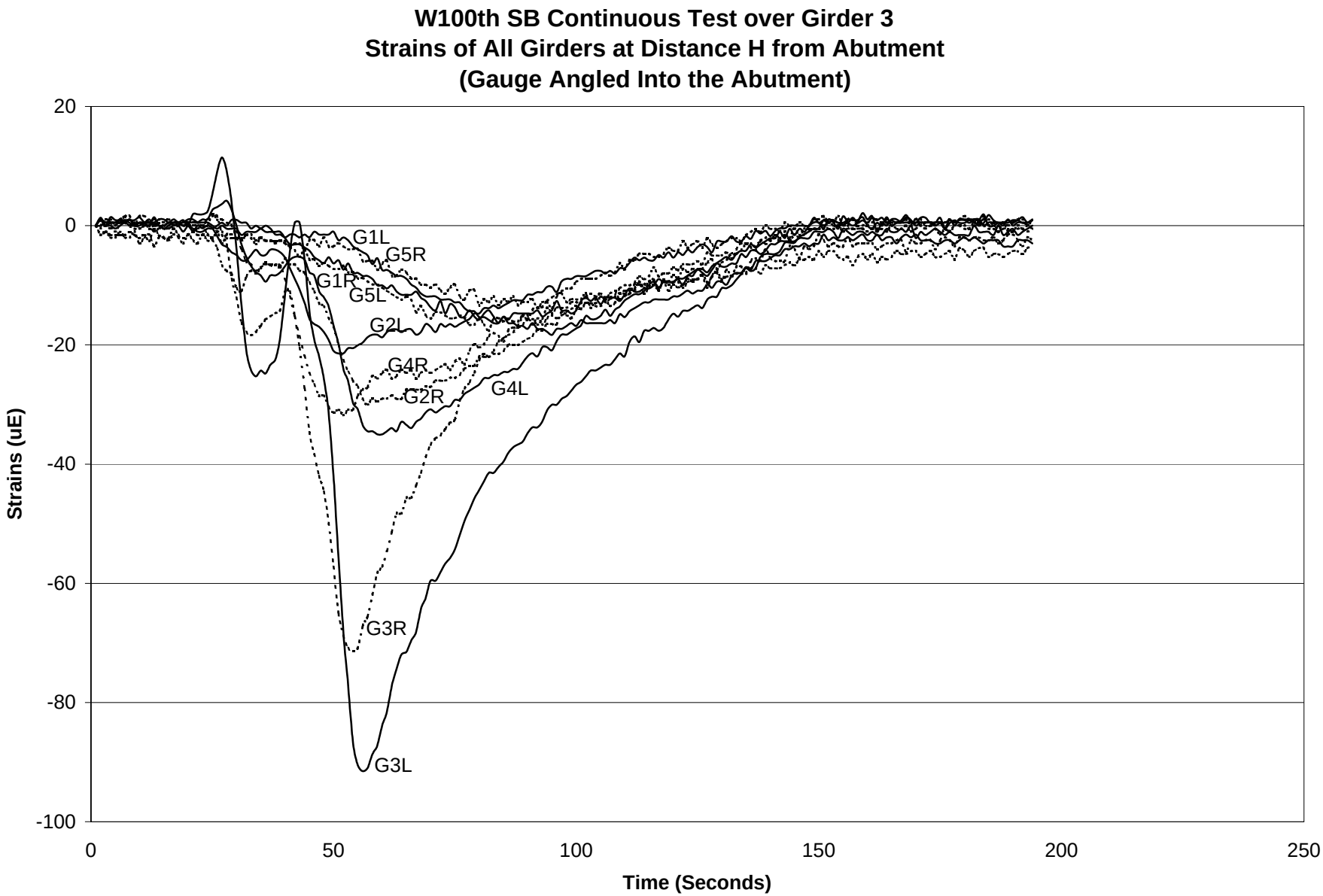
W100th SB Continuous Test over Girder 3
Strains of All Girders at Distance H from Abutment
(Gauge Angled Into the Abutment)
Strains (uE)
Time (Seconds)
20
0
-20
-40
-60
-80
-100
0
50
100
150
200
250
G1L
G5R
G1R
G5L
G2L
G4R
G2R
G4L
G3R
G3L

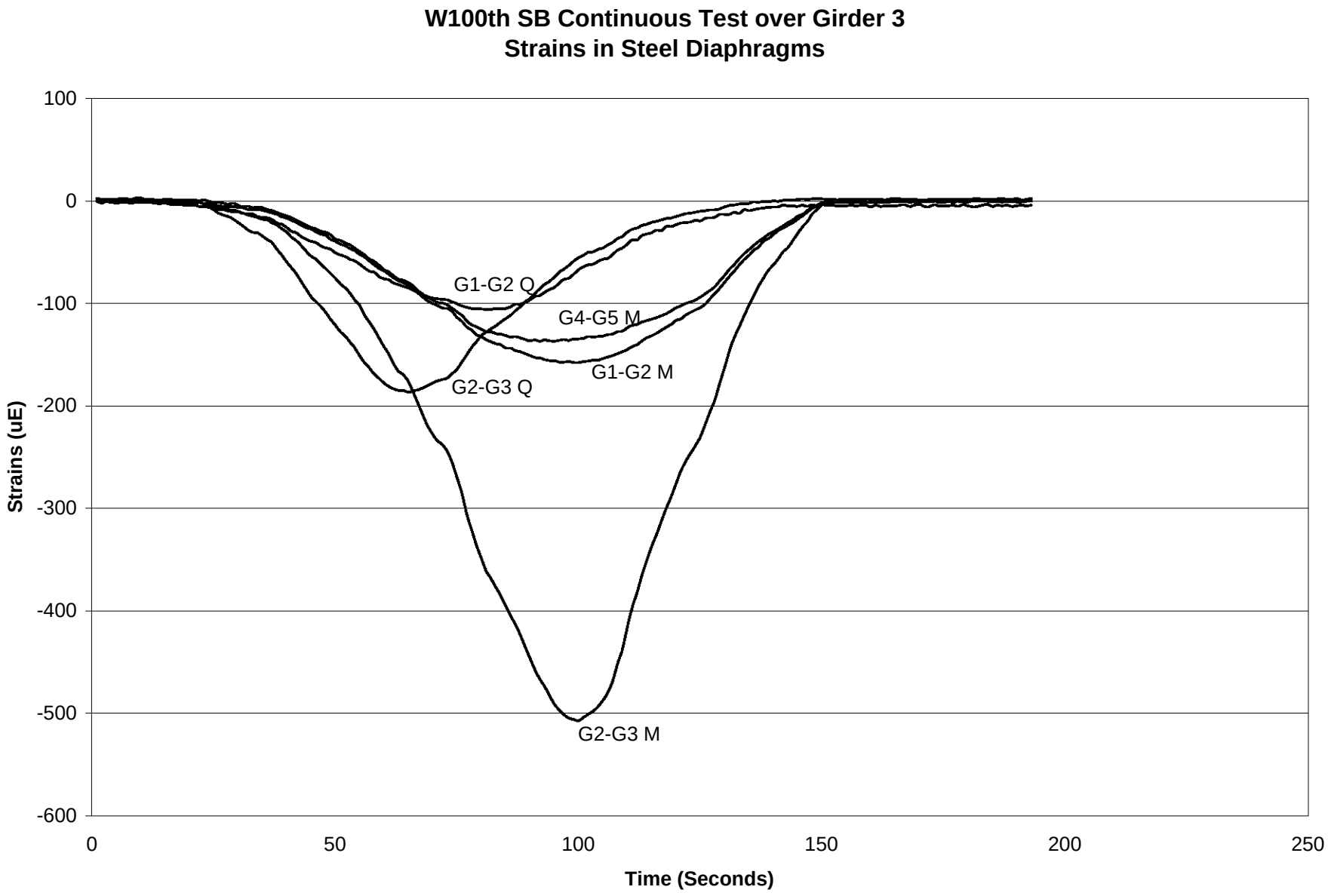
W100th SB Continuous Test over Girder 3
Strains in Steel Diaphragms
100
0
-100
-200
-300
-400
-500
-600
Strains (uE)
0
50
100
150
200
250
Time (Seconds)
G1-G2 Q
G4-G5 M
G1-G2 M
G2-G3 Q
G2-G3 M

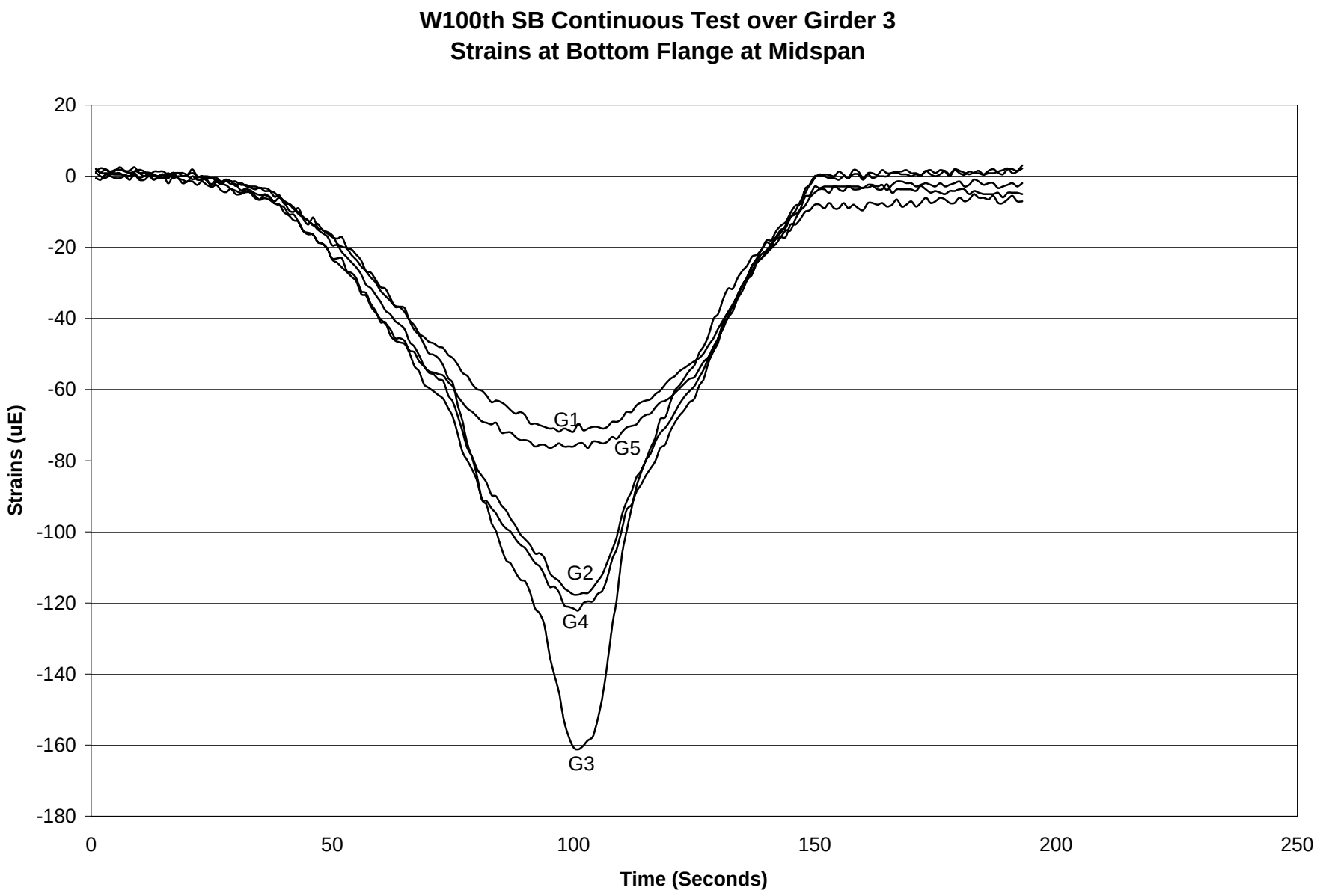
W100th SB Continuous Test over Girder 3
Strains at Bottom Flange at Midspan
Strains (uE)
Time (Seconds)
20
0
-20
-40
-60
-80
-100
-120
-140
-160
-180
0
50
100
150
200
250
G1
G5
G2
G4
G3

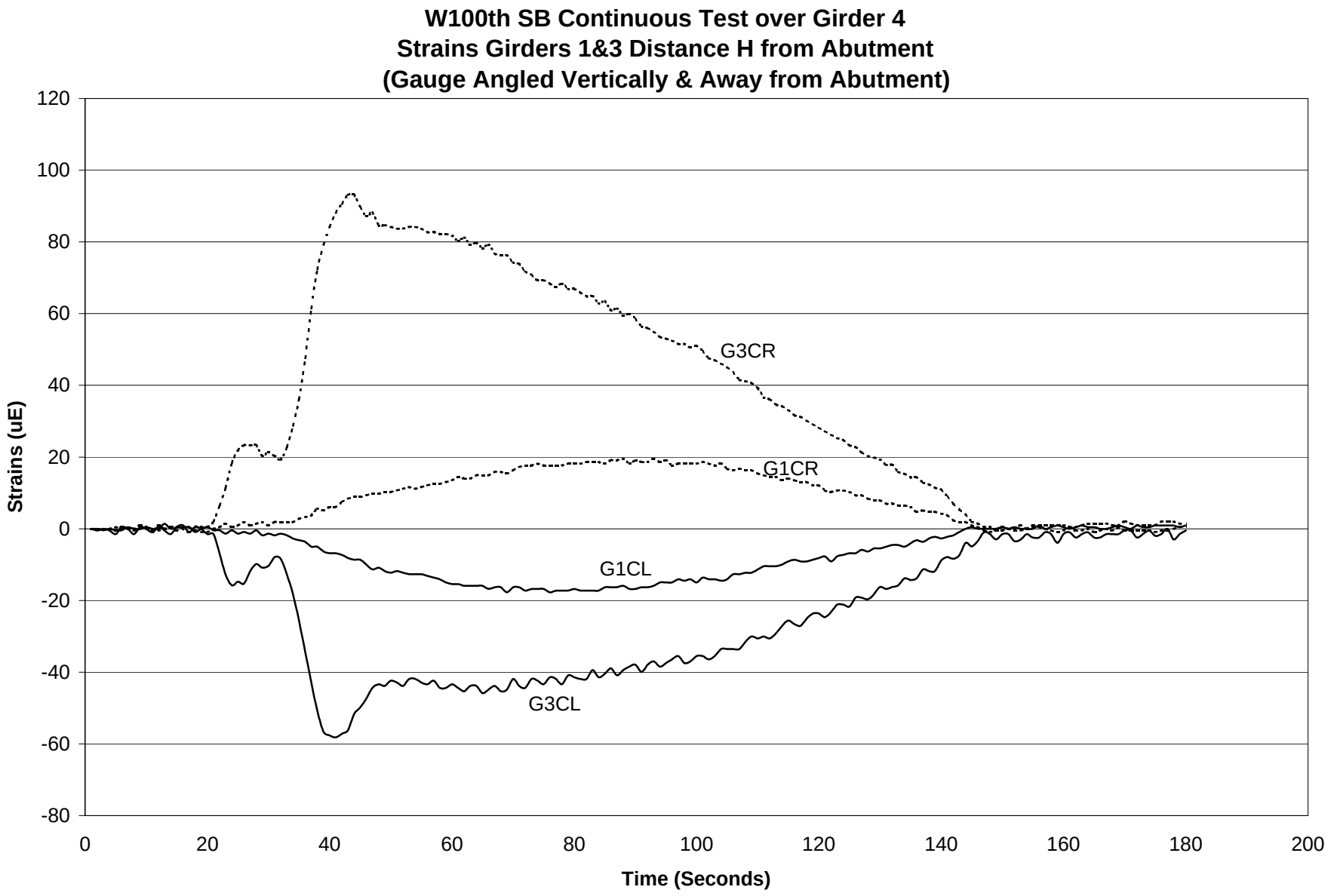
W100th SB Continuous Test over Girder 4
Strains Girders 1&3 Distance H from Abutment
(Gauge Angled Vertically & Away from Abutment)
Strains (uE)
Time (Seconds)
120
100
80
60
40
20
0
-20
-40
-60
-80
0
20
40
60
80
100
120
140
160
180
200
G3CR
G1CR
G1CL
G3CL

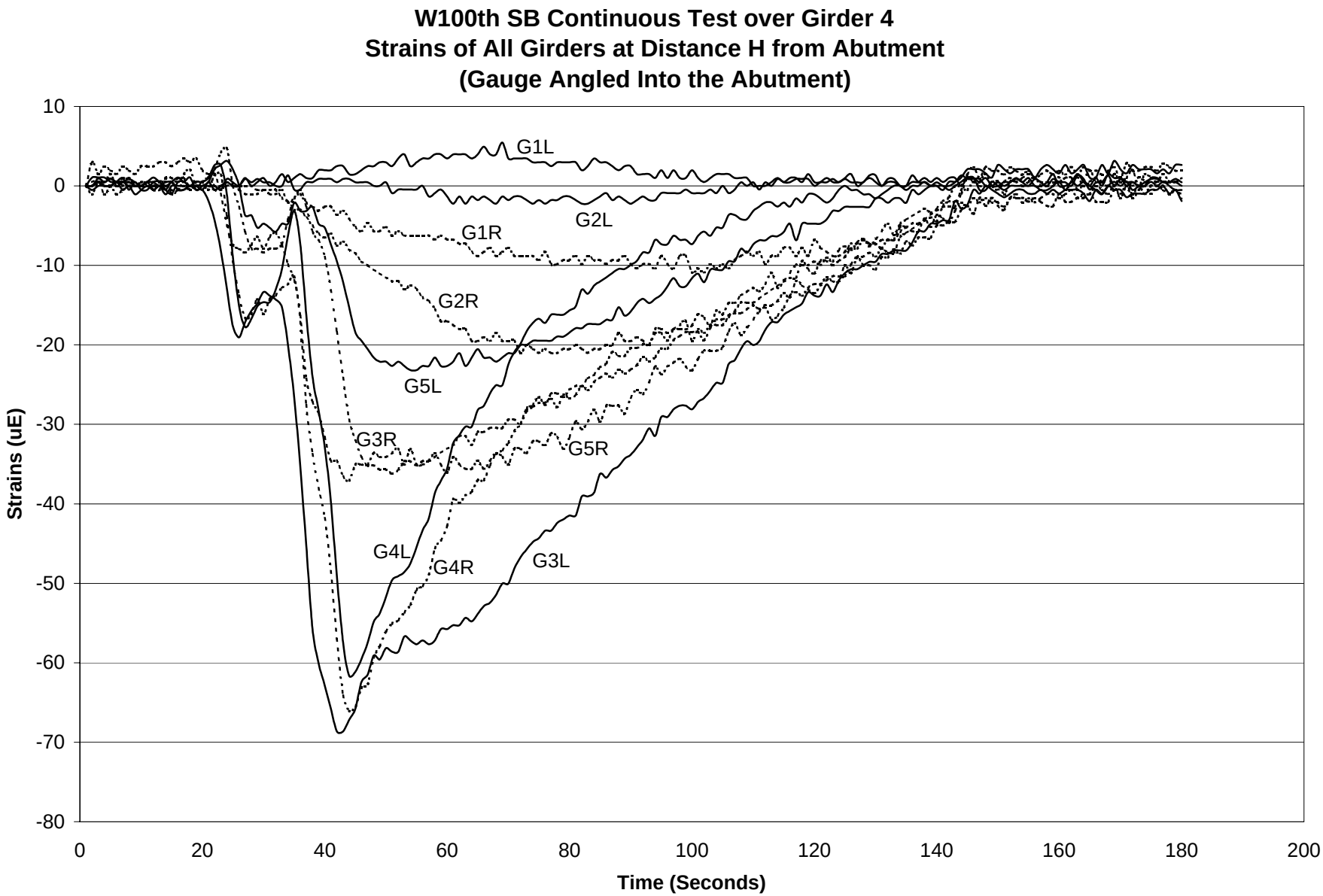
W100th SB Continuous Test over Girder 4
Strains of All Girders at Distance H from Abutment
(Gauge Angled Into the Abutment)
Strains (uE)
Time (Seconds)
10
0
-10
-20
-30
-40
-50
-60
-70
-80
0
20
40
60
80
100
120
140
160
180
200
G1L
G2L
G1R
G2R
G5L
G3R
G5R
G4L
G4R
G3L

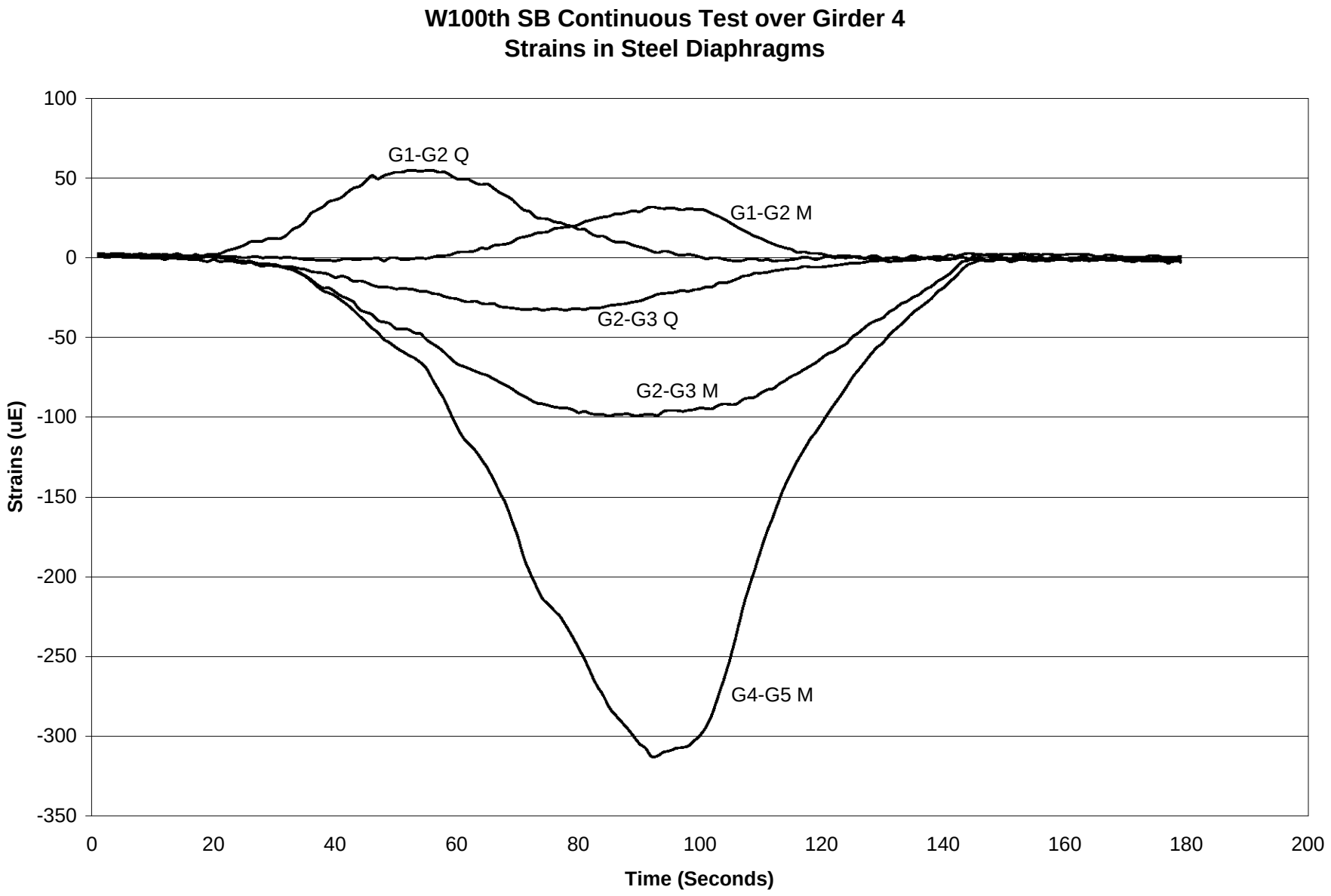
W100th SB Continuous Test over Girder 4
Strains in Steel Diaphragms
G1-G2 Q
G1-G2 M
G2-G3 Q
G2-G3 M
G4-G5 M
Strains (uE)
Time (Seconds)
100
50
0
-50
-100
-150
-200
-250
-300
-350
0
20
40
60
80
100
120
140
160
180
200

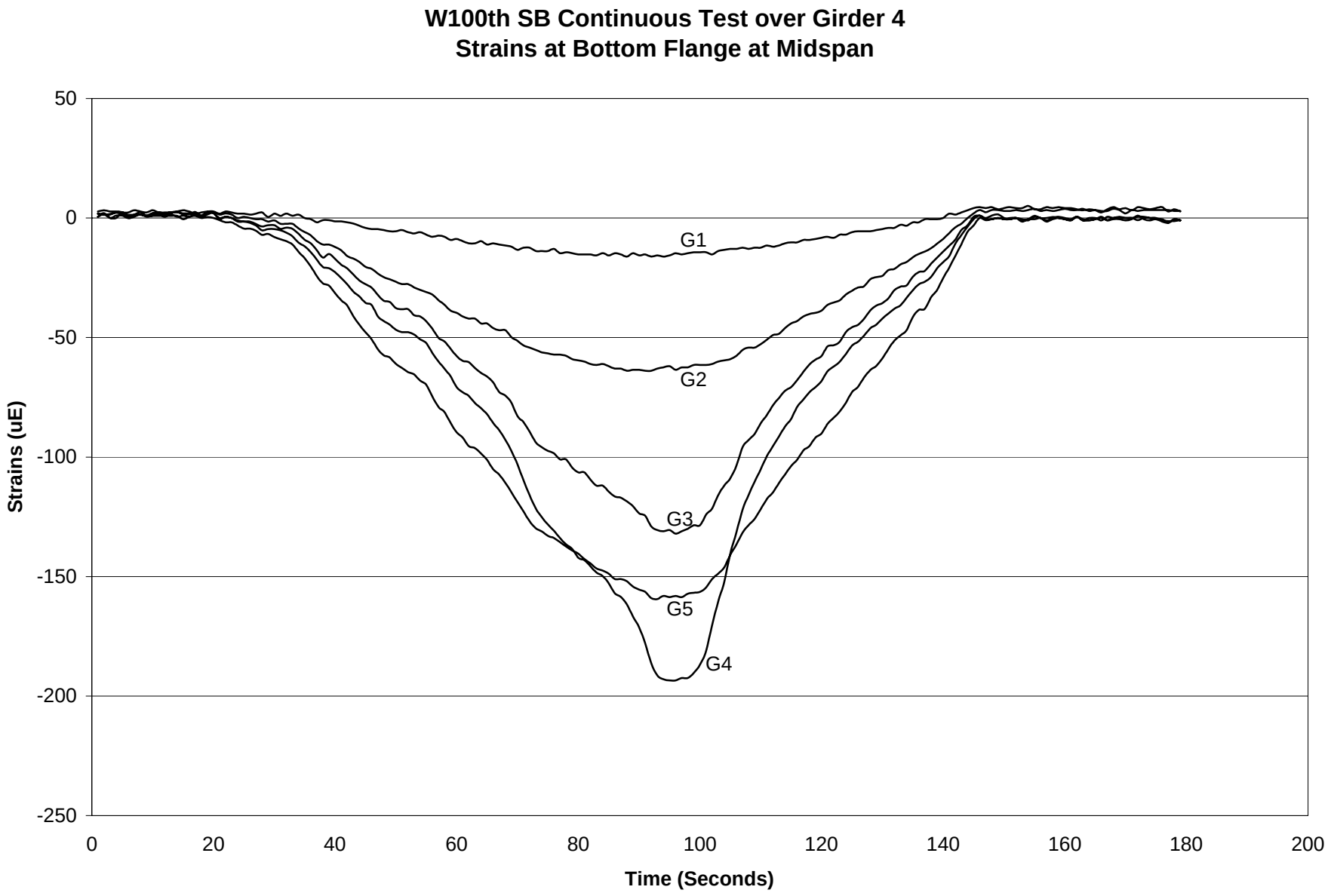
W100th SB Continuous Test over Girder 4
Strains at Bottom Flange at Midspan
Strains (uE)
Time (Seconds)
50
0
-50
-100
-150
-200
-250
0
20
40
60
80
100
120
140
160
180
200
G1
G2
G3
G5
G4

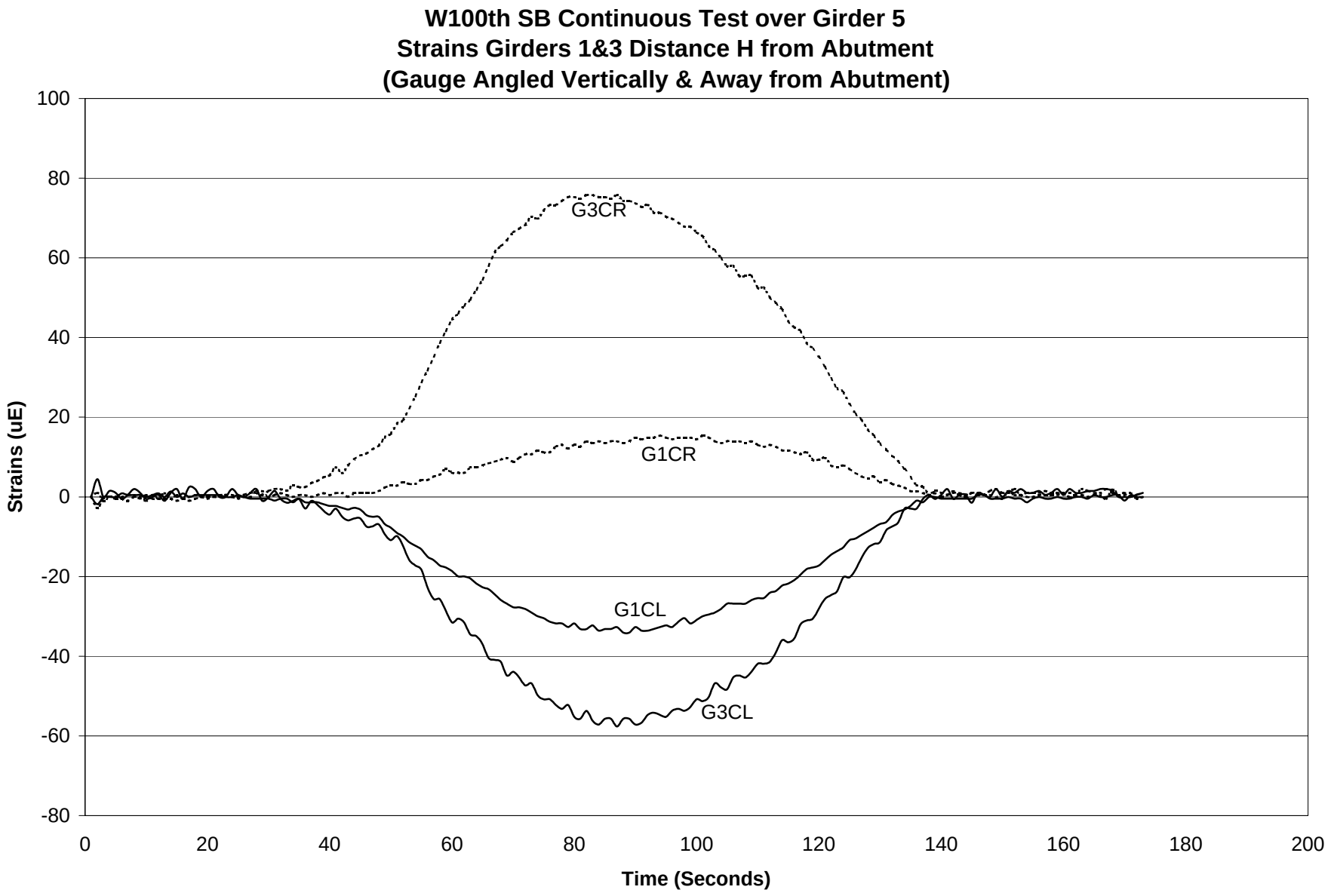
W100th SB Continuous Test over Girder 5
Strains Girders 1&3 Distance H from Abutment
(Gauge Angled Vertically & Away from Abutment)
Strains (uE)
Time (Seconds)
100
80
60
40
20
0
-20
-40
-60
-80
0
20
40
60
80
100
120
140
160
180
200
G3CR
G1CR
G1CL
G3CL

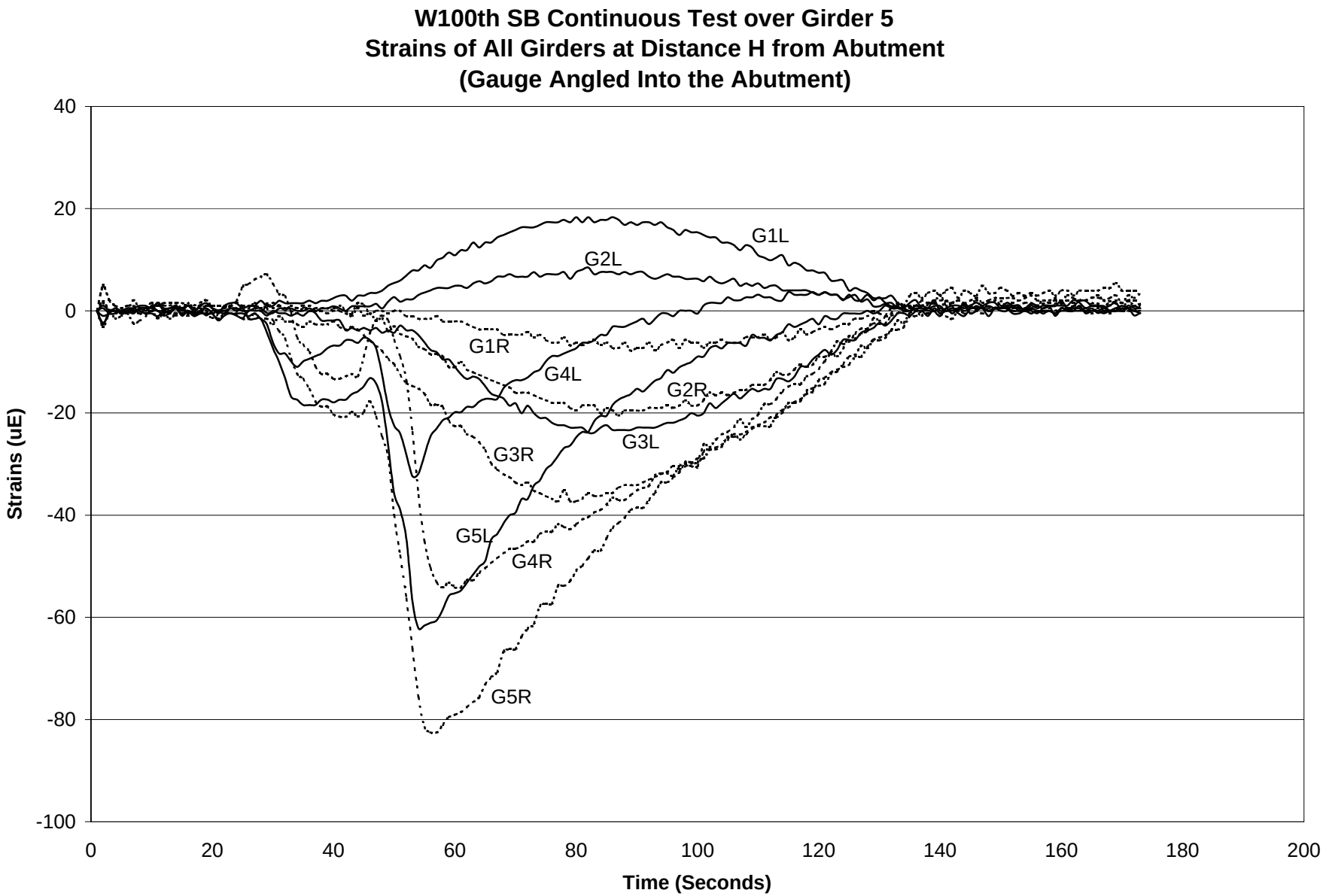
W100th SB Continuous Test over Girder 5
Strains of All Girders at Distance H from Abutment
(Gauge Angled Into the Abutment)
Strains (uE)
Time (Seconds)
40
20
0
-20
-40
-60
-80
-100
0
20
40
60
80
100
120
140
160
180
200
G1L
G2L
G1R
G4L
G2R
G3L
G3R
G5L
G4R
G5R

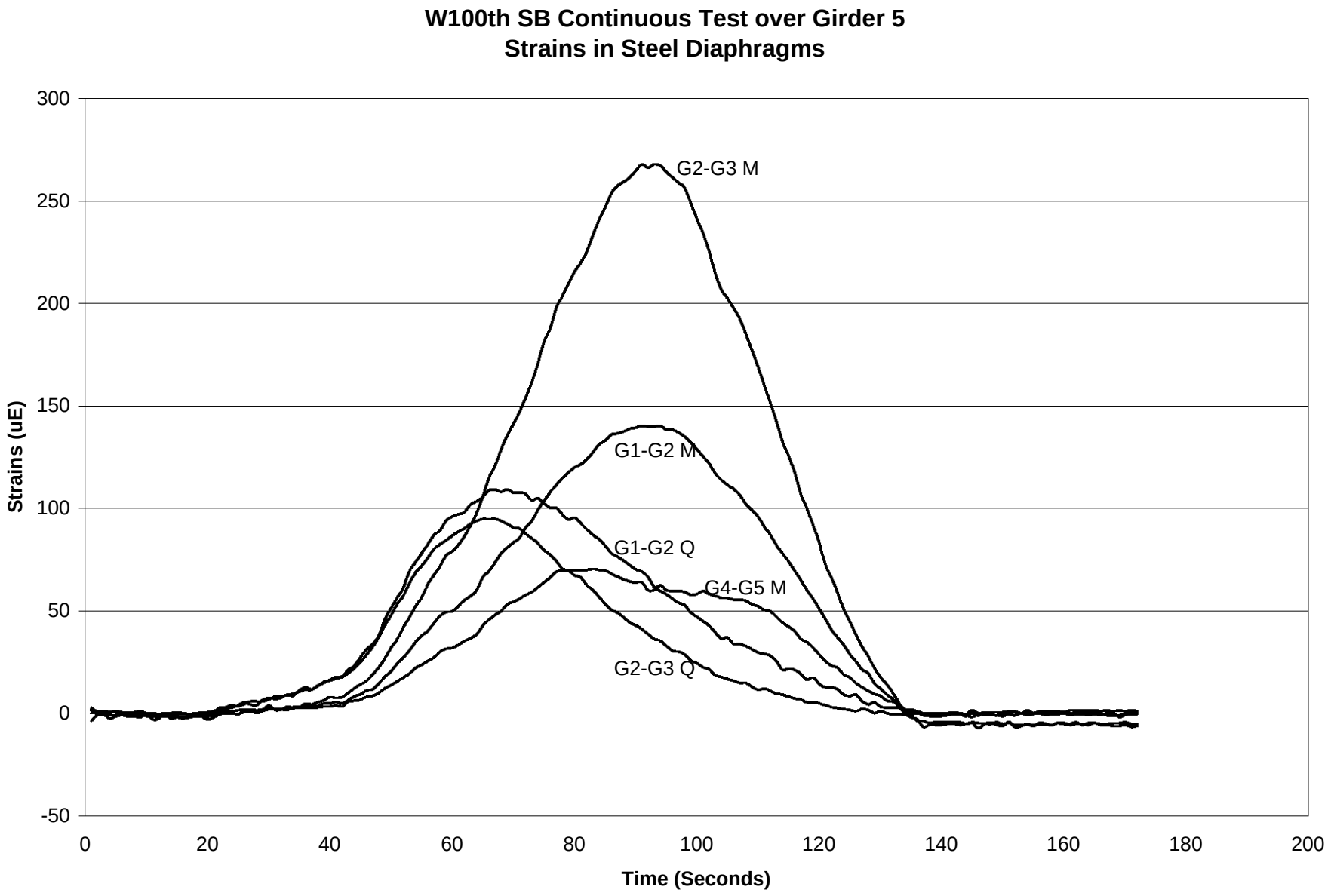
W100th SB Continuous Test over Girder 5
Strains in Steel Diaphragms
Strains (uE)
Time (Seconds)
300
250
200
150
100
50
0
-50
0
20
40
60
80
100
120
140
160
180
200
G2-G3 M
G1-G2 M
G1-G2 Q
G4-G5 M
G2-G3 Q

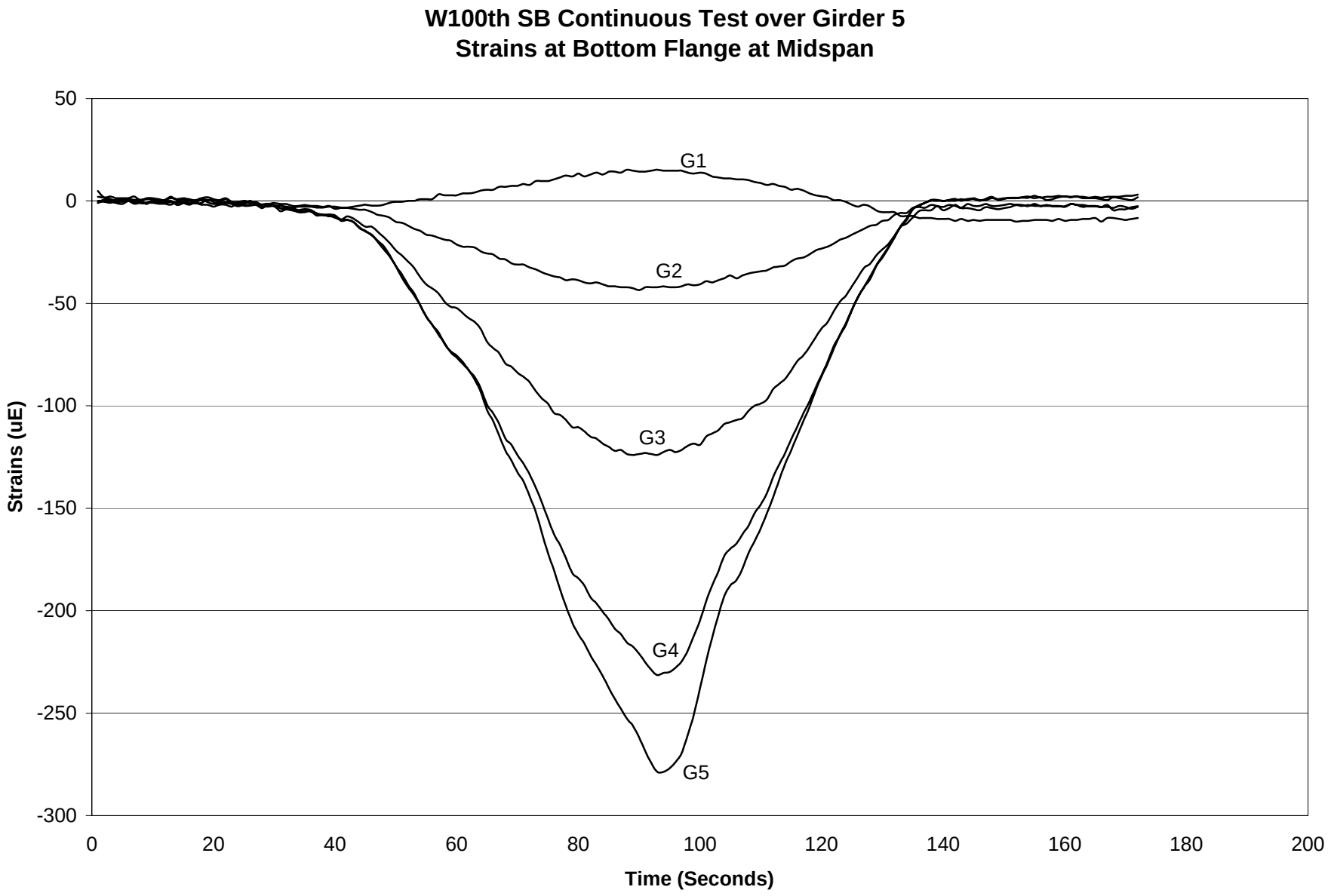
W100th SB Continuous Test over Girder 5
Strains at Bottom Flange at Midspan
Strains (uE)
Time (Seconds)
50
0
-50
-100
-150
-200
-250
-300
0
20
40
60
80
100
120
140
160
180
200
G1
G2
G3
G4
G5

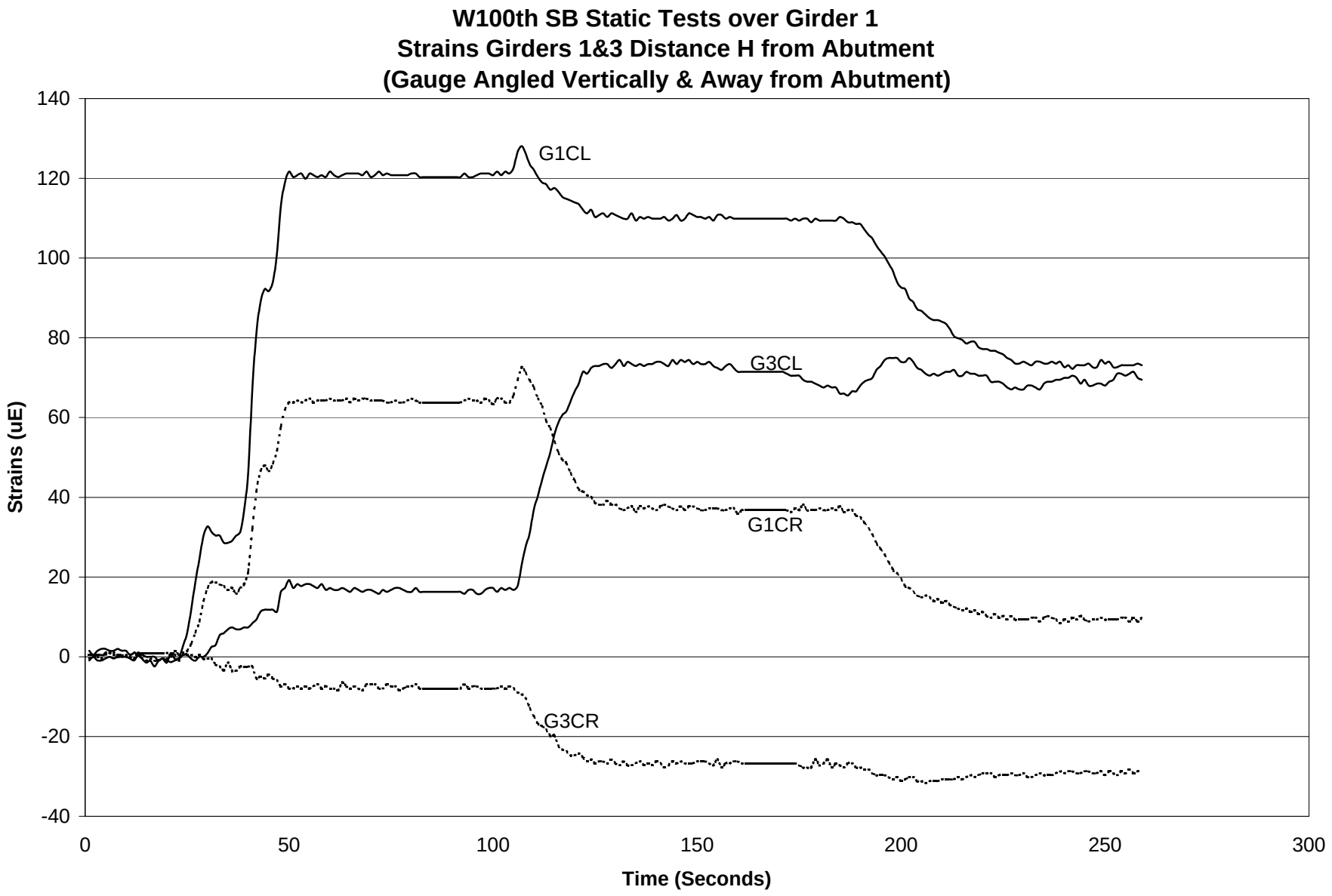
W100th SB Static Tests over Girder 1
Strains Girders 1&3 Distance H from Abutment
(Gauge Angled Vertically & Away from Abutment)
Strains (uE)
Time (Seconds)
G1CL
G3CL
G1CR
G3CR
140
120
100
80
60
40
20
0
-20
-40
0
50
100
150
200
250
300

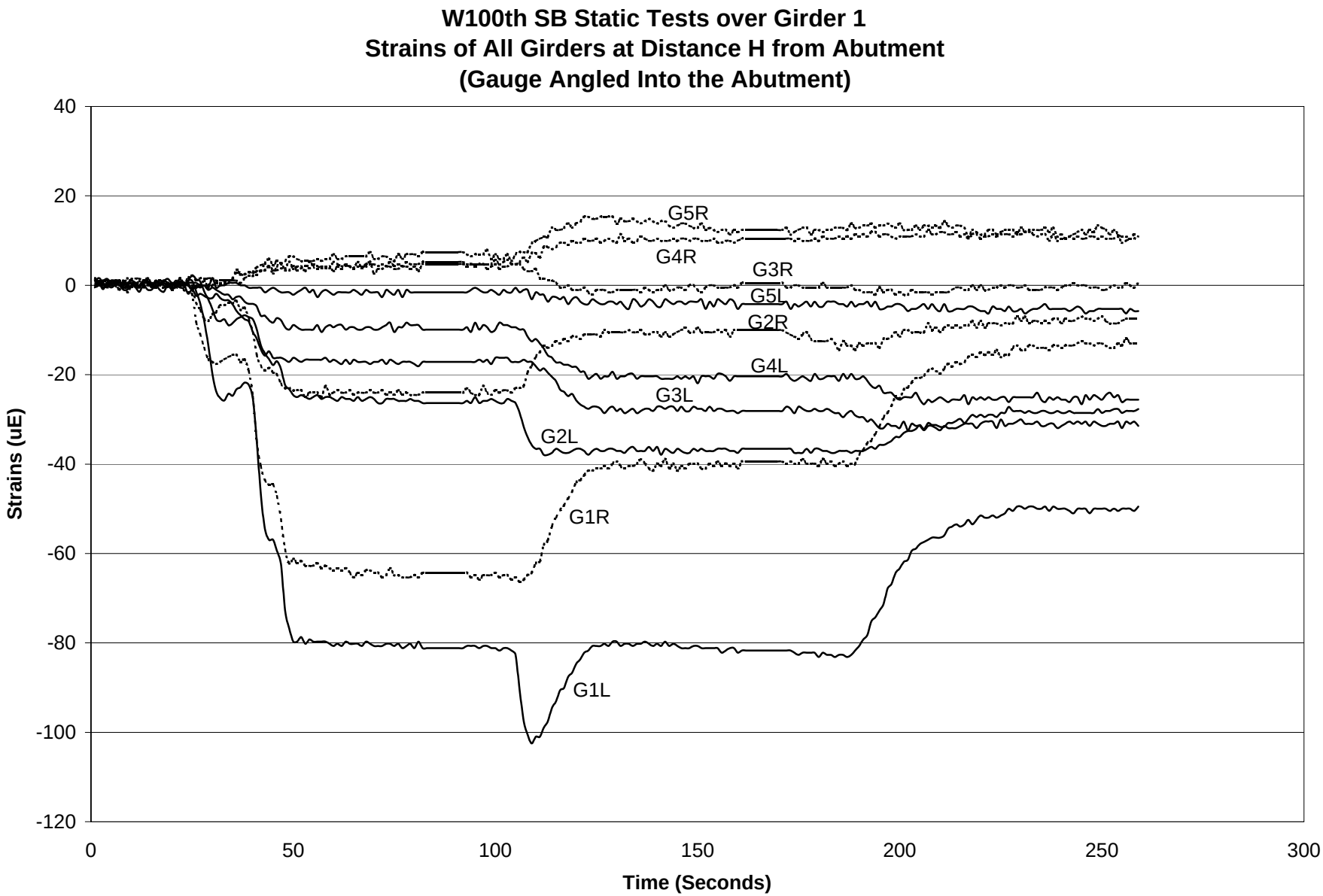
W100th SB Static Tests over Girder 1
Strains of All Girders at Distance H from Abutment
(Gauge Angled Into the Abutment)
Strains (uE)
Time (Seconds)
40
20
0
-20
-40
-60
-80
-100
-120
0
50
100
150
200
250
300
G5R
G4R
G3R
G5L
G2R
G4L
G3L
G2L
G1R
G1L

W100th SB Static Tests over Girder 1
Strains in Steel Diaphragms
Strains (uE)
400
350
300
250
200
150
100
50
0
-50
0
50
100
150
200
250
300
Time (Seconds)
G2-G3 M
G4-G5 M
G1-G2 M
G2-G3 Q
G1-G2 Q

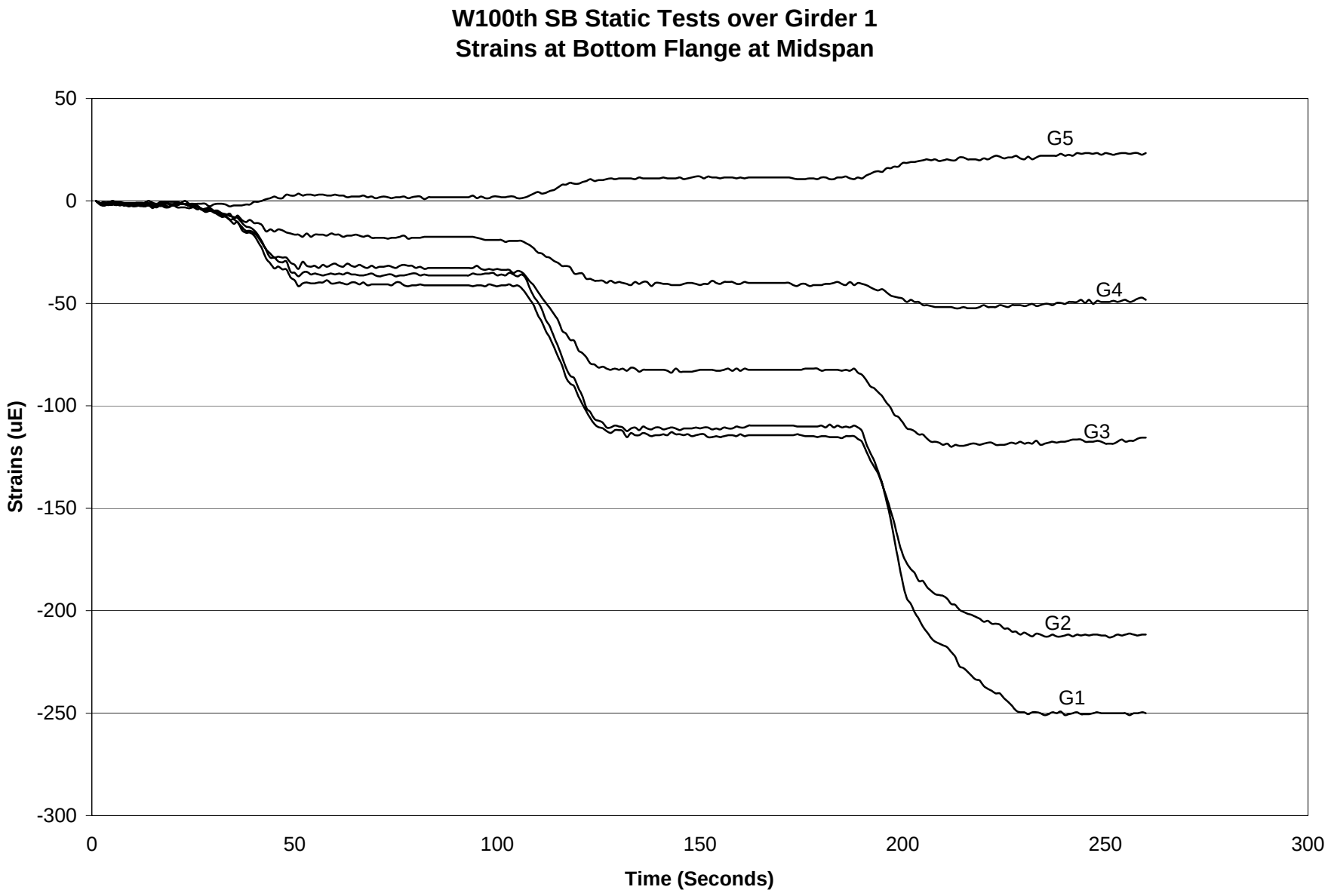
W100th SB Static Tests over Girder 1
Strains at Bottom Flange at Midspan
Strains (uE)
Time (Seconds)
50
0
-50
-100
-150
-200
-250
-300
0
50
100
150
200
250
300
G5
G4
G3
G2
G1

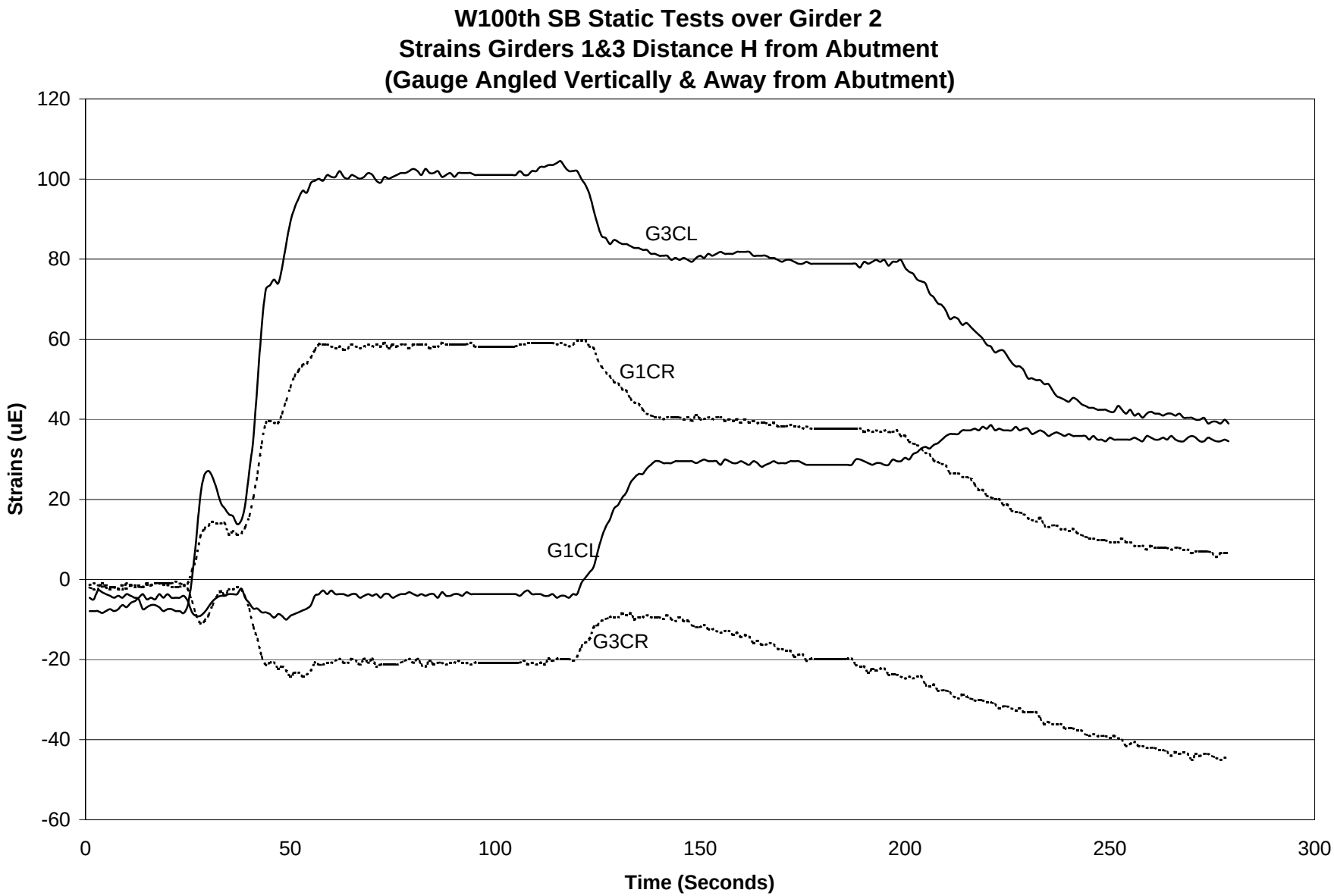
W100th SB Static Tests over Girder 2
Strains Girders 1&3 Distance H from Abutment
(Gauge Angled Vertically & Away from Abutment)
Strains (uE)
Time (Seconds)
120
100
80
60
40
20
0
-20
-40
-60
0
50
100
150
200
250
300
G3CL
G1CR
G1CL
G3CR

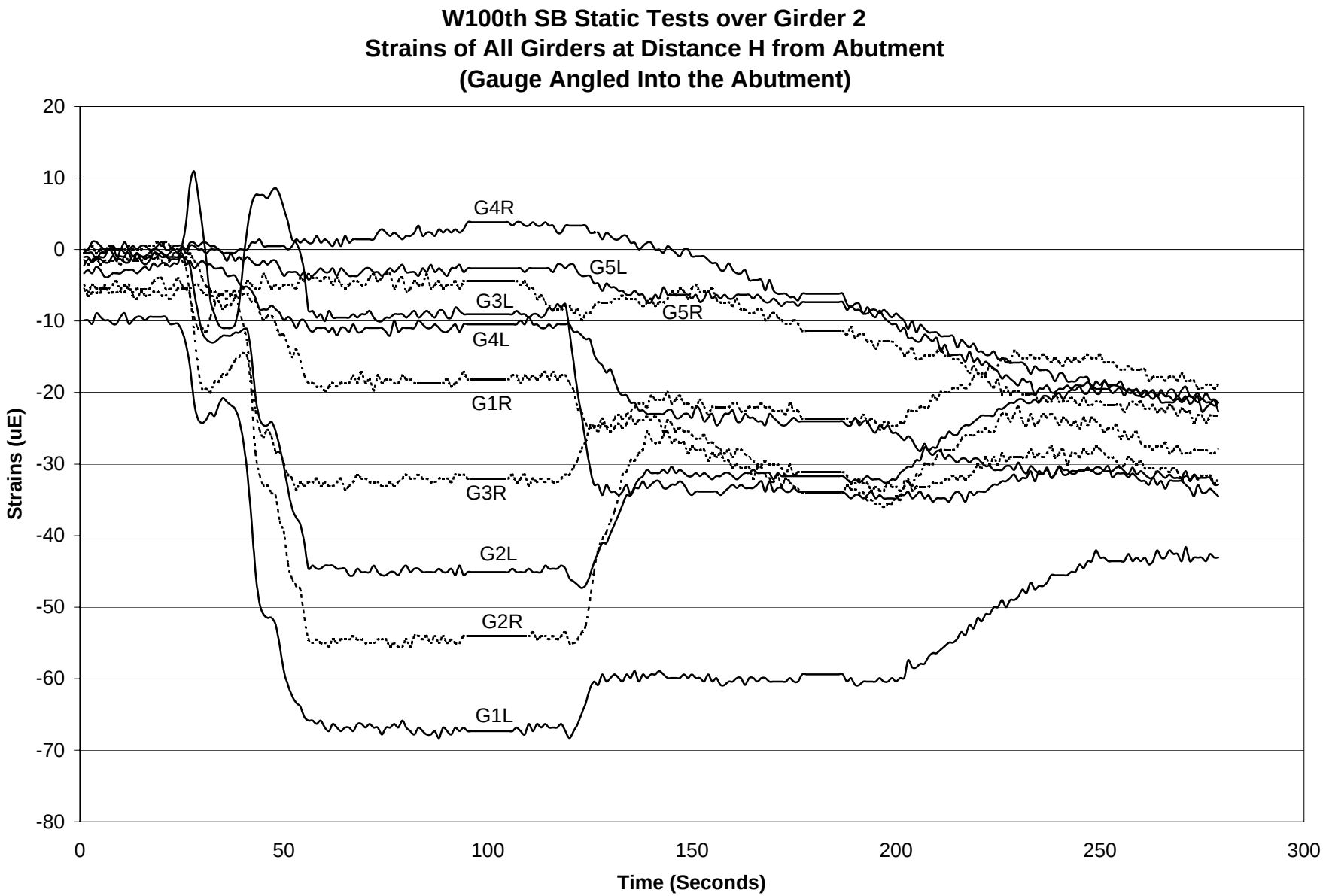
W100th SB Static Tests over Girder 2
Strains of All Girders at Distance H from Abutment
(Gauge Angled Into the Abutment)
Strains (uE)
Time (Seconds)
20
10
0
-10
-20
-30
-40
-50
-60
-70
-80
0
50
100
150
200
250
300
G4R
G5L
G3L
G5R
G4L
G1R
G3R
G2L
G2R
G1L

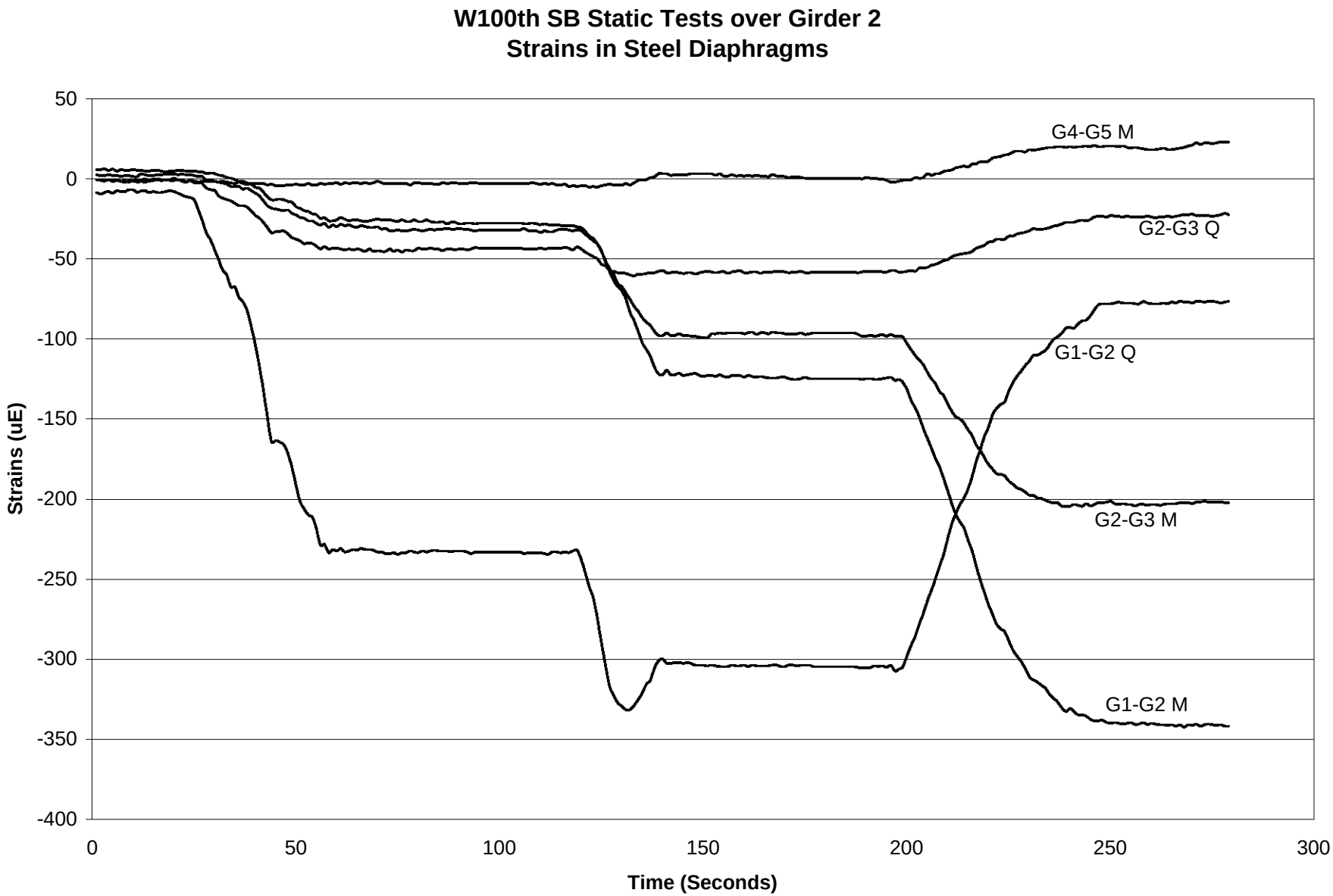
W100th SB Static Tests over Girder 2
Strains in Steel Diaphragms
Strains (uE)
Time (Seconds)
50
0
-50
-100
-150
-200
-250
-300
-350
-400
0
50
100
150
200
250
300
G4-G5 M
G2-G3 Q
G1-G2 Q
G2-G3 M
G1-G2 M

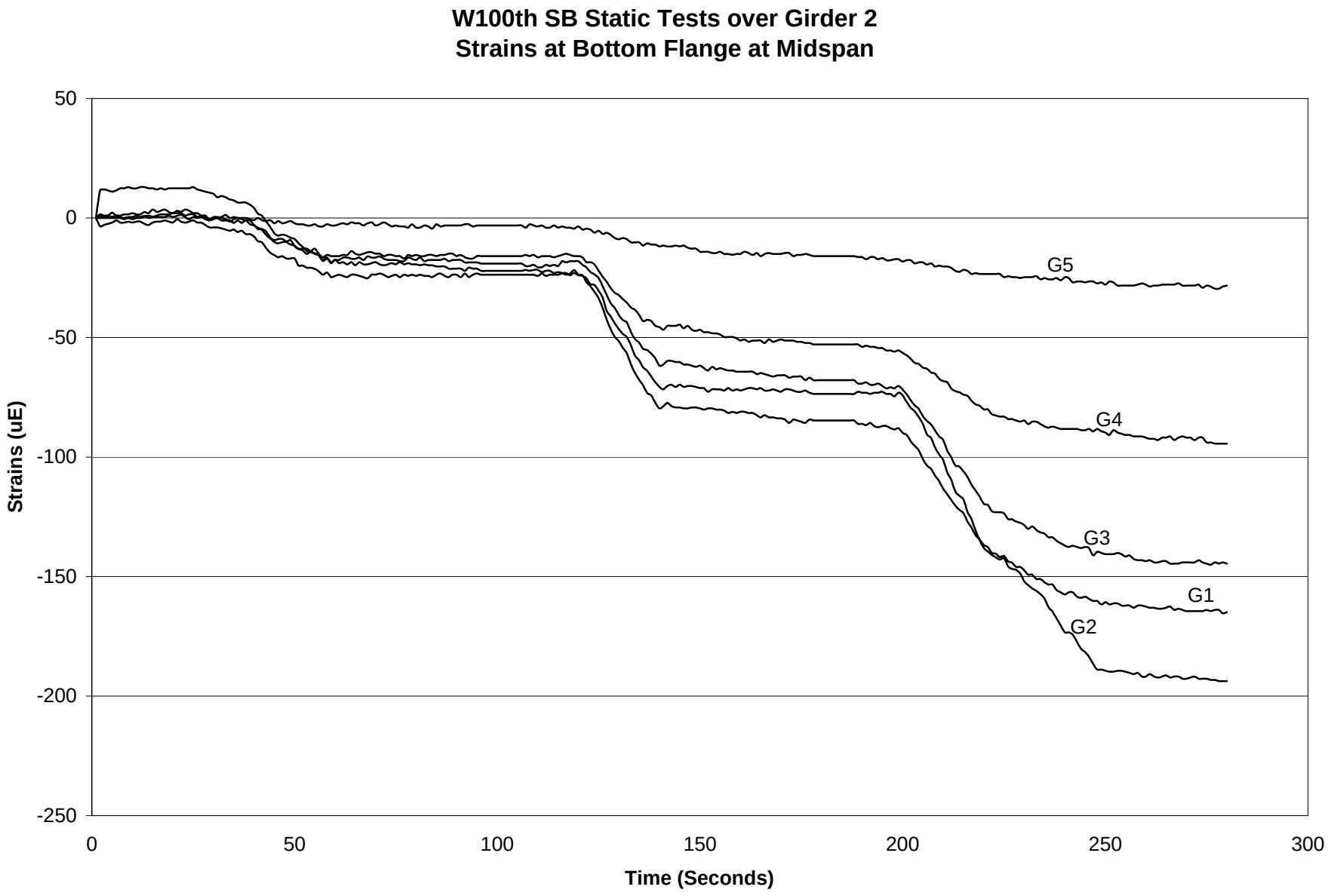
W100th SB Static Tests over Girder 2
Strains at Bottom Flange at Midspan
Strains (uE)
50
0
-50
-100
-150
-200
-250
0
50
100
150
200
250
300
Time (Seconds)
G5
G4
G3
G1
G2

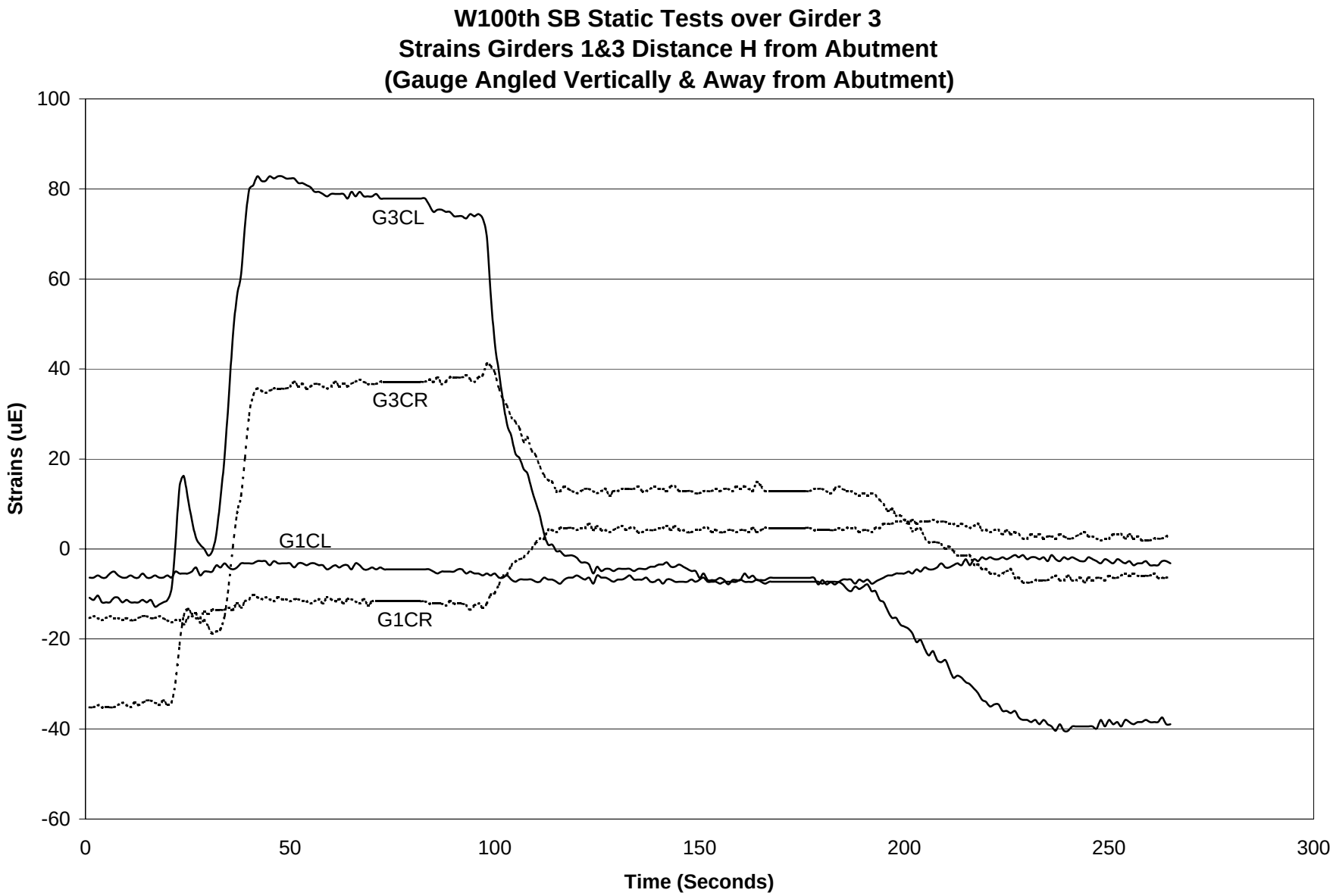
W100th SB Static Tests over Girder 3
Strains Girders 1&3 Distance H from Abutment
(Gauge Angled Vertically & Away from Abutment)
Strains (uE)
Time (Seconds)
100
80
60
40
20
0
-20
-40
-60
0
50
100
150
200
250
300
G3CL
G3CR
G1CL
G1CR

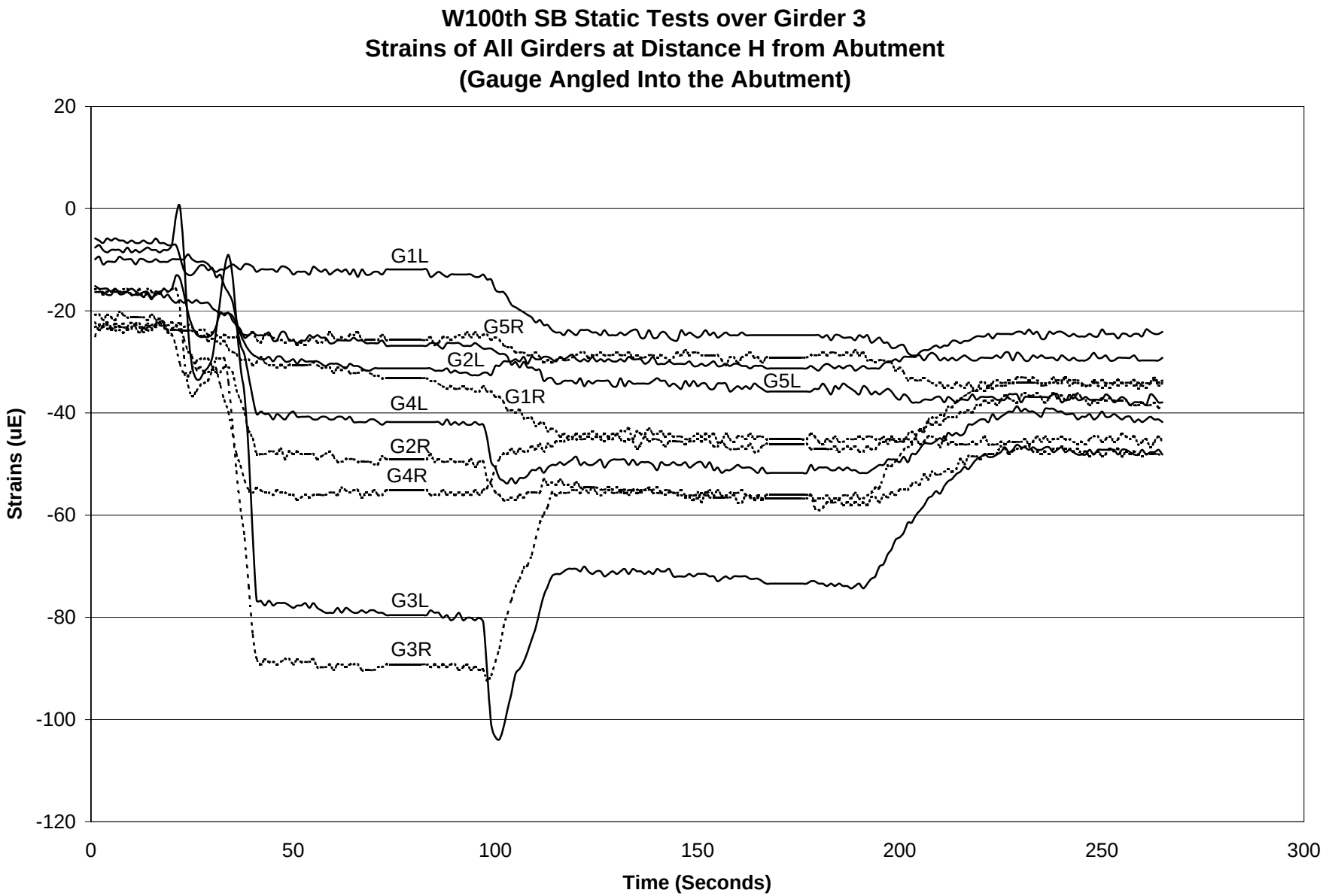
W100th SB Static Tests over Girder 3
Strains of All Girders at Distance H from Abutment
(Gauge Angled Into the Abutment)
Strains (uE)
Time (Seconds)
20
0
-20
-40
-60
-80
-100
-120
0
50
100
150
200
250
300
G1L
G5R
G2L
G5L
G1R
G4L
G2R
G4R
G3L
G3R

W100th SB Static Tests over Girder 3
Strains in Steel Diaphragms
100
0
-100
-200
-300
-400
-500
-600
Strains (uE)
0
50
100
150
200
250
300
Time (Seconds)
G2-G3 Q
G1-G2 Q
G4-G5 M
G1-G2 M
G2-G3 M

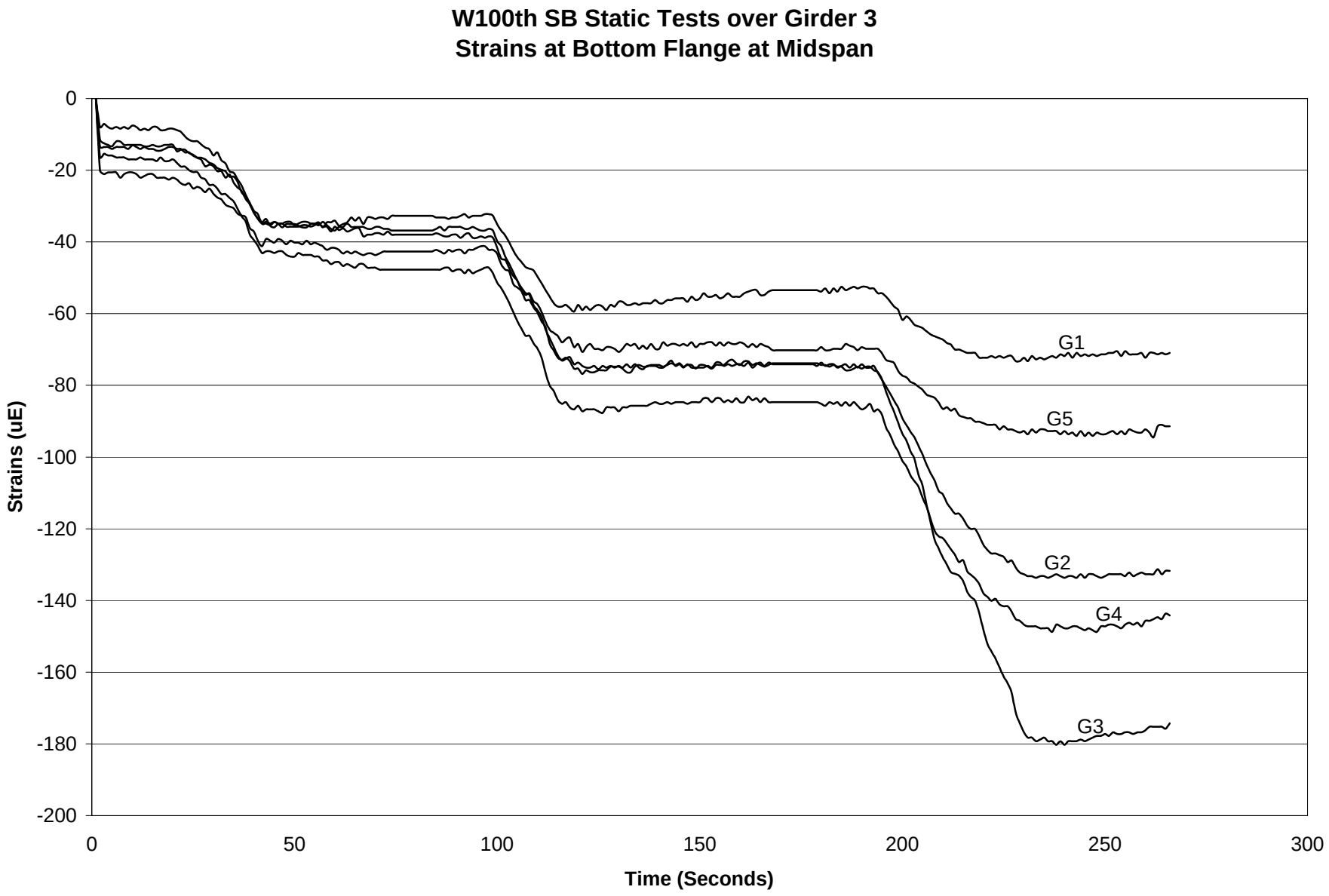
W100th SB Static Tests over Girder 3
Strains at Bottom Flange at Midspan
Strains (uE)
0
-20
-40
-60
-80
-100
-120
-140
-160
-180
-200
0
50
100
150
200
250
300
Time (Seconds)
G1
G5
G2
G4
G3

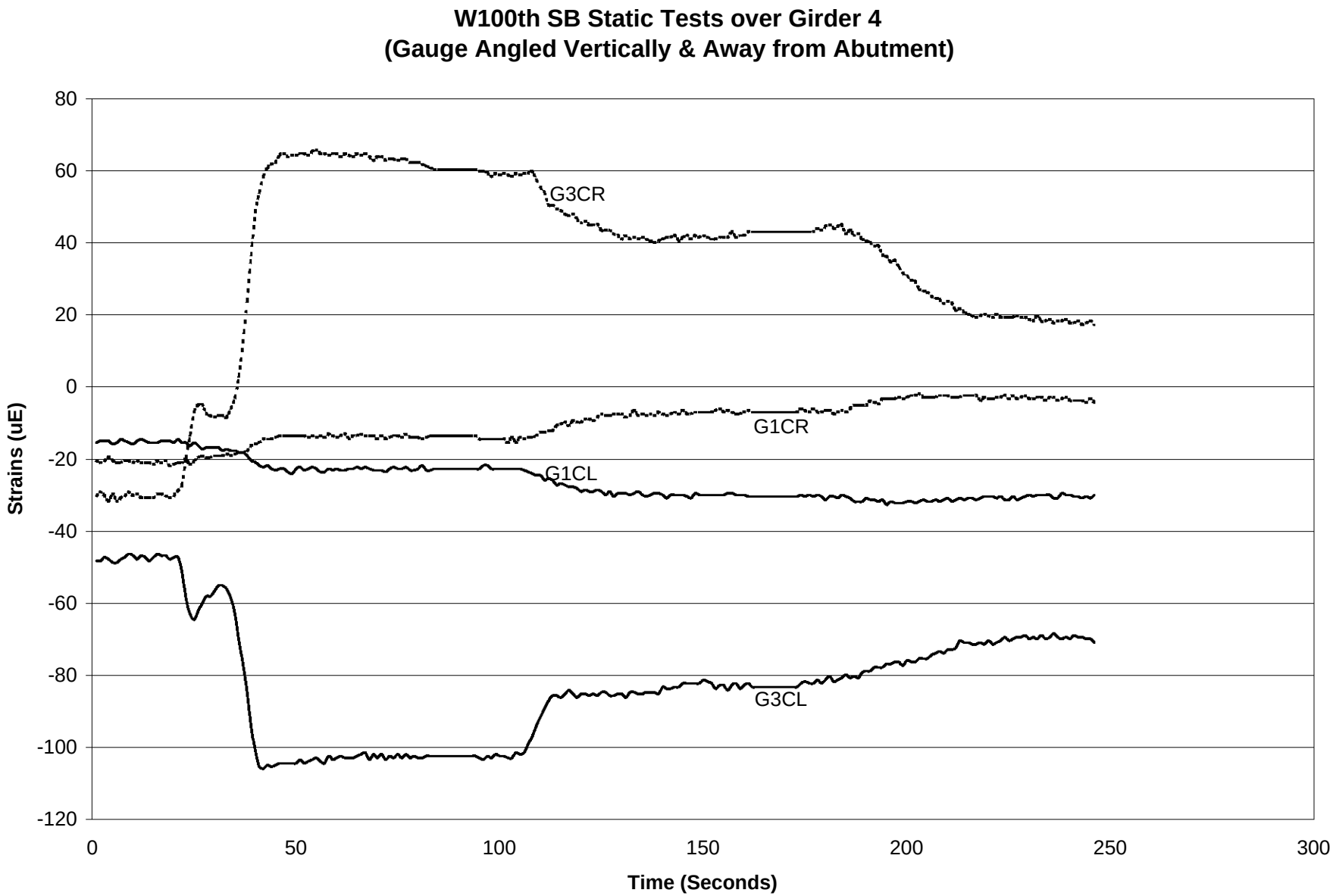
W100th SB Static Tests over Girder 4
(Gauge Angled Vertically & Away from Abutment)
Strains (uE)
Time (Seconds)
80
60
40
20
0
-20
-40
-60
-80
-100
-120
0
50
100
150
200
250
300
G3CR
G1CR
G1CL
G3CL

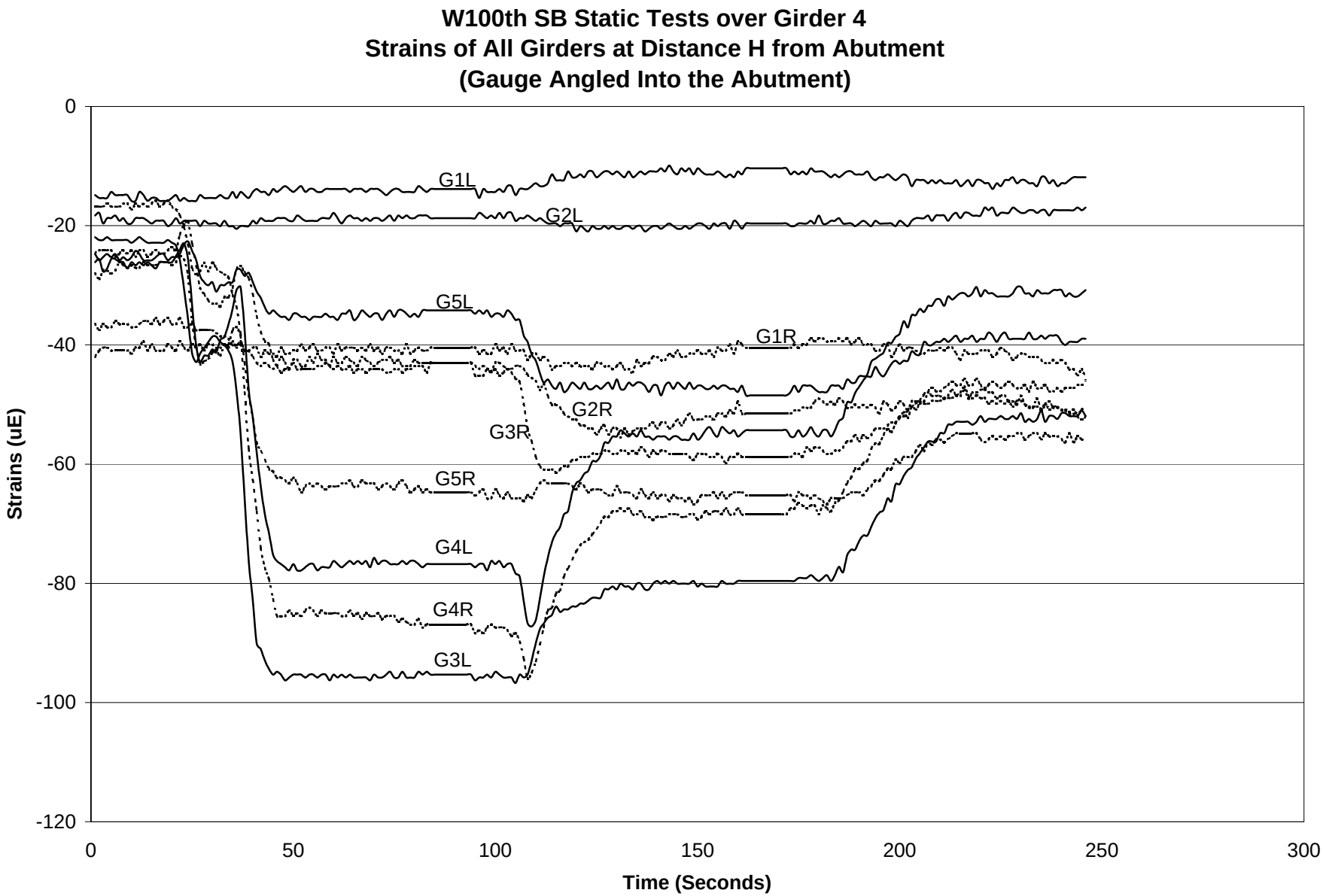
W100th SB Static Tests over Girder 4
Strains of All Girders at Distance H from Abutment
(Gauge Angled Into the Abutment)
Strains (uE)
Time (Seconds)
0
-20
-40
-60
-80
-100
-120
0
50
100
150
200
250
300
G1L
G2L
G5L
G1R
G2R
G3R
G5R
G4L
G4R
G3L

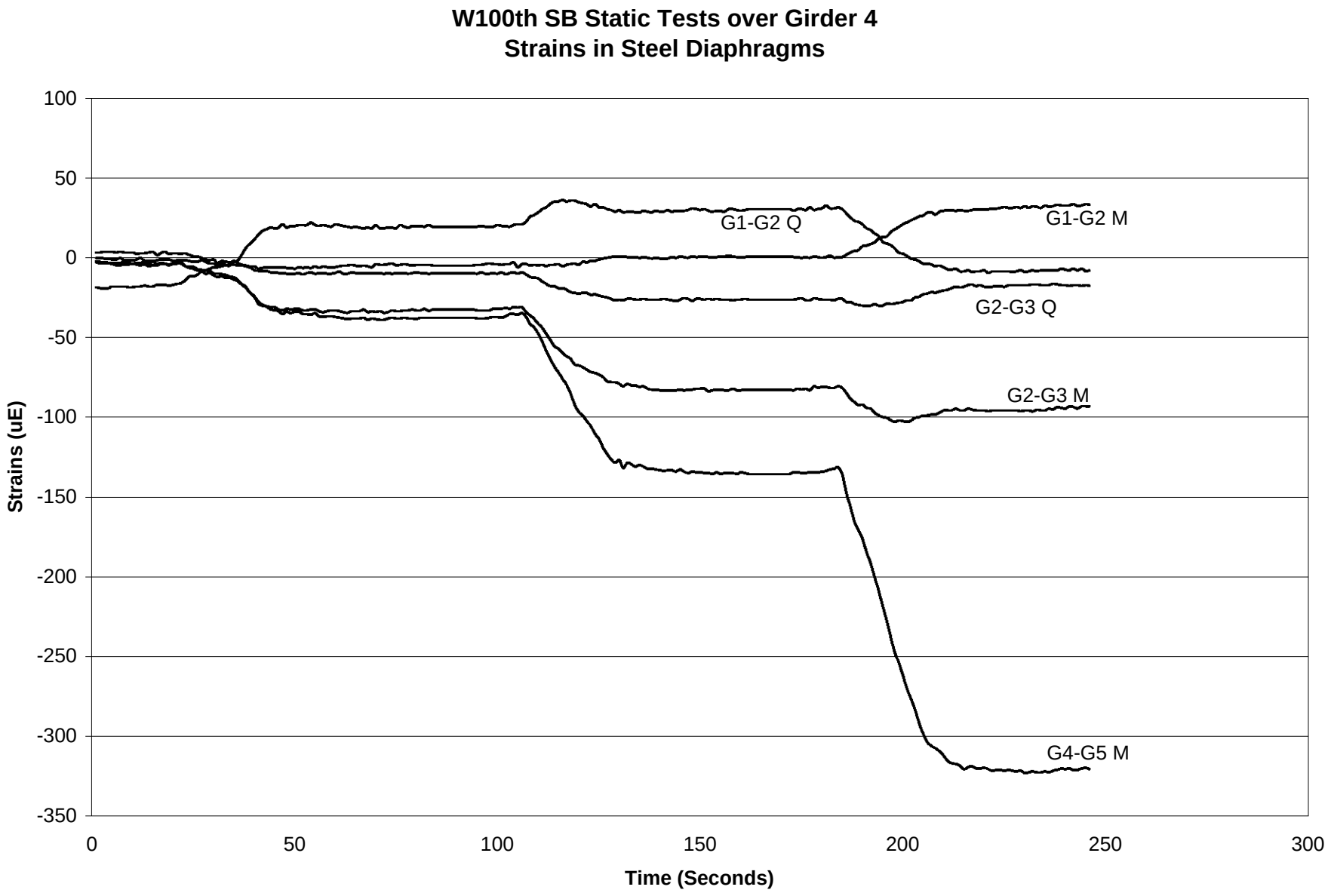
W100th SB Static Tests over Girder 4
Strains in Steel Diaphragms
100
50
0
-50
-100
-150
-200
-250
-300
-350
Strains (uE)
0
50
100
150
200
250
300
Time (Seconds)
G1-G2 Q
G1-G2 M
G2-G3 Q
G2-G3 M
G4-G5 M

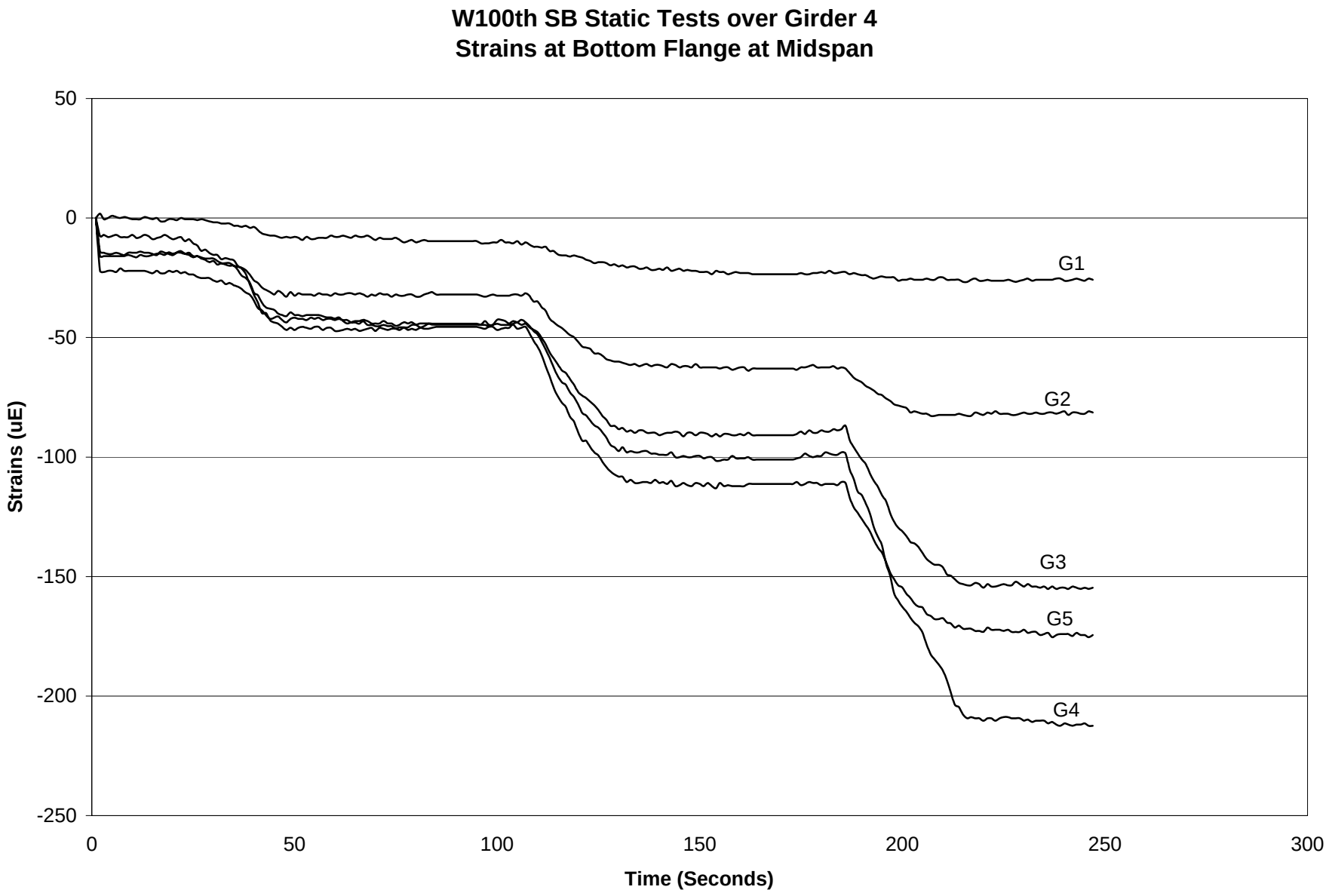
W100th SB Static Tests over Girder 4
Strains at Bottom Flange at Midspan
Strains (uE)
50
0
-50
-100
-150
-200
-250
0
50
100
150
200
250
300
Time (Seconds)
G1
G2
G3
G5
G4

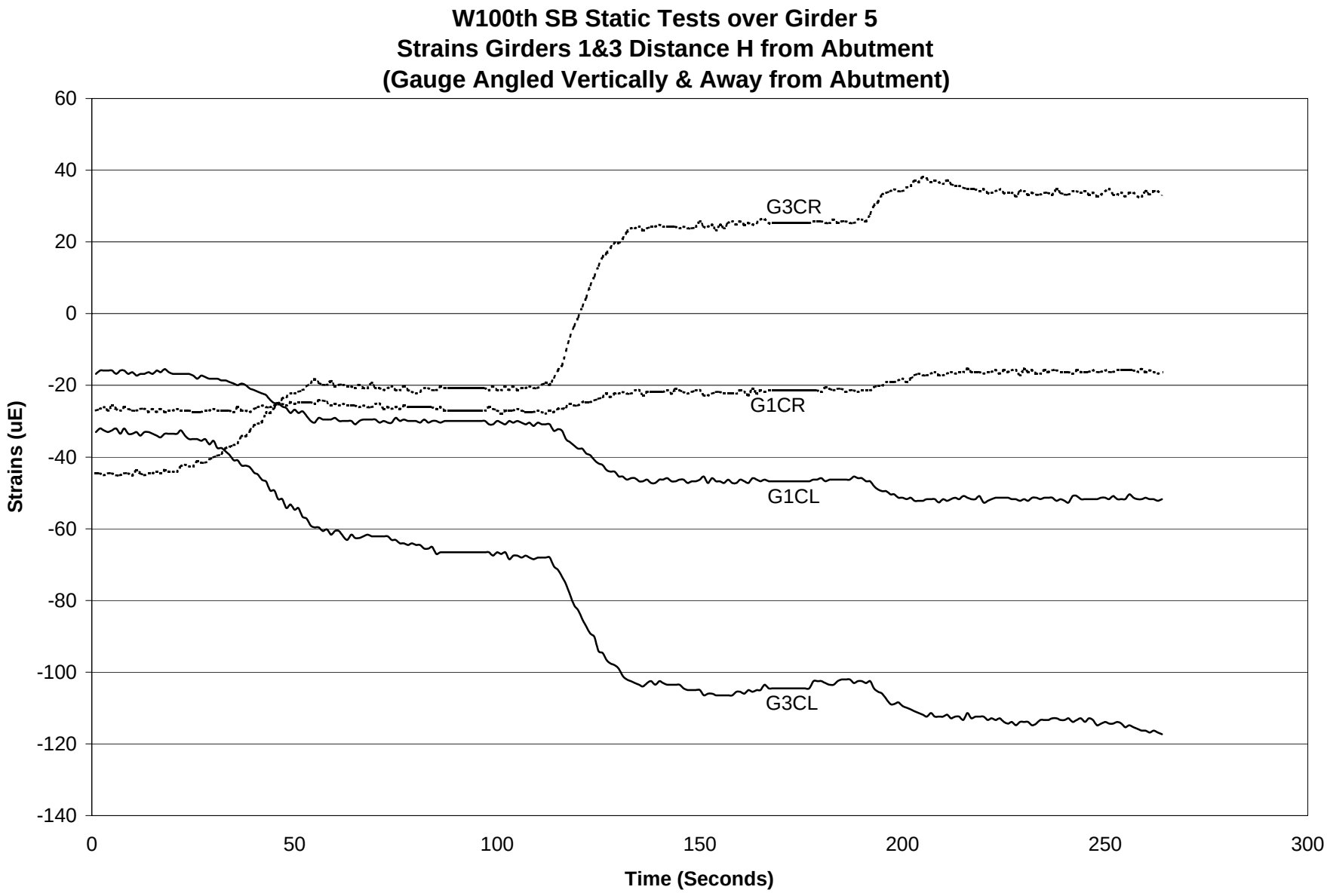
W100th SB Static Tests over Girder 5
Strains Girders 1&3 Distance H from Abutment
(Gauge Angled Vertically & Away from Abutment)
Strains (uE)
Time (Seconds)
60
40
20
0
-20
-40
-60
-80
-100
-120
-140
0
50
100
150
200
250
300
G3CR
G1CR
G1CL
G3CL

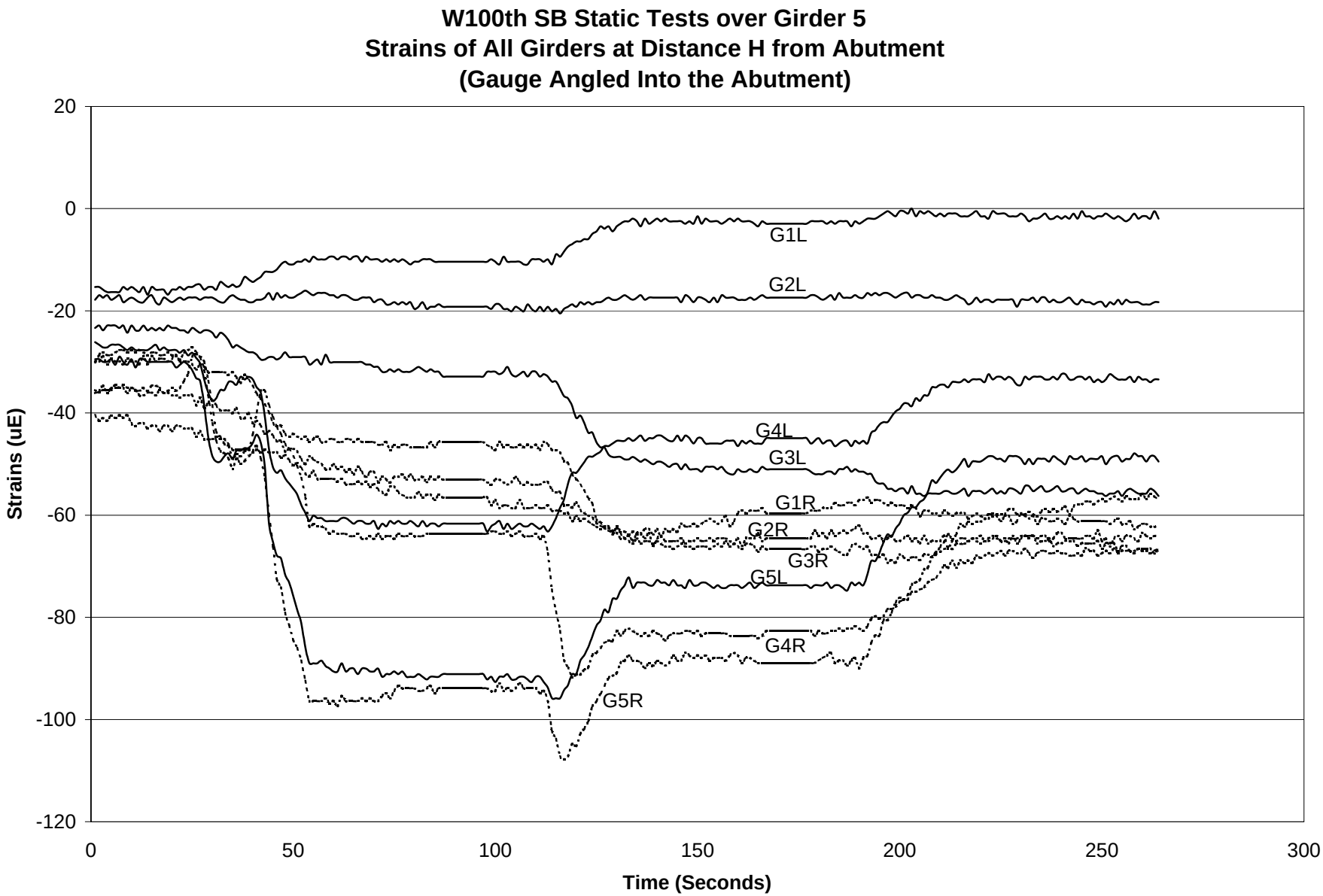
W100th SB Static Tests over Girder 5
Strains of All Girders at Distance H from Abutment
(Gauge Angled Into the Abutment)
Strains (uE)
Time (Seconds)
20
0
-20
-40
-60
-80
-100
-120
0
50
100
150
200
250
300
G1L
G2L
G4L
G3L
G1R
G2R
G3R
G5L
G4R
G5R

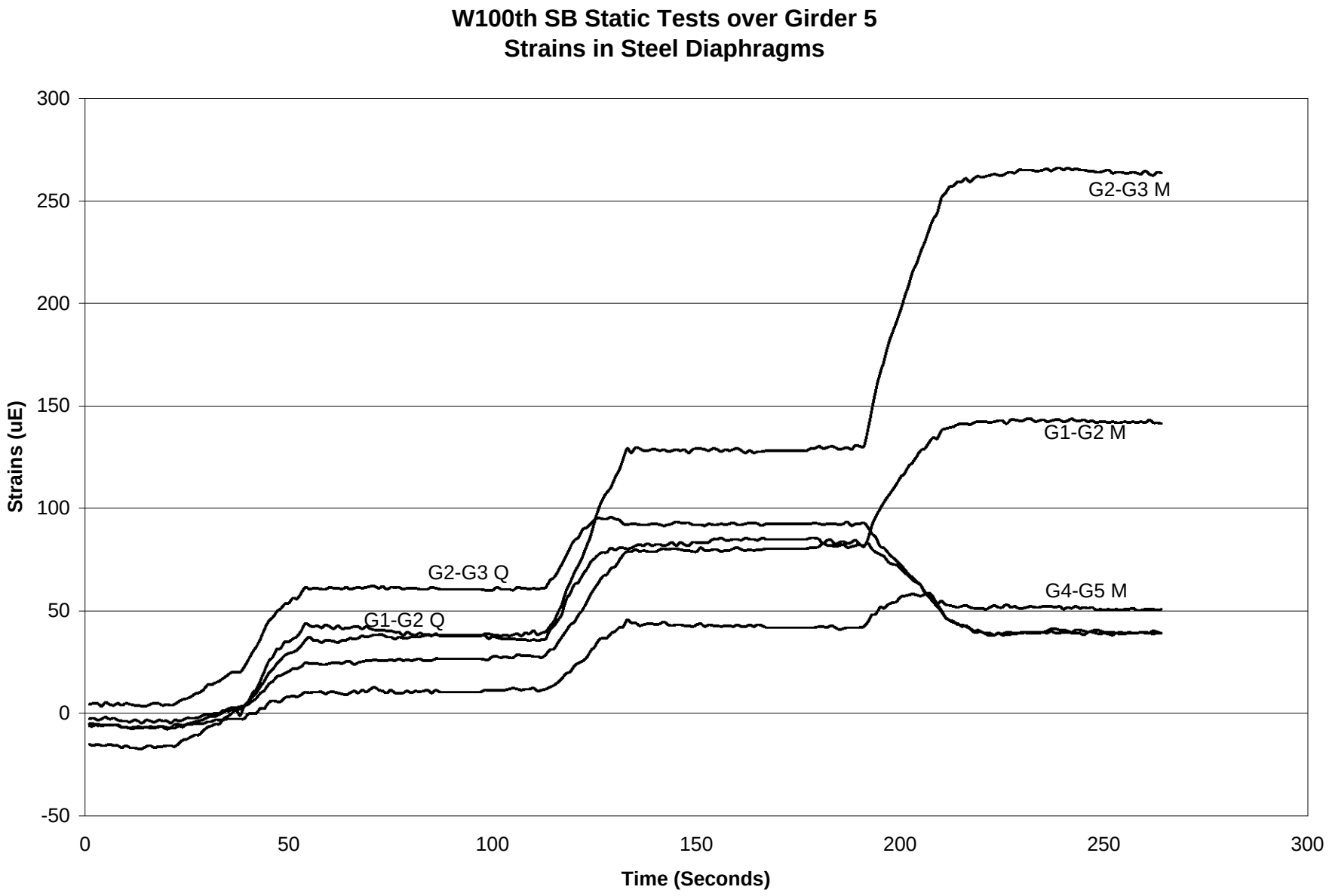
W100th SB Static Tests over Girder 5
Strains in Steel Diaphragms
Strains (uE)
Time (Seconds)
300
250
200
150
100
50
0
-50
0
50
100
150
200
250
300
G2-G3 M
G1-G2 M
G2-G3 Q
G1-G2 Q
G4-G5 M

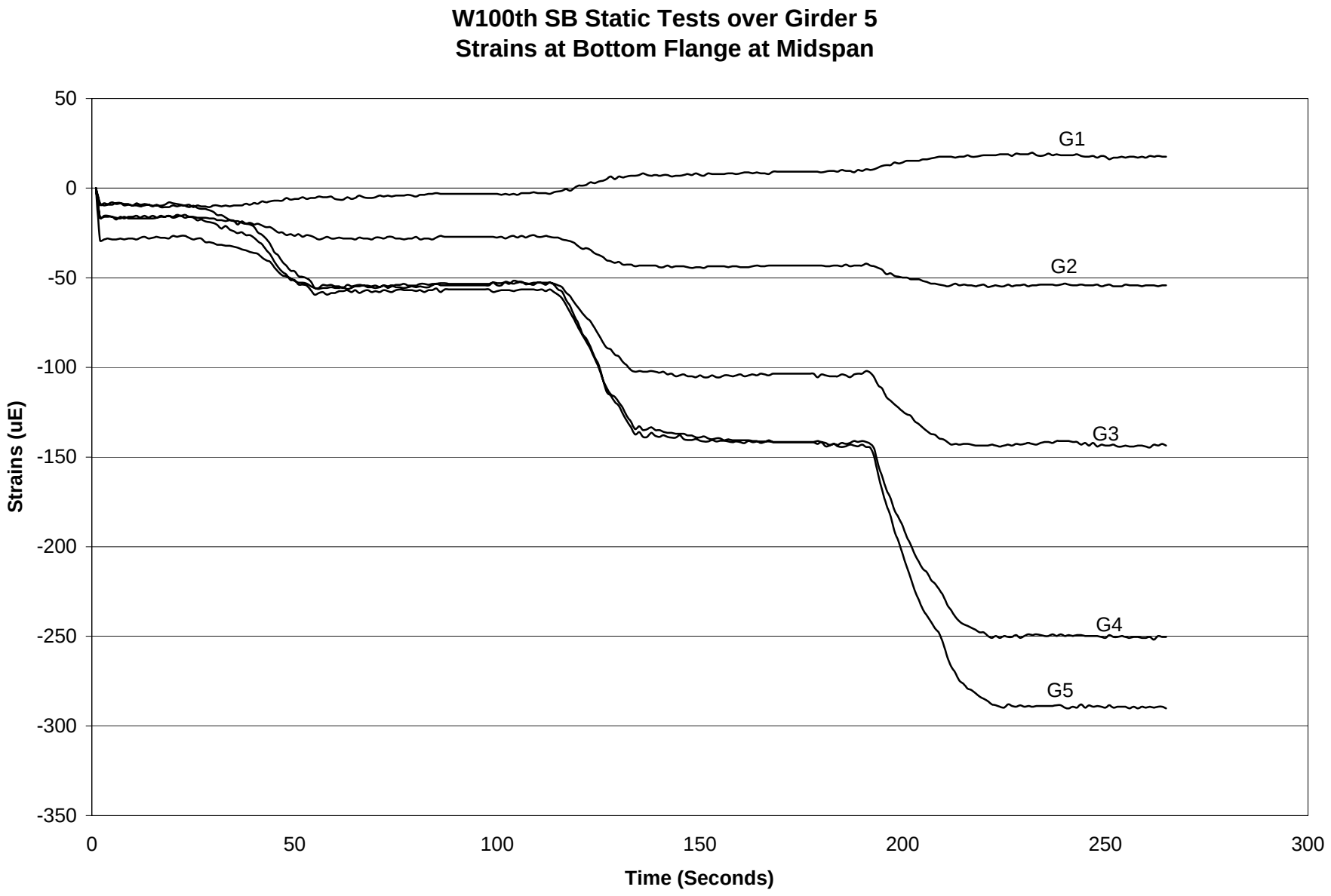
W100th SB Static Tests over Girder 5
Strains at Bottom Flange at Midspan
Strains (uE)
Time (Seconds)
50
0
-50
-100
-150
-200
-250
-300
-350
0
50
100
150
200
250
300
G1
G2
G3
G4
G5

# Campbell NB

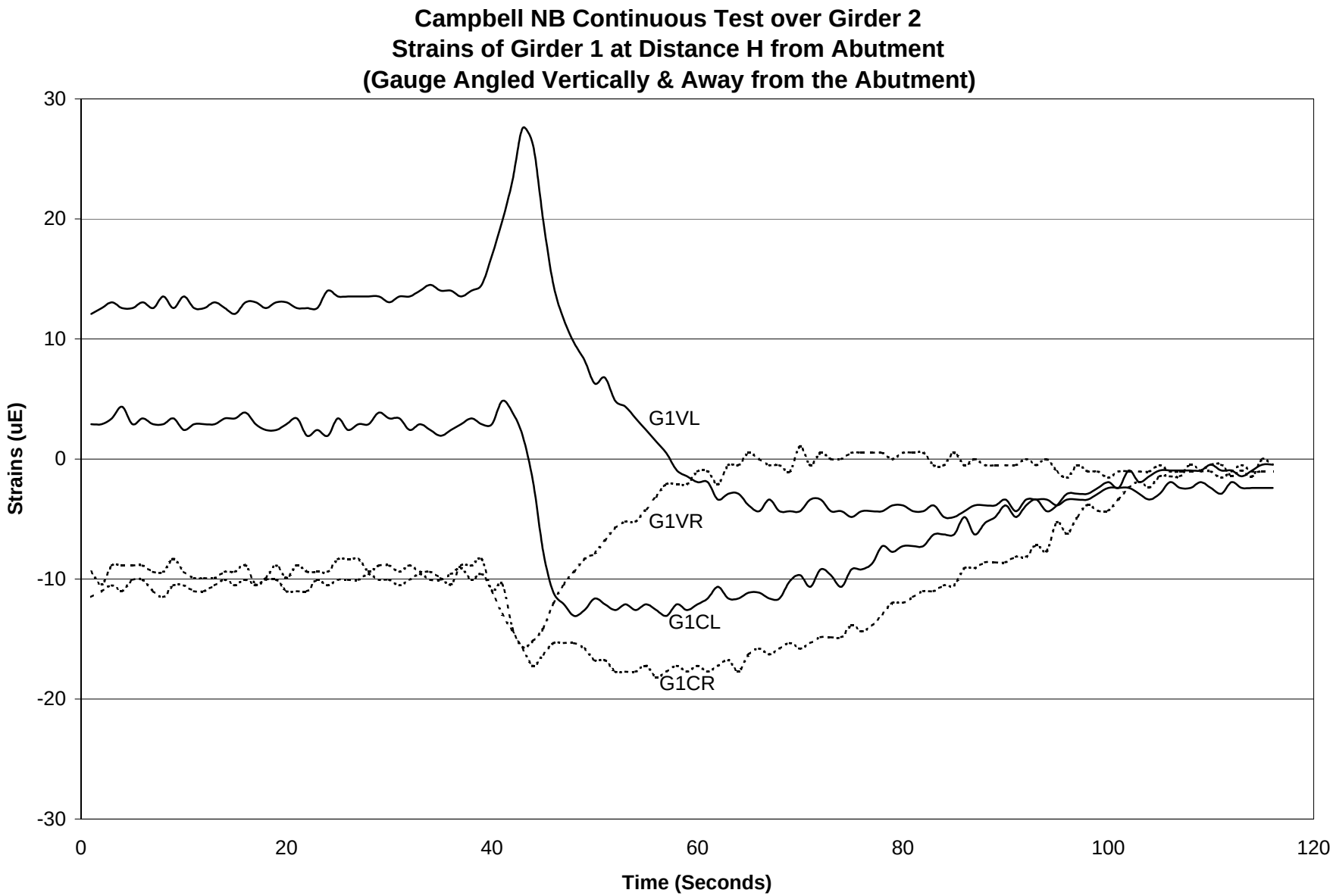
Campbell NB Continuous Test over Girder 2
Strains of Girder 1 at Distance H from Abutment
(Gauge Angled Vertically & Away from the Abutment)
Strains (uE)
30
20
10
0
-10
-20
-30
0
20
40
60
80
100
120
Time (Seconds)
G1VL
G1VR
G1CL
G1CR

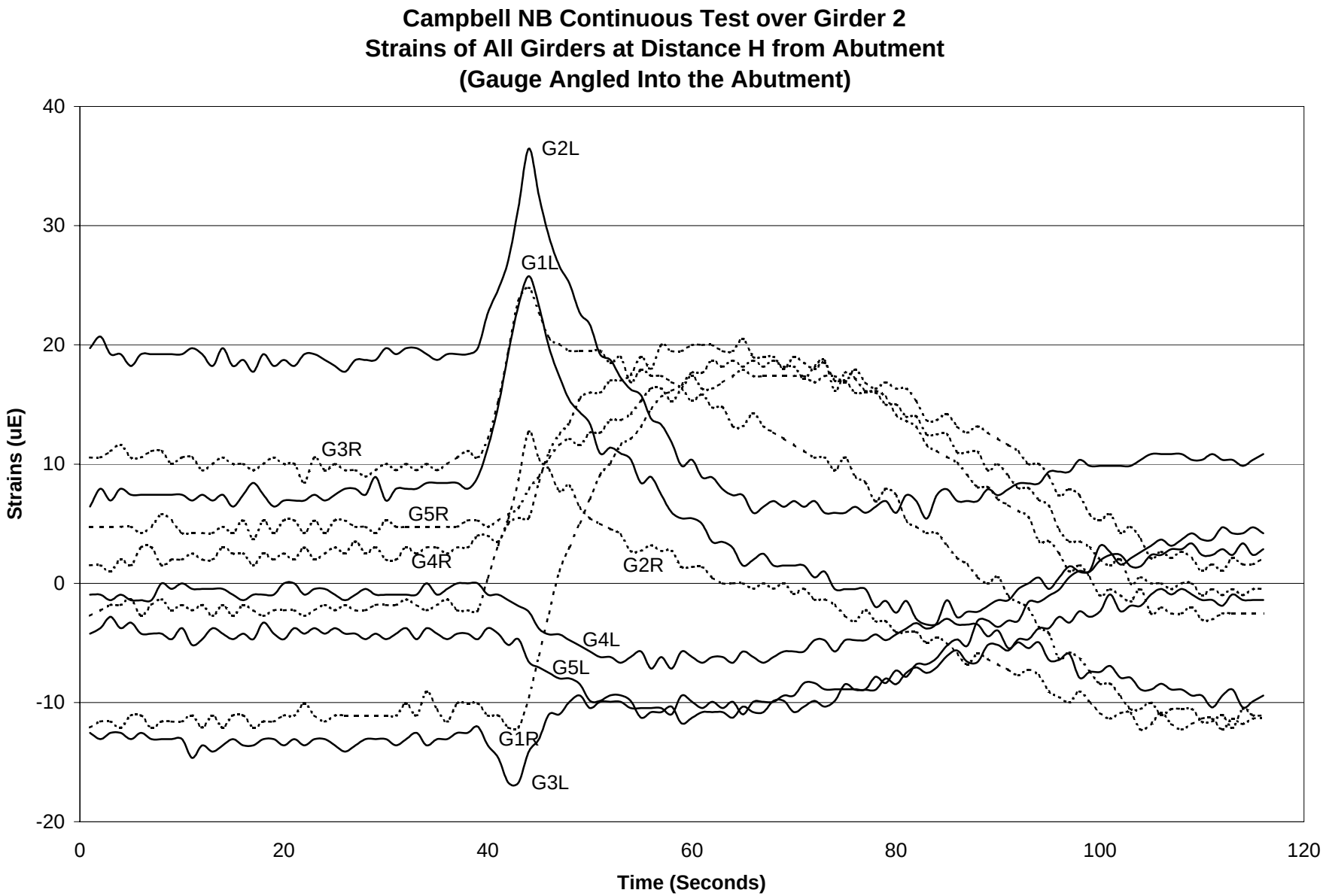
Campbell NB Continuous Test over Girder 2
Strains of All Girders at Distance H from Abutment
(Gauge Angled Into the Abutment)
Strains (uE)
Time (Seconds)
40
30
20
10
0
-10
-20
0
20
40
60
80
100
120
G2L
G1L
G3R
G5R
G4R
G2R
G4L
G5L
G1R
G3L

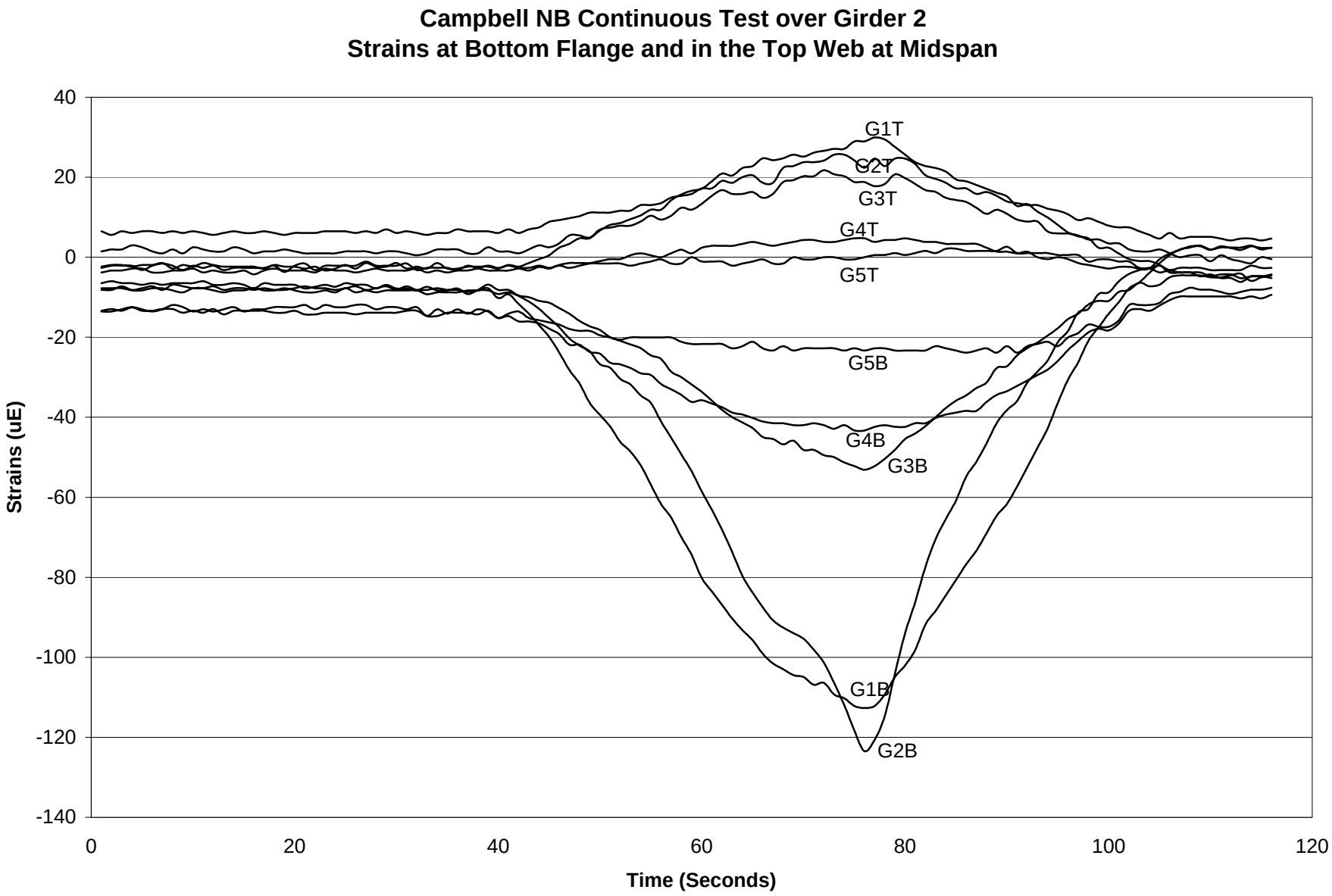
Campbell NB Continuous Test over Girder 2
Strains at Bottom Flange and in the Top Web at Midspan
Strains (uE)
Time (Seconds)
40
20
0
-20
-40
-60
-80
-100
-120
-140
0
20
40
60
80
100
120
G1T
G2T
G3T
G4T
G5T
G5B
G4B
G3B
G1B
G2B

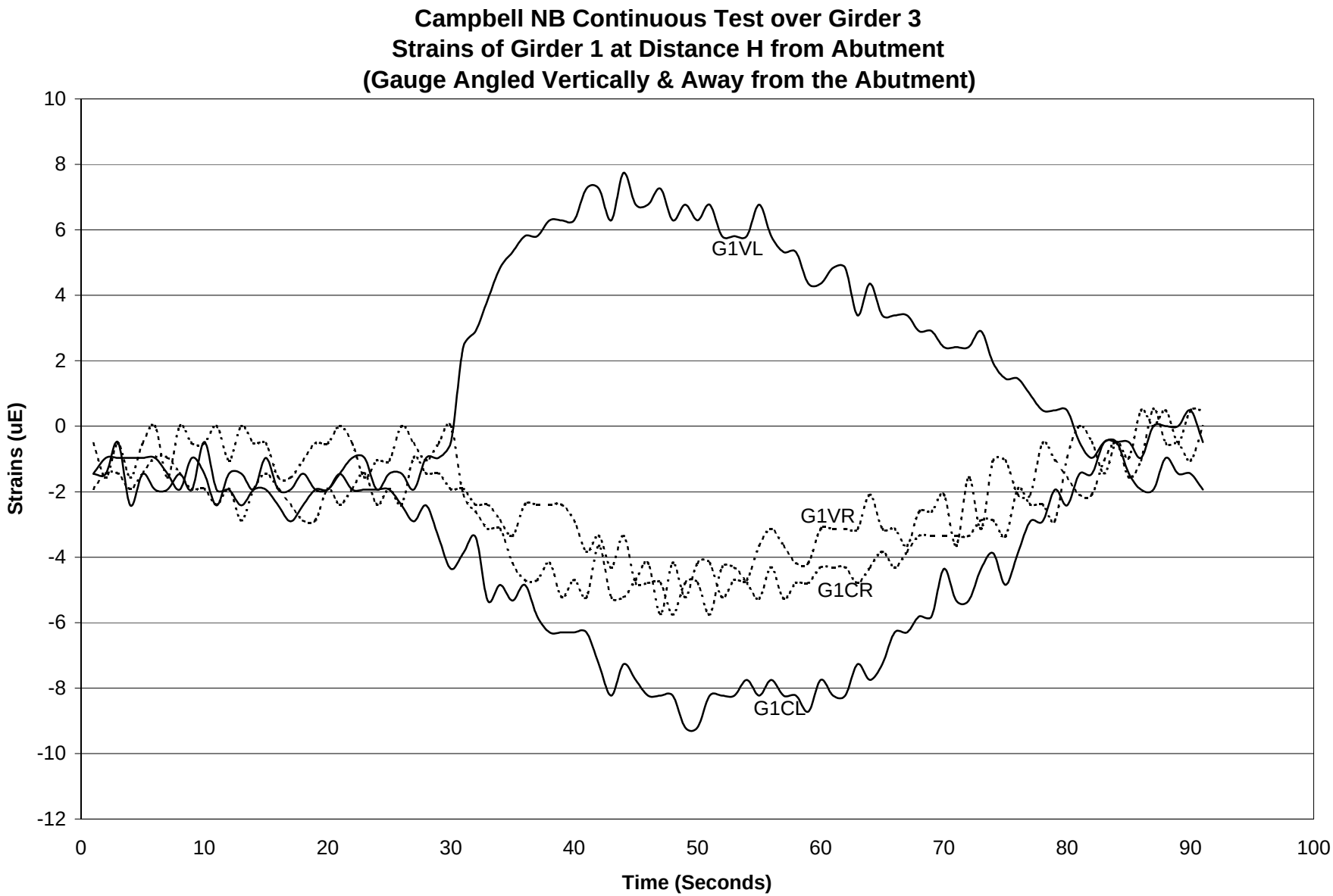
Campbell NB Continuous Test over Girder 3
Strains of Girder 1 at Distance H from Abutment
(Gauge Angled Vertically & Away from the Abutment)
Strains (uE)
Time (Seconds)
G1VL
G1VR
G1CR
G1CL
10
8
6
4
2
0
-2
-4
-6
-8
-10
-12
0
10
20
30
40
50
60
70
80
90
100

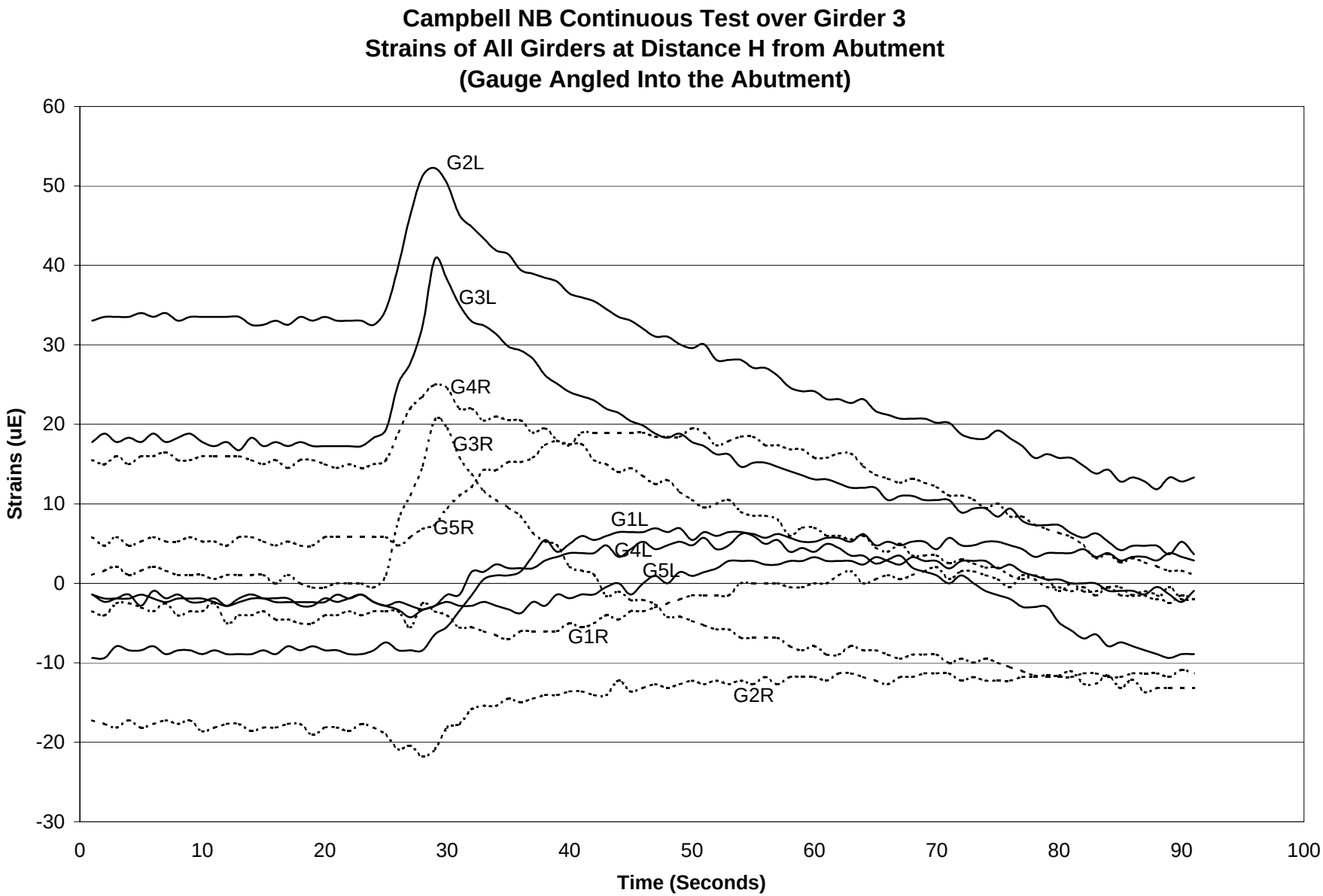
Campbell NB Continuous Test over Girder 3
Strains of All Girders at Distance H from Abutment
(Gauge Angled Into the Abutment)
Strains (uE)
Time (Seconds)
60
50
40
30
20
10
0
-10
-20
-30
0
10
20
30
40
50
60
70
80
90
100
G2L
G3L
G4R
G3R
G5R
G1L
G4L
G5L
G1R
G2R

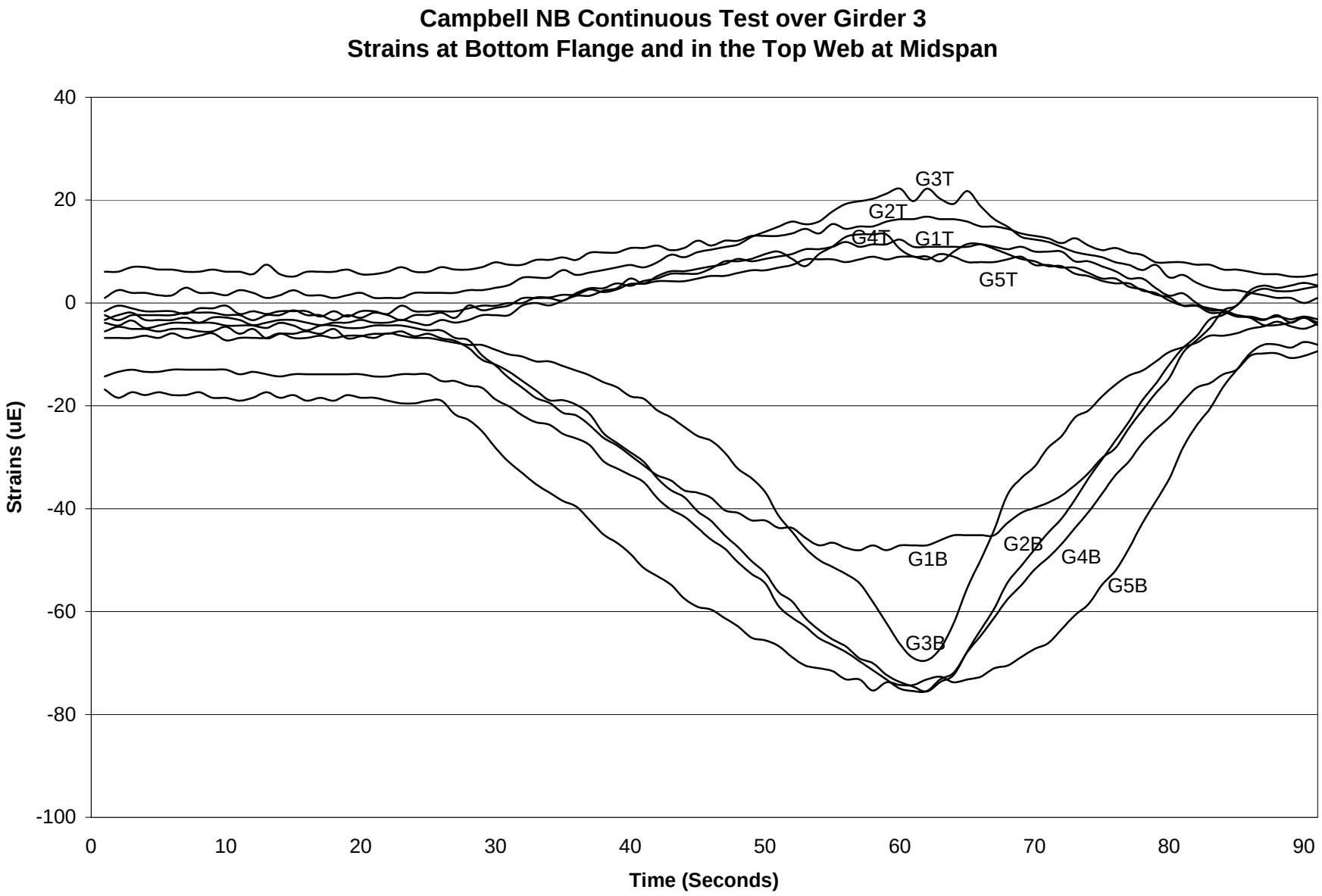
Campbell NB Continuous Test over Girder 3
Strains at Bottom Flange and in the Top Web at Midspan
Strains (uE)
Time (Seconds)
40
20
0
-20
-40
-60
-80
-100
0
10
20
30
40
50
60
70
80
90
G3T
G2T
G4T
G1T
G5T
G1B
G2B
G4B
G5B
G3B

Campbell NB Continuous Test over Girder 4
Strains of Girder 1 at Distance H from Abutment
(Gauge Angled Vertically & Away from the Abutment)
15
10
5
0
-5
-10
Strains (uE)
50
60
70
80
90
100
110
120
130
140
150
Time (Seconds)
G1VL
G1CR
G1VR
G1CL

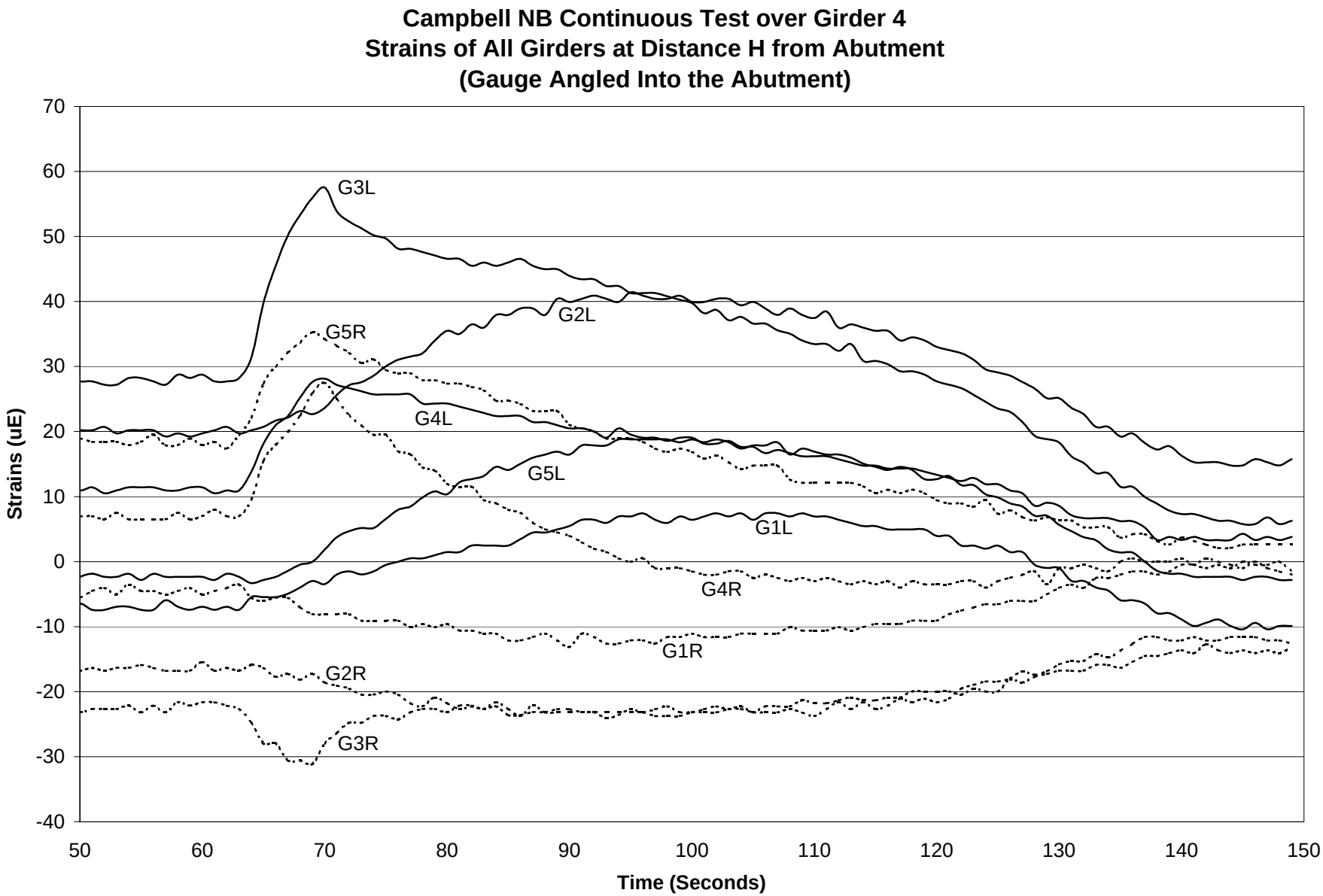
Campbell NB Continuous Test over Girder 4
Strains of All Girders at Distance H from Abutment
(Gauge Angled Into the Abutment)
Strains (uE)
Time (Seconds)
70
60
50
40
30
20
10
0
-10
-20
-30
-40
50
60
70
80
90
100
110
120
130
140
150
G3L
G2L
G5R
G4L
G5L
G1L
G4R
G1R
G2R
G3R

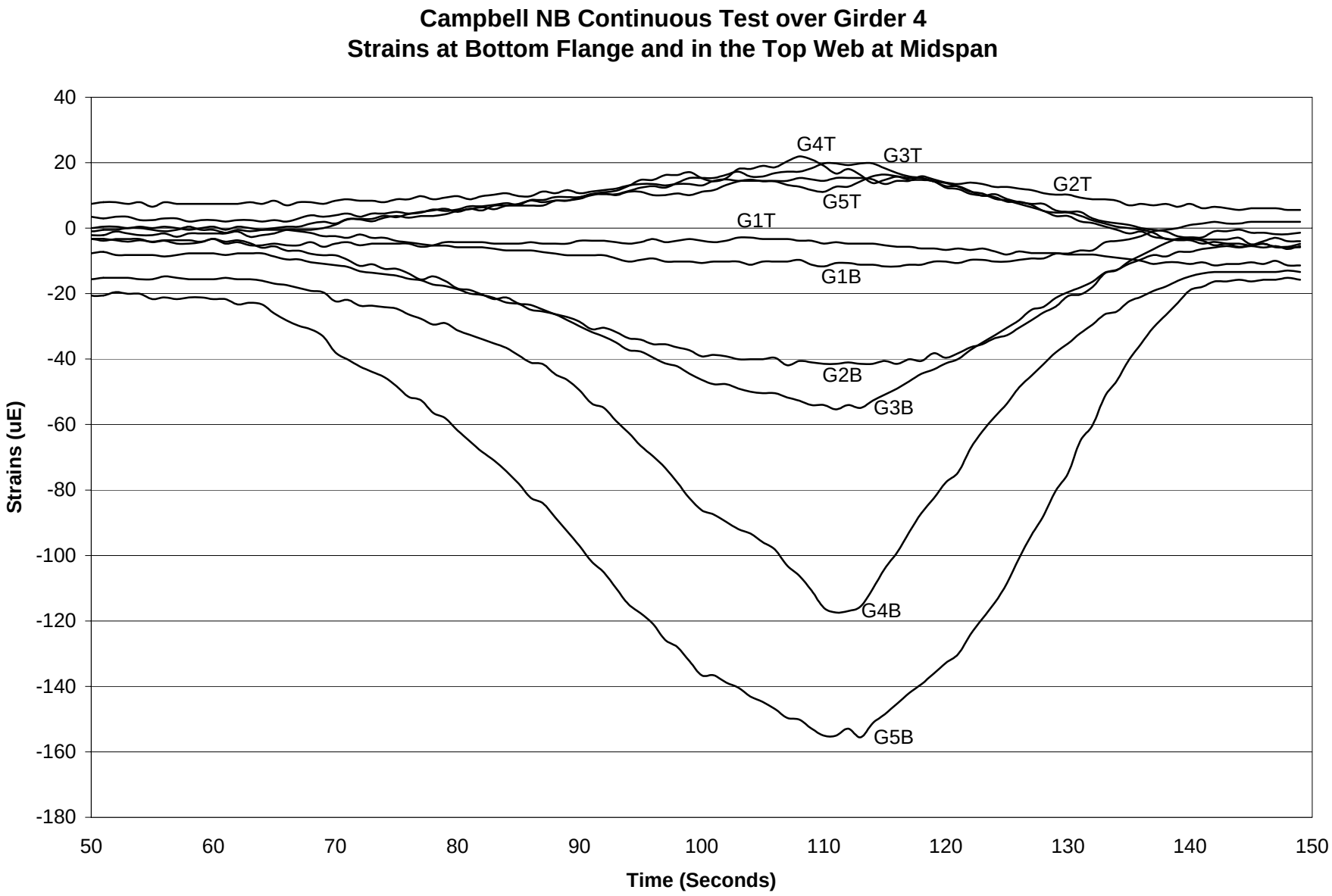
Campbell NB Continuous Test over Girder 4
Strains at Bottom Flange and in the Top Web at Midspan
Strains (uE)
Time (Seconds)
40
20
0
-20
-40
-60
-80
-100
-120
-140
-160
-180
50
60
70
80
90
100
110
120
130
140
150
G4T
G3T
G2T
G5T
G1T
G1B
G2B
G3B
G4B
G5B

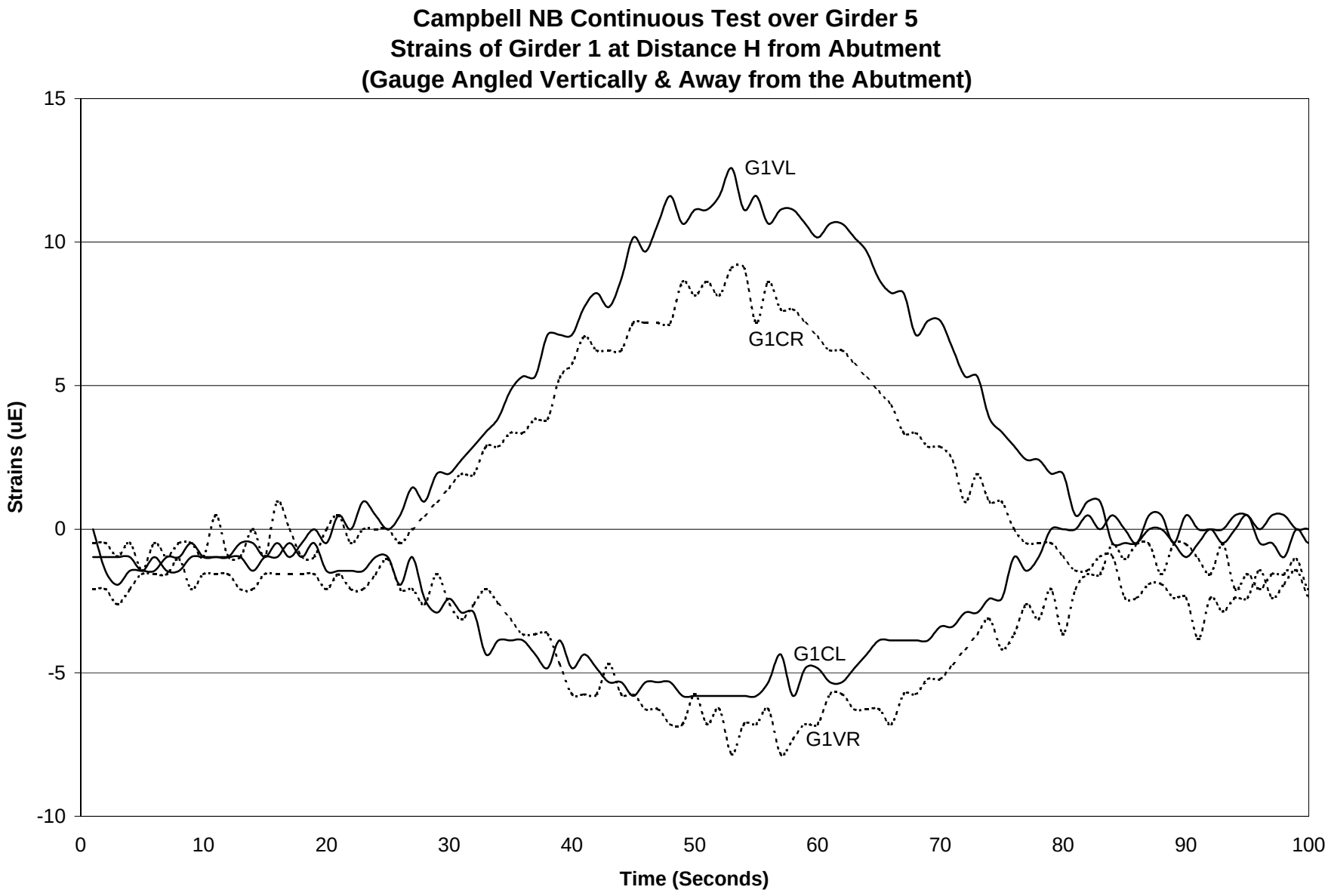
Campbell NB Continuous Test over Girder 5
Strains of Girder 1 at Distance H from Abutment
(Gauge Angled Vertically & Away from the Abutment)
G1VL
G1CR
G1CL
G1VR
Strains (uE)
Time (Seconds)
15
10
5
0
-5
-10
0
10
20
30
40
50
60
70
80
90
100

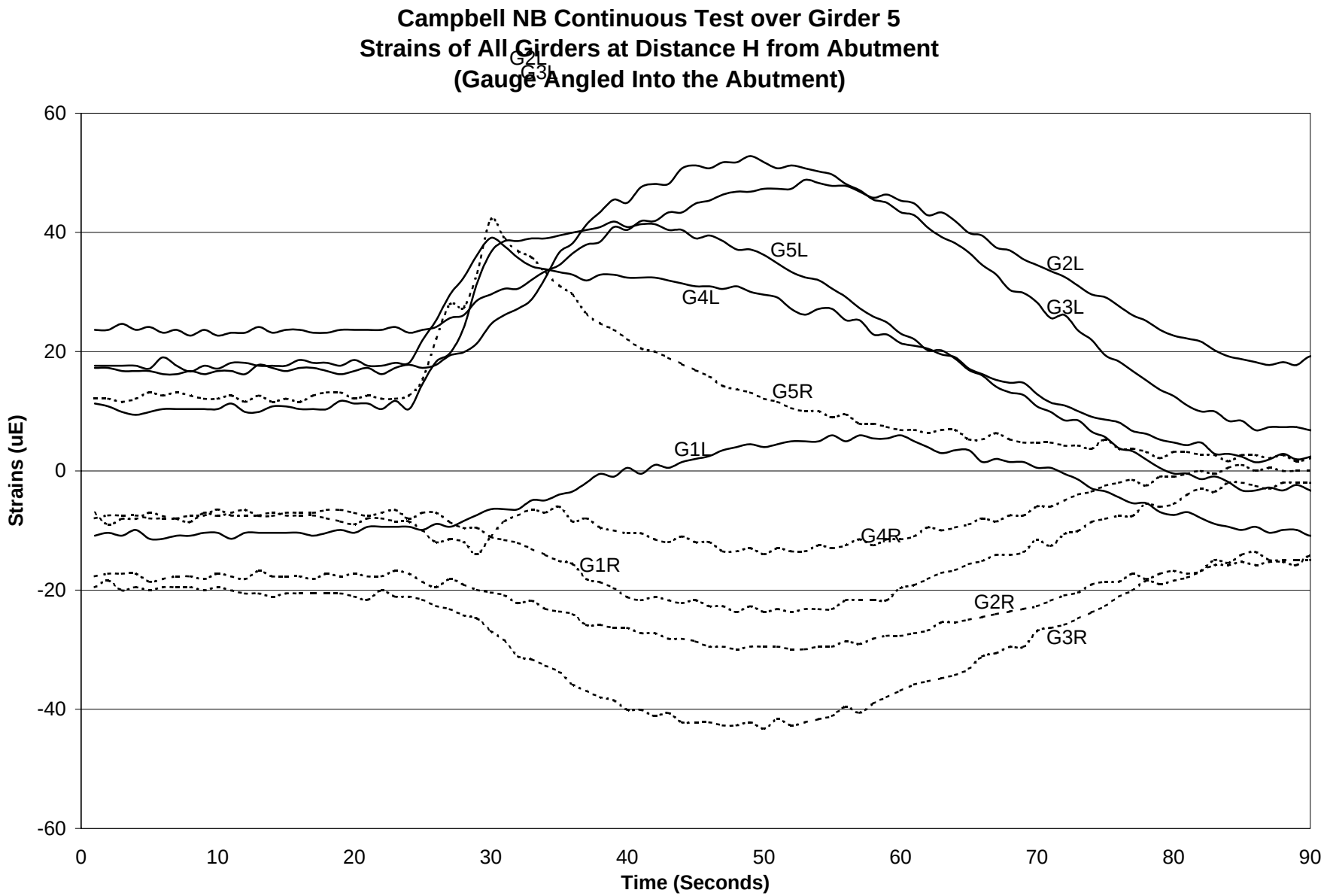
Campbell NB Continuous Test over Girder 5
Strains of All Girders at Distance H from Abutment
(Gauge Angled Into the Abutment)
G2L
G3L
G5L
G4L
G5R
G1L
G4R
G1R
G2R
G3R
Strains (uE)
Time (Seconds)
60
40
20
0
-20
-40
-60
0
10
20
30
40
50
60
70
80
90

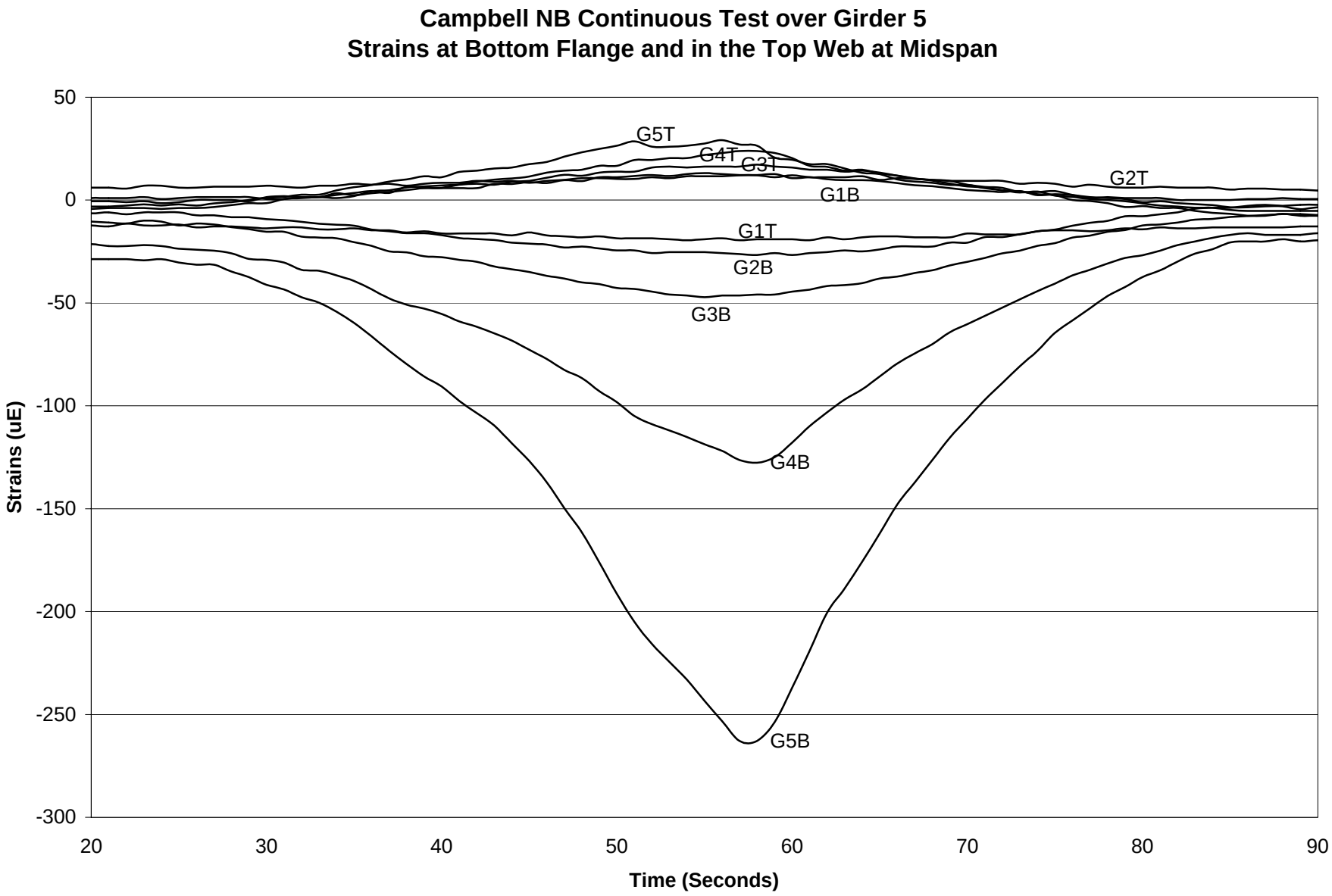
Campbell NB Continuous Test over Girder 5
Strains at Bottom Flange and in the Top Web at Midspan
Strains (uE)
Time (Seconds)
50
0
-50
-100
-150
-200
-250
-300
20
30
40
50
60
70
80
90
G5T
G4T
G3T
G2T
G1B
G1T
G2B
G3B
G4B
G5B

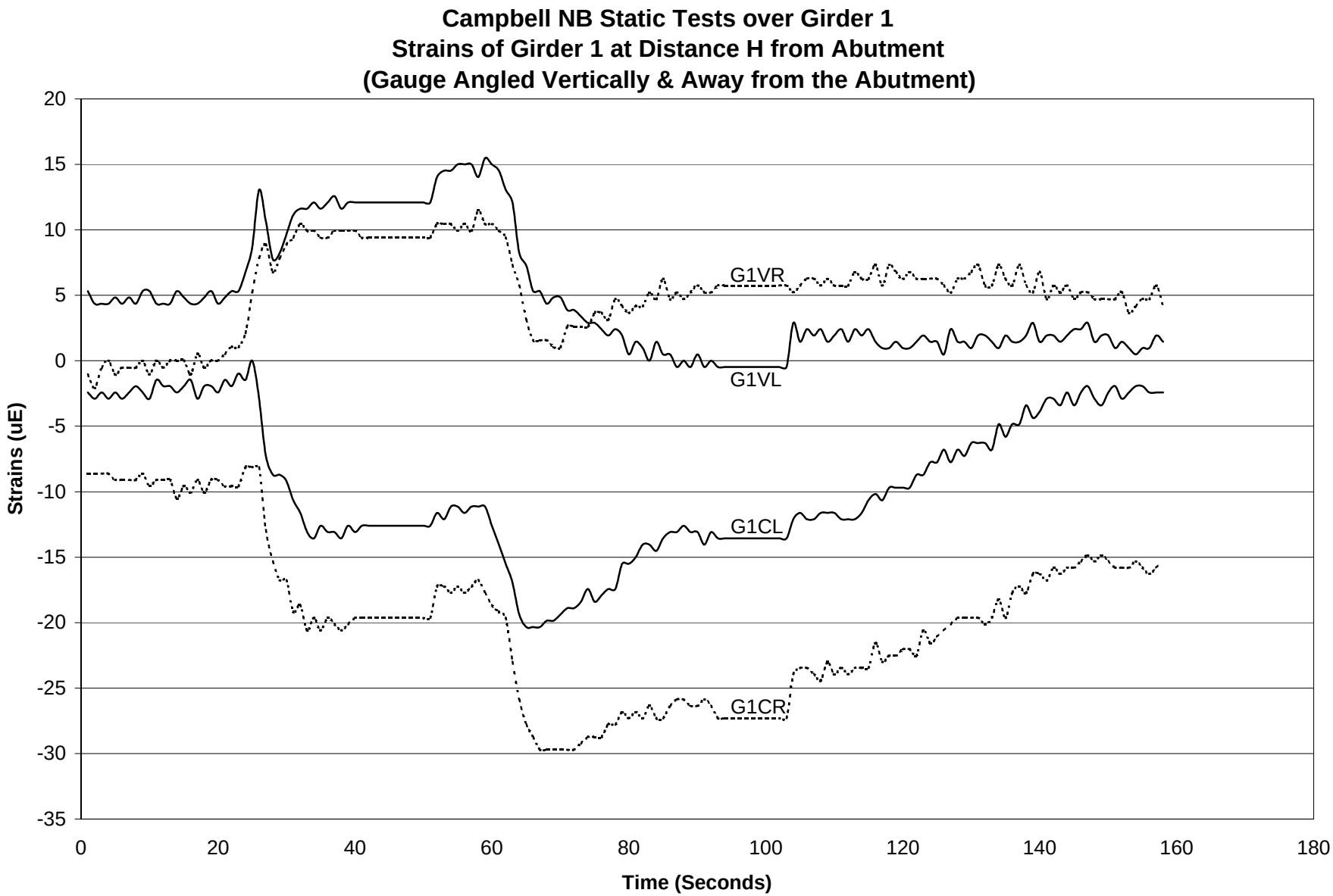
Campbell NB Static Tests over Girder 1
Strains of Girder 1 at Distance H from Abutment
(Gauge Angled Vertically & Away from the Abutment)
Strains (uE)
Time (Seconds)
G1VR
G1VL
G1CL
G1CR
20
15
10
5
0
-5
-10
-15
-20
-25
-30
-35
0
20
40
60
80
100
120
140
160
180

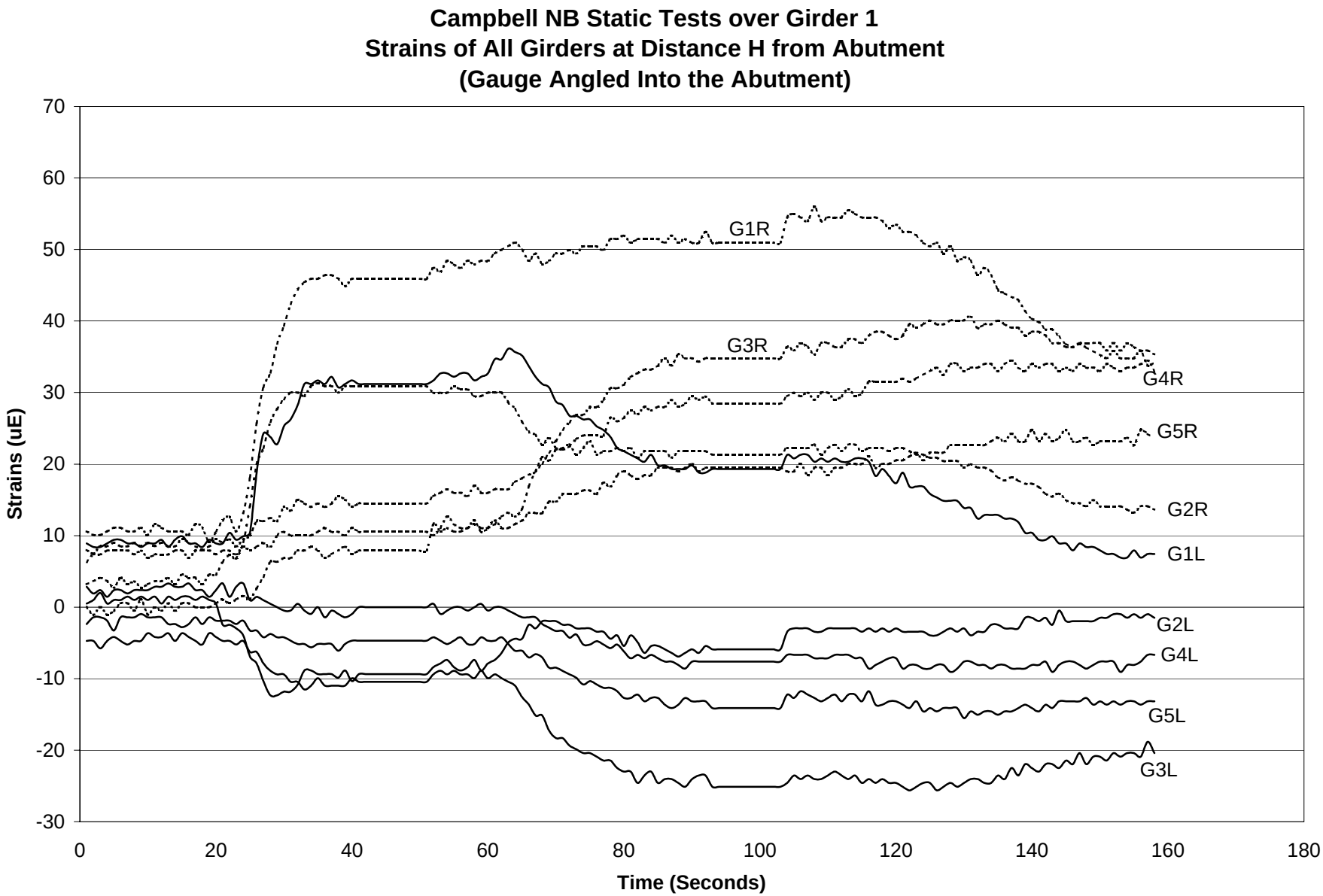
Campbell NB Static Tests over Girder 1
Strains of All Girders at Distance H from Abutment
(Gauge Angled Into the Abutment)
Strains (uE)
Time (Seconds)
70
60
50
40
30
20
10
0
-10
-20
-30
0
20
40
60
80
100
120
140
160
180
G1R
G3R
G4R
G5R
G2R
G1L
G2L
G4L
G5L
G3L

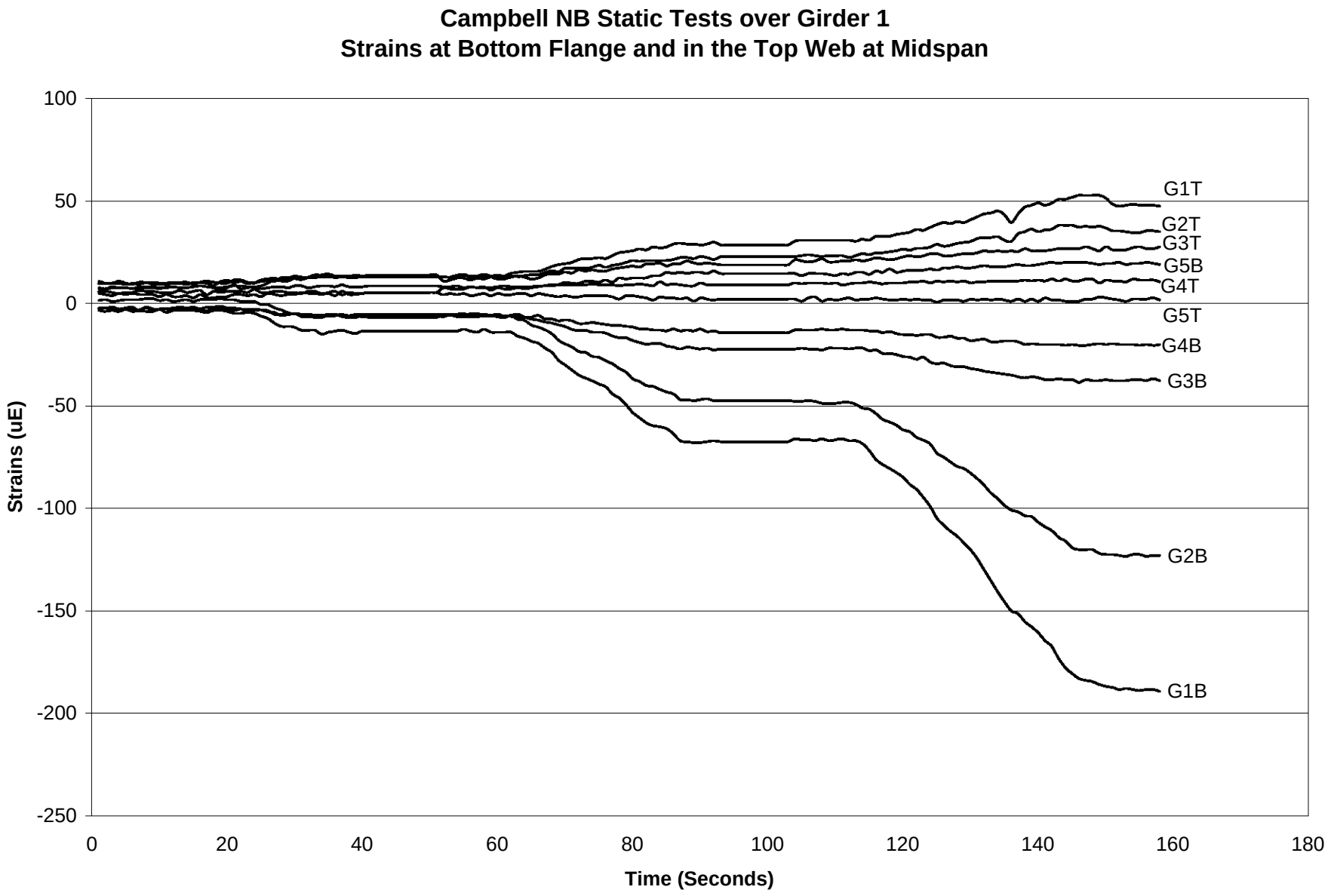
Campbell NB Static Tests over Girder 1
Strains at Bottom Flange and in the Top Web at Midspan
Strains (uE)
Time (Seconds)
100
50
0
-50
-100
-150
-200
-250
0
20
40
60
80
100
120
140
160
180
G1T
G2T
G3T
G5B
G4T
G5T
G4B
G3B
G2B
G1B

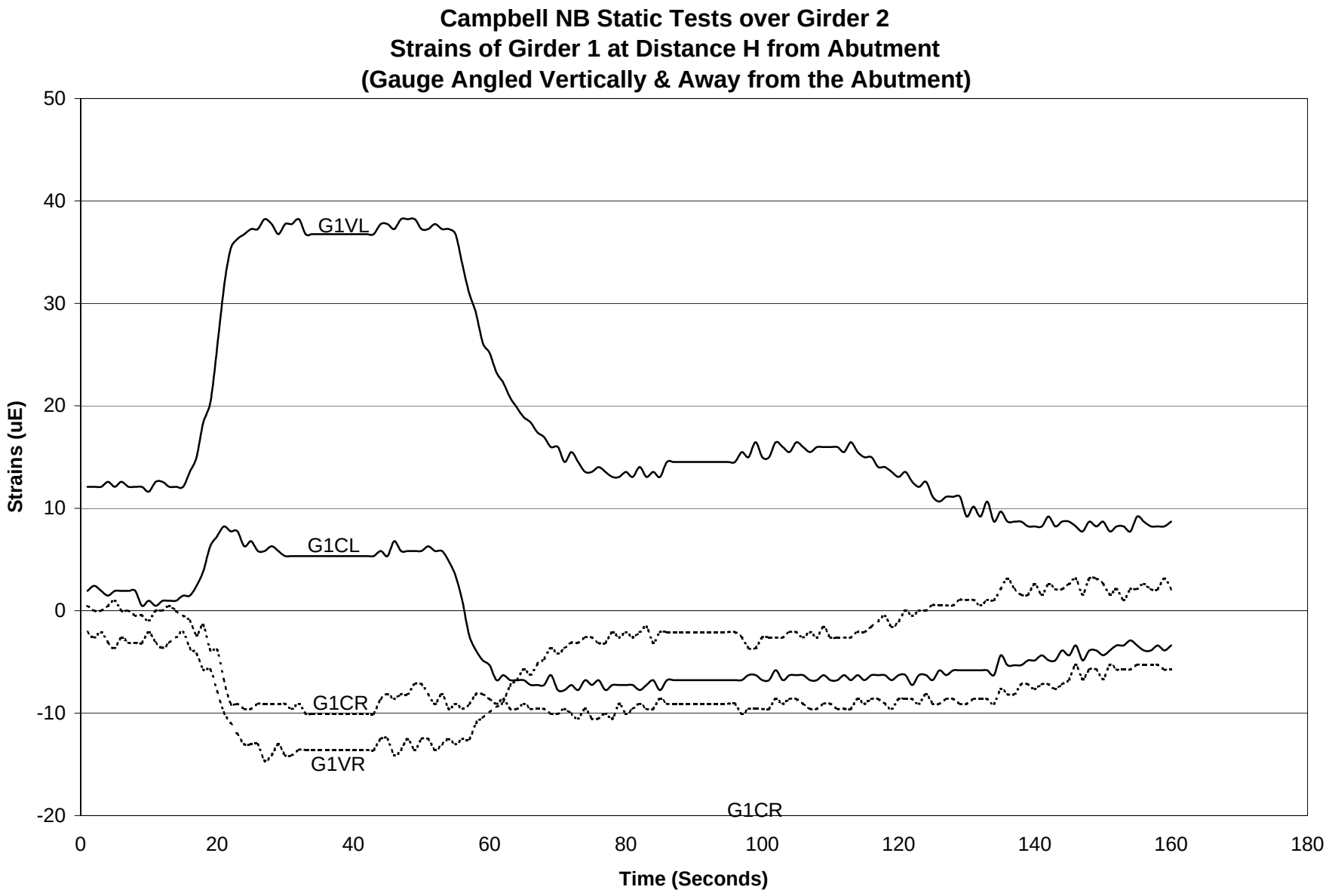
Campbell NB Static Tests over Girder 2
Strains of Girder 1 at Distance H from Abutment
(Gauge Angled Vertically & Away from the Abutment)
Strains (uE)
Time (Seconds)
G1VL
G1CL
G1CR
G1VR
G1CR
50
40
30
20
10
0
-10
-20
0
20
40
60
80
100
120
140
160
180

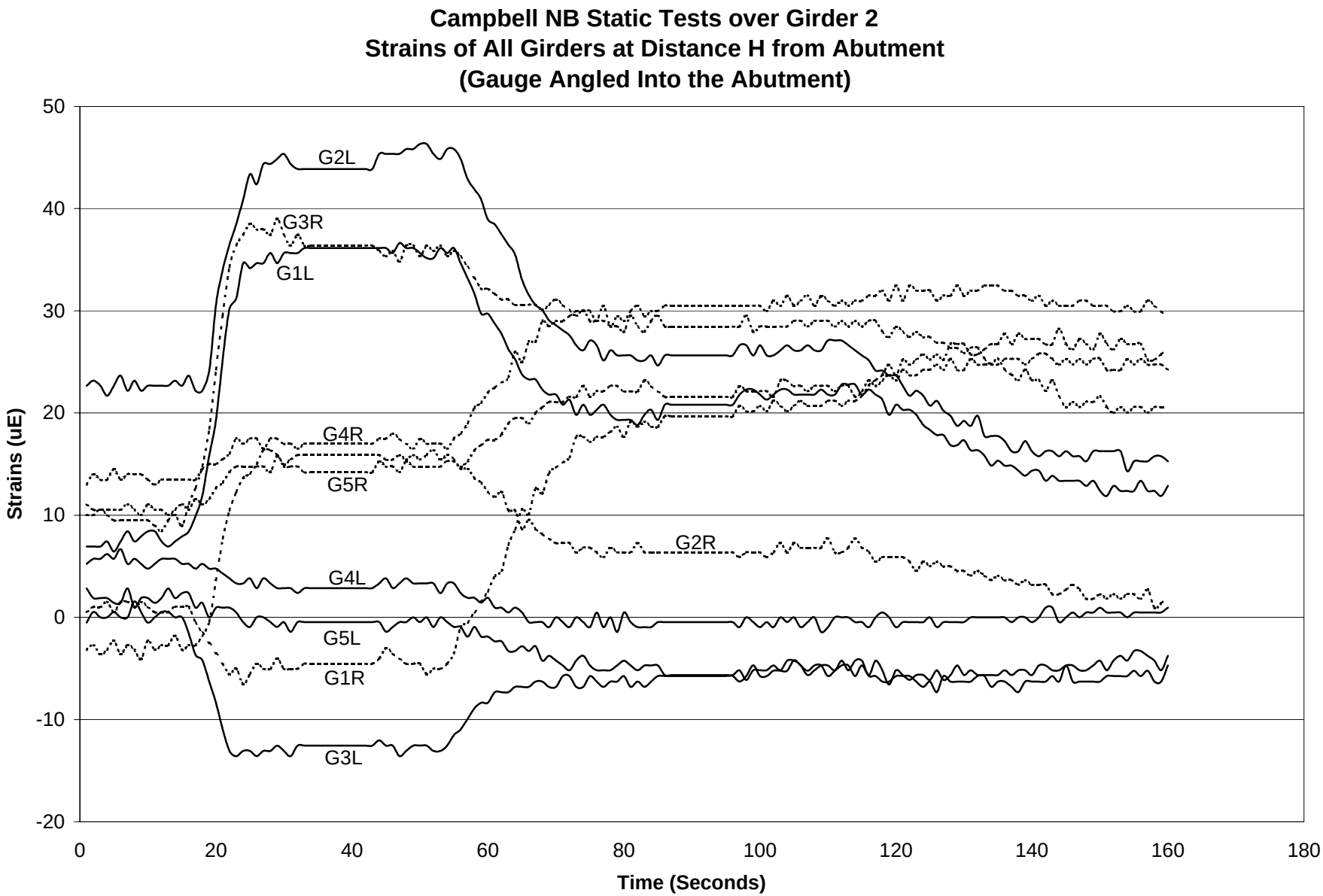
Campbell NB Static Tests over Girder 2
Strains of All Girders at Distance H from Abutment
(Gauge Angled Into the Abutment)
Strains (uE)
Time (Seconds)
50
40
30
20
10
0
-10
-20
0
20
40
60
80
100
120
140
160
180
G2L
G3R
G1L
G4R
G5R
G2R
G4L
G5L
G1R
G3L

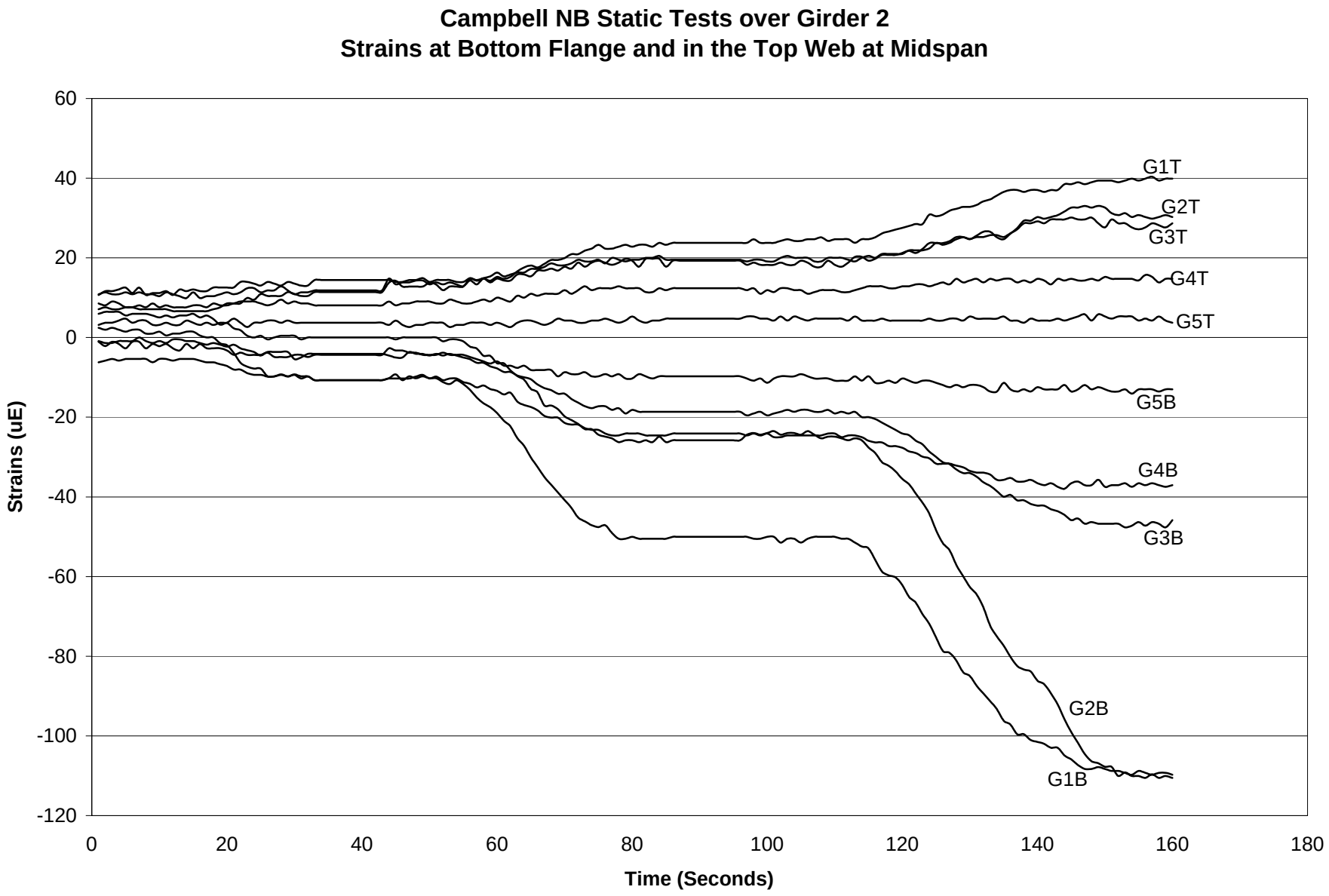
Campbell NB Static Tests over Girder 2
Strains at Bottom Flange and in the Top Web at Midspan
Strains (uE)
Time (Seconds)
60
40
20
0
-20
-40
-60
-80
-100
-120
0
20
40
60
80
100
120
140
160
180
G1T
G2T
G3T
G4T
G5T
G5B
G4B
G3B
G2B
G1B

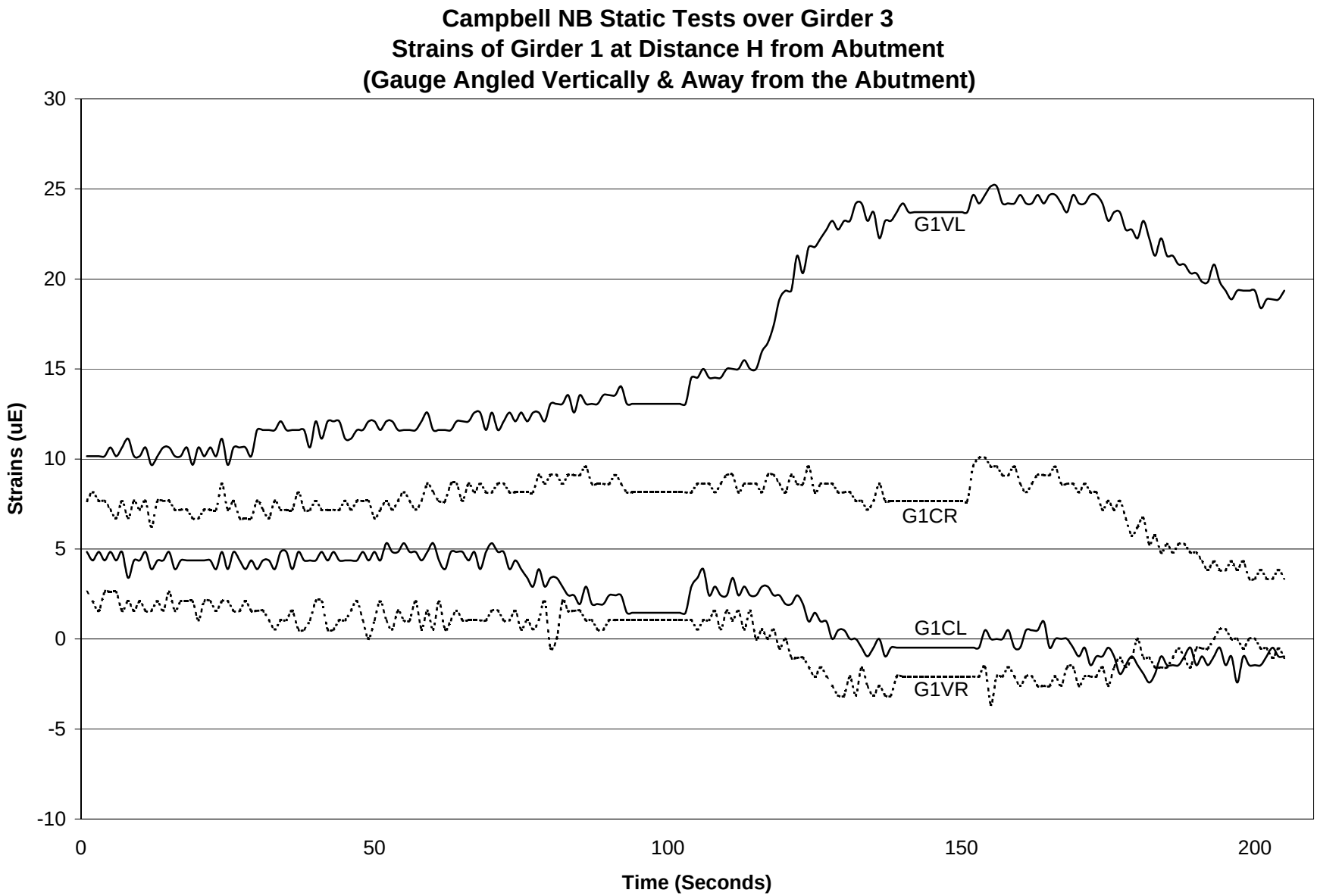
Campbell NB Static Tests over Girder 3
Strains of Girder 1 at Distance H from Abutment
(Gauge Angled Vertically & Away from the Abutment)
Strains (uE)
30
25
20
15
10
5
0
-5
-10
0
50
100
150
200
Time (Seconds)
G1VL
G1CR
G1CL
G1VR

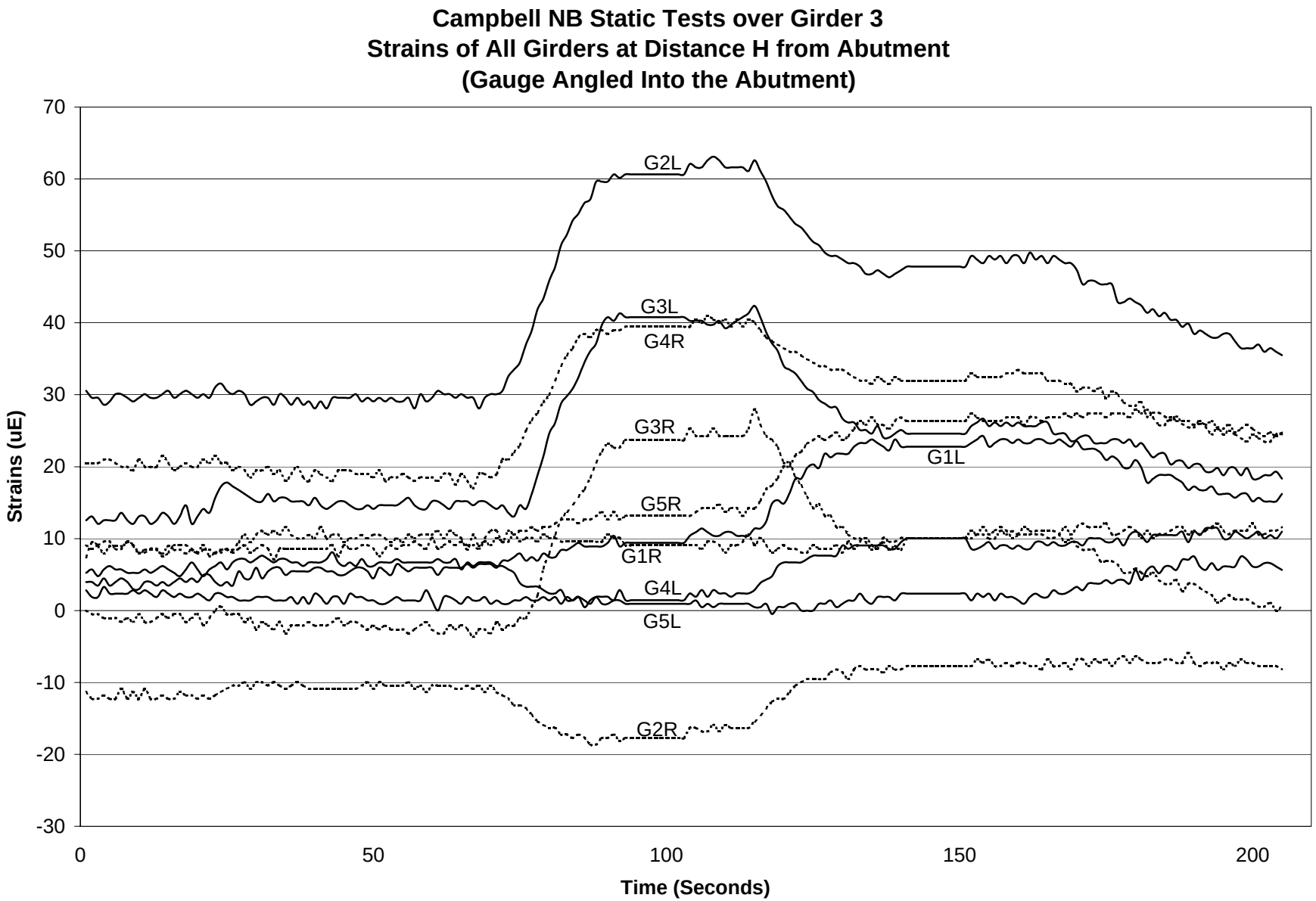
Campbell NB Static Tests over Girder 3
Strains of All Girders at Distance H from Abutment
(Gauge Angled Into the Abutment)
Strains (uE)
Time (Seconds)
70
60
50
40
30
20
10
0
-10
-20
-30
0
50
100
150
200
G2L
G3L
G4R
G3R
G1L
G5R
G1R
G4L
G5L
G2R

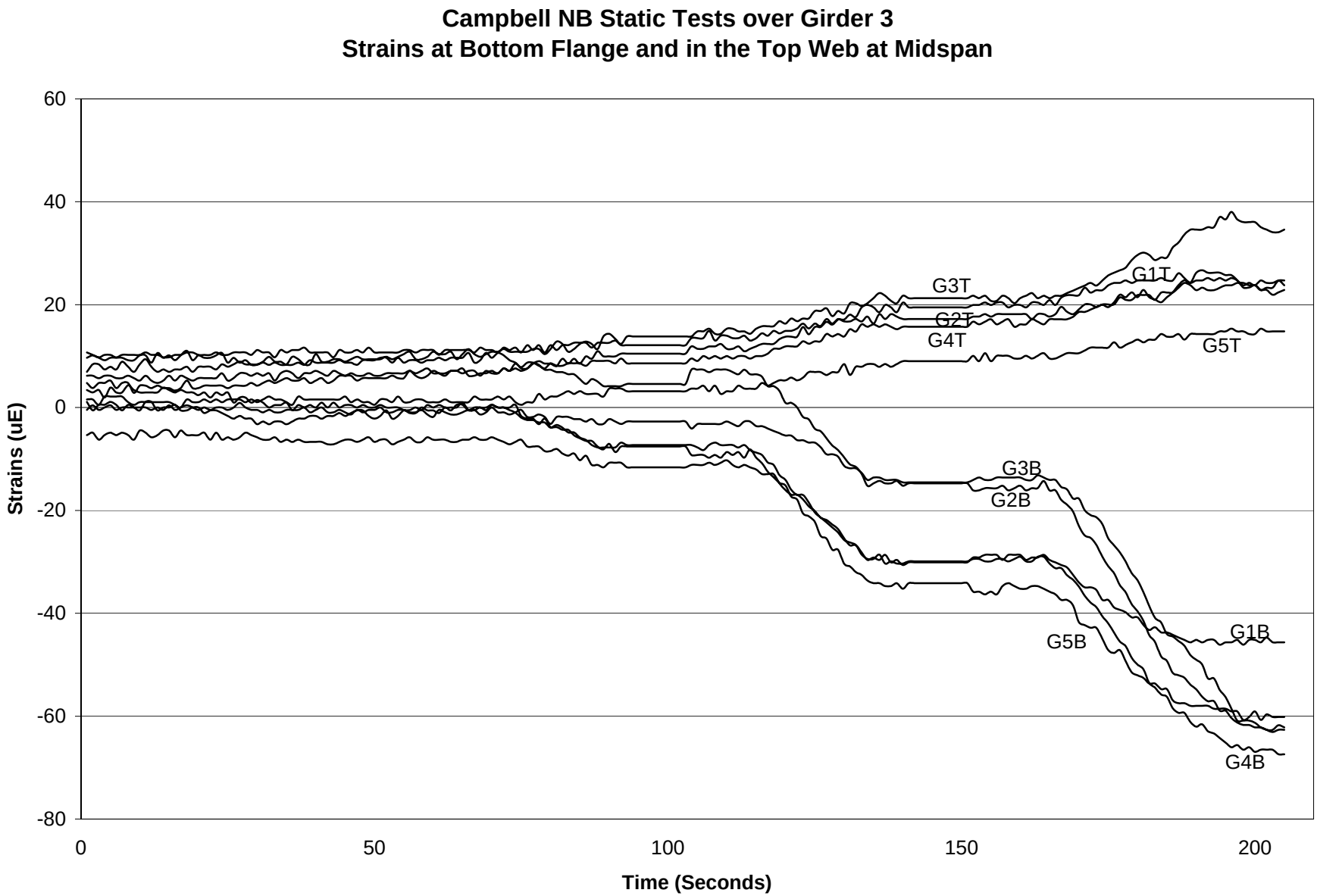
Campbell NB Static Tests over Girder 3
Strains at Bottom Flange and in the Top Web at Midspan
Strains (uE)
Time (Seconds)
60
40
20
0
-20
-40
-60
-80
0
50
100
150
200
G3T
G1T
G2T
G4T
G5T
G3B
G2B
G1B
G5B
G4B

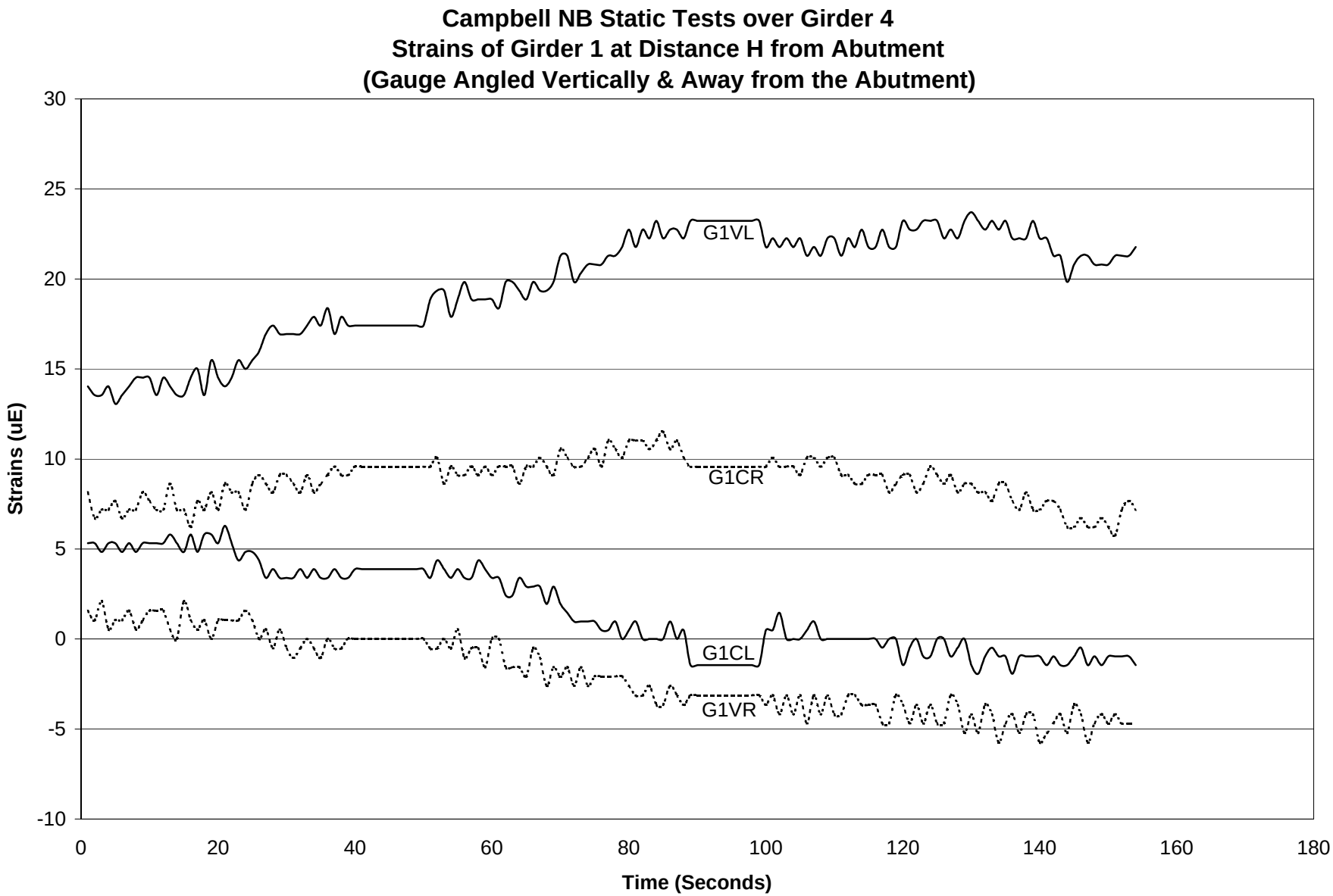
Campbell NB Static Tests over Girder 4
Strains of Girder 1 at Distance H from Abutment
(Gauge Angled Vertically & Away from the Abutment)
Strains (uE)
Time (Seconds)
G1VL
G1CR
G1CL
G1VR
30
25
20
15
10
5
0
-5
-10
0
20
40
60
80
100
120
140
160
180

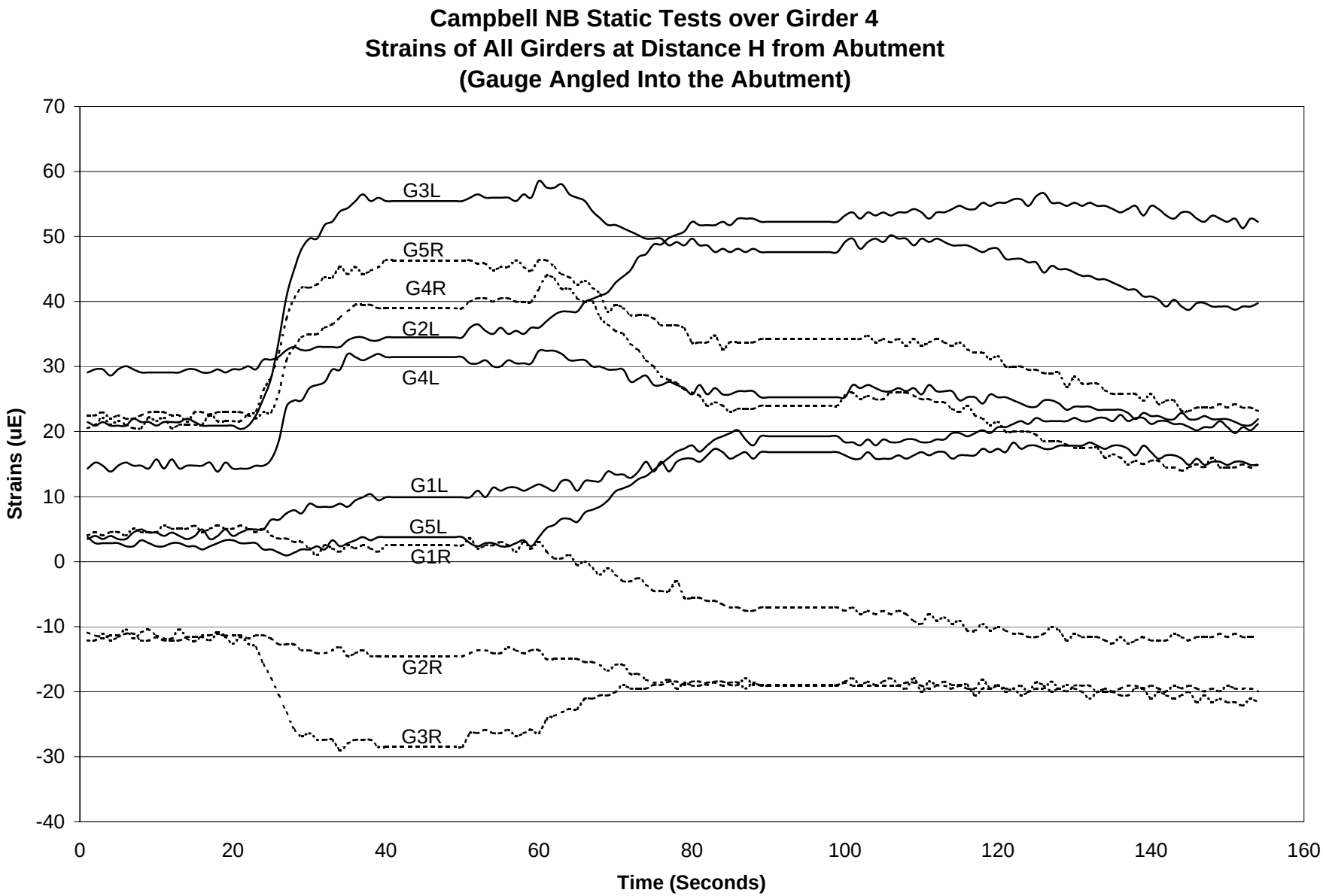
Campbell NB Static Tests over Girder 4
Strains of All Girders at Distance H from Abutment
(Gauge Angled Into the Abutment)
Strains (uE)
Time (Seconds)
70
60
50
40
30
20
10
0
-10
-20
-30
-40
0
20
40
60
80
100
120
140
160
G3L
G5R
G4R
G2L
G4L
G1L
G5L
G1R
G2R
G3R

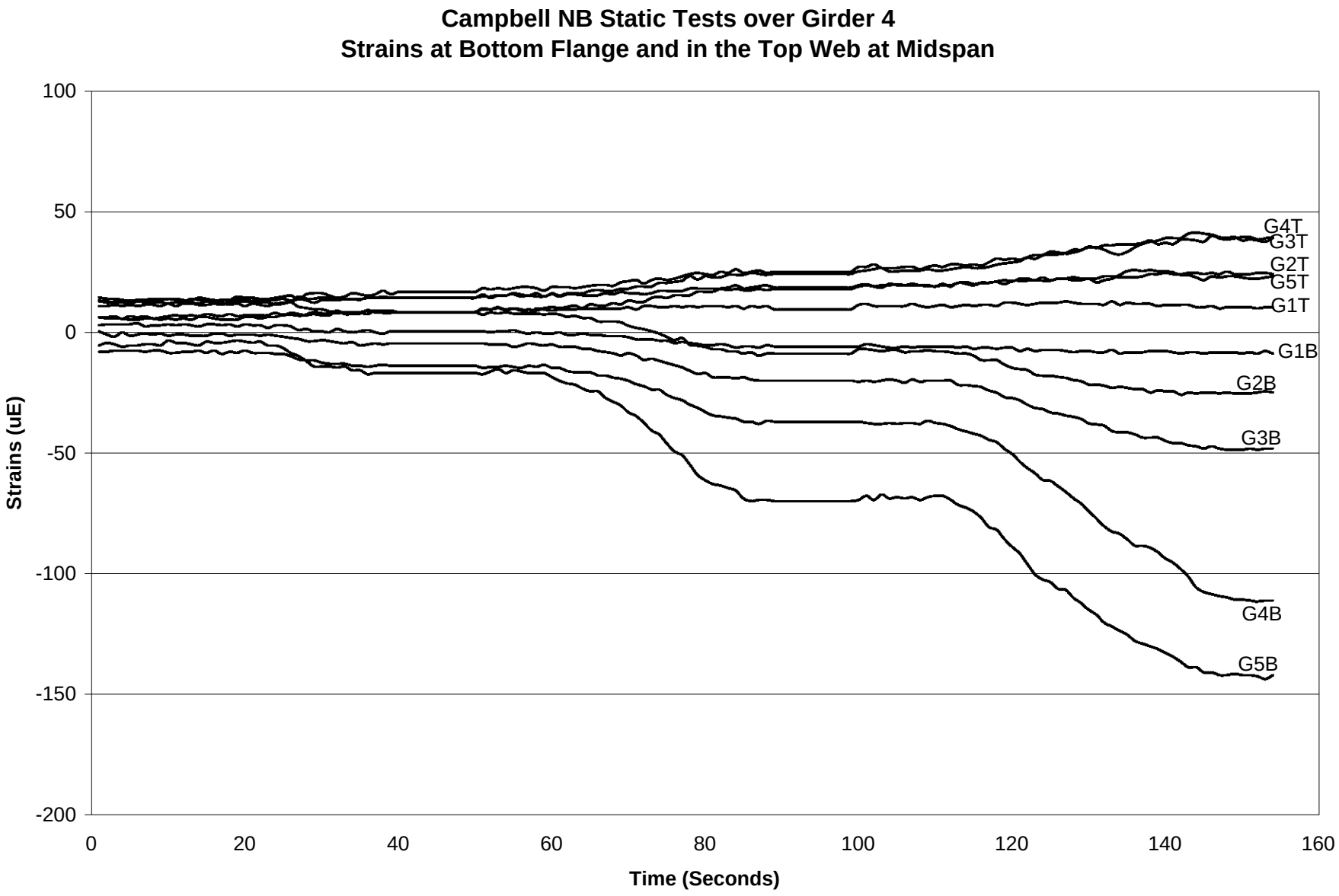
Campbell NB Static Tests over Girder 4
Strains at Bottom Flange and in the Top Web at Midspan
Strains (uE)
Time (Seconds)
100
50
0
-50
-100
-150
-200
0
20
40
60
80
100
120
140
160
G4T
G3T
G2T
G5T
G1T
G1B
G2B
G3B
G4B
G5B

# Campbell SB

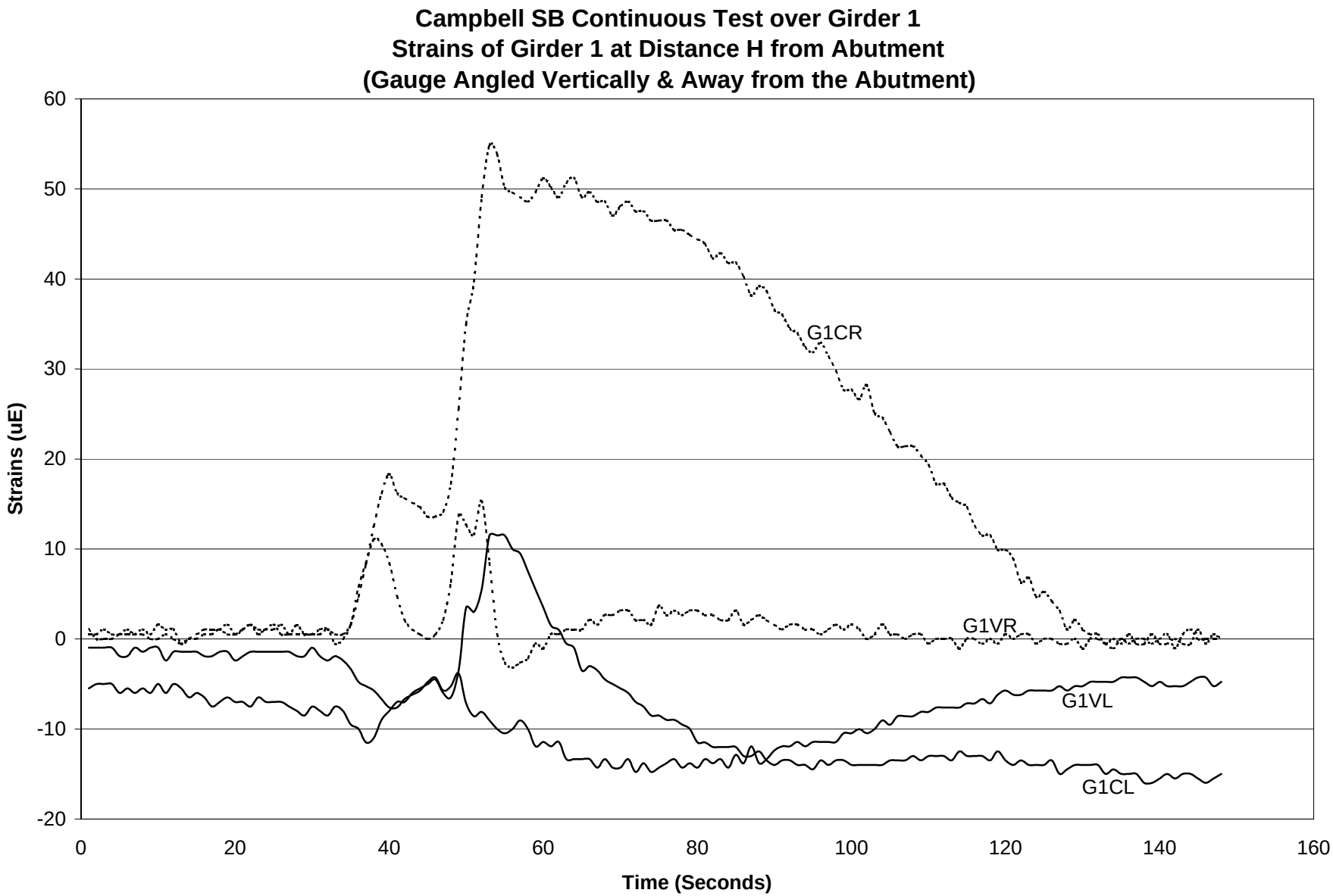
Campbell SB Continuous Test over Girder 1
Strains of Girder 1 at Distance H from Abutment
(Gauge Angled Vertically & Away from the Abutment)
Strains (uE)
Time (Seconds)
60
50
40
30
20
10
0
-10
-20
0
20
40
60
80
100
120
140
160
G1CR
G1VR
G1VL
G1CL

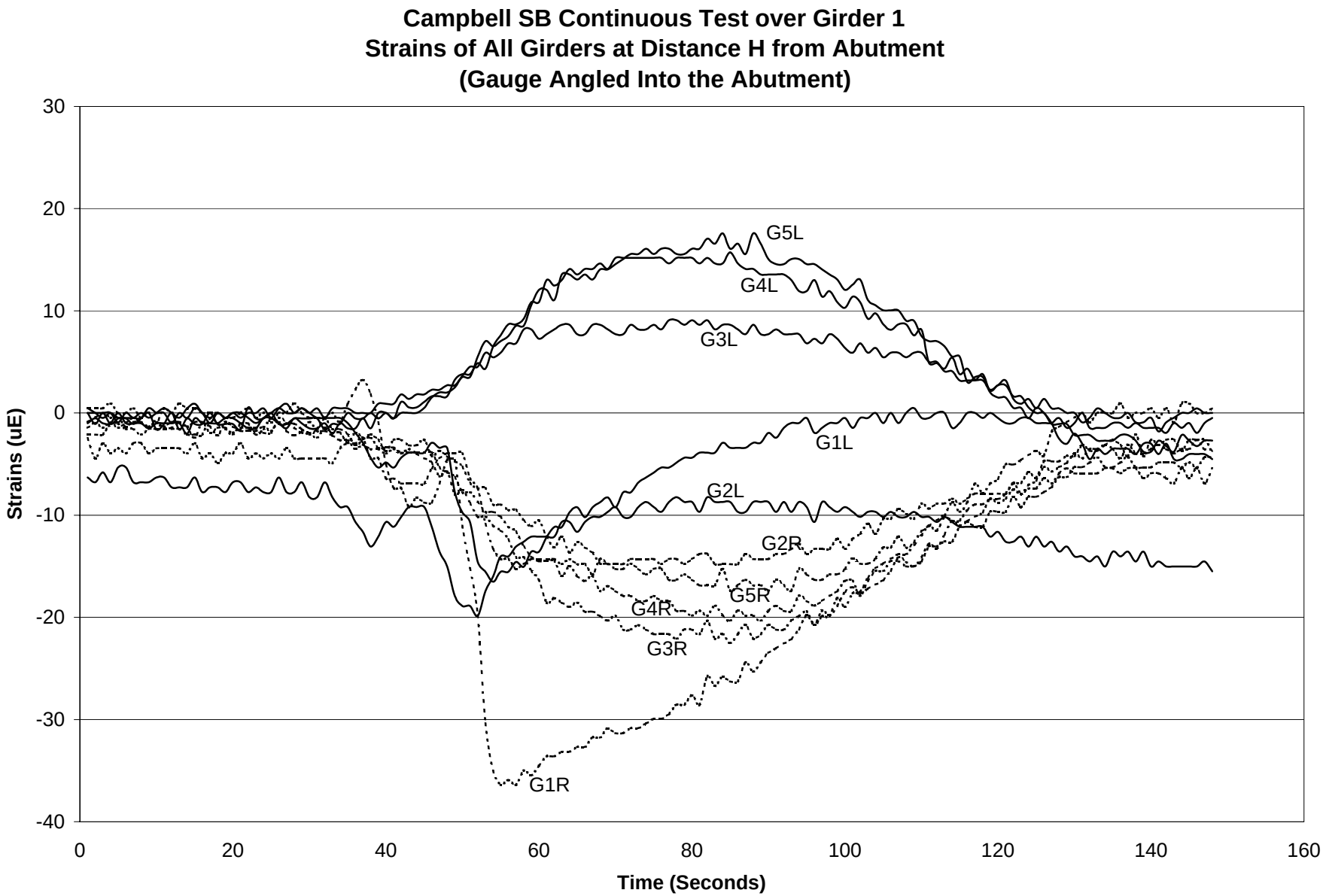
Campbell SB Continuous Test over Girder 1
Strains of All Girders at Distance H from Abutment
(Gauge Angled Into the Abutment)
Strains (uE)
Time (Seconds)
30
20
10
0
-10
-20
-30
-40
0
20
40
60
80
100
120
140
160
G5L
G4L
G3L
G1L
G2L
G2R
G5R
G4R
G3R
G1R

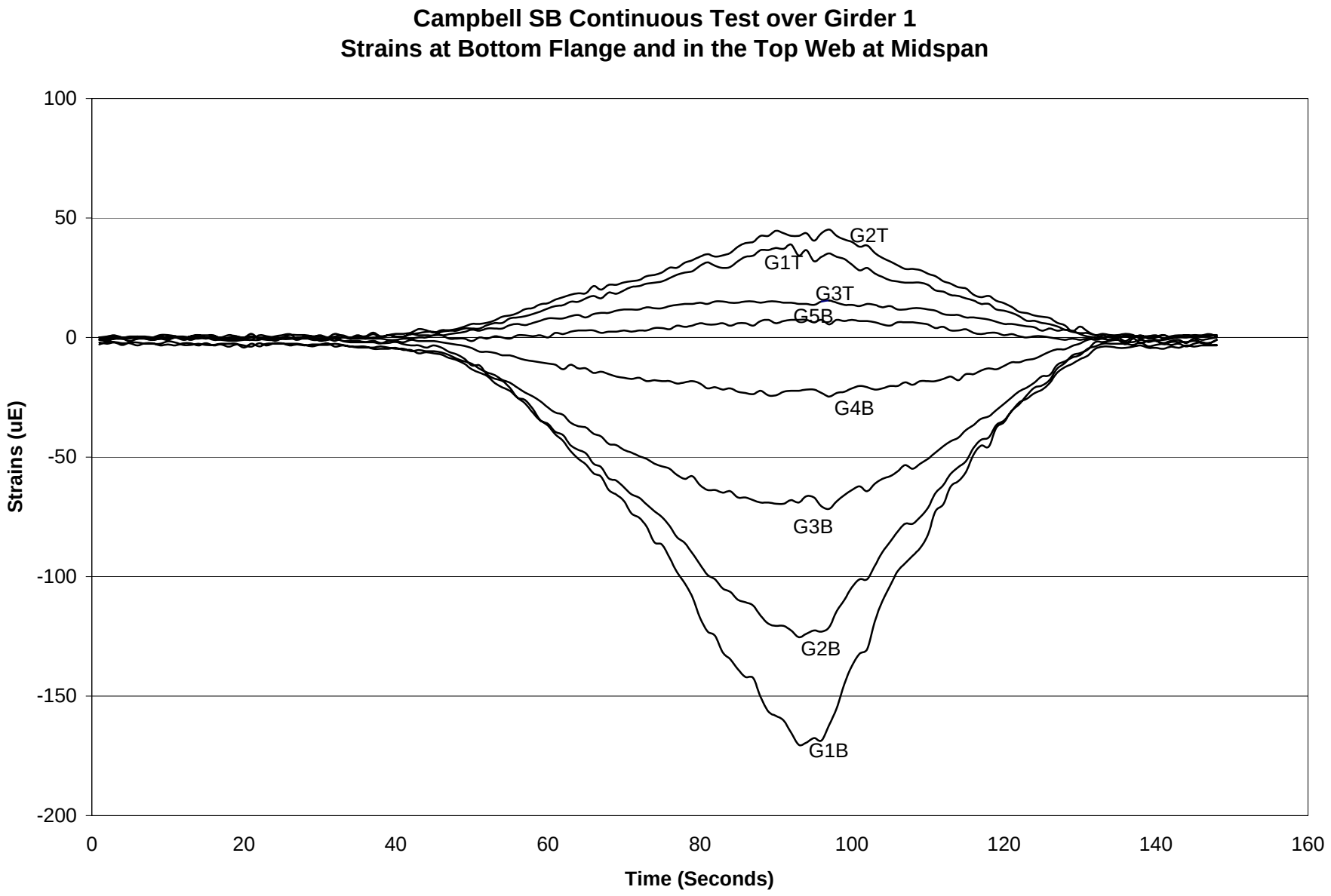
Campbell SB Continuous Test over Girder 1
Strains at Bottom Flange and in the Top Web at Midspan
100
50
0
-50
-100
-150
-200
Strains (uE)
0
20
40
60
80
100
120
140
160
Time (Seconds)
G2T
G1T
G3T
G5B
G4B
G3B
G2B
G1B

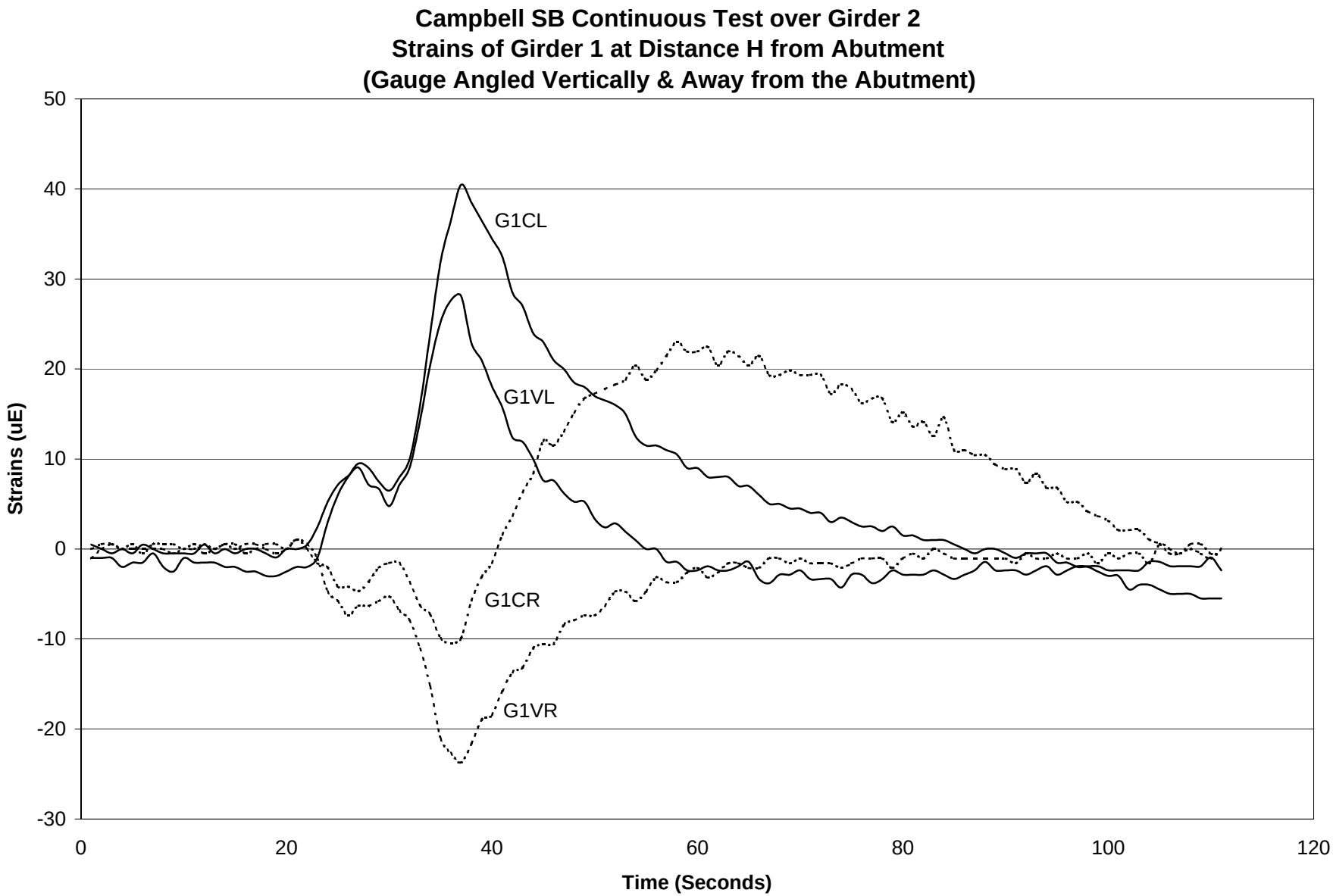
Campbell SB Continuous Test over Girder 2
Strains of Girder 1 at Distance H from Abutment
(Gauge Angled Vertically & Away from the Abutment)
Strains (uE)
Time (Seconds)
G1CL
G1VL
G1CR
G1VR
50
40
30
20
10
0
-10
-20
-30
0
20
40
60
80
100
120

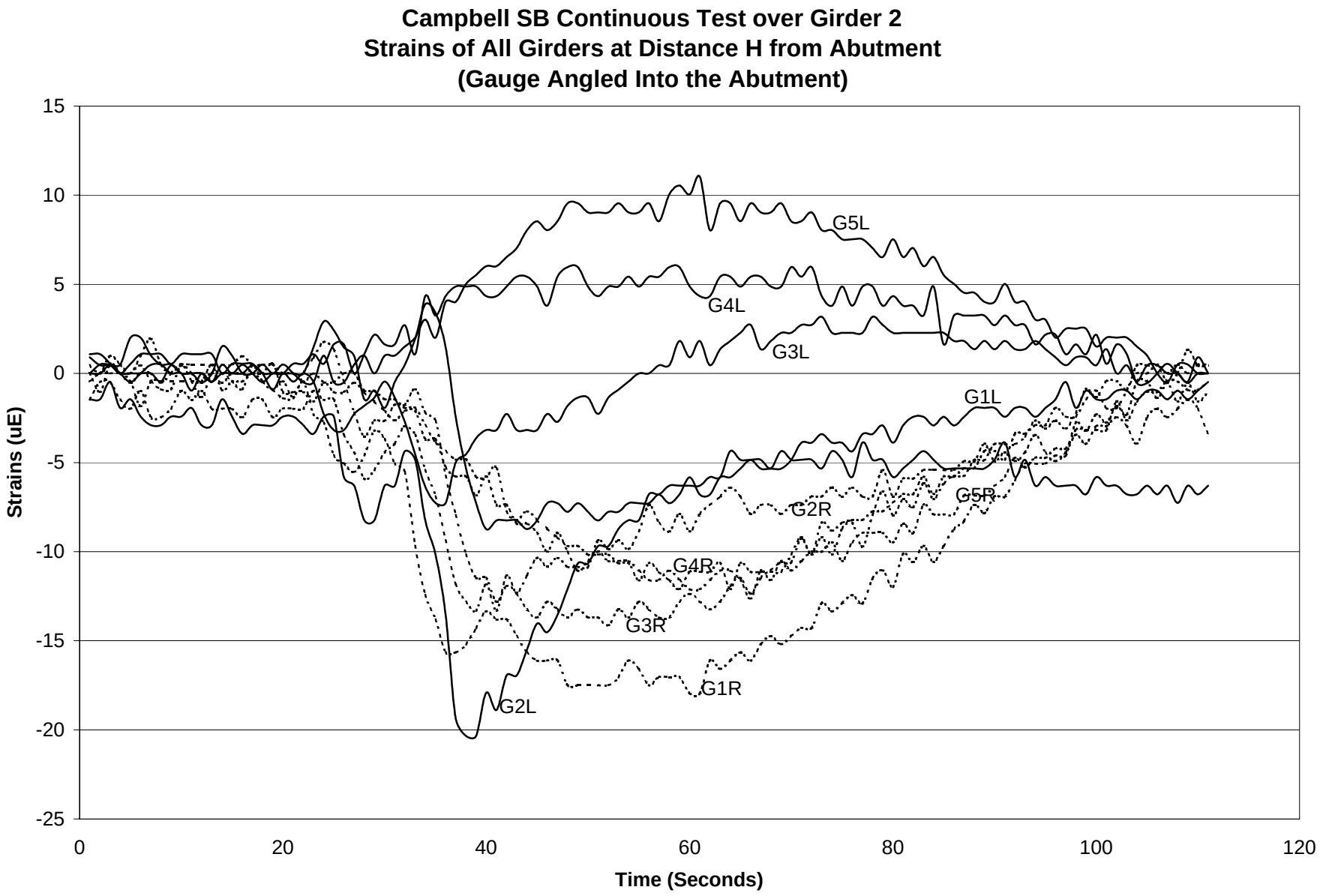
Campbell SB Continuous Test over Girder 2
Strains of All Girders at Distance H from Abutment
(Gauge Angled Into the Abutment)
Strains (uE)
Time (Seconds)
15
10
5
0
-5
-10
-15
-20
-25
0
20
40
60
80
100
120
G5L
G4L
G3L
G1L
G5R
G2R
G4R
G3R
G1R
G2L

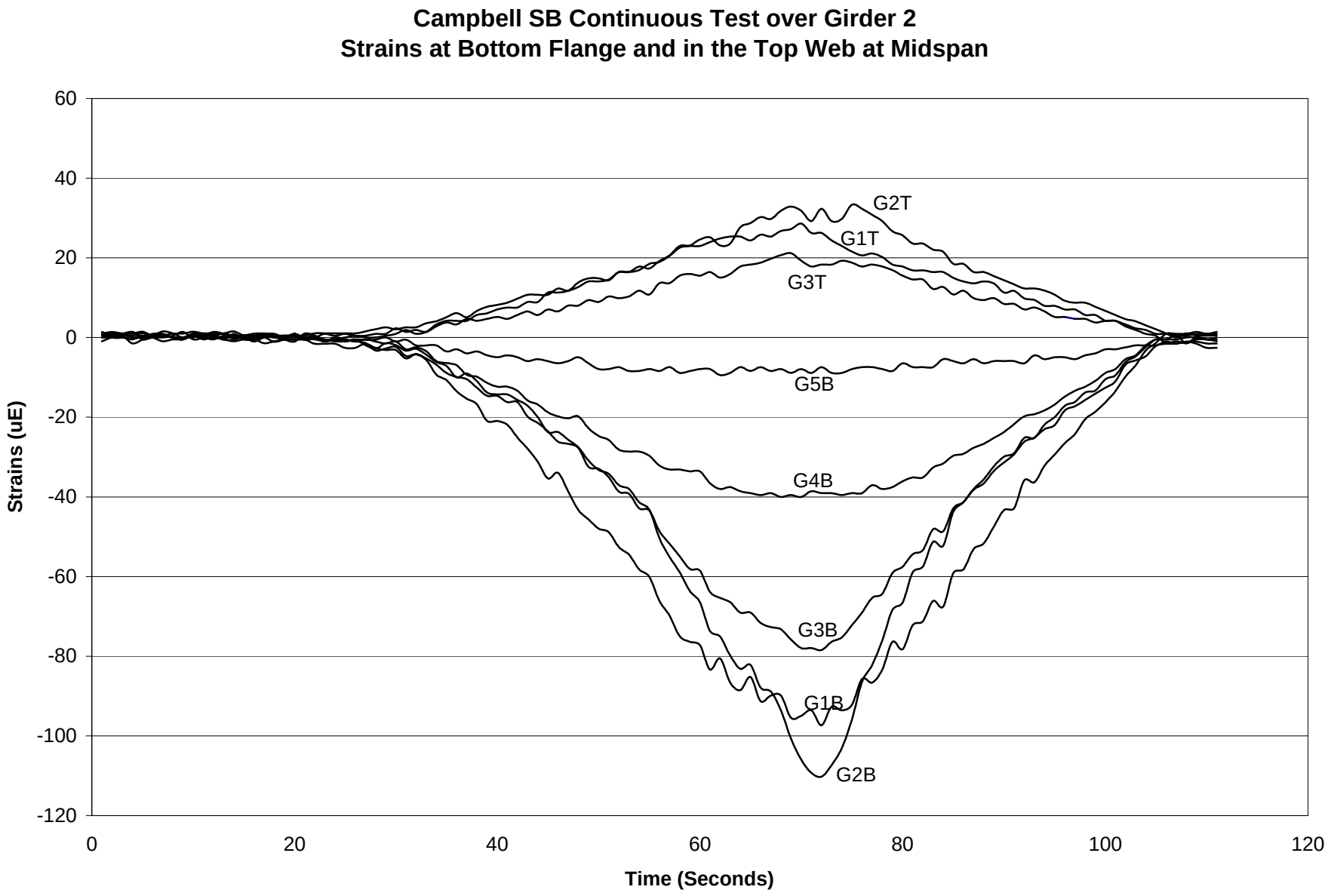
Campbell SB Continuous Test over Girder 2
Strains at Bottom Flange and in the Top Web at Midspan
Strains (uE)
Time (Seconds)
60
40
20
0
-20
-40
-60
-80
-100
-120
0
20
40
60
80
100
120
G2T
G1T
G3T
G5B
G4B
G3B
G1B
G2B

Campbell SB Continuous Test over Girder 3
Strains of Girder 1 at Distance H from Abutment
(Gauge Angled Vertically & Away from the Abutment)
Strains (uE)
Time (Seconds)
25
20
15
10
5
0
-5
-10
0
20
40
60
80
100
120
140
G1CL
G1VL
G1CR
G1VR

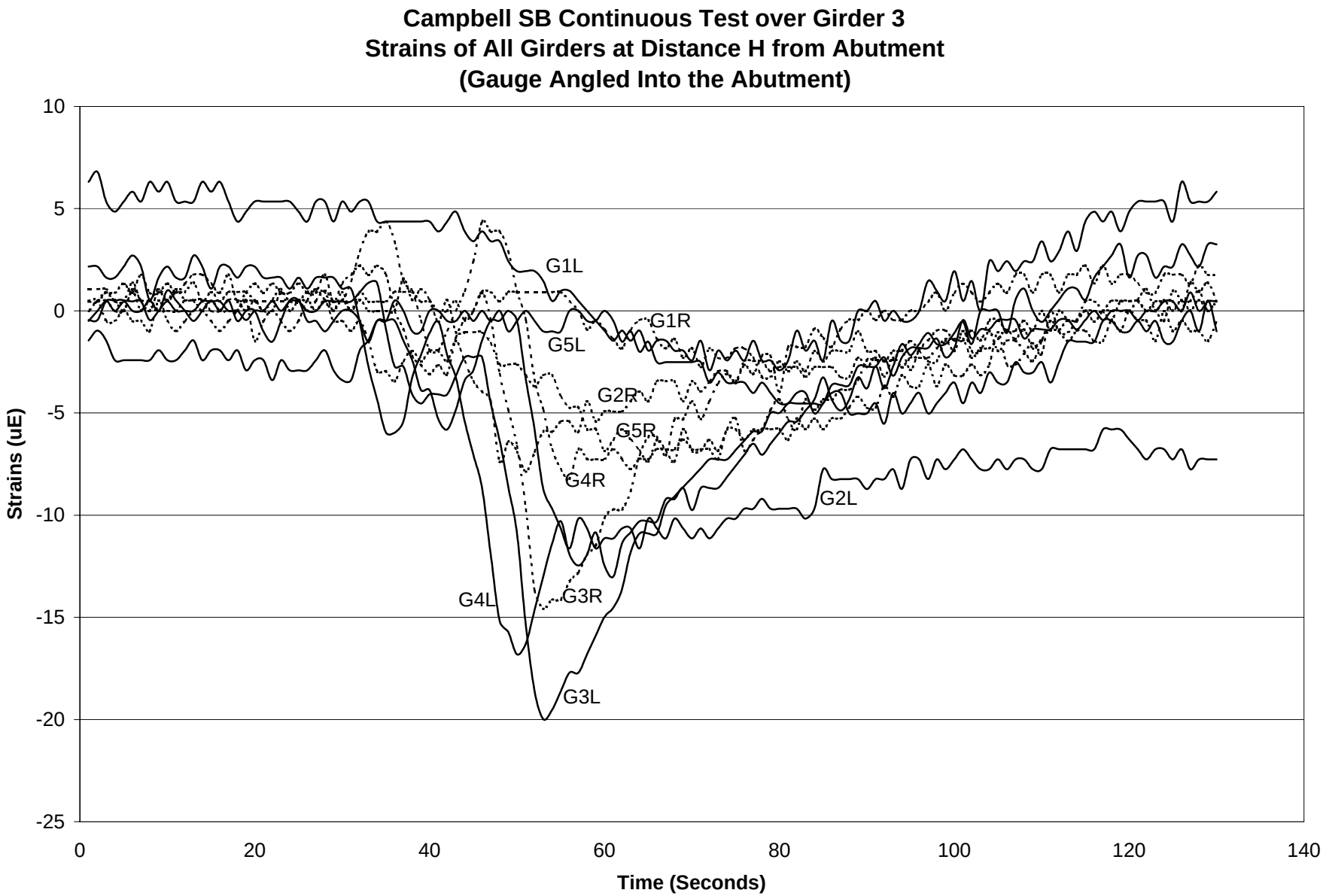
Campbell SB Continuous Test over Girder 3
Strains of All Girders at Distance H from Abutment
(Gauge Angled Into the Abutment)
Strains (uE)
Time (Seconds)
10
5
0
-5
-10
-15
-20
-25
0
20
40
60
80
100
120
140
G1L
G1R
G5L
G2R
G5R
G4R
G2L
G4L
G3R
G3L

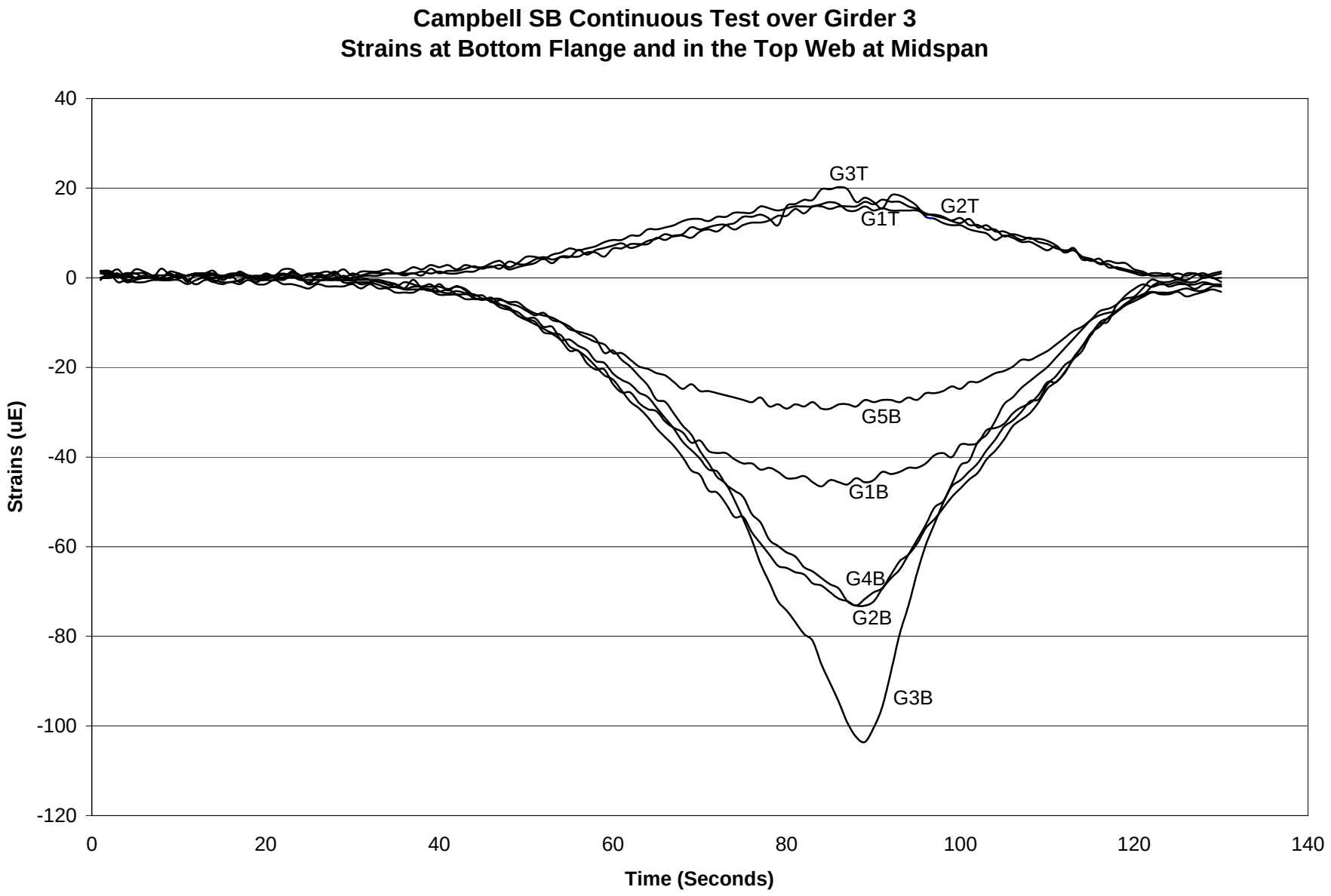
Campbell SB Continuous Test over Girder 3
Strains at Bottom Flange and in the Top Web at Midspan
Strains (uE)
Time (Seconds)
40
20
0
-20
-40
-60
-80
-100
-120
0
20
40
60
80
100
120
140
G3T
G2T
G1T
G5B
G1B
G4B
G2B
G3B

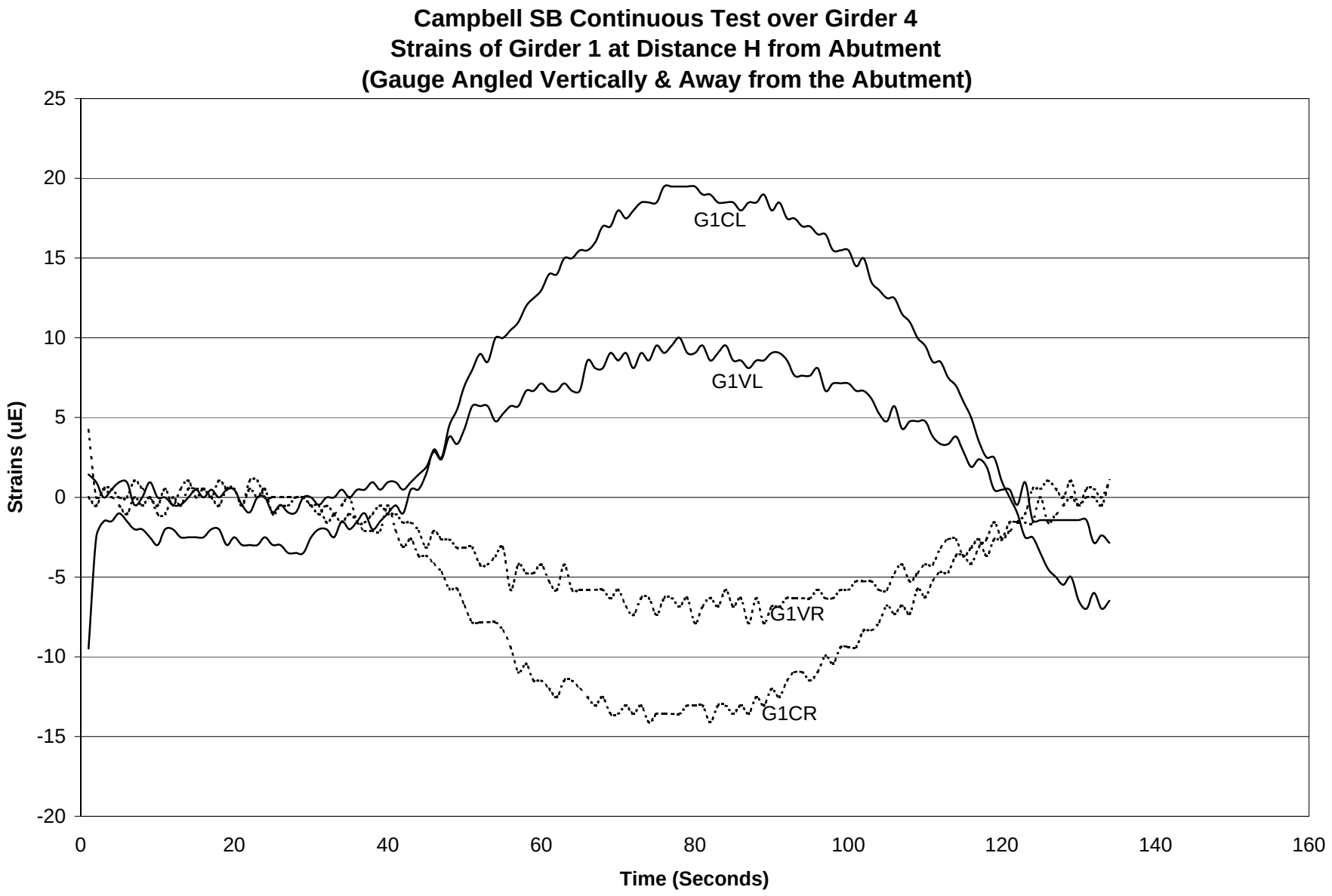
Campbell SB Continuous Test over Girder 4
Strains of Girder 1 at Distance H from Abutment
(Gauge Angled Vertically & Away from the Abutment)
Strains (uE)
Time (Seconds)
G1CL
G1VL
G1VR
G1CR
25
20
15
10
5
0
-5
-10
-15
-20
0
20
40
60
80
100
120
140
160

Campbell SB Continuous Test over Girder 4
Strains of All Girders at Distance H from Abutment
(Gauge Angled Into the Abutment)
Strains (uE)
Time (Seconds)
10
5
0
-5
-10
-15
-20
-25
-30
-35
-40
-45
0
20
40
60
80
100
120
140
160
G1R
G3R
G2R
G5R
G1L
G2L
G3L
G4R
G5L
G4L

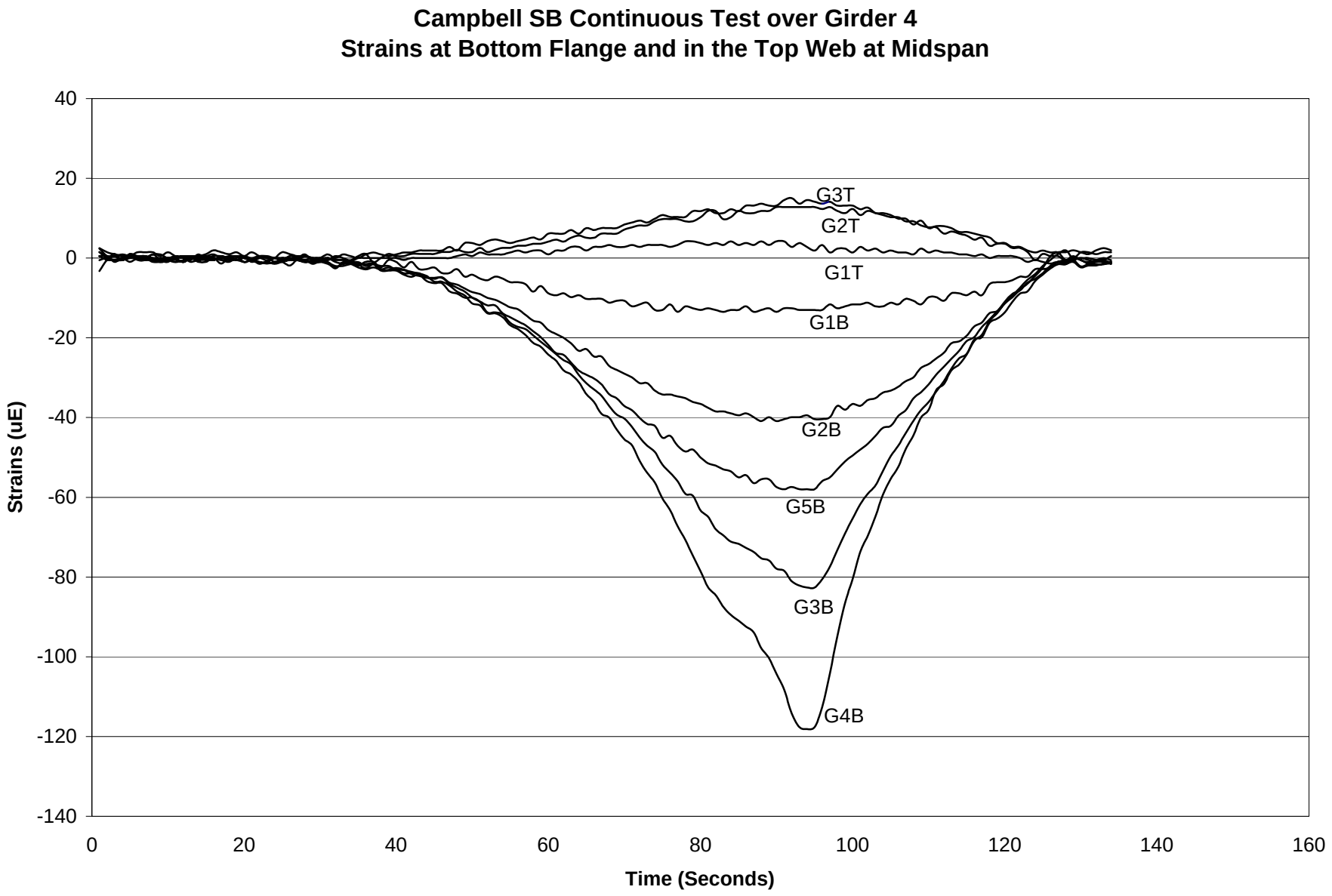
Campbell SB Continuous Test over Girder 4
Strains at Bottom Flange and in the Top Web at Midspan
Strains (uE)
Time (Seconds)
40
20
0
-20
-40
-60
-80
-100
-120
-140
0
20
40
60
80
100
120
140
160
G3T
G2T
G1T
G1B
G2B
G5B
G3B
G4B

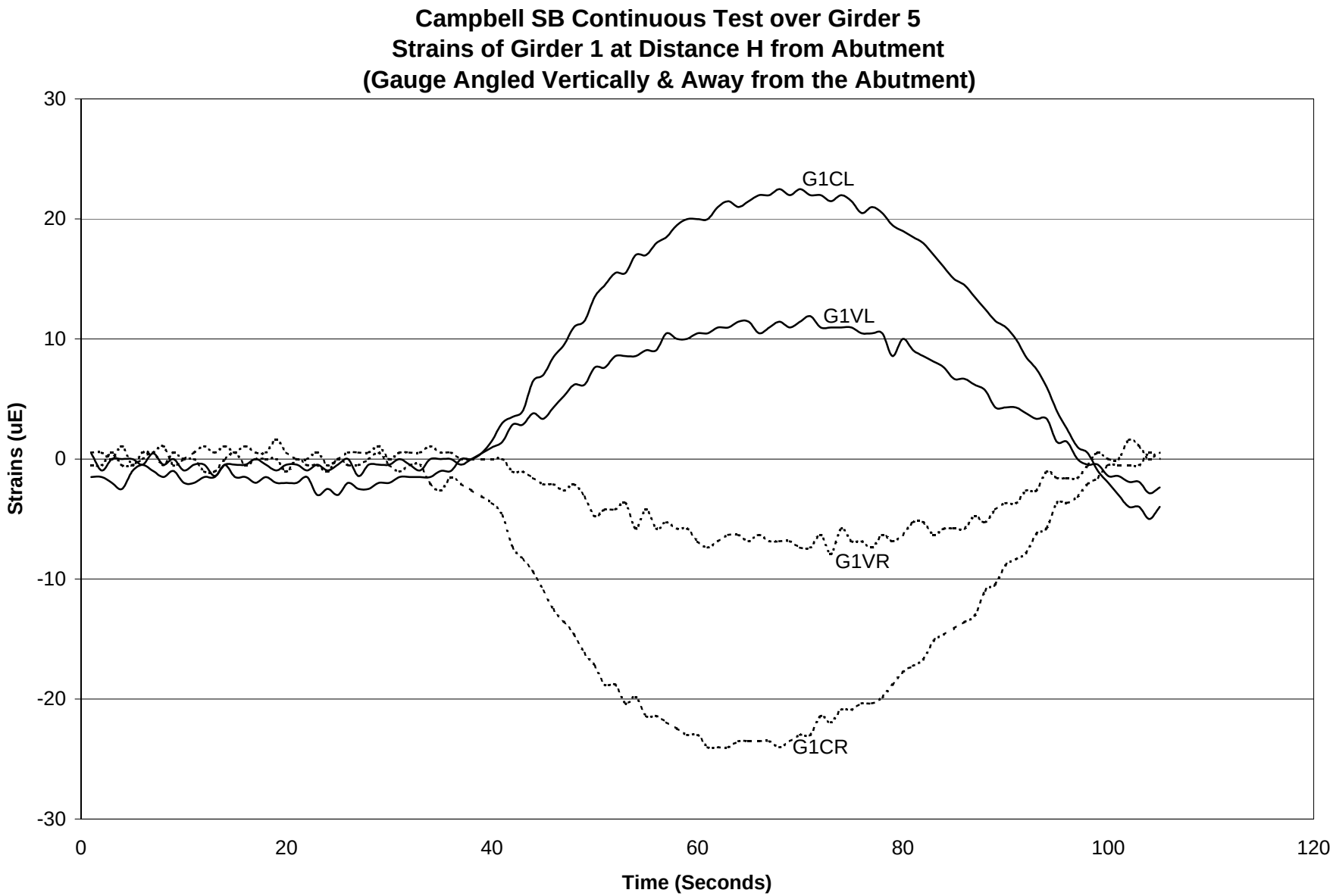
Campbell SB Continuous Test over Girder 5
Strains of Girder 1 at Distance H from Abutment
(Gauge Angled Vertically & Away from the Abutment)
Strains (uE)
Time (Seconds)
30
20
10
0
-10
-20
-30
0
20
40
60
80
100
120
G1CL
G1VL
G1VR
G1CR

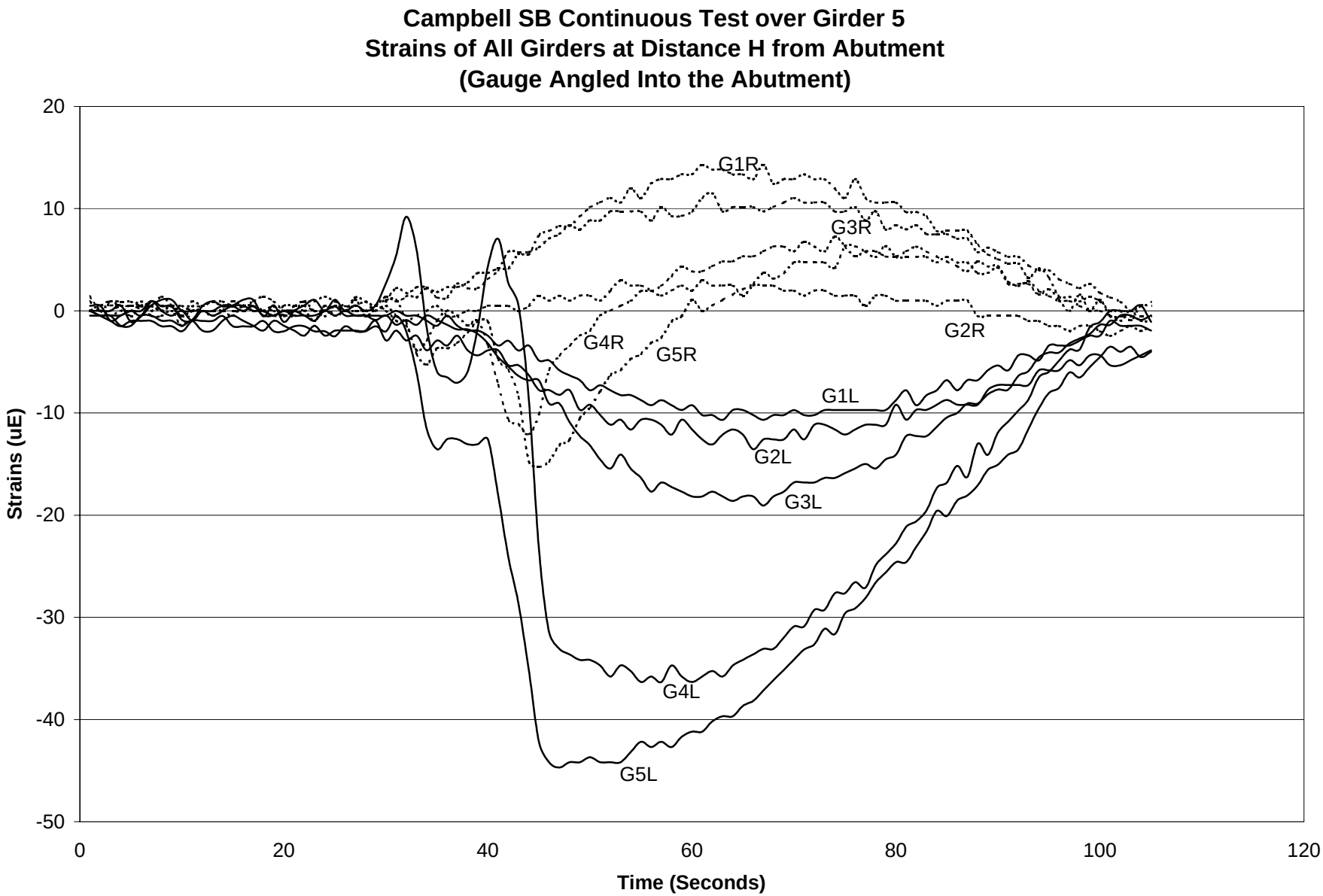
Campbell SB Continuous Test over Girder 5
Strains of All Girders at Distance H from Abutment
(Gauge Angled Into the Abutment)
Strains (uE)
Time (Seconds)
20
10
0
-10
-20
-30
-40
-50
0
20
40
60
80
100
120
G1R
G3R
G2R
G4R
G5R
G1L
G2L
G3L
G4L
G5L

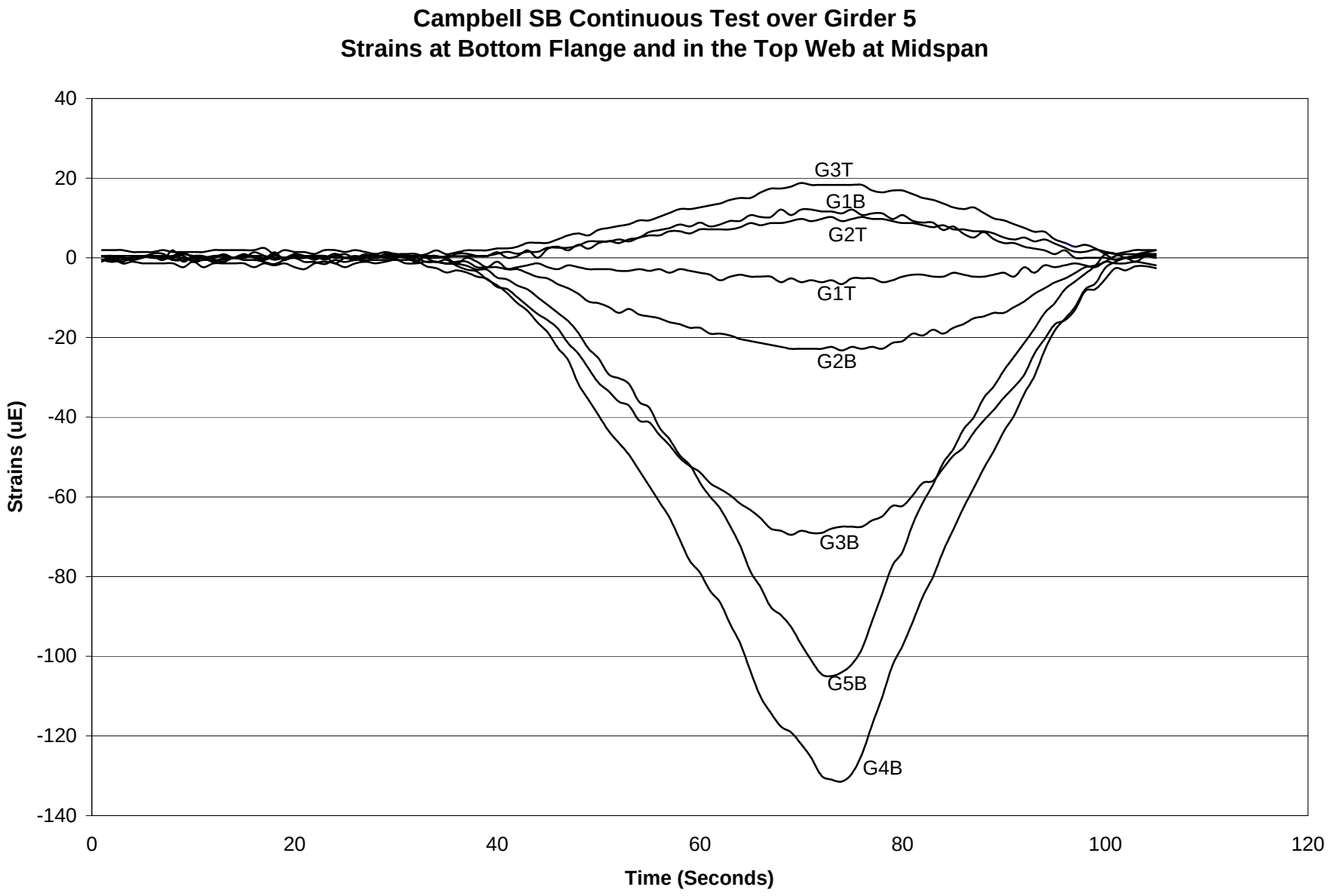
Campbell SB Continuous Test over Girder 5
Strains at Bottom Flange and in the Top Web at Midspan
Strains (uE)
Time (Seconds)
40
20
0
-20
-40
-60
-80
-100
-120
-140
0
20
40
60
80
100
120
G3T
G1B
G2T
G1T
G2B
G3B
G5B
G4B

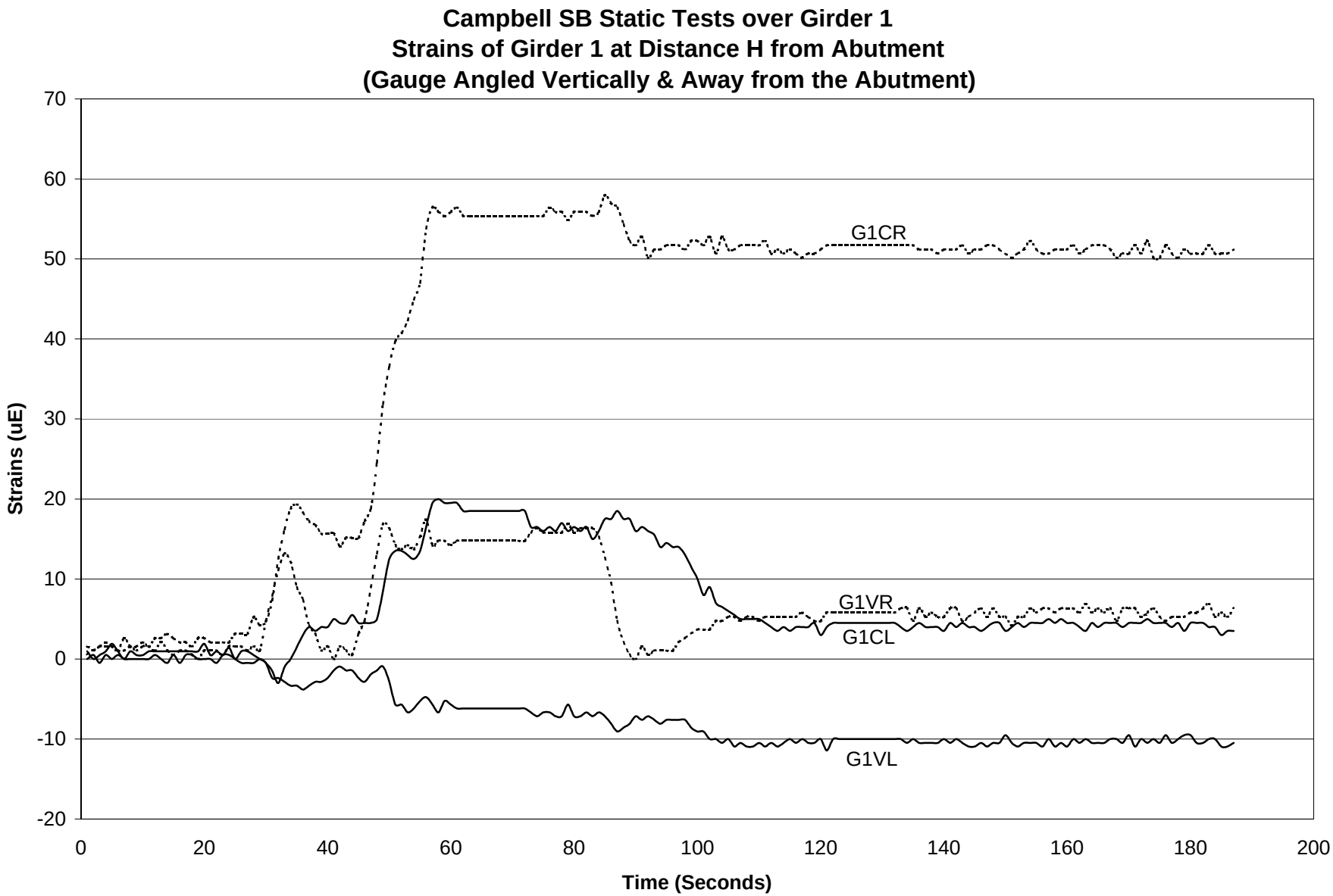
Campbell SB Static Tests over Girder 1
Strains of Girder 1 at Distance H from Abutment
(Gauge Angled Vertically & Away from the Abutment)
Strains (uE)
Time (Seconds)
G1CR
G1VR
G1CL
G1VL
70
60
50
40
30
20
10
0
-10
-20
0
20
40
60
80
100
120
140
160
180
200

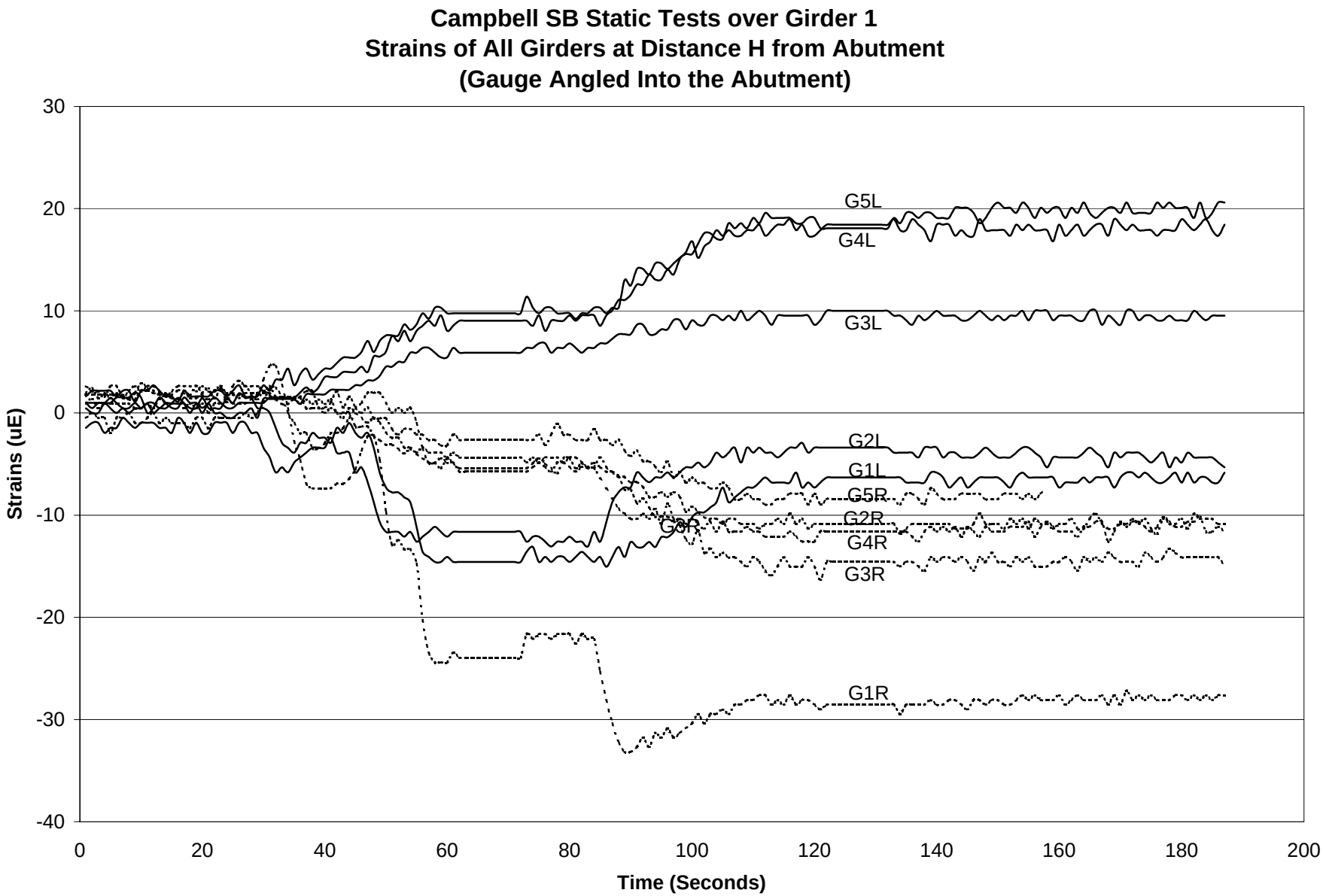
Campbell SB Static Tests over Girder 1
Strains of All Girders at Distance H from Abutment
(Gauge Angled Into the Abutment)
Strains (uE)
Time (Seconds)
30
20
10
0
-10
-20
-30
-40
0
20
40
60
80
100
120
140
160
180
200
G5L
G4L
G3L
G2L
G1L
G5R
G2R
G6R
G4R
G3R
G1R

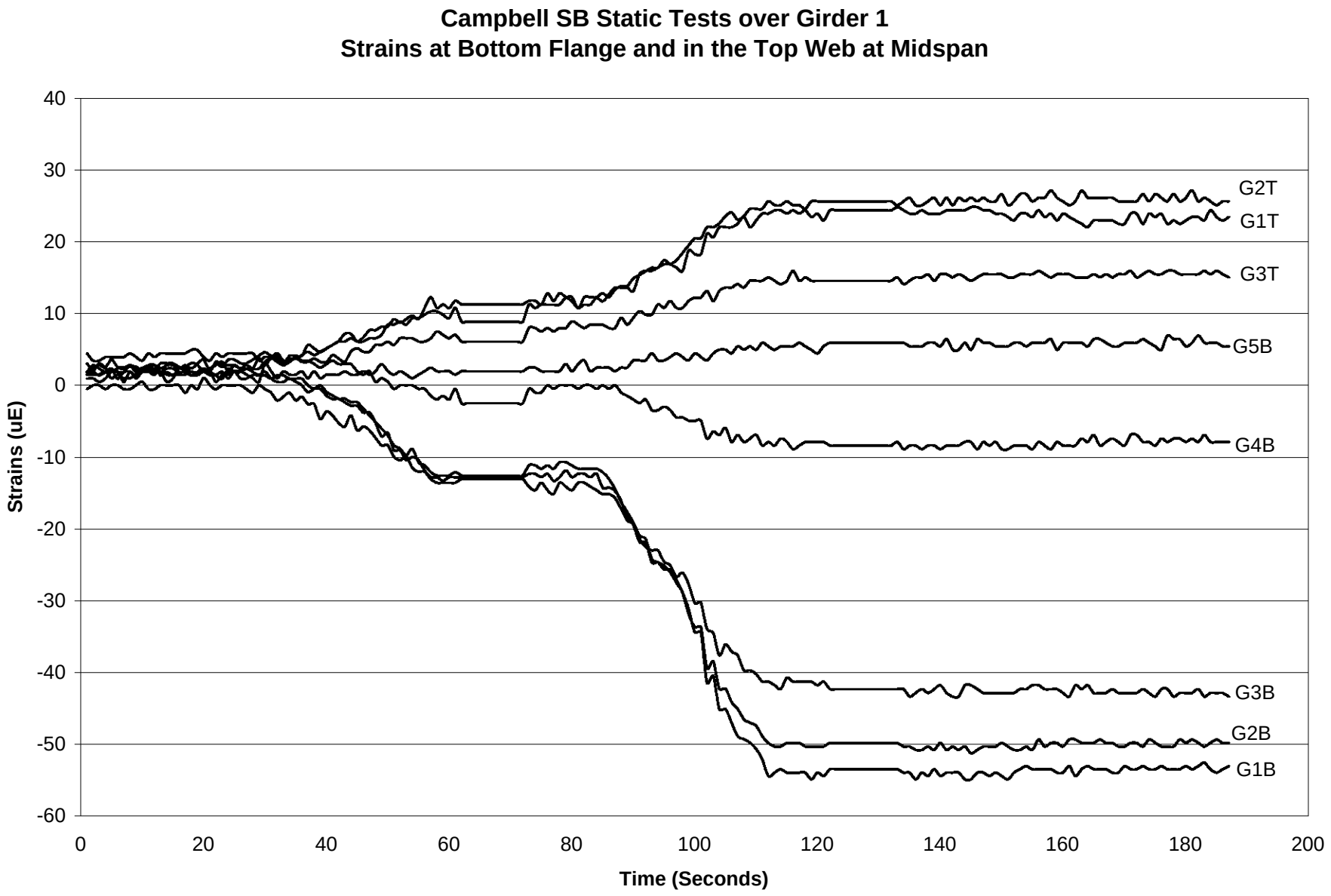
Campbell SB Static Tests over Girder 1
Strains at Bottom Flange and in the Top Web at Midspan
Strains (uE)
Time (Seconds)
40
30
20
10
0
-10
-20
-30
-40
-50
-60
0
20
40
60
80
100
120
140
160
180
200
G2T
G1T
G3T
G5B
G4B
G3B
G2B
G1B

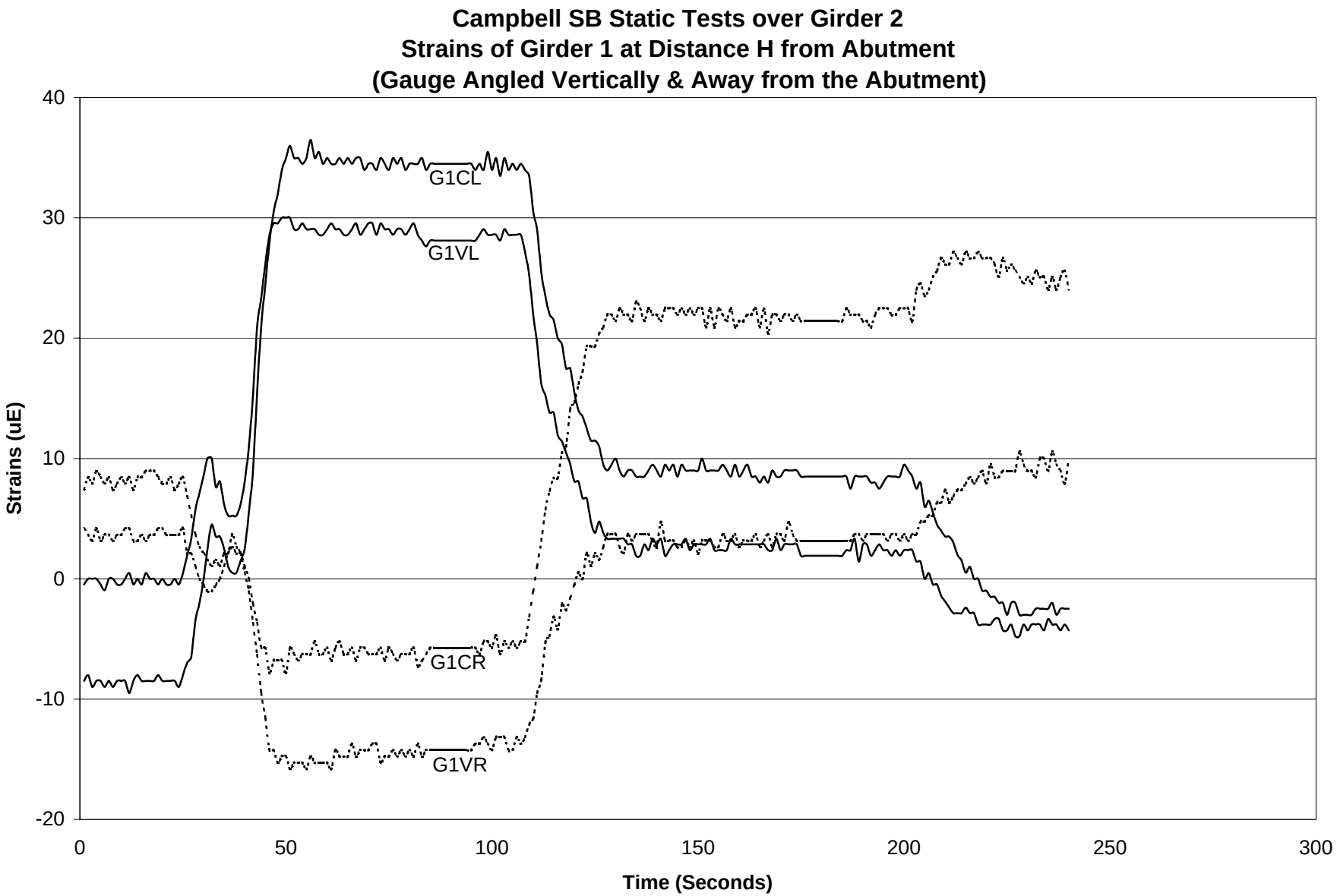
Campbell SB Static Tests over Girder 2
Strains of Girder 1 at Distance H from Abutment
(Gauge Angled Vertically & Away from the Abutment)
Strains (uE)
Time (Seconds)
G1CL
G1VL
G1CR
G1VR
40
30
20
10
0
-10
-20
0
50
100
150
200
250
300

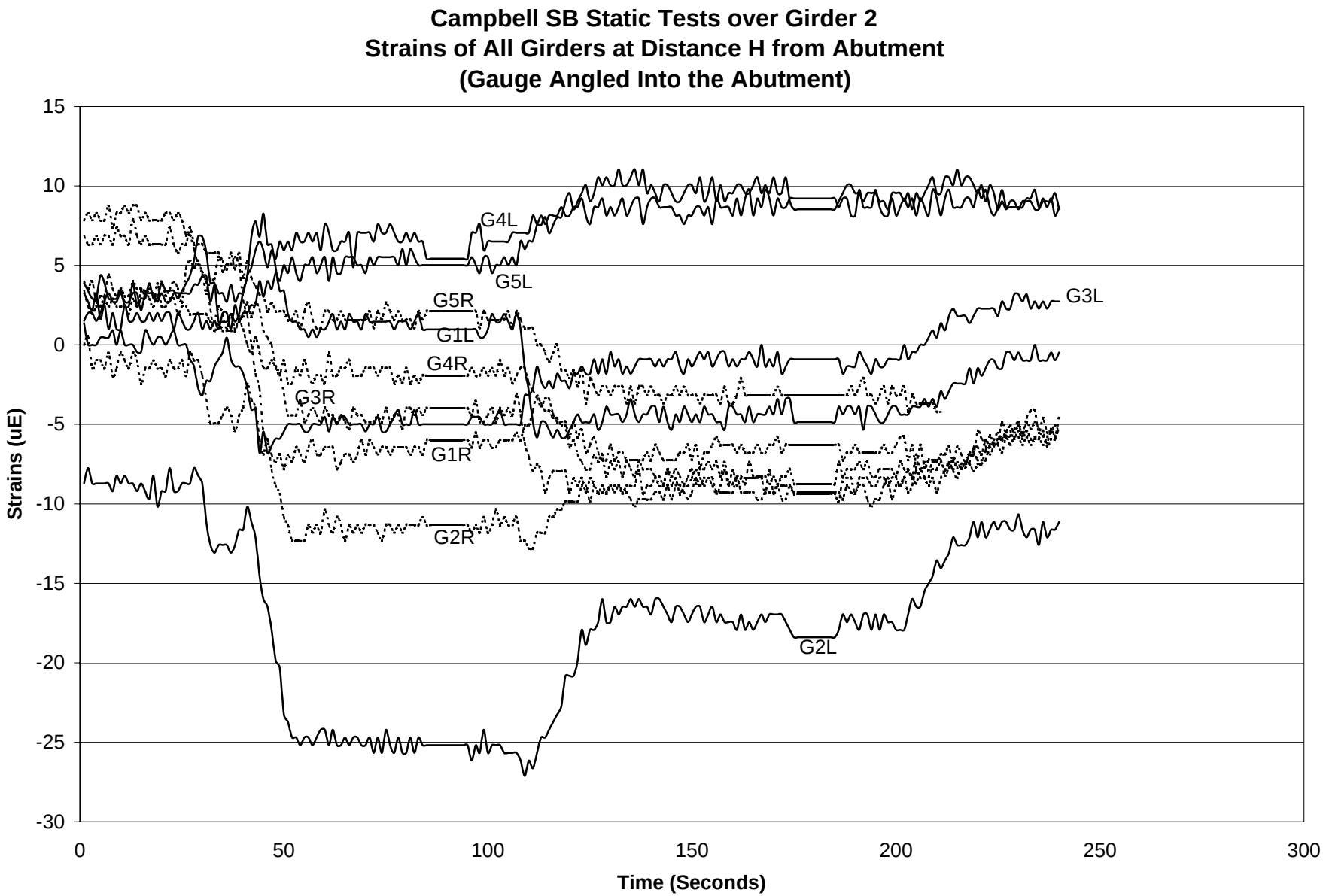
Campbell SB Static Tests over Girder 2
Strains of All Girders at Distance H from Abutment
(Gauge Angled Into the Abutment)
Strains (uE)
Time (Seconds)
15
10
5
0
-5
-10
-15
-20
-25
-30
0
50
100
150
200
250
300
G4L
G5L
G5R
G1L
G4R
G3R
G1R
G2R
G3L
G2L

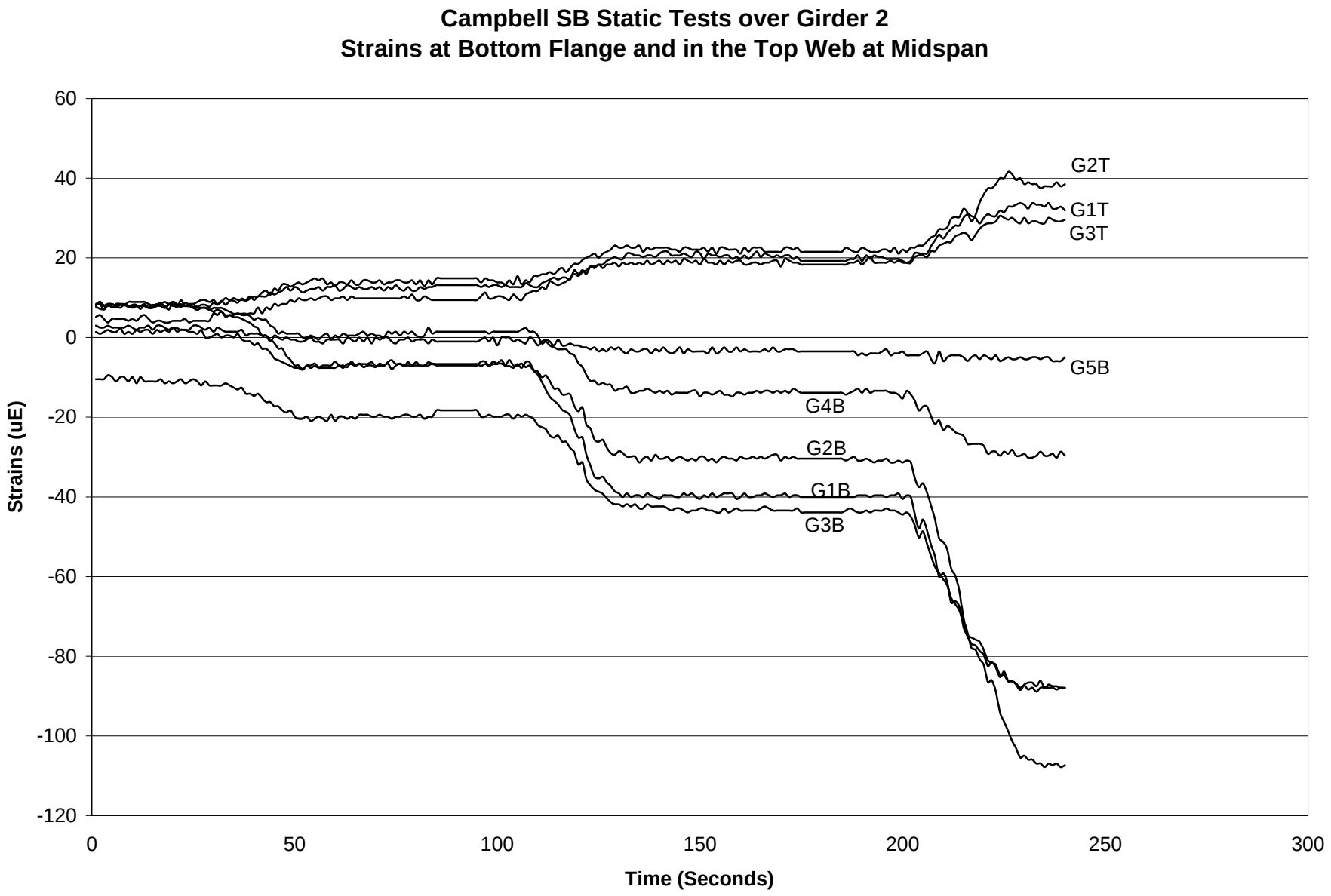
Campbell SB Static Tests over Girder 2
Strains at Bottom Flange and in the Top Web at Midspan
Strains (uE)
Time (Seconds)
60
40
20
0
-20
-40
-60
-80
-100
-120
0
50
100
150
200
250
300
G2T
G1T
G3T
G5B
G4B
G2B
G1B
G3B

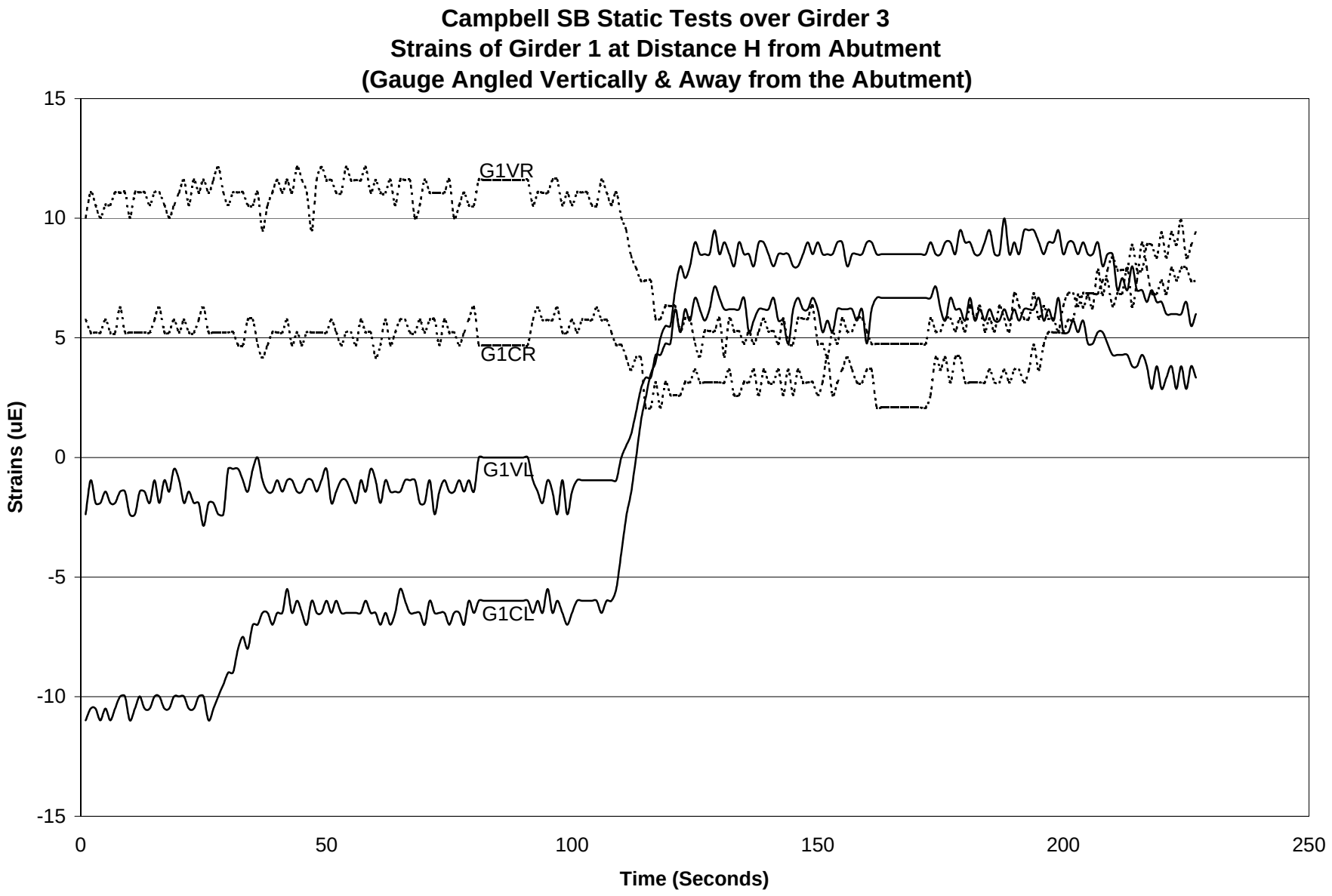
Campbell SB Static Tests over Girder 3
Strains of Girder 1 at Distance H from Abutment
(Gauge Angled Vertically & Away from the Abutment)
G1VR
G1CR
G1VL
G1CL
Strains (uE)
Time (Seconds)
15
10
5
0
-5
-10
-15
0
50
100
150
200
250

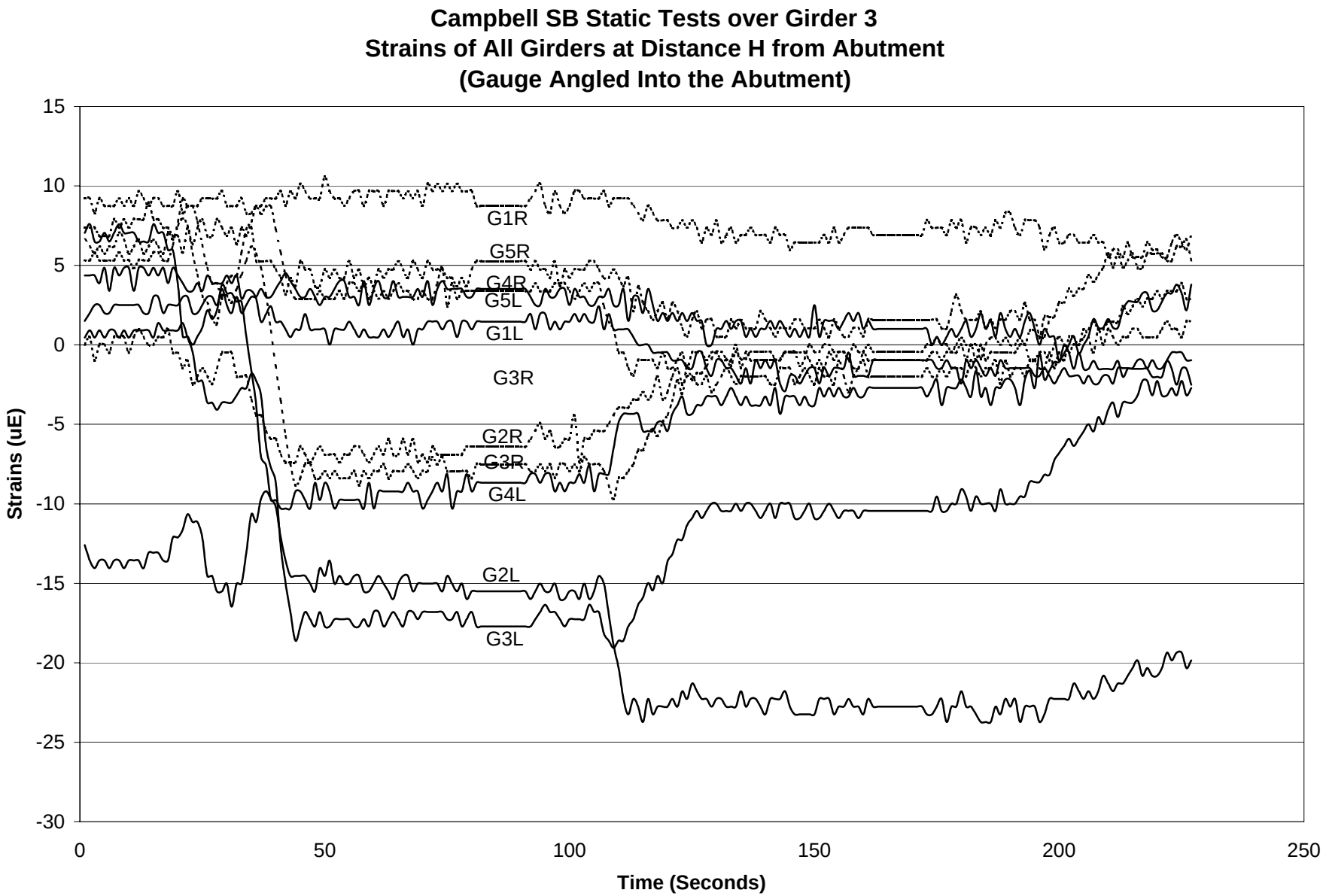
Campbell SB Static Tests over Girder 3
Strains of All Girders at Distance H from Abutment
(Gauge Angled Into the Abutment)
Strains (uE)
Time (Seconds)
15
10
5
0
-5
-10
-15
-20
-25
-30
0
50
100
150
200
250
G1R
G5R
G4R
G5L
G1L
G3R
G2R
G3R
G4L
G2L
G3L

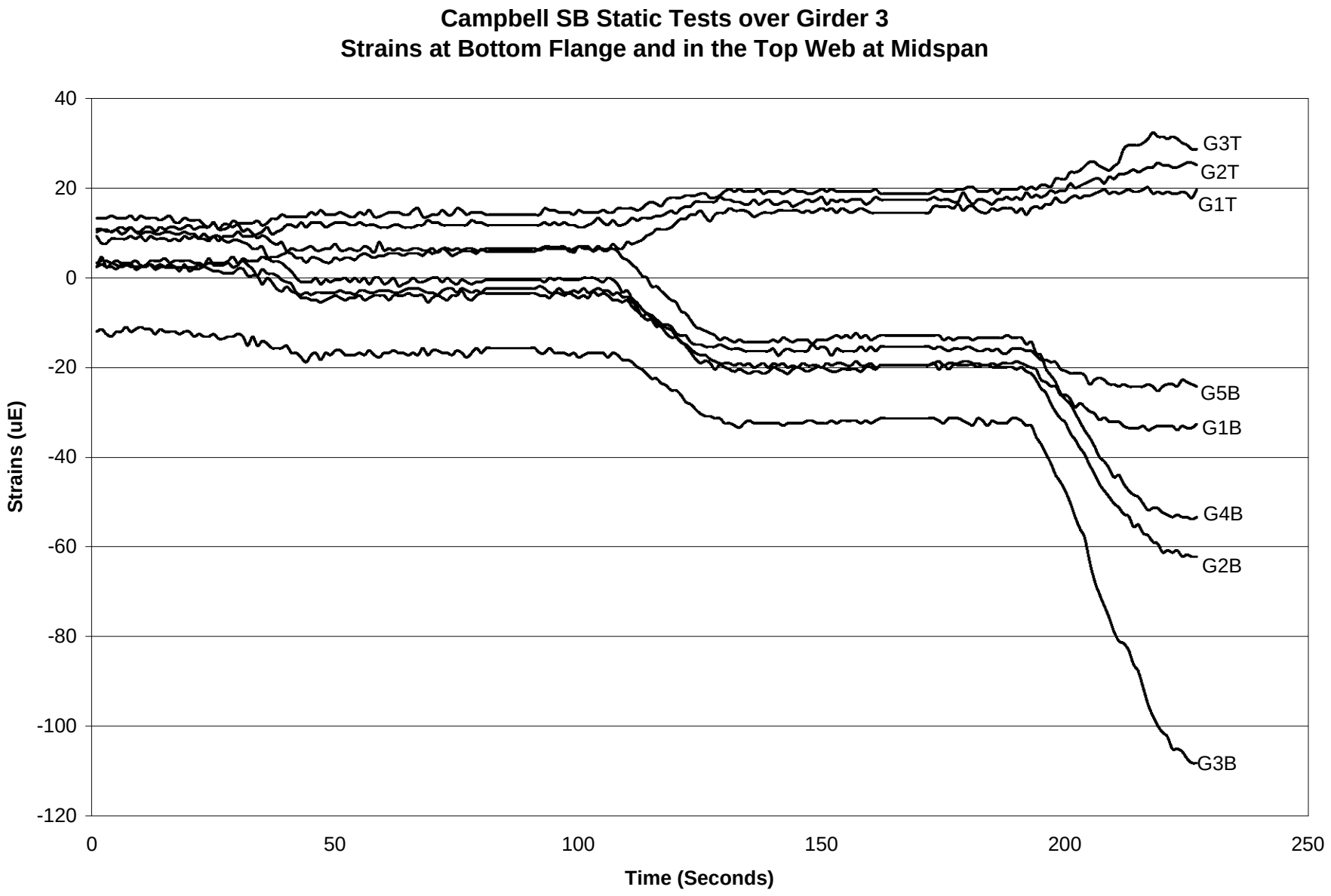
Campbell SB Static Tests over Girder 3
Strains at Bottom Flange and in the Top Web at Midspan
Strains (uE)
Time (Seconds)
40
20
0
-20
-40
-60
-80
-100
-120
0
50
100
150
200
250
G3T
G2T
G1T
G5B
G1B
G4B
G2B
G3B

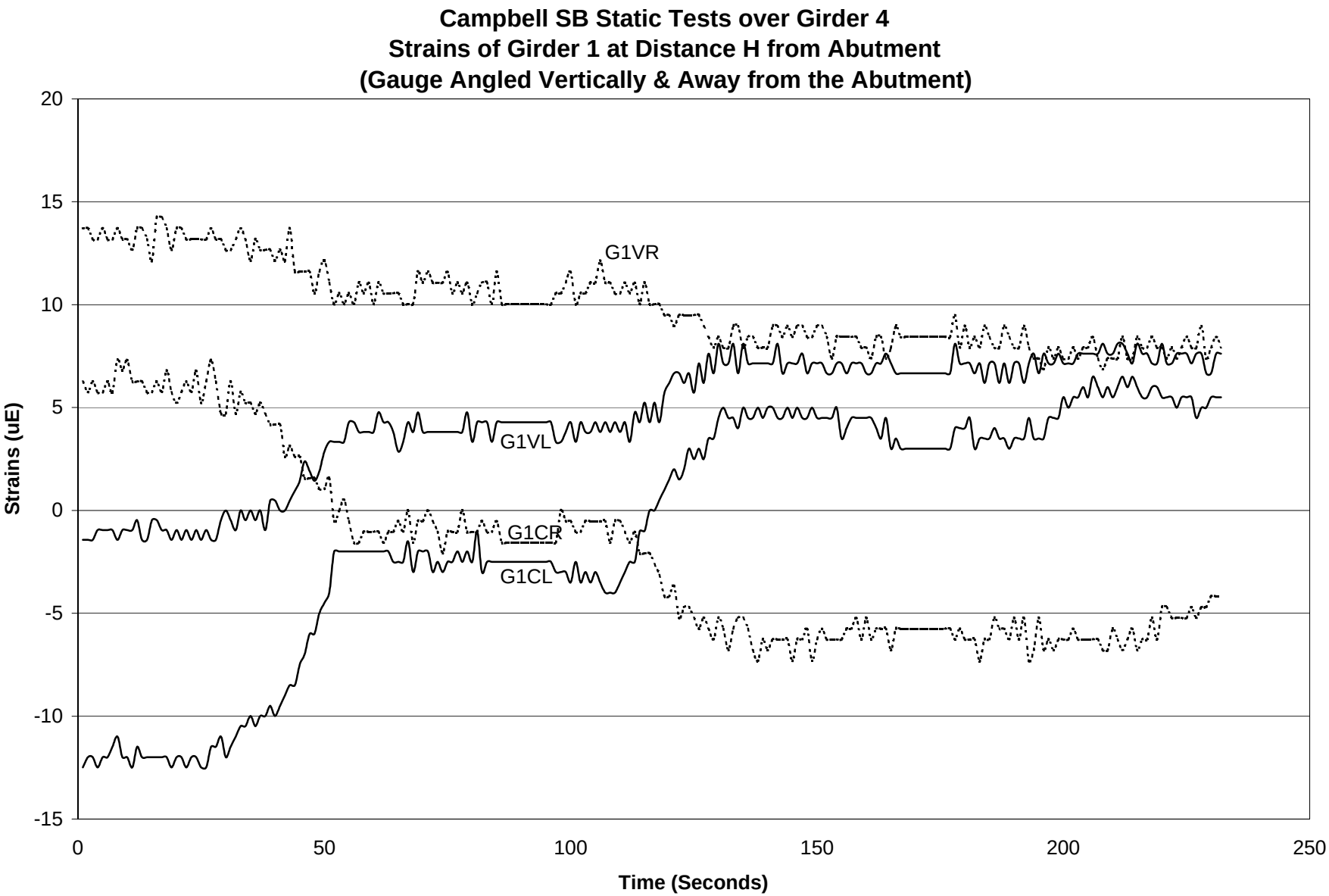
Campbell SB Static Tests over Girder 4
Strains of Girder 1 at Distance H from Abutment
(Gauge Angled Vertically & Away from the Abutment)
Strains (uE)
Time (Seconds)
20
15
10
5
0
-5
-10
-15
0
50
100
150
200
250
G1VR
G1VL
G1CR
G1CL

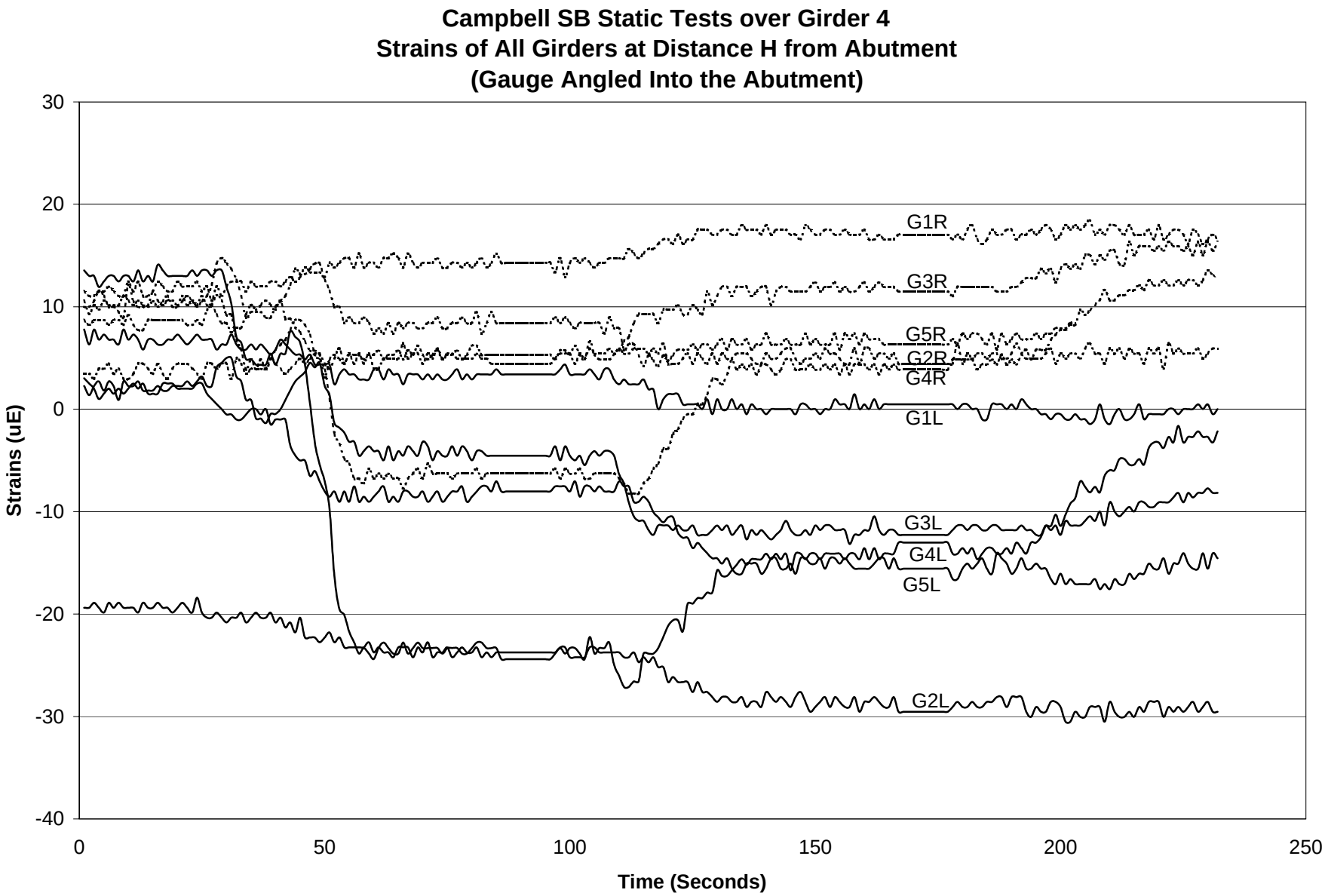
Campbell SB Static Tests over Girder 4
Strains of All Girders at Distance H from Abutment
(Gauge Angled Into the Abutment)
Strains (uE)
Time (Seconds)
30
20
10
0
-10
-20
-30
-40
0
50
100
150
200
250
G1R
G3R
G5R
G2R
G4R
G1L
G3L
G4L
G5L
G2L

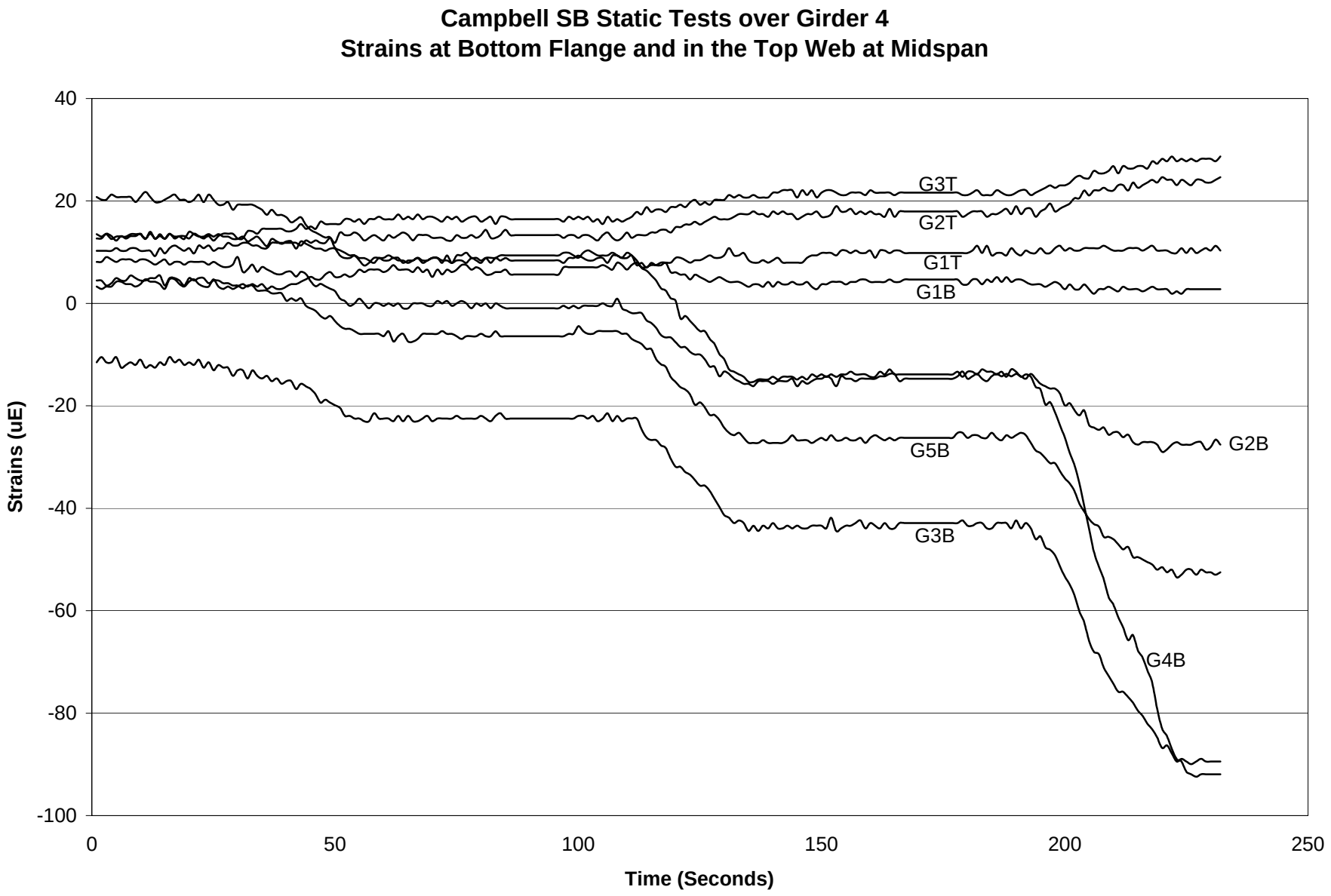
Campbell SB Static Tests over Girder 4
Strains at Bottom Flange and in the Top Web at Midspan
Strains (uE)
Time (Seconds)
40
20
0
-20
-40
-60
-80
-100
0
50
100
150
200
250
G3T
G2T
G1T
G1B
G2B
G5B
G3B
G4B

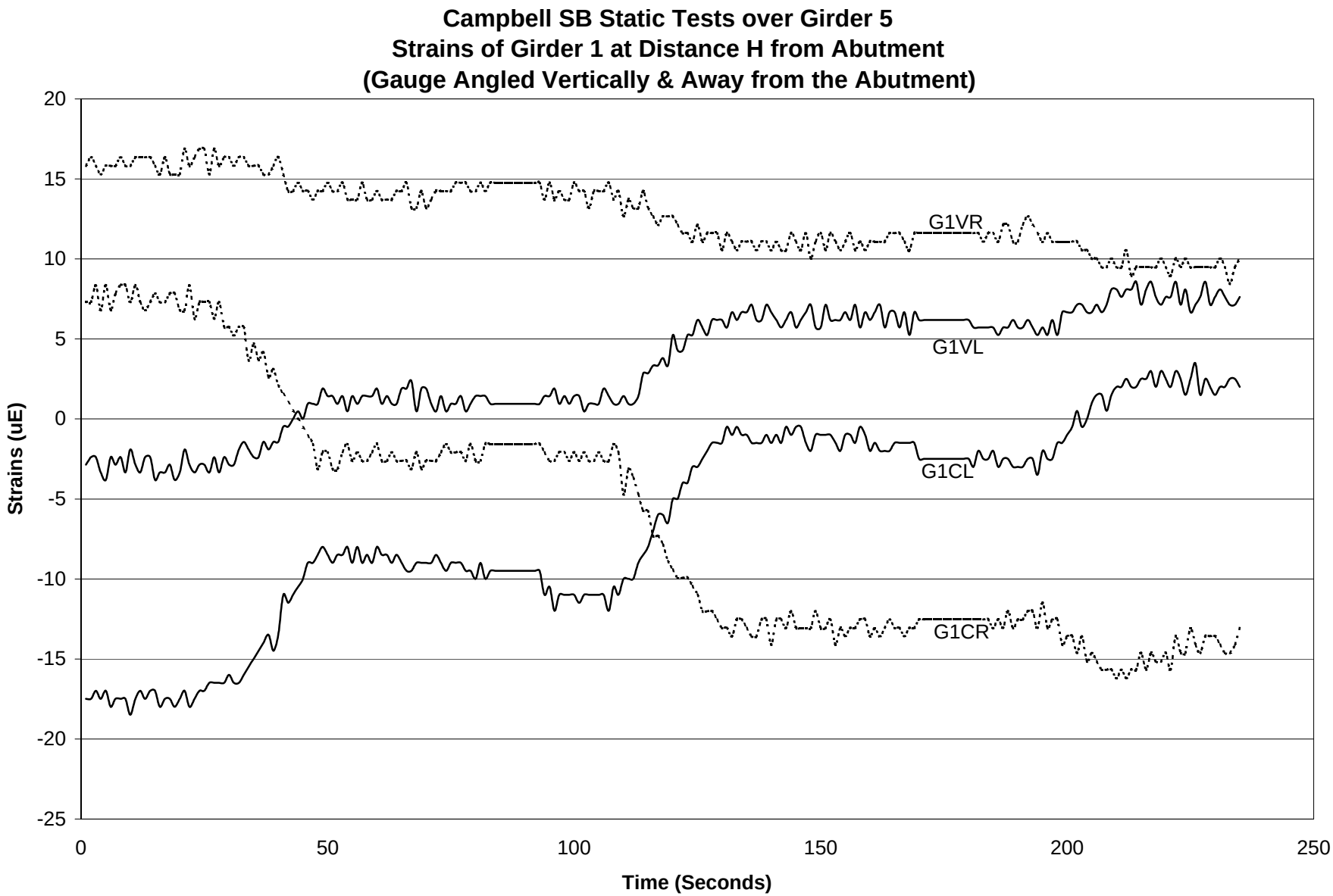
Campbell SB Static Tests over Girder 5
Strains of Girder 1 at Distance H from Abutment
(Gauge Angled Vertically & Away from the Abutment)
Strains (uE)
Time (Seconds)
20
15
10
5
0
-5
-10
-15
-20
-25
0
50
100
150
200
250
G1VR
G1VL
G1CL
G1CR

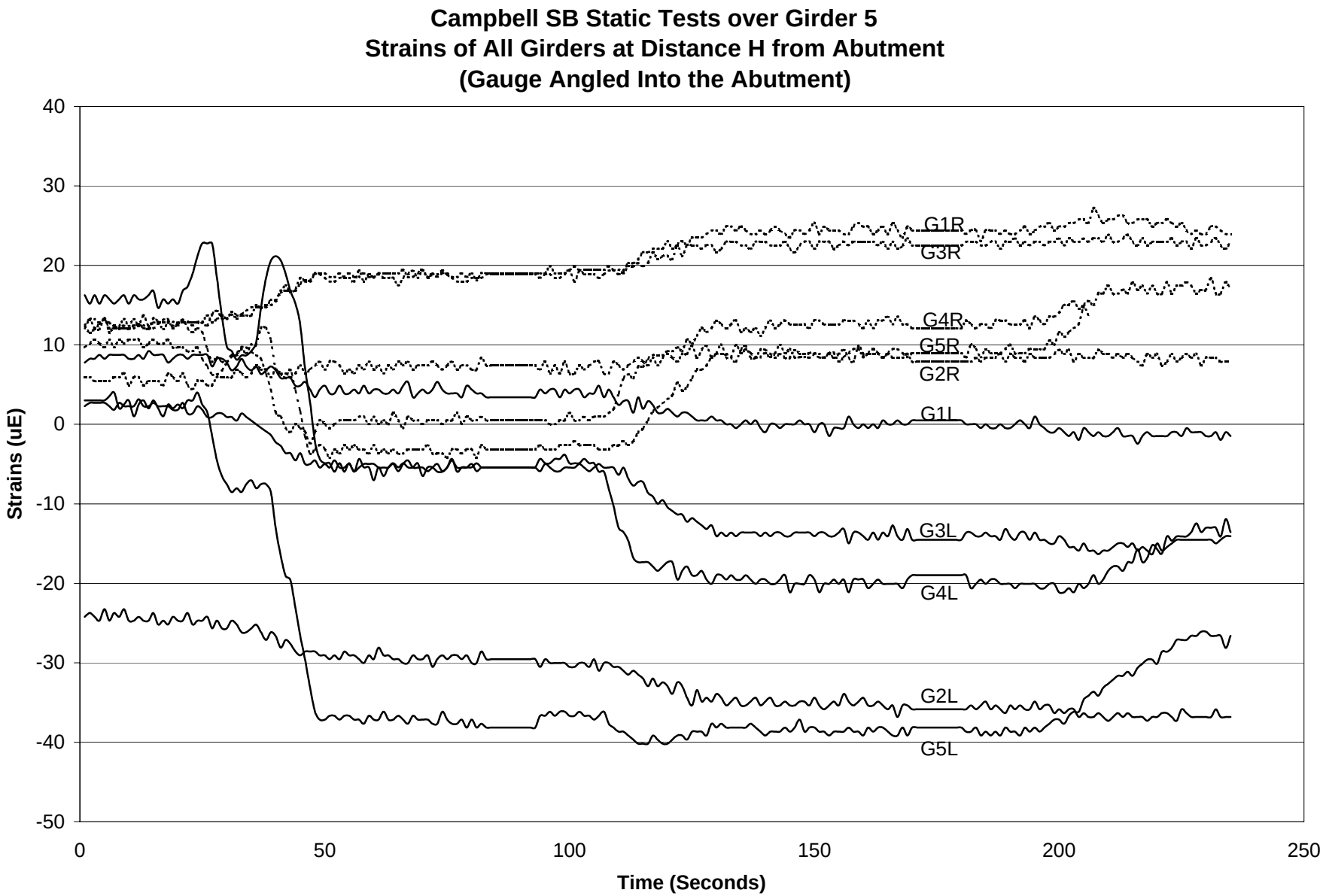
Campbell SB Static Tests over Girder 5
Strains of All Girders at Distance H from Abutment
(Gauge Angled Into the Abutment)
Strains (uE)
Time (Seconds)
40
30
20
10
0
-10
-20
-30
-40
-50
0
50
100
150
200
250
G1R
G3R
G4R
G5R
G2R
G1L
G3L
G4L
G2L
G5L

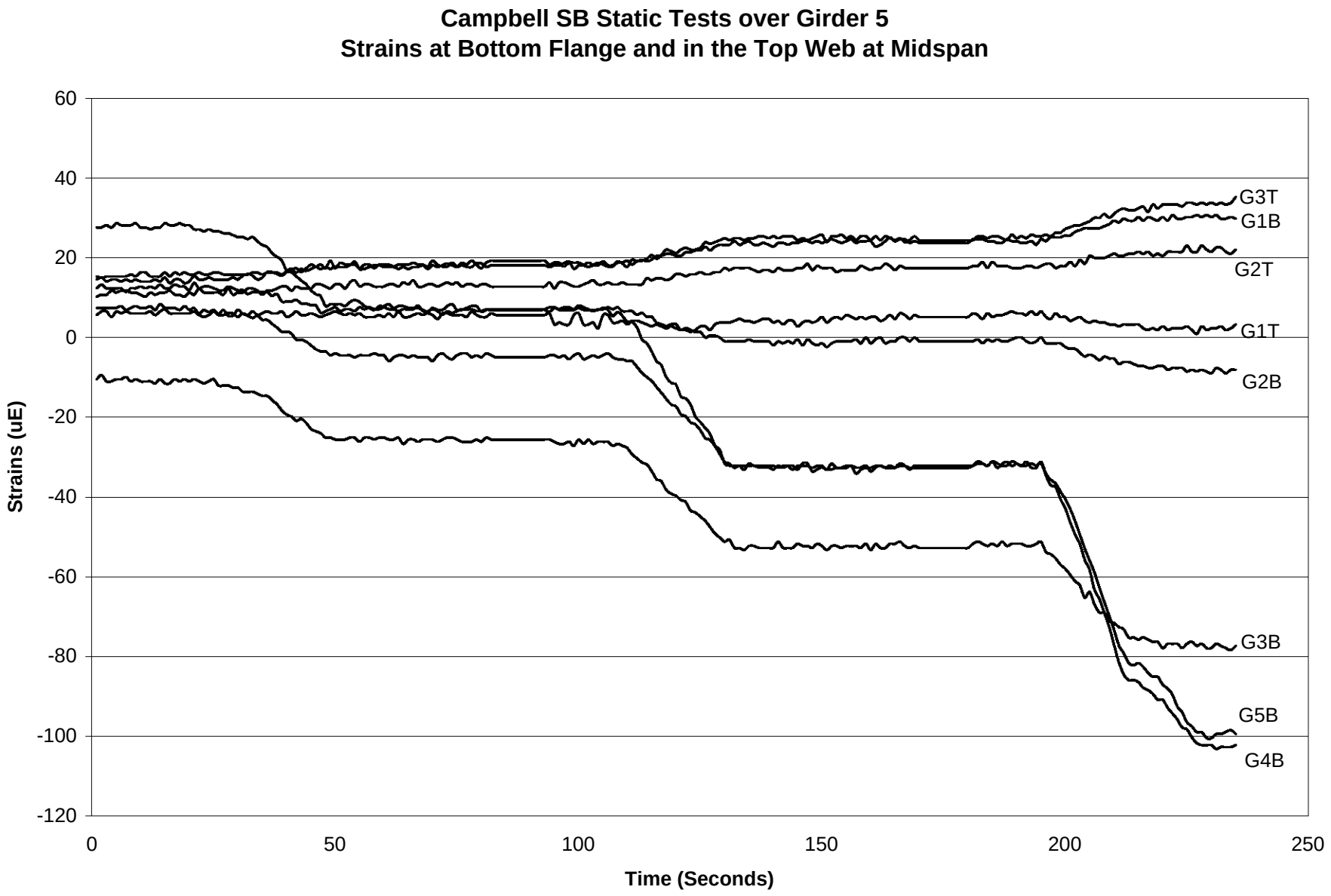
Campbell SB Static Tests over Girder 5
Strains at Bottom Flange and in the Top Web at Midspan
Strains (uE)
Time (Seconds)
60
40
20
0
-20
-40
-60
-80
-100
-120
0
50
100
150
200
250
G3T
G1B
G2T
G1T
G2B
G3B
G5B
G4B

# Huffman NB

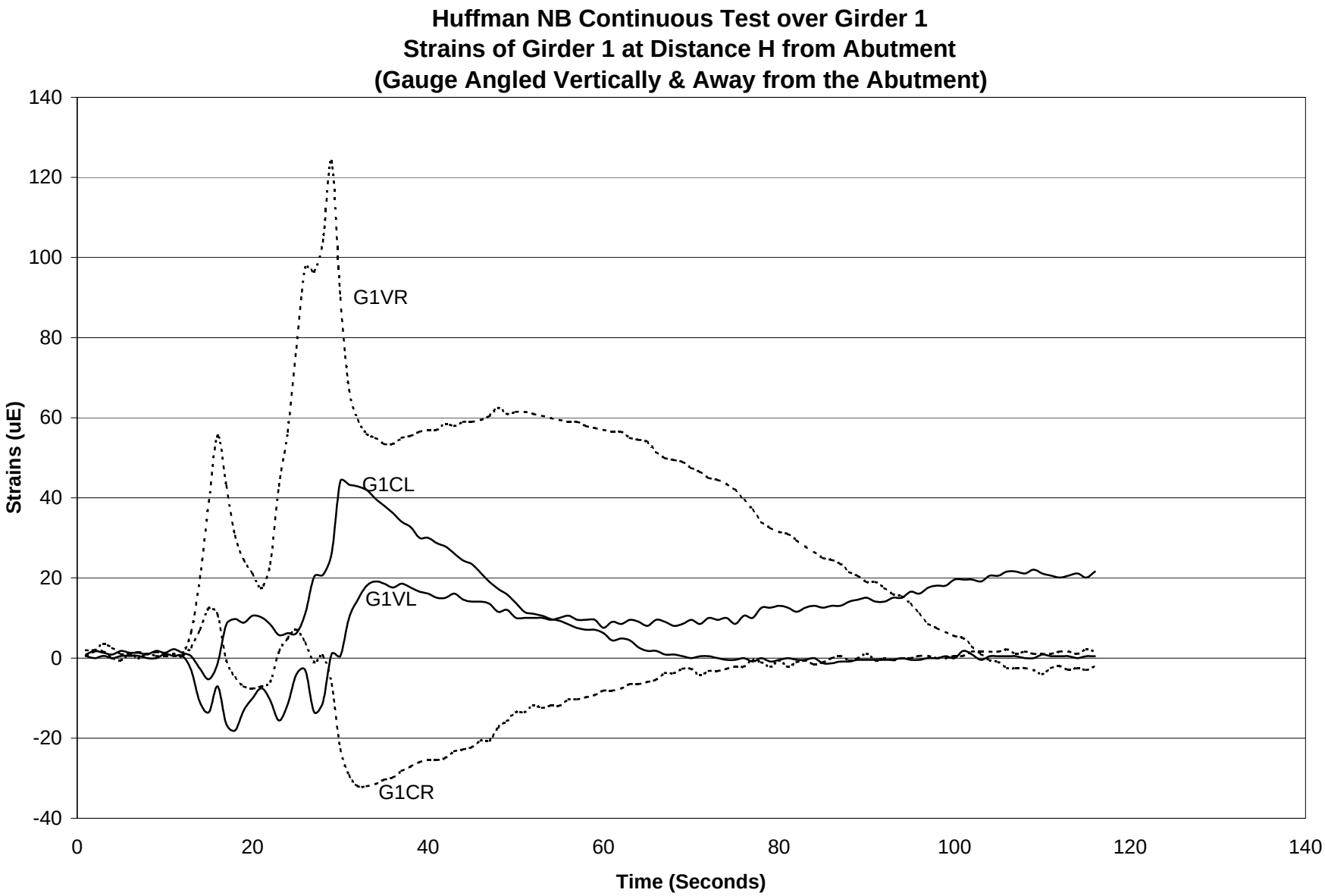
Huffman NB Continuous Test over Girder 1
Strains of Girder 1 at Distance H from Abutment
(Gauge Angled Vertically & Away from the Abutment)
Strains (uE)
Time (Seconds)
140
120
100
80
60
40
20
0
-20
-40
0
20
40
60
80
100
120
140
G1VR
G1CL
G1VL
G1CR

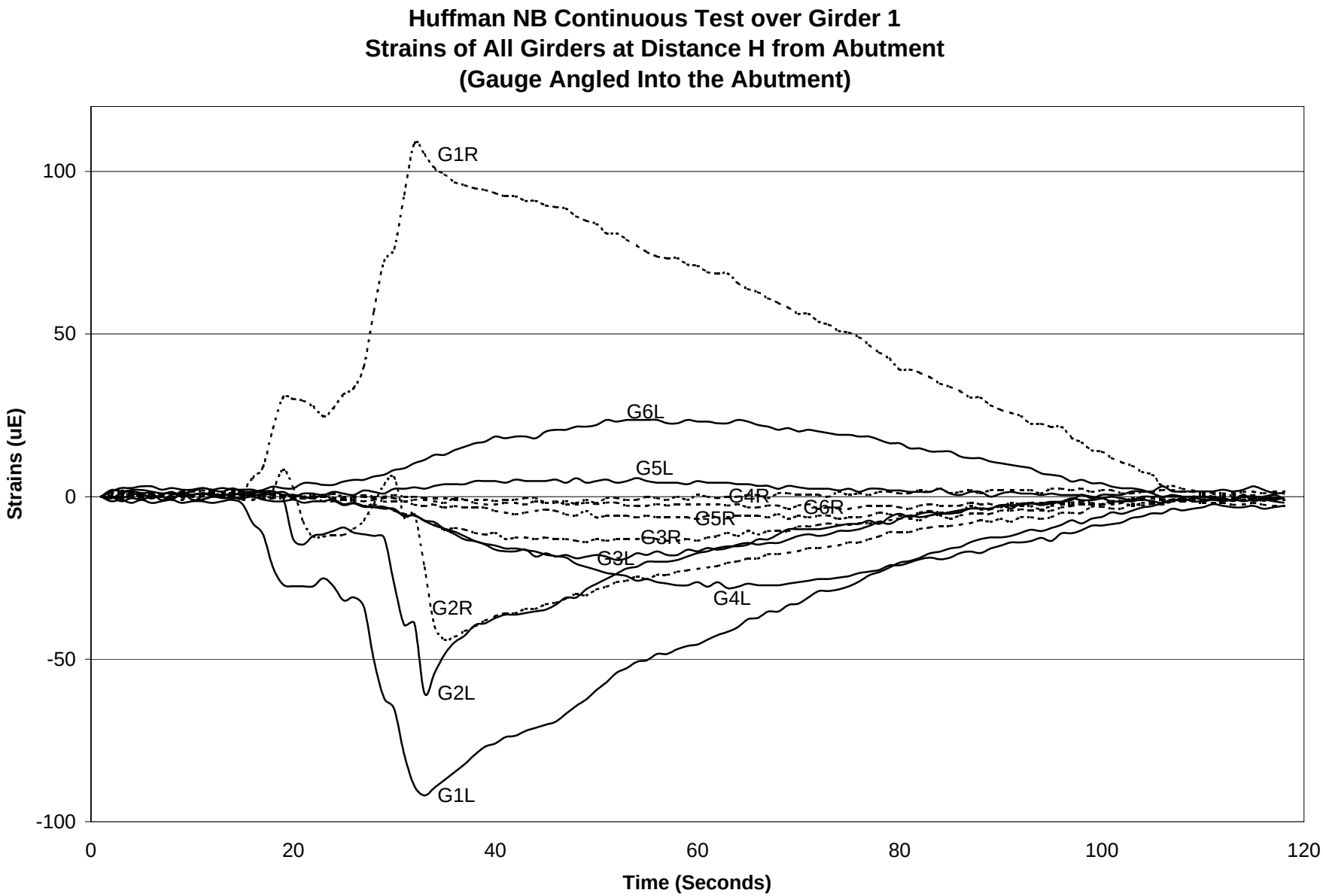
Huffman NB Continuous Test over Girder 1
Strains of All Girders at Distance H from Abutment
(Gauge Angled Into the Abutment)
Strains (uE)
Time (Seconds)
100
50
0
-50
-100
0
20
40
60
80
100
120
G1R
G6L
G5L
G4R
G6R
G5R
G3R
G3L
G4L
G2R
G2L
G1L

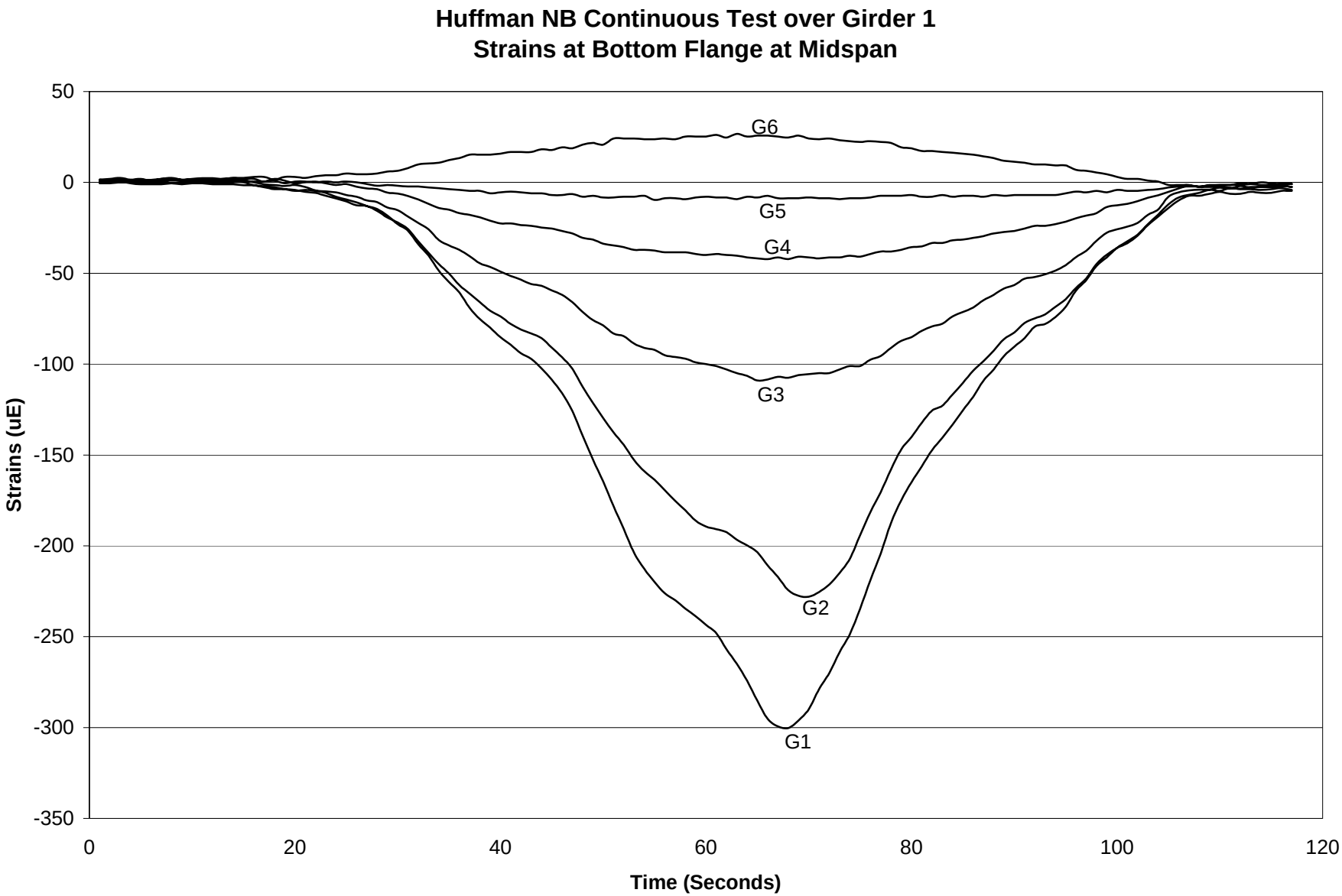
Huffman NB Continuous Test over Girder 1
Strains at Bottom Flange at Midspan
50
0
-50
-100
-150
-200
-250
-300
-350
Strains (uE)
0
20
40
60
80
100
120
Time (Seconds)
G6
G5
G4
G3
G2
G1

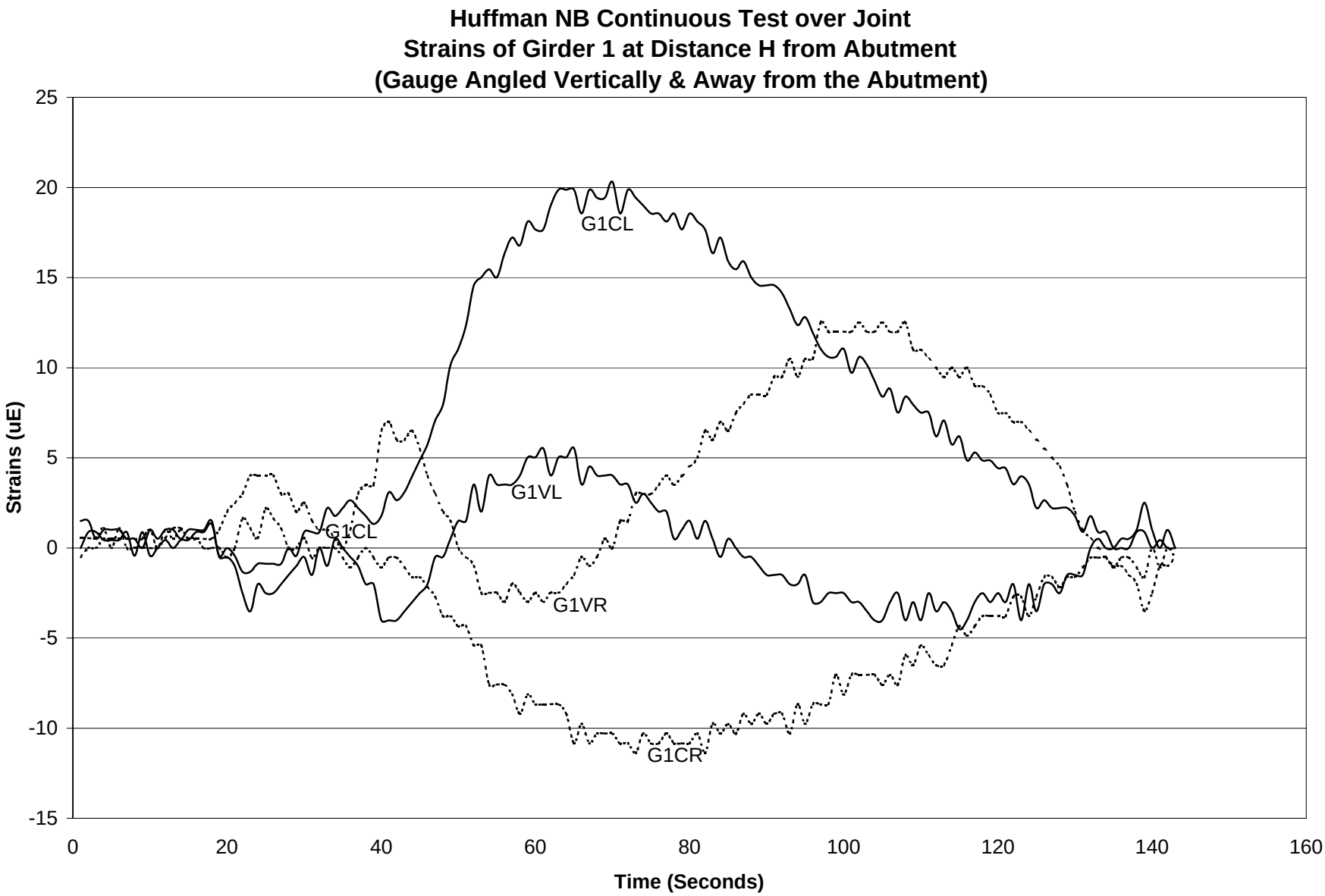
Huffman NB Continuous Test over Joint
Strains of Girder 1 at Distance H from Abutment
(Gauge Angled Vertically & Away from the Abutment)
Strains (uE)
Time (Seconds)
25
20
15
10
5
0
-5
-10
-15
0
20
40
60
80
100
120
140
160
G1CL
G1VL
G1CL
G1VR
G1CR

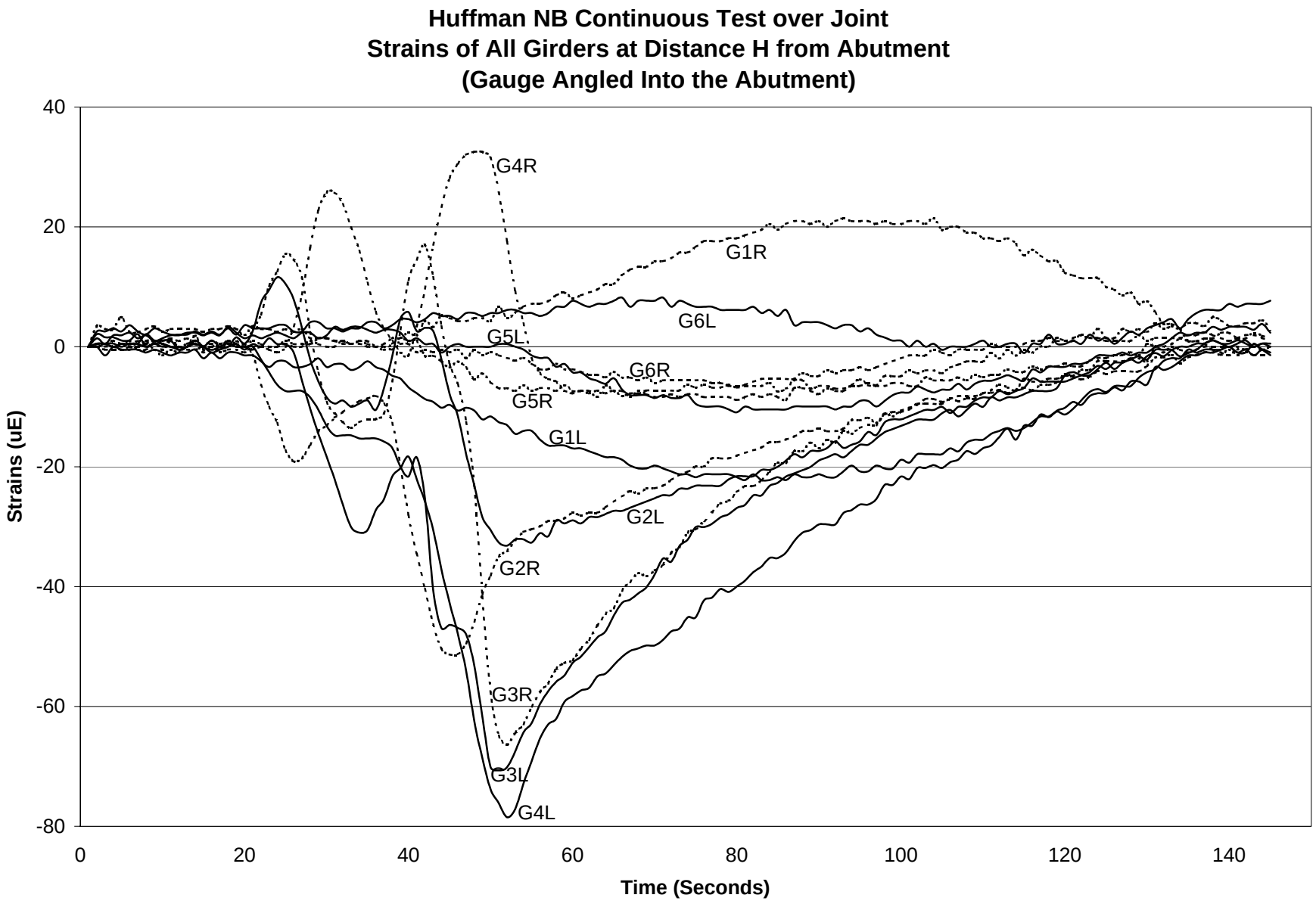
Huffman NB Continuous Test over Joint
Strains of All Girders at Distance H from Abutment
(Gauge Angled Into the Abutment)
Strains (uE)
Time (Seconds)
40
20
0
-20
-40
-60
-80
0
20
40
60
80
100
120
140
G4R
G1R
G6L
G5L
G6R
G5R
G1L
G2L
G2R
G3R
G3L
G4L

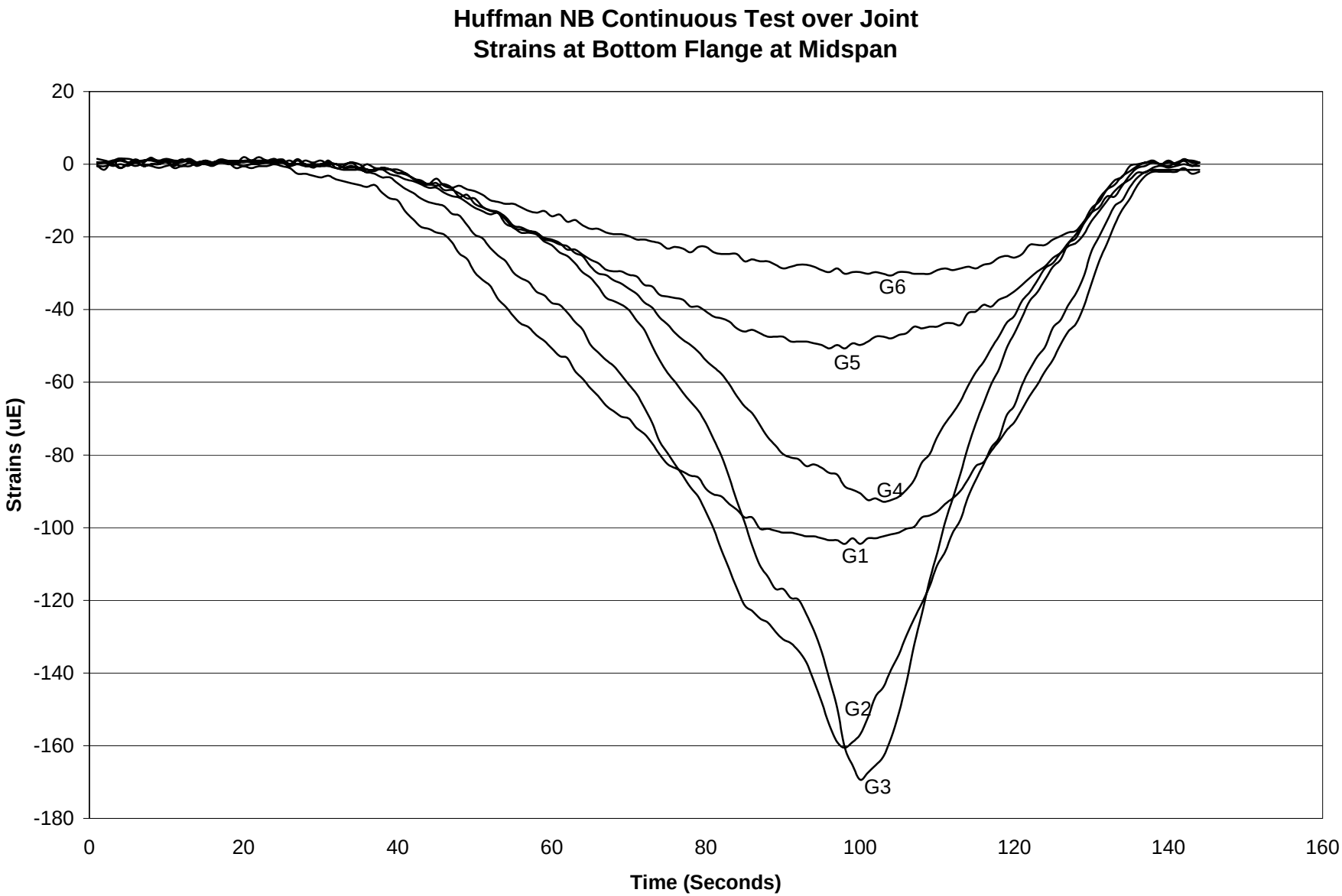
Huffman NB Continuous Test over Joint
Strains at Bottom Flange at Midspan
Strains (uE)
Time (Seconds)
20
0
-20
-40
-60
-80
-100
-120
-140
-160
-180
0
20
40
60
80
100
120
140
160
G6
G5
G4
G1
G2
G3

Huffman NB Continuous Test over Center
Strains of Girder 1 at Distance H from Abutment
(Gauge Angled Vertically & Away from the Abutment)
Strains (uE)
Time (Seconds)
G1CL
G1VL
G1VR
G1CR
20
15
10
5
0
-5
-10
0
20
40
60
80
100
120
140

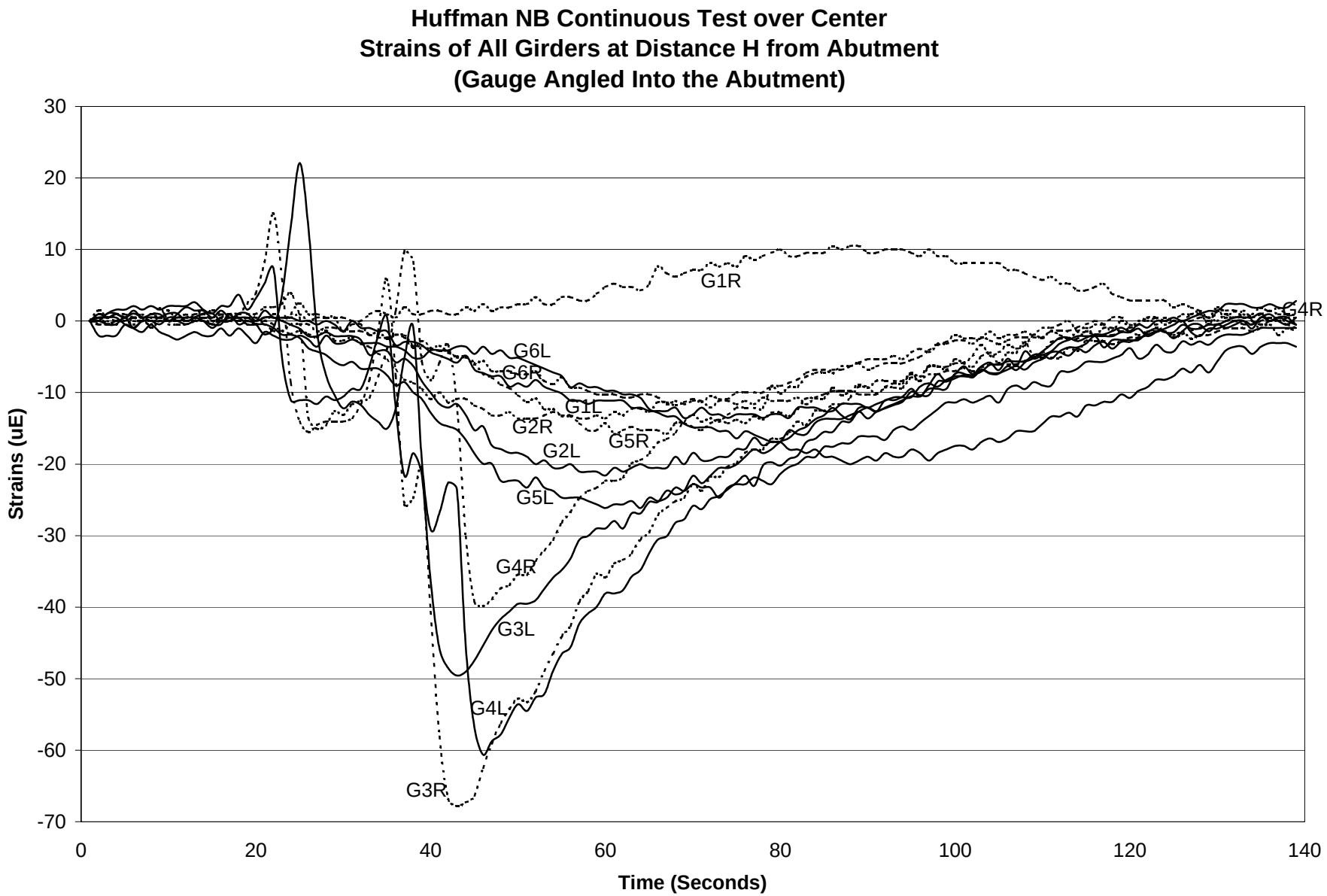
Huffman NB Continuous Test over Center
Strains of All Girders at Distance H from Abutment
(Gauge Angled Into the Abutment)
Strains (uE)
Time (Seconds)
30
20
10
0
-10
-20
-30
-40
-50
-60
-70
0
20
40
60
80
100
120
140
G1R
G4R
G6L
G6R
G1L
G2R
G5R
G2L
G5L
G4R
G3L
G4L
G3R

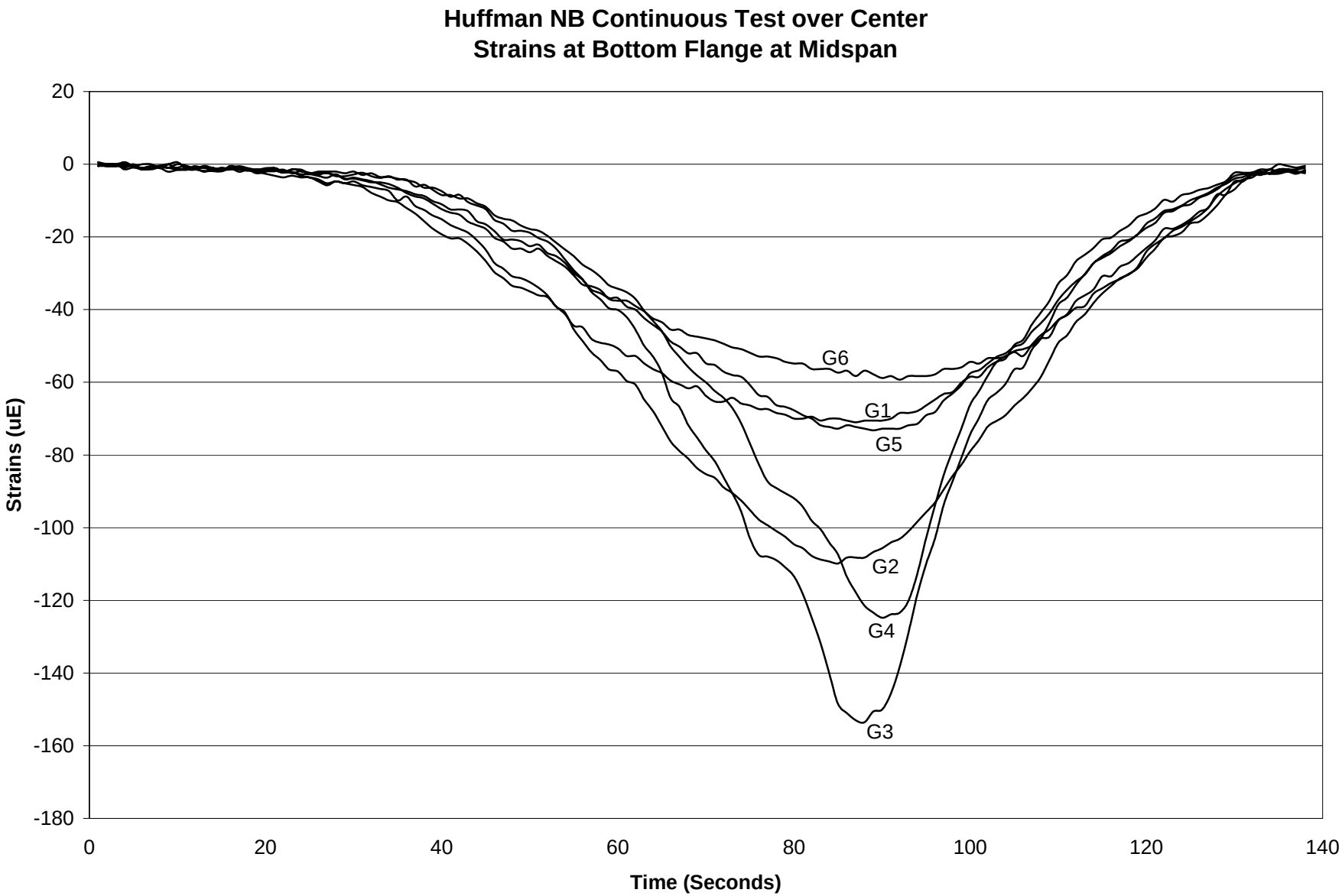
Huffman NB Continuous Test over Center
Strains at Bottom Flange at Midspan
Strains (uE)
Time (Seconds)
20
0
-20
-40
-60
-80
-100
-120
-140
-160
-180
0
20
40
60
80
100
120
140
G6
G1
G5
G2
G4
G3

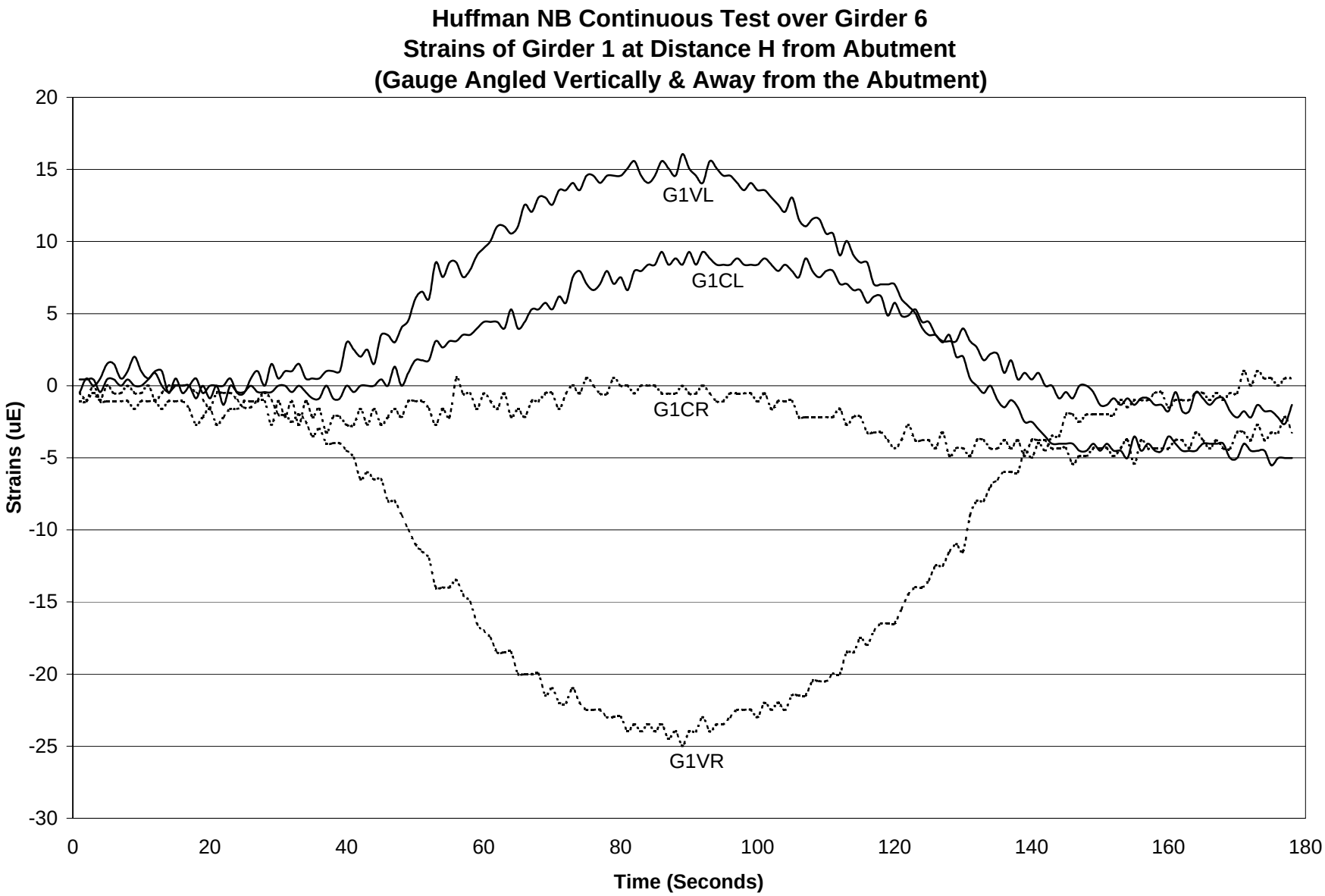
Huffman NB Continuous Test over Girder 6
Strains of Girder 1 at Distance H from Abutment
(Gauge Angled Vertically & Away from the Abutment)
Strains (uE)
Time (Seconds)
G1VL
G1CL
G1CR
G1VR
20
15
10
5
0
-5
-10
-15
-20
-25
-30
0
20
40
60
80
100
120
140
160
180

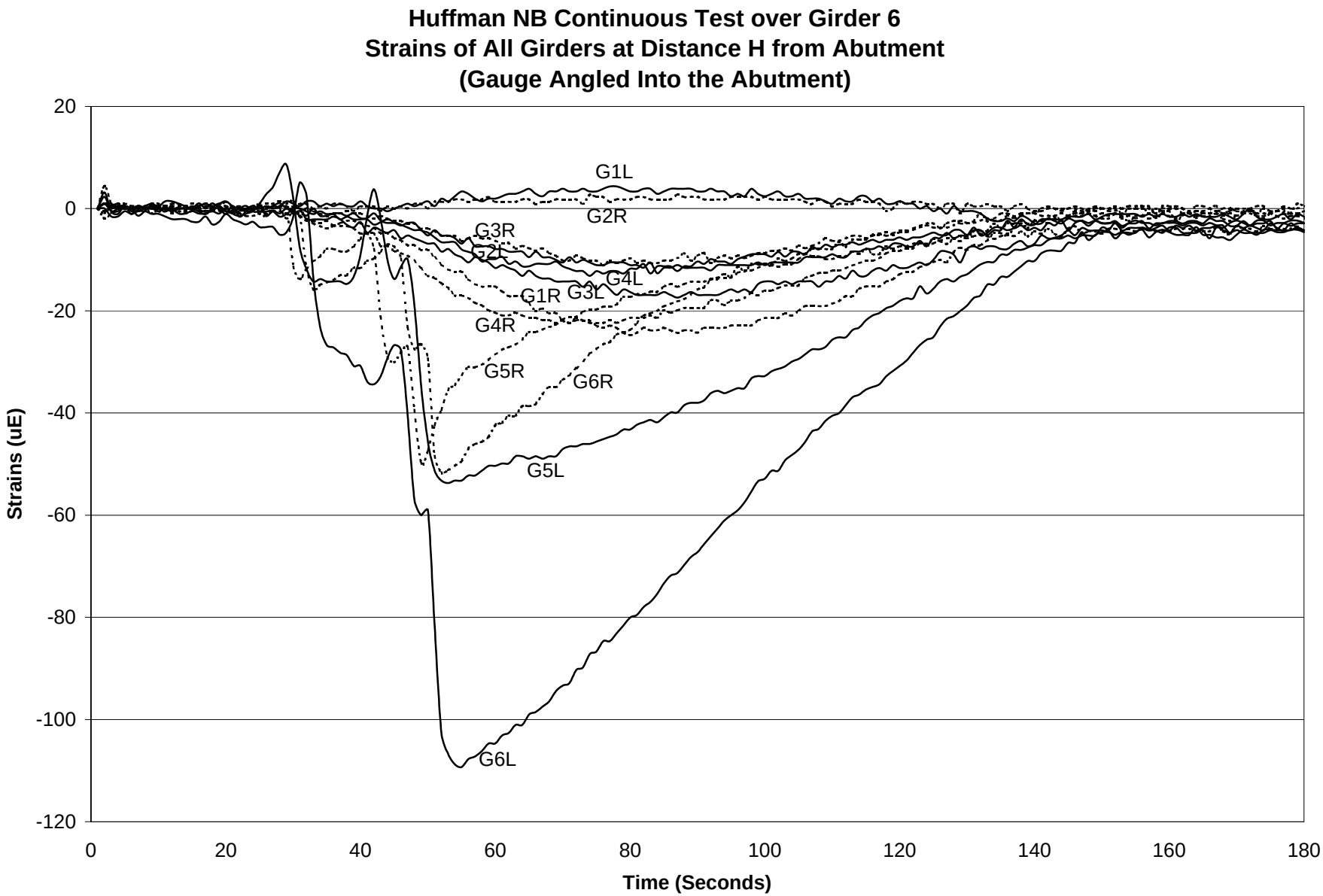
Huffman NB Continuous Test over Girder 6
Strains of All Girders at Distance H from Abutment
(Gauge Angled Into the Abutment)
Strains (uE)
Time (Seconds)
20
0
-20
-40
-60
-80
-100
-120
0
20
40
60
80
100
120
140
160
180
G1L
G2R
G3R
G2L
G4L
G1R
G3L
G4R
G5R
G6R
G5L
G6L

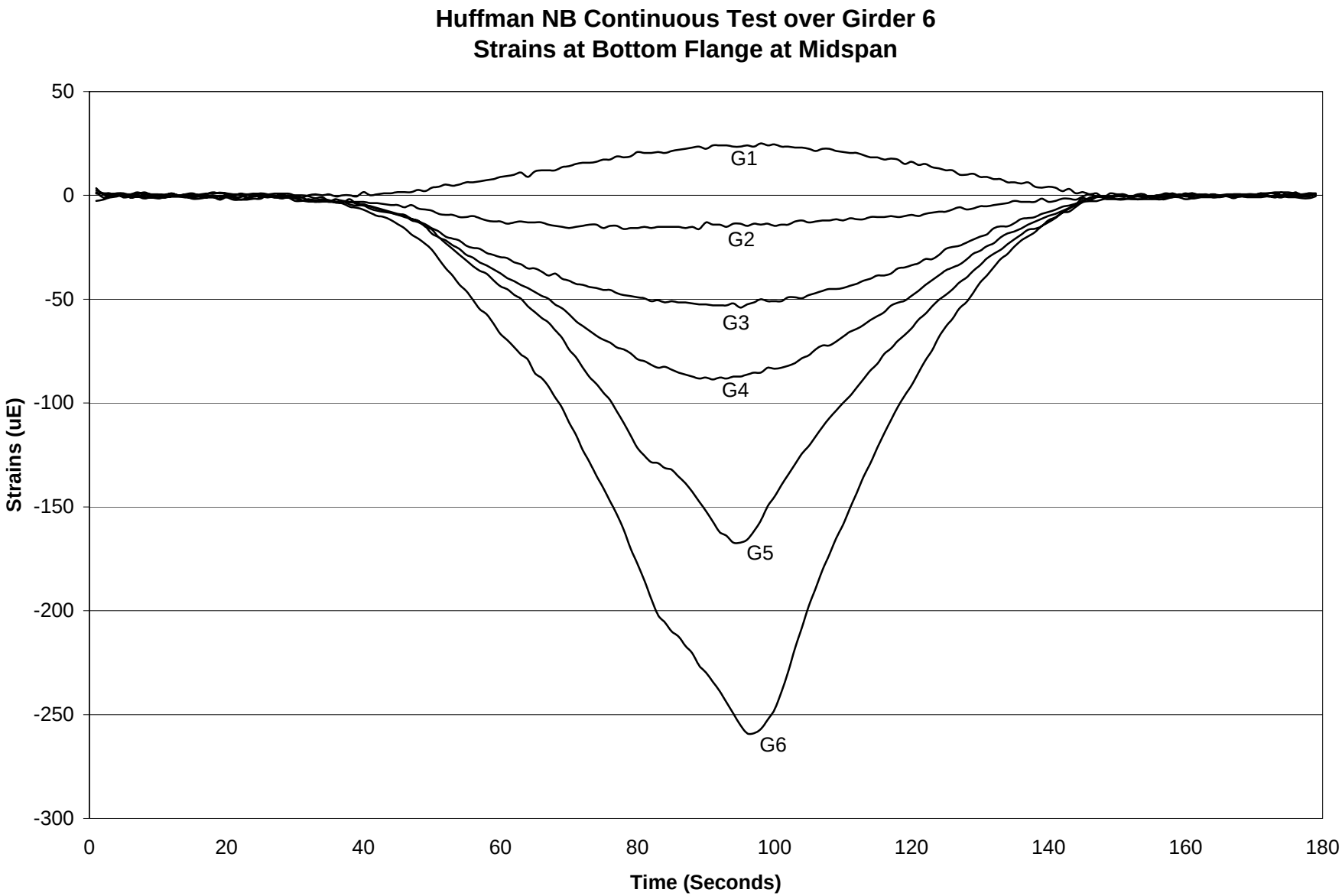
Huffman NB Continuous Test over Girder 6
Strains at Bottom Flange at Midspan
50
0
-50
-100
-150
-200
-250
-300
Strains (uE)
0
20
40
60
80
100
120
140
160
180
Time (Seconds)
G1
G2
G3
G4
G5
G6

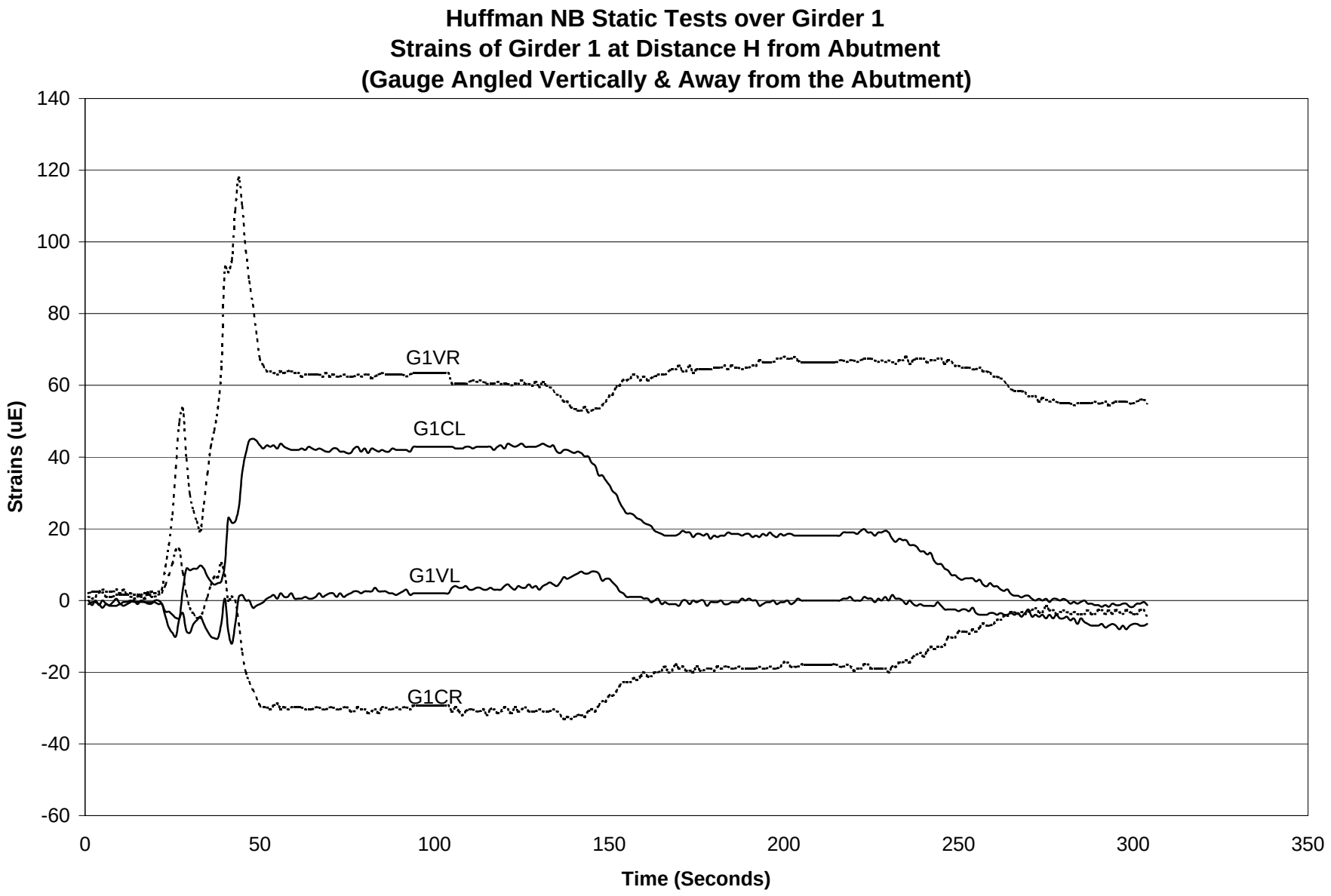
Huffman NB Static Tests over Girder 1
Strains of Girder 1 at Distance H from Abutment
(Gauge Angled Vertically & Away from the Abutment)
Strains (uE)
Time (Seconds)
G1VR
G1CL
G1VL
G1CR
140
120
100
80
60
40
20
0
-20
-40
-60
0
50
100
150
200
250
300
350

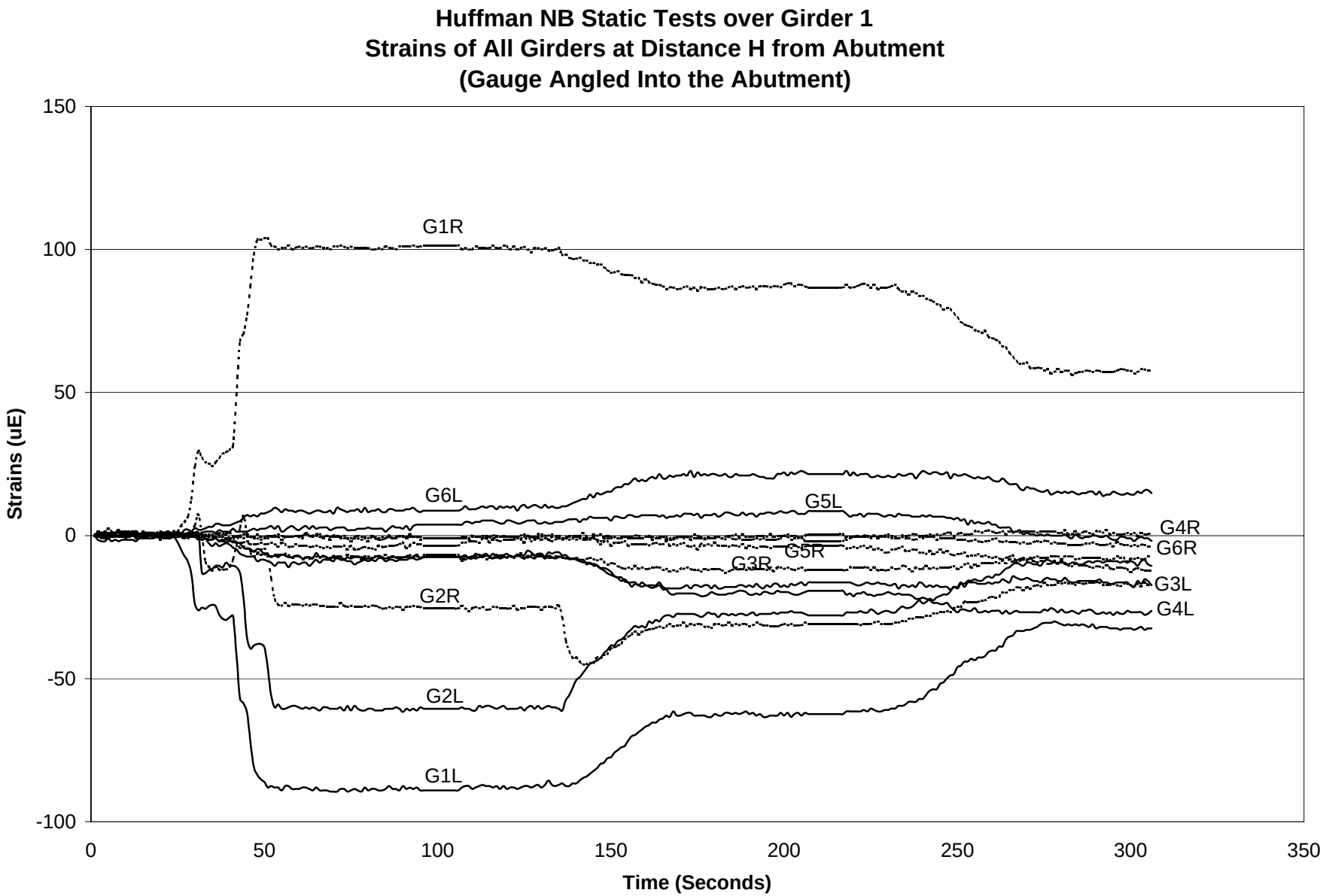
Huffman NB Static Tests over Girder 1
Strains of All Girders at Distance H from Abutment
(Gauge Angled Into the Abutment)
Strains (uE)
Time (Seconds)
150
100
50
0
-50
-100
0
50
100
150
200
250
300
350
G1R
G6L
G5L
G4R
G6R
G5R
G3R
G3L
G2R
G4L
G2L
G1L

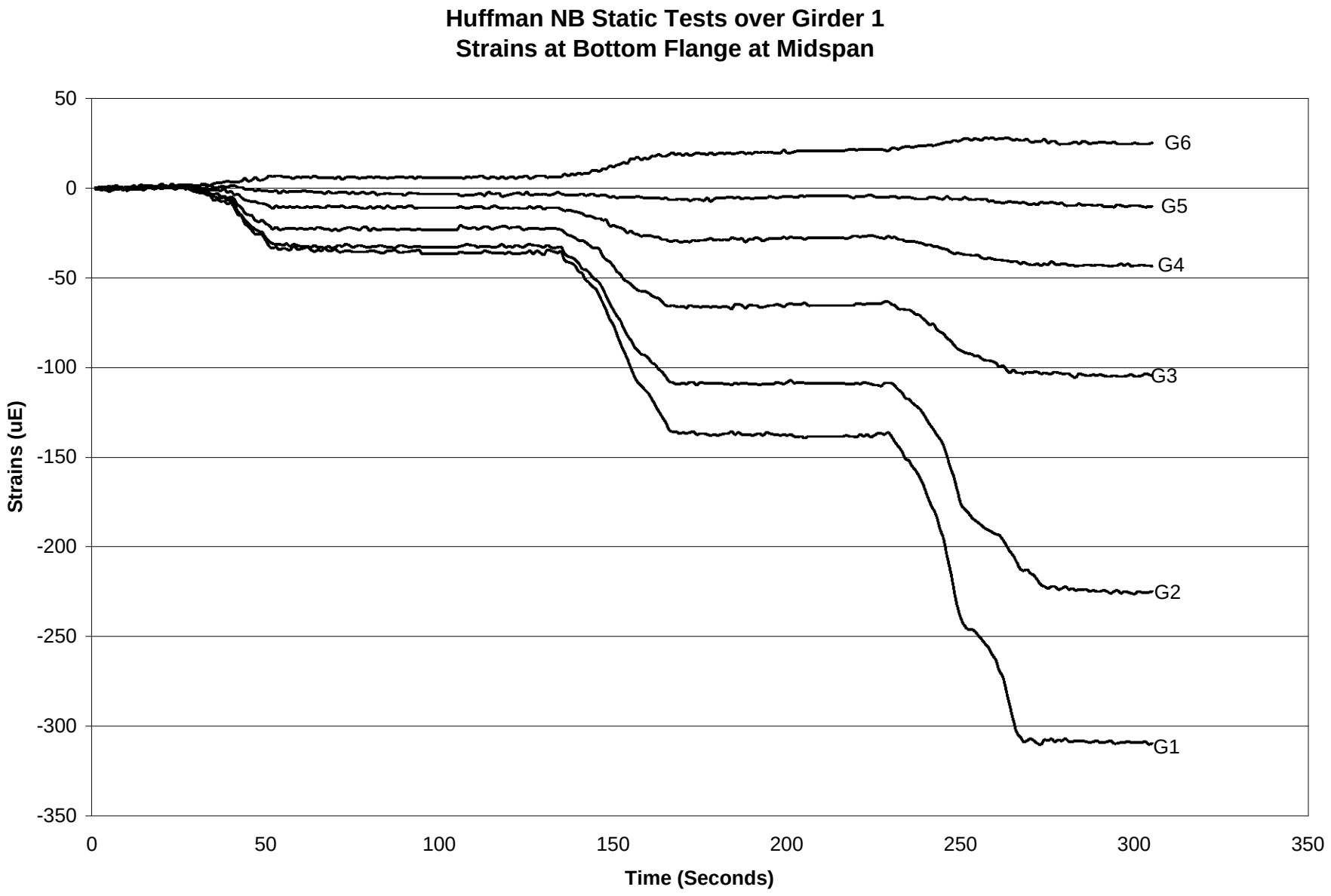
Huffman NB Static Tests over Girder 1
Strains at Bottom Flange at Midspan
Strains (uE)
Time (Seconds)
50
0
-50
-100
-150
-200
-250
-300
-350
0
50
100
150
200
250
300
350
G6
G5
G4
G3
G2
G1

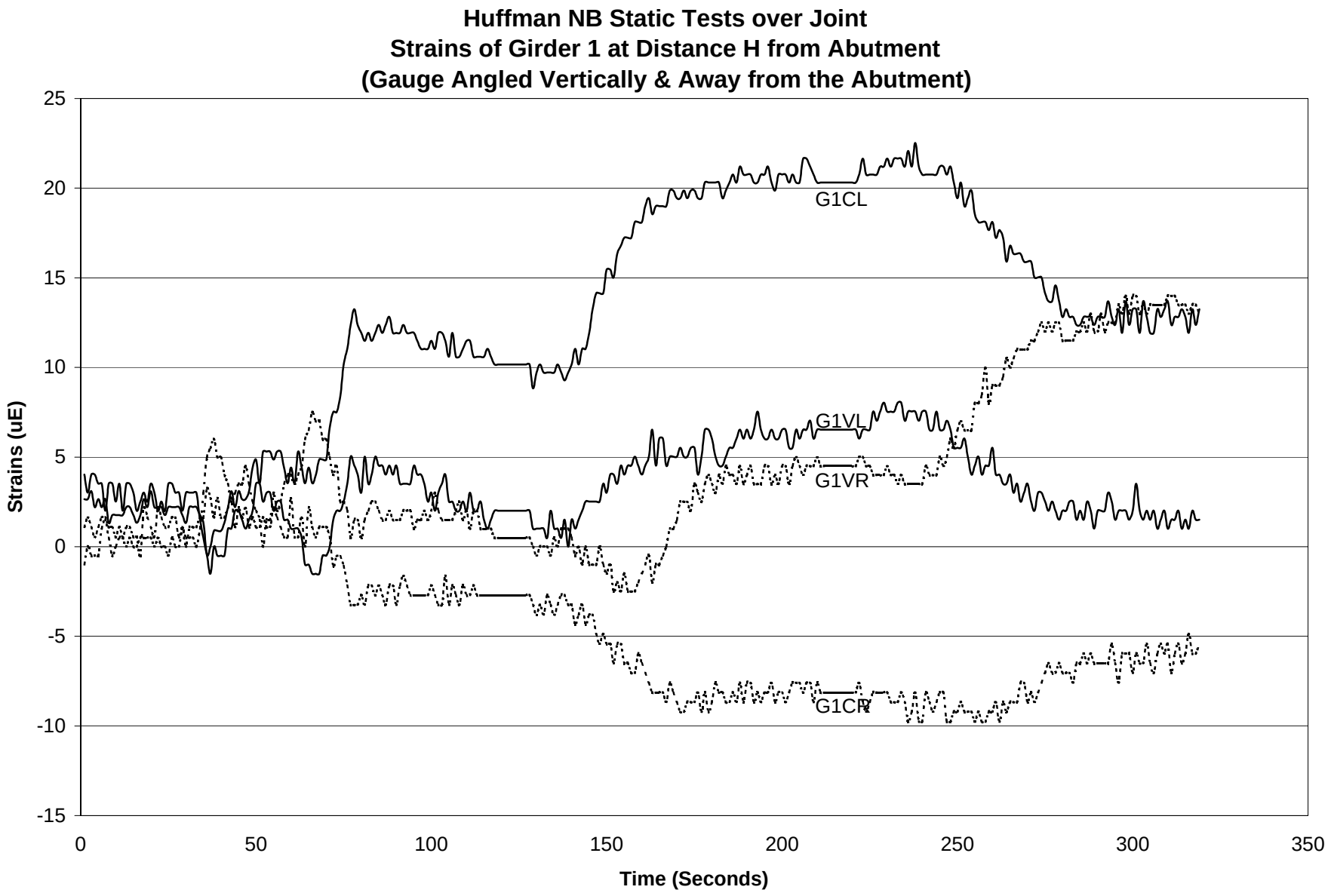
Huffman NB Static Tests over Joint
Strains of Girder 1 at Distance H from Abutment
(Gauge Angled Vertically & Away from the Abutment)
Strains (uE)
Time (Seconds)
G1CL
G1VL
G1VR
G1CR
25
20
15
10
5
0
-5
-10
-15
0
50
100
150
200
250
300
350

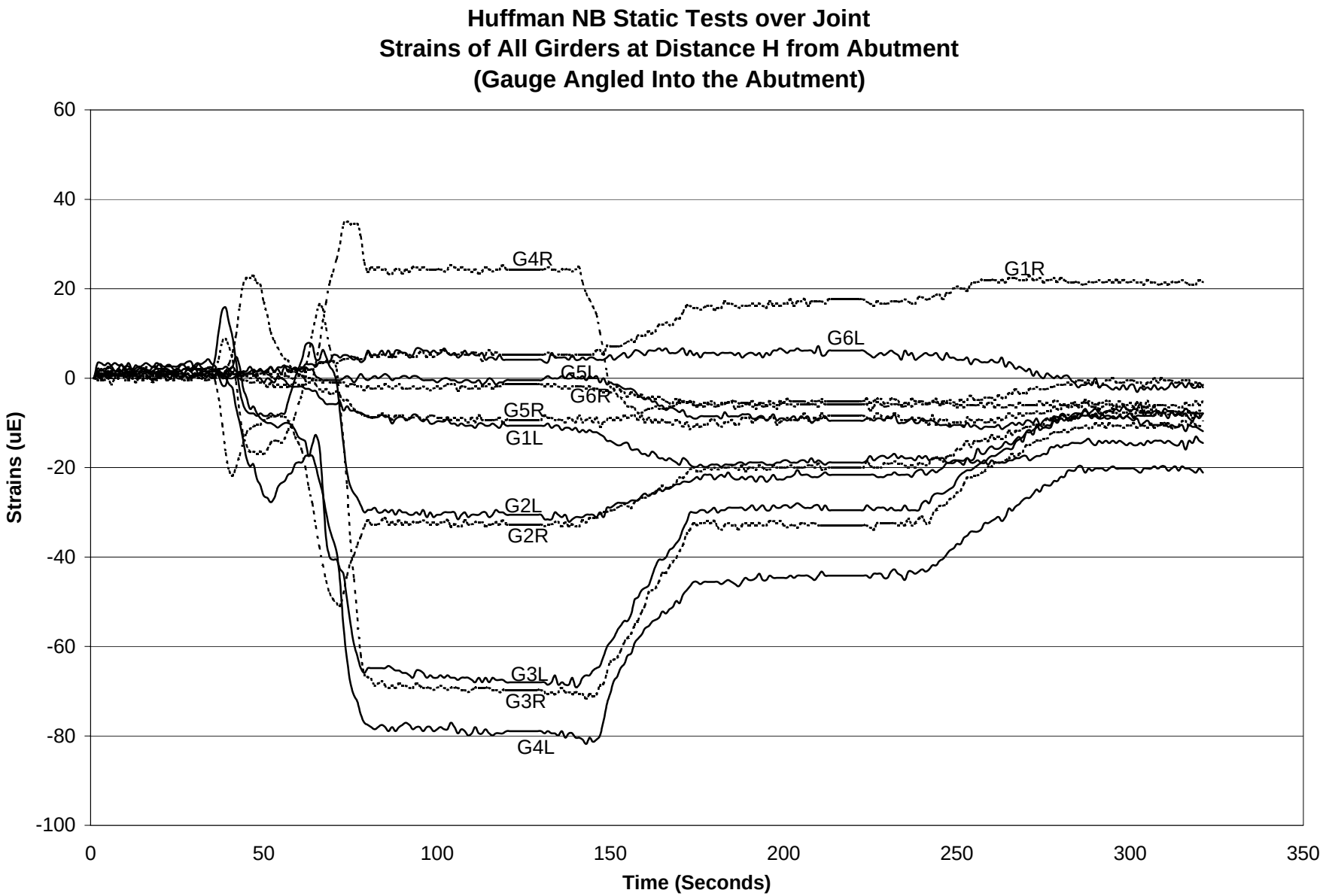
Huffman NB Static Tests over Joint
Strains of All Girders at Distance H from Abutment
(Gauge Angled Into the Abutment)
Strains (uE)
Time (Seconds)
60
40
20
0
-20
-40
-60
-80
-100
0
50
100
150
200
250
300
350
G4R
G1R
G6L
G5L
G6R
G5R
G1L
G2L
G2R
G3L
G3R
G4L

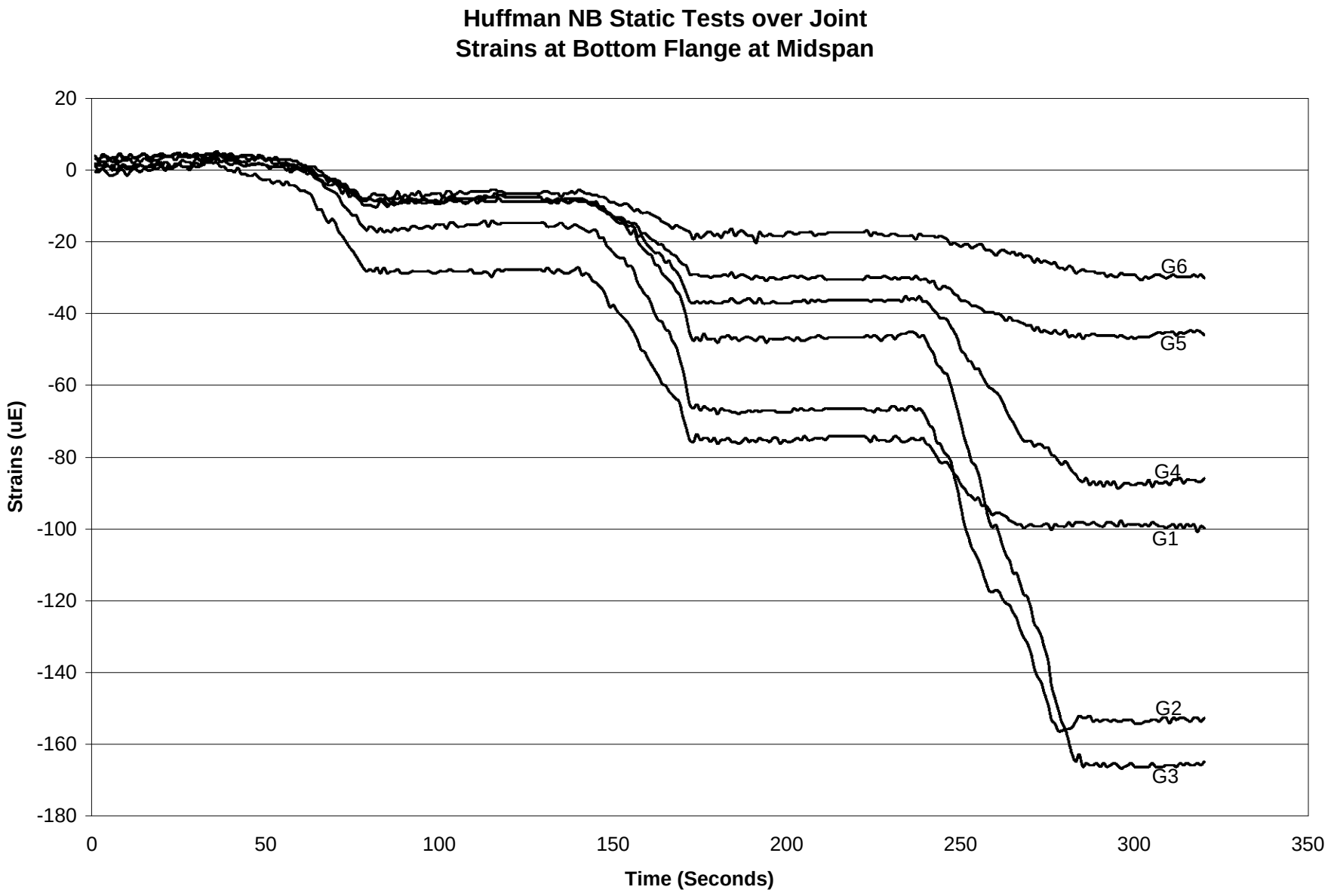
Huffman NB Static Tests over Joint
Strains at Bottom Flange at Midspan
Strains (uE)
Time (Seconds)
20
0
-20
-40
-60
-80
-100
-120
-140
-160
-180
0
50
100
150
200
250
300
350
G6
G5
G4
G1
G2
G3

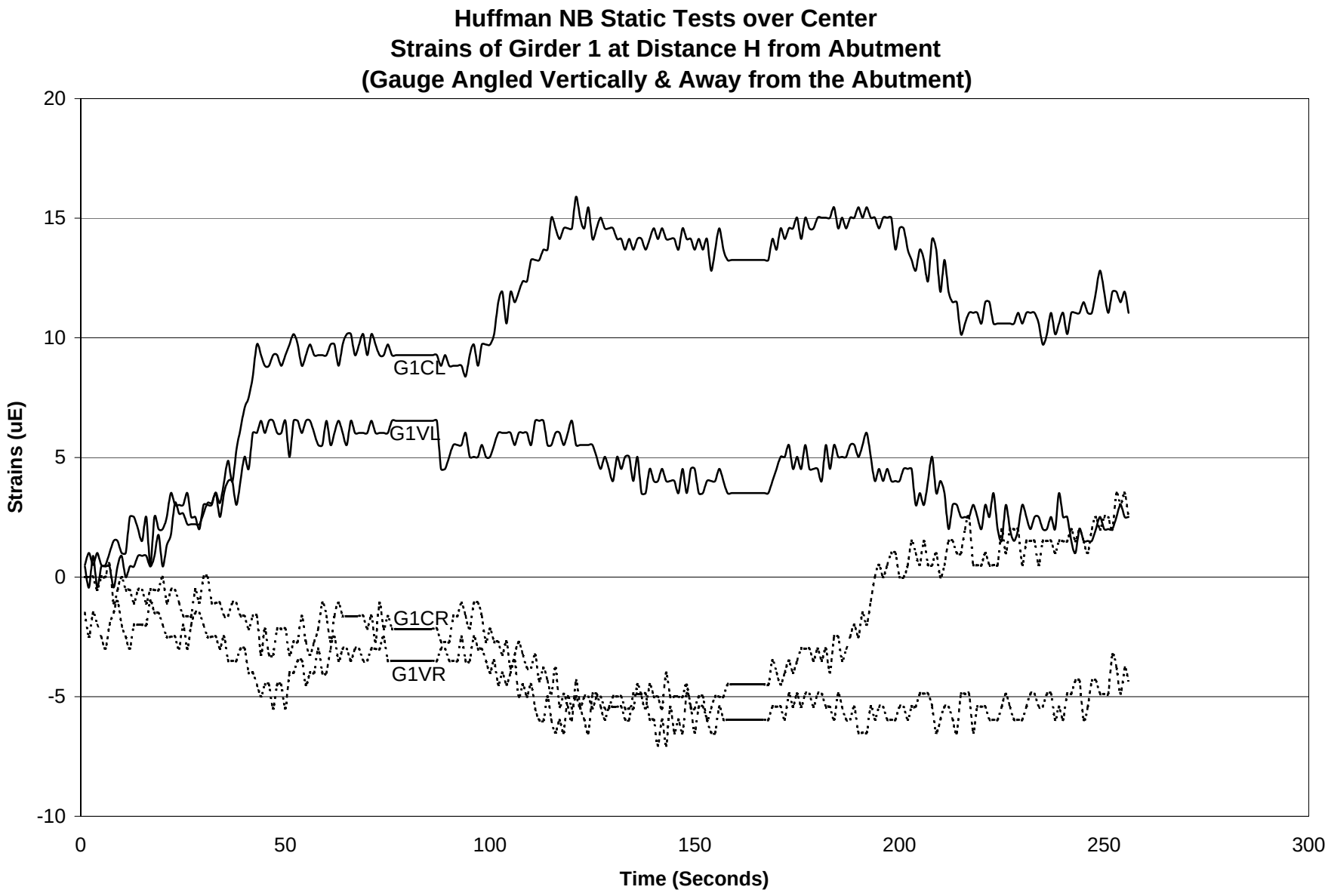
Huffman NB Static Tests over Center
Strains of Girder 1 at Distance H from Abutment
(Gauge Angled Vertically & Away from the Abutment)
Strains (uE)
Time (Seconds)
20
15
10
5
0
-5
-10
0
50
100
150
200
250
300
G1CL
G1VL
G1CR
G1VR

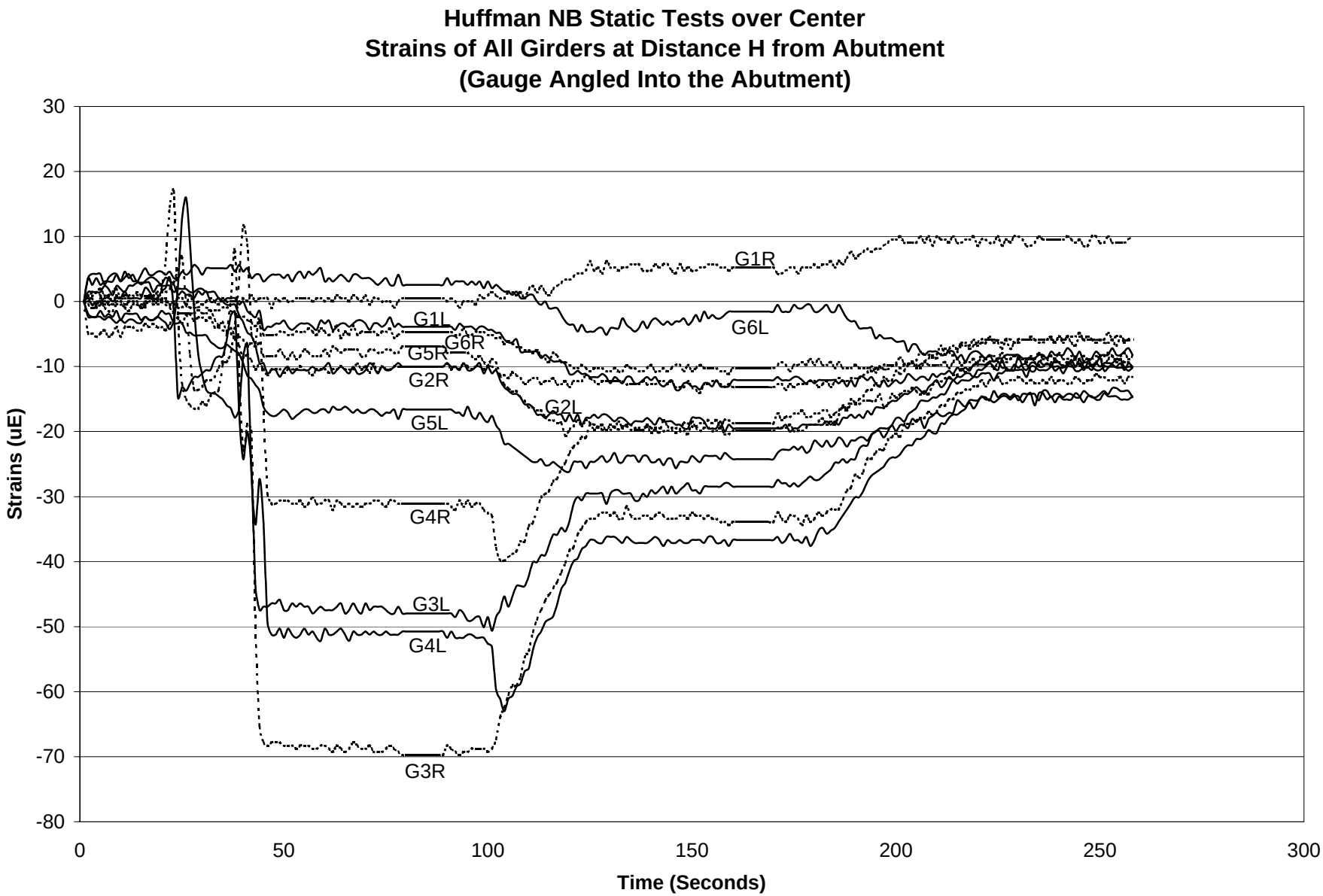
Huffman NB Static Tests over Center
Strains of All Girders at Distance H from Abutment
(Gauge Angled Into the Abutment)
Strains (uE)
Time (Seconds)
30
20
10
0
-10
-20
-30
-40
-50
-60
-70
-80
0
50
100
150
200
250
300
G1R
G6L
G1L
G6R
G5R
G2R
G2L
G5L
G4R
G3L
G4L
G3R

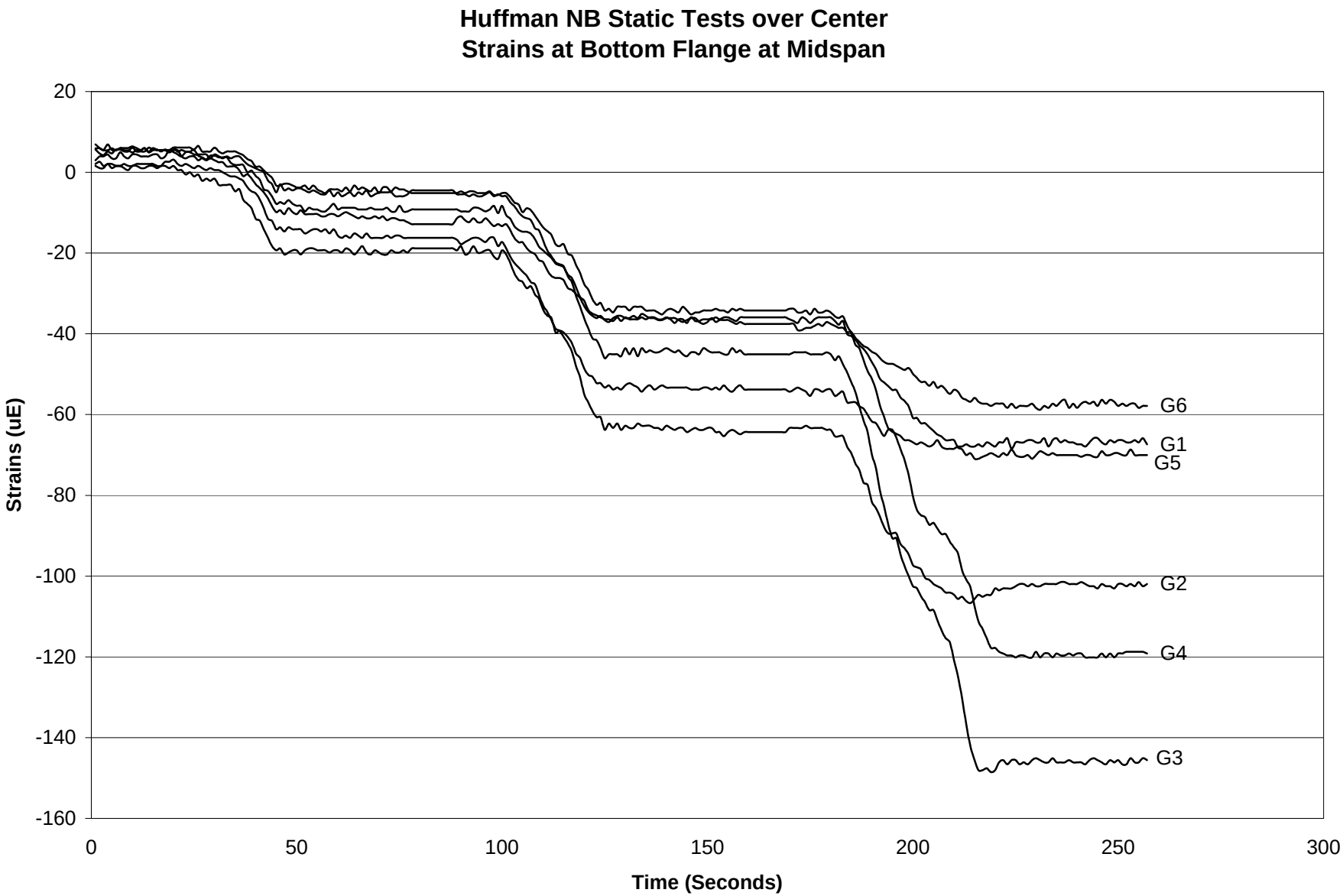
Huffman NB Static Tests over Center
Strains at Bottom Flange at Midspan
Strains (uE)
Time (Seconds)
20
0
-20
-40
-60
-80
-100
-120
-140
-160
0
50
100
150
200
250
300
G6
G1
G5
G2
G4
G3

Huffman NB Static Tests over Girder 6
Strains of Girder 1 at Distance H from Abutment
(Gauge Angled Vertically & Away from the Abutment)
Strains (uE)
Time (Seconds)
G1VL
G1CL
G1CR
G1VR
25
20
15
10
5
0
-5
-10
-15
-20
-25
0
50
100
150
200
250
300

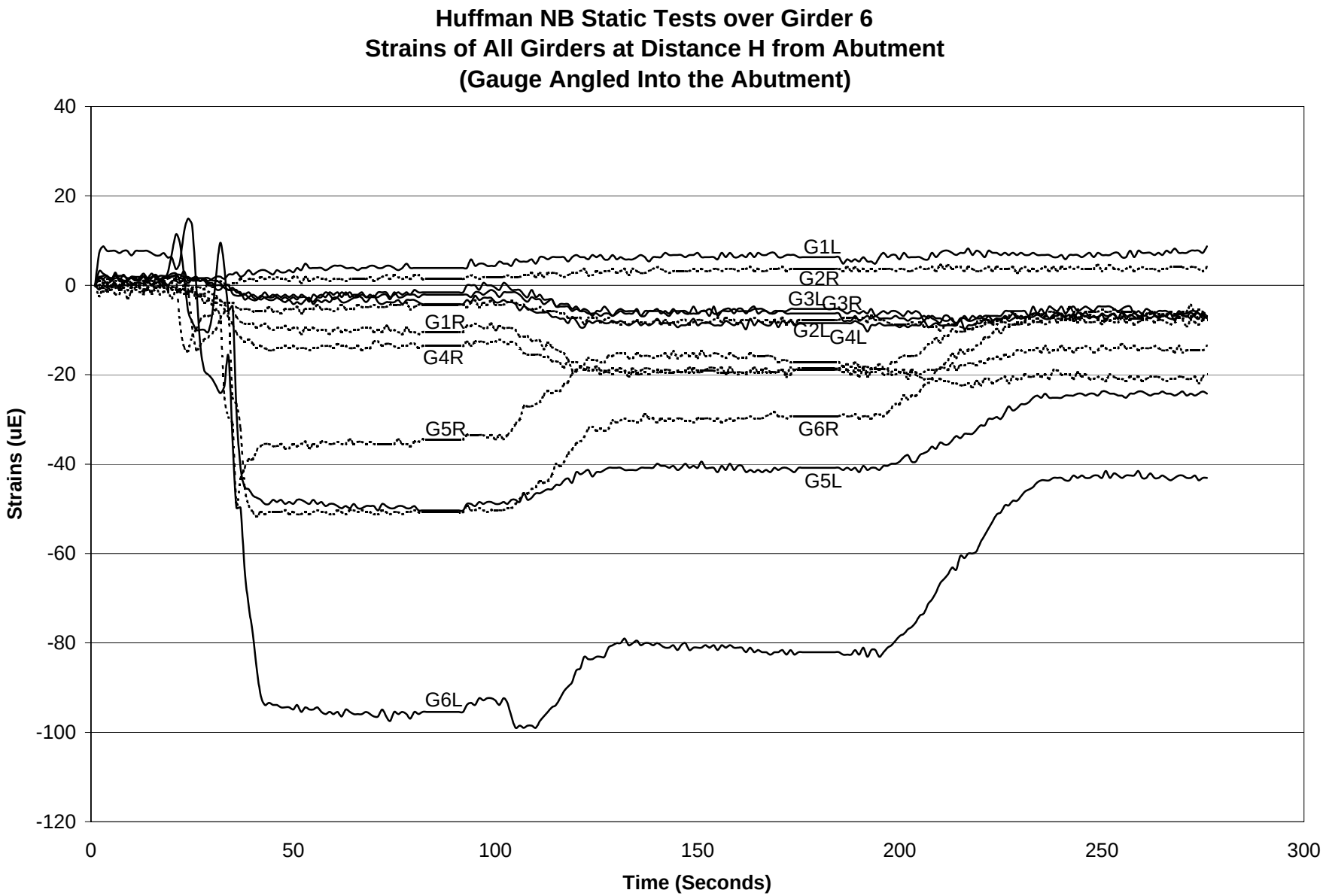
Huffman NB Static Tests over Girder 6
Strains of All Girders at Distance H from Abutment
(Gauge Angled Into the Abutment)
Strains (uE)
Time (Seconds)
40
20
0
-20
-40
-60
-80
-100
-120
0
50
100
150
200
250
300
G1L
G2R
G3L
G3R
G1R
G2L
G4L
G4R
G5R
G6R
G5L
G6L

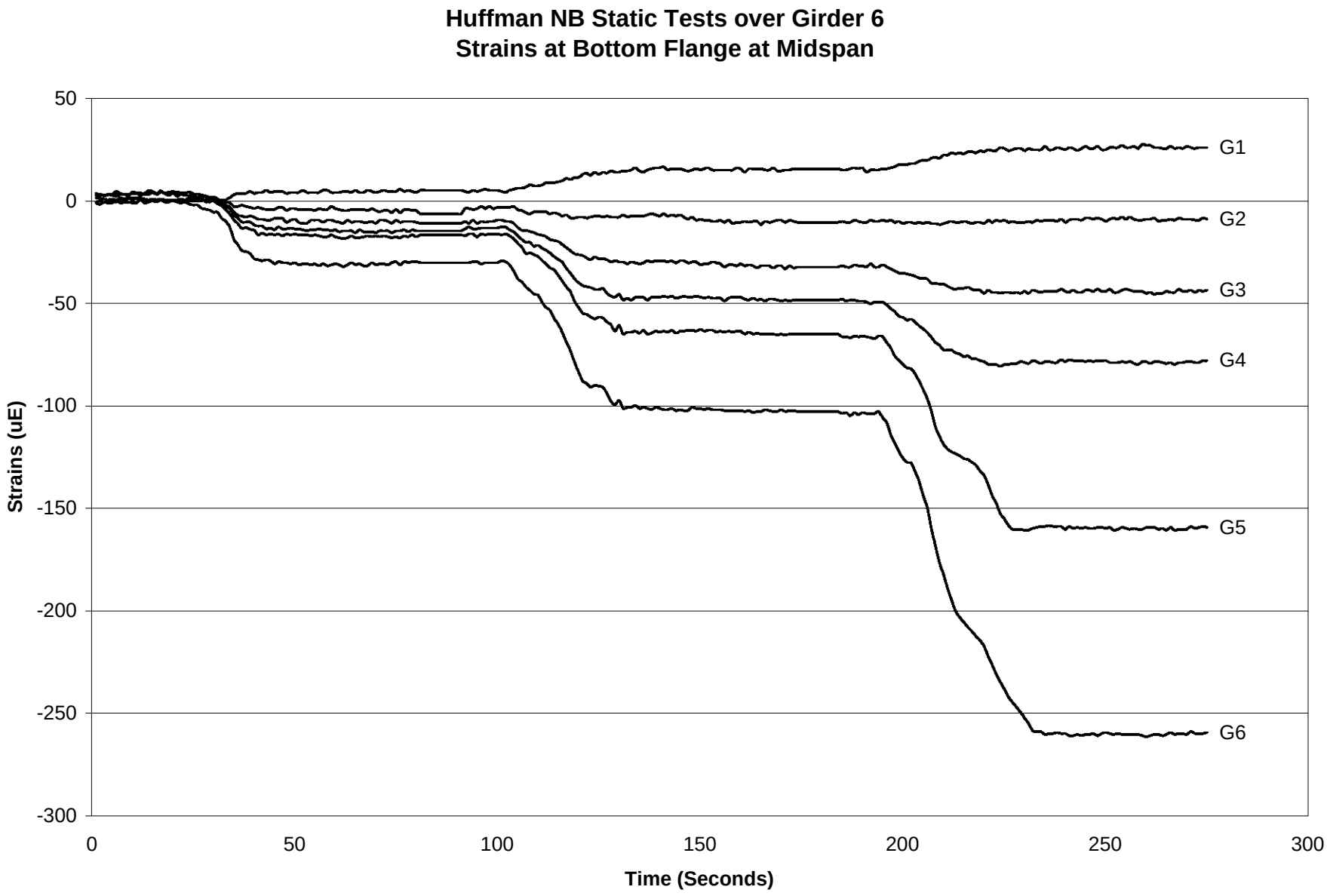
Huffman NB Static Tests over Girder 6
Strains at Bottom Flange at Midspan
Strains (uE)
Time (Seconds)
50
0
-50
-100
-150
-200
-250
-300
0
50
100
150
200
250
300
G1
G2
G3
G4
G5
G6

# Huffman SB

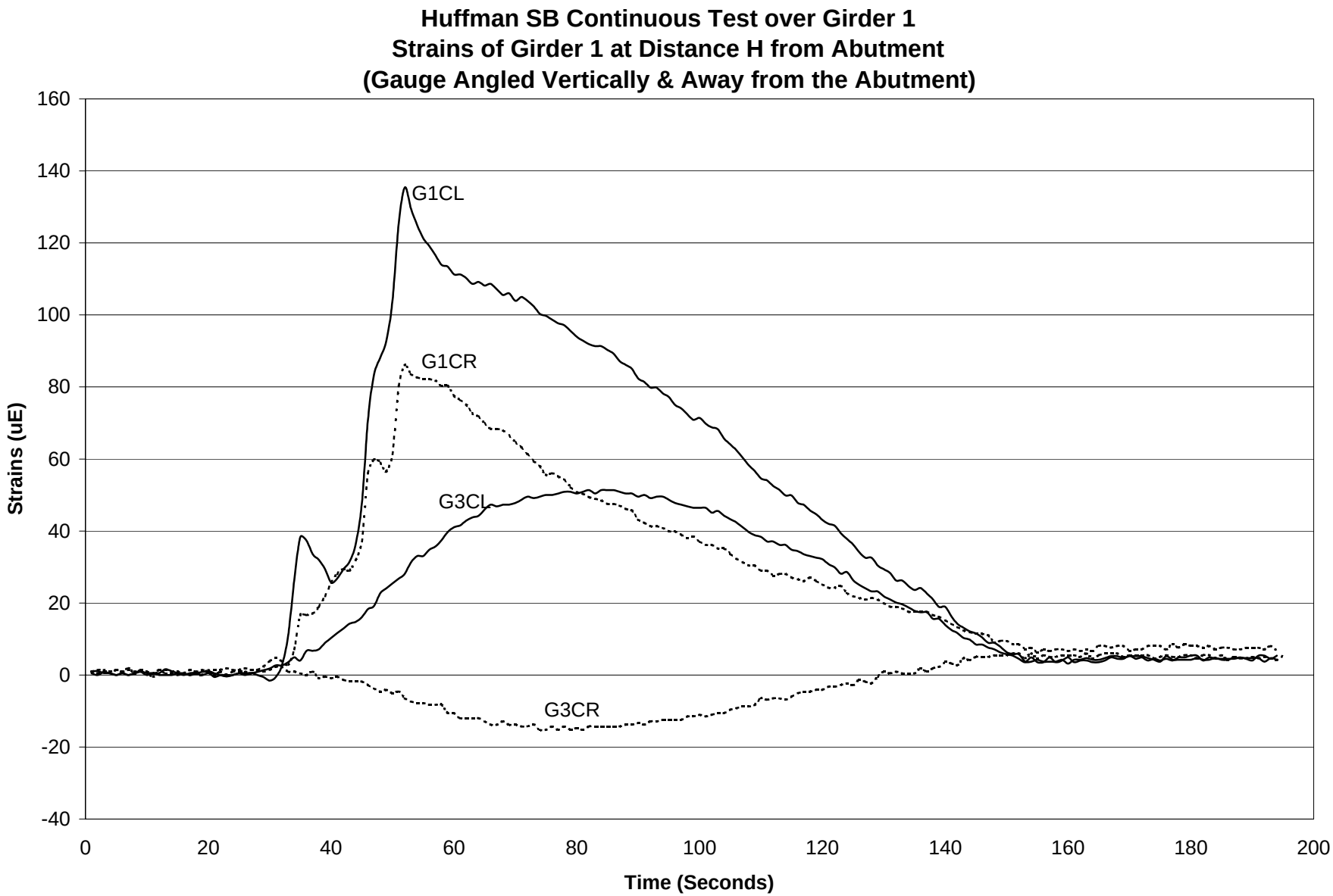
Huffman SB Continuous Test over Girder 1
Strains of Girder 1 at Distance H from Abutment
(Gauge Angled Vertically & Away from the Abutment)
Strains (uE)
Time (Seconds)
G1CL
G1CR
G3CL
G3CR
160
140
120
100
80
60
40
20
0
-20
-40
0
20
40
60
80
100
120
140
160
180
200

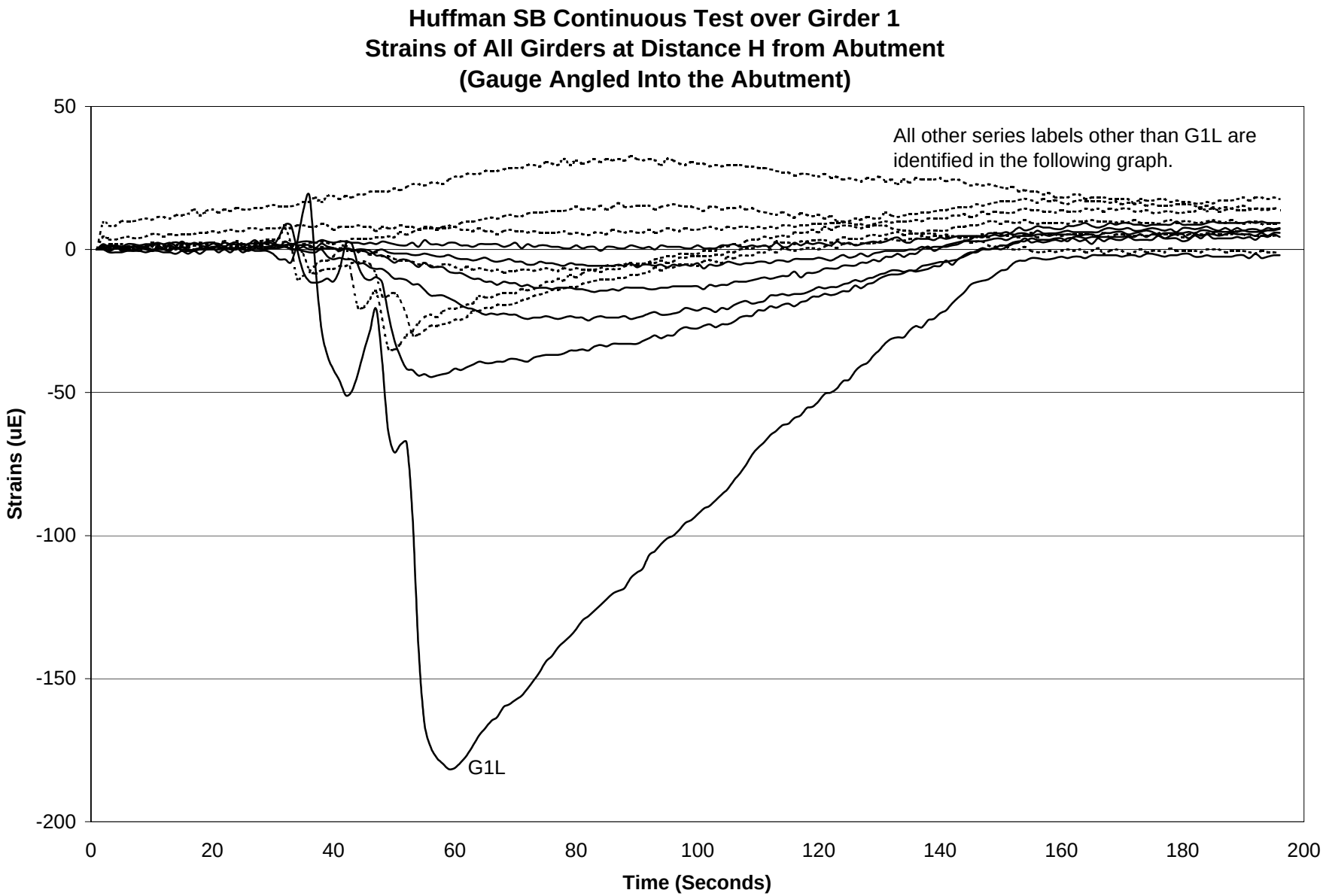
Huffman SB Continuous Test over Girder 1
Strains of All Girders at Distance H from Abutment
(Gauge Angled Into the Abutment)
All other series labels other than G1L are identified in the following graph.
G1L
Strains (uE)
Time (Seconds)
50
0
-50
-100
-150
-200
0
20
40
60
80
100
120
140
160
180
200

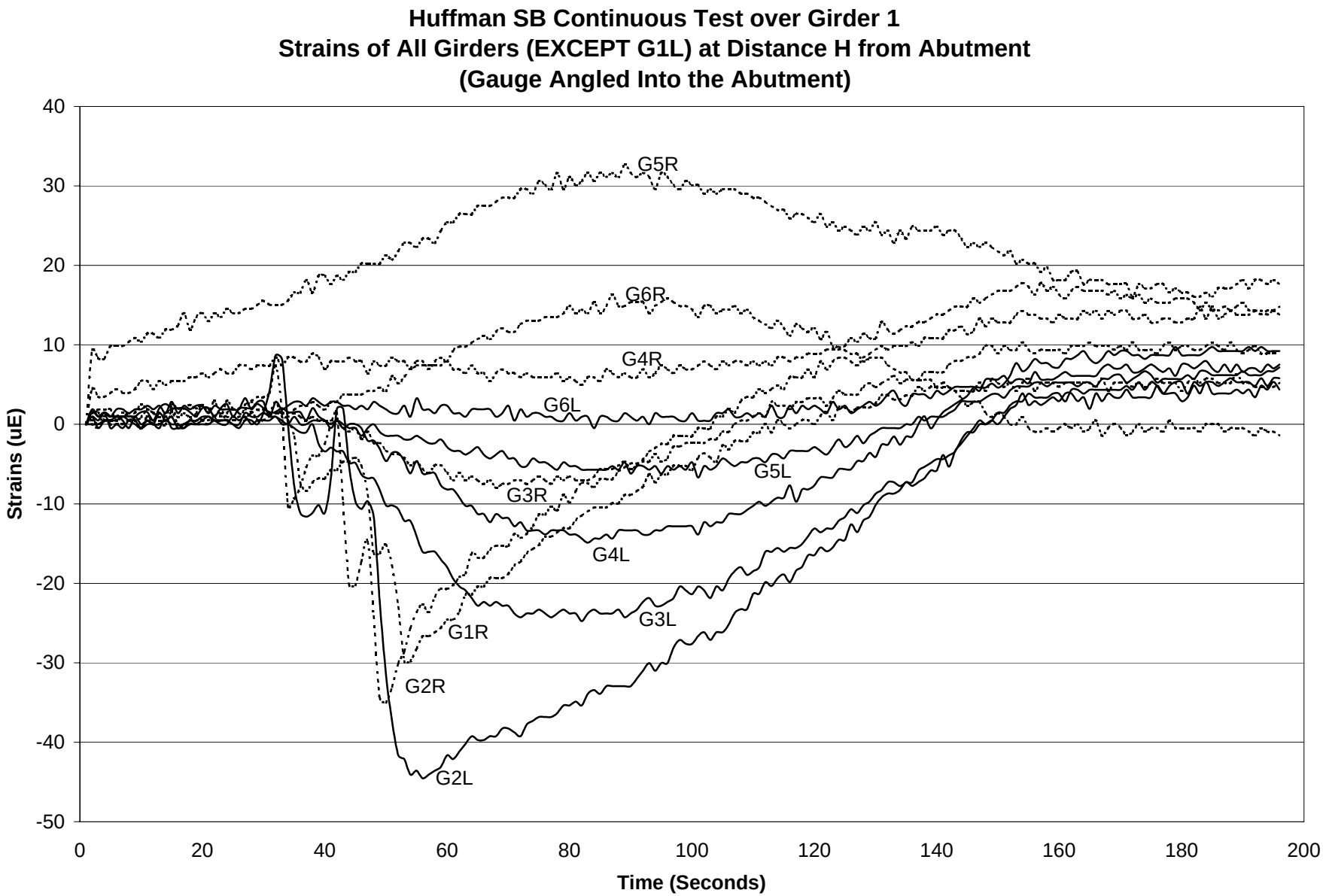
Huffman SB Continuous Test over Girder 1
Strains of All Girders (EXCEPT G1L) at Distance H from Abutment
(Gauge Angled Into the Abutment)
Strains (uE)
Time (Seconds)
40
30
20
10
0
-10
-20
-30
-40
-50
0
20
40
60
80
100
120
140
160
180
200
G5R
G6R
G4R
G6L
G5L
G3R
G4L
G3L
G1R
G2R
G2L

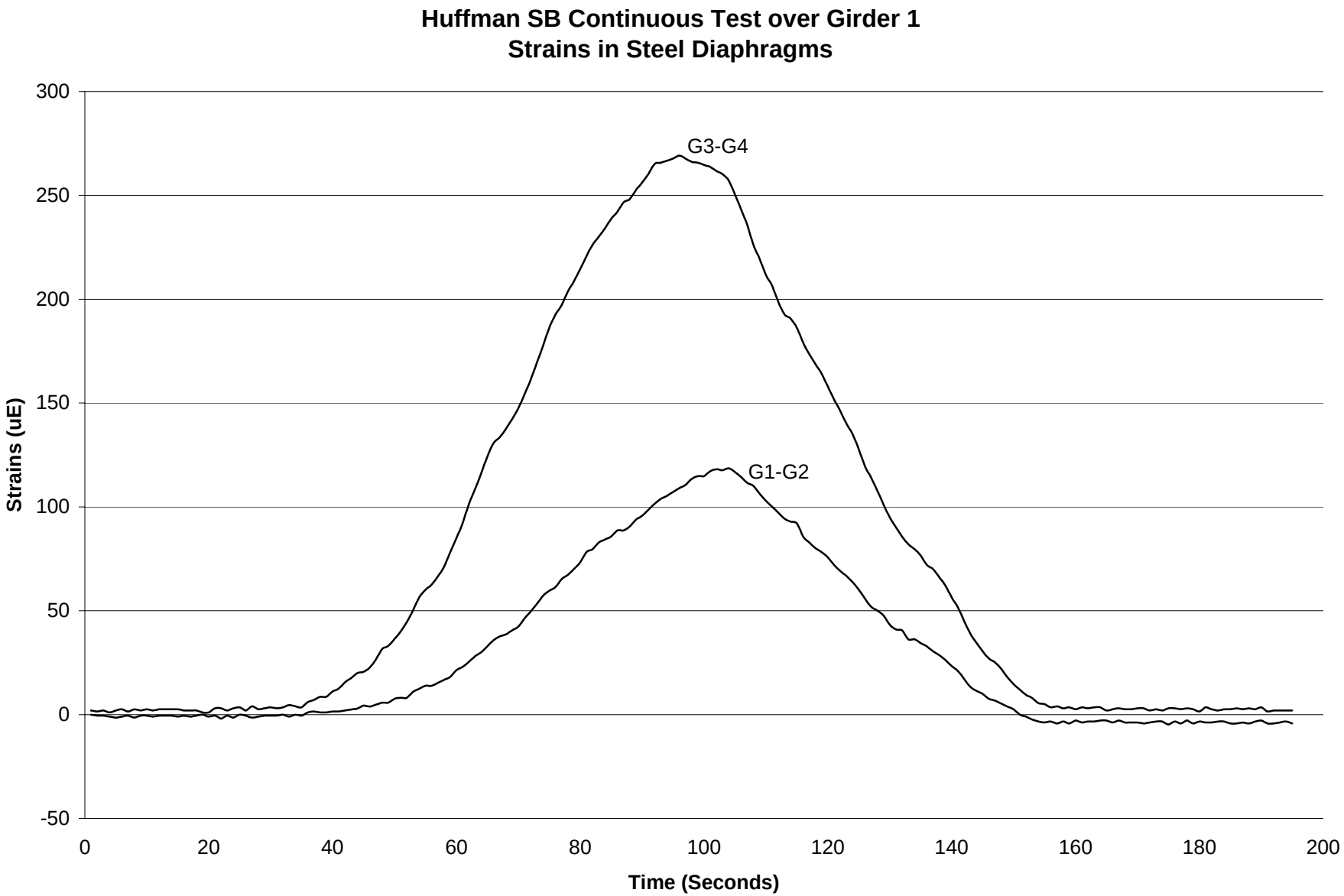
Huffman SB Continuous Test over Girder 1
Strains in Steel Diaphragms
G3-G4
G1-G2
Strains (uE)
Time (Seconds)
300
250
200
150
100
50
0
-50
0
20
40
60
80
100
120
140
160
180
200

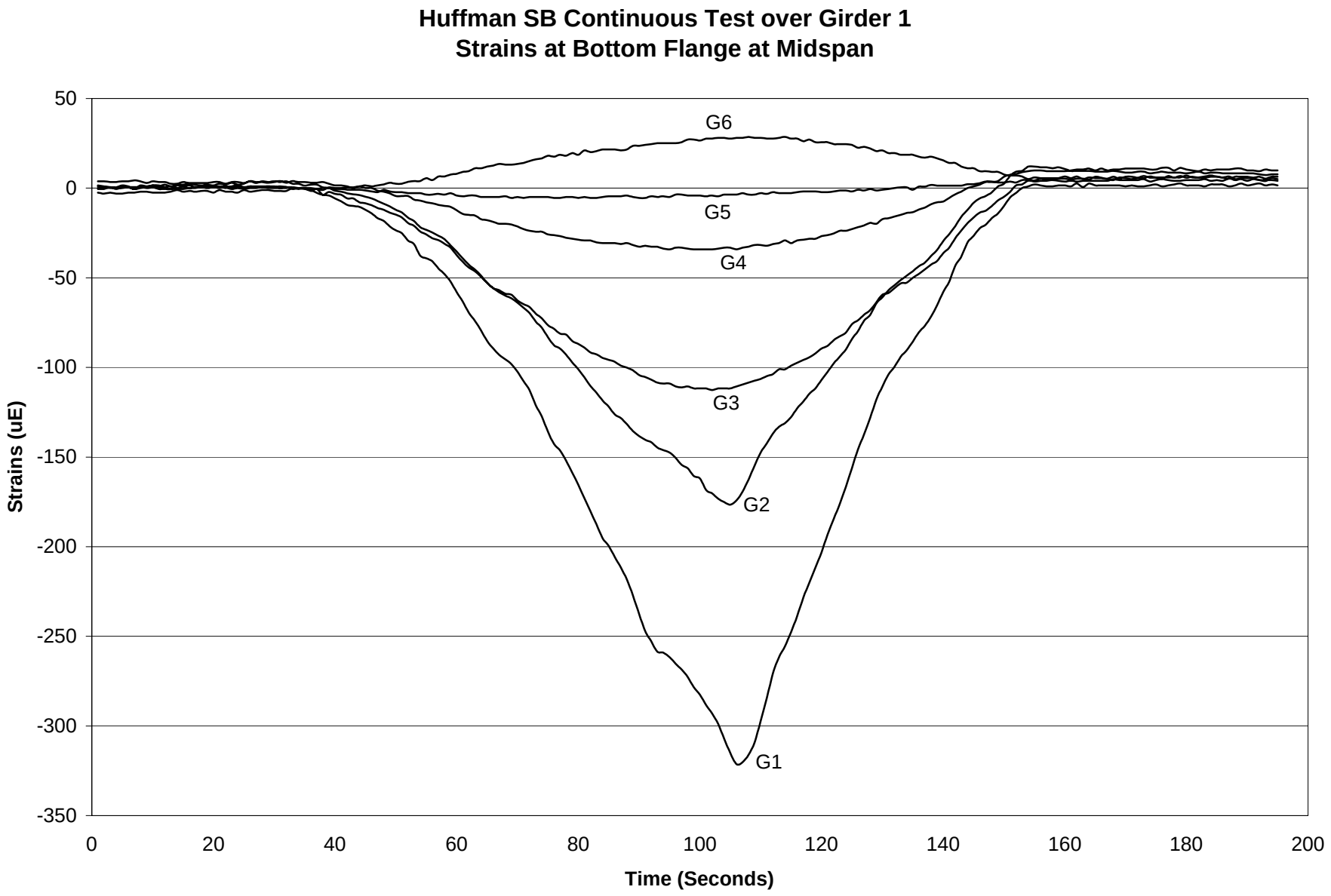
Huffman SB Continuous Test over Girder 1
Strains at Bottom Flange at Midspan
Strains (uE)
Time (Seconds)
50
0
-50
-100
-150
-200
-250
-300
-350
0
20
40
60
80
100
120
140
160
180
200
G6
G5
G4
G3
G2
G1

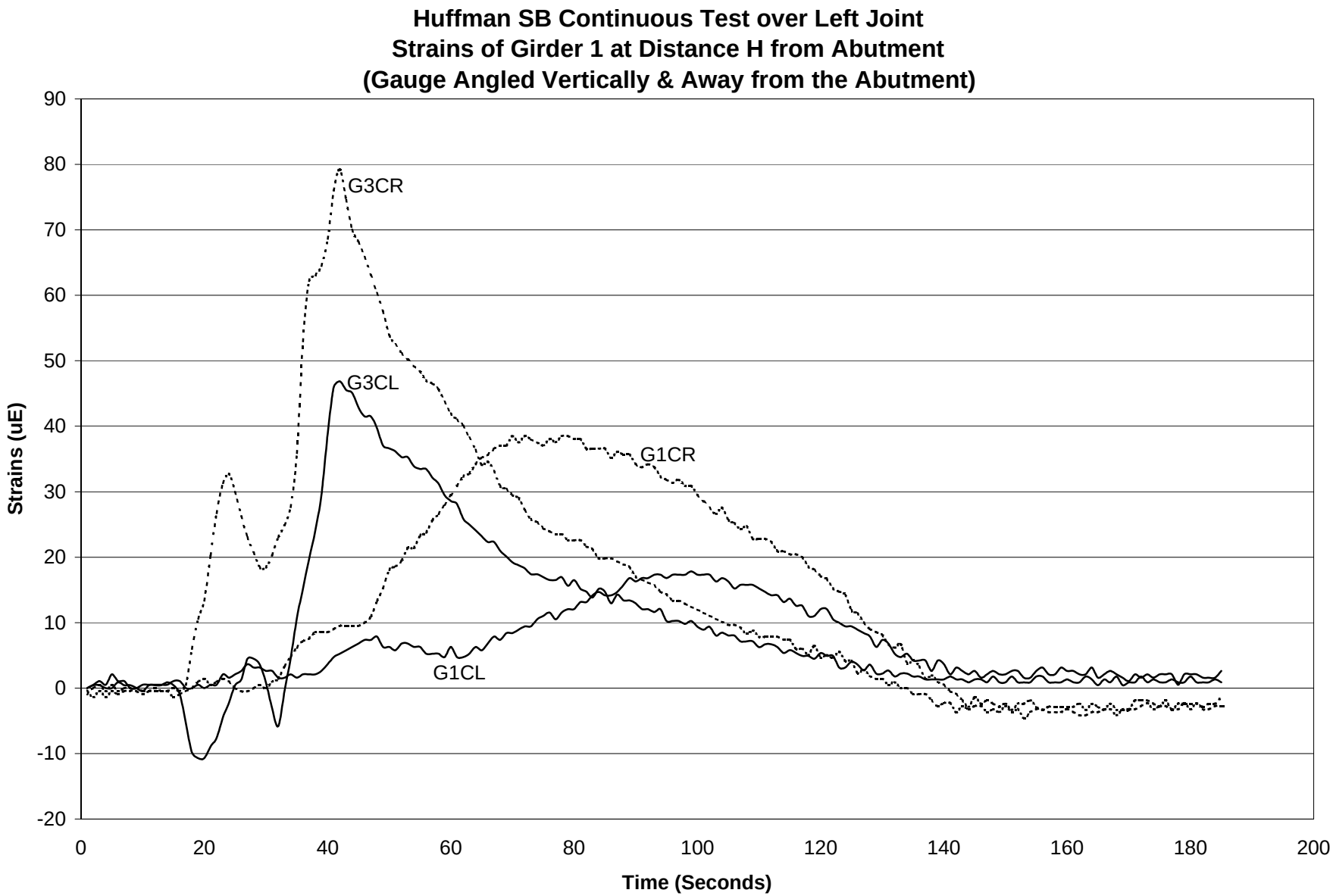
Huffman SB Continuous Test over Left Joint
Strains of Girder 1 at Distance H from Abutment
(Gauge Angled Vertically & Away from the Abutment)
Strains (uE)
Time (Seconds)
G3CR
G3CL
G1CR
G1CL
90
80
70
60
50
40
30
20
10
0
-10
-20
0
20
40
60
80
100
120
140
160
180
200

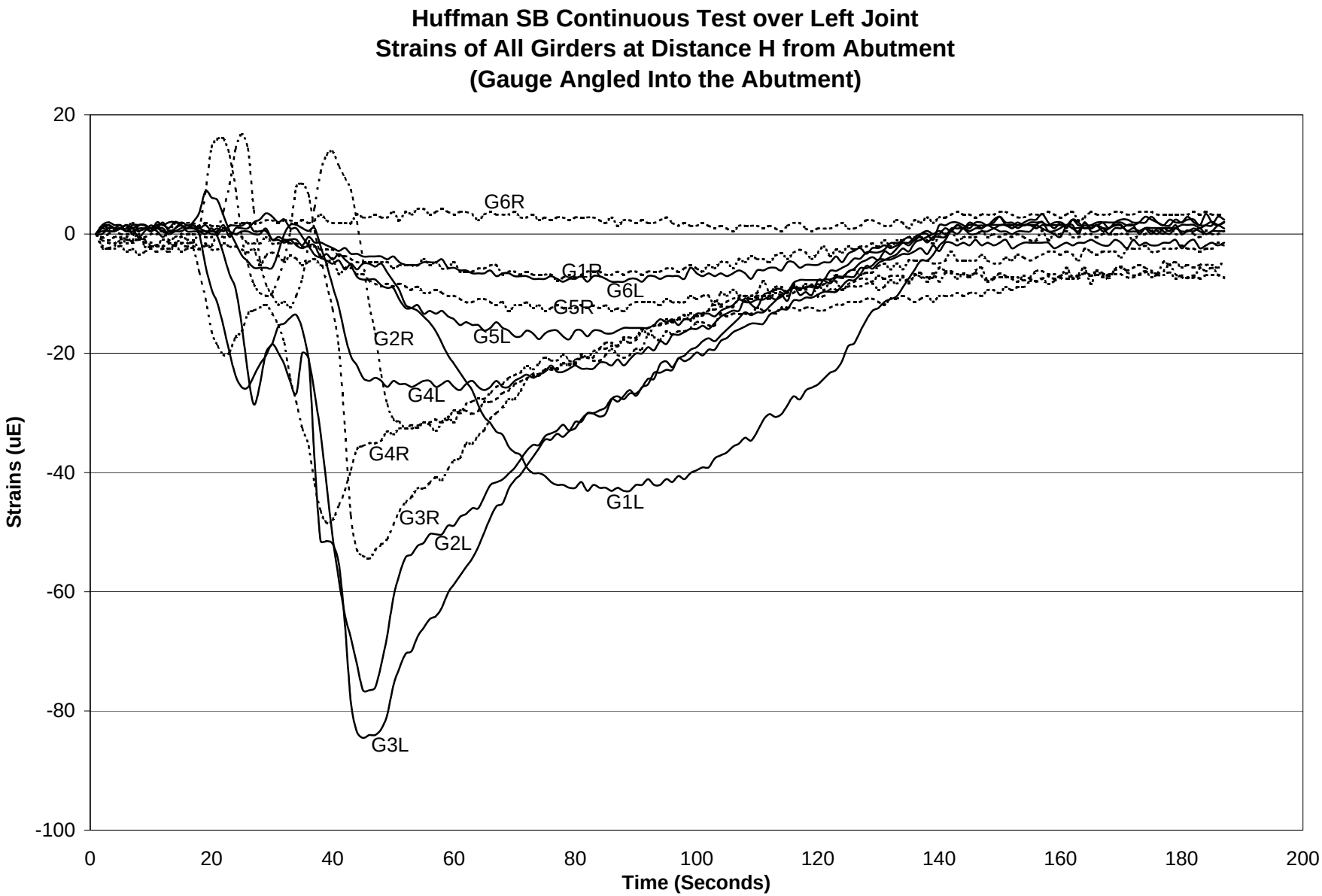
Huffman SB Continuous Test over Left Joint
Strains of All Girders at Distance H from Abutment
(Gauge Angled Into the Abutment)
Strains (uE)
Time (Seconds)
20
0
-20
-40
-60
-80
-100
0
20
40
60
80
100
120
140
160
180
200
G6R
G1R
G6L
G5R
G5L
G2R
G4L
G4R
G1L
G3R
G2L
G3L

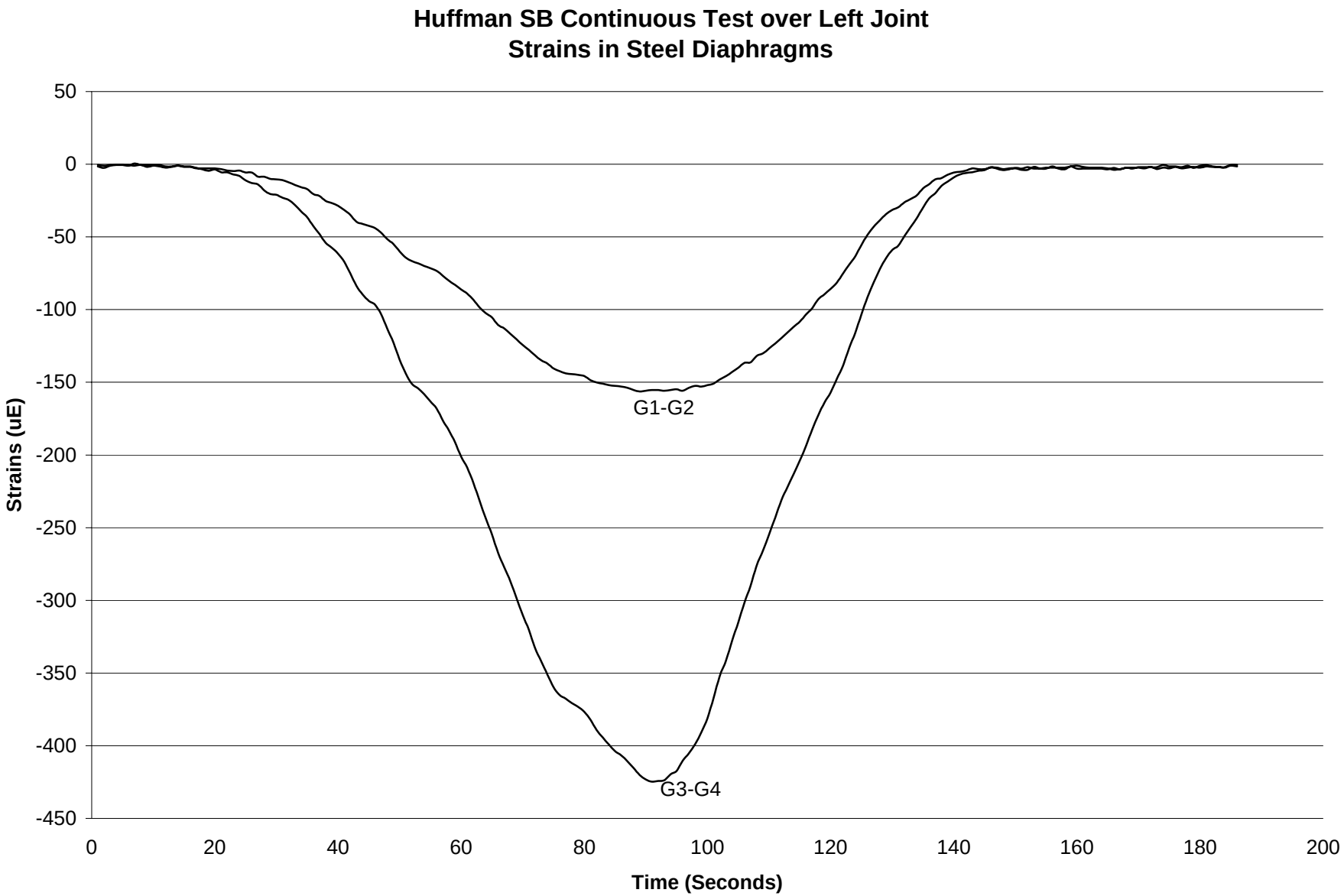
Huffman SB Continuous Test over Left Joint
Strains in Steel Diaphragms
50
0
-50
-100
-150
-200
-250
-300
-350
-400
-450
Strains (uE)
G1-G2
G3-G4
0
20
40
60
80
100
120
140
160
180
200
Time (Seconds)

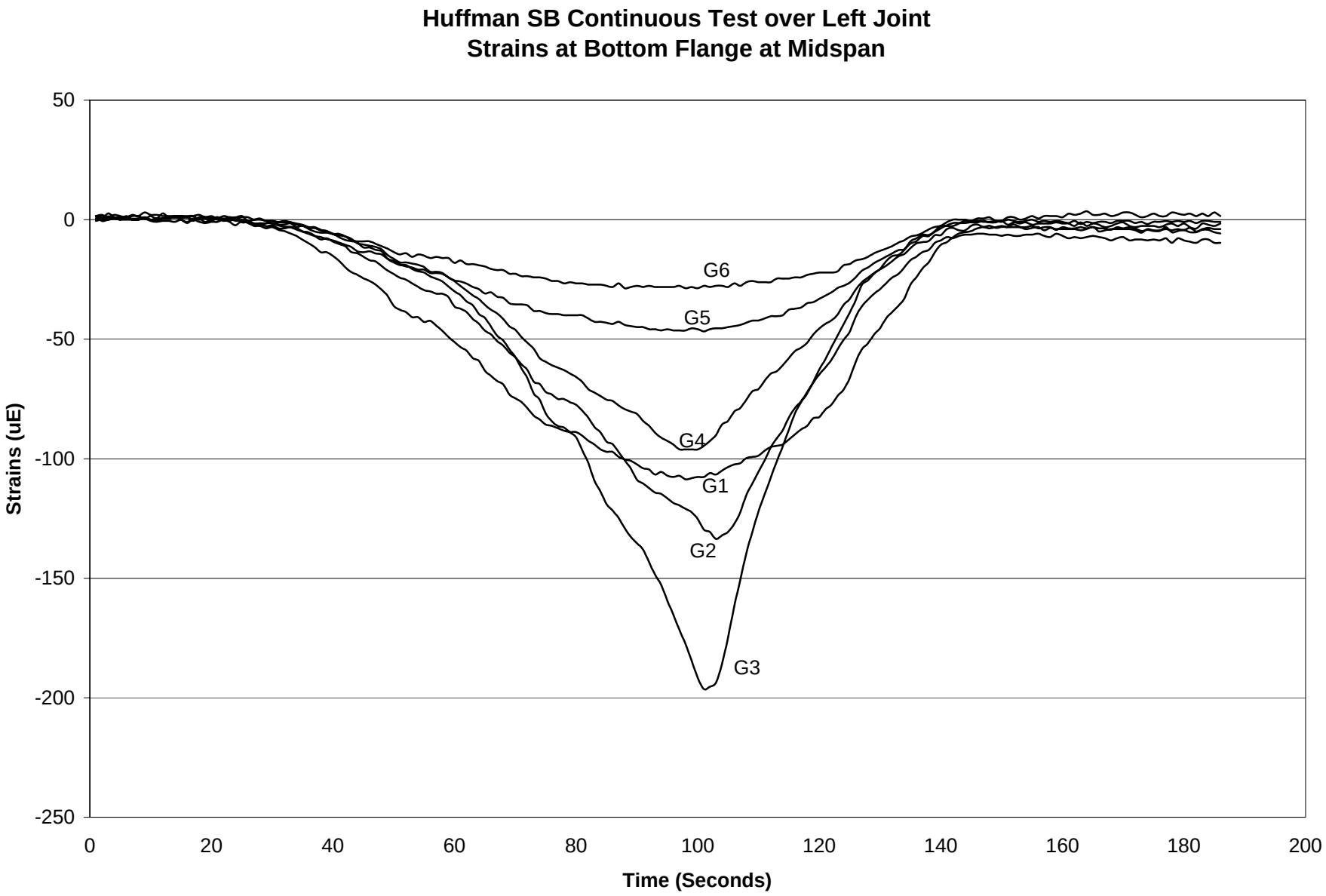
Huffman SB Continuous Test over Left Joint
Strains at Bottom Flange at Midspan
Strains (uE)
Time (Seconds)
50
0
-50
-100
-150
-200
-250
0
20
40
60
80
100
120
140
160
180
200
G6
G5
G4
G1
G2
G3

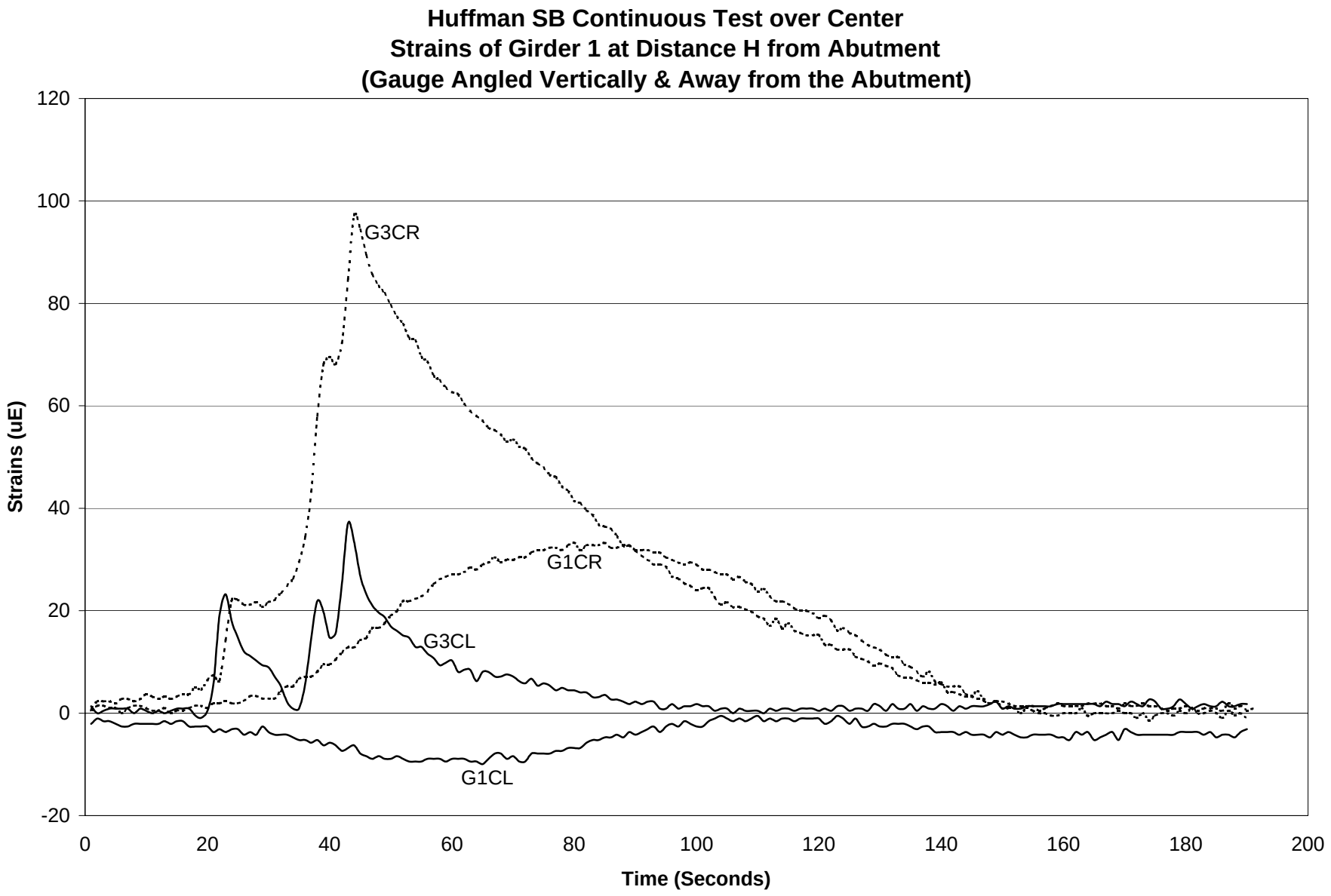
Huffman SB Continuous Test over Center
Strains of Girder 1 at Distance H from Abutment
(Gauge Angled Vertically & Away from the Abutment)
Strains (uE)
Time (Seconds)
G3CR
G1CR
G3CL
G1CL
120
100
80
60
40
20
0
-20
0
20
40
60
80
100
120
140
160
180
200

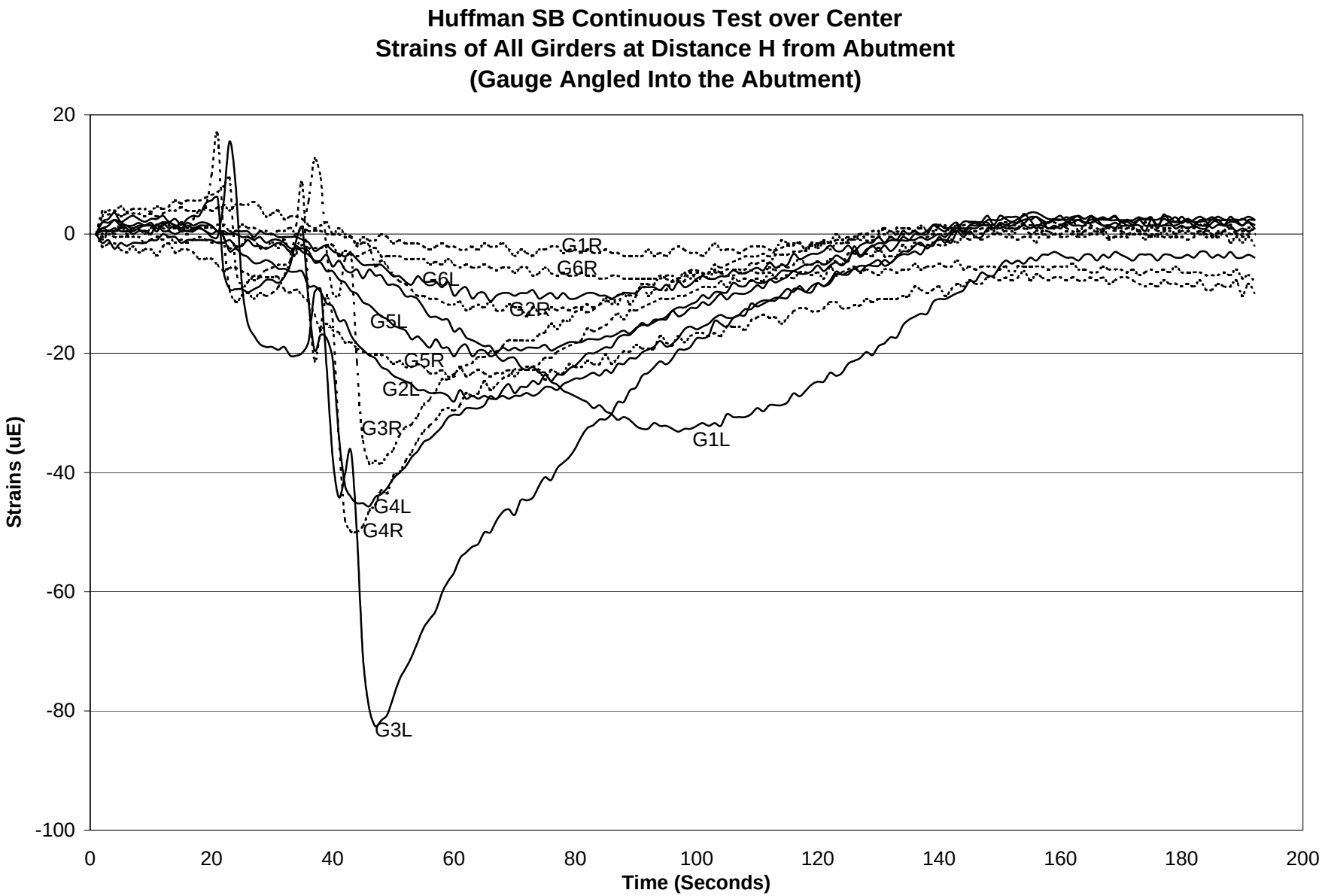
Huffman SB Continuous Test over Center
Strains of All Girders at Distance H from Abutment
(Gauge Angled Into the Abutment)
Strains (uE)
Time (Seconds)
20
0
-20
-40
-60
-80
-100
0
20
40
60
80
100
120
140
160
180
200
G1R
G6R
G6L
G2R
G5L
G5R
G2L
G3R
G1L
G4L
G4R
G3L

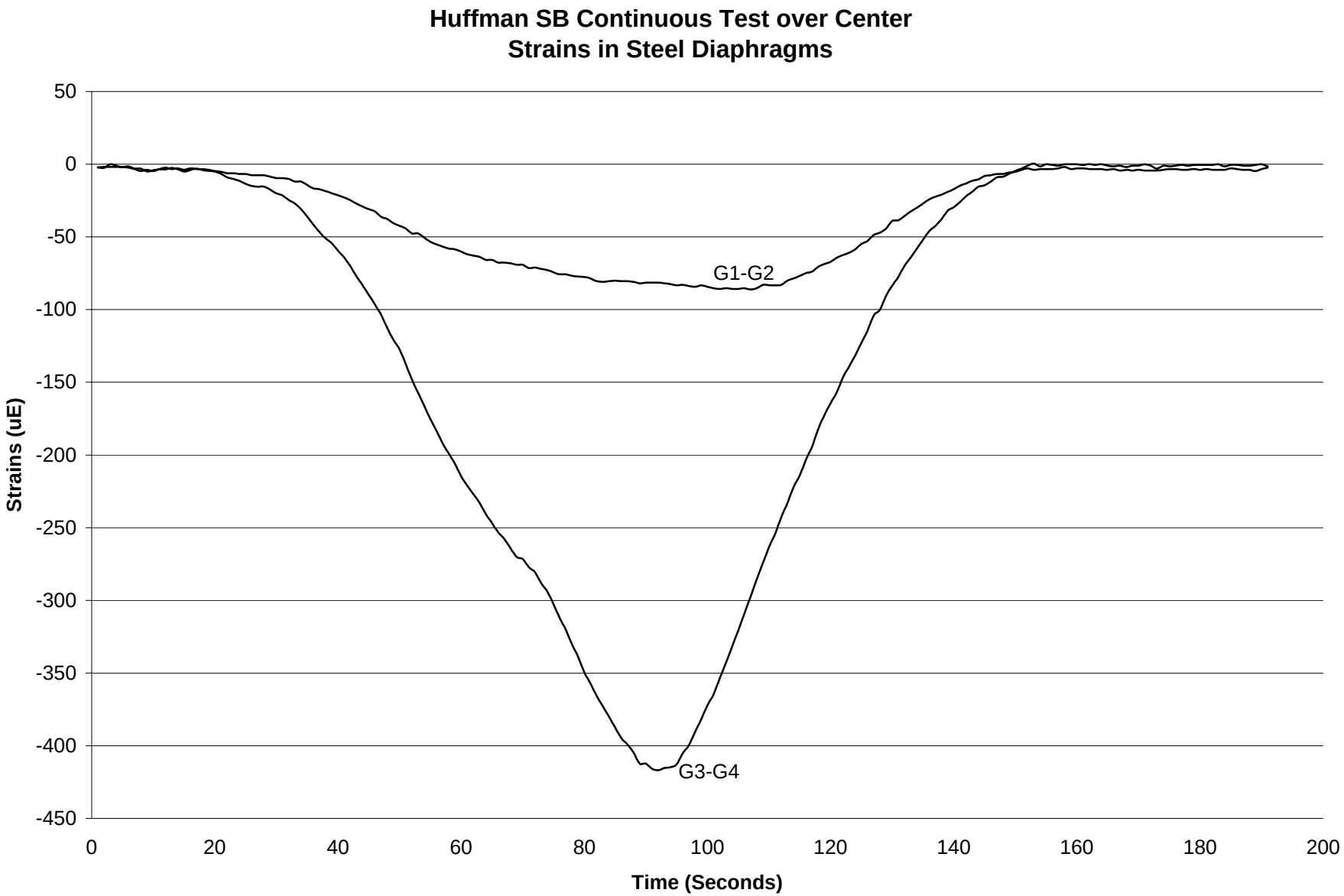
Huffman SB Continuous Test over Center
Strains in Steel Diaphragms
50
0
-50
-100
-150
-200
-250
-300
-350
-400
-450
Strains (uE)
0
20
40
60
80
100
120
140
160
180
200
Time (Seconds)
G1-G2
G3-G4

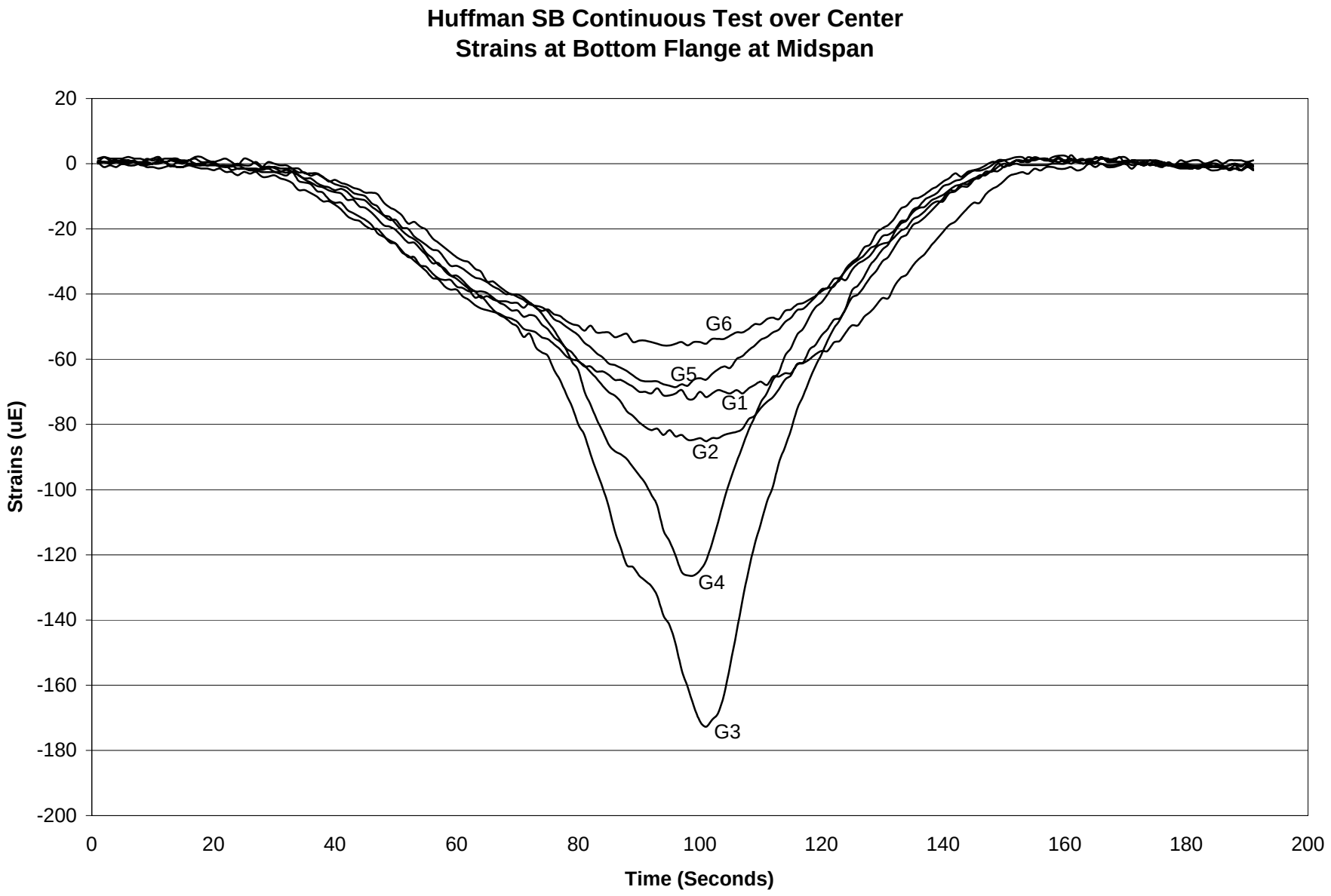
Huffman SB Continuous Test over Center
Strains at Bottom Flange at Midspan
Strains (uE)
Time (Seconds)
20
0
-20
-40
-60
-80
-100
-120
-140
-160
-180
-200
0
20
40
60
80
100
120
140
160
180
200
G6
G5
G1
G2
G4
G3

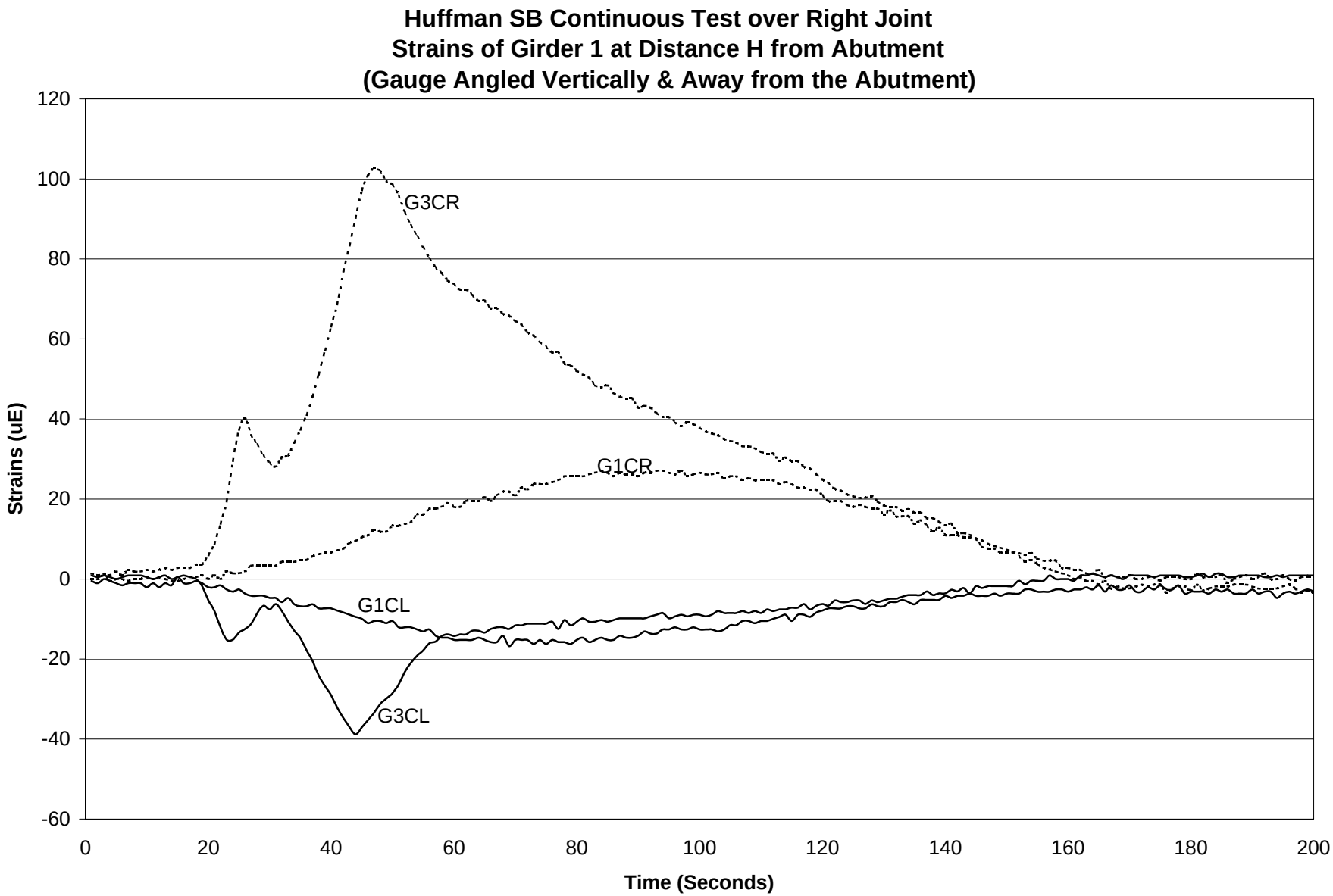
Huffman SB Continuous Test over Right Joint
Strains of Girder 1 at Distance H from Abutment
(Gauge Angled Vertically & Away from the Abutment)
Strains (uE)
Time (Seconds)
G3CR
G1CR
G1CL
G3CL
120
100
80
60
40
20
0
-20
-40
-60
0
20
40
60
80
100
120
140
160
180
200

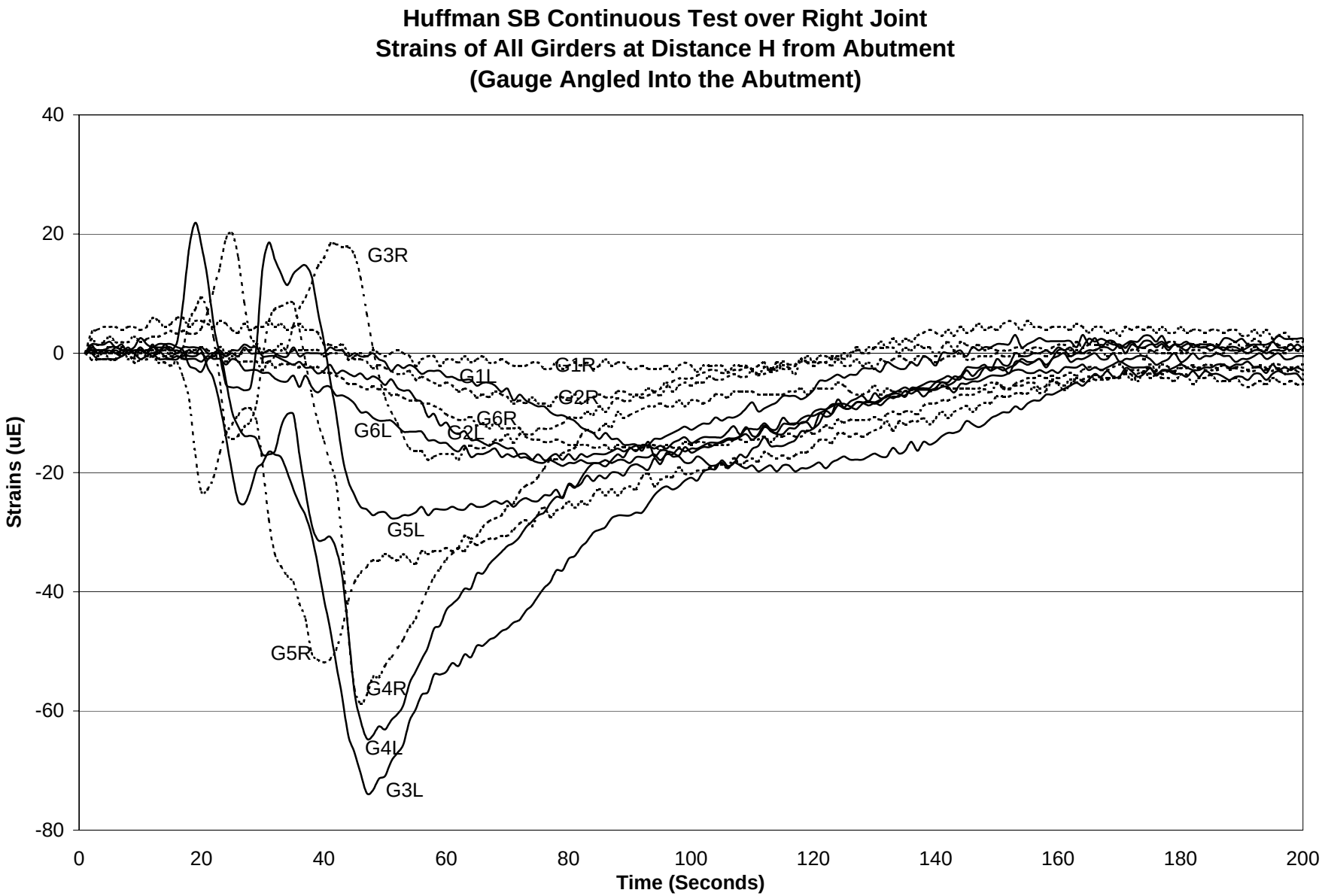
Huffman SB Continuous Test over Right Joint
Strains of All Girders at Distance H from Abutment
(Gauge Angled Into the Abutment)
Strains (uE)
Time (Seconds)
40
20
0
-20
-40
-60
-80
0
20
40
60
80
100
120
140
160
180
200
G3R
G1R
G1L
G2R
G6R
G6L
G2L
G5L
G5R
G4R
G4L
G3L

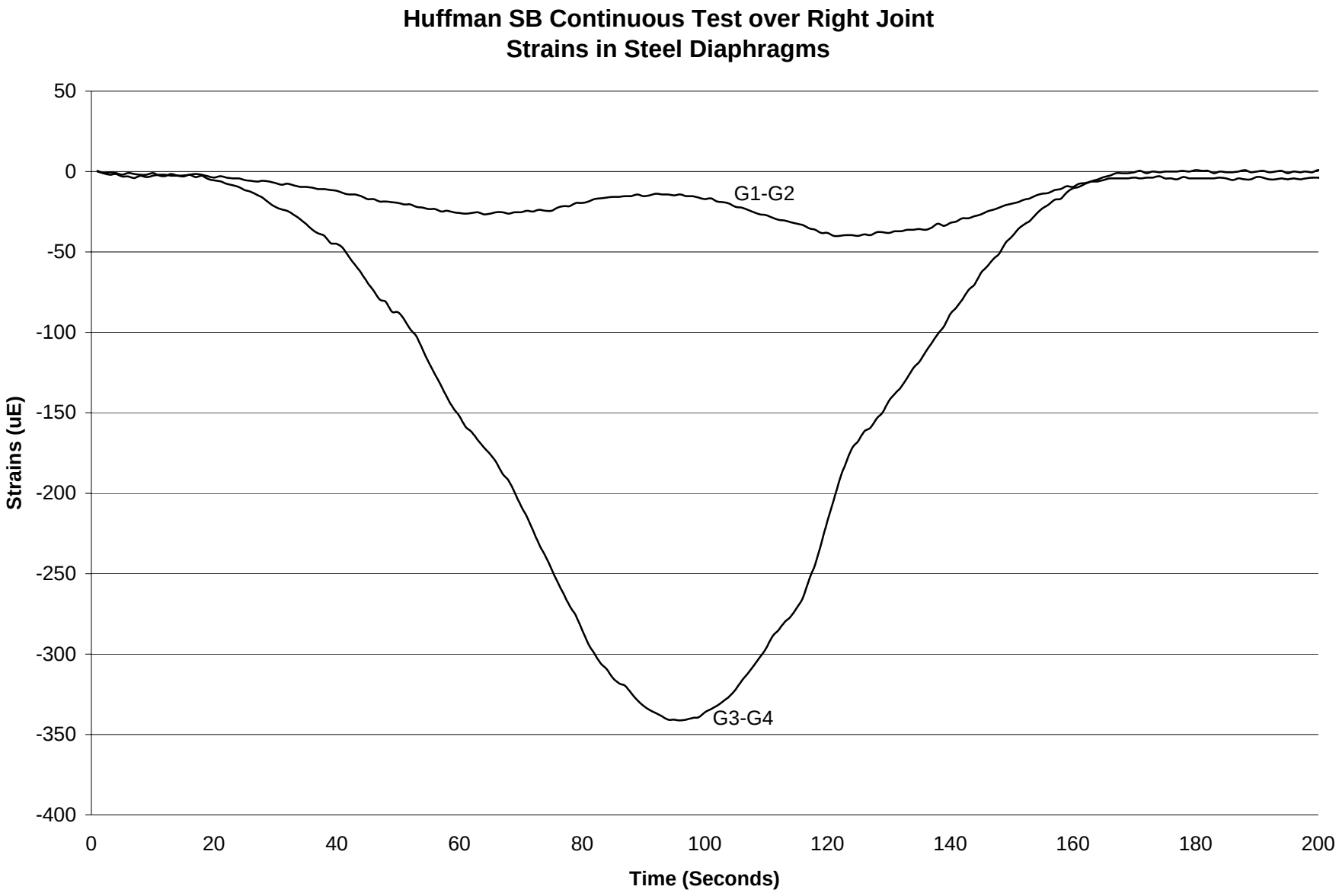
Huffman SB Continuous Test over Right Joint
Strains in Steel Diaphragms
50
0
-50
-100
-150
-200
-250
-300
-350
-400
Strains (uE)
0
20
40
60
80
100
120
140
160
180
200
Time (Seconds)
G1-G2
G3-G4

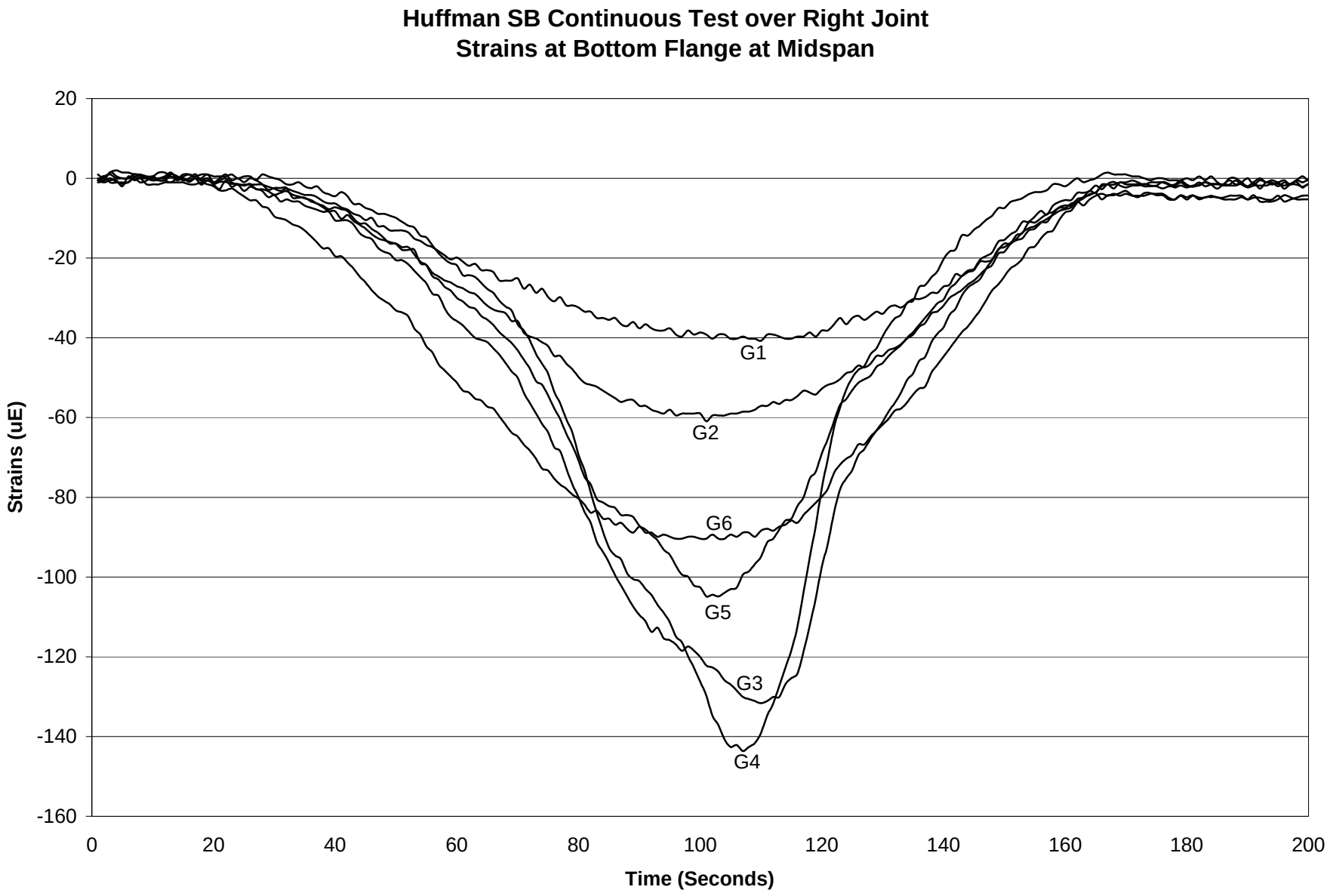
Huffman SB Continuous Test over Right Joint
Strains at Bottom Flange at Midspan
Strains (uE)
Time (Seconds)
20
0
-20
-40
-60
-80
-100
-120
-140
-160
0
20
40
60
80
100
120
140
160
180
200
G1
G2
G6
G5
G3
G4

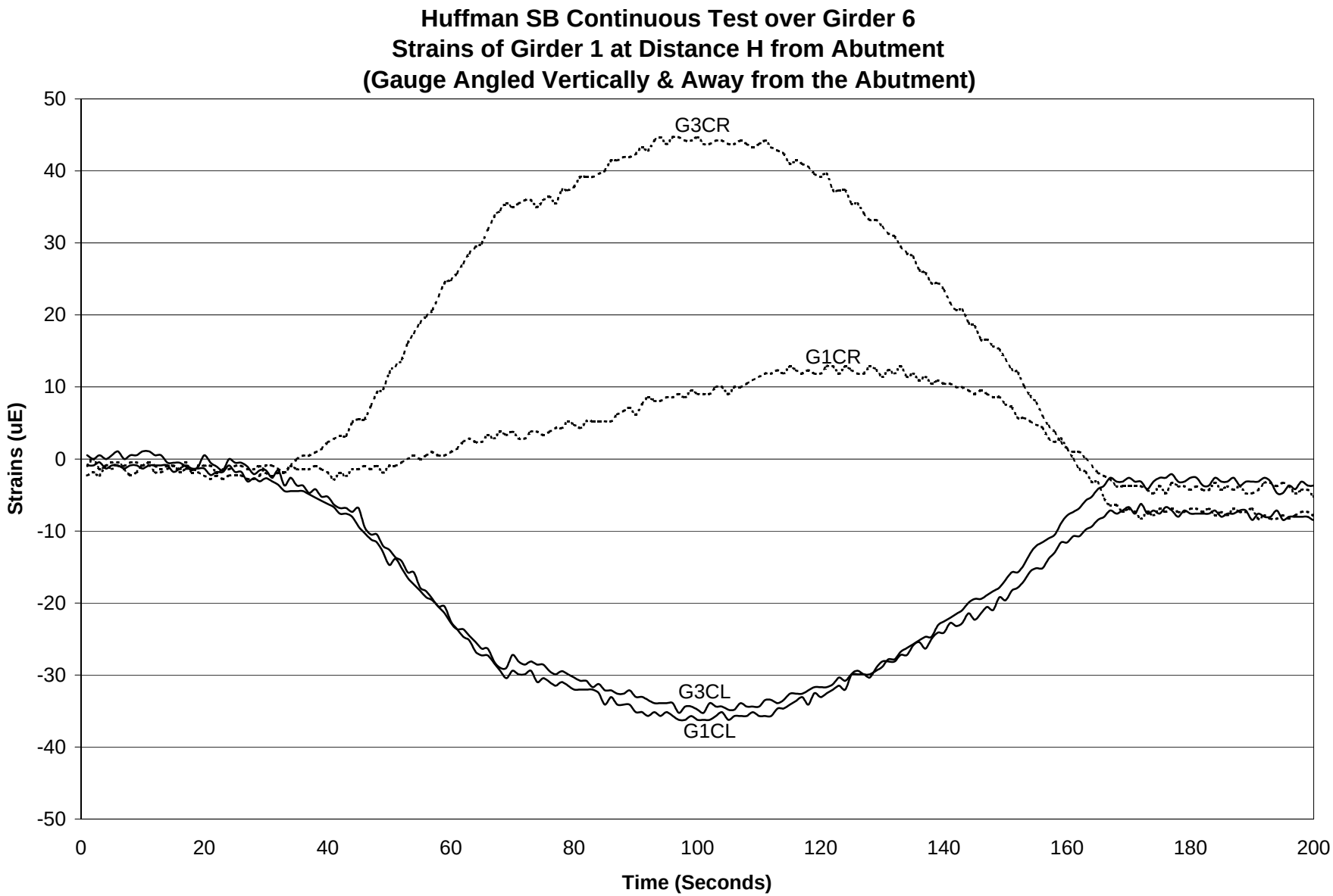
Huffman SB Continuous Test over Girder 6
Strains of Girder 1 at Distance H from Abutment
(Gauge Angled Vertically & Away from the Abutment)
G3CR
G1CR
G3CL
G1CL
Strains (uE)
Time (Seconds)
50
40
30
20
10
0
-10
-20
-30
-40
-50
0
20
40
60
80
100
120
140
160
180
200

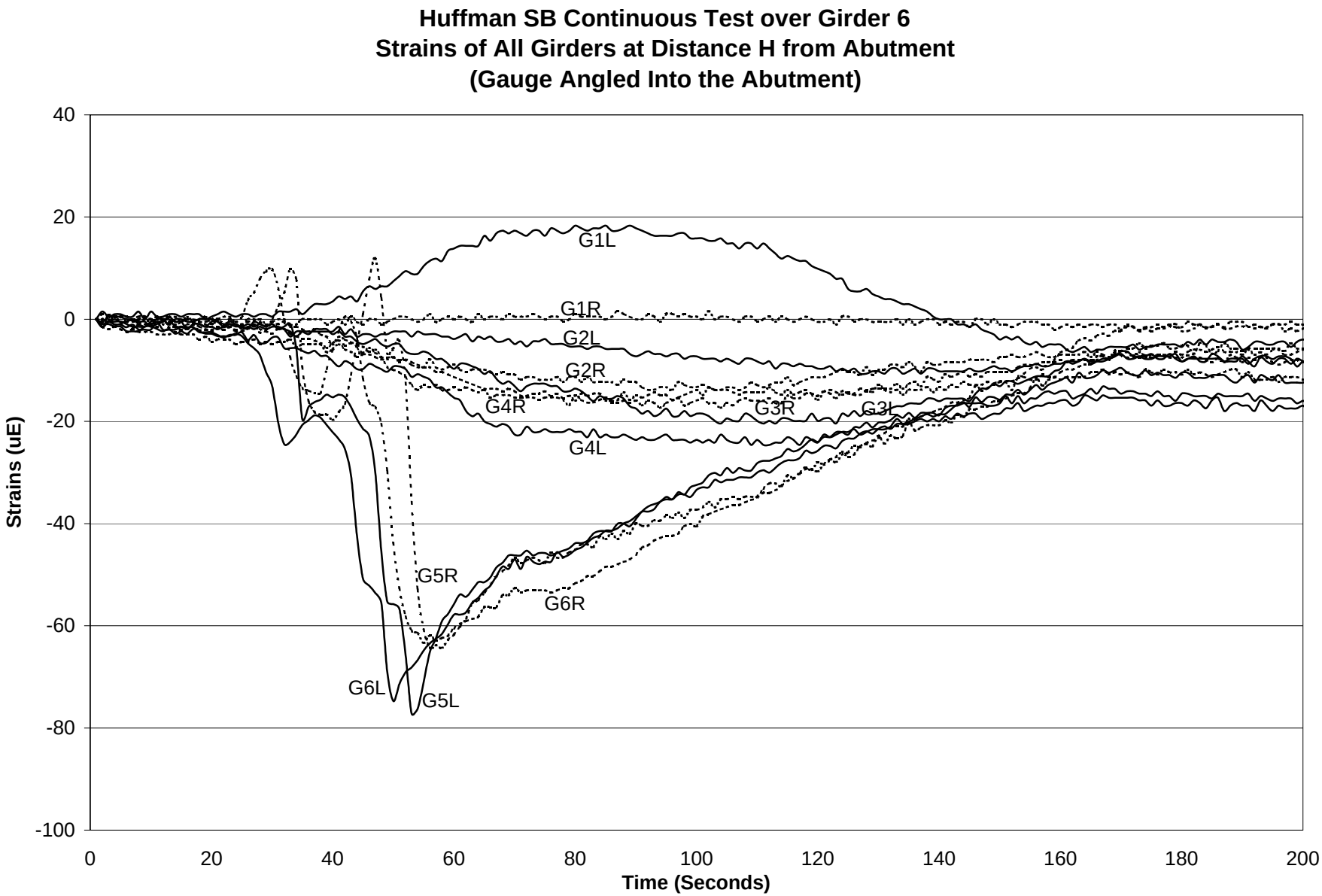
Huffman SB Continuous Test over Girder 6
Strains of All Girders at Distance H from Abutment
(Gauge Angled Into the Abutment)
Strains (uE)
Time (Seconds)
40
20
0
-20
-40
-60
-80
-100
0
20
40
60
80
100
120
140
160
180
200
G1L
G1R
G2L
G2R
G4R
G3R
G3L
G4L
G5R
G6R
G6L
G5L

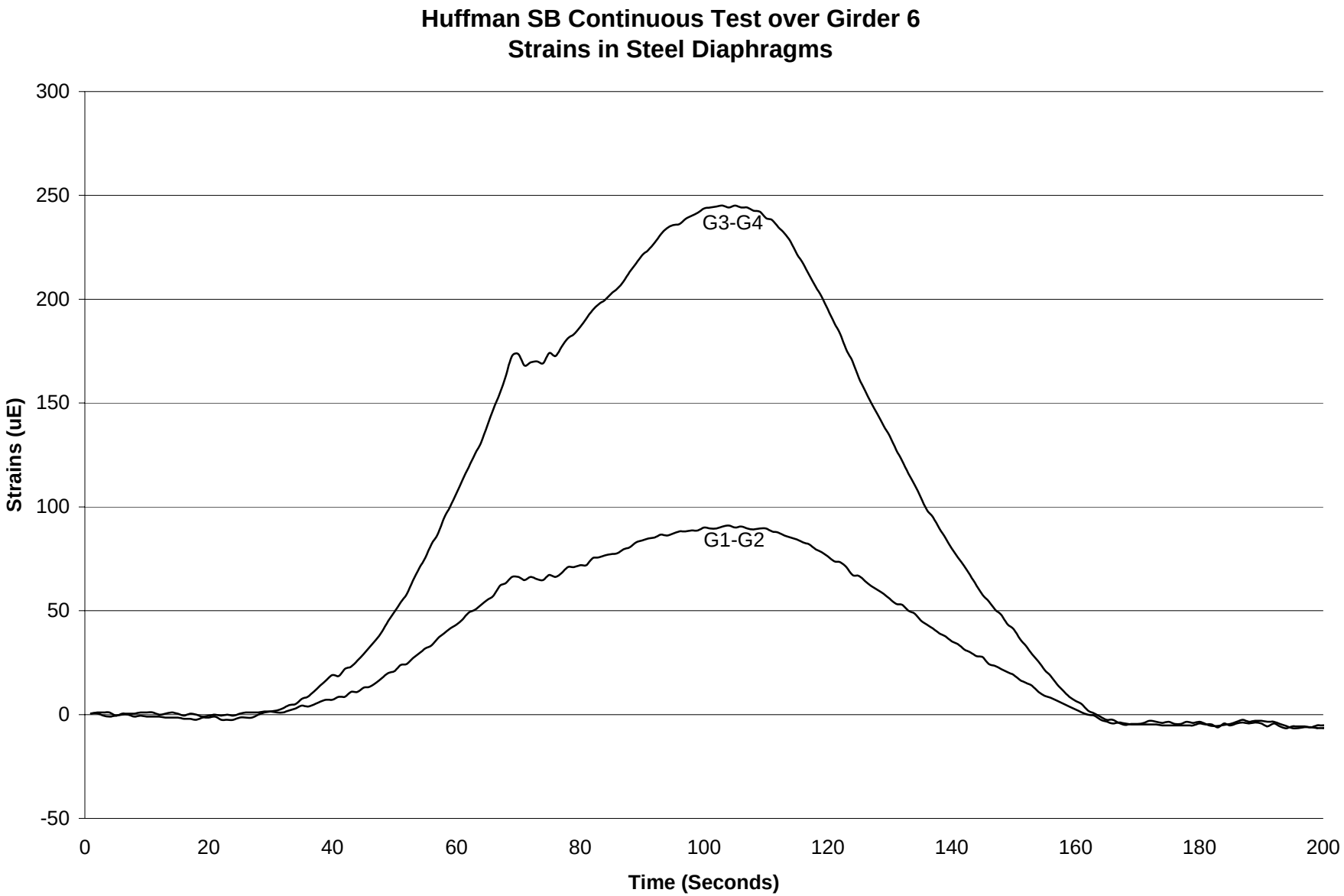
Huffman SB Continuous Test over Girder 6
Strains in Steel Diaphragms
300
250
200
150
100
50
0
-50
Strains (uE)
G3-G4
G1-G2
0
20
40
60
80
100
120
140
160
180
200
Time (Seconds)

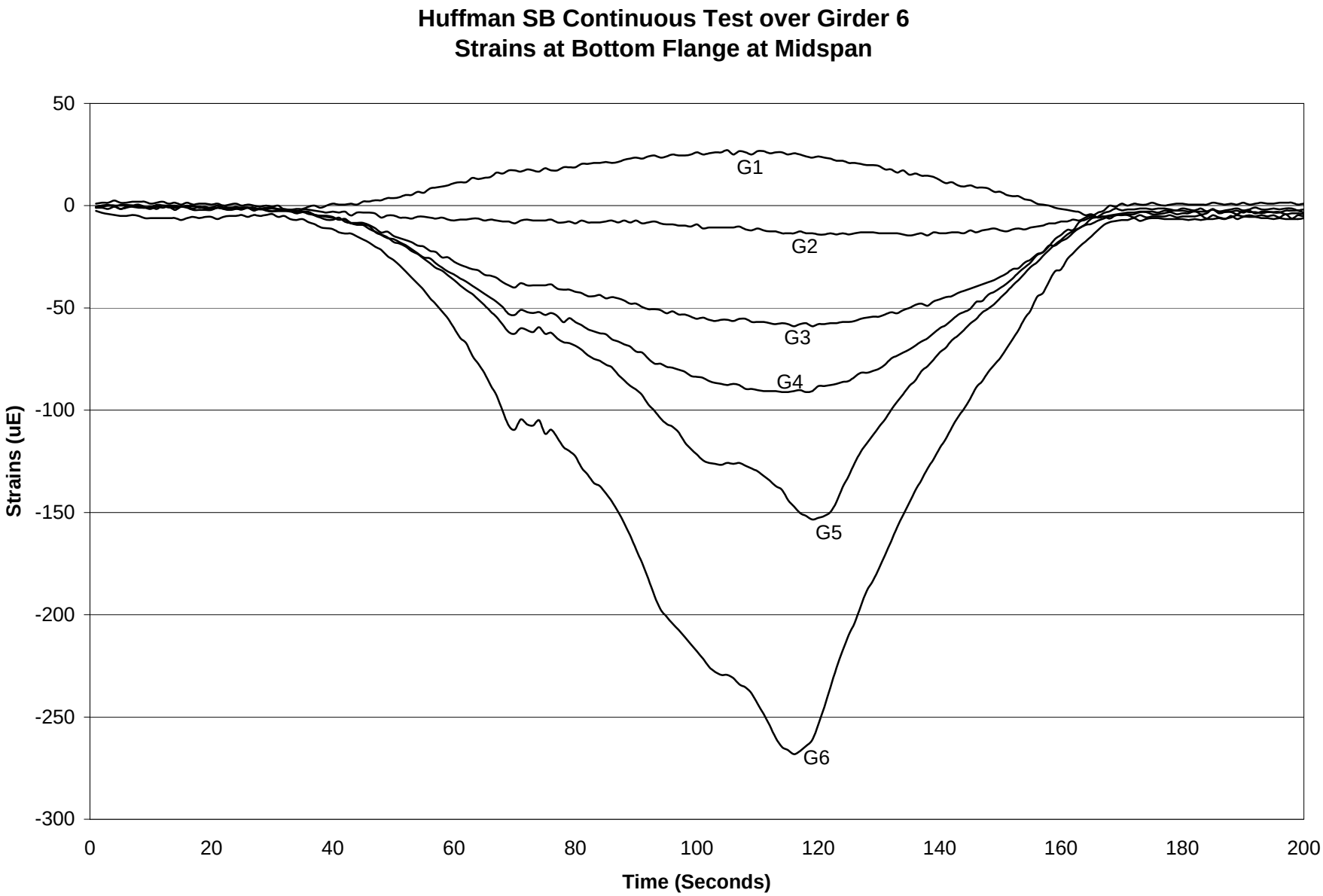
Huffman SB Continuous Test over Girder 6
Strains at Bottom Flange at Midspan
Strains (uE)
Time (Seconds)
50
0
-50
-100
-150
-200
-250
-300
0
20
40
60
80
100
120
140
160
180
200
G1
G2
G3
G4
G5
G6

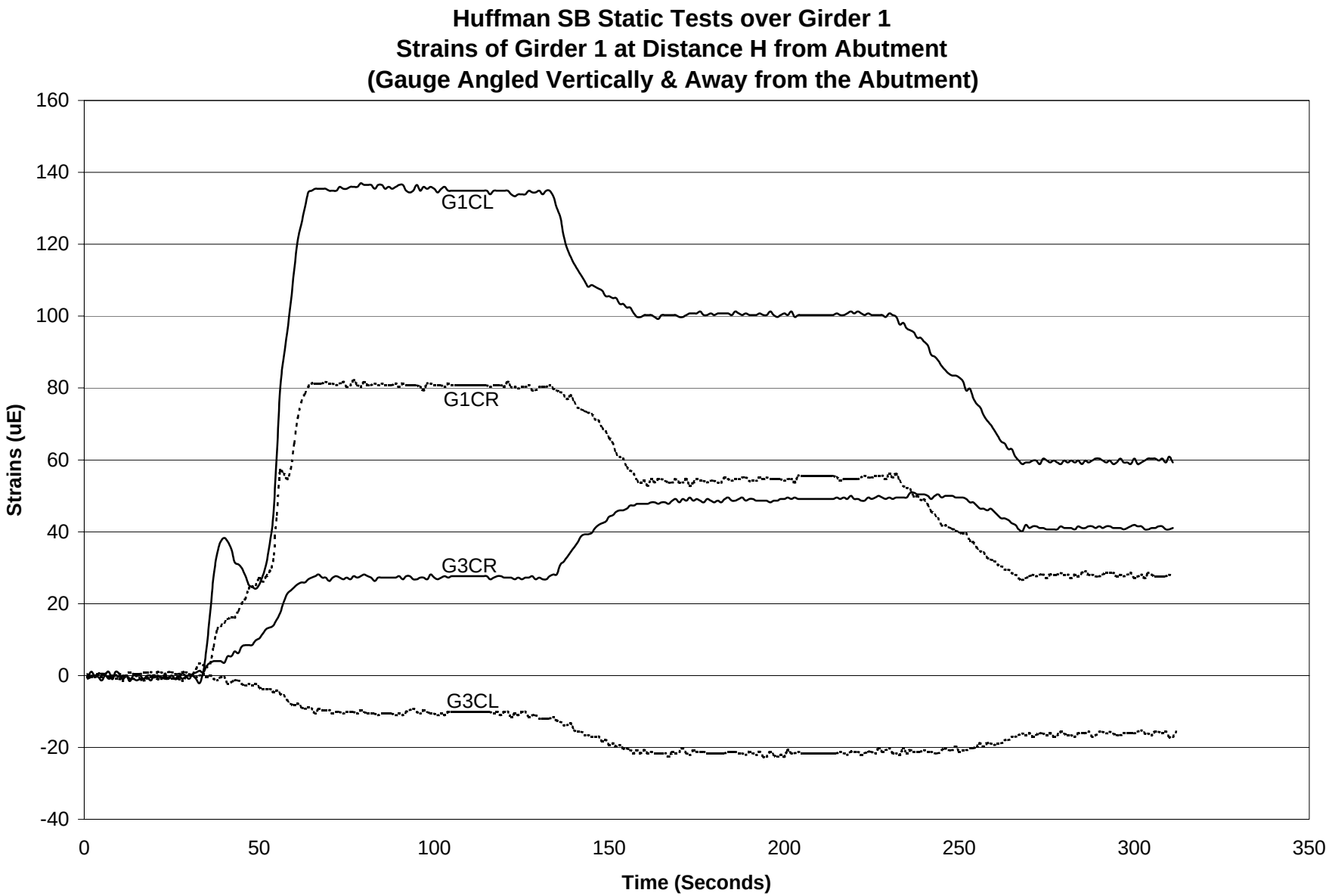
Huffman SB Static Tests over Girder 1
Strains of Girder 1 at Distance H from Abutment
(Gauge Angled Vertically & Away from the Abutment)
Strains (uE)
Time (Seconds)
G1CL
G1CR
G3CR
G3CL
160
140
120
100
80
60
40
20
0
-20
-40
0
50
100
150
200
250
300
350

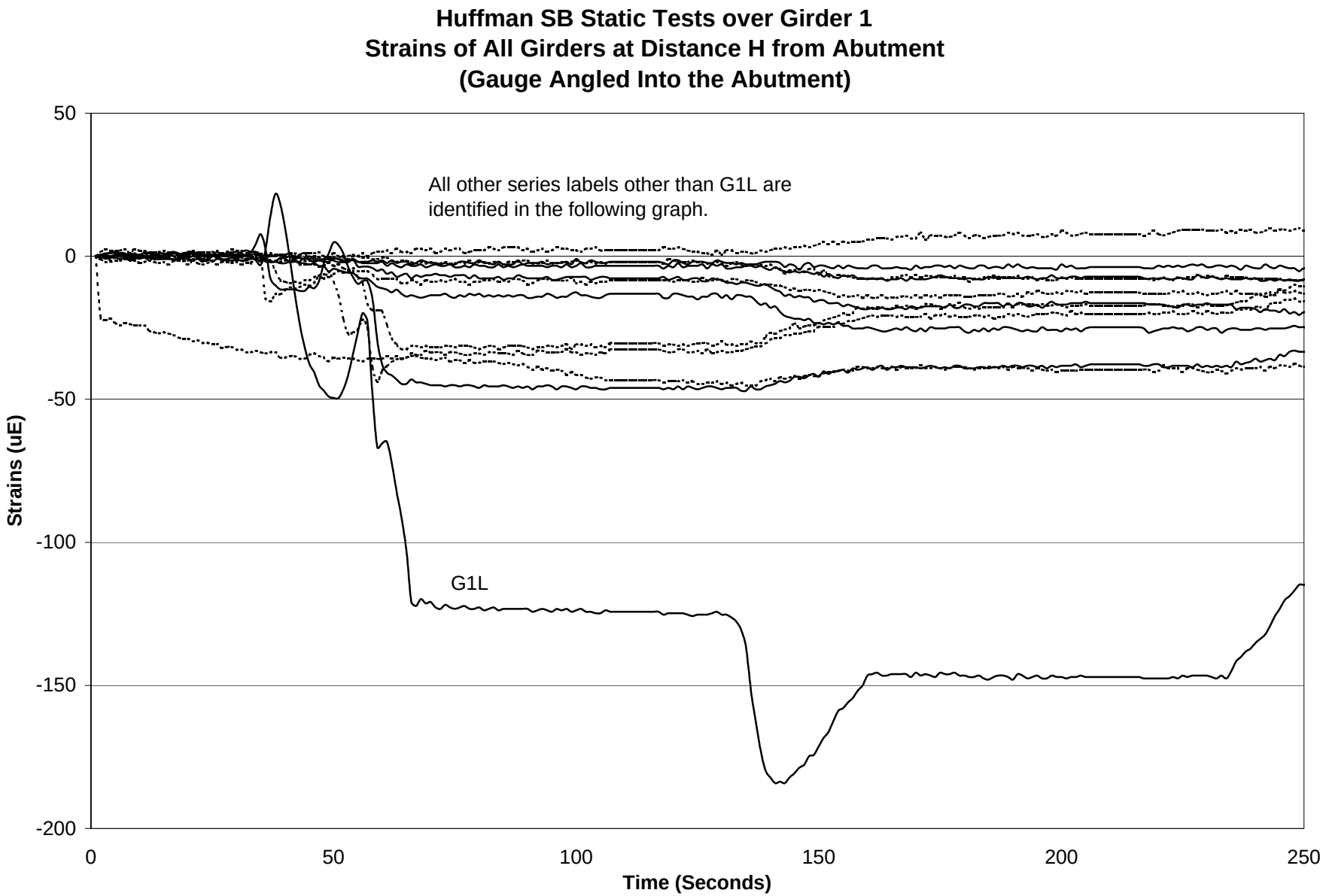
Huffman SB Static Tests over Girder 1
Strains of All Girders at Distance H from Abutment
(Gauge Angled Into the Abutment)
All other series labels other than G1L are identified in the following graph.
G1L
Strains (uE)
Time (Seconds)
50
0
-50
-100
-150
-200
0
50
100
150
200
250

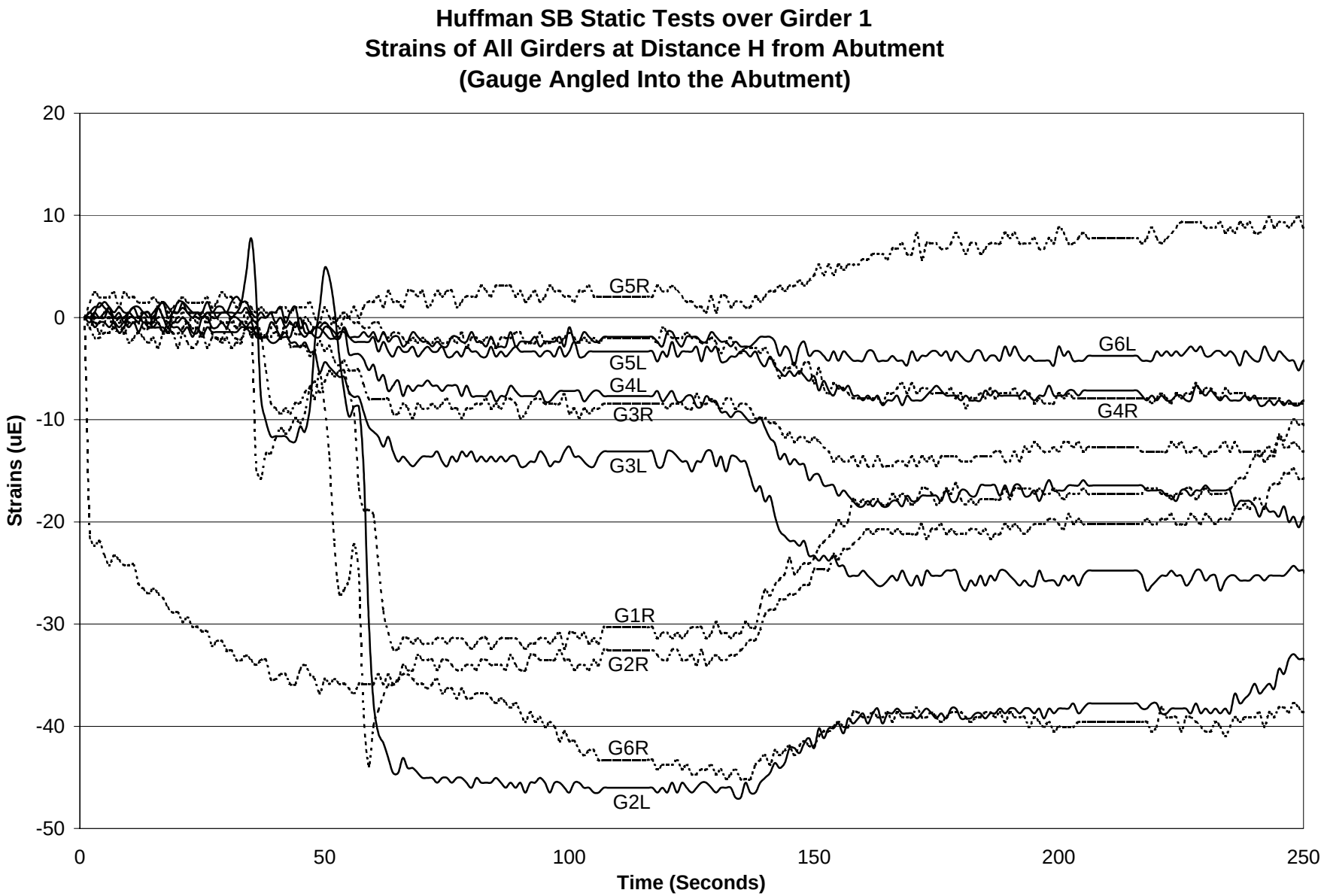
Huffman SB Static Tests over Girder 1
Strains of All Girders at Distance H from Abutment
(Gauge Angled Into the Abutment)
Strains (uE)
Time (Seconds)
20
10
0
-10
-20
-30
-40
-50
0
50
100
150
200
250
G5R
G6L
G5L
G4L
G4R
G3R
G3L
G1R
G2R
G6R
G2L

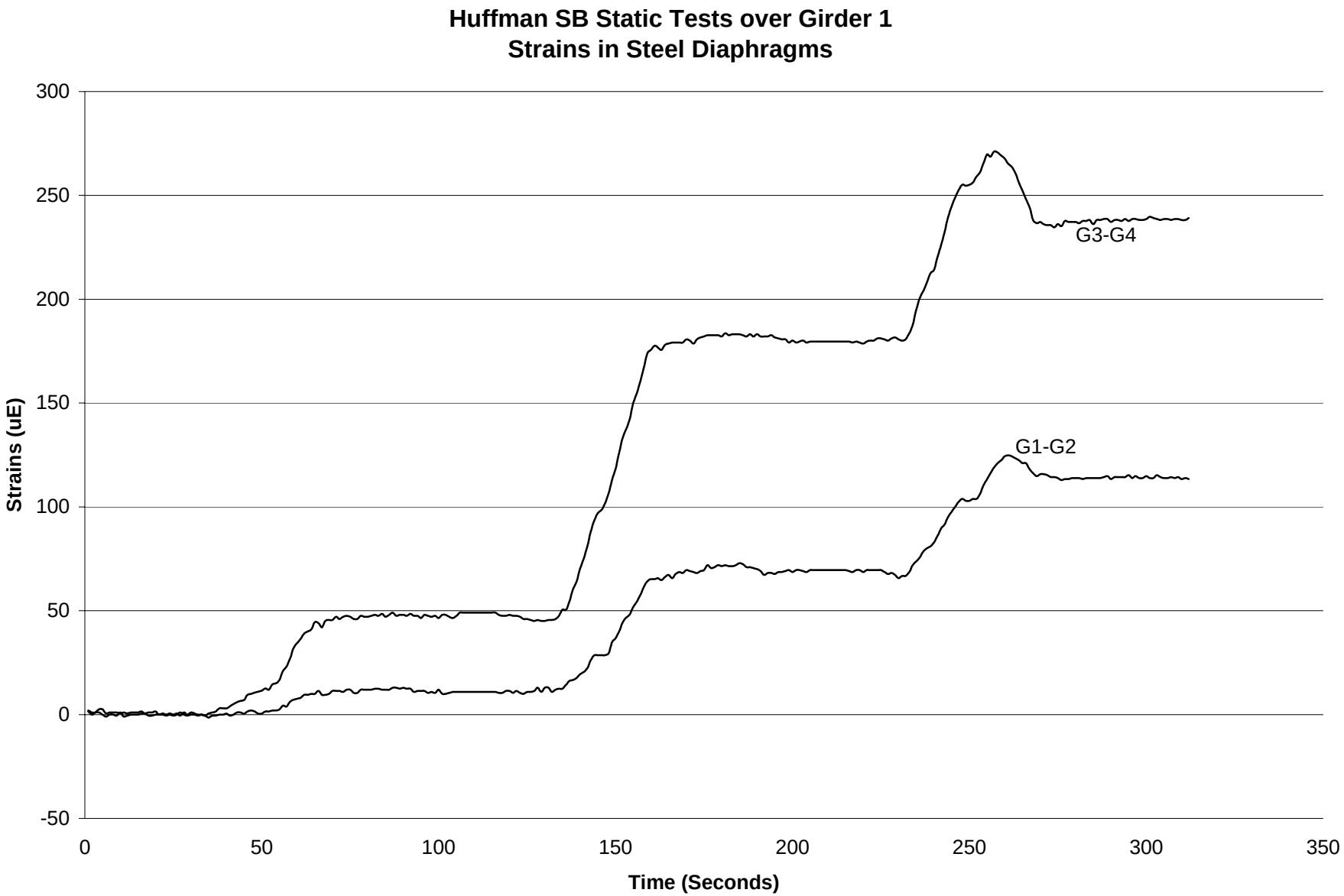
Huffman SB Static Tests over Girder 1
Strains in Steel Diaphragms
300
250
200
150
100
50
0
-50
Strains (uE)
0
50
100
150
200
250
300
350
Time (Seconds)
G3-G4
G1-G2

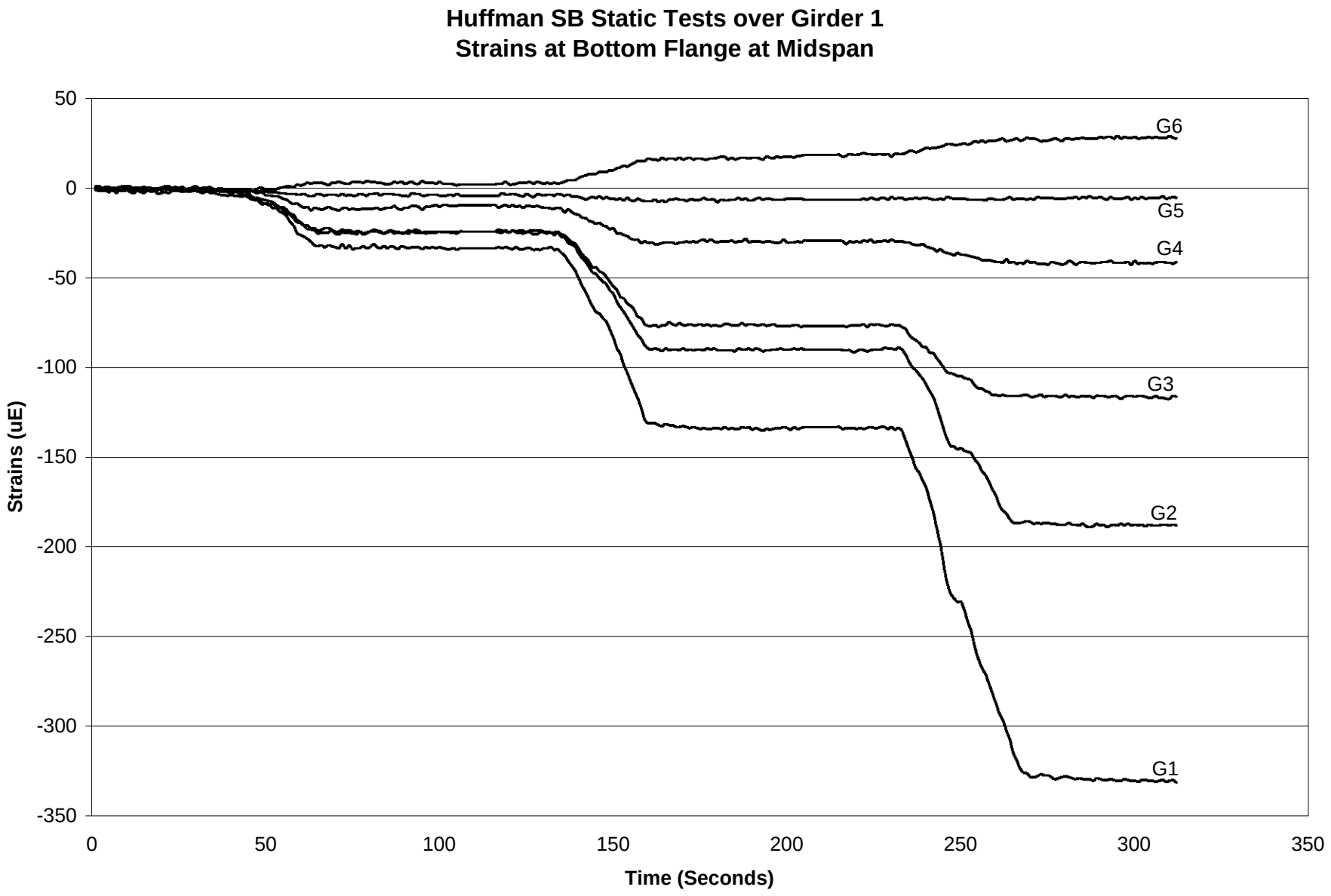
Huffman SB Static Tests over Girder 1
Strains at Bottom Flange at Midspan
Strains (uE)
Time (Seconds)
50
0
-50
-100
-150
-200
-250
-300
-350
0
50
100
150
200
250
300
350
G6
G5
G4
G3
G2
G1

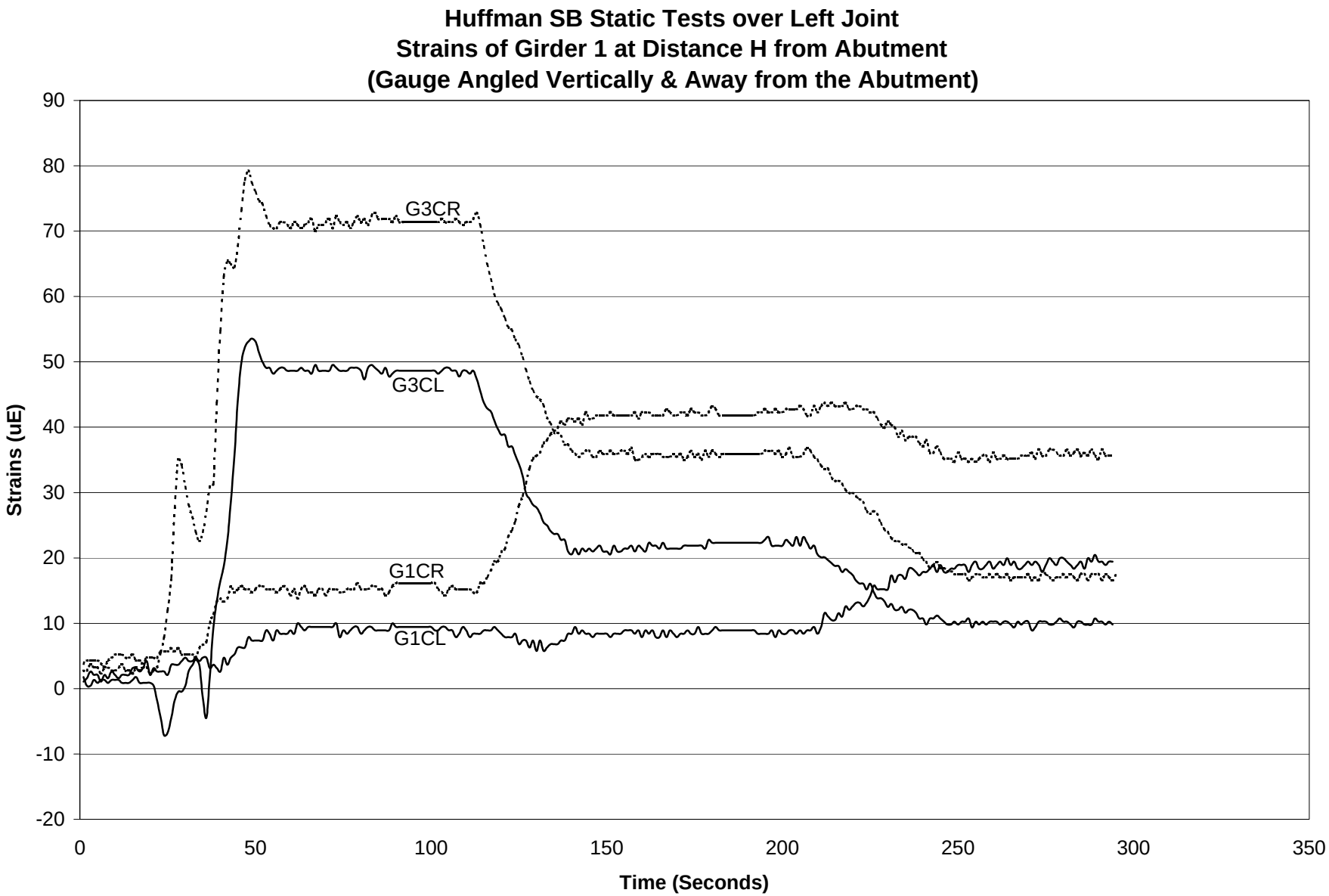
Huffman SB Static Tests over Left Joint
Strains of Girder 1 at Distance H from Abutment
(Gauge Angled Vertically & Away from the Abutment)
Strains (uE)
Time (Seconds)
G3CR
G3CL
G1CR
G1CL
90
80
70
60
50
40
30
20
10
0
-10
-20
0
50
100
150
200
250
300
350

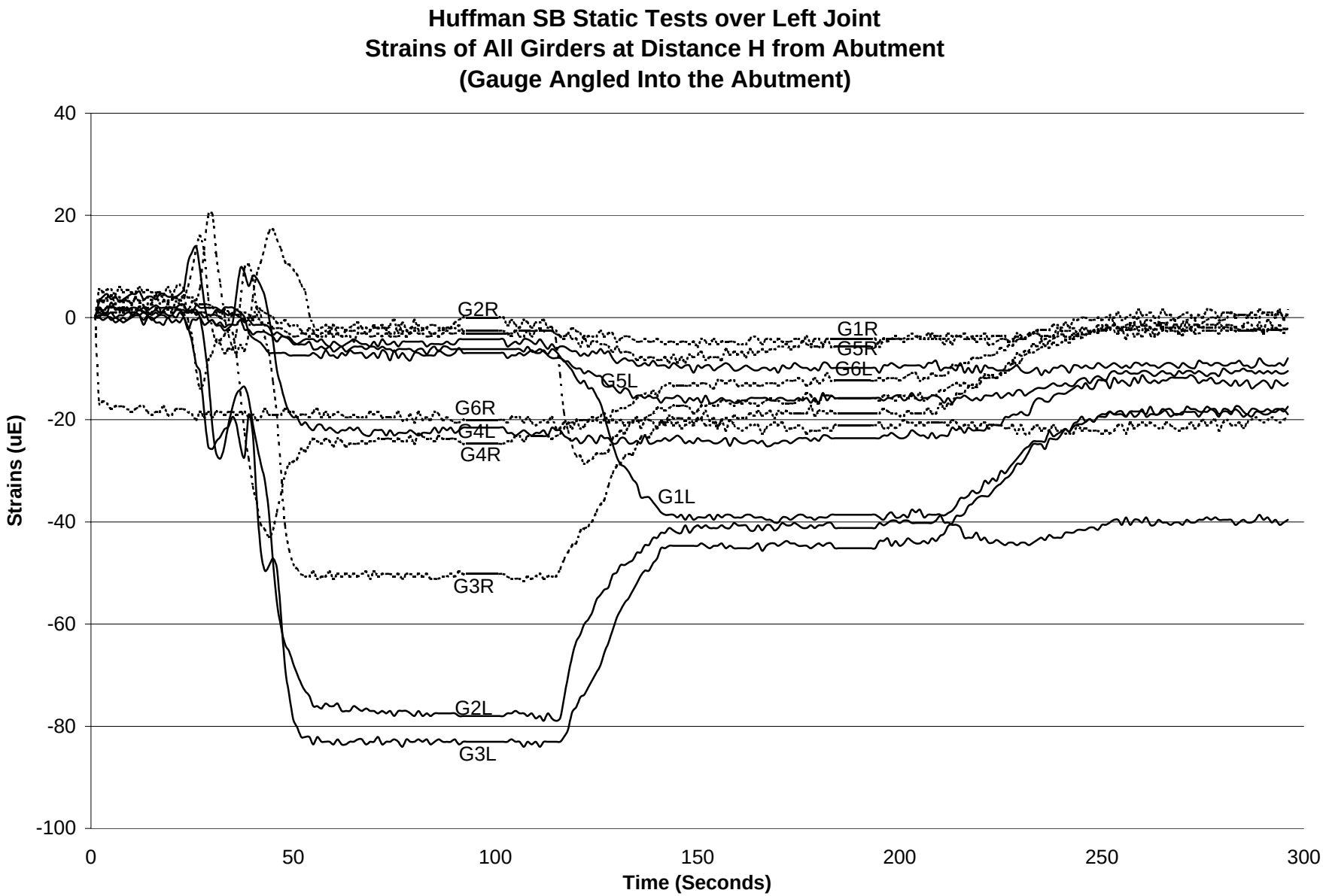
Huffman SB Static Tests over Left Joint
Strains of All Girders at Distance H from Abutment
(Gauge Angled Into the Abutment)
Strains (uE)
Time (Seconds)
40
20
0
-20
-40
-60
-80
-100
0
50
100
150
200
250
300
G2R
G1R
G5R
G6L
G5L
G6R
G4L
G4R
G1L
G3R
G2L
G3L

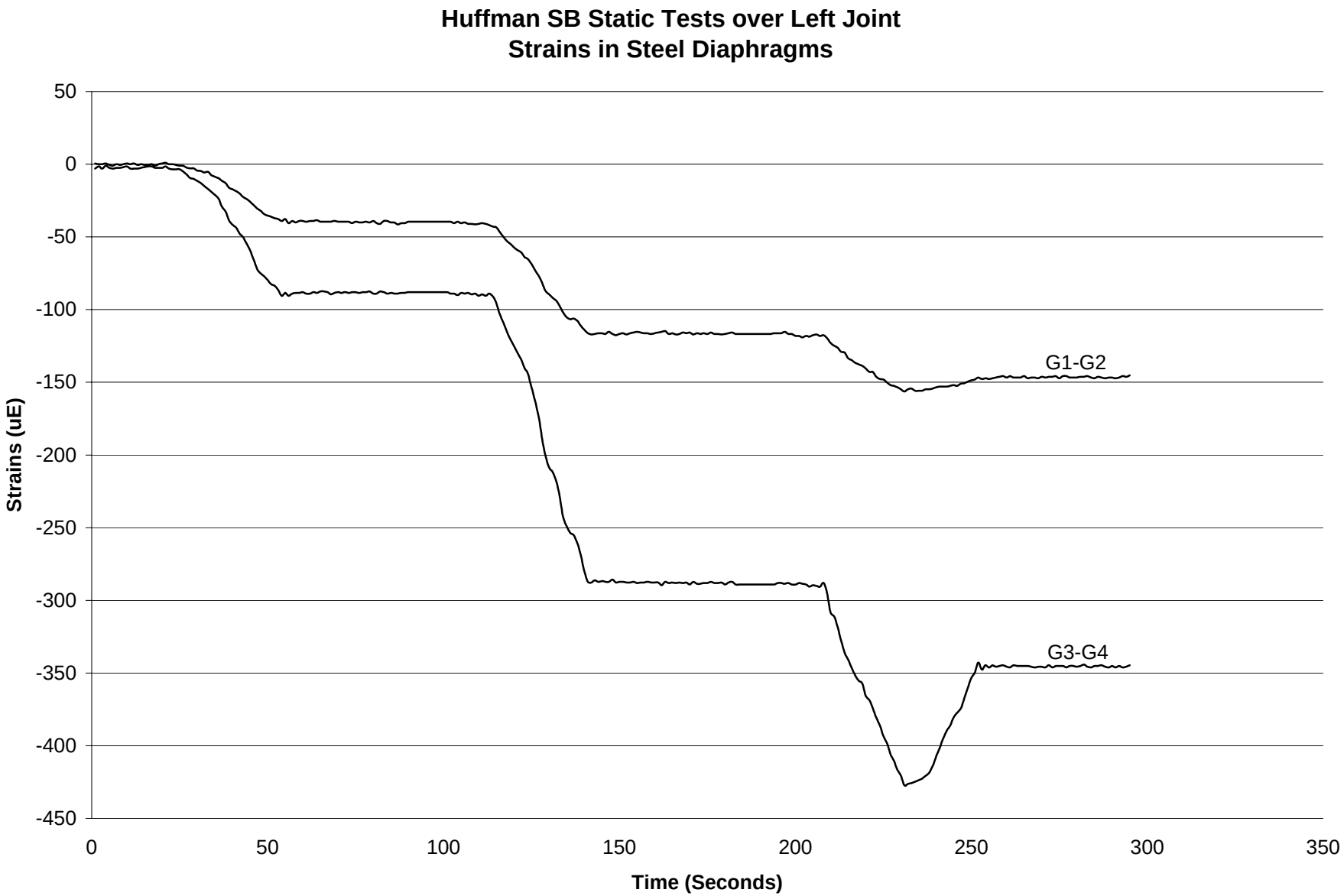
Huffman SB Static Tests over Left Joint
Strains in Steel Diaphragms
50
0
-50
-100
-150
-200
-250
-300
-350
-400
-450
Strains (uE)
0
50
100
150
200
250
300
350
Time (Seconds)
G1-G2
G3-G4

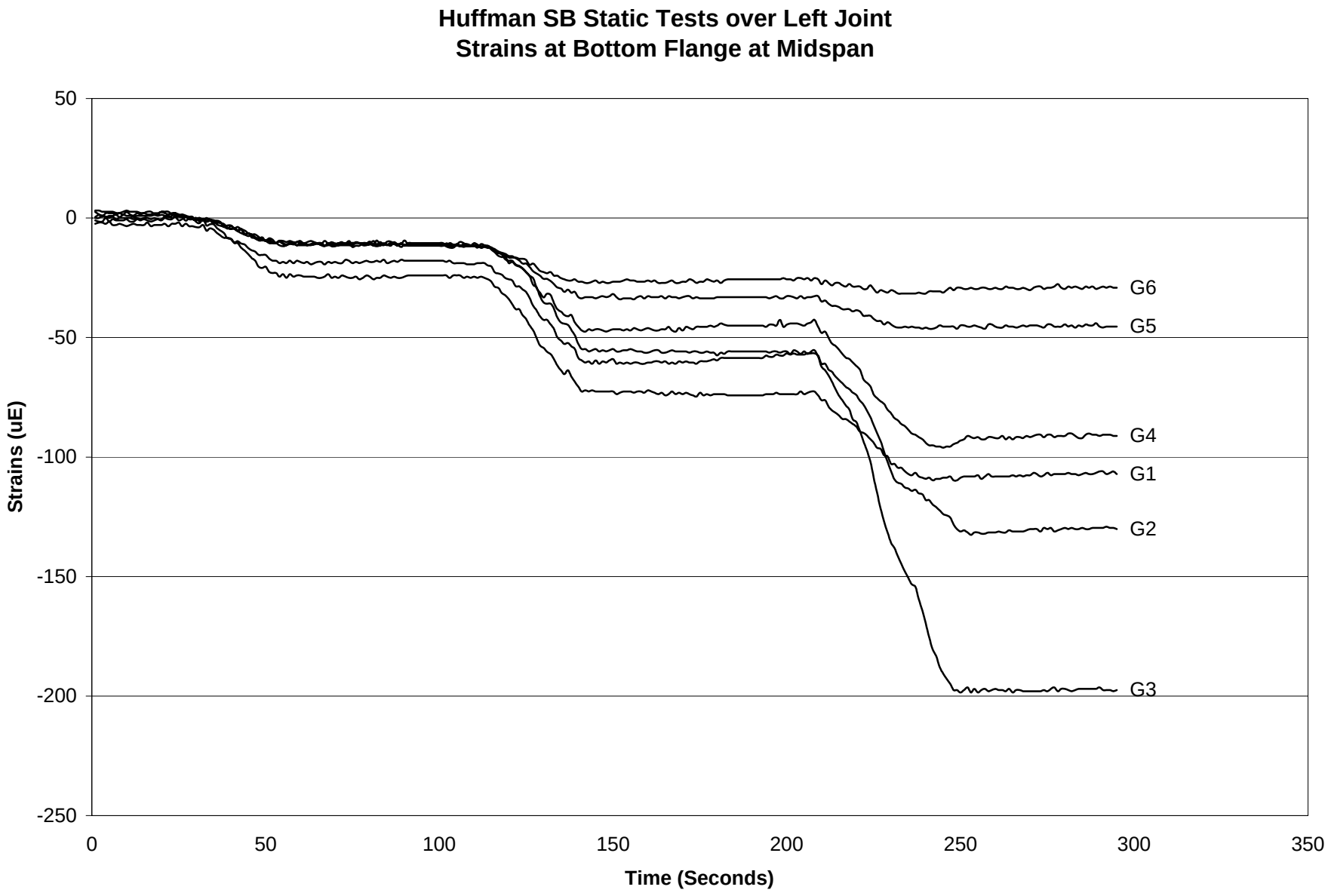
Huffman SB Static Tests over Left Joint
Strains at Bottom Flange at Midspan
Strains (uE)
50
0
-50
-100
-150
-200
-250
0
50
100
150
200
250
300
350
Time (Seconds)
G6
G5
G4
G1
G2
G3

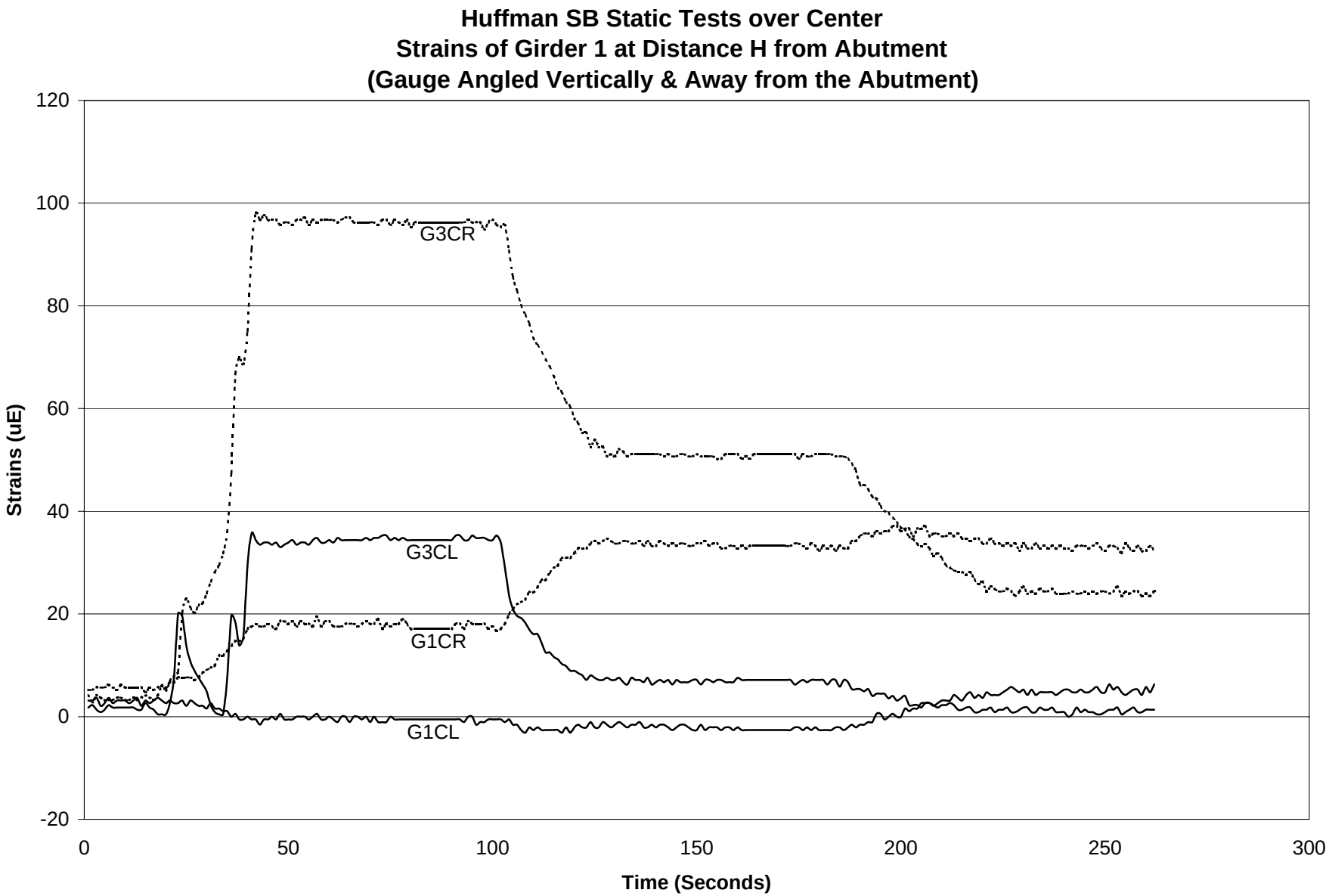
Huffman SB Static Tests over Center
Strains of Girder 1 at Distance H from Abutment
(Gauge Angled Vertically & Away from the Abutment)
Strains (uE)
Time (Seconds)
120
100
80
60
40
20
0
-20
0
50
100
150
200
250
300
G3CR
G3CL
G1CR
G1CL

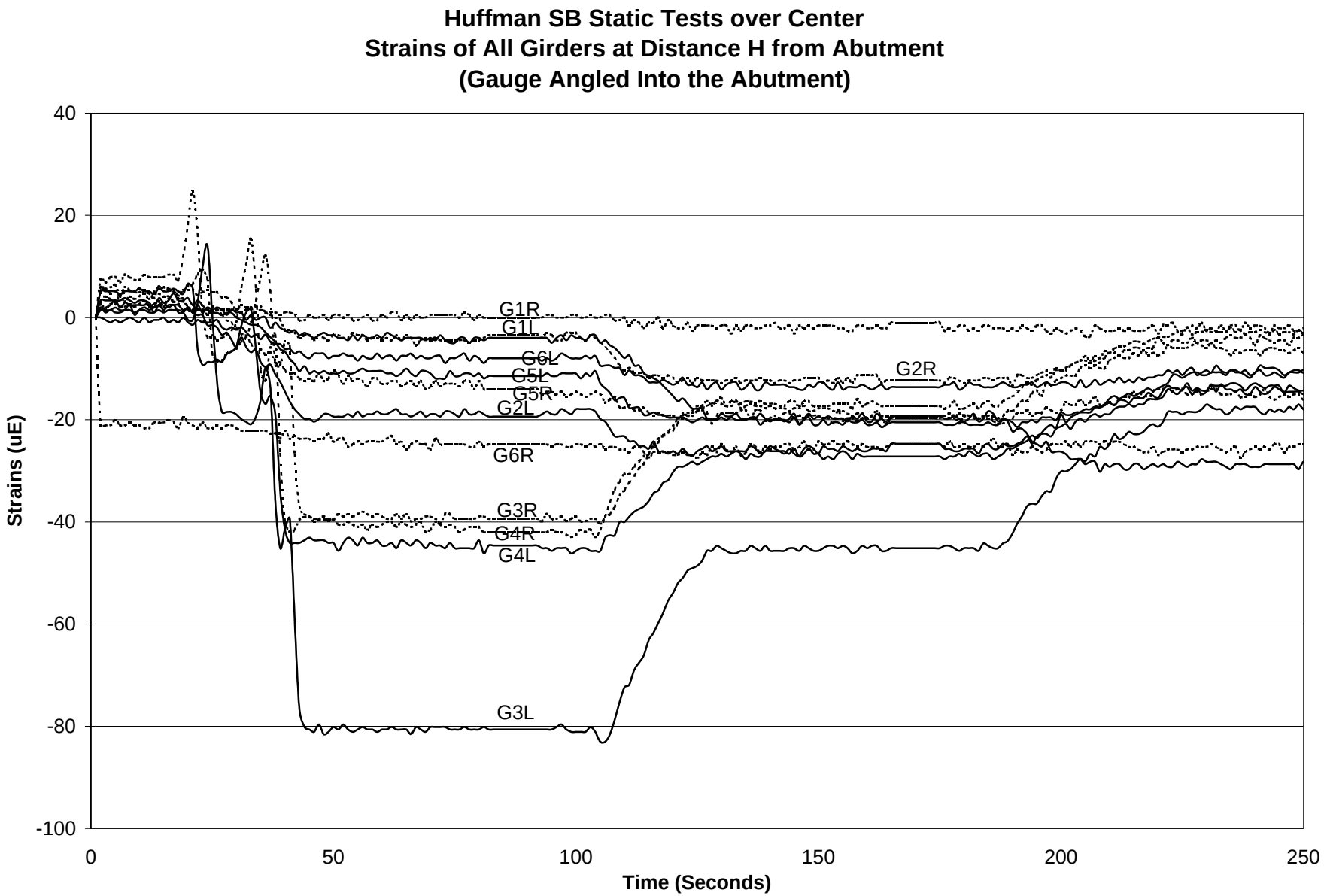
Huffman SB Static Tests over Center
Strains of All Girders at Distance H from Abutment
(Gauge Angled Into the Abutment)
Strains (uE)
Time (Seconds)
40
20
0
-20
-40
-60
-80
-100
0
50
100
150
200
250
G1R
G1L
G6L
G5L
G5R
G2L
G6R
G3R
G4R
G4L
G3L
G2R

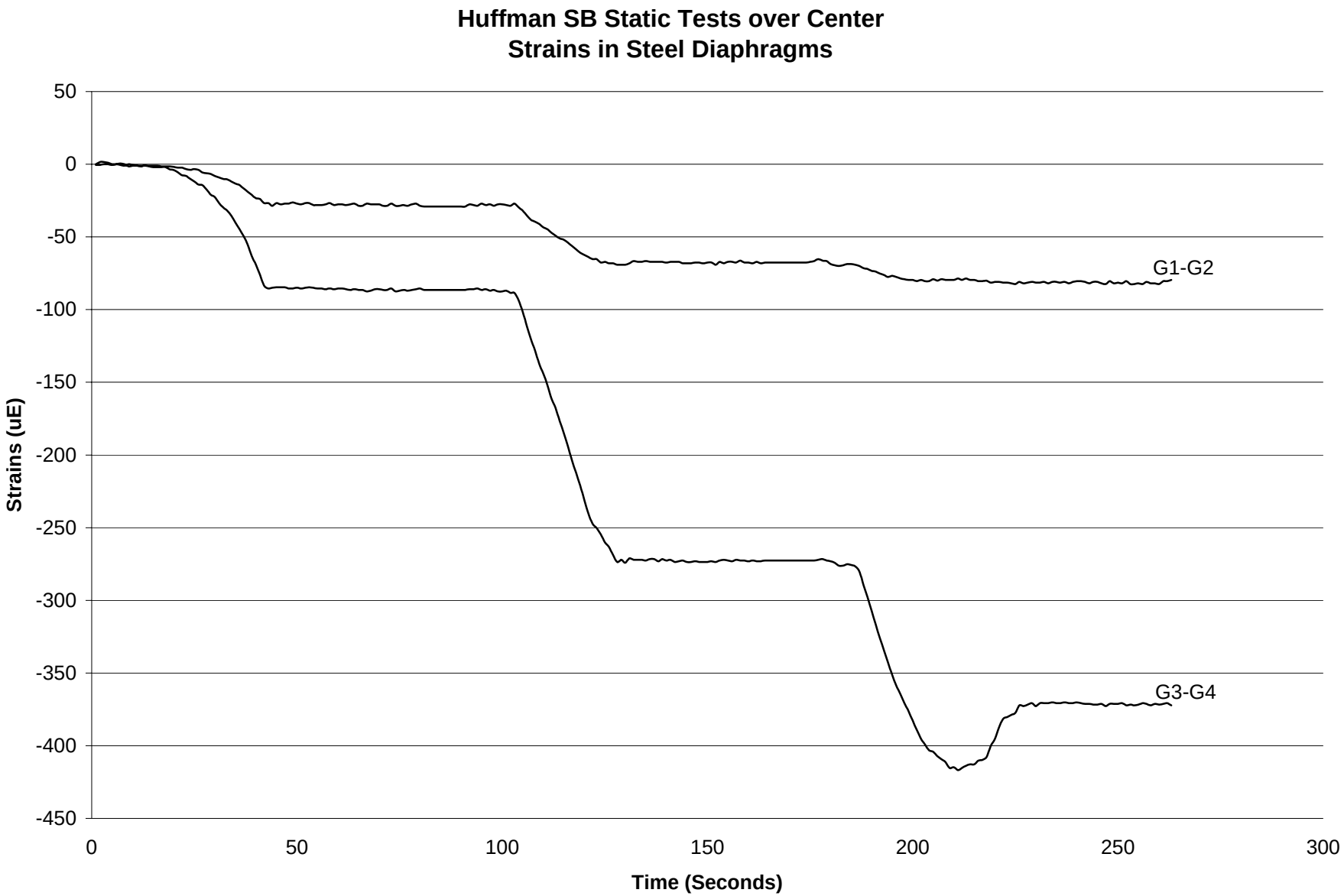
Huffman SB Static Tests over Center
Strains in Steel Diaphragms
50
0
-50
-100
-150
-200
-250
-300
-350
-400
-450
Strains (uE)
0
50
100
150
200
250
300
Time (Seconds)
G1-G2
G3-G4

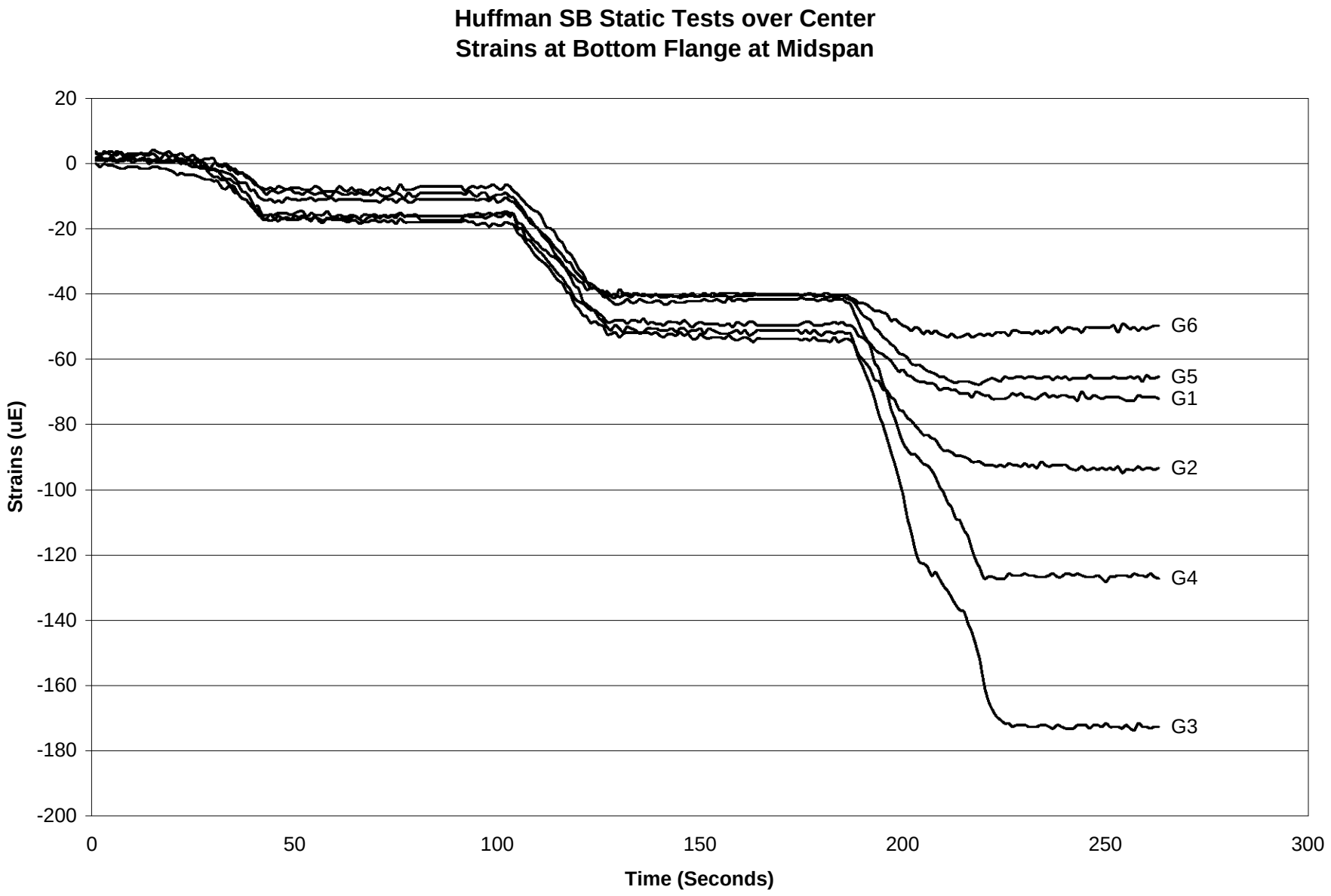
Huffman SB Static Tests over Center
Strains at Bottom Flange at Midspan
Strains (uE)
Time (Seconds)
20
0
-20
-40
-60
-80
-100
-120
-140
-160
-180
-200
0
50
100
150
200
250
300
G6
G5
G1
G2
G4
G3

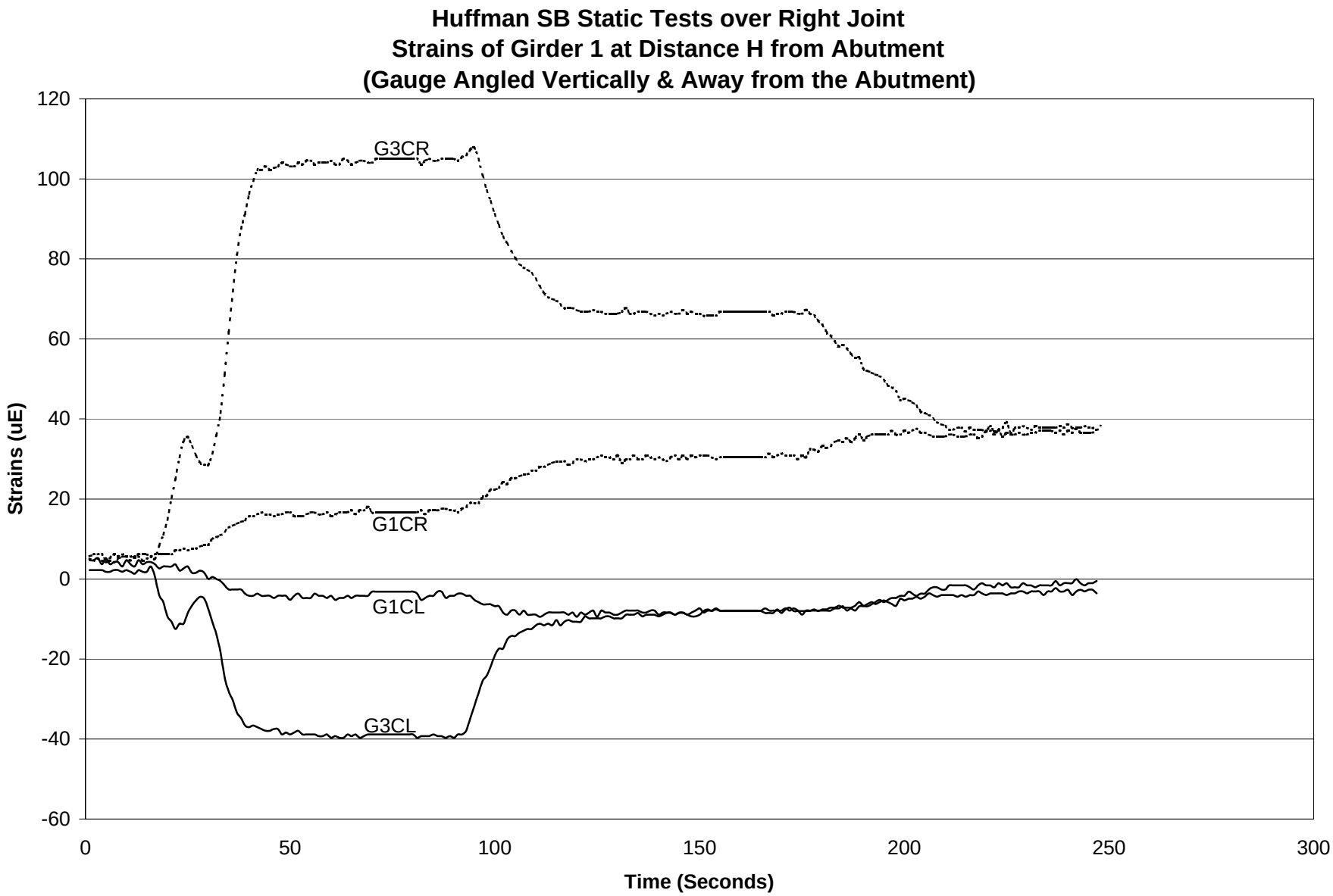
Huffman SB Static Tests over Right Joint
Strains of Girder 1 at Distance H from Abutment
(Gauge Angled Vertically & Away from the Abutment)
Strains (uE)
Time (Seconds)
G3CR
G1CR
G1CL
G3CL
120
100
80
60
40
20
0
-20
-40
-60
0
50
100
150
200
250
300

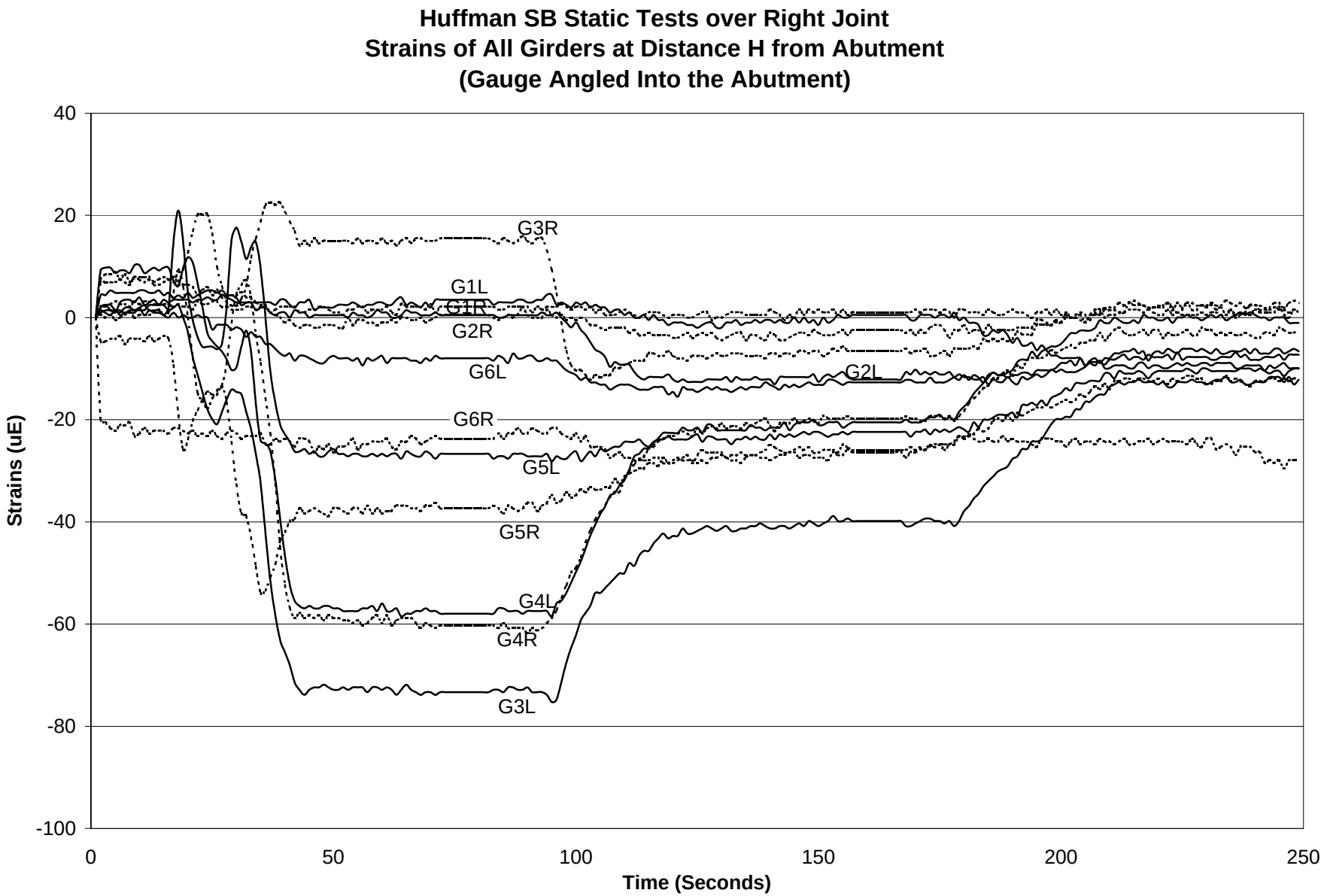
Huffman SB Static Tests over Right Joint
Strains of All Girders at Distance H from Abutment
(Gauge Angled Into the Abutment)
Strains (uE)
Time (Seconds)
40
20
0
-20
-40
-60
-80
-100
0
50
100
150
200
250
G3R
G1L
G1R
G2R
G6L
G2L
G6R
G5L
G5R
G4L
G4R
G3L

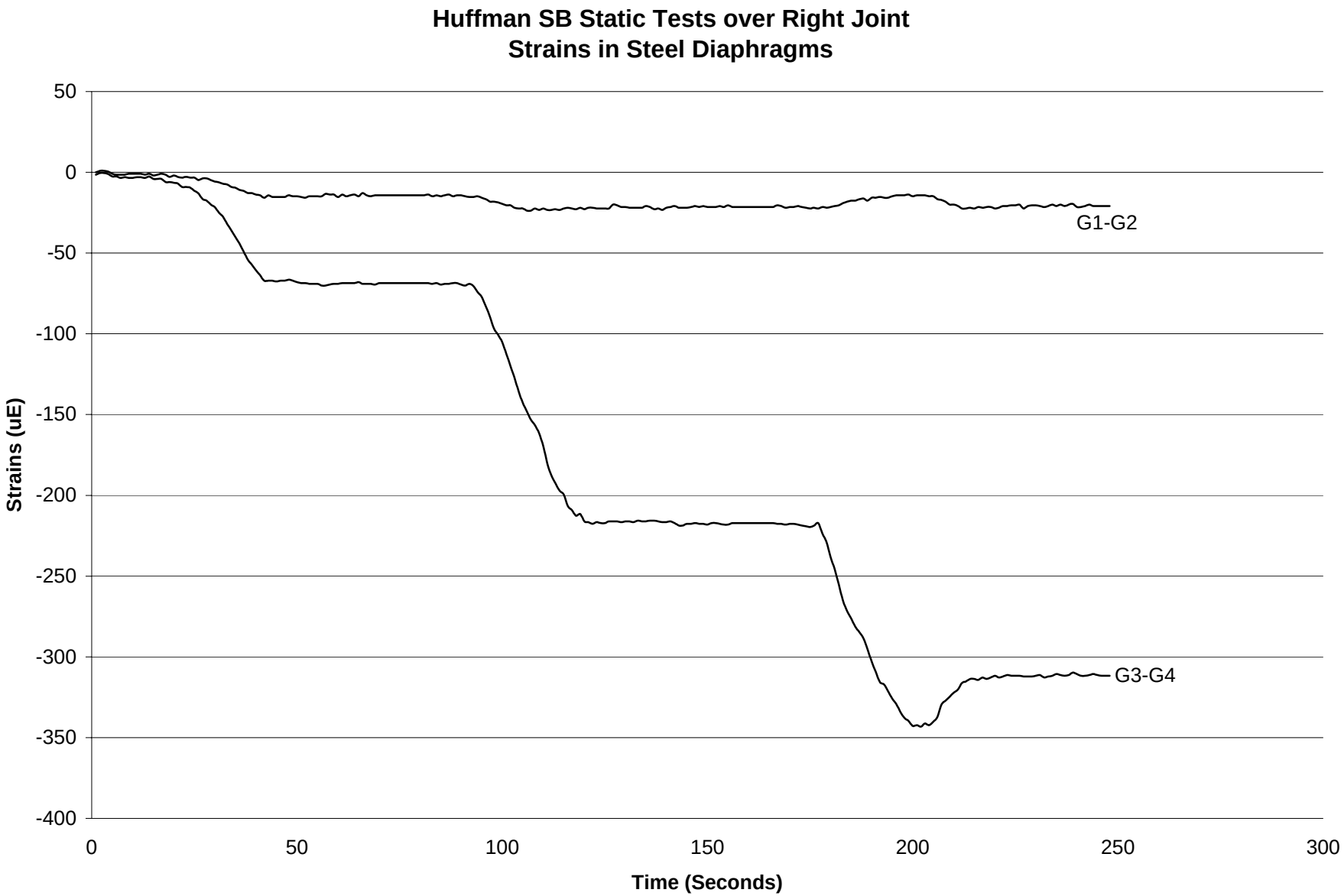
Huffman SB Static Tests over Right Joint
Strains in Steel Diaphragms
50
0
-50
-100
-150
-200
-250
-300
-350
-400
Strains (uE)
0
50
100
150
200
250
300
Time (Seconds)
G1-G2
G3-G4

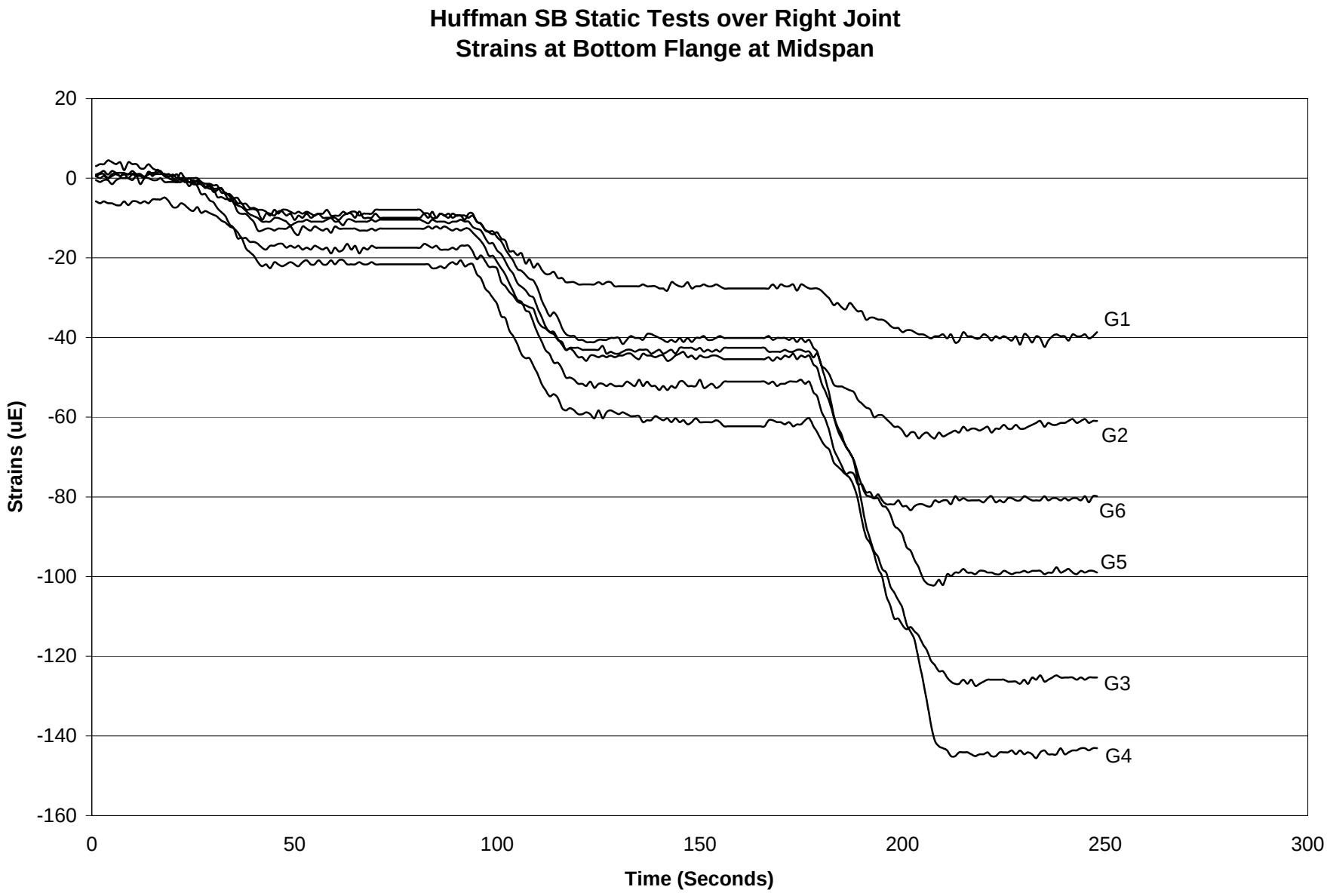
Huffman SB Static Tests over Right Joint
Strains at Bottom Flange at Midspan
Strains (uE)
20
0
-20
-40
-60
-80
-100
-120
-140
-160
0
50
100
150
200
250
300
Time (Seconds)
G1
G2
G6
G5
G3
G4

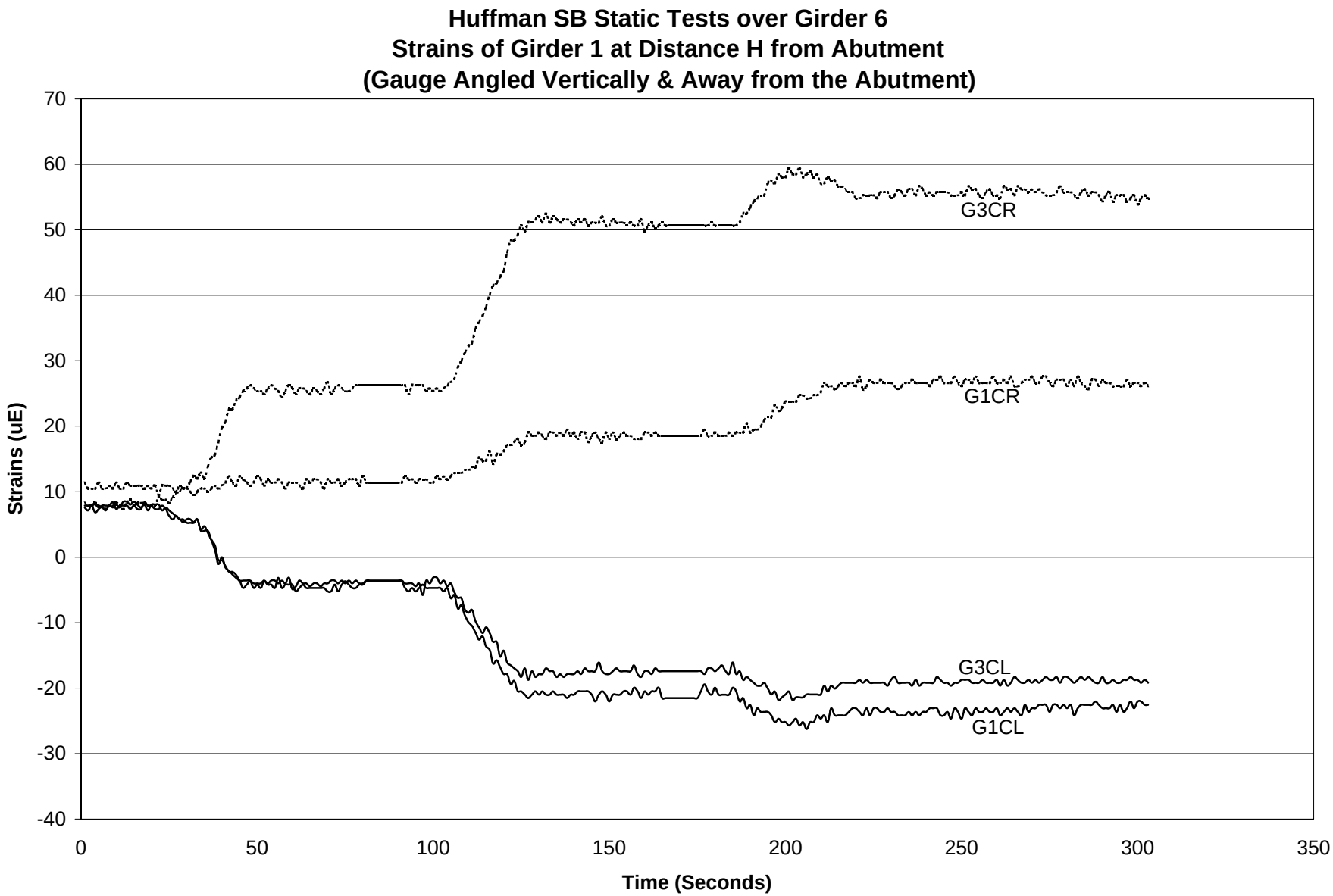
Huffman SB Static Tests over Girder 6
Strains of Girder 1 at Distance H from Abutment
(Gauge Angled Vertically & Away from the Abutment)
Strains (uE)
Time (Seconds)
70
60
50
40
30
20
10
0
-10
-20
-30
-40
0
50
100
150
200
250
300
350
G3CR
G1CR
G3CL
G1CL

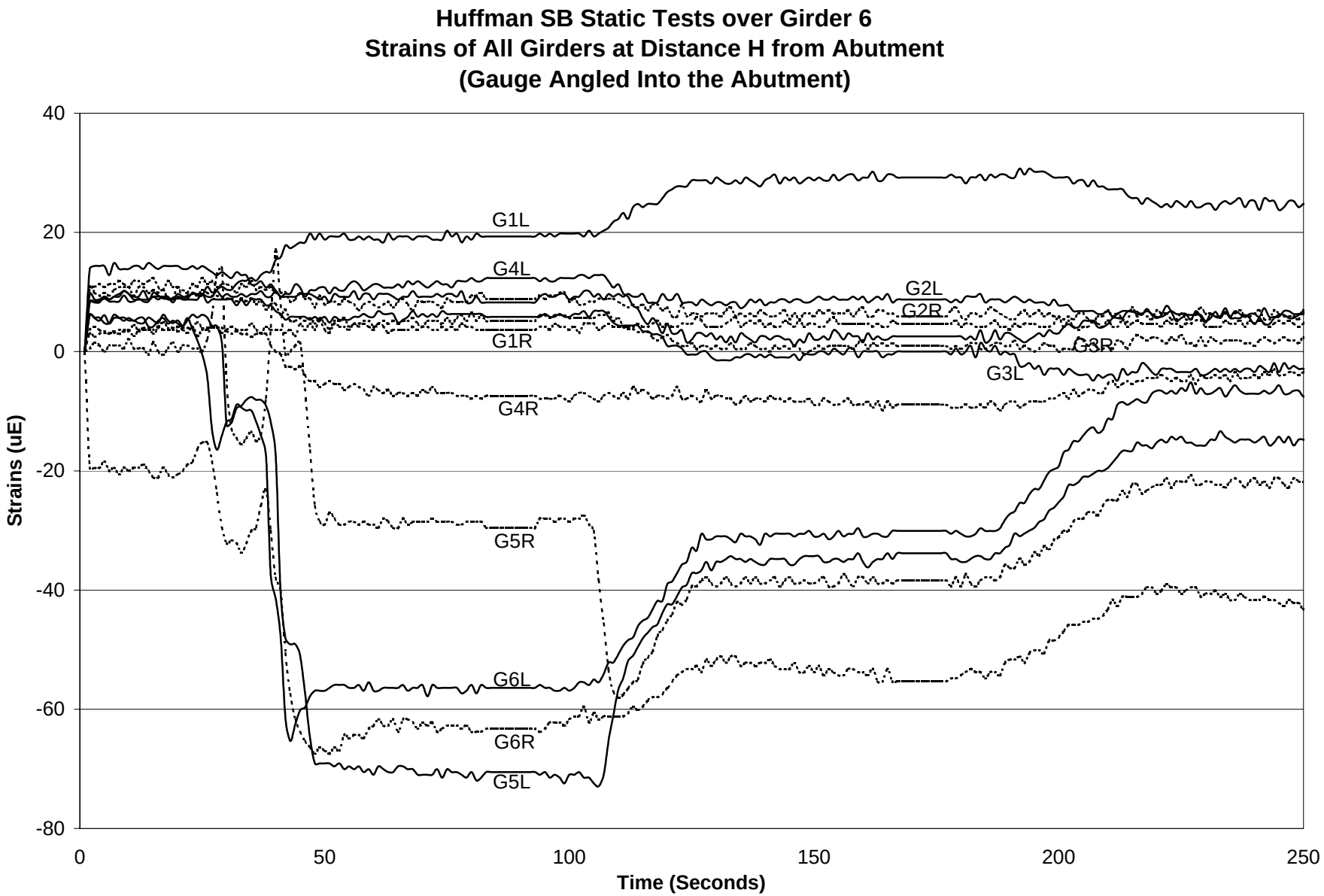
Huffman SB Static Tests over Girder 6
Strains of All Girders at Distance H from Abutment
(Gauge Angled Into the Abutment)
Strains (uE)
Time (Seconds)
40
20
0
-20
-40
-60
-80
0
50
100
150
200
250
G1L
G4L
G2L
G2R
G1R
G3R
G3L
G4R
G5R
G6L
G6R
G5L

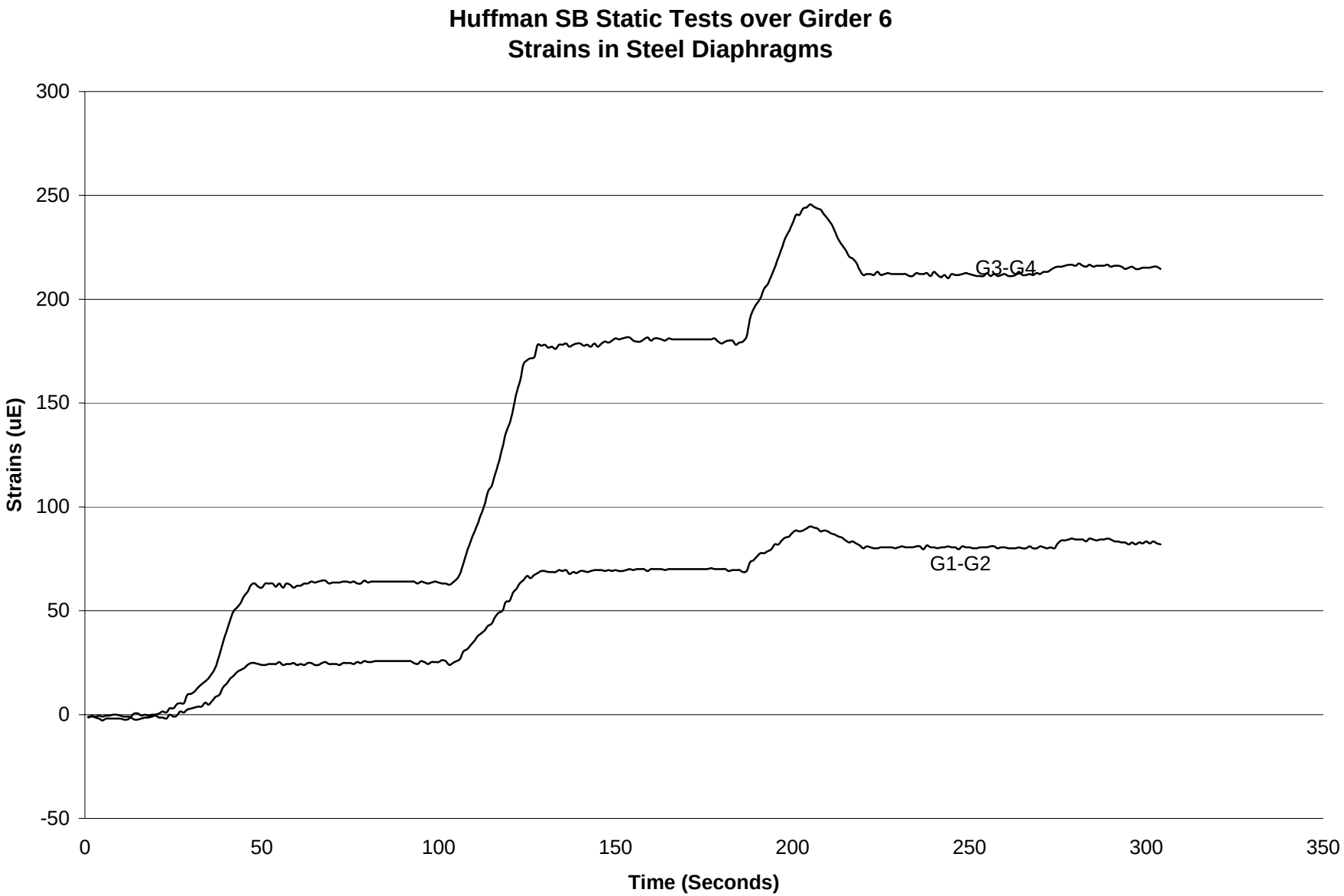
Huffman SB Static Tests over Girder 6
Strains in Steel Diaphragms
300
250
200
150
100
50
0
-50
Strains (uE)
0
50
100
150
200
250
300
350
Time (Seconds)
G3-G4
G1-G2

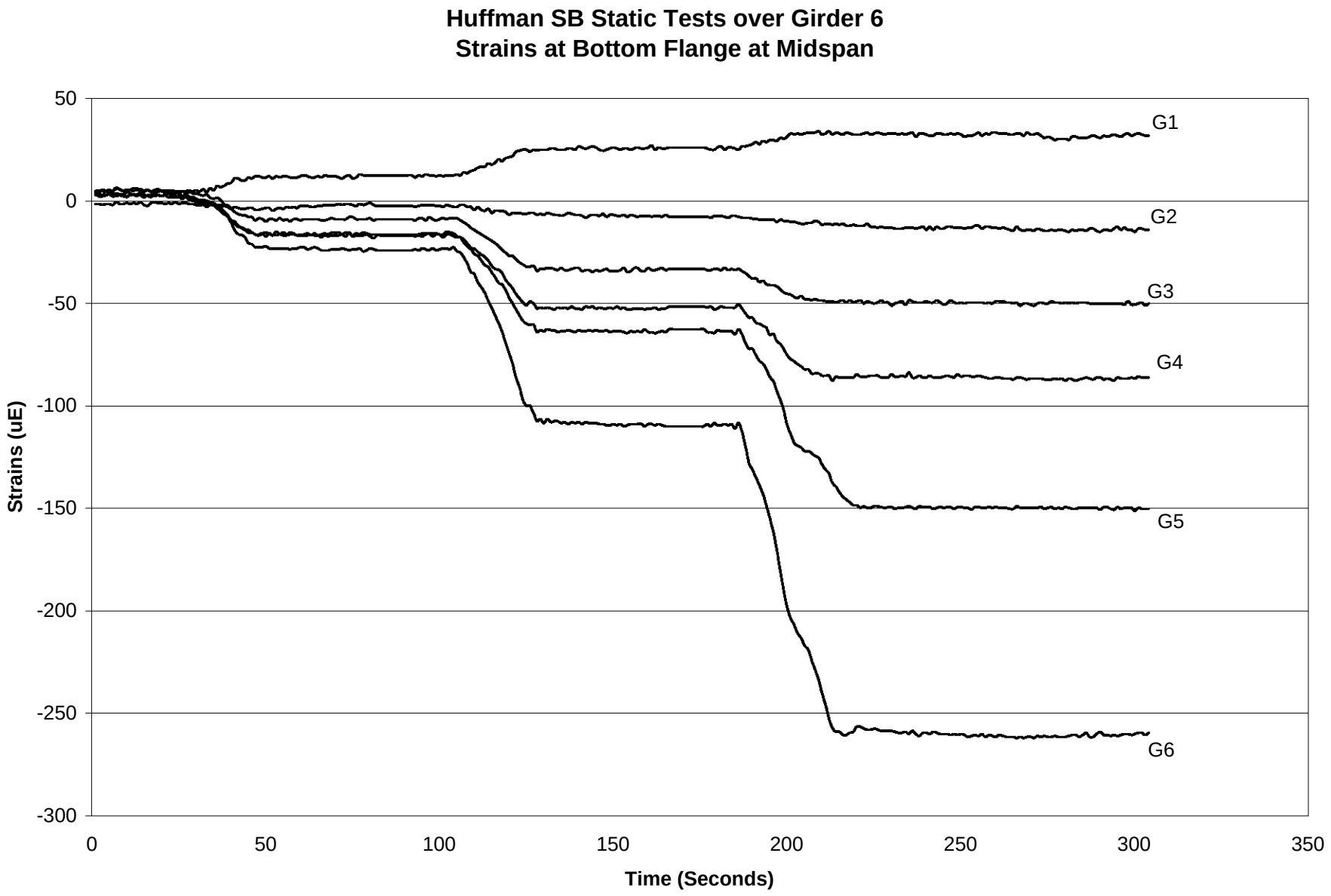
Huffman SB Static Tests over Girder 6
Strains at Bottom Flange at Midspan
Strains (uE)
Time (Seconds)
50
0
-50
-100
-150
-200
-250
-300
0
50
100
150
200
250
300
350
G1
G2
G3
G4
G5
G6

# Diamond

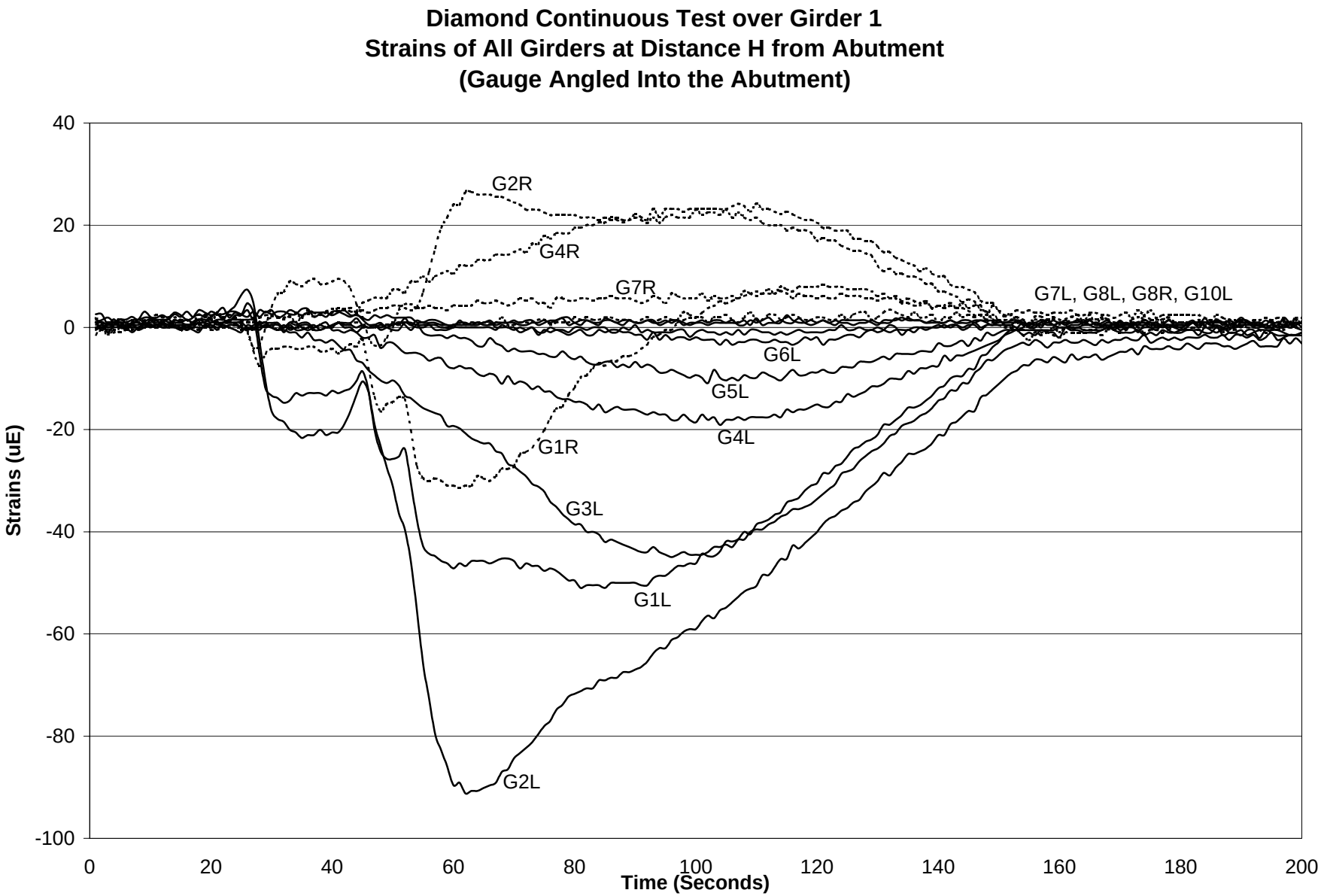
Diamond Continuous Test over Girder 1
Strains of All Girders at Distance H from Abutment
(Gauge Angled Into the Abutment)
Strains (uE)
Time (Seconds)
40
20
0
-20
-40
-60
-80
-100
0
20
40
60
80
100
120
140
160
180
200
G2R
G4R
G7R
G7L, G8L, G8R, G10L
G6L
G5L
G4L
G1R
G3L
G1L
G2L

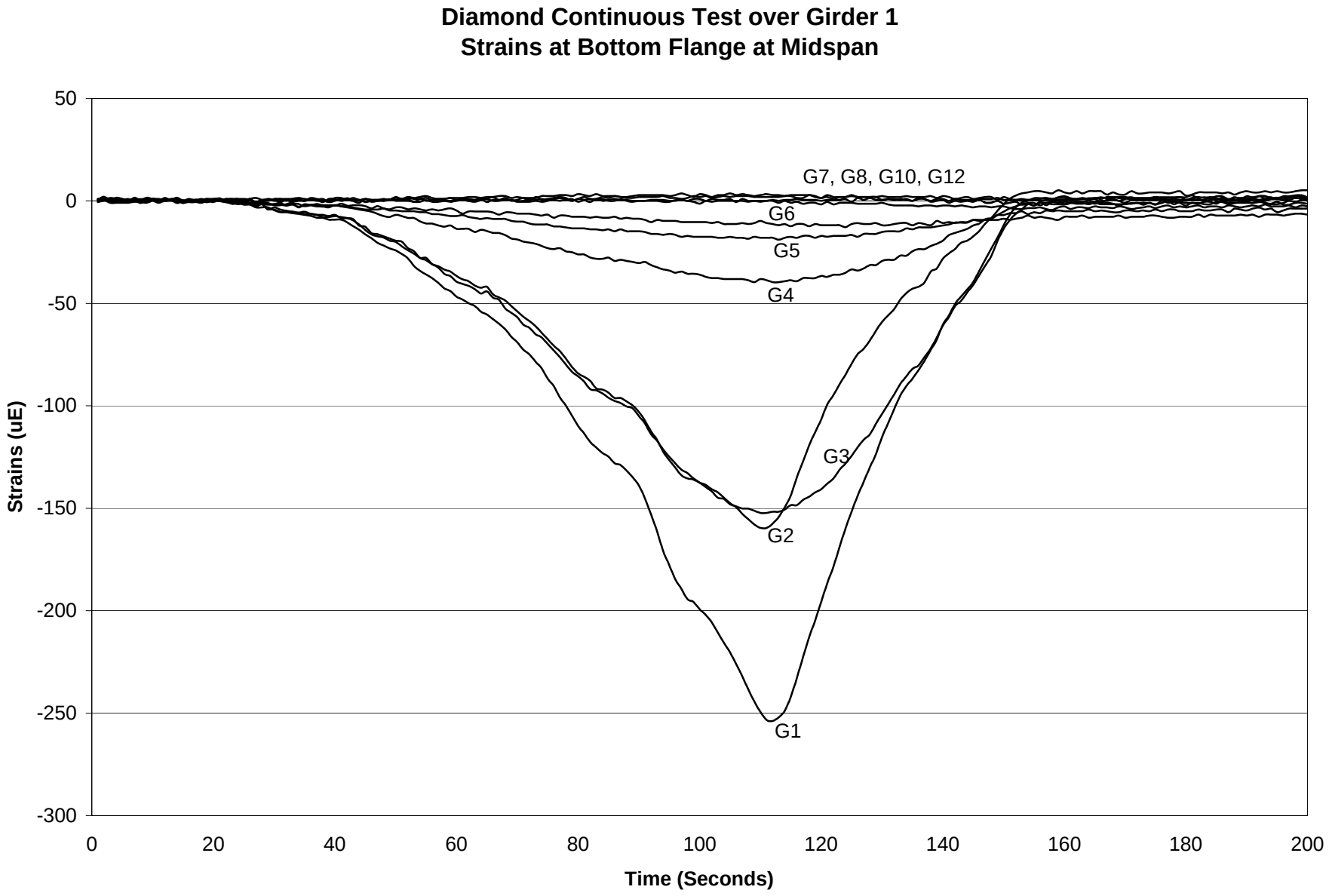
Diamond Continuous Test over Girder 1
Strains at Bottom Flange at Midspan
Strains (uE)
Time (Seconds)
50
0
-50
-100
-150
-200
-250
-300
0
20
40
60
80
100
120
140
160
180
200
G7, G8, G10, G12
G6
G5
G4
G3
G2
G1

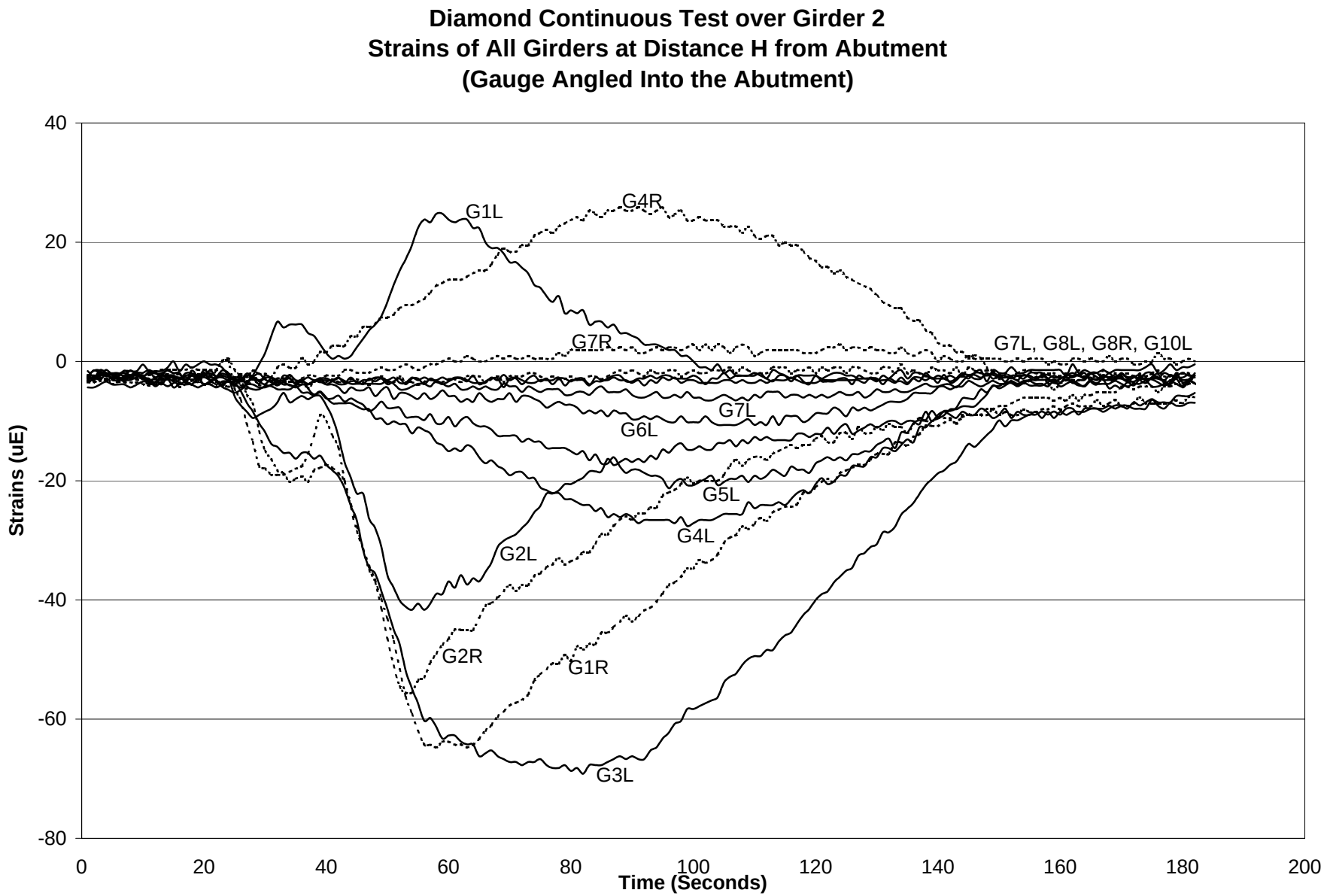
Diamond Continuous Test over Girder 2
Strains of All Girders at Distance H from Abutment
(Gauge Angled Into the Abutment)
Strains (uE)
Time (Seconds)
40
20
0
-20
-40
-60
-80
0
20
40
60
80
100
120
140
160
180
200
G1L
G4R
G7R
G7L, G8L, G8R, G10L
G7L
G6L
G5L
G4L
G2L
G2R
G1R
G3L

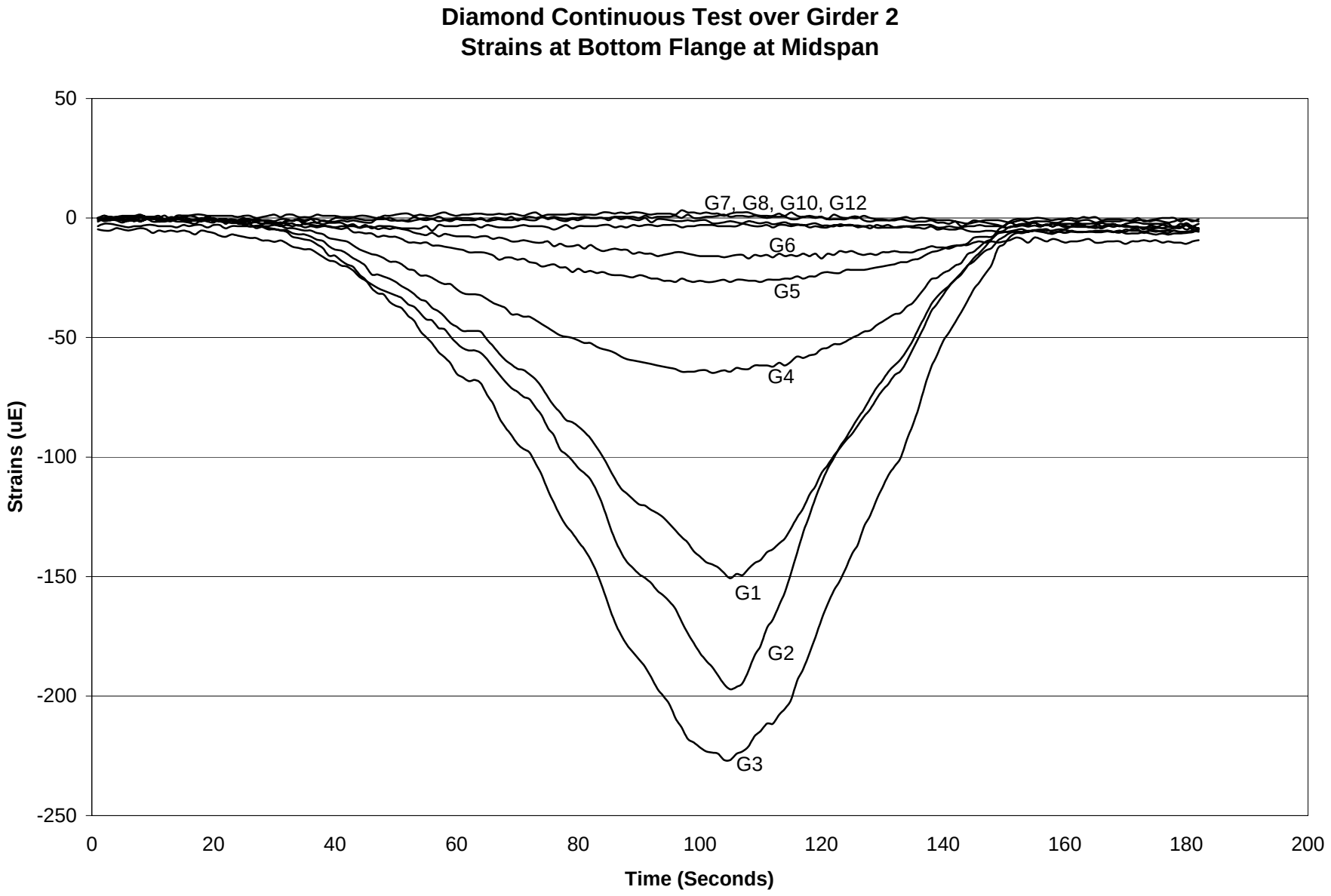
Diamond Continuous Test over Girder 2
Strains at Bottom Flange at Midspan
Strains (uE)
Time (Seconds)
50
0
-50
-100
-150
-200
-250
0
20
40
60
80
100
120
140
160
180
200
G7, G8, G10, G12
G6
G5
G4
G1
G2
G3

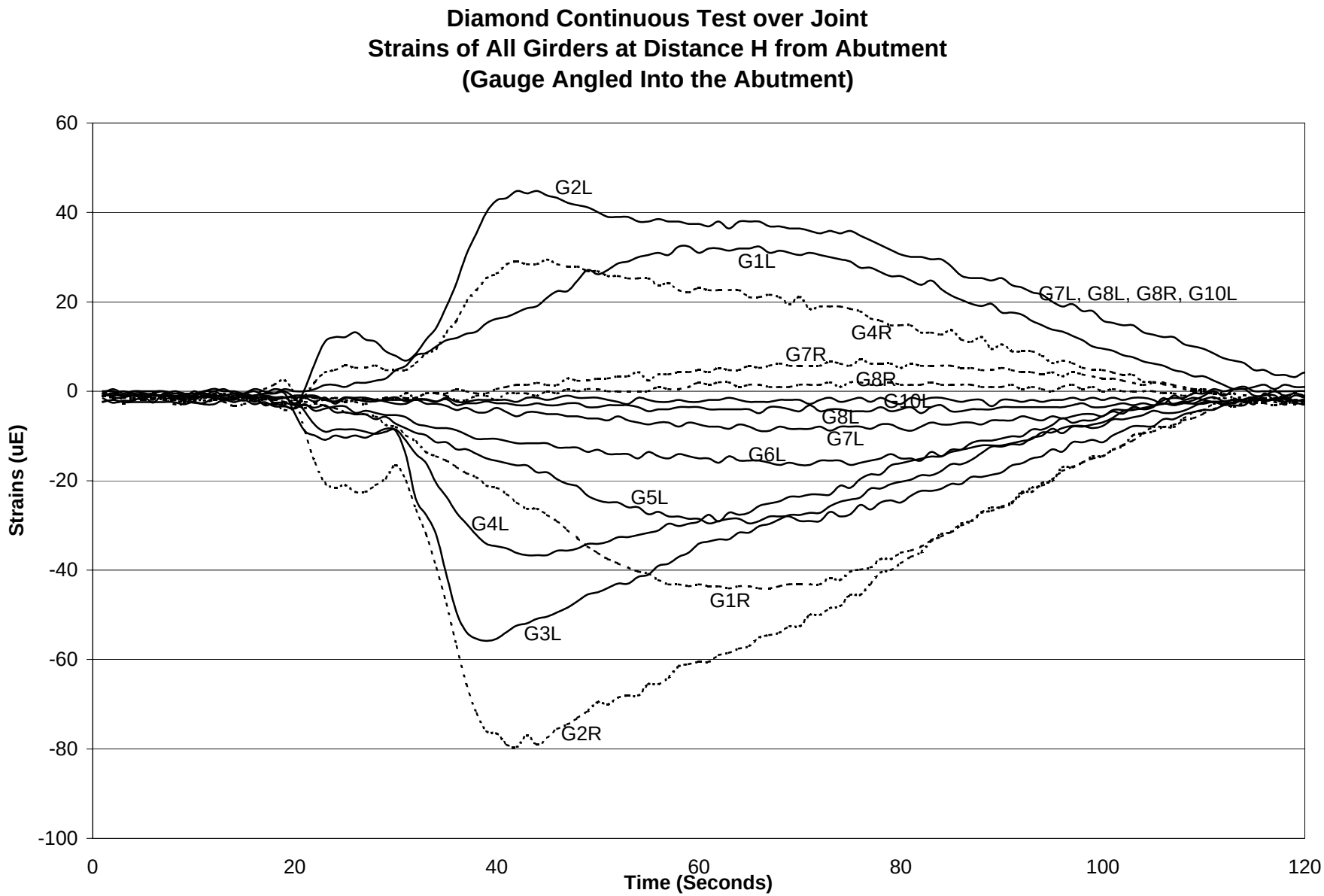
Diamond Continuous Test over Joint
Strains of All Girders at Distance H from Abutment
(Gauge Angled Into the Abutment)
Strains (uE)
Time (Seconds)
60
40
20
0
-20
-40
-60
-80
-100
0
20
40
60
80
100
120
G2L
G1L
G7L, G8L, G8R, G10L
G4R
G7R
G8R
G10L
G8L
G7L
G6L
G5L
G4L
G1R
G3L
G2R

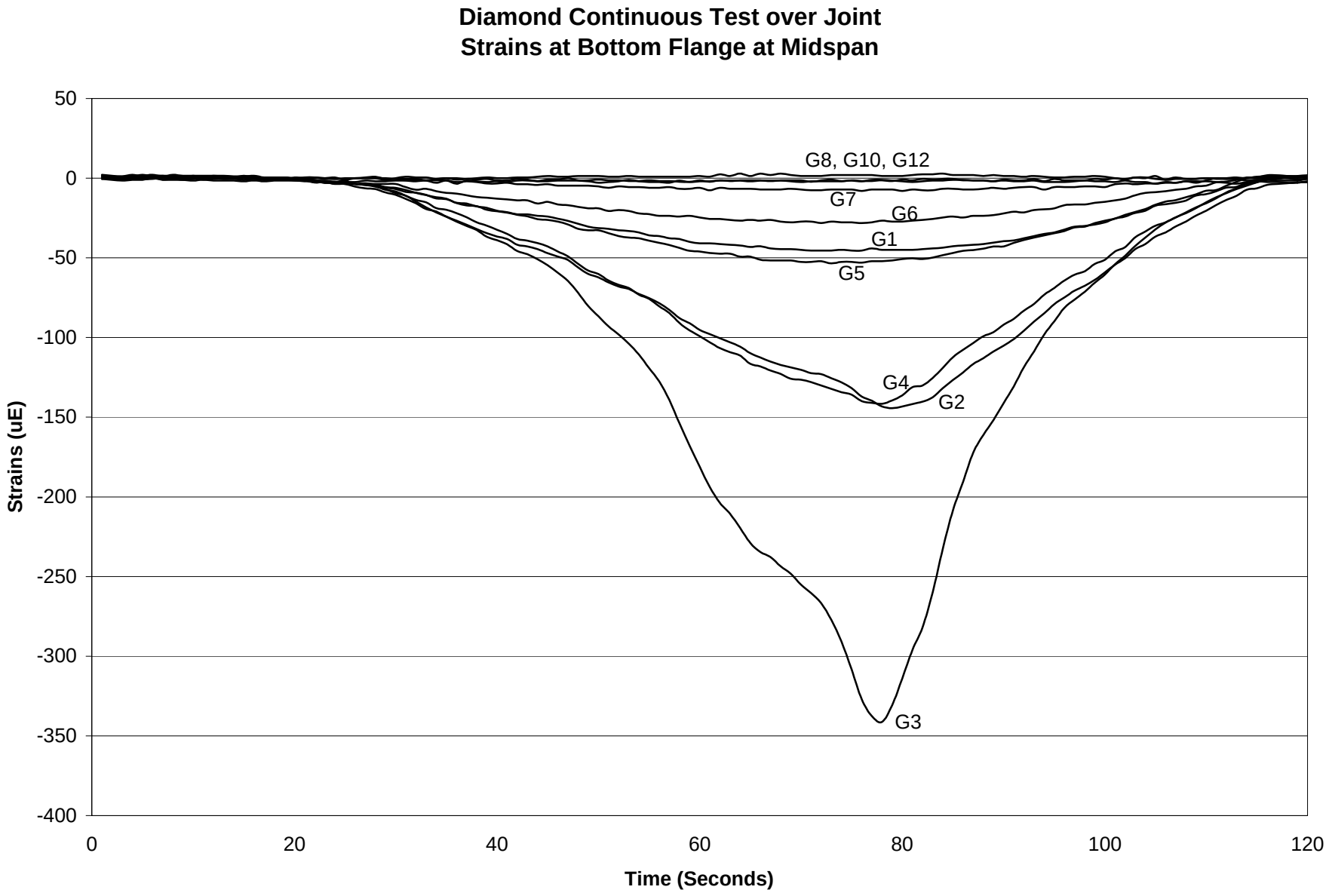
Diamond Continuous Test over Joint
Strains at Bottom Flange at Midspan
Strains (uE)
Time (Seconds)
50
0
-50
-100
-150
-200
-250
-300
-350
-400
0
20
40
60
80
100
120
G8, G10, G12
G7
G6
G1
G5
G4
G2
G3

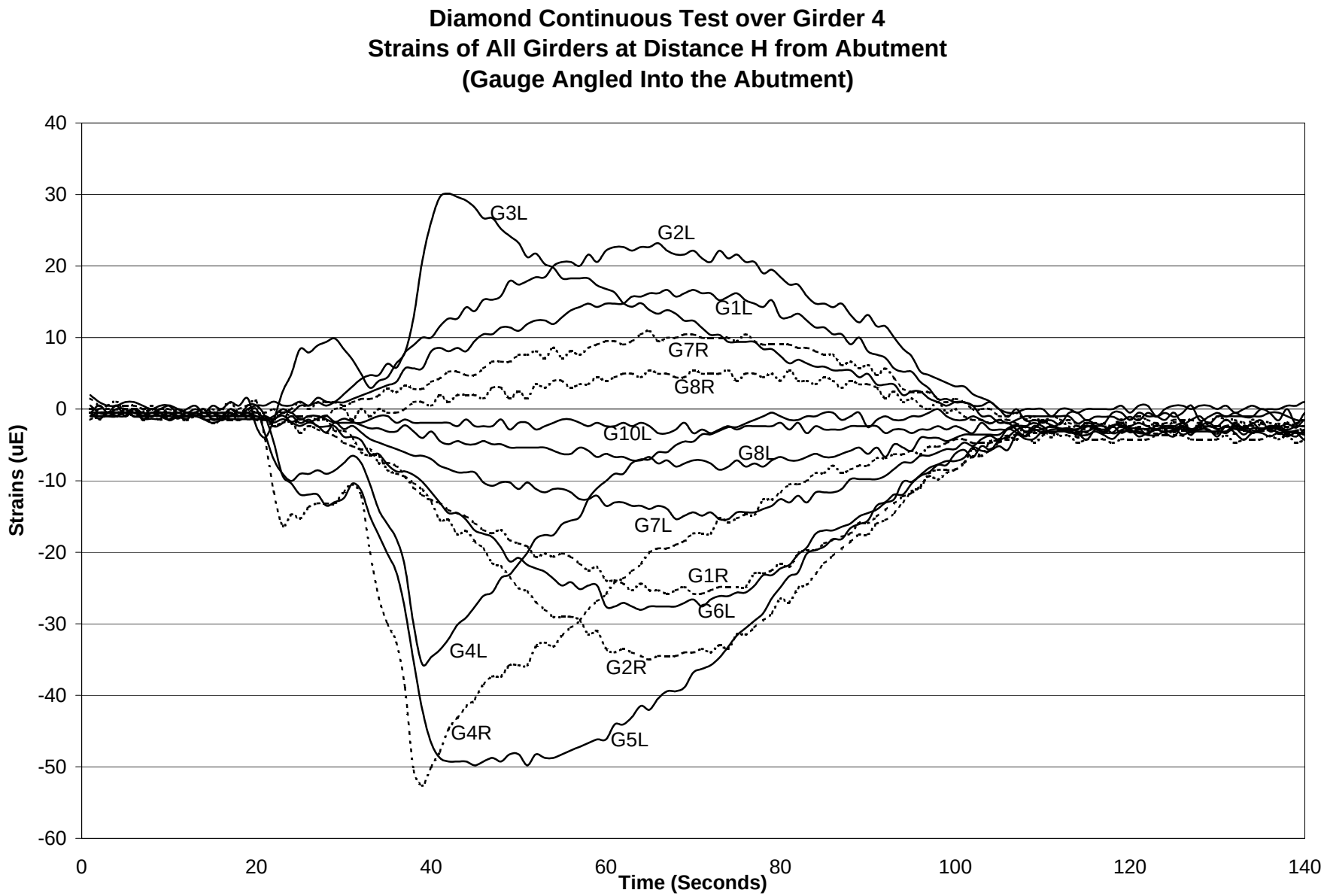
Diamond Continuous Test over Girder 4
Strains of All Girders at Distance H from Abutment
(Gauge Angled Into the Abutment)
Strains (uE)
Time (Seconds)
40
30
20
10
0
-10
-20
-30
-40
-50
-60
0
20
40
60
80
100
120
140
G3L
G2L
G1L
G7R
G8R
G10L
G8L
G7L
G1R
G6L
G4L
G2R
G4R
G5L

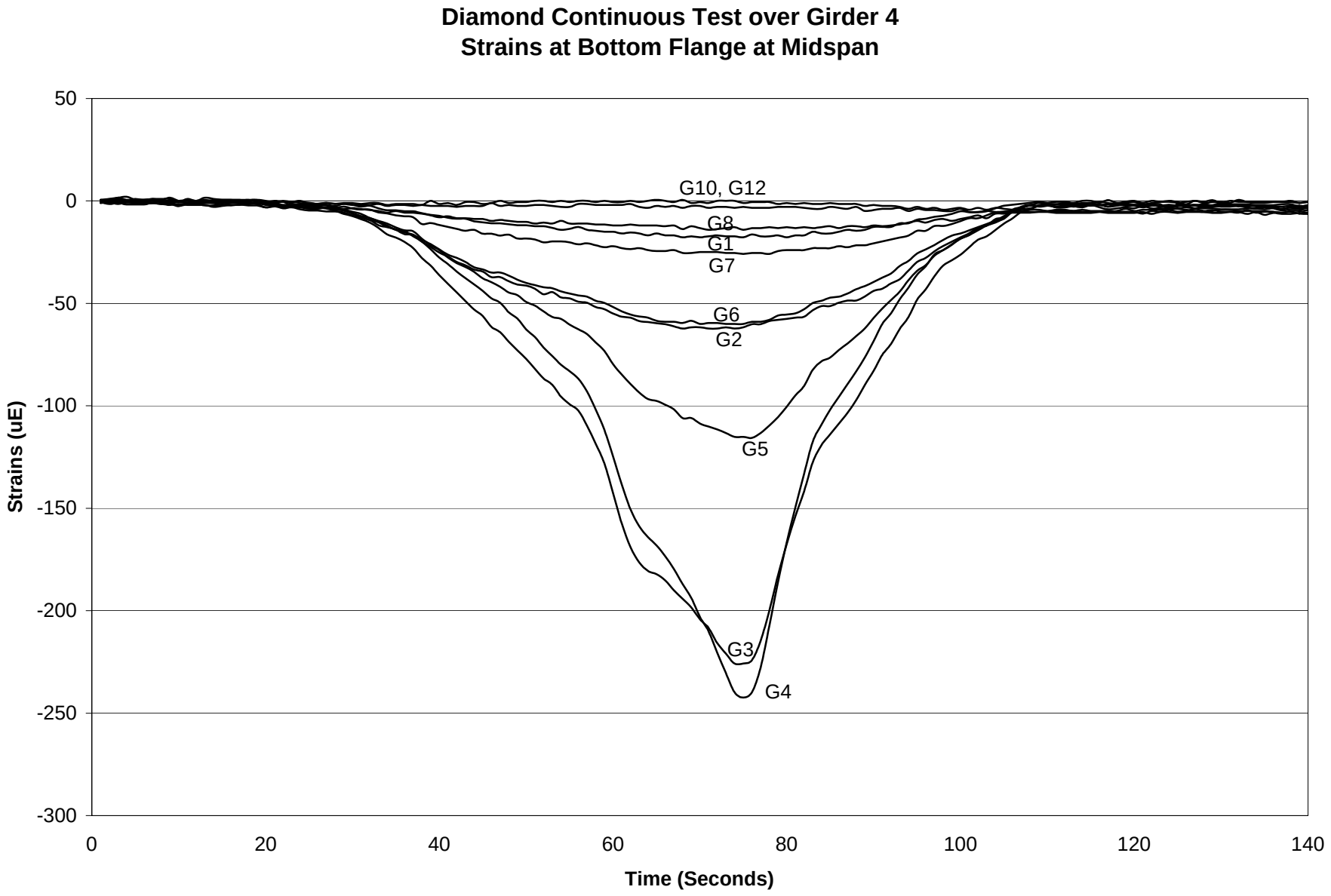
Diamond Continuous Test over Girder 4
Strains at Bottom Flange at Midspan
Strains (uE)
Time (Seconds)
50
0
-50
-100
-150
-200
-250
-300
0
20
40
60
80
100
120
140
G10, G12
G8
G1
G7
G6
G2
G5
G3
G4

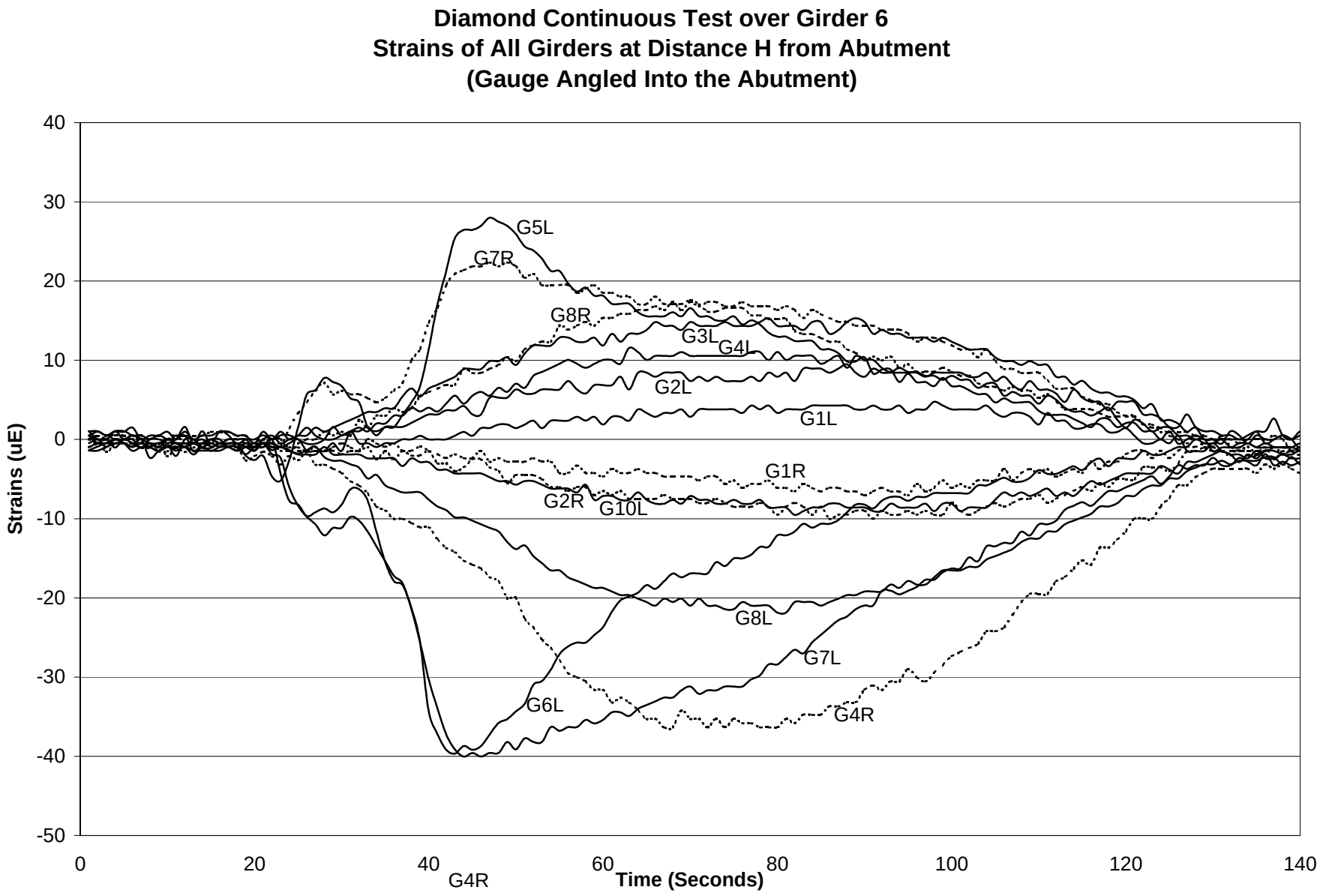
Diamond Continuous Test over Girder 6
Strains of All Girders at Distance H from Abutment
(Gauge Angled Into the Abutment)
Strains (uE)
Time (Seconds)
40
30
20
10
0
-10
-20
-30
-40
-50
0
20
40
60
80
100
120
140
G5L
G7R
G8R
G3L
G4L
G2L
G1L
G1R
G2R
G10L
G8L
G7L
G6L
G4R
G4R

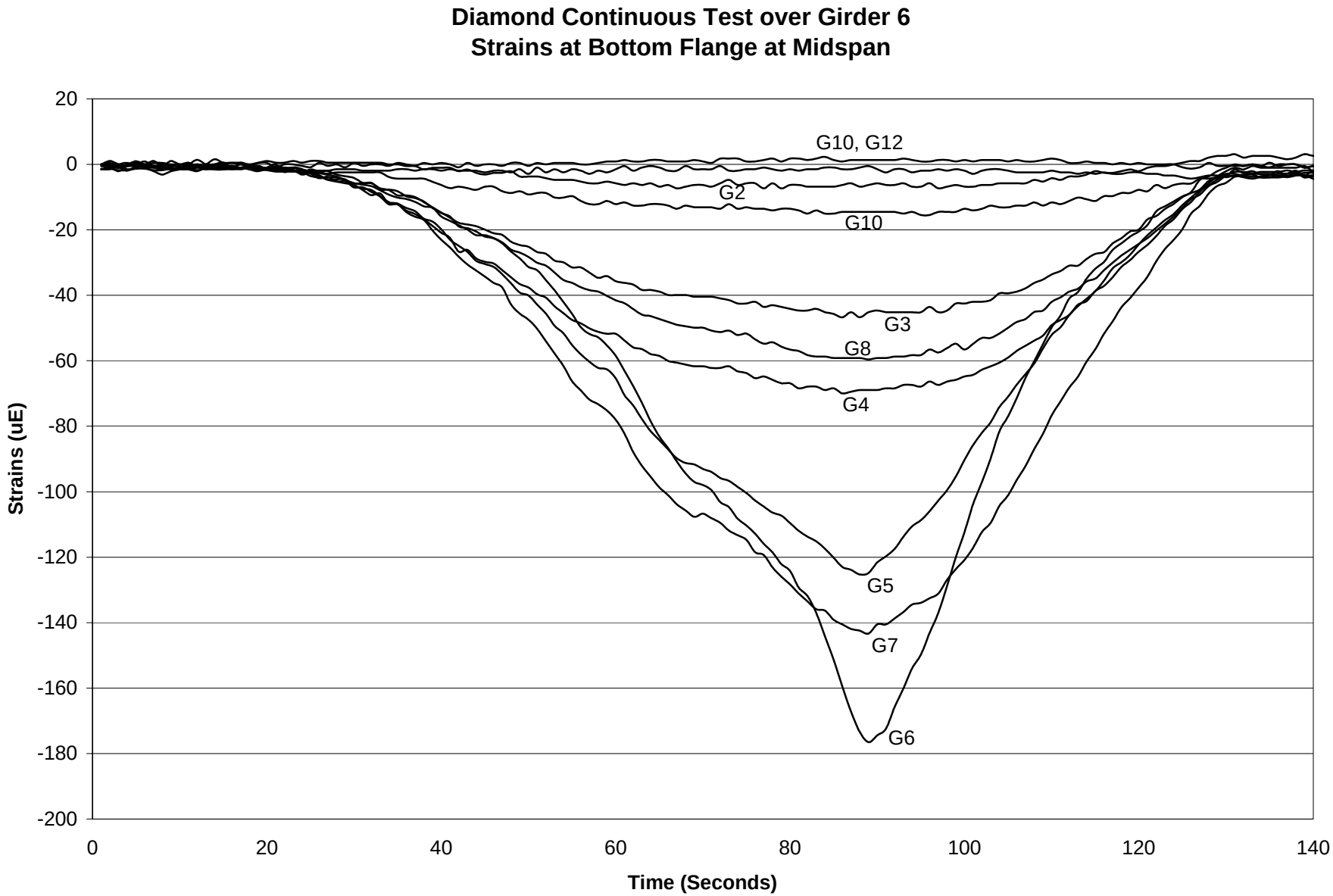
Diamond Continuous Test over Girder 6
Strains at Bottom Flange at Midspan
Strains (uE)
Time (Seconds)
20
0
-20
-40
-60
-80
-100
-120
-140
-160
-180
-200
0
20
40
60
80
100
120
140
G10, G12
G2
G10
G3
G8
G4
G5
G7
G6

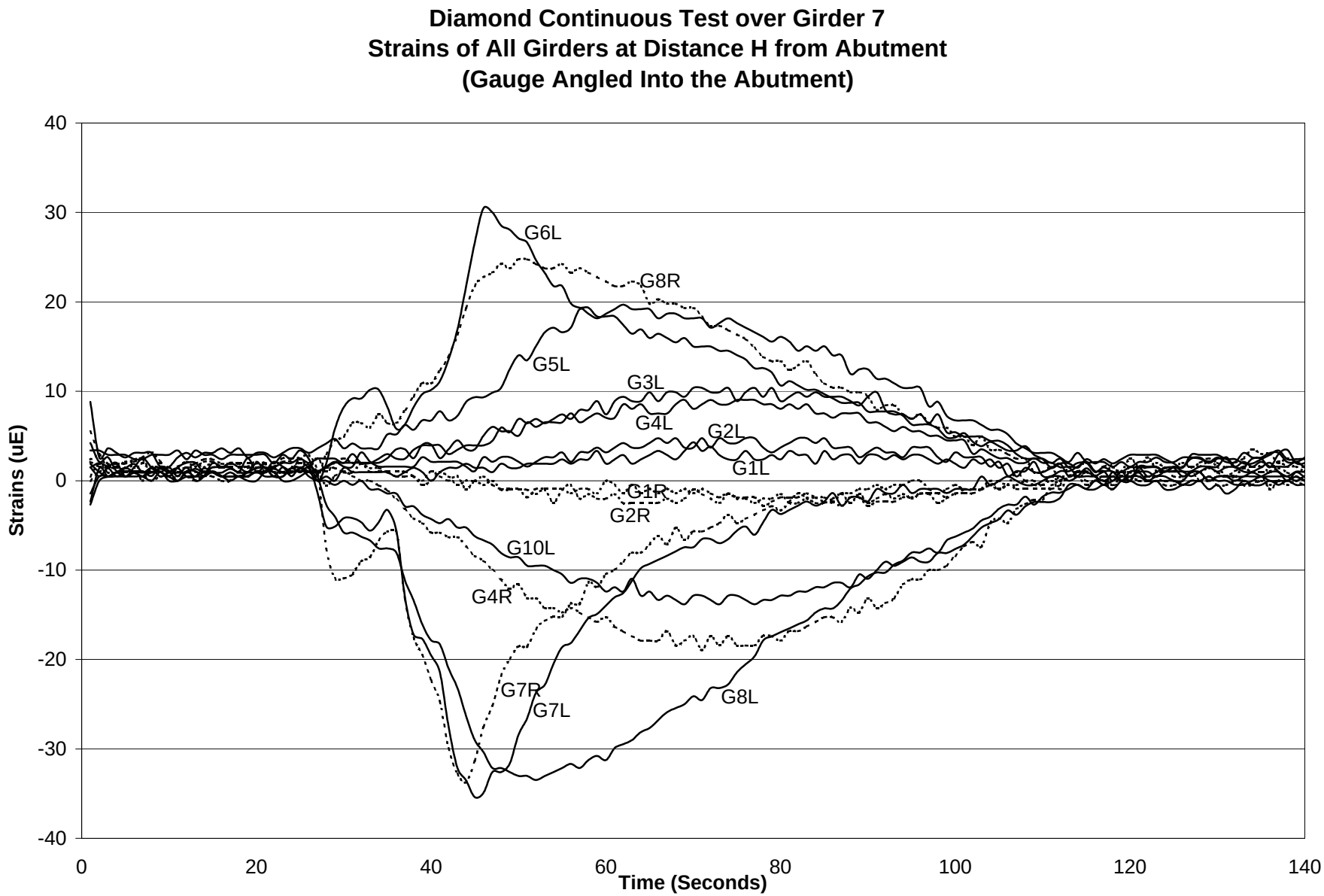
Diamond Continuous Test over Girder 7
Strains of All Girders at Distance H from Abutment
(Gauge Angled Into the Abutment)
Strains (uE)
Time (Seconds)
40
30
20
10
0
-10
-20
-30
-40
0
20
40
60
80
100
120
140
G6L
G8R
G5L
G3L
G4L
G2L
G1L
G1R
G2R
G10L
G4R
G7R
G7L
G8L

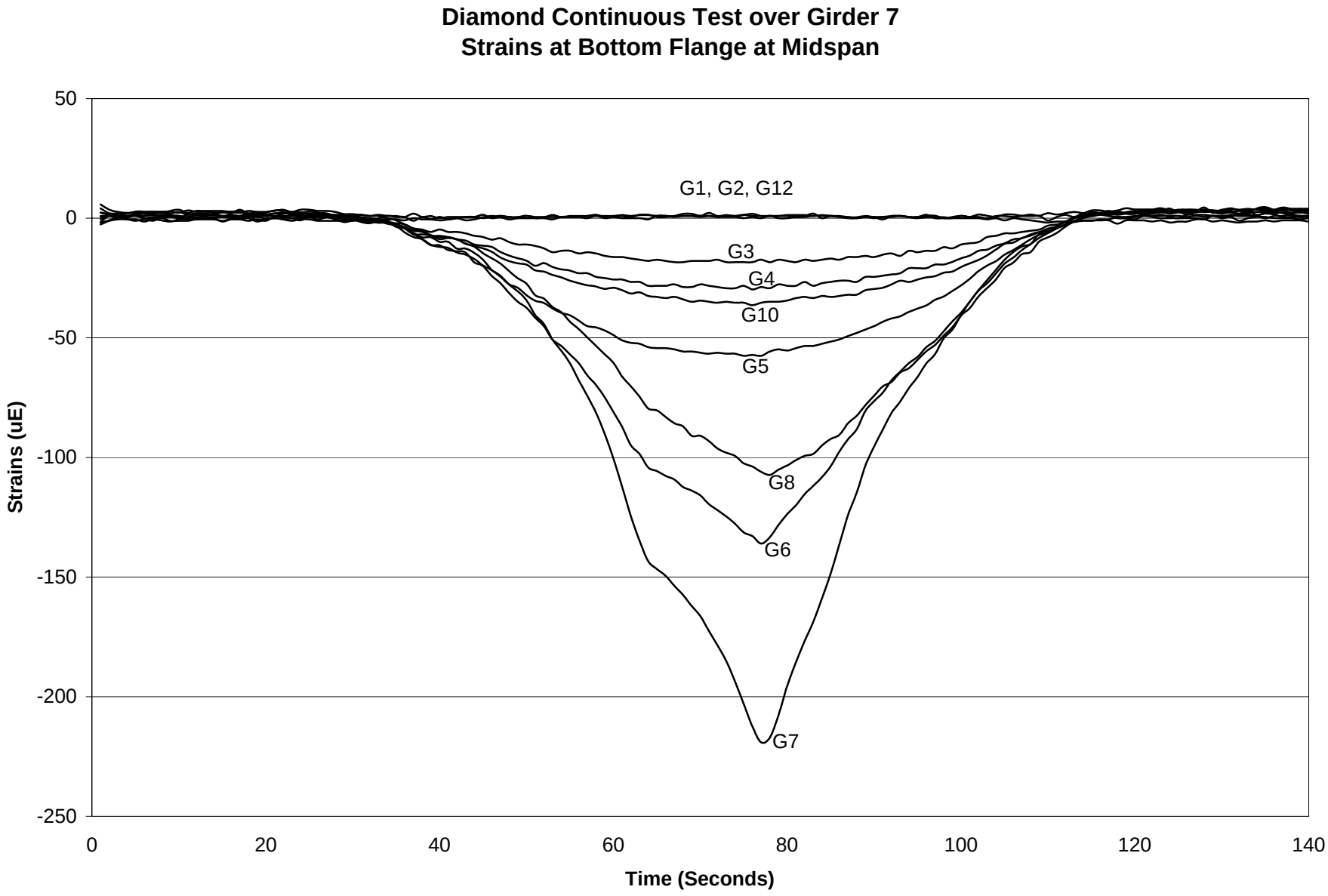
Diamond Continuous Test over Girder 7
Strains at Bottom Flange at Midspan
50
0
-50
-100
-150
-200
-250
Strains (uE)
0
20
40
60
80
100
120
140
Time (Seconds)
G1, G2, G12
G3
G4
G10
G5
G8
G6
G7

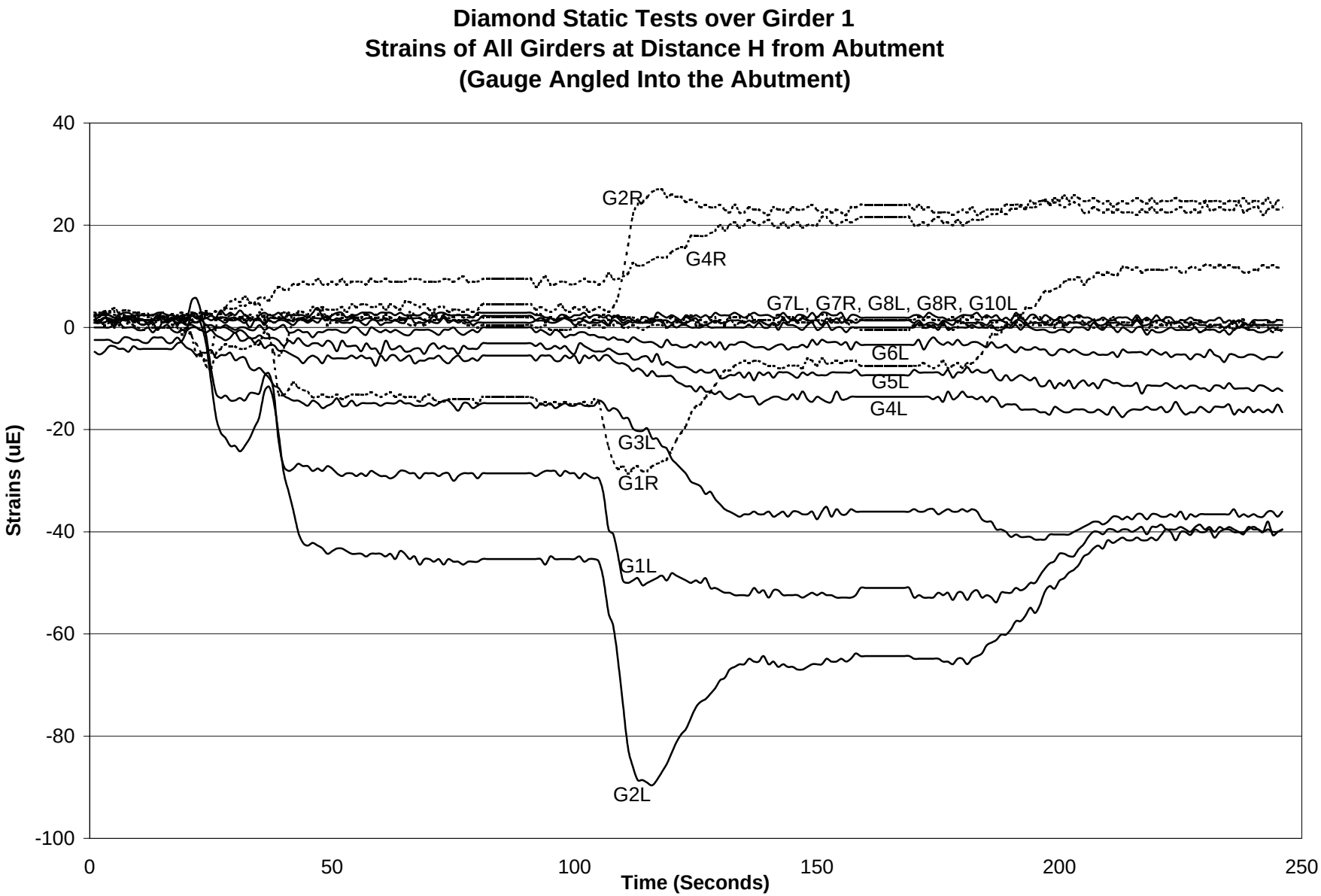
Diamond Static Tests over Girder 1
Strains of All Girders at Distance H from Abutment
(Gauge Angled Into the Abutment)
Strains (uE)
Time (Seconds)
40
20
0
-20
-40
-60
-80
-100
0
50
100
150
200
250
G2R
G4R
G7L, G7R, G8L, G8R, G10L
G6L
G5L
G4L
G3L
G1R
G1L
G2L

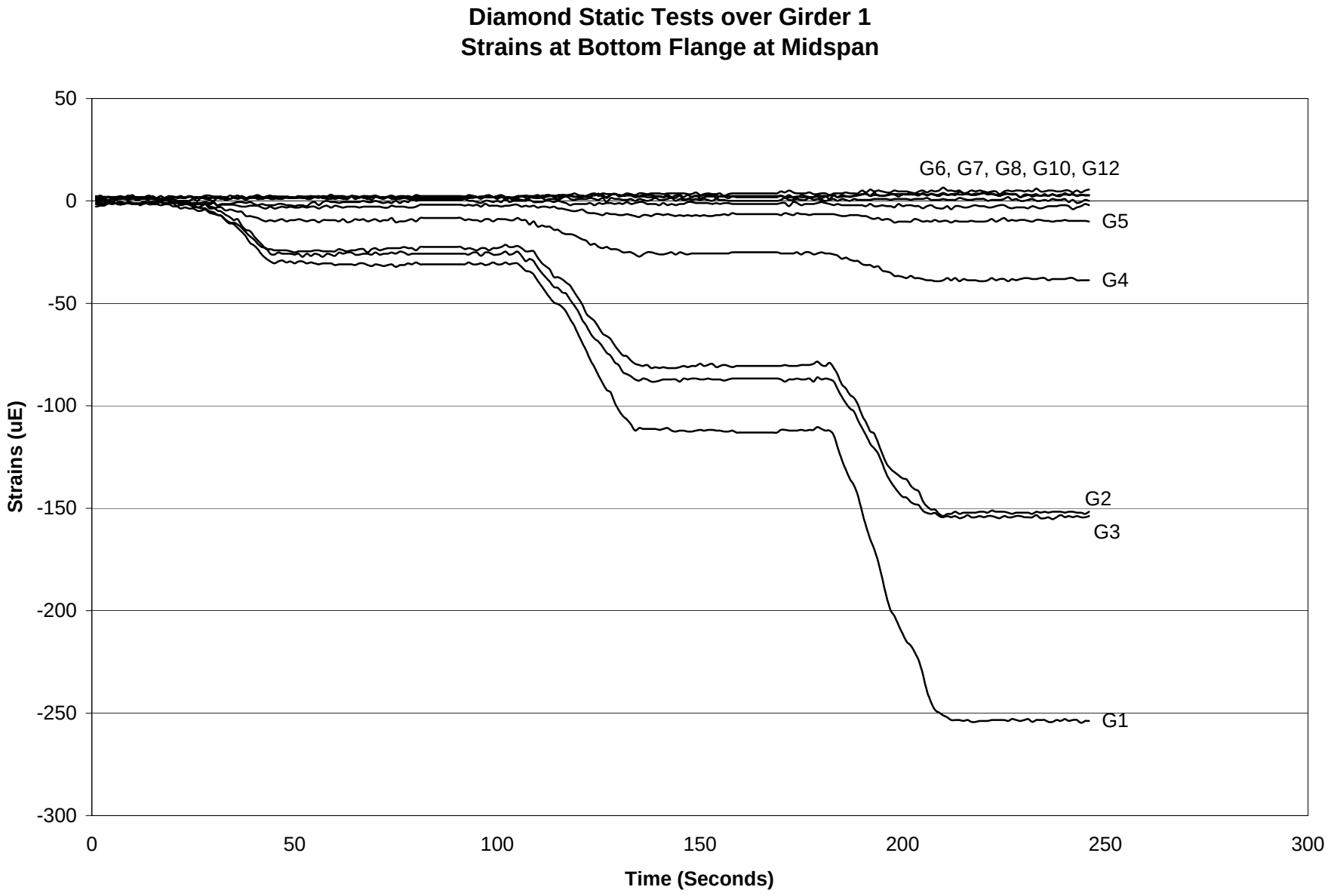
Diamond Static Tests over Girder 1
Strains at Bottom Flange at Midspan
50
0
-50
-100
-150
-200
-250
-300
Strains (uE)
0
50
100
150
200
250
300
Time (Seconds)
G6, G7, G8, G10, G12
G5
G4
G2
G3
G1

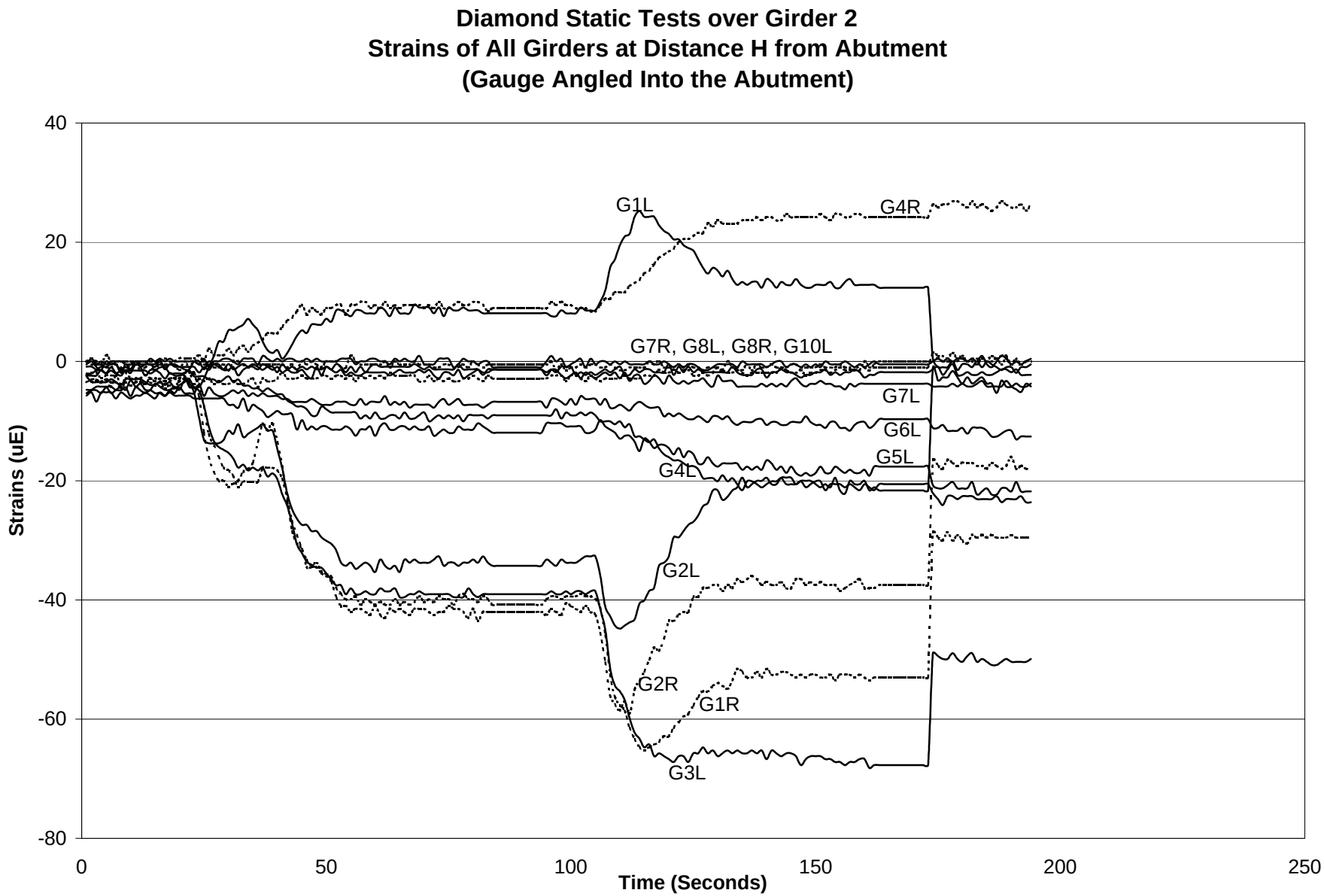
Diamond Static Tests over Girder 2
Strains of All Girders at Distance H from Abutment
(Gauge Angled Into the Abutment)
Strains (uE)
Time (Seconds)
40
20
0
-20
-40
-60
-80
0
50
100
150
200
250
G1L
G4R
G7R, G8L, G8R, G10L
G7L
G6L
G5L
G4L
G2L
G2R
G1R
G3L

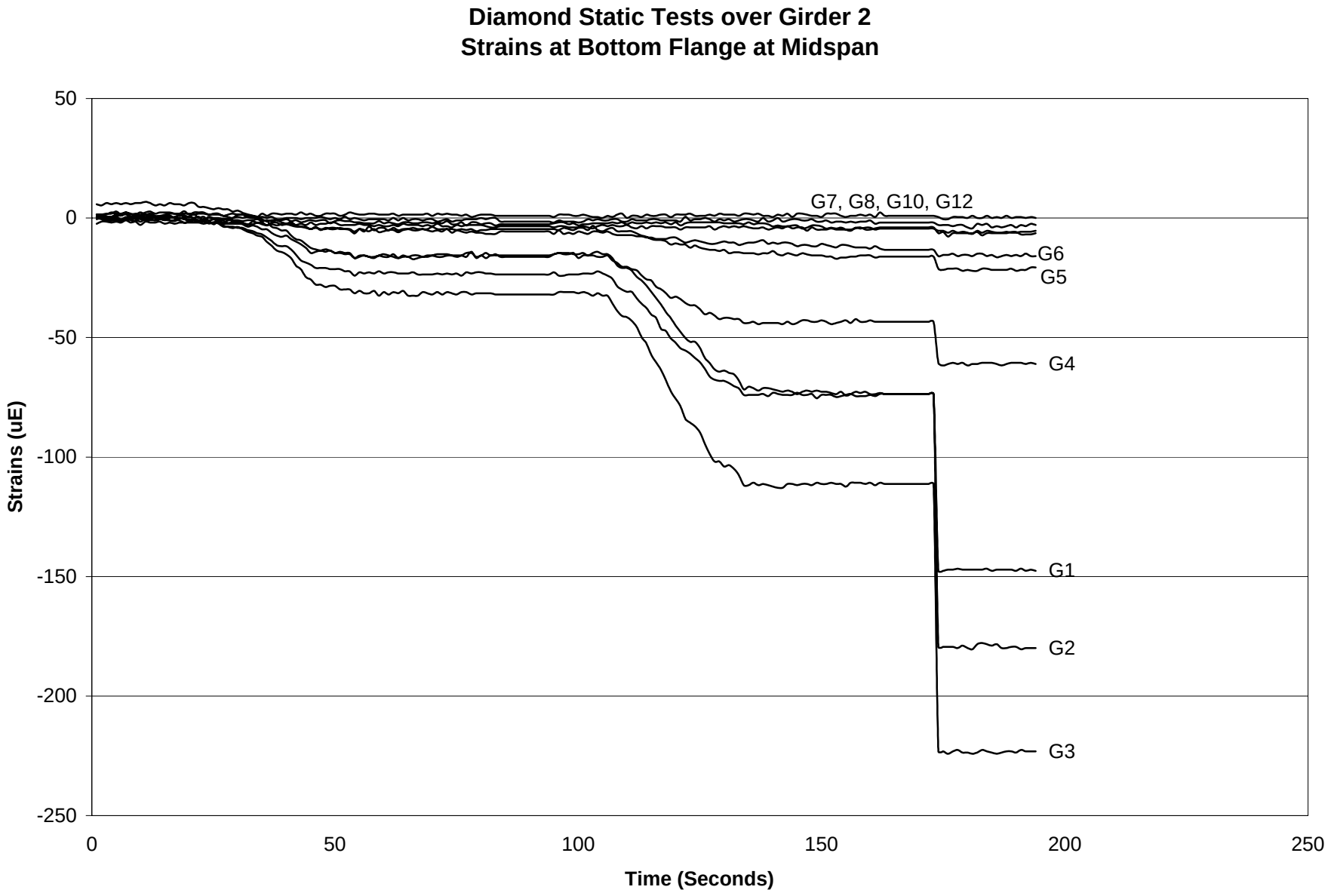
Diamond Static Tests over Girder 2
Strains at Bottom Flange at Midspan
50
0
-50
-100
-150
-200
-250
Strains (uE)
0
50
100
150
200
250
Time (Seconds)
G7, G8, G10, G12
G6
G5
G4
G1
G2
G3

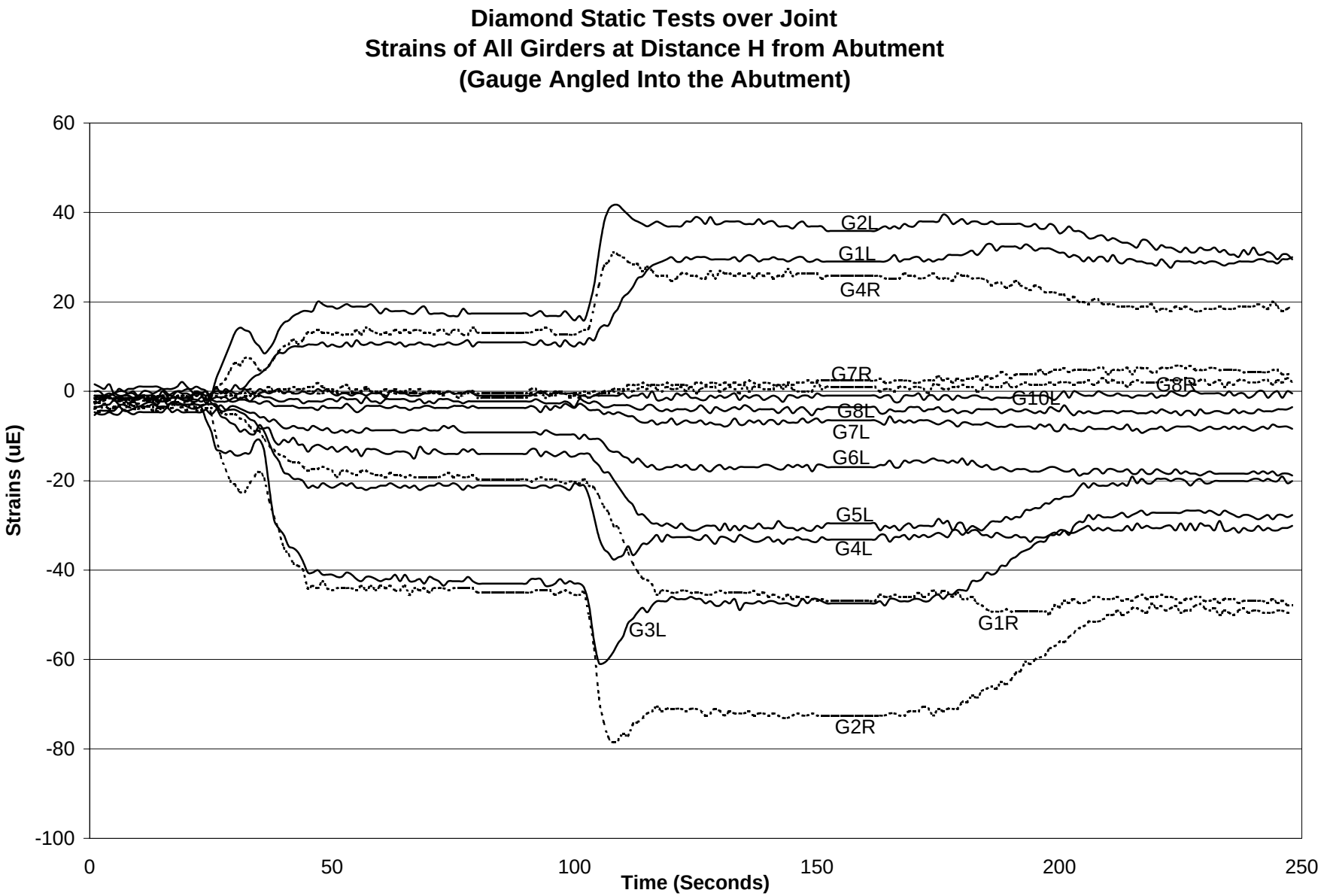
Diamond Static Tests over Joint
Strains of All Girders at Distance H from Abutment
(Gauge Angled Into the Abutment)
Strains (uE)
Time (Seconds)
60
40
20
0
-20
-40
-60
-80
-100
0
50
100
150
200
250
G2L
G1L
G4R
G7R
G8R
G10L
G8L
G7L
G6L
G5L
G4L
G3L
G1R
G2R

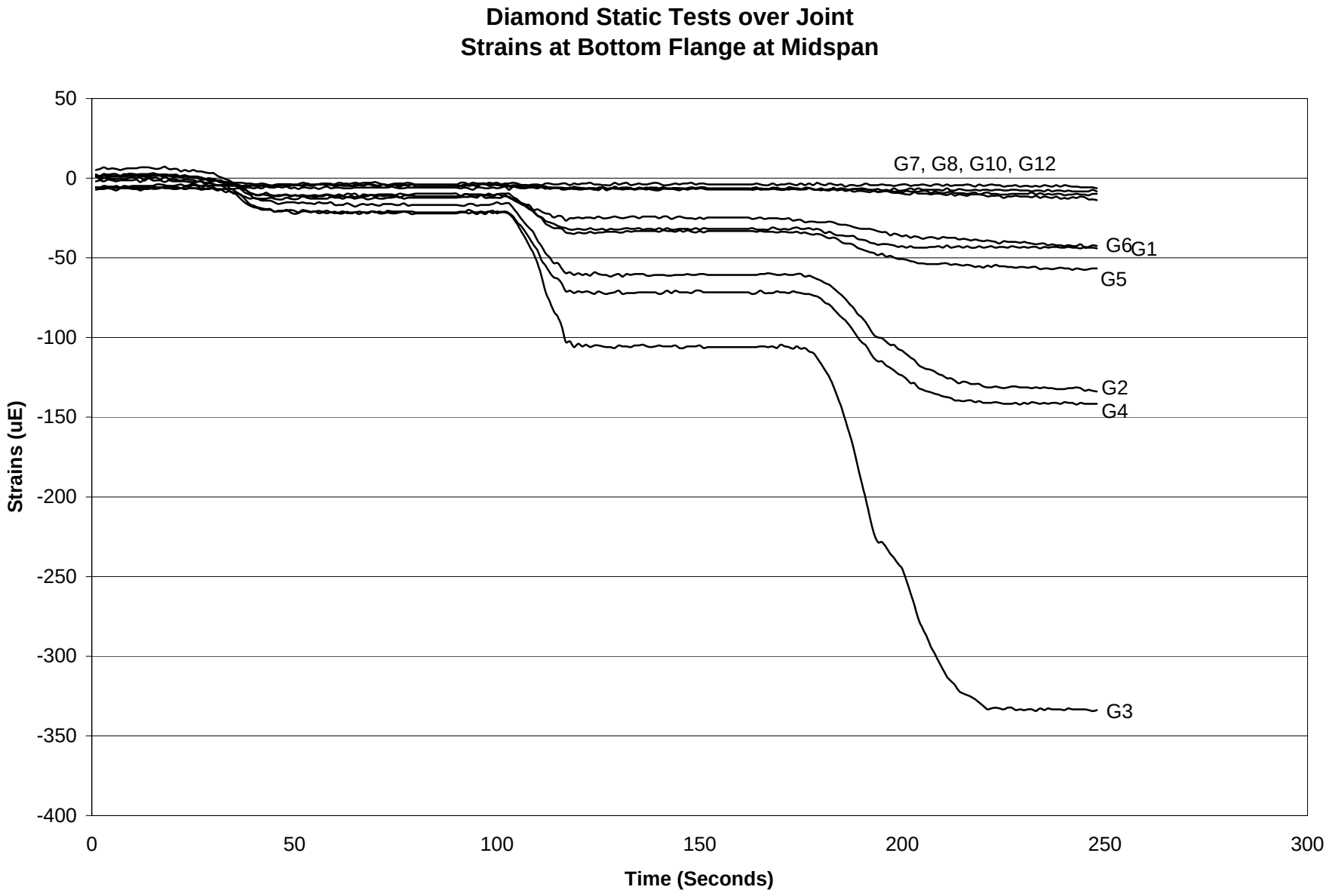
Diamond Static Tests over Joint
Strains at Bottom Flange at Midspan
Strains (uE)
Time (Seconds)
50
0
-50
-100
-150
-200
-250
-300
-350
-400
0
50
100
150
200
250
300
G7, G8, G10, G12
G6
G1
G5
G2
G4
G3

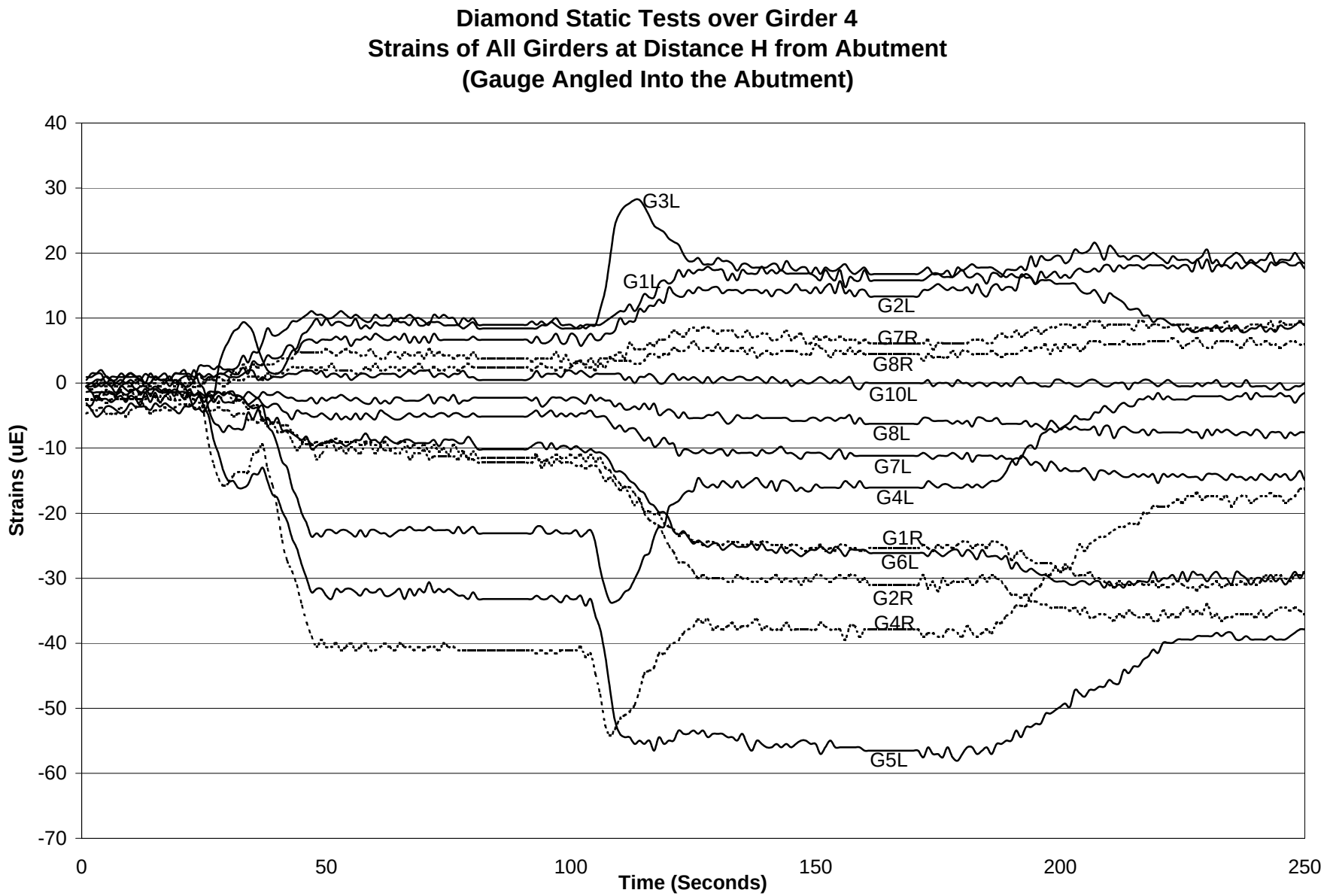
Diamond Static Tests over Girder 4
Strains of All Girders at Distance H from Abutment
(Gauge Angled Into the Abutment)
Strains (uE)
Time (Seconds)
40
30
20
10
0
-10
-20
-30
-40
-50
-60
-70
0
50
100
150
200
250
G3L
G1L
G2L
G7R
G8R
G10L
G8L
G7L
G4L
G1R
G6L
G2R
G4R
G5L

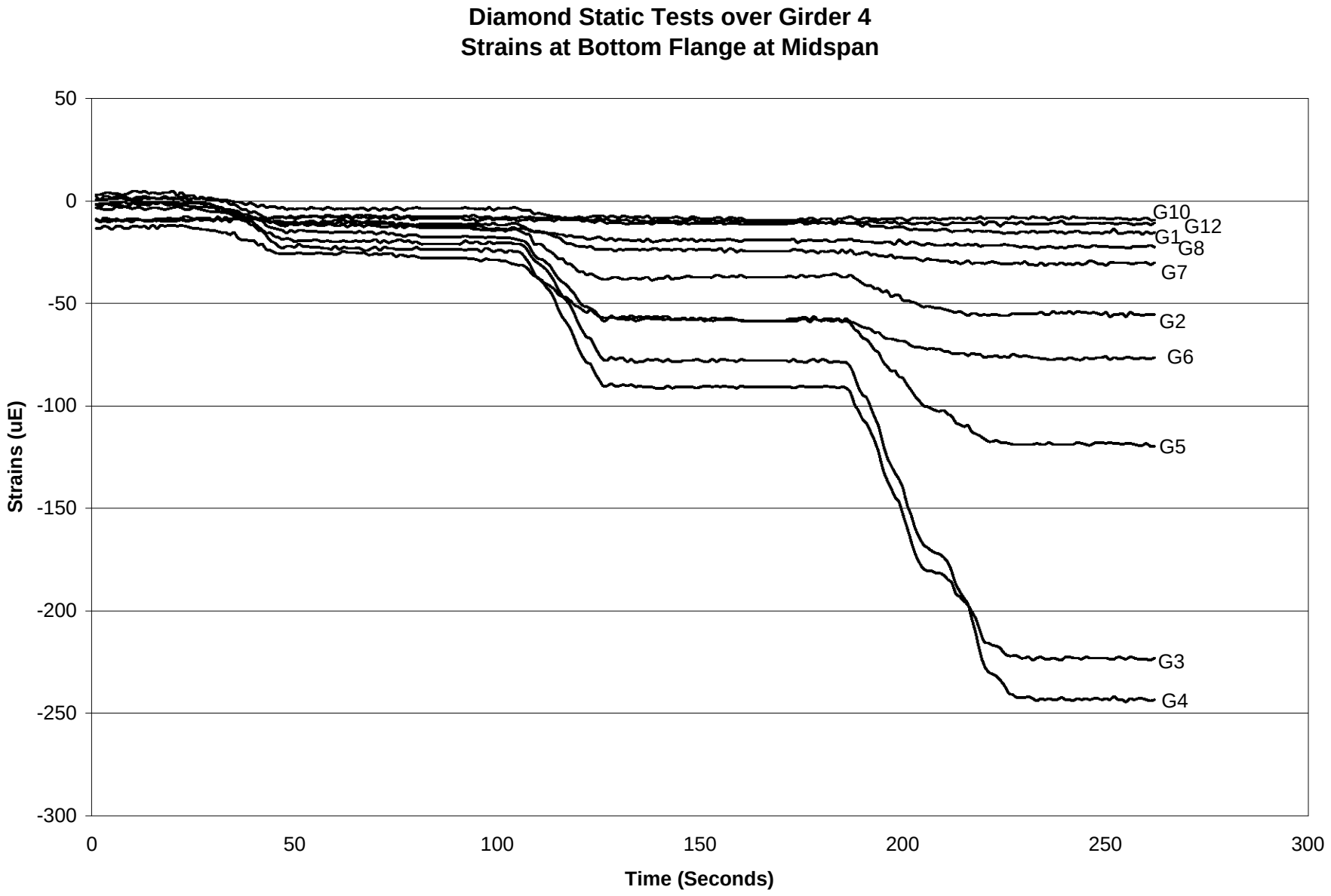
Diamond Static Tests over Girder 4
Strains at Bottom Flange at Midspan
Strains (uE)
Time (Seconds)
50
0
-50
-100
-150
-200
-250
-300
0
50
100
150
200
250
300
G10
G12
G1
G8
G7
G2
G6
G5
G3
G4

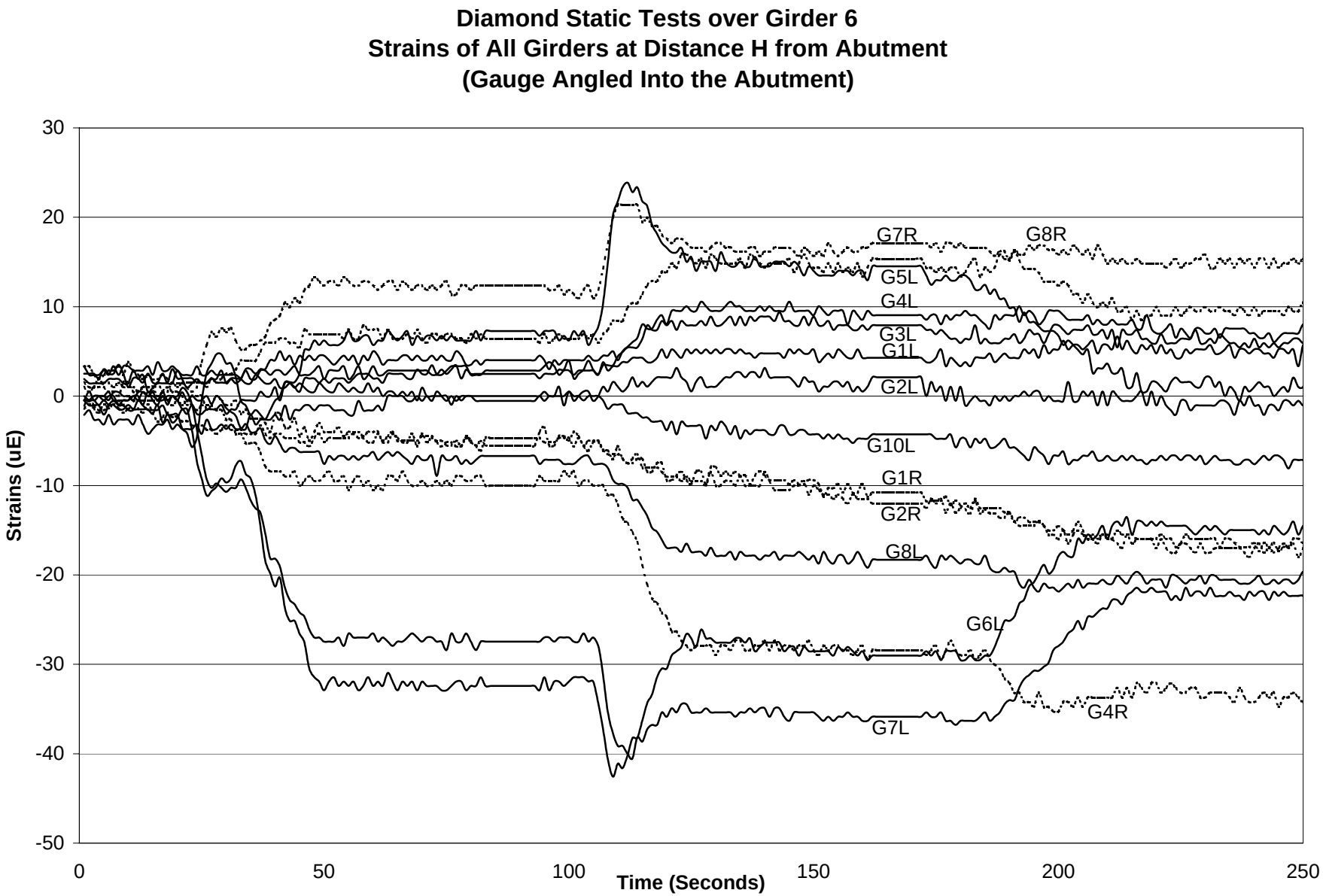
Diamond Static Tests over Girder 6
Strains of All Girders at Distance H from Abutment
(Gauge Angled Into the Abutment)
Strains (uE)
Time (Seconds)
30
20
10
0
-10
-20
-30
-40
-50
0
50
100
150
200
250
G7R
G8R
G5L
G4L
G3L
G1L
G2L
G10L
G1R
G2R
G8L
G6L
G4R
G7L

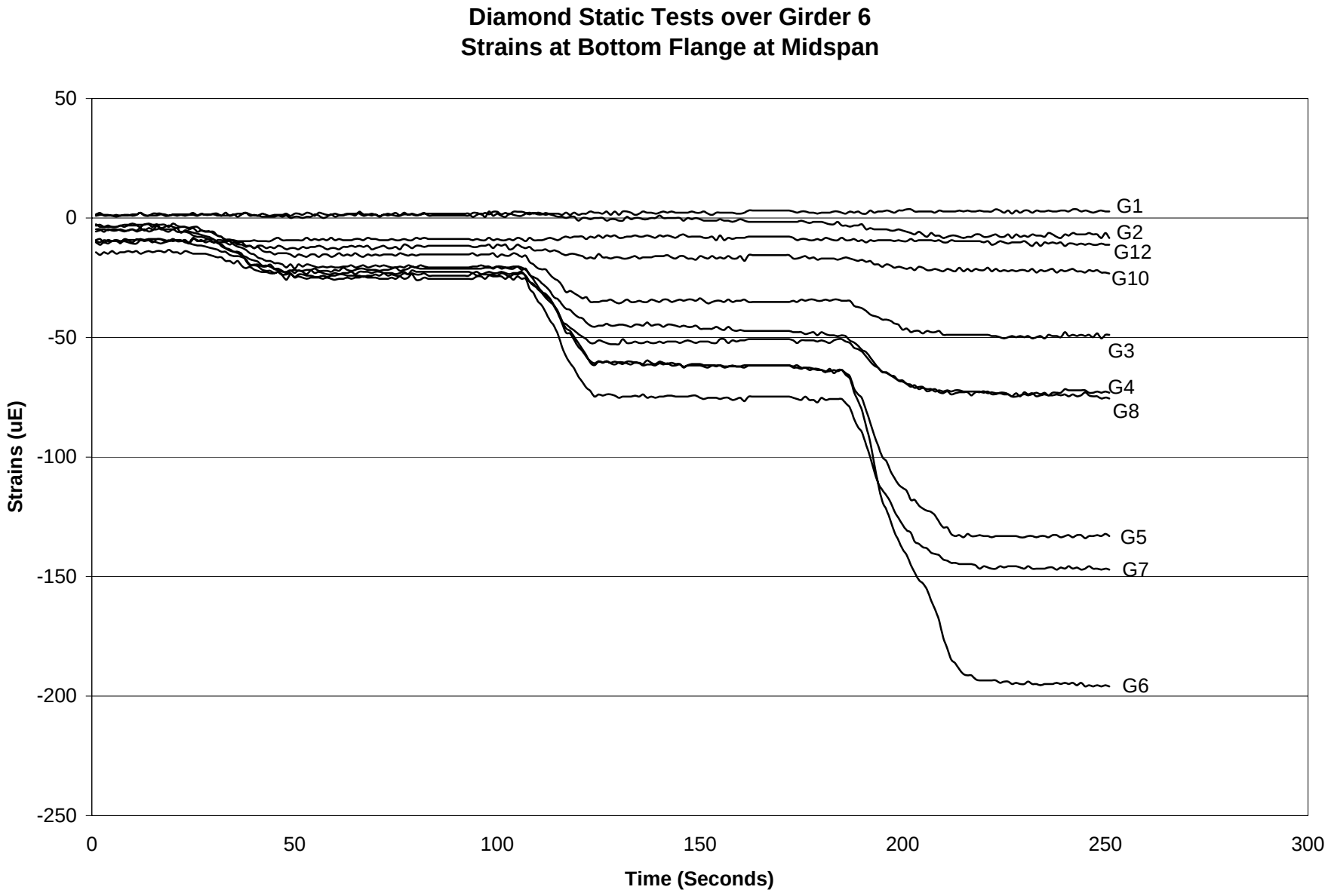
Diamond Static Tests over Girder 6
Strains at Bottom Flange at Midspan
Strains (uE)
Time (Seconds)
50
0
-50
-100
-150
-200
-250
0
50
100
150
200
250
300
G1
G2
G12
G10
G3
G4
G8
G5
G7
G6

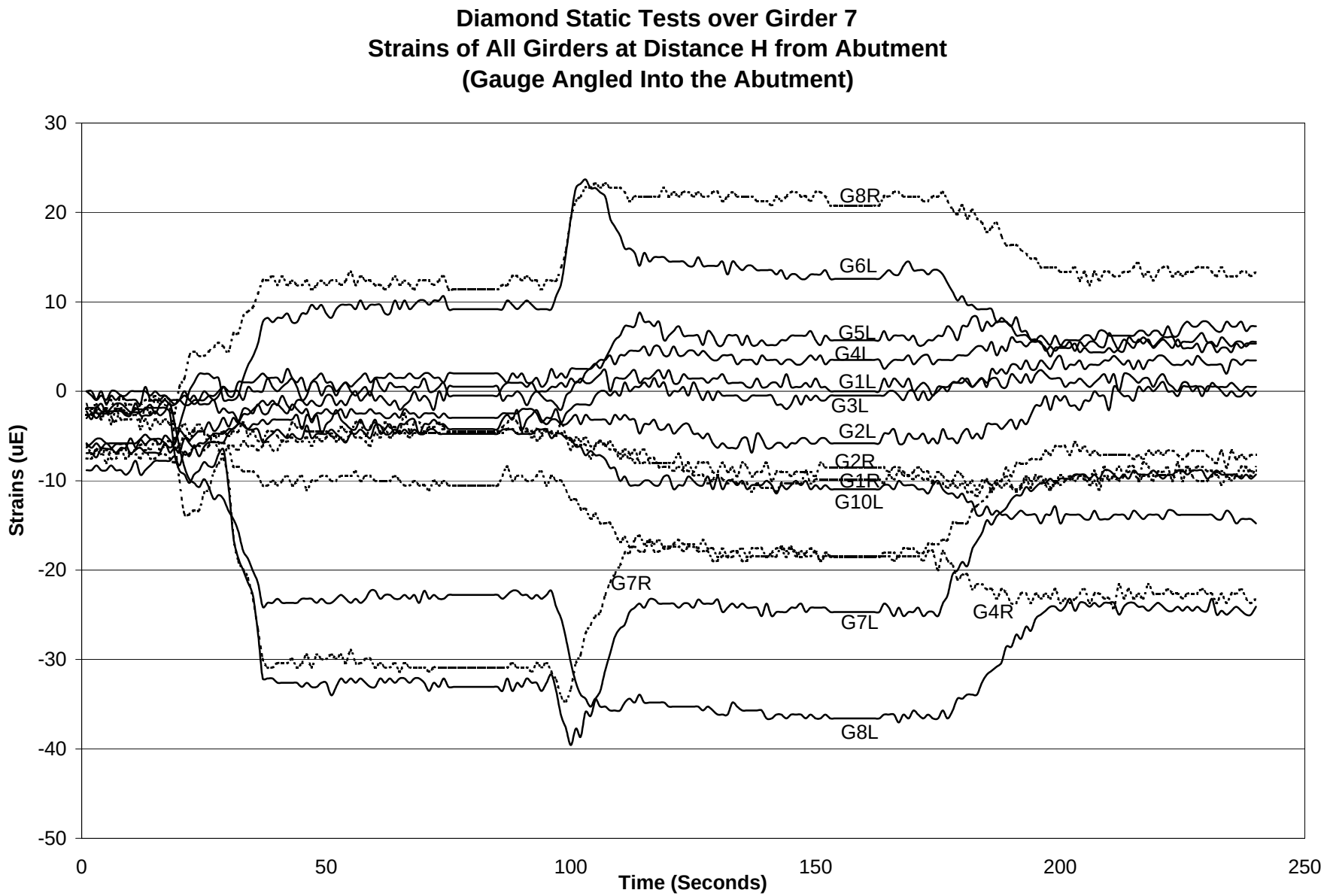
Diamond Static Tests over Girder 7
Strains of All Girders at Distance H from Abutment
(Gauge Angled Into the Abutment)
Strains (uE)
Time (Seconds)
30
20
10
0
-10
-20
-30
-40
-50
0
50
100
150
200
250
G8R
G6L
G5L
G4L
G1L
G3L
G2L
G2R
G1R
G10L
G7R
G7L
G4R
G8L

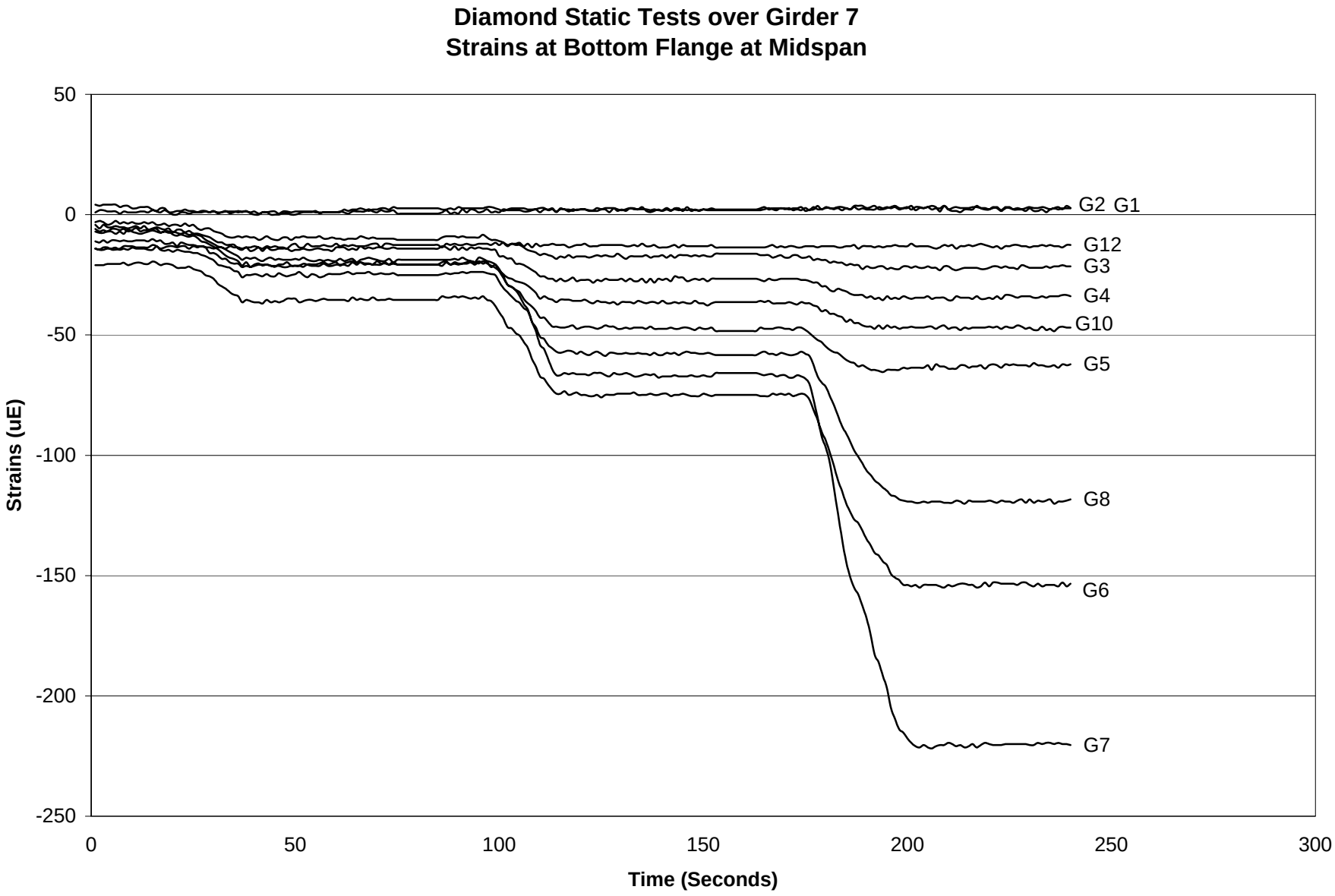
Diamond Static Tests over Girder 7
Strains at Bottom Flange at Midspan
Strains (uE)
Time (Seconds)
50
0
-50
-100
-150
-200
-250
0
50
100
150
200
250
300
G2
G1
G12
G3
G4
G10
G5
G8
G6
G7

# Dowling

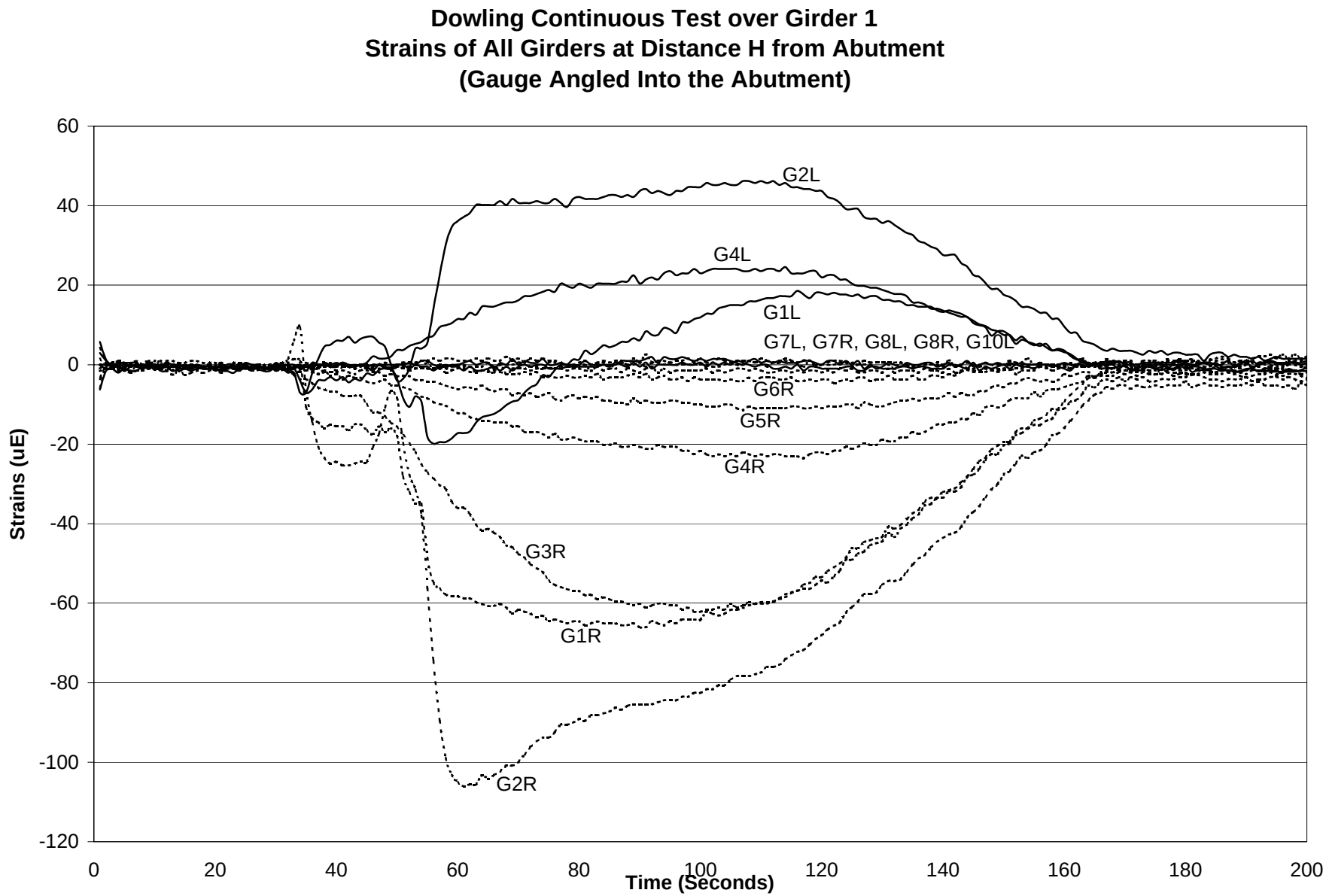
Dowling Continuous Test over Girder 1
Strains of All Girders at Distance H from Abutment
(Gauge Angled Into the Abutment)
Strains (uE)
Time (Seconds)
60
40
20
0
-20
-40
-60
-80
-100
-120
0
20
40
60
80
100
120
140
160
180
200
G2L
G4L
G1L
G7L, G7R, G8L, G8R, G10L
G6R
G5R
G4R
G3R
G1R
G2R

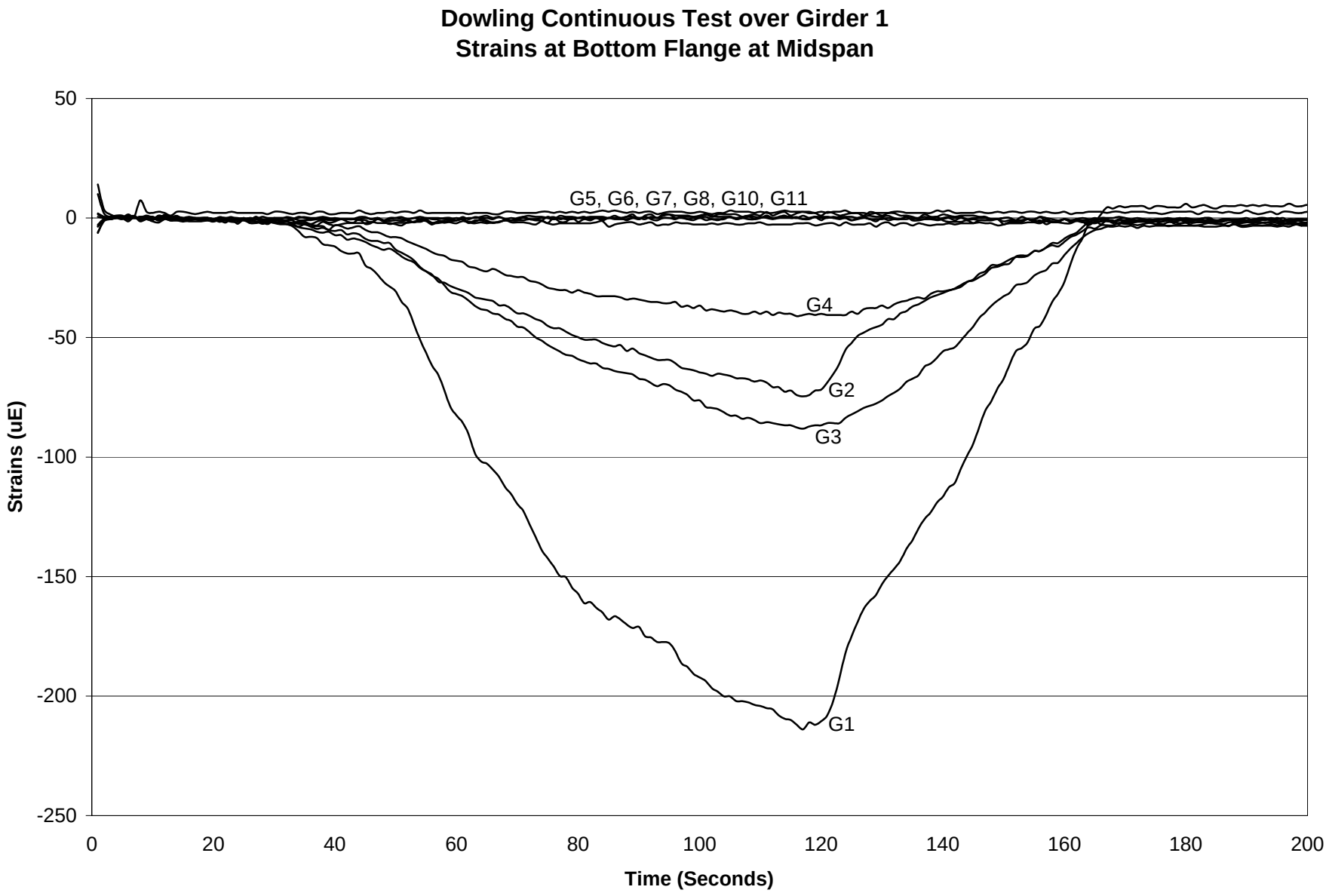
Dowling Continuous Test over Girder 1
Strains at Bottom Flange at Midspan
50
0
-50
-100
-150
-200
-250
Strains (uE)
0
20
40
60
80
100
120
140
160
180
200
Time (Seconds)
G5, G6, G7, G8, G10, G11
G4
G2
G3
G1

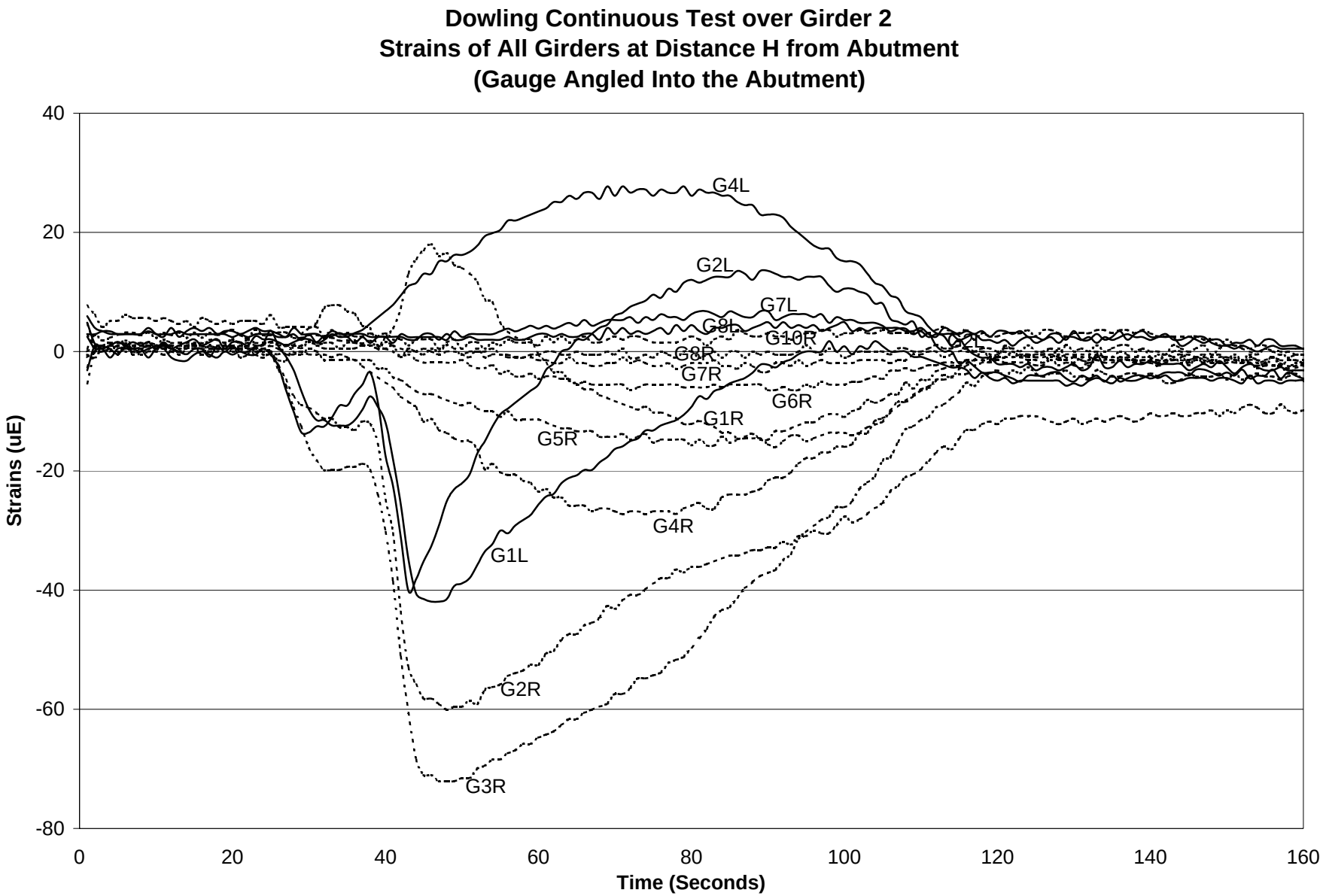
Dowling Continuous Test over Girder 2
Strains of All Girders at Distance H from Abutment
(Gauge Angled Into the Abutment)
Strains (uE)
Time (Seconds)
40
20
0
-20
-40
-60
-80
0
20
40
60
80
100
120
140
160
G4L
G2L
G7L
G9L
G10R
G8R
G7R
G6R
G1R
G5R
G4R
G1L
G2R
G3R

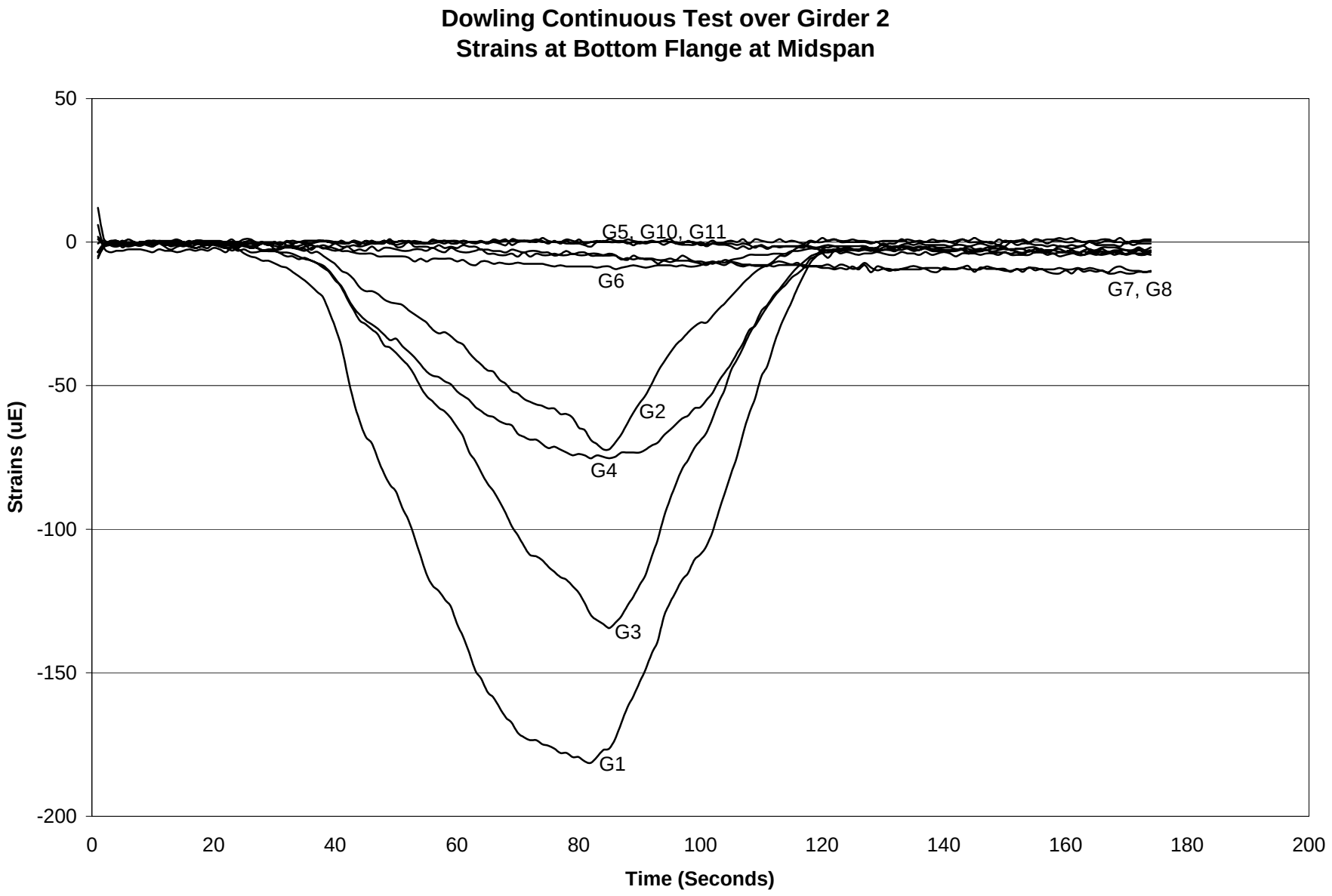
Dowling Continuous Test over Girder 2
Strains at Bottom Flange at Midspan
Strains (uE)
Time (Seconds)
50
0
-50
-100
-150
-200
0
20
40
60
80
100
120
140
160
180
200
G5, G10, G11
G6
G7, G8
G2
G4
G3
G1

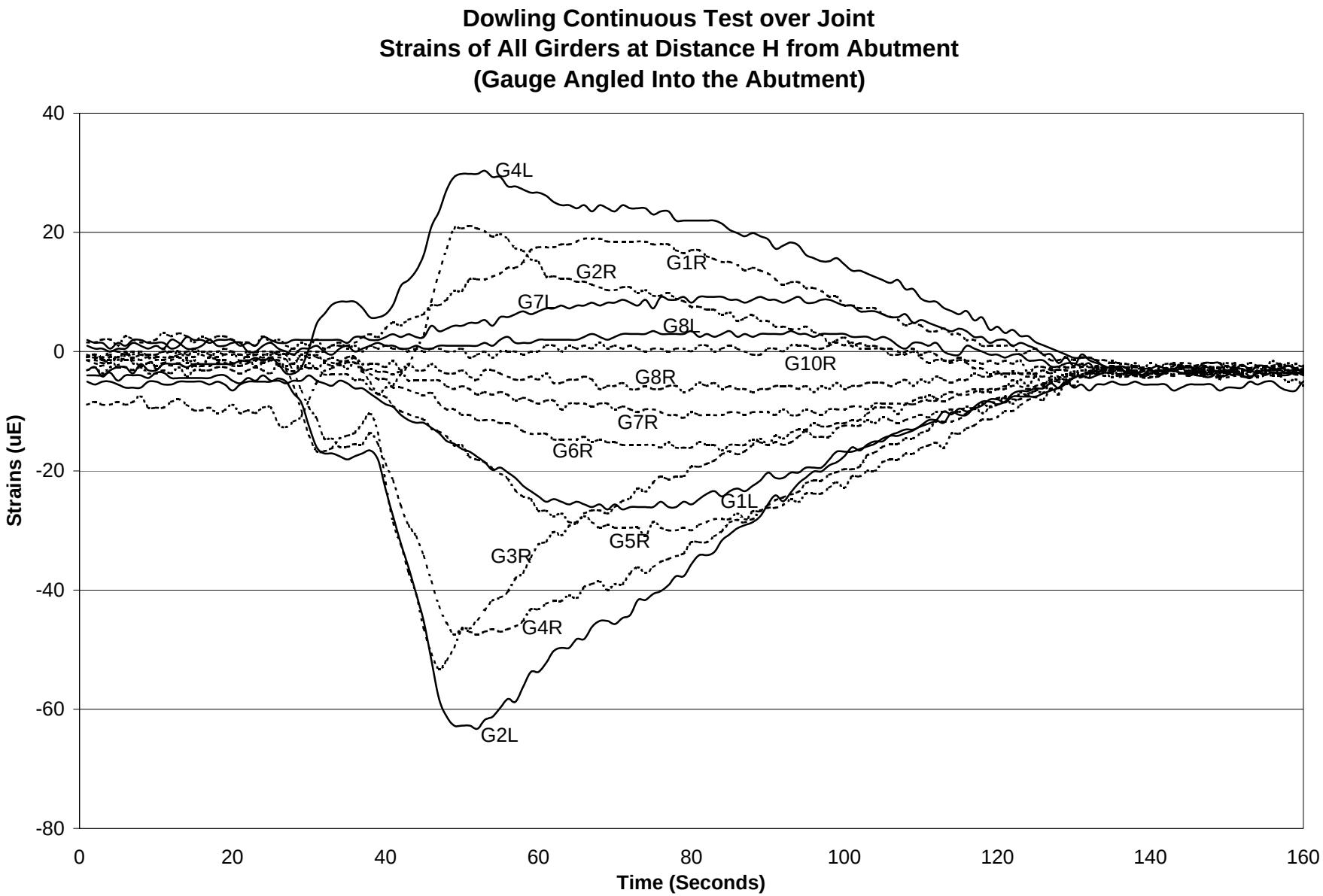
Dowling Continuous Test over Joint
Strains of All Girders at Distance H from Abutment
(Gauge Angled Into the Abutment)
Strains (uE)
Time (Seconds)
40
20
0
-20
-40
-60
-80
0
20
40
60
80
100
120
140
160
G4L
G1R
G2R
G7L
G8L
G10R
G8R
G7R
G6R
G1L
G5R
G3R
G4R
G2L

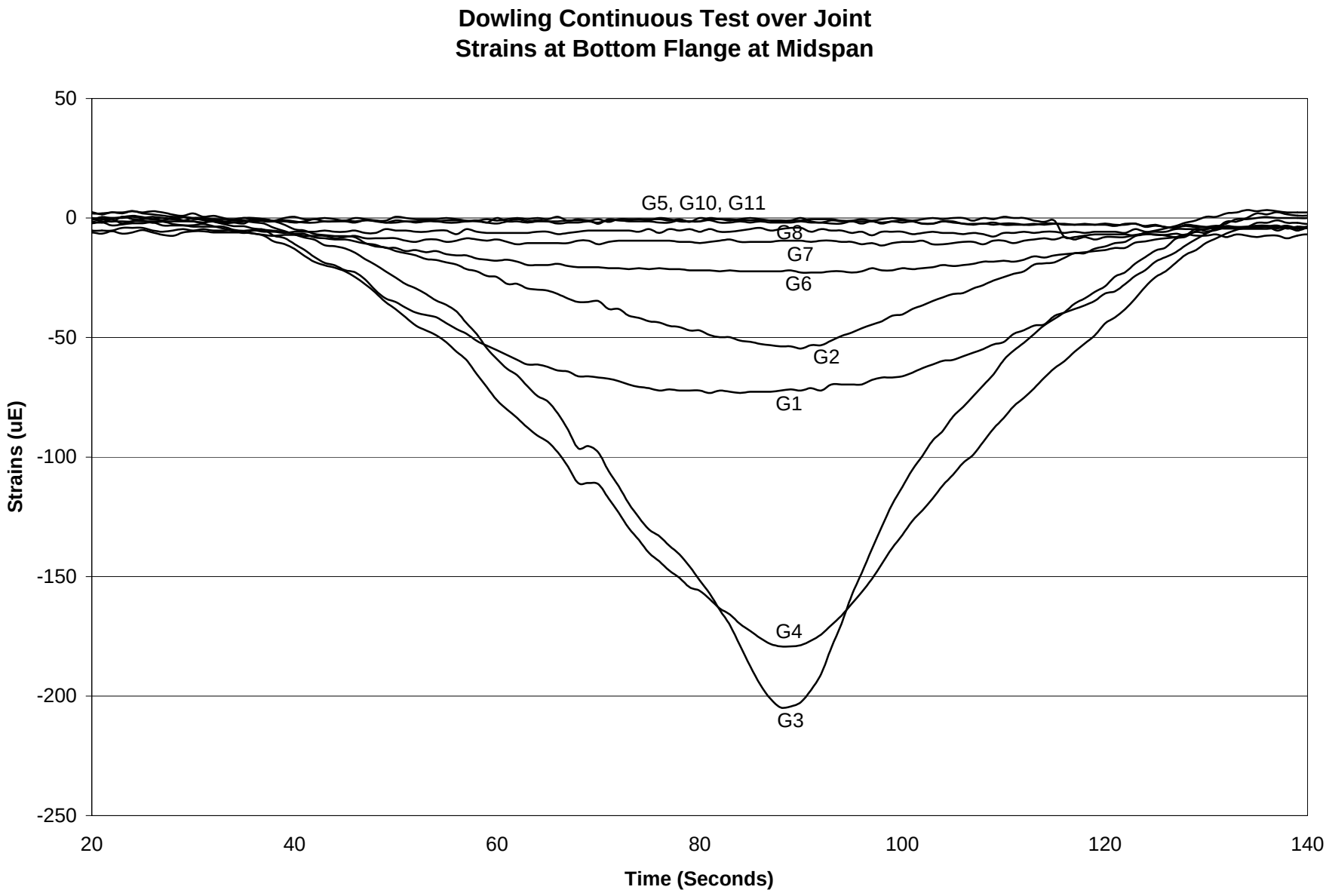
Dowling Continuous Test over Joint
Strains at Bottom Flange at Midspan
50
0
-50
-100
-150
-200
-250
Strains (uE)
20
40
60
80
100
120
140
Time (Seconds)
G5, G10, G11
G8
G7
G6
G2
G1
G4
G3

Dowling Continuous Test over Girder 4
Strains of All Girders at Distance H from Abutment
(Gauge Angled Into the Abutment)
Strains (uE)
Time (Seconds)
40
30
20
10
0
-10
-20
-30
-40
-50
-60
0
20
40
60
80
100
120
140
160
G3R
G2R
G1R
G7L
G8L
G8R
G10R
G1L
G7R
G4R
G6R
G2L
G4L
G5R

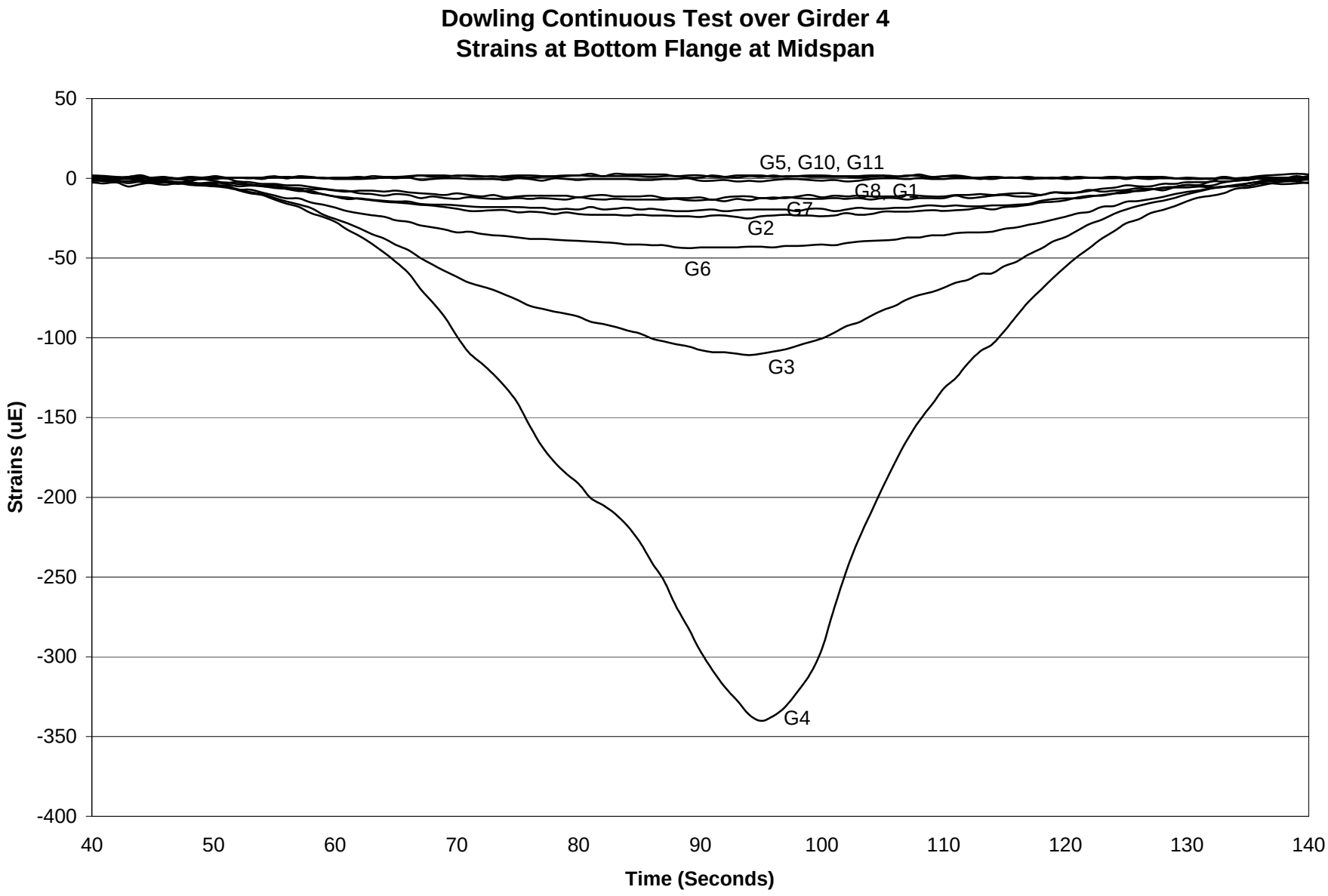
Dowling Continuous Test over Girder 4
Strains at Bottom Flange at Midspan
Strains (uE)
Time (Seconds)
50
0
-50
-100
-150
-200
-250
-300
-350
-400
40
50
60
70
80
90
100
110
120
130
140
G5, G10, G11
G8, G1
G7
G2
G6
G3
G4

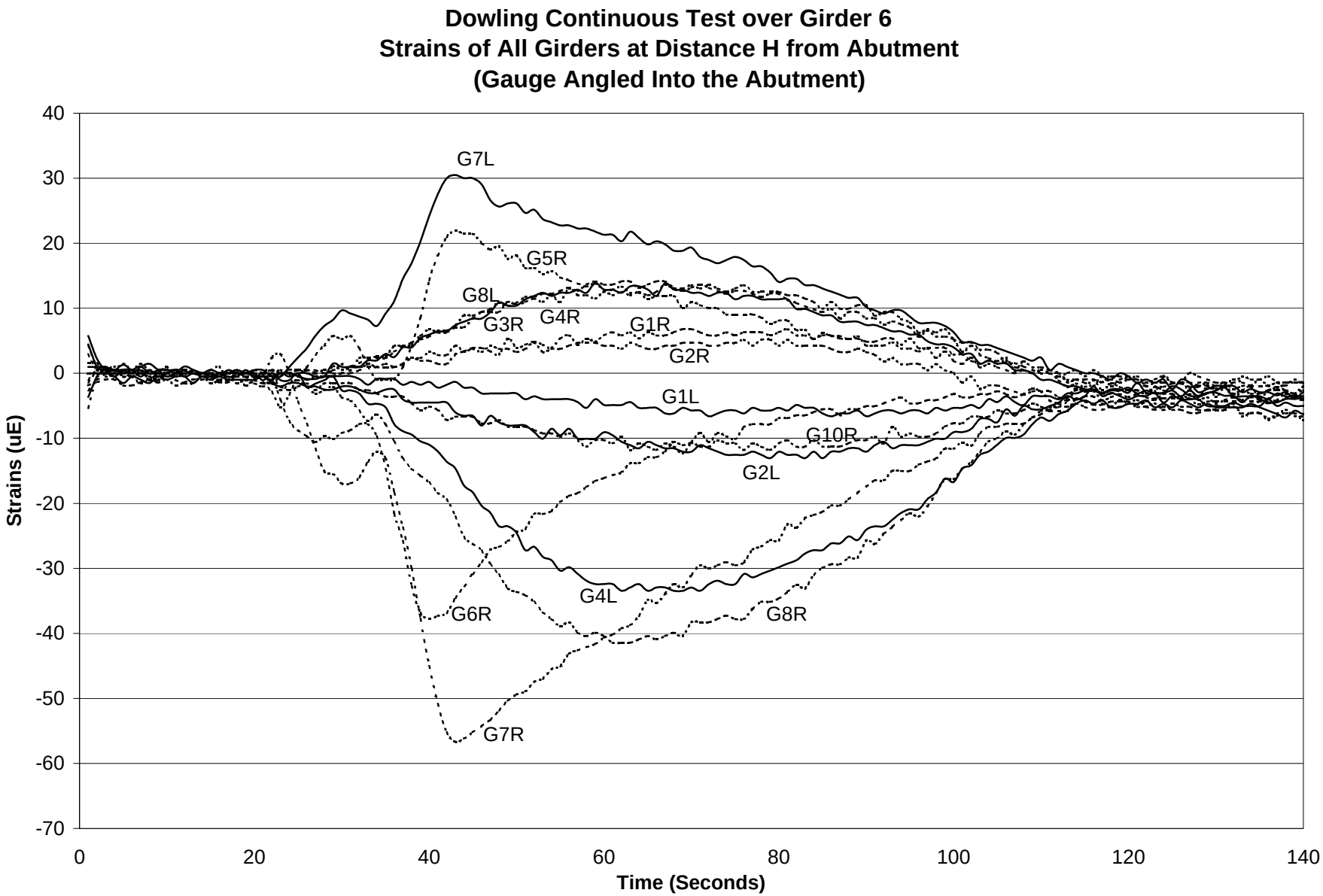
Dowling Continuous Test over Girder 6
Strains of All Girders at Distance H from Abutment
(Gauge Angled Into the Abutment)
Strains (uE)
Time (Seconds)
40
30
20
10
0
-10
-20
-30
-40
-50
-60
-70
0
20
40
60
80
100
120
140
G7L
G5R
G8L
G3R
G4R
G1R
G2R
G1L
G10R
G2L
G4L
G6R
G8R
G7R

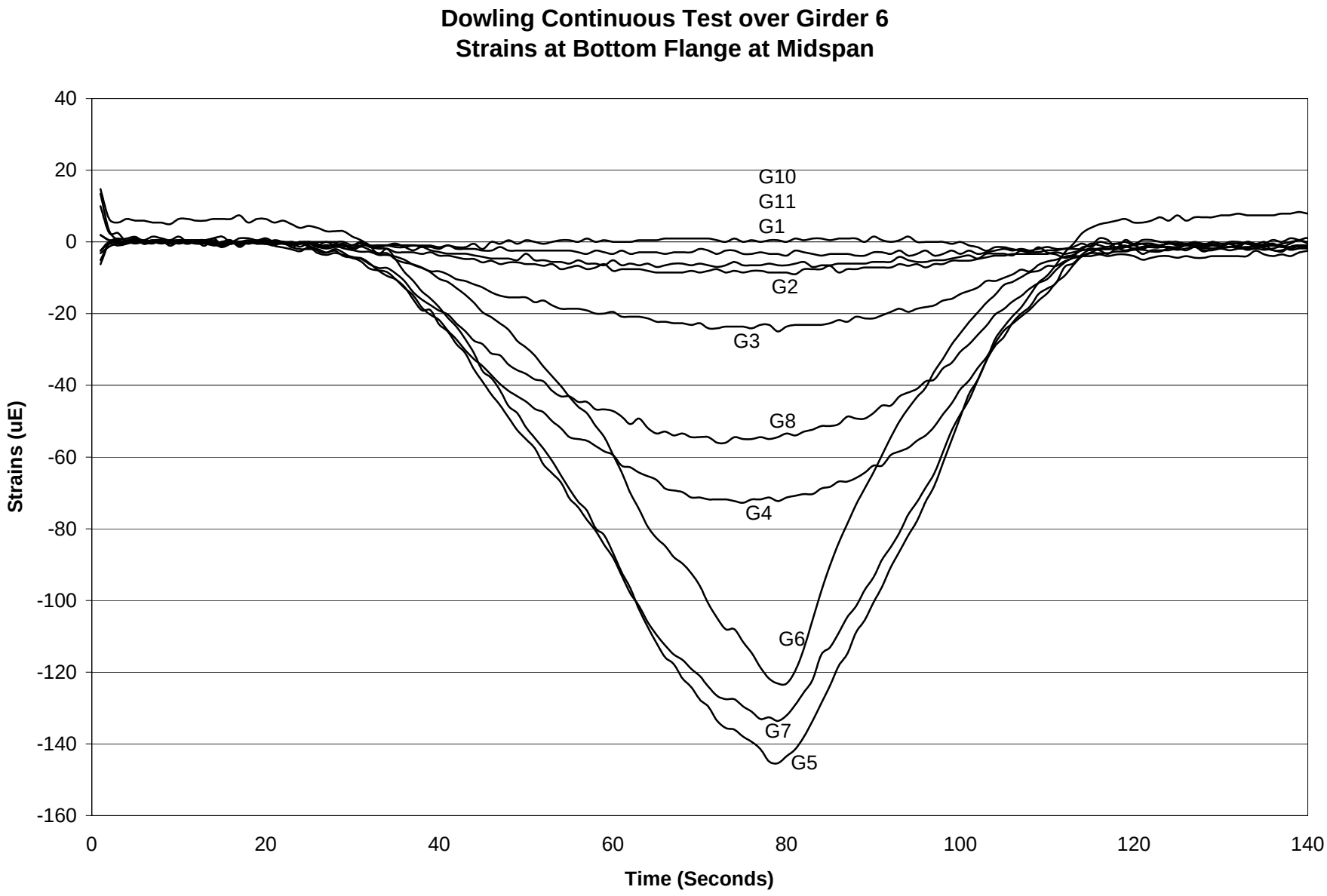
Dowling Continuous Test over Girder 6
Strains at Bottom Flange at Midspan
Strains (uE)
Time (Seconds)
40
20
0
-20
-40
-60
-80
-100
-120
-140
-160
0
20
40
60
80
100
120
140
G10
G11
G1
G2
G3
G8
G4
G6
G7
G5

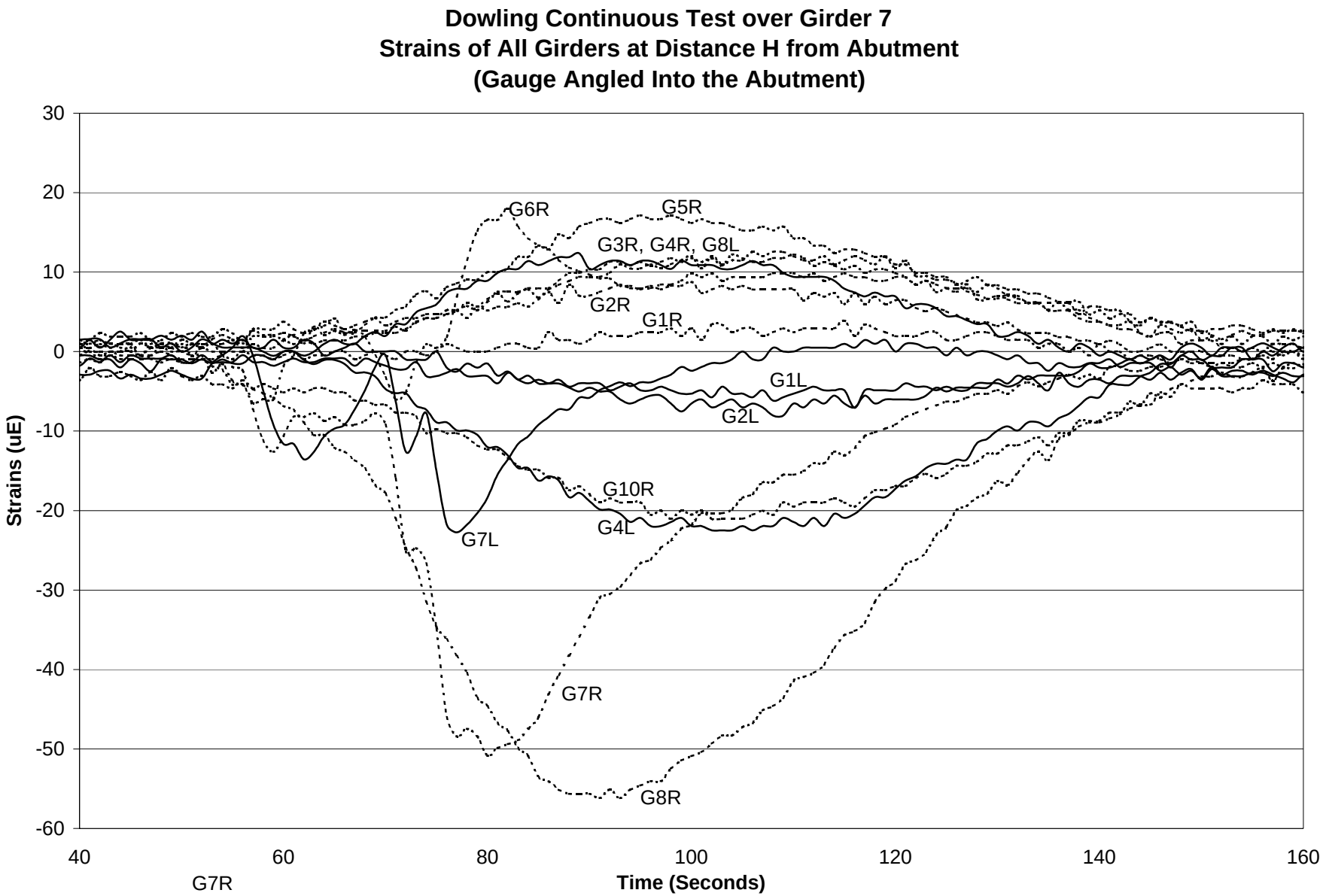
Dowling Continuous Test over Girder 7
Strains of All Girders at Distance H from Abutment
(Gauge Angled Into the Abutment)
Strains (uE)
Time (Seconds)
30
20
10
0
-10
-20
-30
-40
-50
-60
40
60
80
100
120
140
160
G7R
G6R
G5R
G3R, G4R, G8L
G2R
G1R
G1L
G2L
G10R
G4L
G7L
G7R
G8R

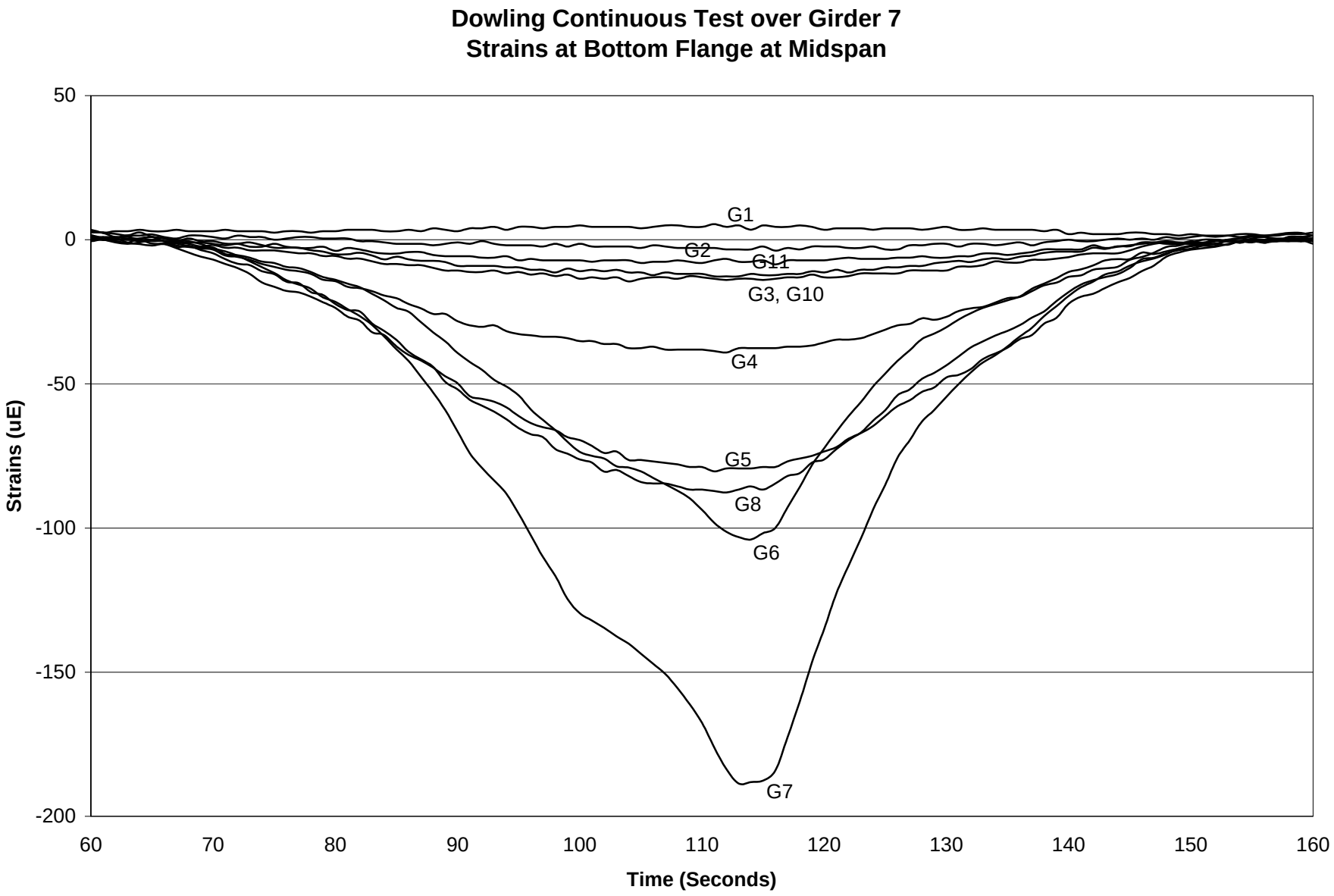
Dowling Continuous Test over Girder 7
Strains at Bottom Flange at Midspan
Strains (uE)
Time (Seconds)
50
0
-50
-100
-150
-200
60
70
80
90
100
110
120
130
140
150
160
G1
G2
G11
G3, G10
G4
G5
G8
G6
G7

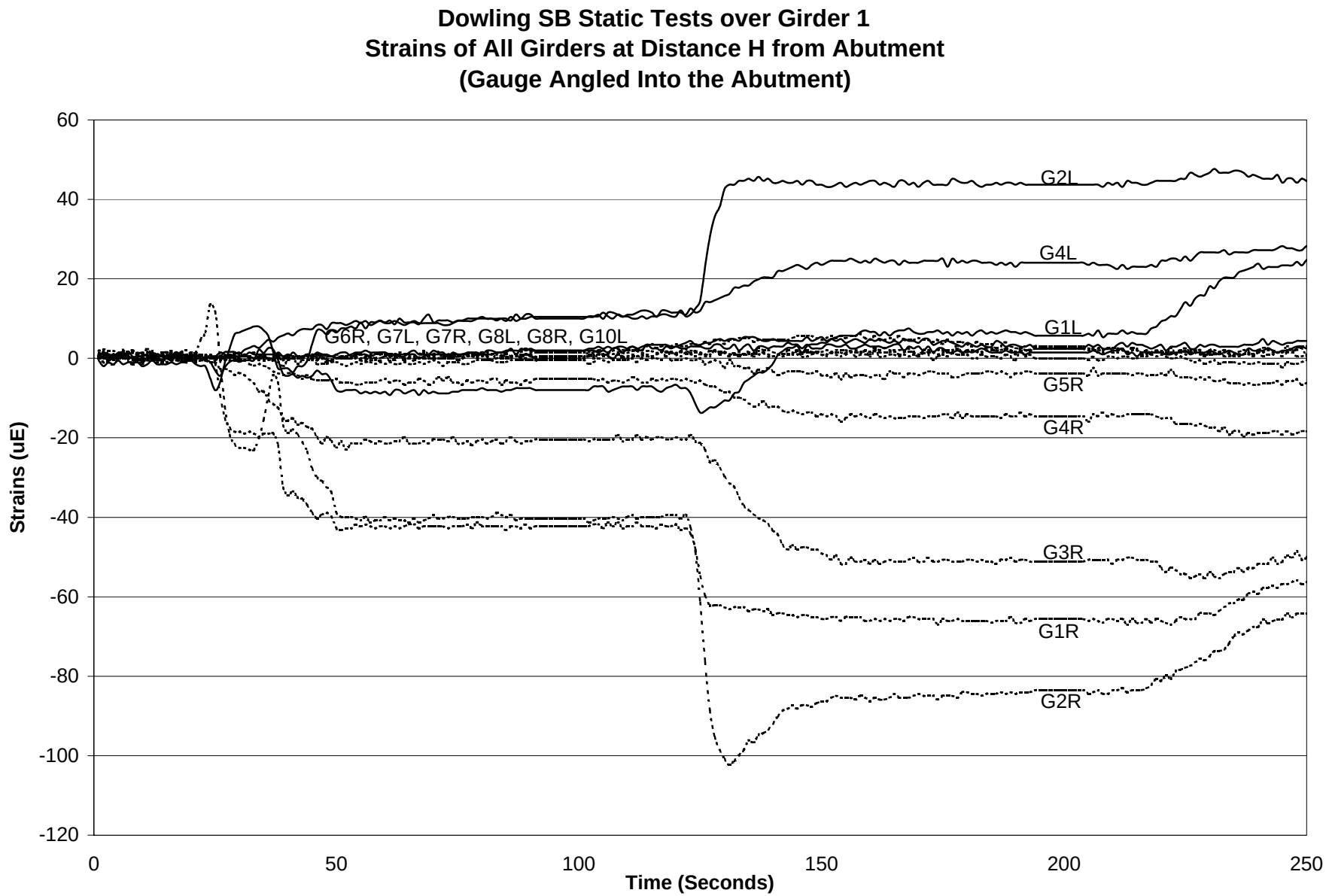
Dowling SB Static Tests over Girder 1
Strains of All Girders at Distance H from Abutment
(Gauge Angled Into the Abutment)
Strains (uE)
Time (Seconds)
60
40
20
0
-20
-40
-60
-80
-100
-120
0
50
100
150
200
250
G2L
G4L
G1L
G6R, G7L, G7R, G8L, G8R, G10L
G5R
G4R
G3R
G1R
G2R

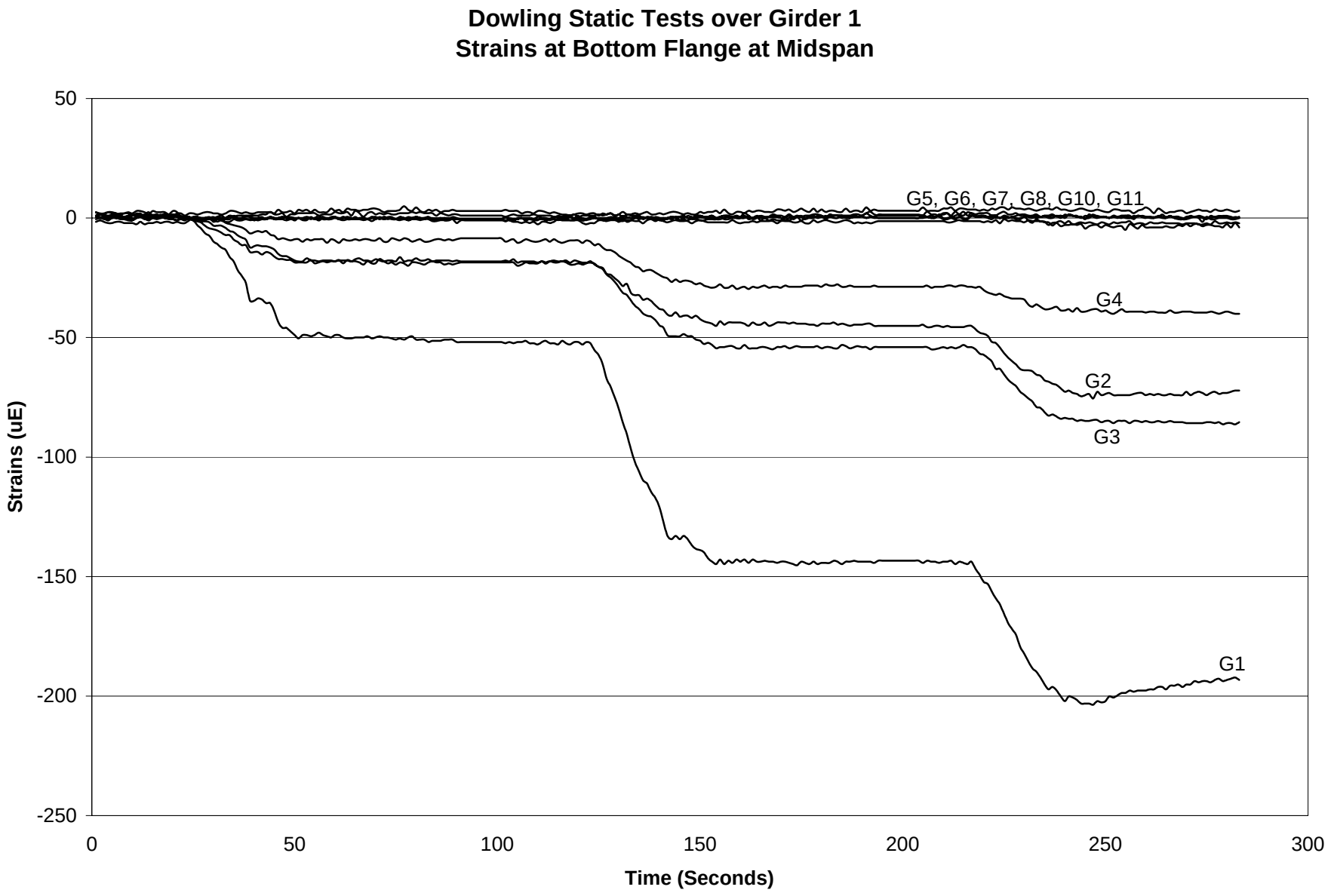
Dowling Static Tests over Girder 1
Strains at Bottom Flange at Midspan
50
0
-50
-100
-150
-200
-250
Strains (uE)
0
50
100
150
200
250
300
Time (Seconds)
G5, G6, G7, G8, G10, G11
G4
G2
G3
G1

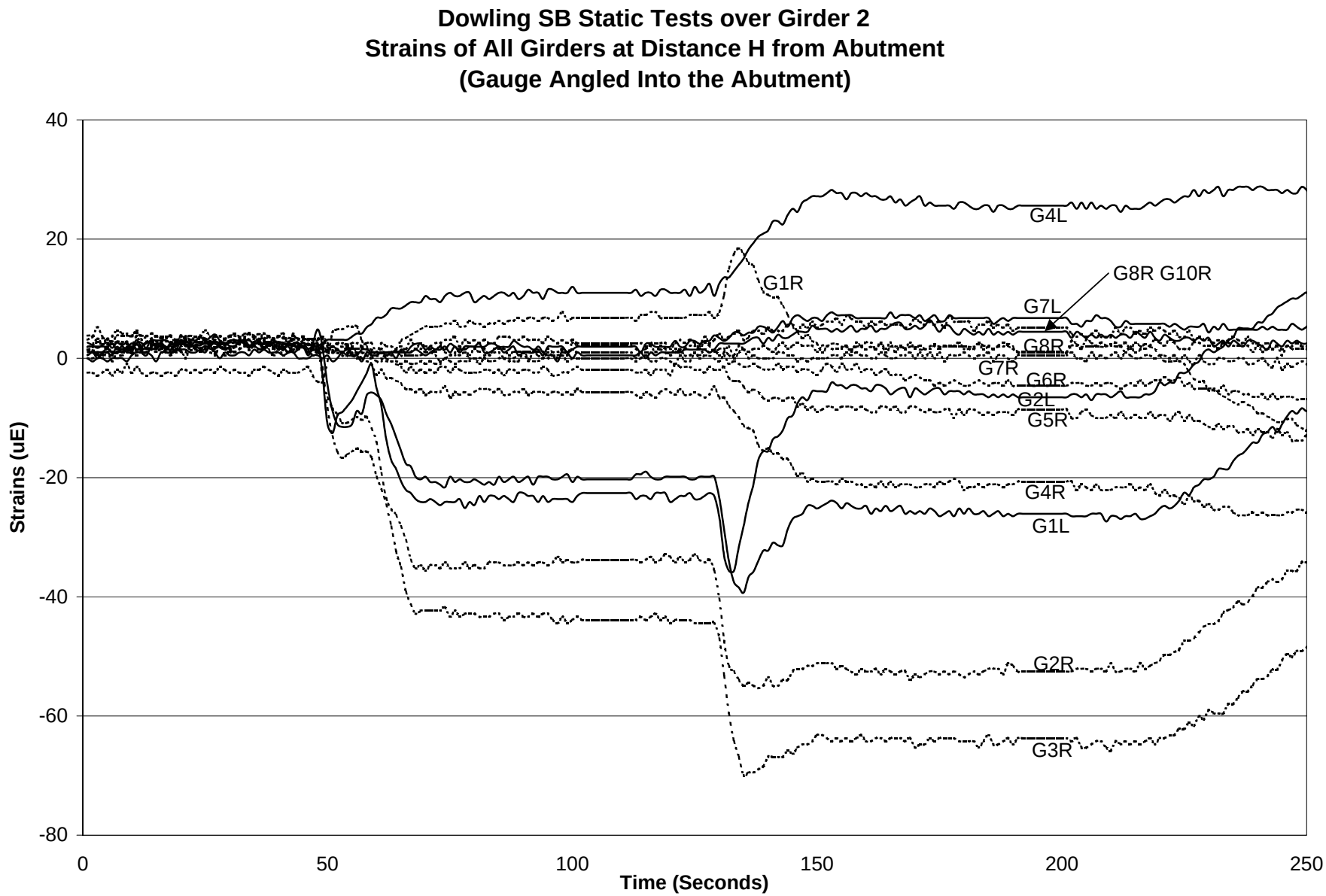
Dowling SB Static Tests over Girder 2
Strains of All Girders at Distance H from Abutment
(Gauge Angled Into the Abutment)
Strains (uE)
Time (Seconds)
40
20
0
-20
-40
-60
-80
0
50
100
150
200
250
G4L
G1R
G8R G10R
G7L
G8R
G7R
G6R
G2L
G5R
G4R
G1L
G2R
G3R

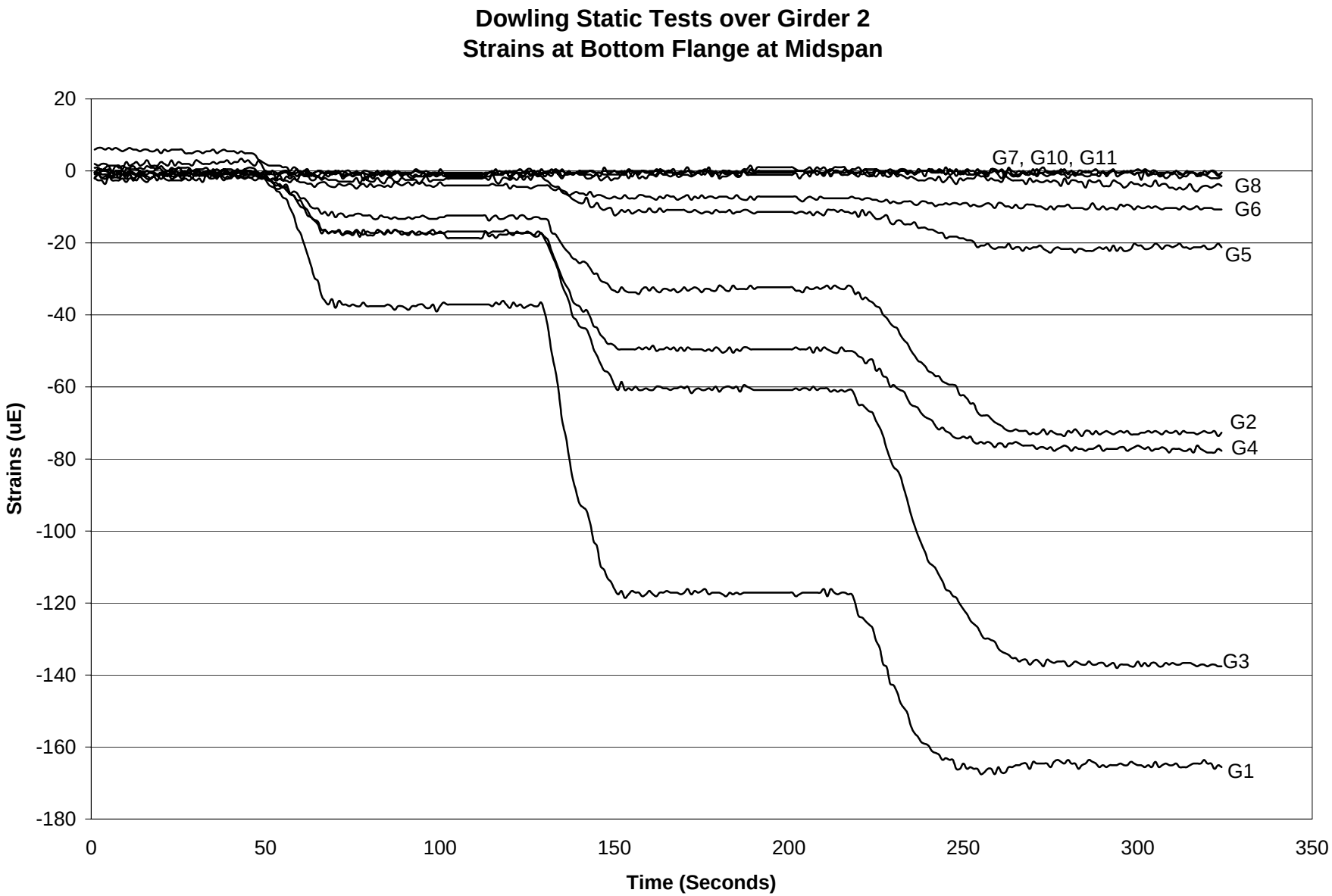
Dowling Static Tests over Girder 2
Strains at Bottom Flange at Midspan
Strains (uE)
Time (Seconds)
20
0
-20
-40
-60
-80
-100
-120
-140
-160
-180
0
50
100
150
200
250
300
350
G7, G10, G11
G8
G6
G5
G2
G4
G3
G1

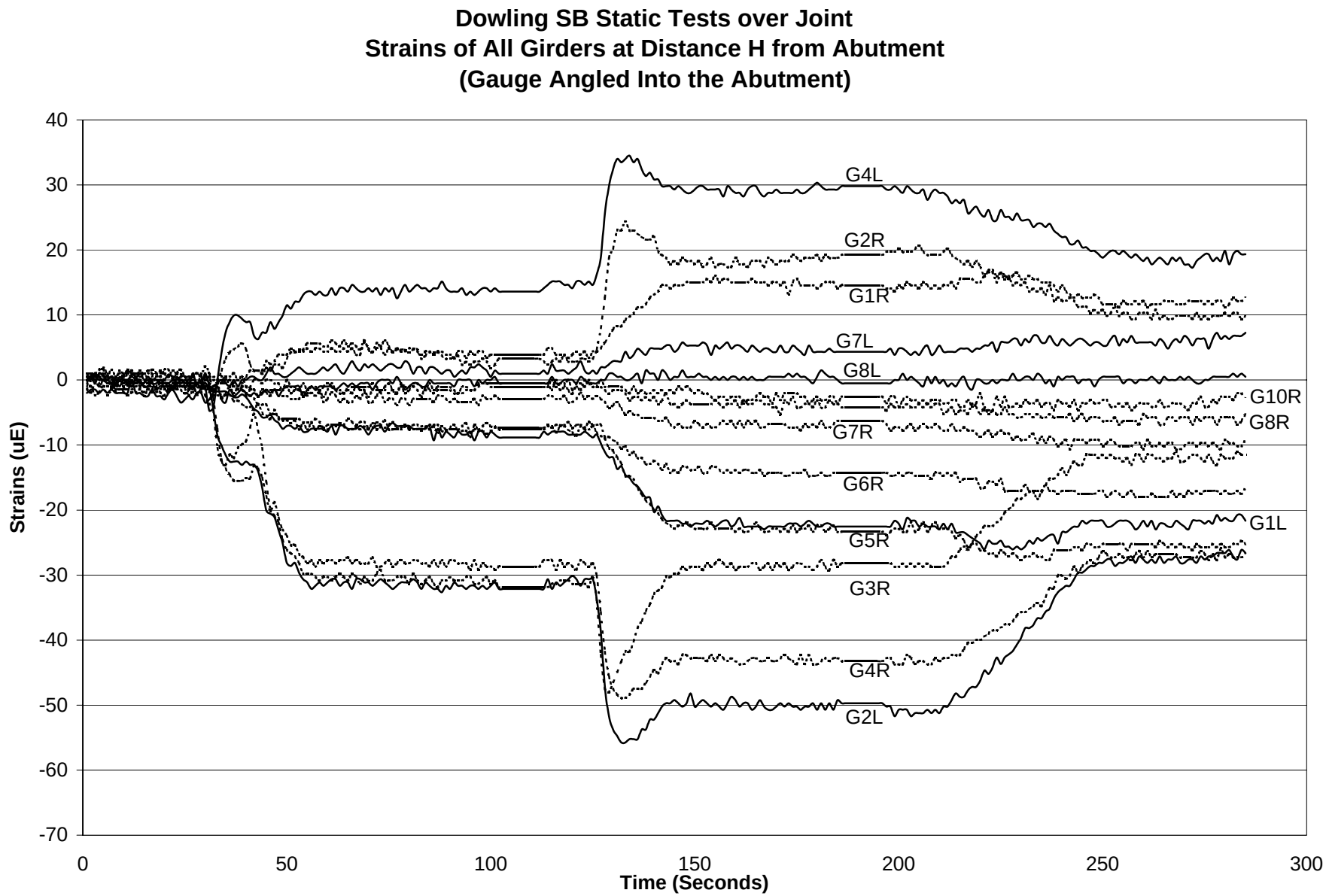
Dowling SB Static Tests over Joint
Strains of All Girders at Distance H from Abutment
(Gauge Angled Into the Abutment)
Strains (uE)
Time (Seconds)
40
30
20
10
0
-10
-20
-30
-40
-50
-60
-70
0
50
100
150
200
250
300
G4L
G2R
G1R
G7L
G8L
G10R
G8R
G7R
G6R
G1L
G5R
G3R
G4R
G2L

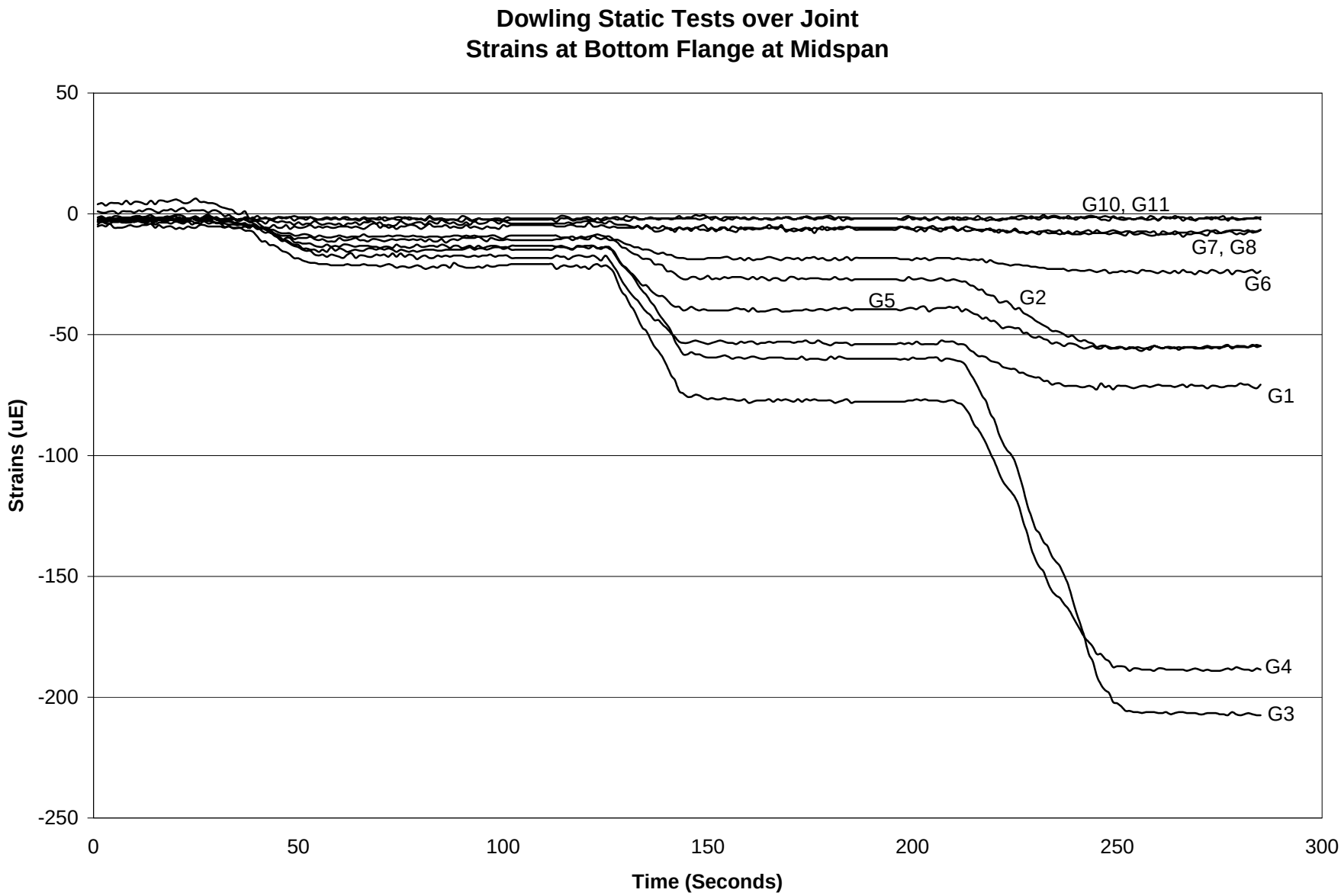
Dowling Static Tests over Joint
Strains at Bottom Flange at Midspan
Strains (uE)
Time (Seconds)
50
0
-50
-100
-150
-200
-250
0
50
100
150
200
250
300
G10, G11
G7, G8
G6
G5
G2
G1
G4
G3

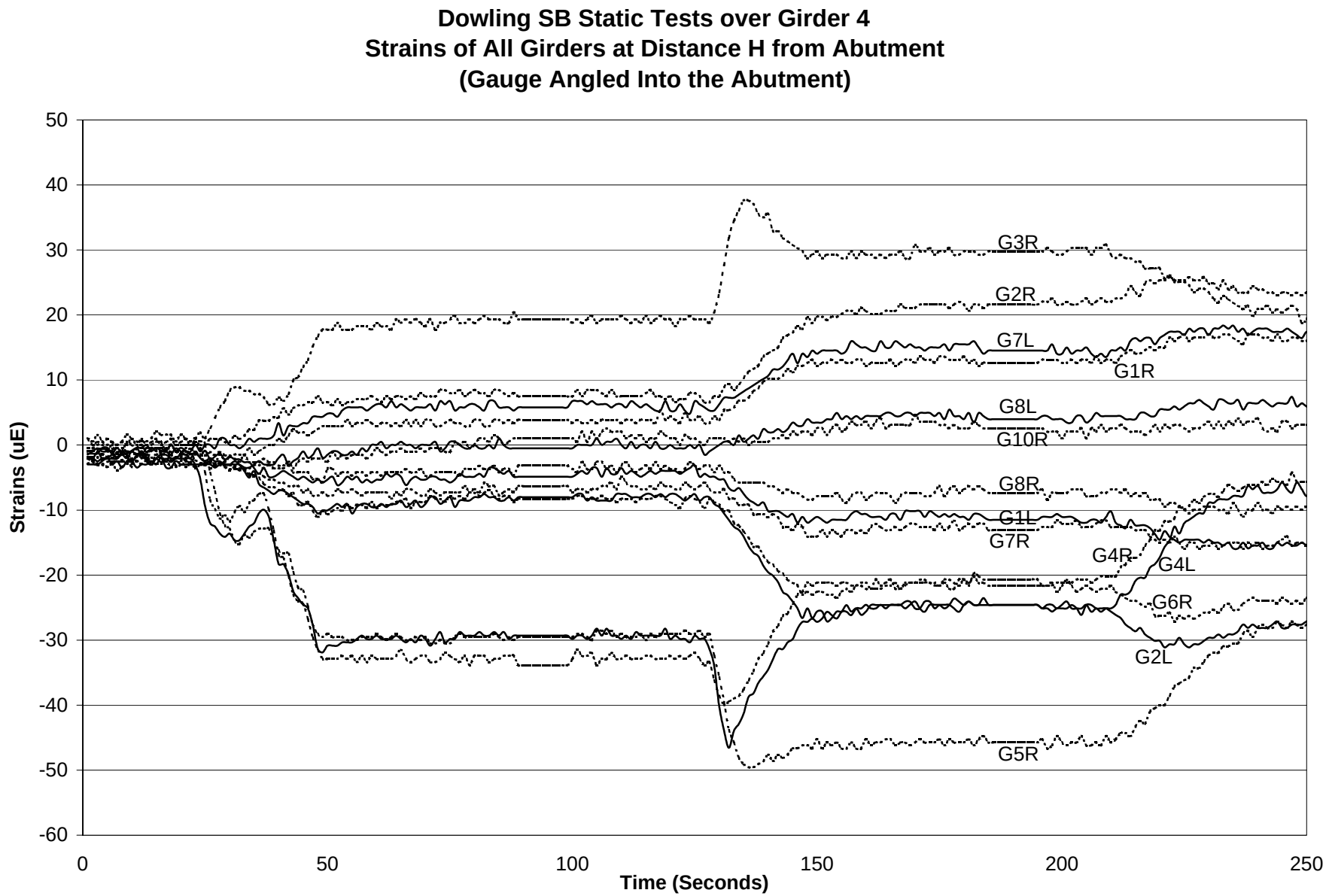
Dowling SB Static Tests over Girder 4
Strains of All Girders at Distance H from Abutment
(Gauge Angled Into the Abutment)
Strains (uE)
Time (Seconds)
50
40
30
20
10
0
-10
-20
-30
-40
-50
-60
0
50
100
150
200
250
G3R
G2R
G7L
G1R
G8L
G10R
G8R
G1L
G7R
G4R
G4L
G6R
G2L
G5R

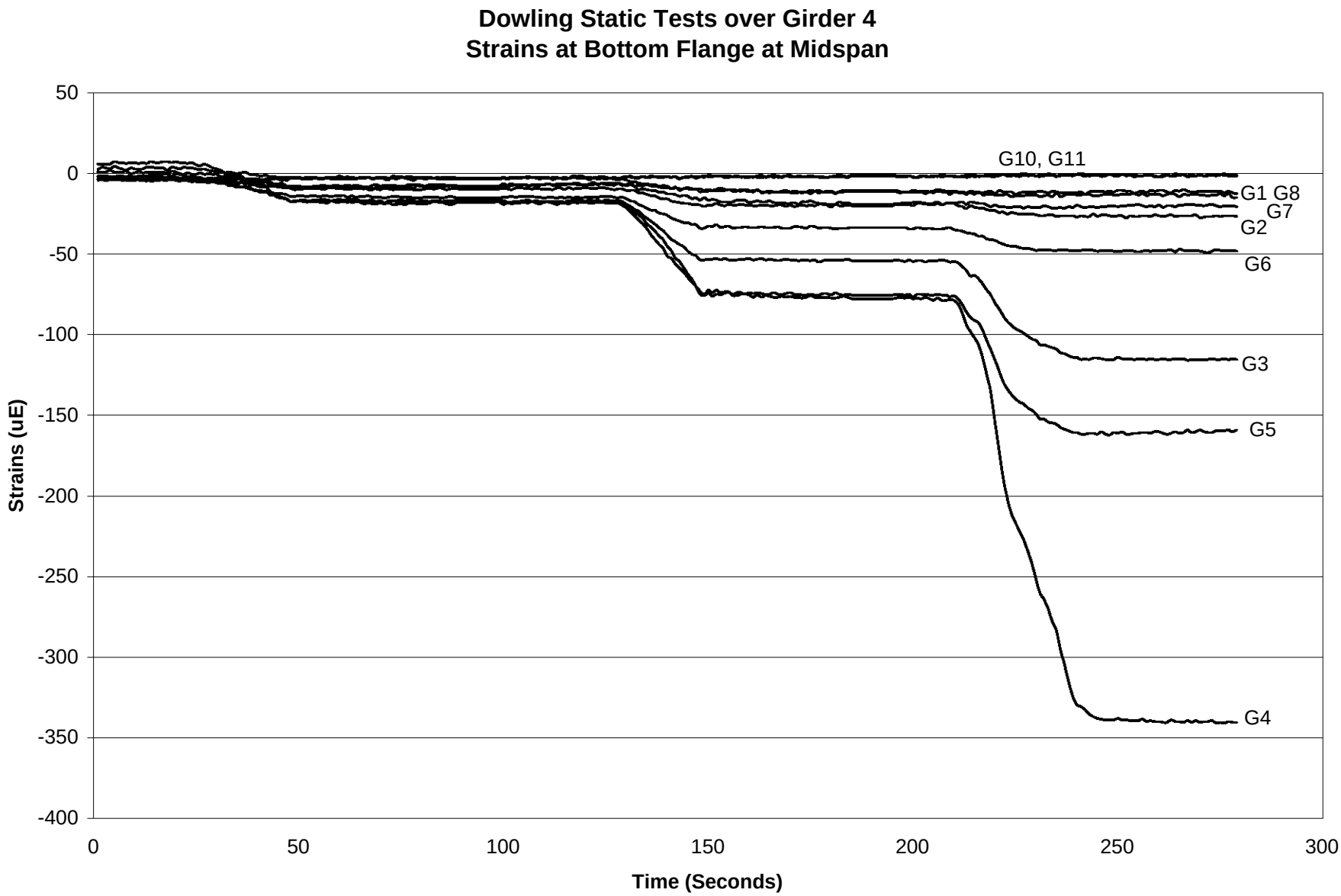
Dowling Static Tests over Girder 4
Strains at Bottom Flange at Midspan
Strains (uE)
Time (Seconds)
50
0
-50
-100
-150
-200
-250
-300
-350
-400
0
50
100
150
200
250
300
G10, G11
G1 G8
G7
G2
G6
G3
G5
G4

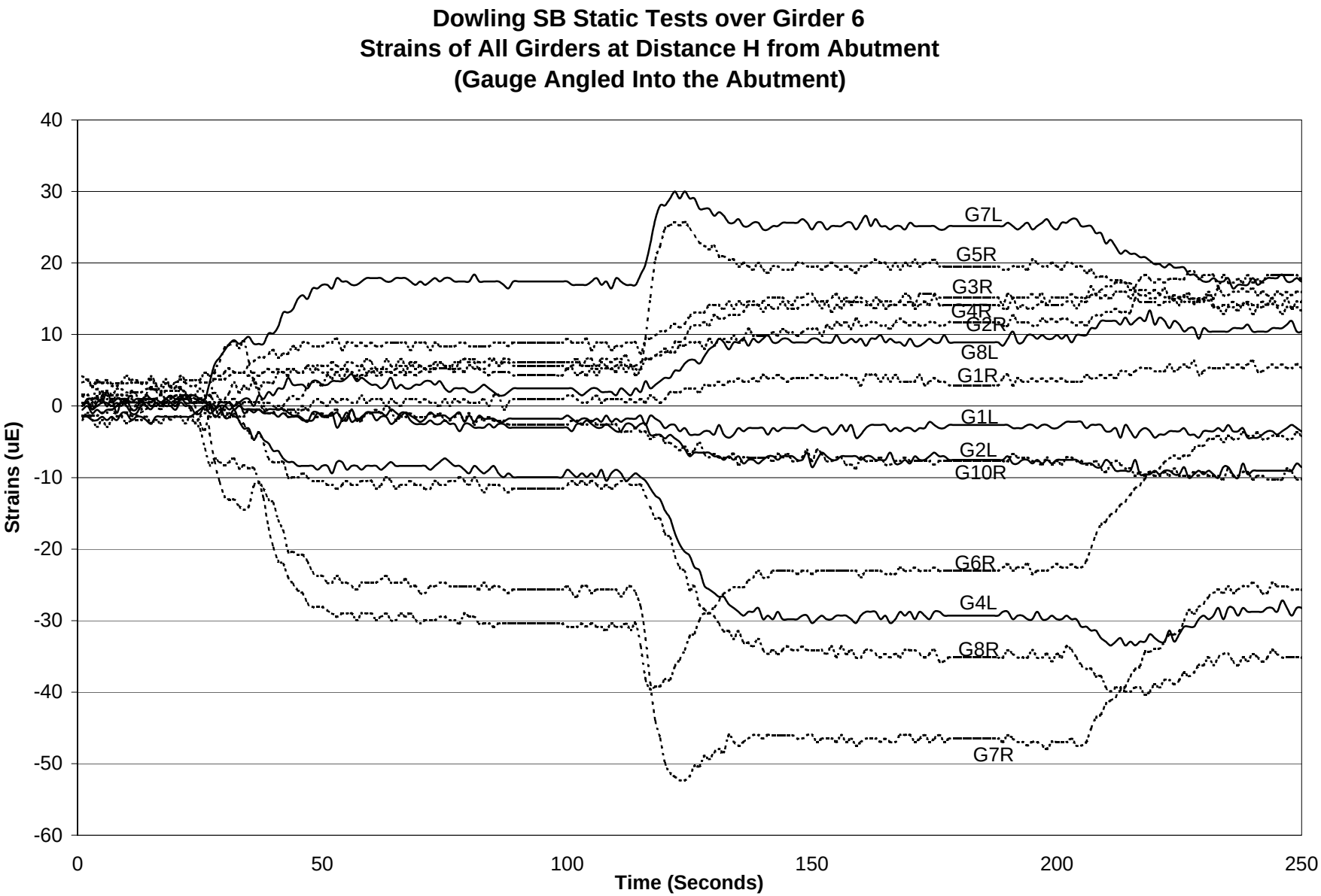
Dowling SB Static Tests over Girder 6
Strains of All Girders at Distance H from Abutment
(Gauge Angled Into the Abutment)
Strains (uE)
Time (Seconds)
40
30
20
10
0
-10
-20
-30
-40
-50
-60
0
50
100
150
200
250
G7L
G5R
G3R
G4R
G2R
G8L
G1R
G1L
G2L
G10R
G6R
G4L
G8R
G7R

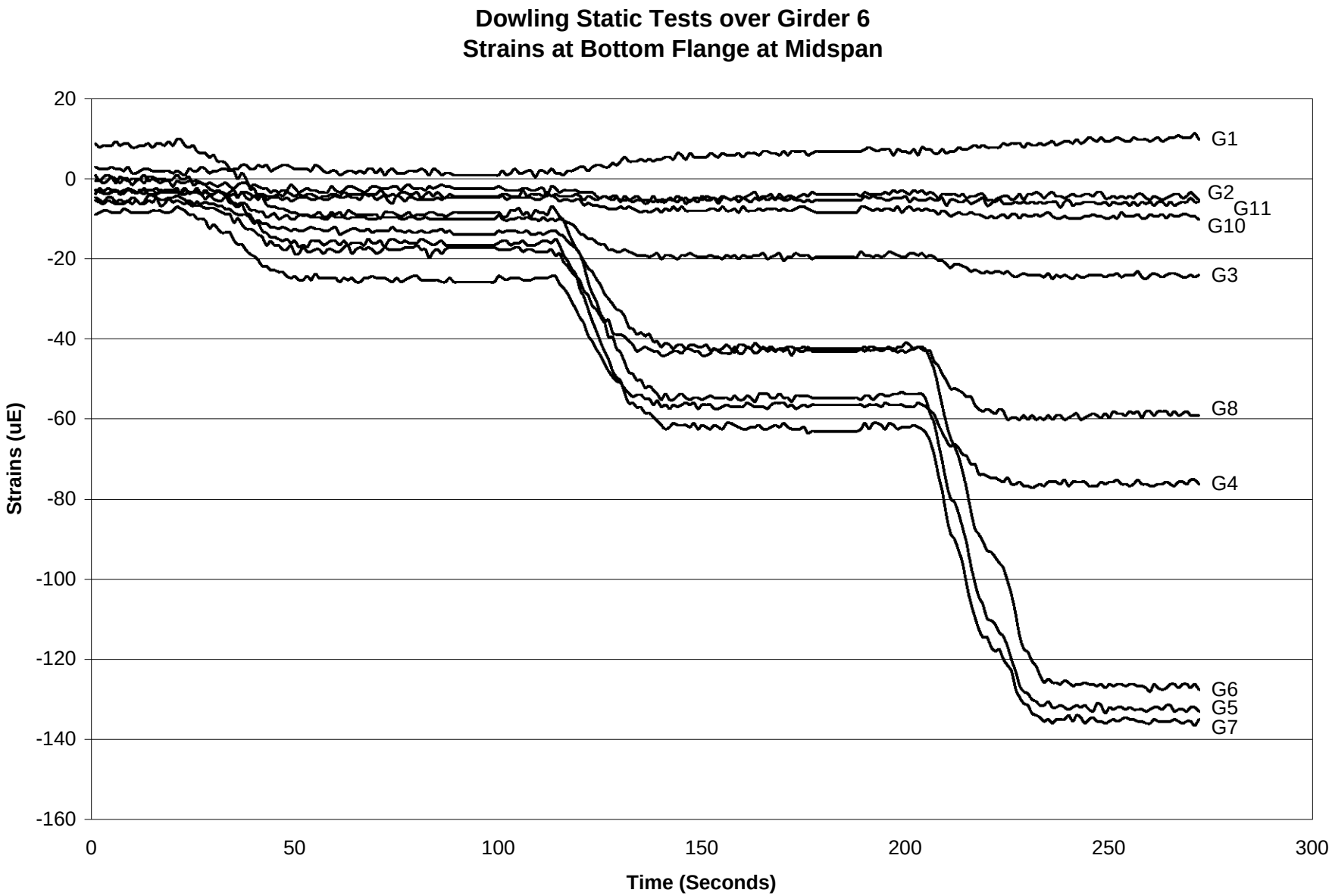
Dowling Static Tests over Girder 6
Strains at Bottom Flange at Midspan
Strains (uE)
Time (Seconds)
20
0
-20
-40
-60
-80
-100
-120
-140
-160
0
50
100
150
200
250
300
G1
G2
G11
G10
G3
G8
G4
G6
G5
G7

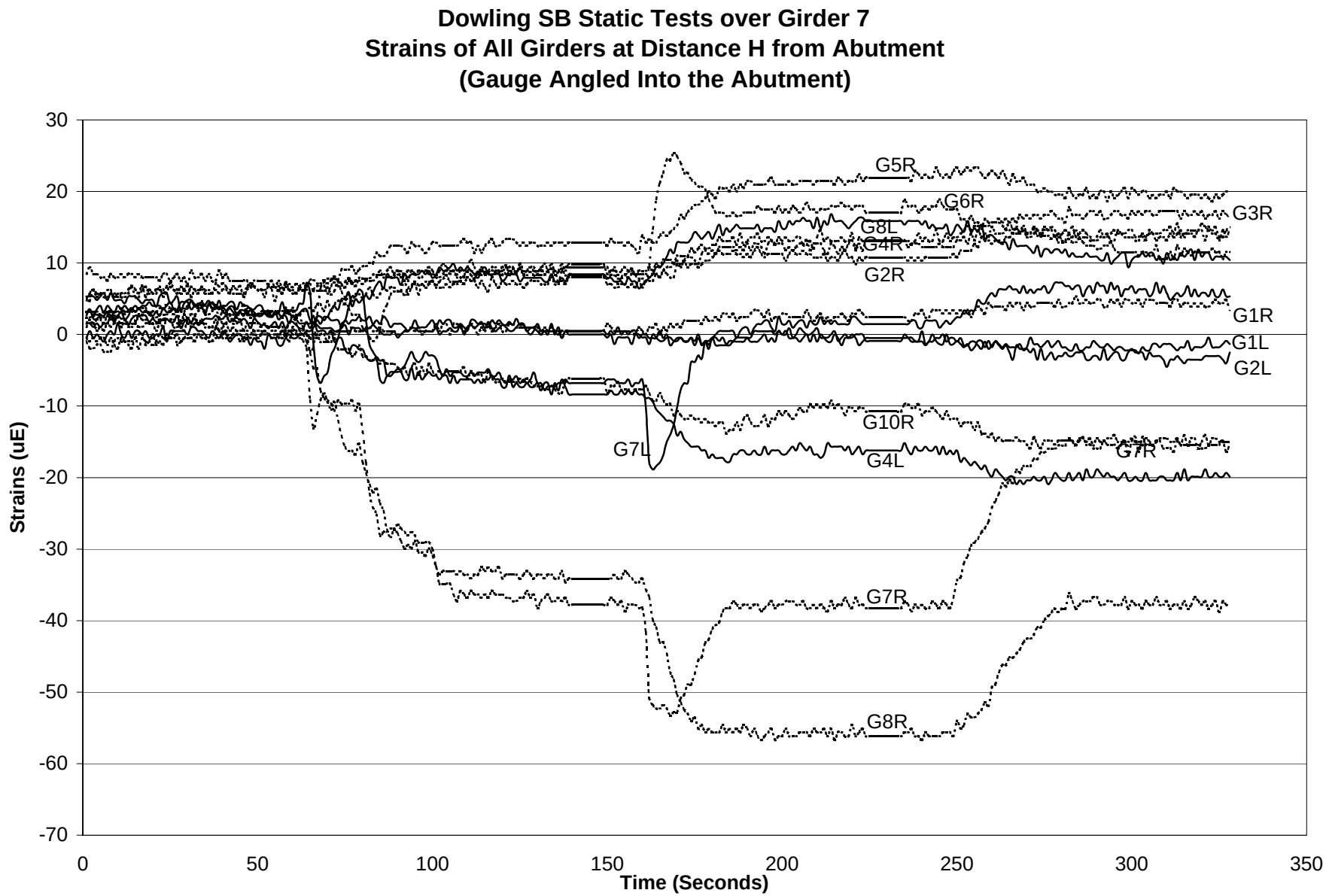
Dowling SB Static Tests over Girder 7
Strains of All Girders at Distance H from Abutment
(Gauge Angled Into the Abutment)
Strains (uE)
Time (Seconds)
30
20
10
0
-10
-20
-30
-40
-50
-60
-70
0
50
100
150
200
250
300
350
G5R
G6R
G3R
G8L
G4R
G2R
G1R
G1L
G2L
G10R
G7L
G4L
G7R
G7R
G8R

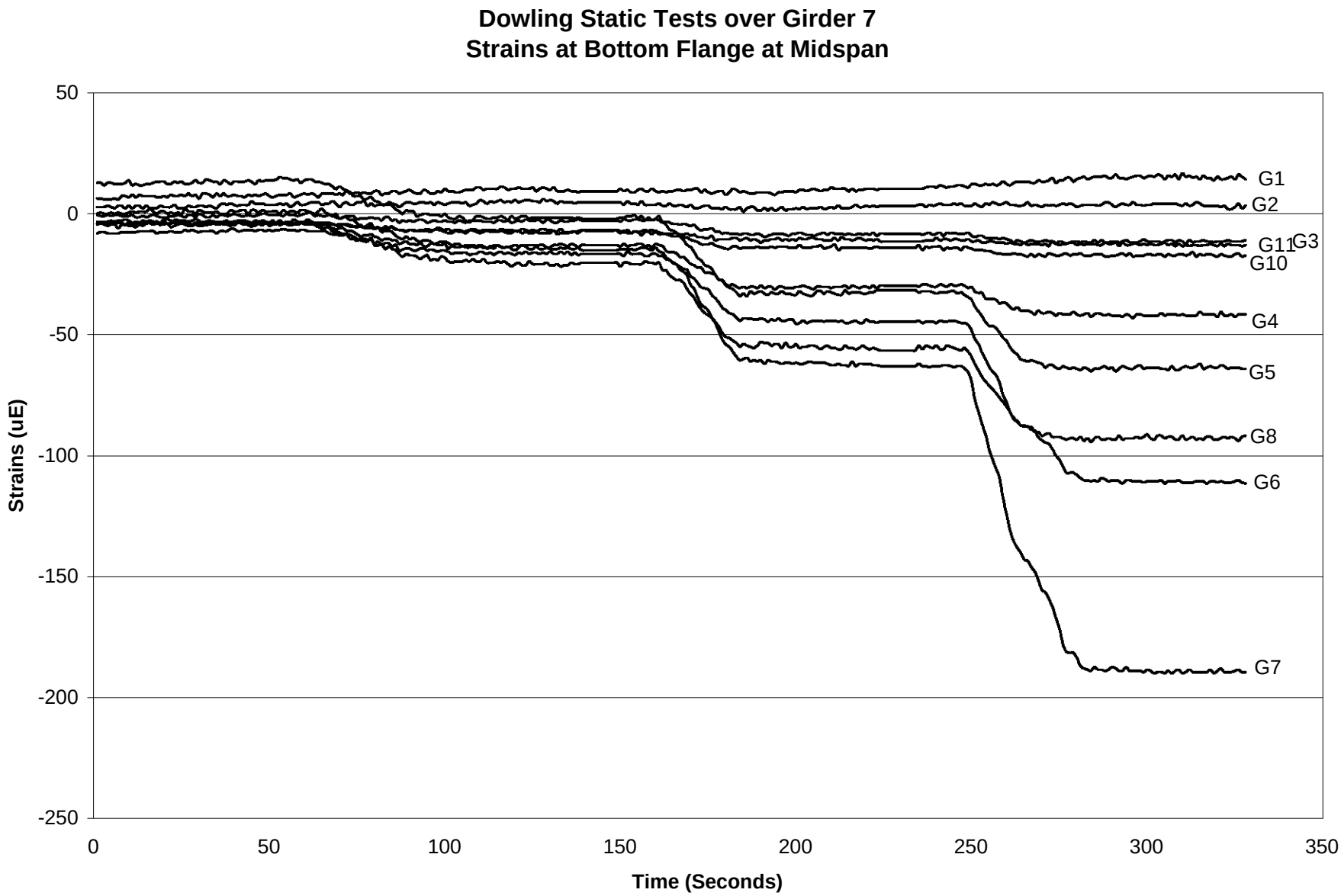
Dowling Static Tests over Girder 7
Strains at Bottom Flange at Midspan
Strains (uE)
Time (Seconds)
50
0
-50
-100
-150
-200
-250
0
50
100
150
200
250
300
350
G1
G2
G3
G11
G10
G4
G5
G8
G6
G7

# CHAPTER 3 – DEVELOPMENT OF 3D FE MODELS

One of the research objectives was to develop analytical models that could be used to analyze how load is distributed to the girders for the Alaska decked bulb-tee girder highway bridges. When developing load distribution factors for AASHTO LRFD Specifications, three levels of analysis were used. The development of 3D finite element model and the 2D grillage model is based on a similar idea.

## 3.1 Three-Dimensional (3D) FE Model Development

The finite element (FE) method offers an improvement over most other methods. A three-dimensional (3D) model can accommodate interaction between girders, decks, shear connector joints, intermediate steel diaphragms and supports. This type of model treats the bridge deck as a three-dimensional system. Bearings are modeled at actual locations. Each girder cross section may be modeled using a different mesh density. The mesh density is based on the location of the girder relative to the load position. This section provides a comparison between predictions by the 3D FE model and field test results.

### 3.1.1 Elements and Mesh

A three-dimensional (3D) finite element (FE) model was prepared for each bridge using ABAQUS Version 6.3 software available at the Arctic Region Supercomputing Centre at UAF (http://www.arsc.edu). ABAQUS Version 6.3 contains a library of solid elements for three dimensional applications. The library of solid elements in ABAQUS contains first and second order isoparametric elements. These isoparametric elements are generally referred for most cases because they are usually the most cost effective of the elements that are provided in the ABAQUS. In the ABAQUS elements library there are different types of schemes. One is the Reduced Integration, Full Integration and Incompatible Scheme. After a detailed study of the elements and the scheme it has been found that Reduced Integration scheme with 20 node solid elements yields the most accurate results. The advantages of Reduced Integration scheme over Incompatible mode scheme are that the former produces consistent results even after a considerable deformation of the elements. The reason that Reduced Integration scheme is preferred over full integration is because it requires less computational time and the added accuracy. The 20-node brick element, as shown in Figure 3.1, was used to model the bulb-tee girders because it has an improved inter-element compatibility.

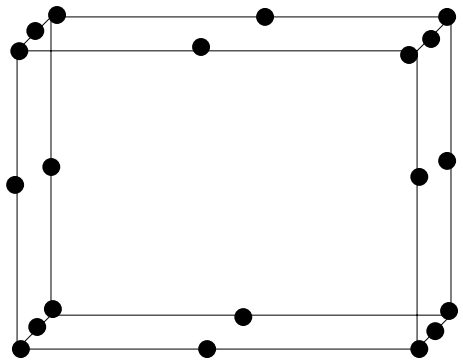

Fig. 3.1 The 20-node Solid Element

Mesh size and shape is a very important parameter when using a finite element analysis. Coarse meshes are likely to yield inaccurate results. A sufficiently refined mesh was used to ensure that the results from ABAQUS simulation are adequate. This was achieved by studying the influence of mesh refine on the resulting accuracy. The initial mesh density was doubled and solutions checked. If the increase changes the results by less than 5% then the mesh was said to be refined. Figure 3.2 shows one example of the refined mesh.

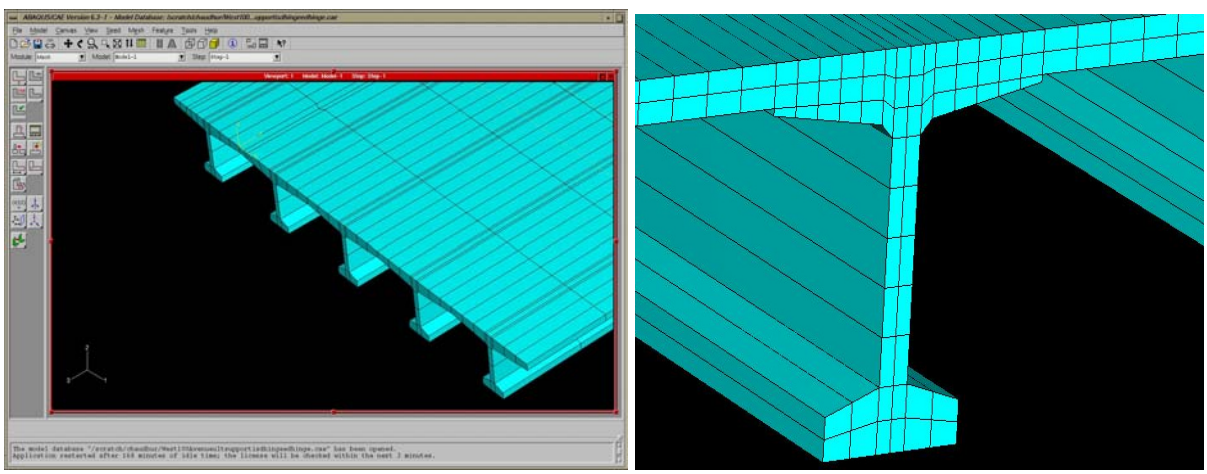

Fig. 3.2 Refined Mesh Example

### 3.1.2 Scheme Used

Elements in the ABAQUS are available with full or reduced integration and incompatible modes. Gauss integration is almost always used with second order isoparametric elements because it is efficient and the Gauss points corresponding to reduced integration are the points at which the strains are most accurately predicted if the elements are well shaped.

Full integration means that the Gauss scheme chosen will integrate the stiffness matrix of an element with uniform material behavior exactly, if the Jacobian of the mapping from the

isoparametric coordinates to the physical coordinates is constant throughout the element. This means that the faces in three dimensional elements must be parallel and in the cases of the second-order elements, the midside nodes are at the middle of the element sides.

Reduced integration usually means that the integration scheme one order less than the full scheme is used to integrate the element's internal forces and stiffness. Reduced integration reduces the number of constraints introduced by an element when there are internal constraints in the continuum theory being modeled i.e. if solid elements are used to analyze bending problems.

The incompatible mode elements which is used for 8 node Elements are an attempt to overcome the problems of shear locking in fully integrated, first order elements. Since shear locking is caused by the inability of the element's displacement field to model the kinematics associated with bending, additional degrees of freedom. The incompatible mode elements perform almost as well as second order elements if the elements have an approximately rectangular shape. The performance is considerably less if the elements have a parallelogram shape and for trapezoidal element shapes the performance is not much better than the performance of regular displacement elements. Since the Alaska style decked bulb tee girder bridges with many inclined faces it is obvious that the elements will be trapezoidal in shape. Owing to this fact the models are not analyzed using this scheme.

Reduced integration scheme is followed over single integration scheme because reduced integration lowers the cost of forming an element: for example, a fully integrated second order, three dimensional elements requires integration at 27 points while the reduced integration version of the same element only uses 8 points, and therefore costs less than 30% of the fully integrated version. This cost saving is especially significant in the element formation costs dominate the overall costs, i.e. in which the constitutive models require lengthy calculations and provides accurate results.

### 3.1.3 Shear Connectors

Between decked bulb-tee girders, there are two types of connections: shear connectors and intermediate steel diaphragms. The spacing of the connectors is 4 ft throughout the entire length of the structure. They were made of steel angles welded together by ¼" thick steel plates through the girder's top flange. These angles, 6 inches long in the longitudinal traffic direction, are embedded into the girder concrete through #4 steel bars. Figures 3.3 and 3.4 show a sketch of a typical shear connector.

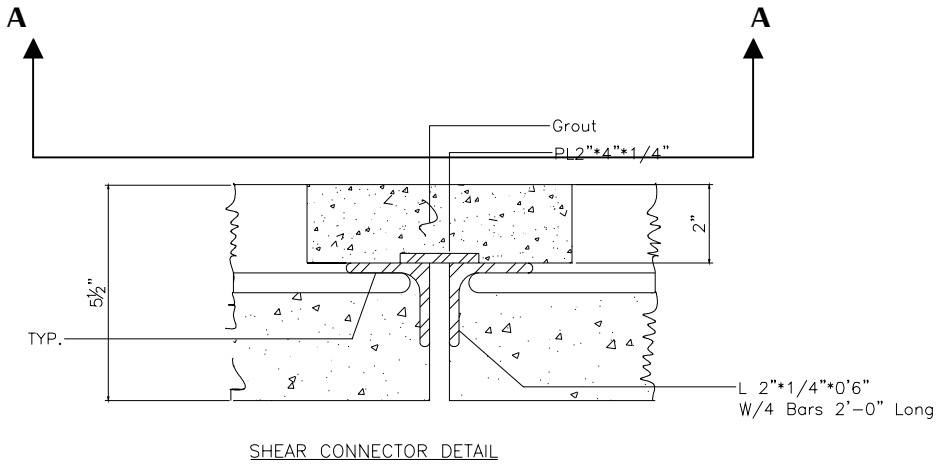


Fig. 3.3 Cross Section of the Shear Connection

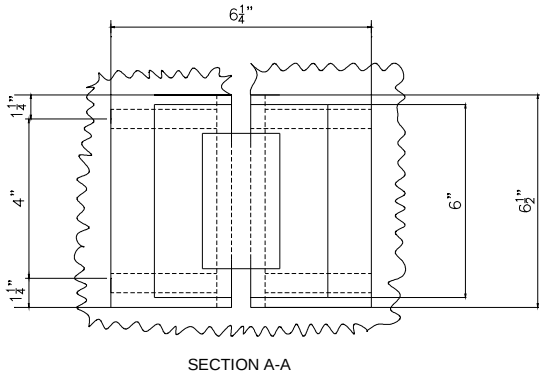


Fig. 3.4 Plan View of the Shear Connectors

In the 3D FE model, 2-node hinge-connector elements were used to model shear connectors. The hinges are located at a longitudinal spacing of 4 feet. Since the steel plates are 6 inches wide, the hinges have an influence radius of the same width, as shown in Figure 3.5. The hinges have only unconstrained rotation of motion in the "x" axis, i.e. in the longitudinal direction of the bridge.

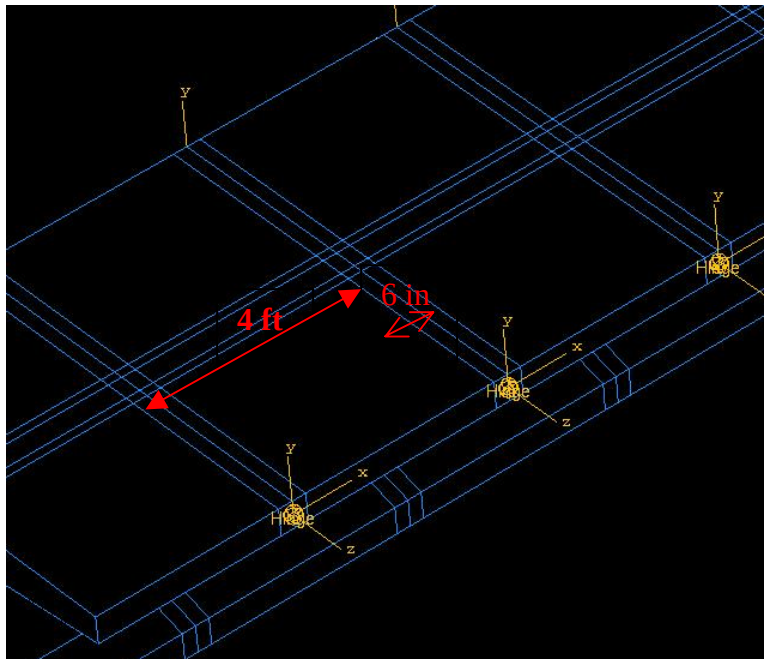


Fig. 3.5 Model of Shear Connectors

The shear connectors are attached to the girders by the above mechanism. The following procedures are followed to find out the elasticity of the hinges.

In one case it is modeled as a plate having dimensions of 4” in length, 2” in width and ¼” inches in depth, and the other having a dimension of 4 “ in length , ½ “ in width and ¼ “ inches in depth. In the first case it has been assumed that the span extends from one half of the angle section to the other half. In the second case the span length is the gap between the top flanges of the girders.

A uniformly applied load acts on one end of the plate of the magnitude 1 kip/ inch in the longitudinal direction. One end of the plate is fixed in all direction while the other end is released in the vertical direction. The plate consists of 3D, 20 node solid elements. Under these conditions the displacement in the vertical direction is measured for end which is released. These displacements are computed for all nodes lying on that face. The average displacement is found out by using the following formula: $\partial = \sum_{i=1}^{i=n} \partial / n$ where $n$ is the number of nodes and $\partial$ is the deflection.
Using the above formula we can evaluate the spring constant $k$.

$F = k\partial$ , where $F$ is the total load applied on one node. Using the value of $k$ obtained from the above equation; it is used in giving the spring constant of the hinge in 3D finite element modeling.

### 3.1.4 Intermediate Steel Diaphragms

The concrete girder elements are modeled with three dimensional solid elements. These solid elements have three degrees of freedom, i.e. three translational (x, y, z axes). The intermediate steel diaphragms are steel members connected to the girders by means of bolts, as shown in Figure 3.6. Hence these steel diaphragms act as truss members. To avoid any incompatibility at the junction in the 3D FE model, 3D truss elements were used to model the intermediate steel diaphragms, as shown in Figure 3.7.

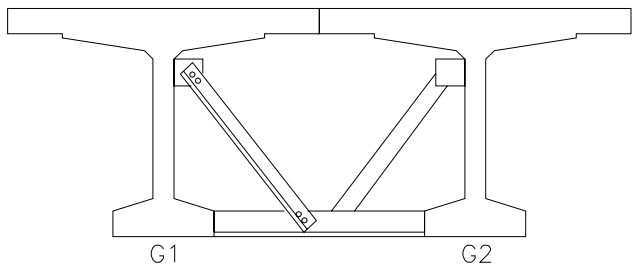


Fig. 3.6 Girders connected by Intermediate Steel Diaphragms

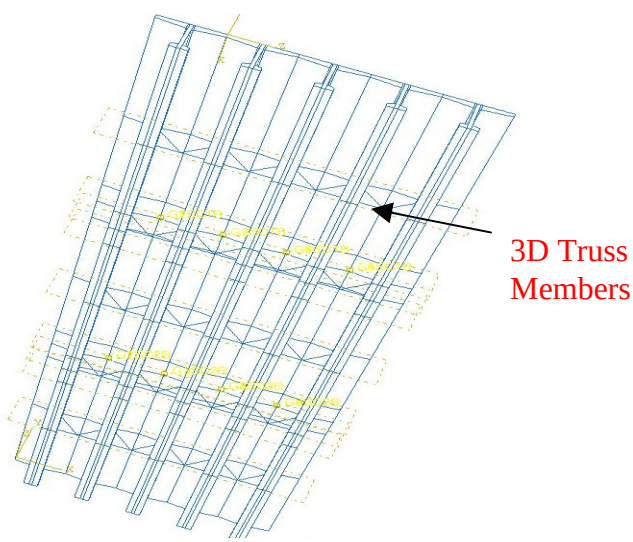


Fig. 3.7 Modeling Intermediate Steel Diaphragms

### 3.1.5 Boundary Conditions

The following boundary conditions were assumed in the 3D FE model. The model is placed in spatially so the longitudinal axis of the bridge is described by “X”, “Y” is vertically upward and “Z” is perpendicular to the “X-Y” plane. The bridge is assumed to be supported by a pin-roller system. This means at one end of the bride, the bottom flange of the girder is restrained in the vertical (“Y”) and transverse (“Z”) directions. At the other end, the bottom

flange is restrained in all three directions (“X”, “Y”, and “Z”). To model the end diaphragms, the two end sections of the girder are assumed to be restrained in the transverse direction (“Z”). The above assumptions are adopted in case of straight bridge. A slight modification is made in terms of skew bridges. For the pinned support, displacements along the skew direction, in the vertical direction and in the direction perpendicular to the skew is made equal to zero. For the roller support displacements in the vertical direction as well as in the direction of the skew is made equal to zero.

### 3.1.6 Modeling Constants

The modulus of elasticity “E” is calculated by the formula:

$$E = 33 \times (145.0)^{1.5} \sqrt{f_c^{'}} \qquad (3.1)$$

where $\mathbf{f_c'}$ is the concrete strength at 28 days, taken as 6500 psi as per the shop drawings.

Other material properties include the Poisson’s ratio of the concrete, and it was taken as 0.2.

## 3.2 3D FE Model Verification

Four 3D FE models, one for each tested bridge, were prepared using the above discussed modeling technique. The 3D FE model was used to simulate the field tests. These results were compared to the experimental data. Figures 3.8 and 3.9 show example models of two tested bridges.

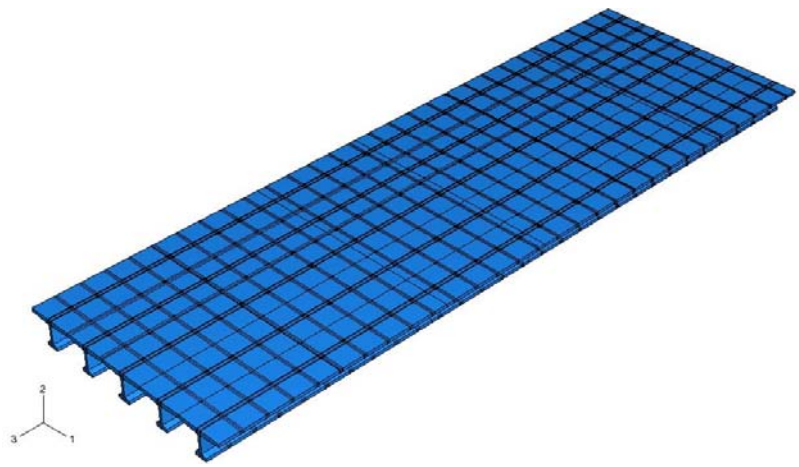

Fig. 3.8 3D FE Model of the West 100th Avenue Bridge

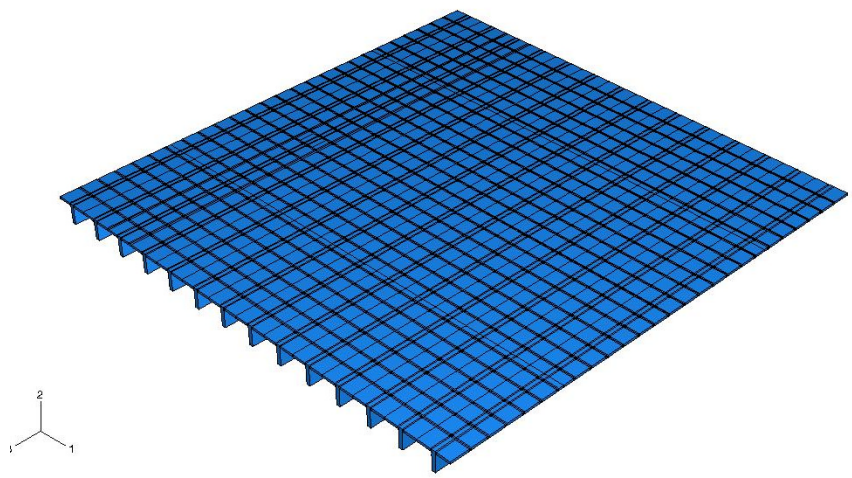

Fig. 3.9 3D FE Model of the Dimond & Dowling Bridge

Comparisons between the 3D FE model results and experimental results are shown in the next four sections which correspond to four sets of bridges tested.

### 3.2.1 Comparisons with Set 1 Bridges

In the field testing, flexural strains were measured by placing the strain gauges in the direction of the bridge at the bottom of the girder. In the 3D FE modeling, 3D solid elements were used, which have six faces. For any given loading, stresses can be generated for all the six faces. Stresses or strains are taken from the faces of the elements which have the same orientation as that in the field testing. Comparison of flexural strains is relatively easy comparing to the comparison of shear strains since gauges measuring the flexural strains in the field testing are located in the same face and orientation as in the solid elements. However, for the shear strain comparison we cannot make the direct comparison. Instead, the strain transformation was used first to convert strains from modeling results.

Figure 3.10 shows the comparison of flexural strains between model results and testing results. Using the Loading Key defined in Section 2.3.3 of this report, the loading position for the comparison is shown in the title of the figure. For example, "100$^{th}$ NB and SB-3-G1/G5" in Figure 3.10 means that this figure shows the results from 100$^{th}$ NB and 100$^{th}$ SB bridges when the truck load is positioned near the midspan ("3") over two edge girders, Girder 1 (G1) and Girder 5 (G5). Please note that for shear strain comparisons the left face (e.g. "G1_Left" = the left face of the Girder 1) of the girder and the right face of the same girder (e.g. "G1_Right" = the right face of the Girder 1) are compared in different figures.

The dotted lines in all figures show the model results while the firm lines show the experimental results. The x-axis refers to the girder number while the y-axis refers to the flexural strains. The strains are in the order of $10^{-3}$ (i.e. in micro-strain uE). The experimental strains are directly tabulated from the BDI strain gauges which were connected to the computer. The model strains are evaluated from the 3D FE models. Negative strains refer to tension whereas positive refers to compression. It should be noted that always the point of interest is the girder upon where the load is placed. Say for example if the loading key refers to G1, then the point of interest will be Girder 1. Similarly for G2, it will be Girder 2 and so on. This is applicable for all figures in this Section.

*Comparison of Flexural Strains:*

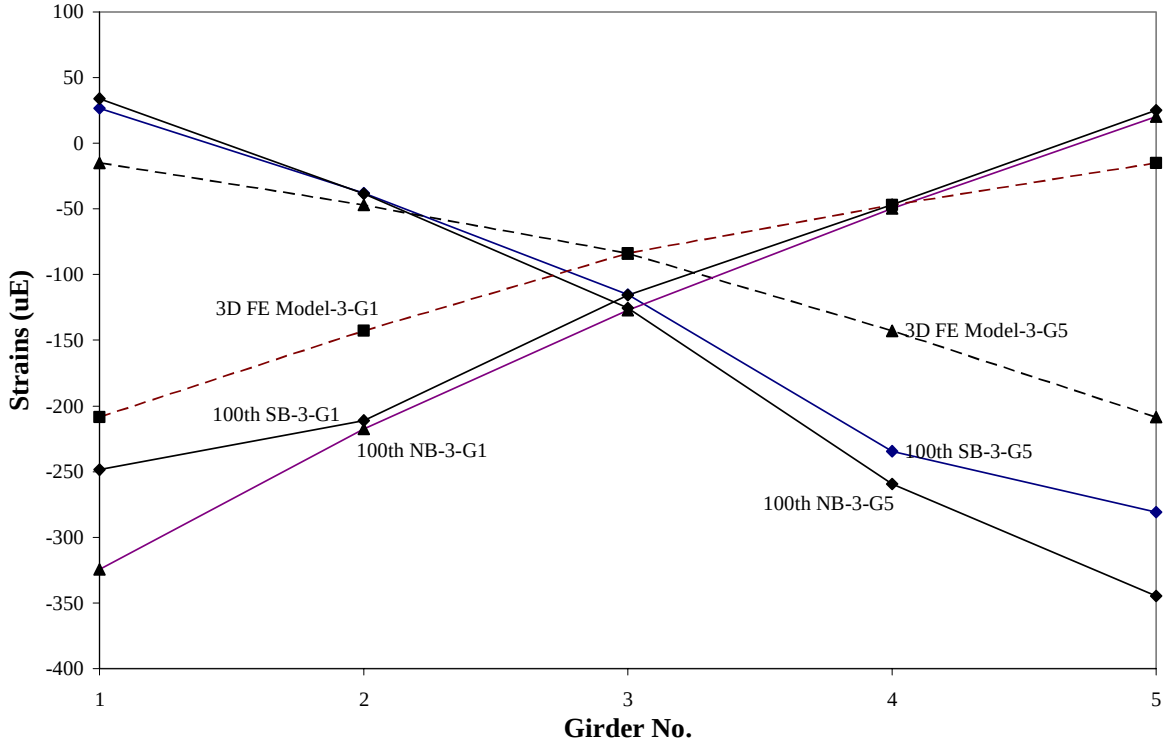


Fig. 3.10 Comparison of Flexural Strains (100th NB and SB-3-G1/G5)

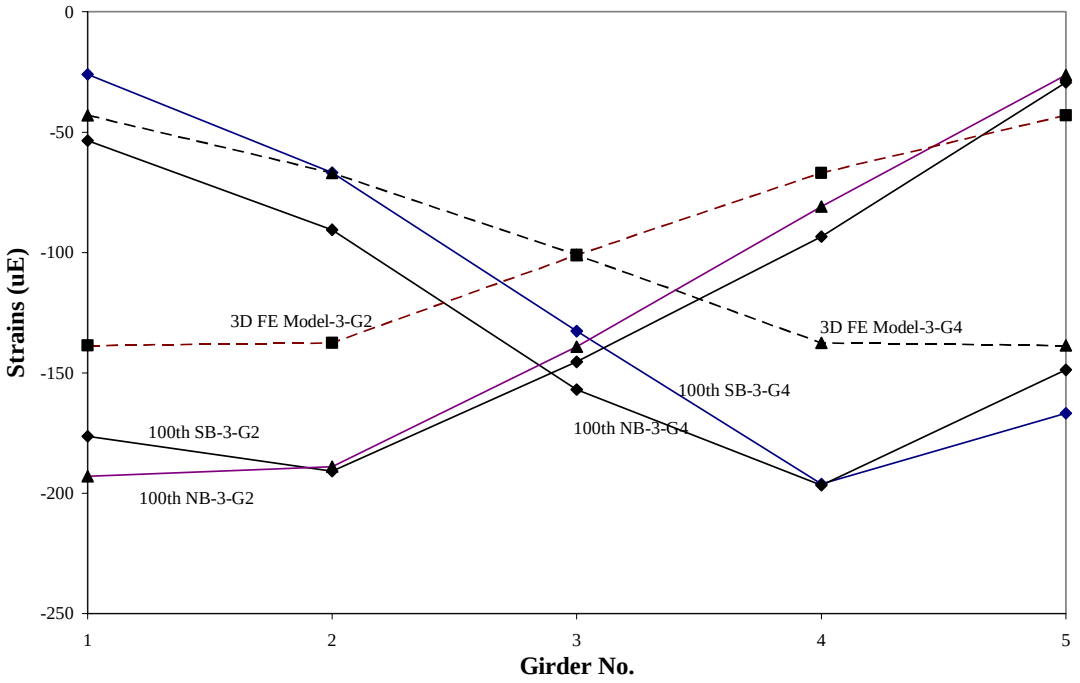


Fig. 3.11 Comparison of Flexural Strains (100th NB and SB-3-G2/G4)

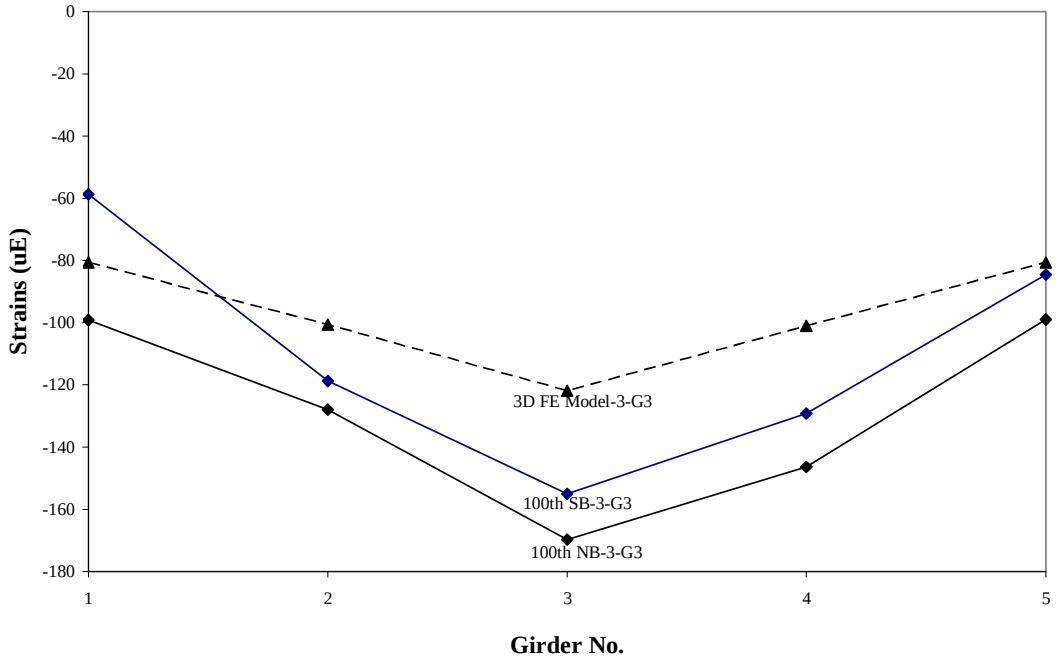


Fig. 3.12 Comparison of Flexural Strains (100th NB and SB-3-G3)

*Comparison of Shear Strains:*

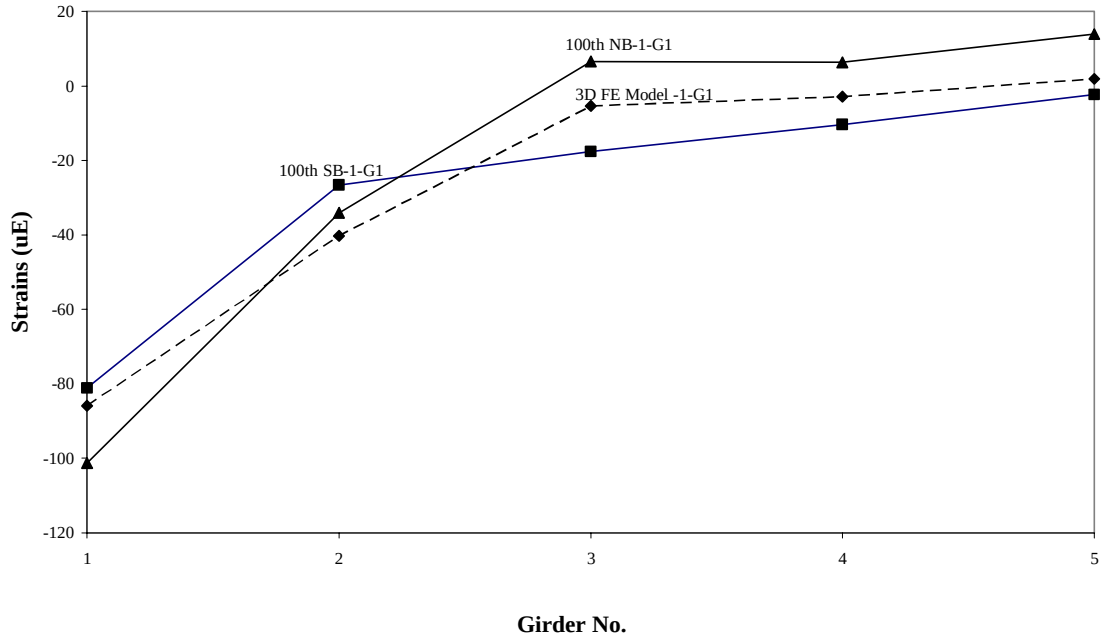


Fig. 3.13 Comparison of Shear Strains (100th NB and SB-1-G1_Left)

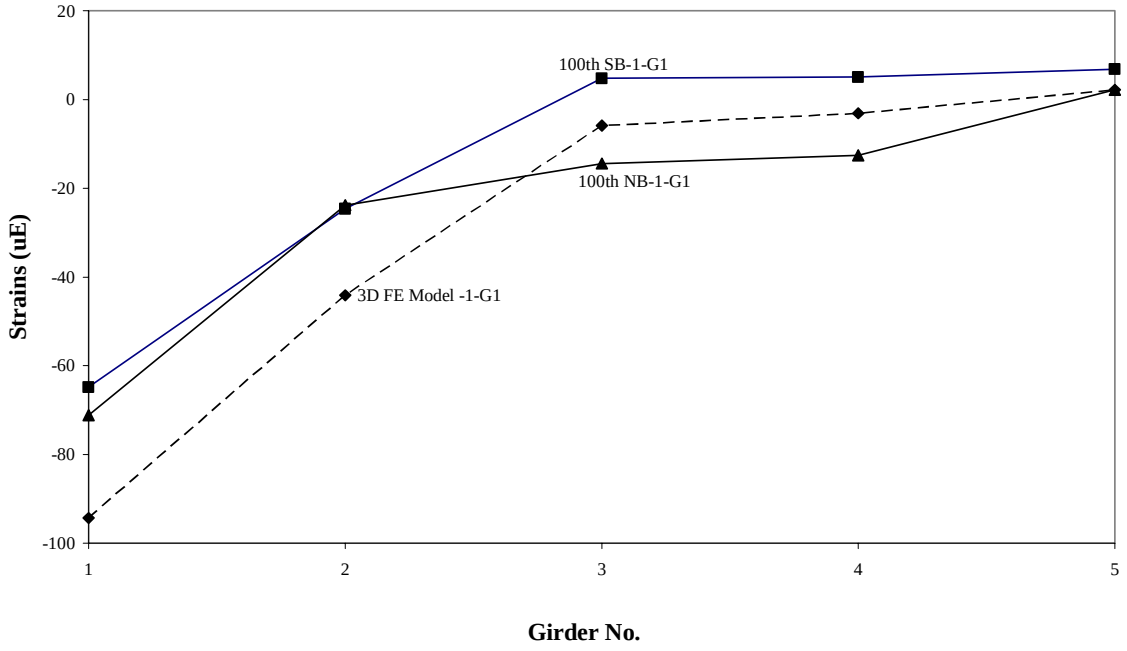


Fig. 3.14 Comparison of Shear Strains (100th NB and SB-1-G1_Right)

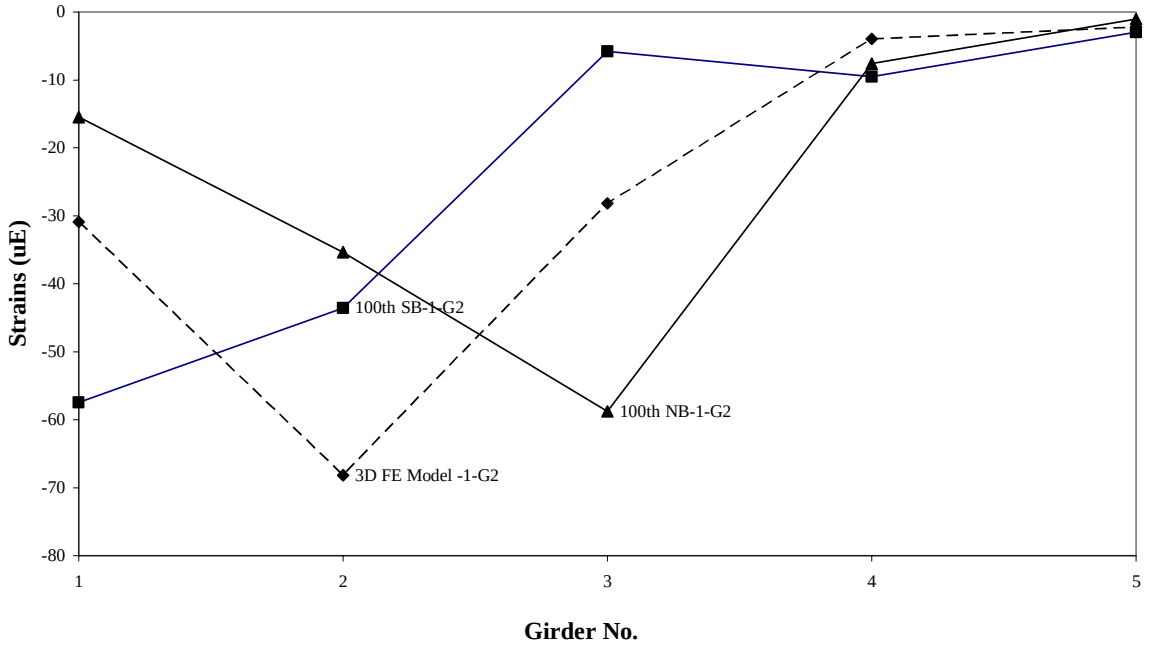


Fig. 3.15 Comparison of Shear Strains (100th NB and SB-1-G2_Left)

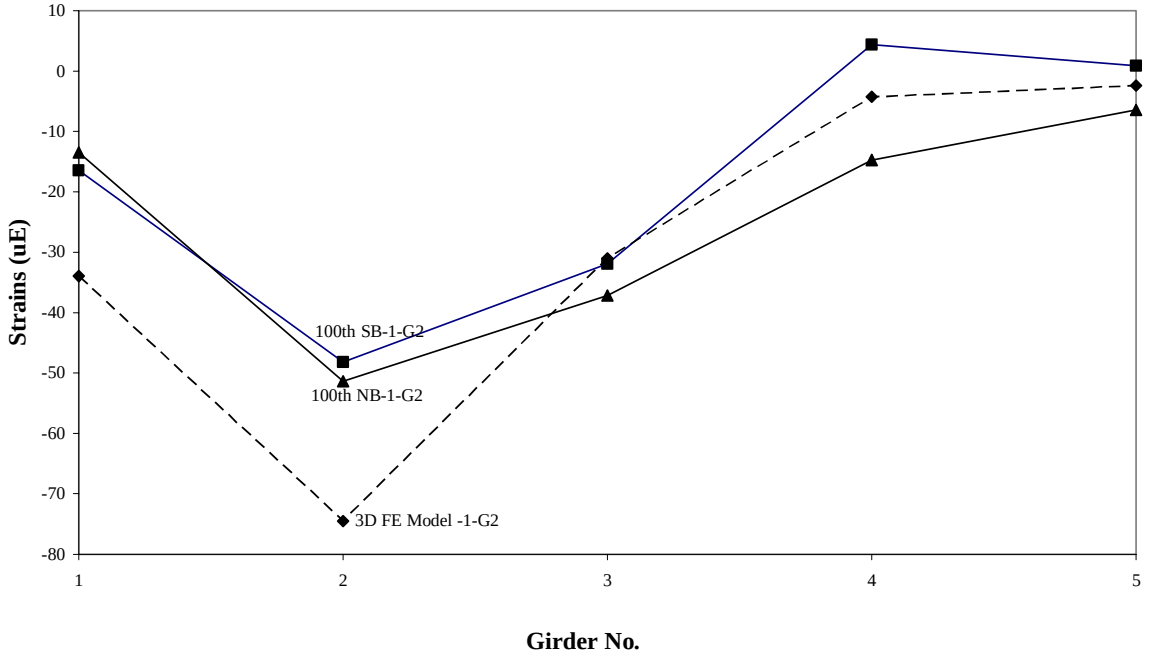


Fig. 3.16 Comparison of Shear Strains (100th NB and SB-1-G2_Right)

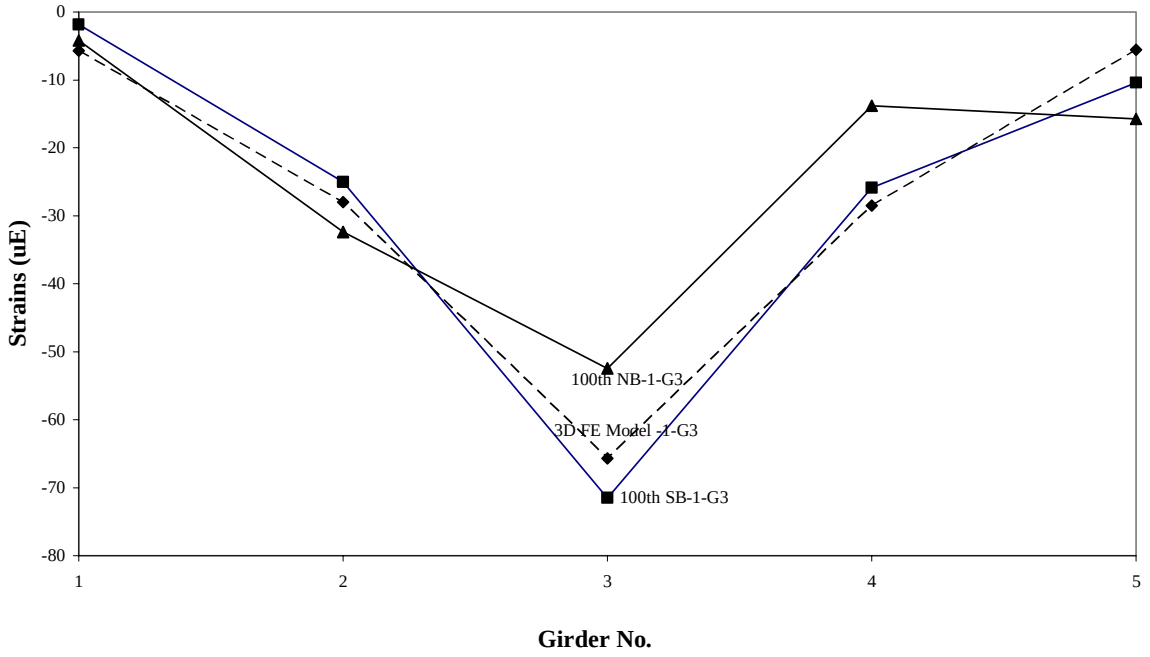


Fig. 3.17 Comparison of Shear Strains (100th NB and SB-1-G3_Left)

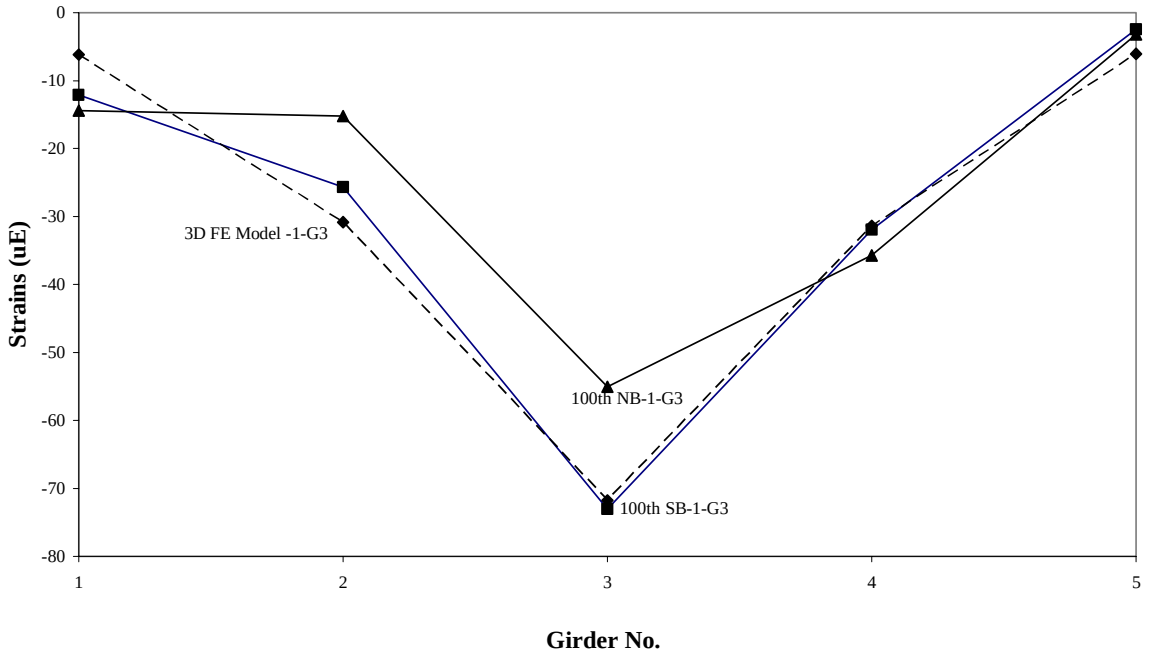


Fig. 3.18 Comparison of Shear Strains (100th NB and SB-1-G3_Right)

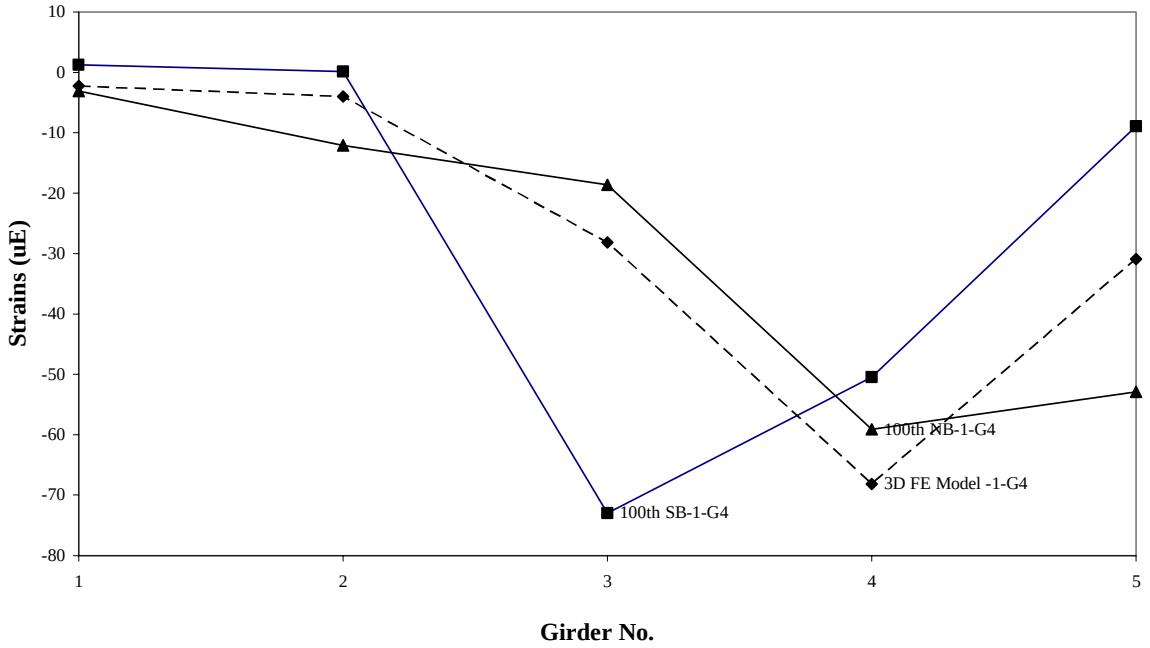


Fig. 3.19 Comparison of Shear Strains (100th NB and SB-1-G4_Left)

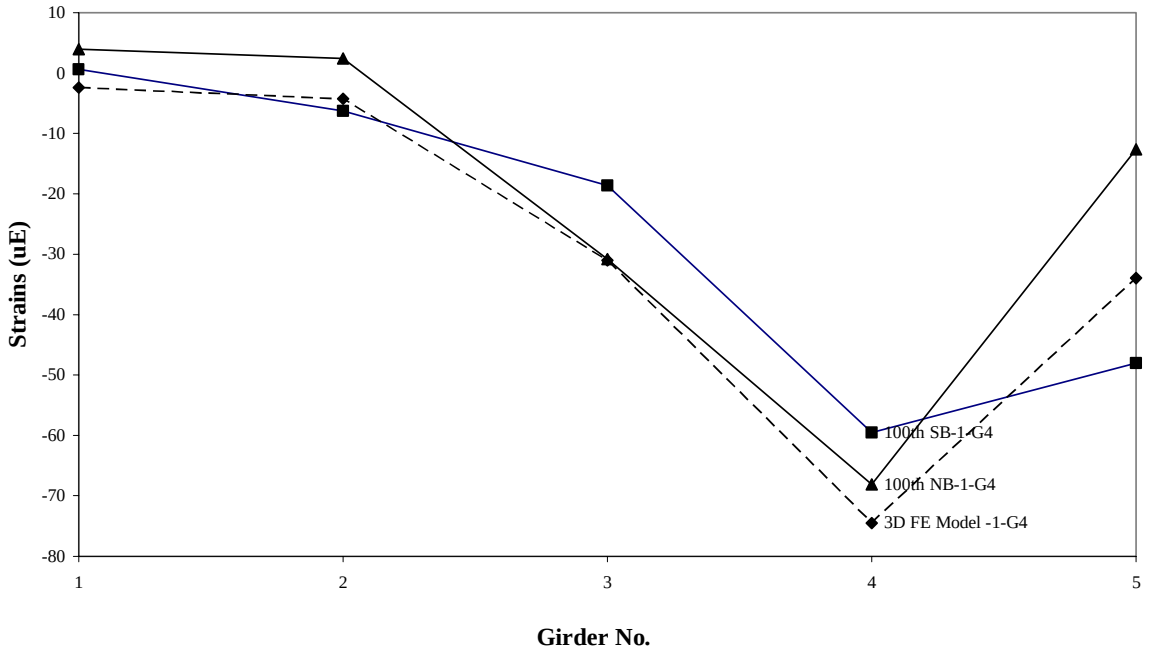


Fig. 3.20 Comparison of Shear Strains (100th NB and SB-1-G4_Right)

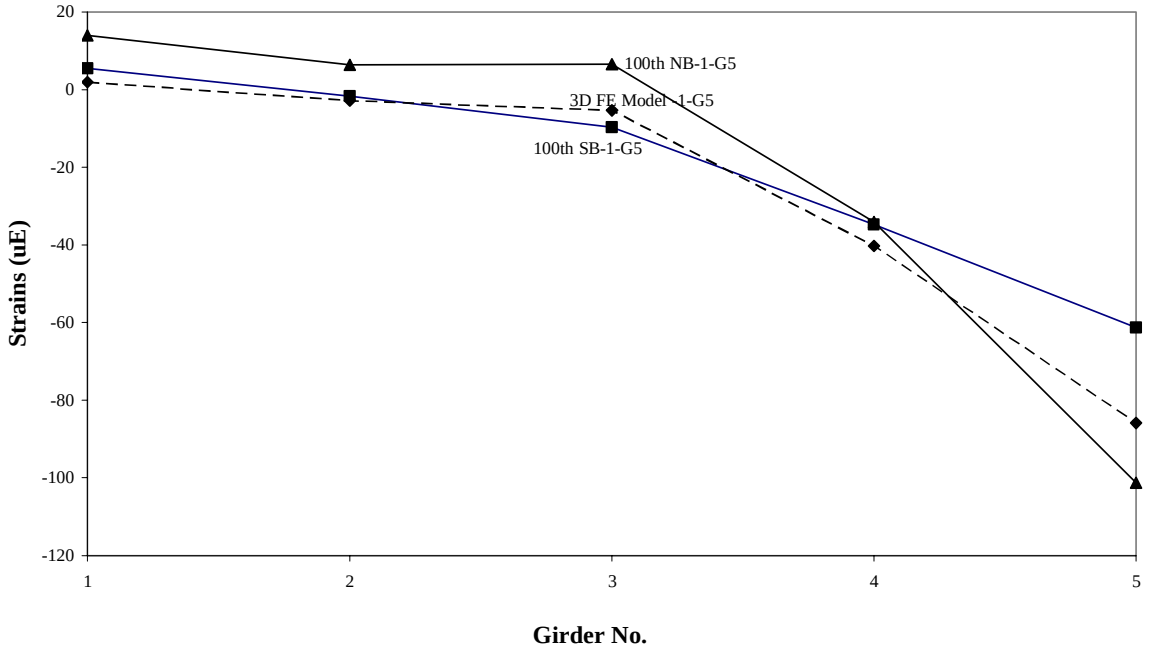


Fig. 3.21 Comparison of Shear Strains (100th NB and SB-1-G5_Left)

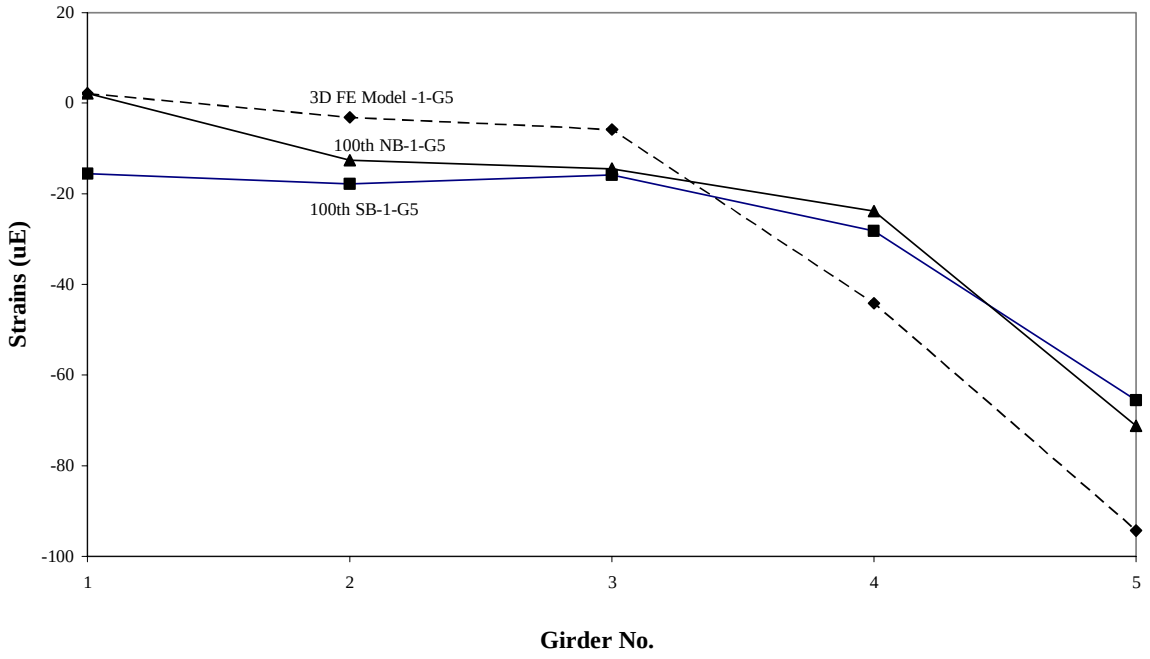


Fig. 3.22 Comparison of Shear Strains (100th NB and SB-1-G5_Right)

### 3.2.2 Comparisons with Set 2 Bridges

*Comparison of Flexural Strains:*

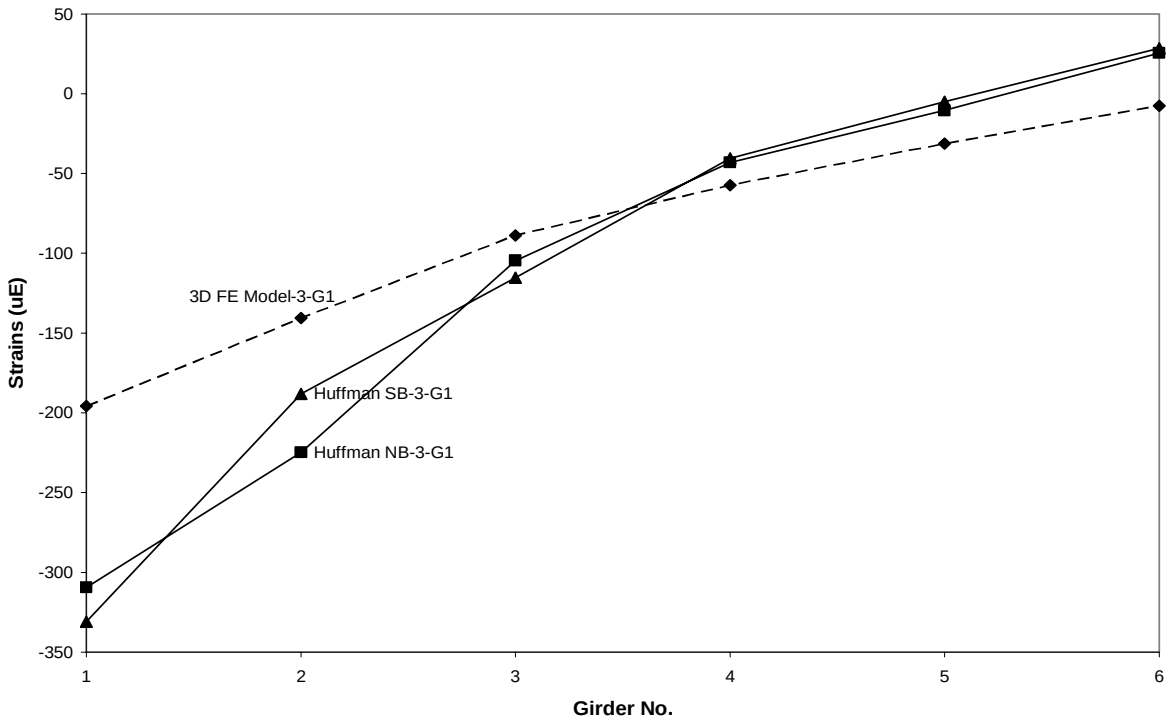


Fig. 3.23 Comparison of Flexural Strains (Huffman NB and SB-3-G1)

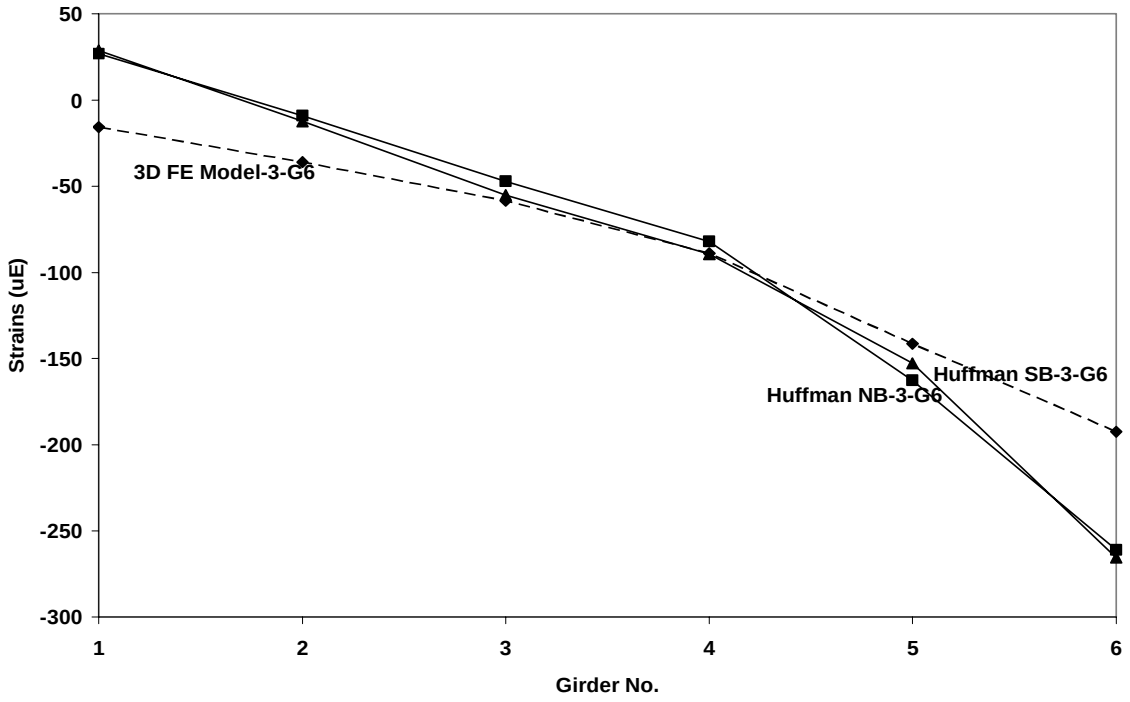


Fig. 3.24 Comparison of Flexural Strains (Huffman NB and SB-3-G6)

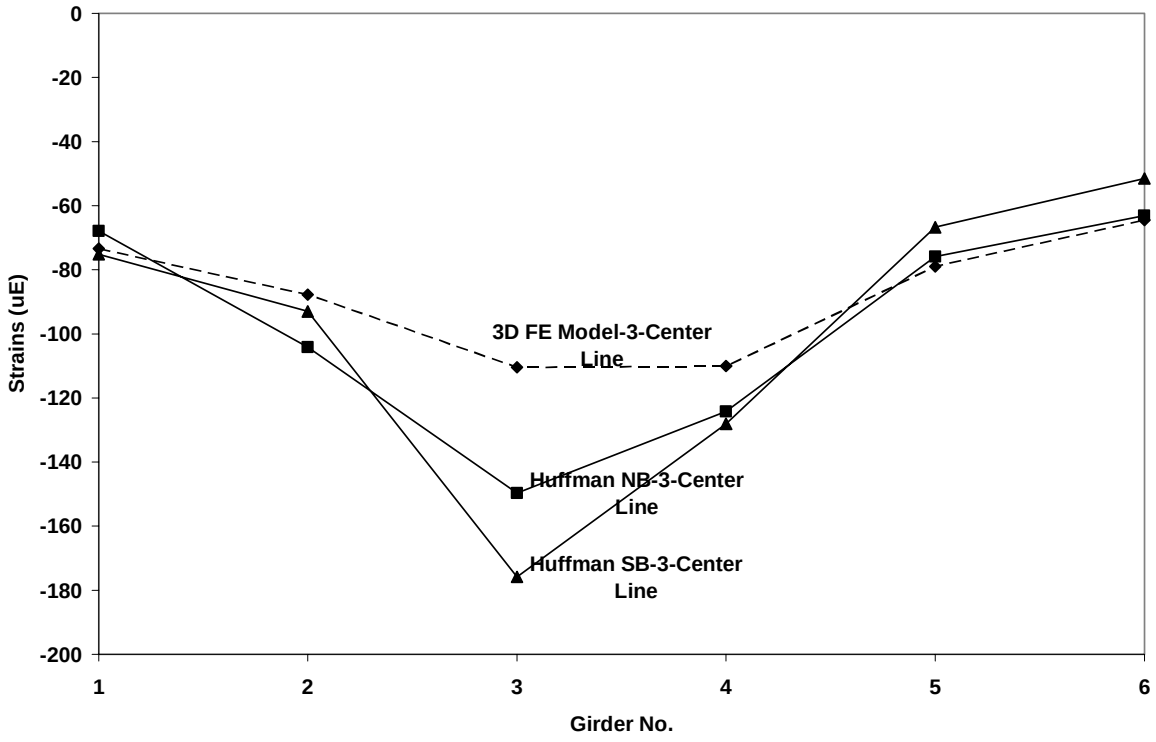


Fig. 3.25 Comparison of Flexural Strains (Huffman NB and SB-3-Center Line)

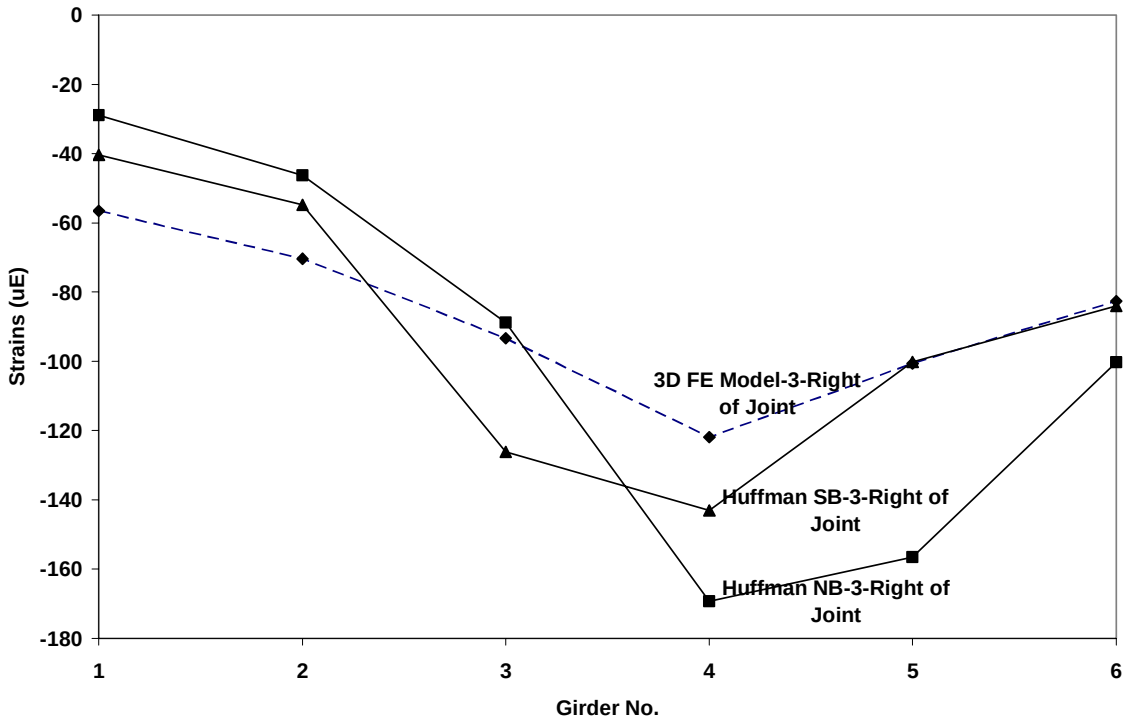


Fig. 3.26 Comparison of Flexural Strains (Huffman NB and SB-3-Right of Joint)

*Comparison of Shear Strains:*

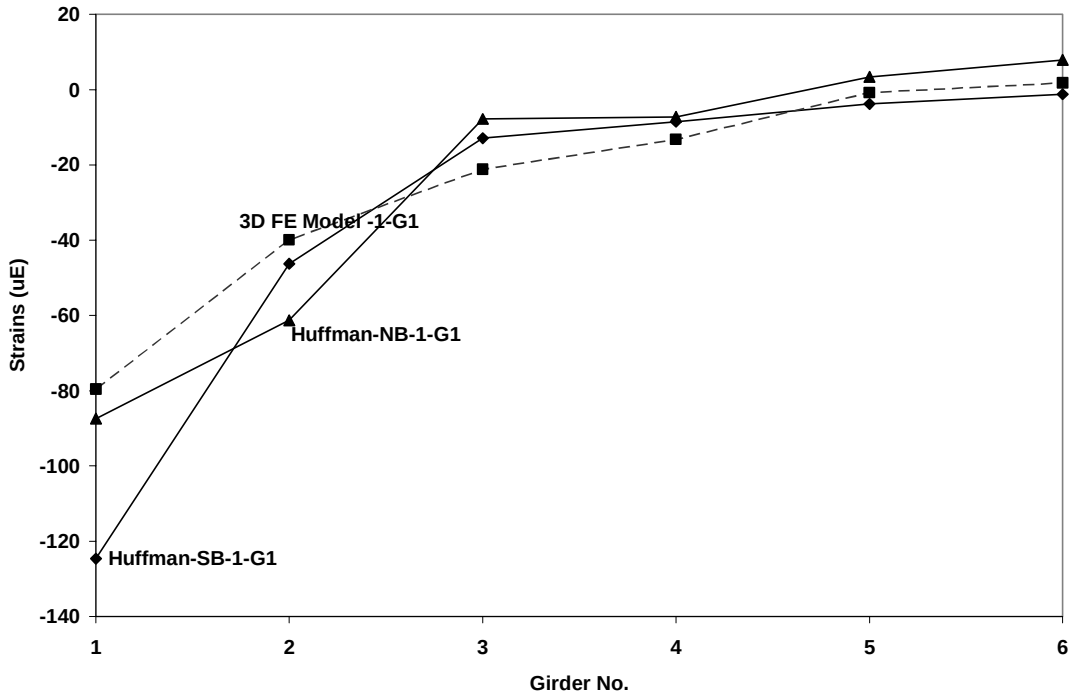


Fig. 3.27 Comparison of Shear Strains (Huffman NB and SB-1-G1_Left)

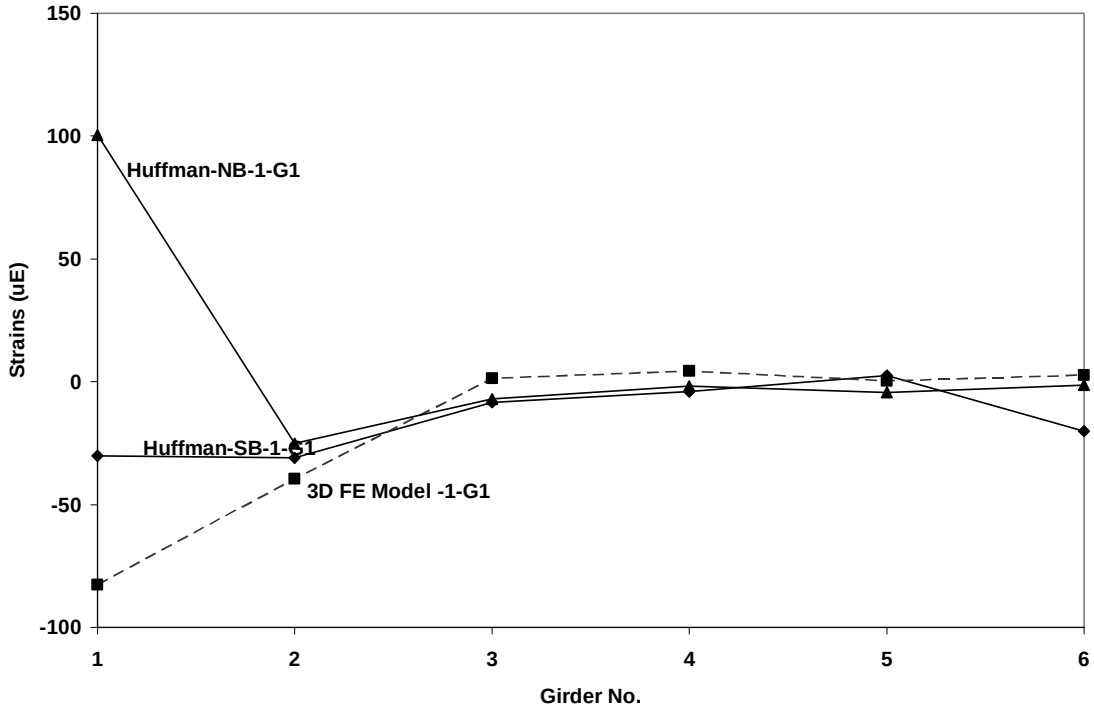


Fig. 3.28 Comparison of Shear Strains (Huffman NB and SB-1-G1_Right)

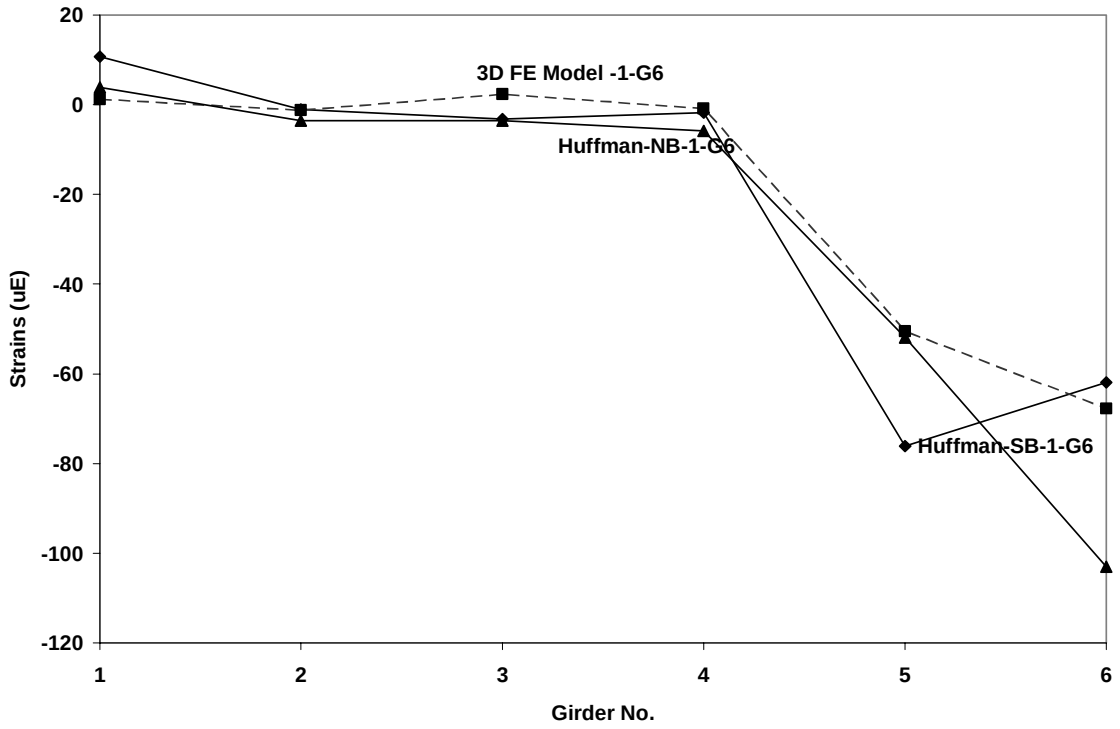


Fig. 3.29 Comparison of Shear Strains (Huffman NB and SB-1-G6_Left)

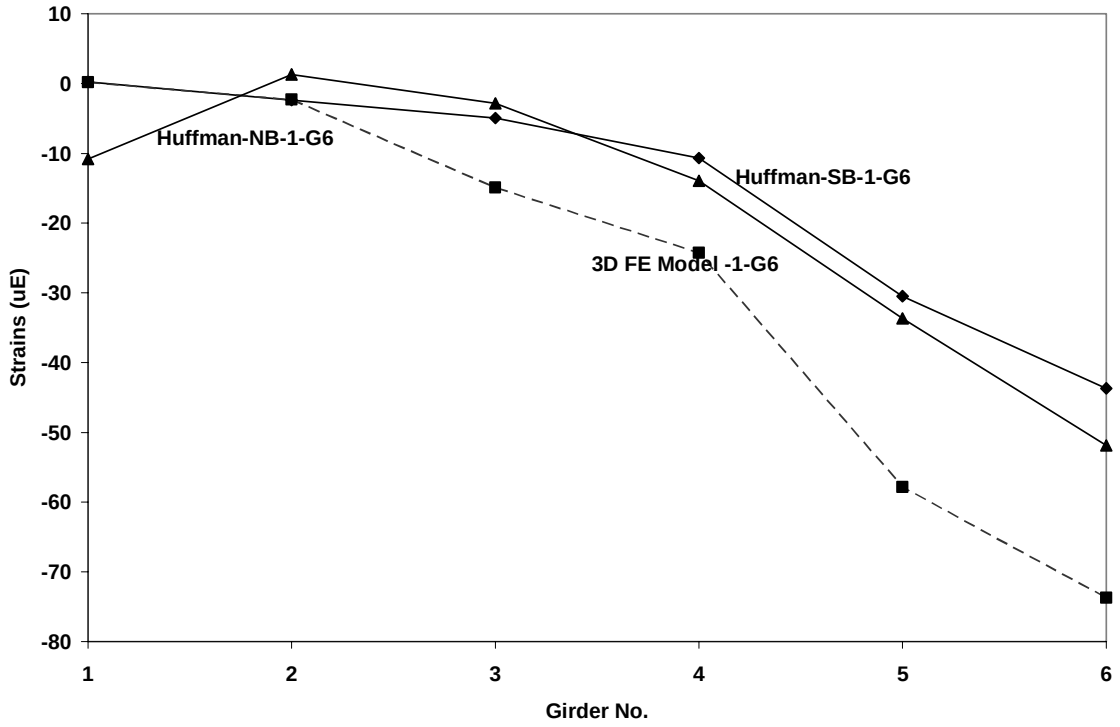


Fig. 3.30 Comparison of Shear Strains (Huffman NB and SB-1-G6_Right)

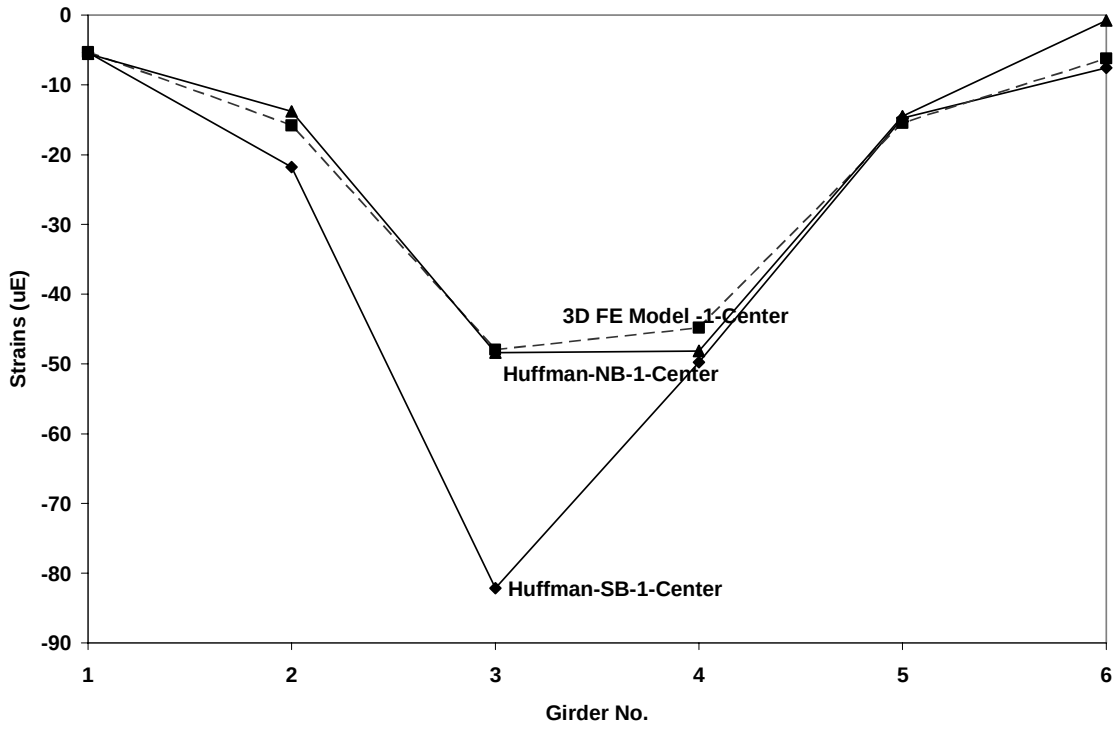


Fig. 3.31 Comparison of Shear Strains (Huffman NB and SB-1-Center_Left)

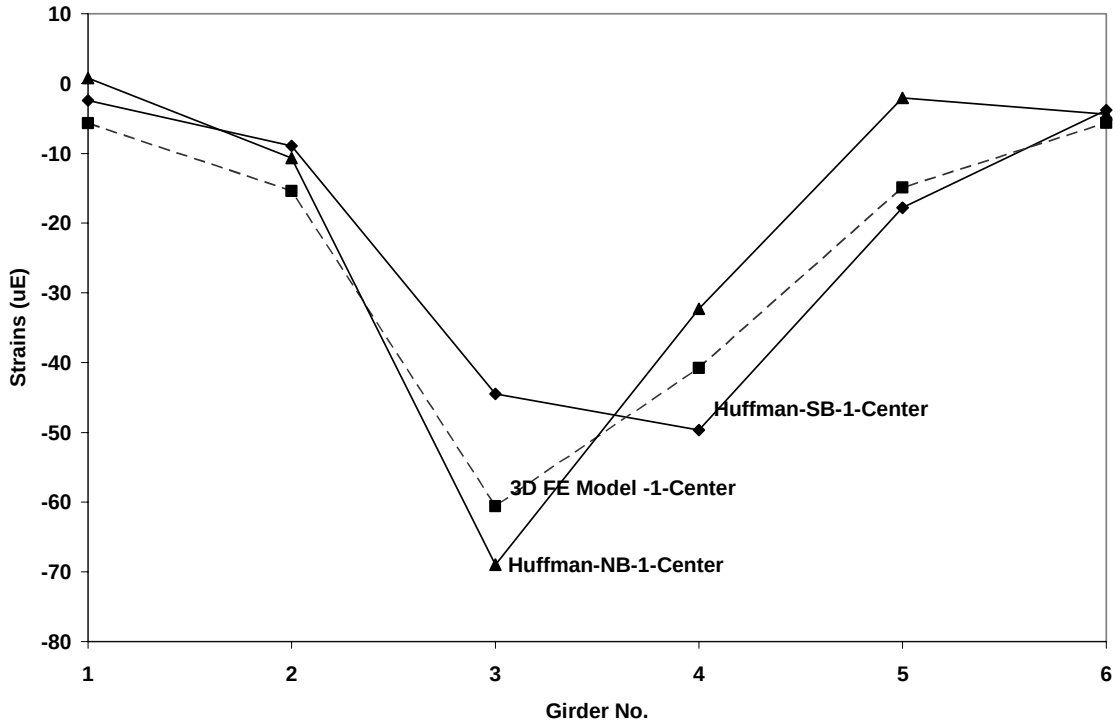


Fig. 3.32 Comparison of Shear Strains (Huffman NB and SB-1-Center_Right)

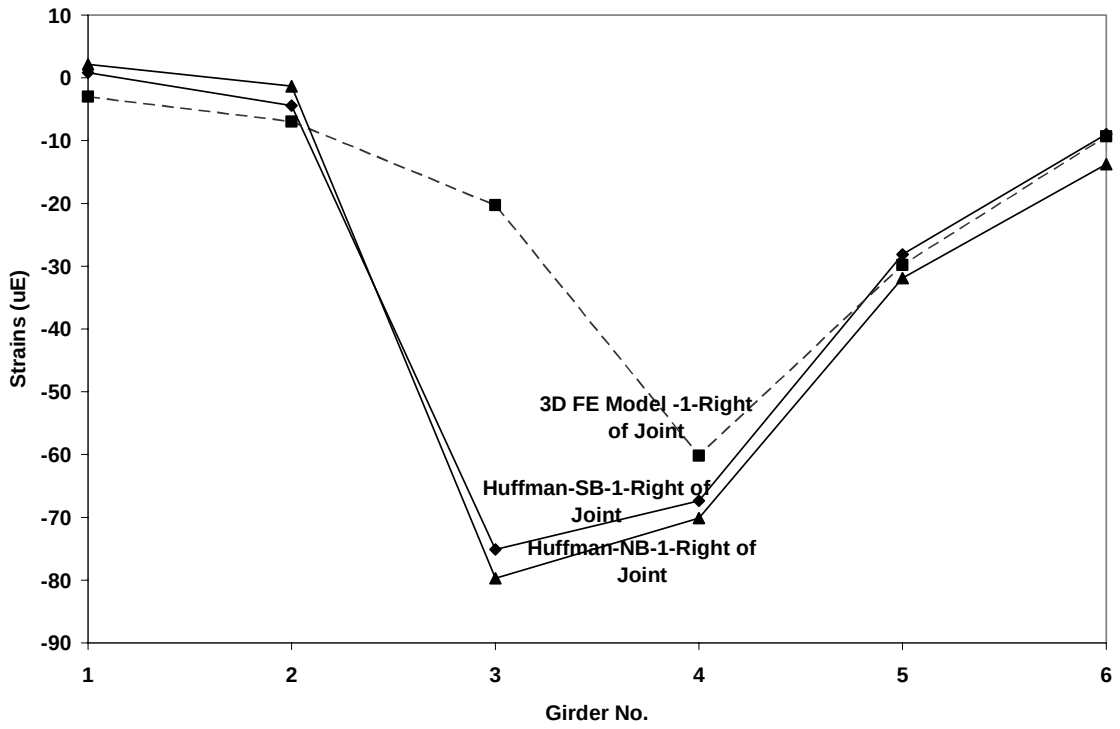


Fig. 3.33 Comparison of Shear Strains (Huffman NB & SB-1-RightofJoint_Left)

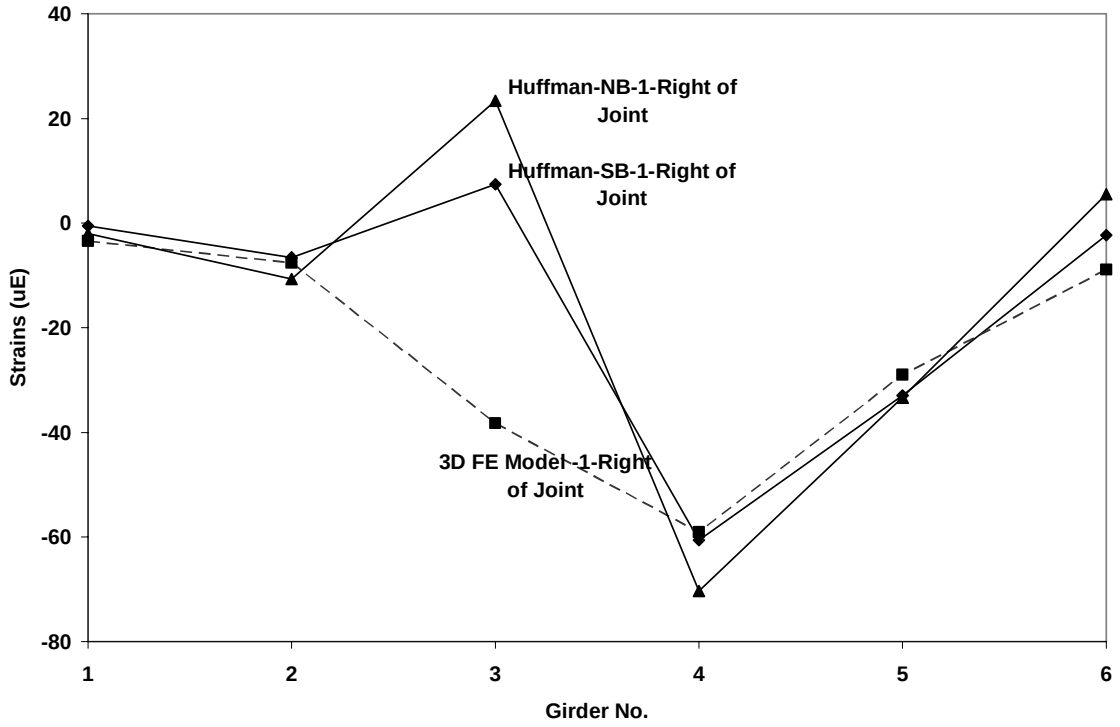


Fig. 3.34 Comparison of Shear Strains (Huffman NB & SB-1-RightofJoint_Right)

3.2.3 Comparisons with Set 3 Bridges

*Comparison of Flexural Strains:*

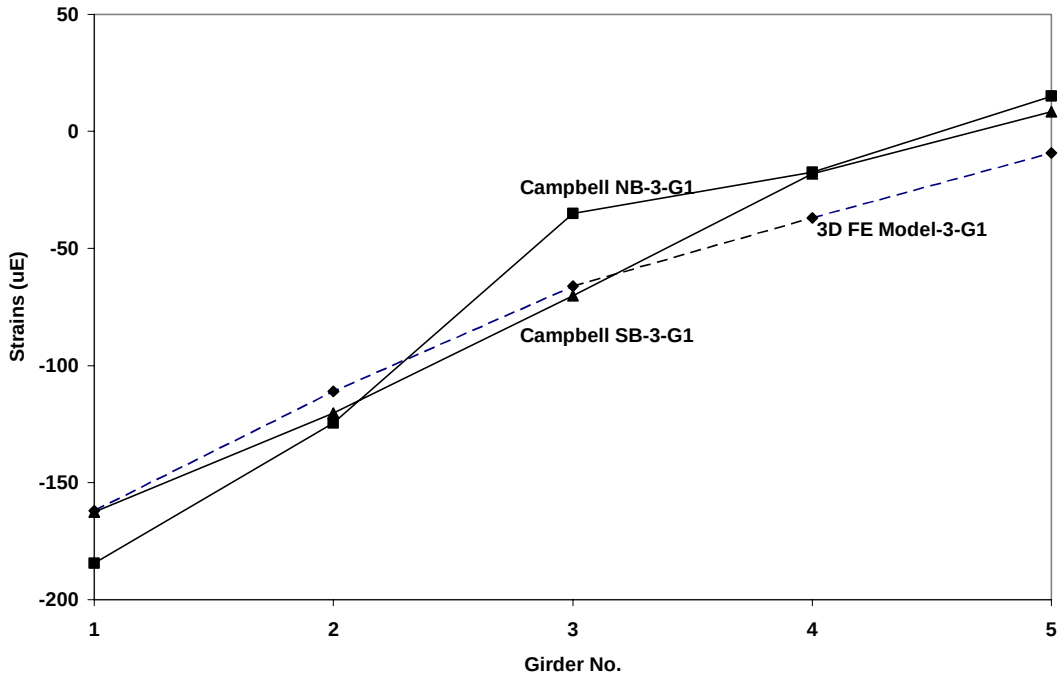


Fig. 3.35 Comparison of Flexural Strains (Campbell NB and SB-3-G1)

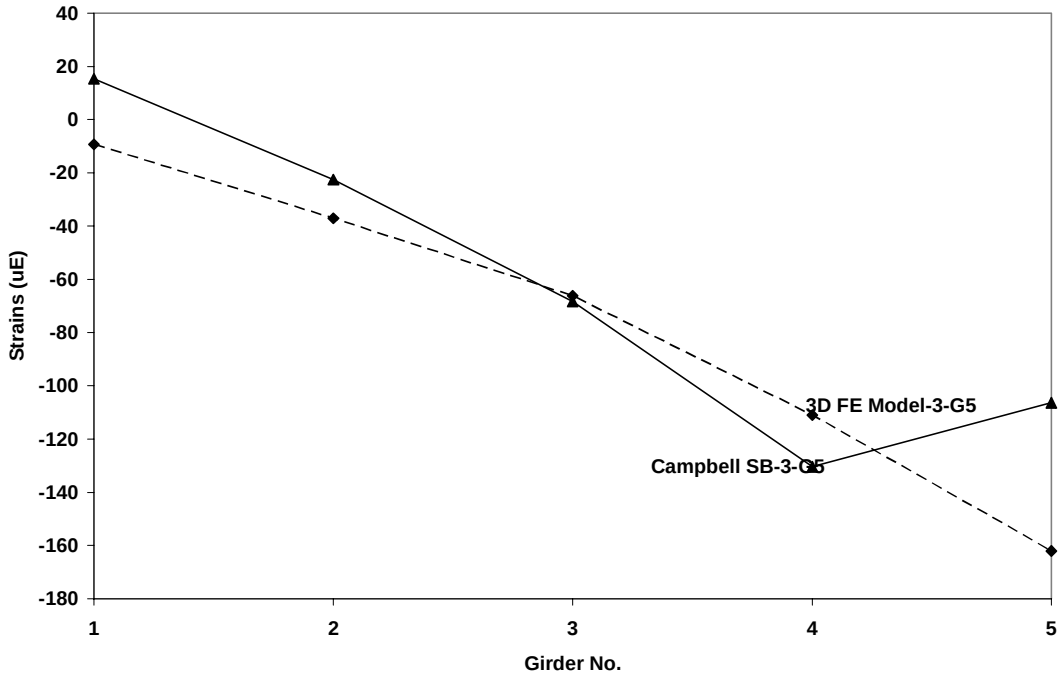


Fig. 3.36 Comparison of Flexural Strains (Campbell SB-3-G5)

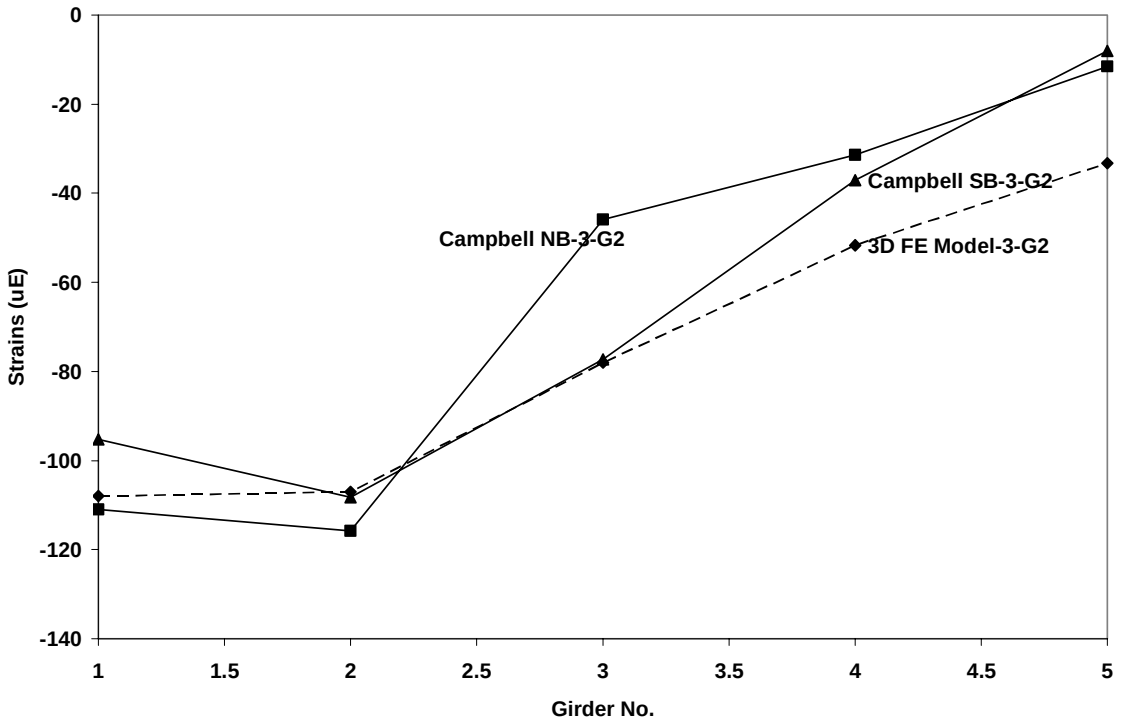


Fig. 3.37 Comparison of Flexural Strains (Campbell NB & SB-3-G2)

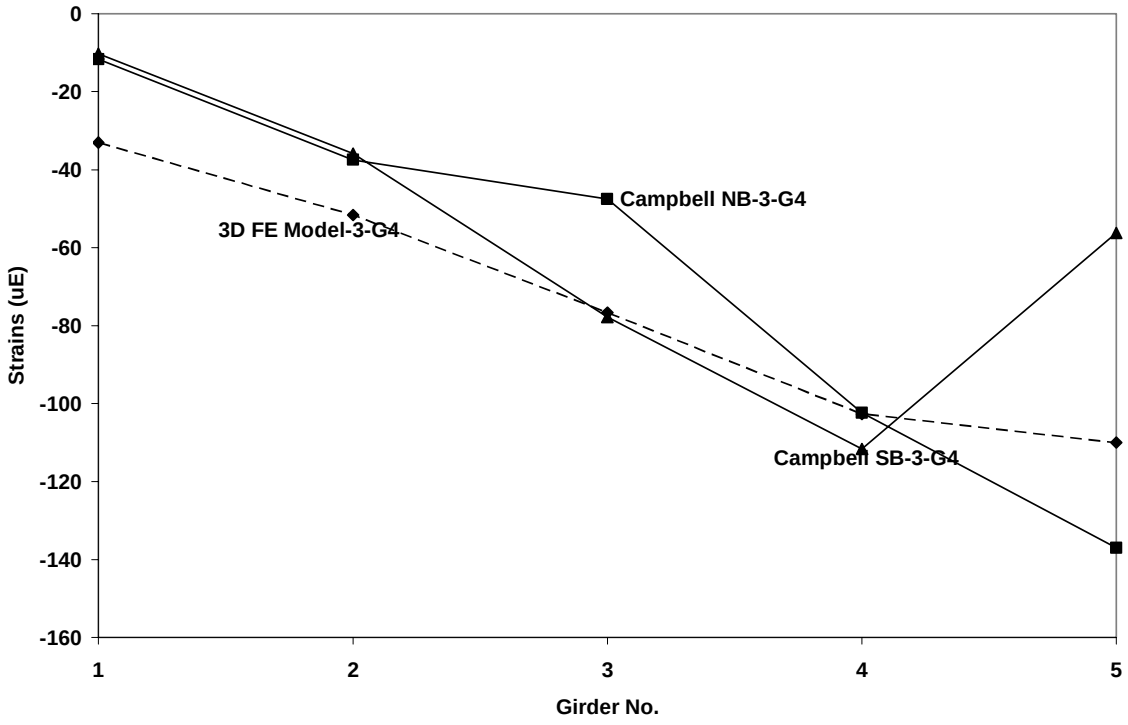


Fig. 3.38 Comparison of Flexural Strains (Campbell NB & SB-3-G4)

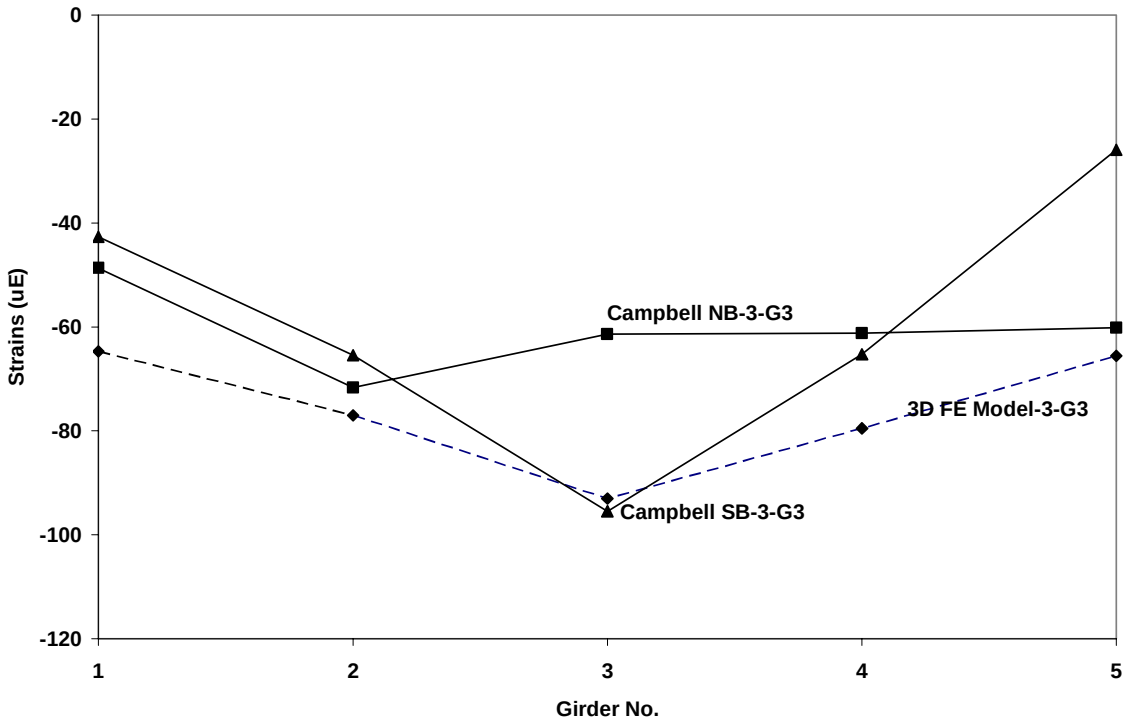


Fig. 3.39 Comparison of Flexural Strains (Campbell NB & SB-3-G3)

*Comparison of Shear Strains:*

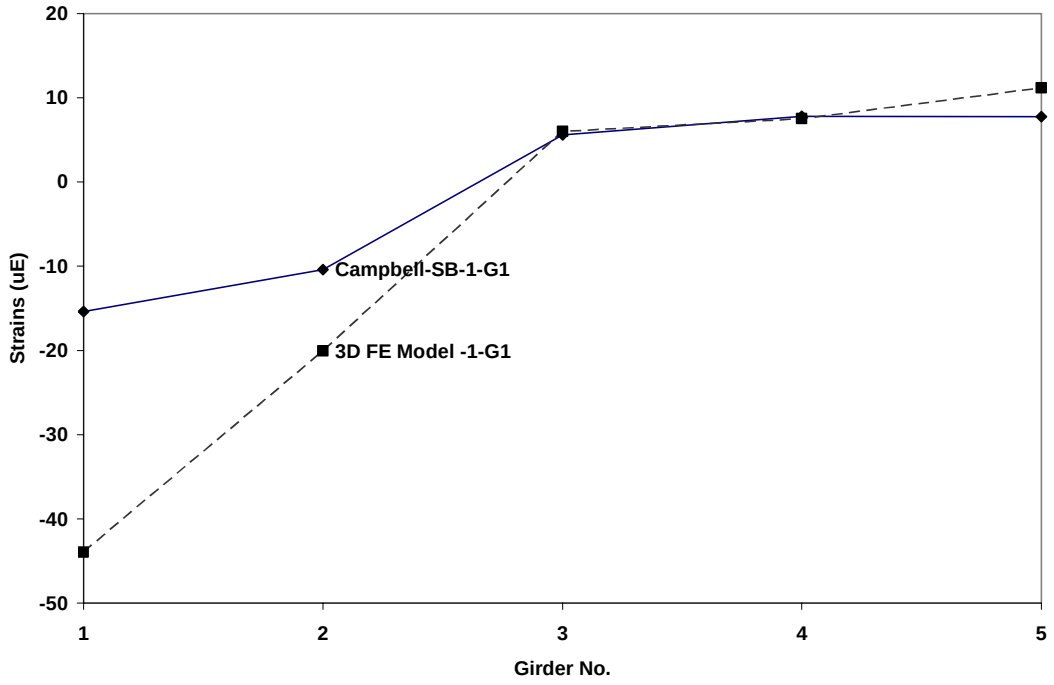


Fig. 3.40 Comparison of Shear Strains (Campbell SB-1-G1_Left)

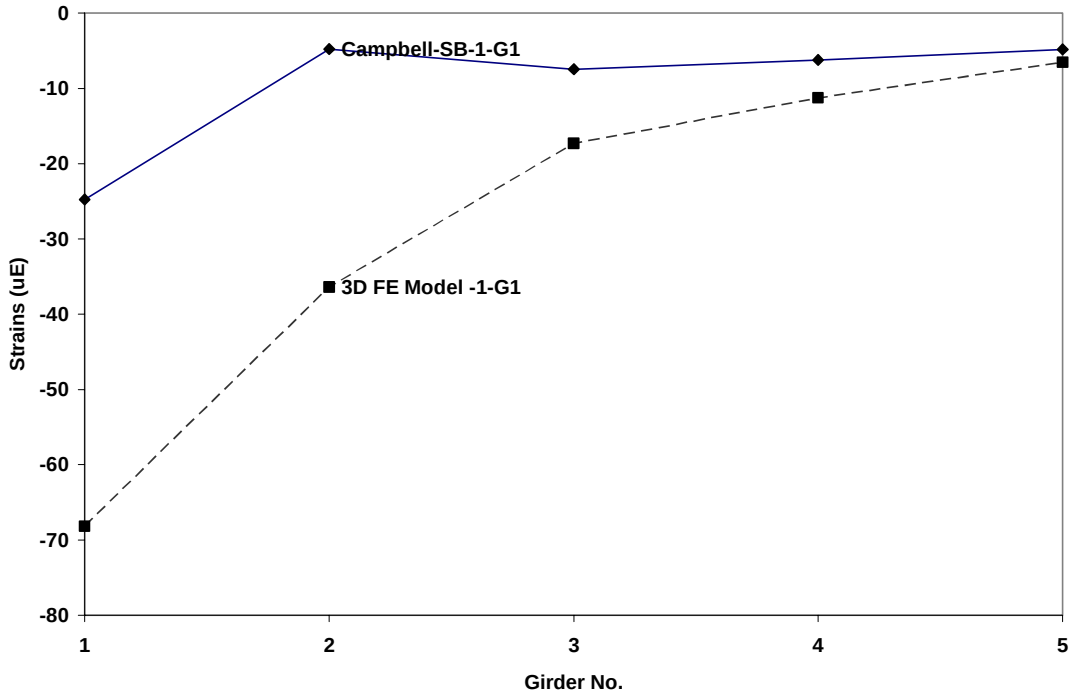


Fig. 3.41 Comparison of Shear Strains (Campbell SB-1-G1_Right)

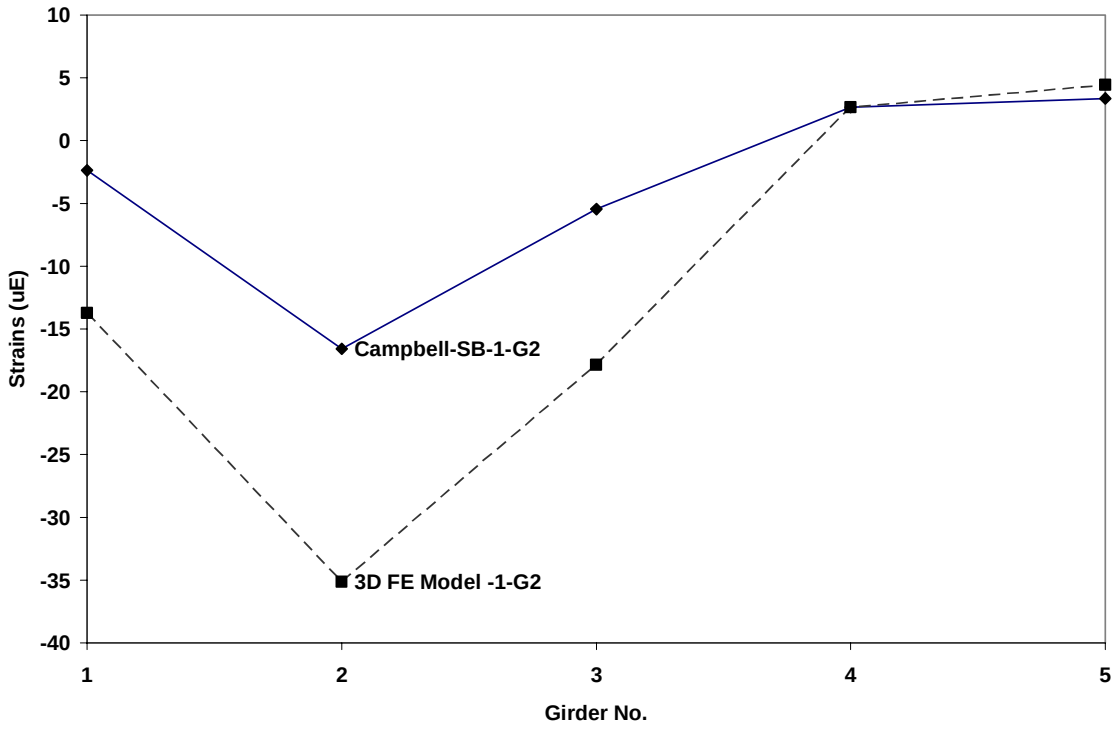


Fig. 3.42 Comparison of Shear Strains (Campbell SB-1-G2_Left)

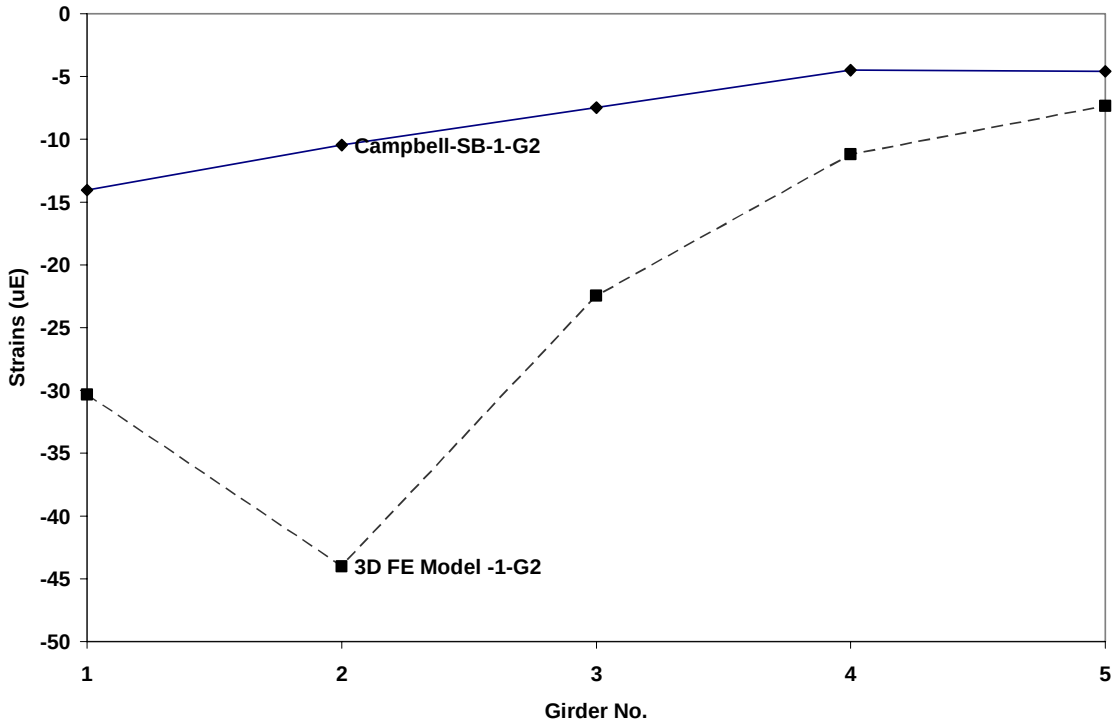


Fig. 3.43 Comparison of Shear Strains (Campbell SB-1-G2_Right)

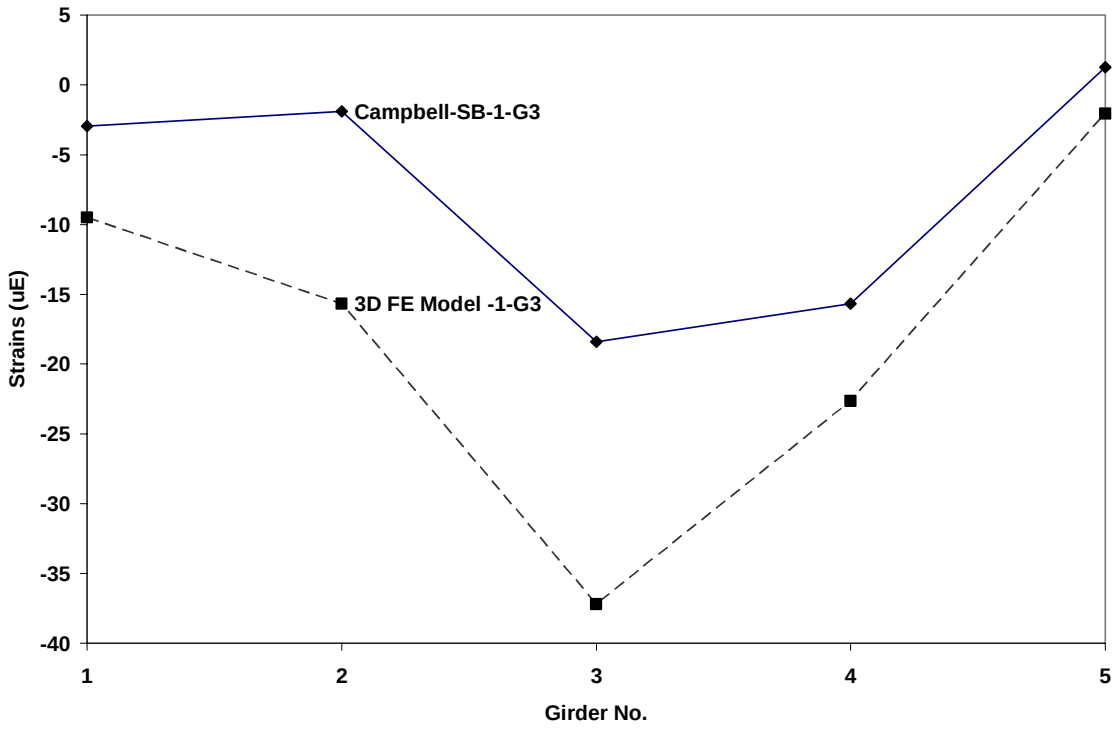


Fig. 3.44 Comparison of Shear Strains (Campbell SB-1-G3_Left)

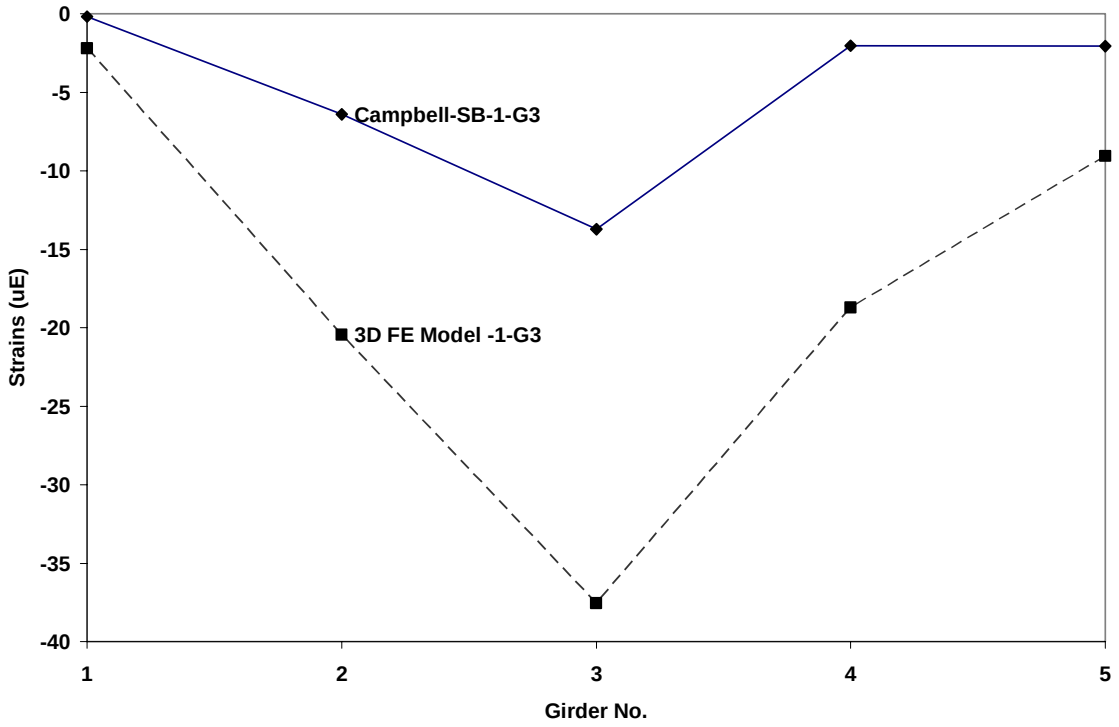


Fig. 3.45 Comparison of Shear Strains (Campbell SB-1-G3_Right)

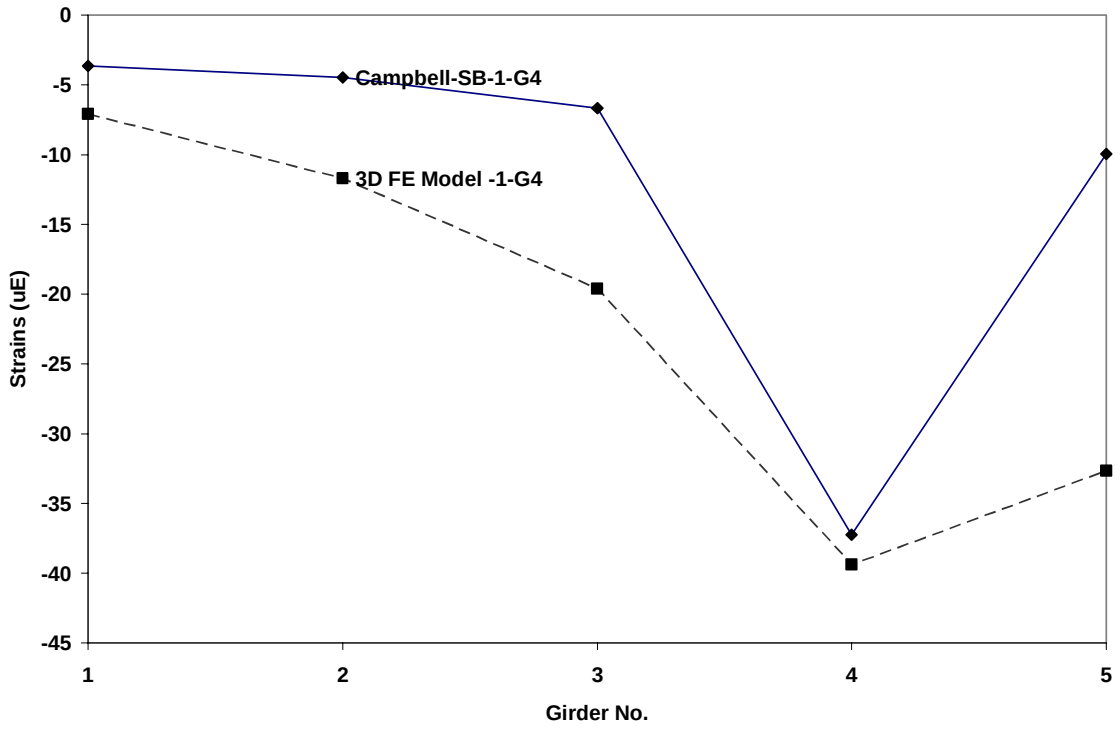


Fig. 3.46 Comparison of Shear Strains (Campbell SB-1-G4_Left)

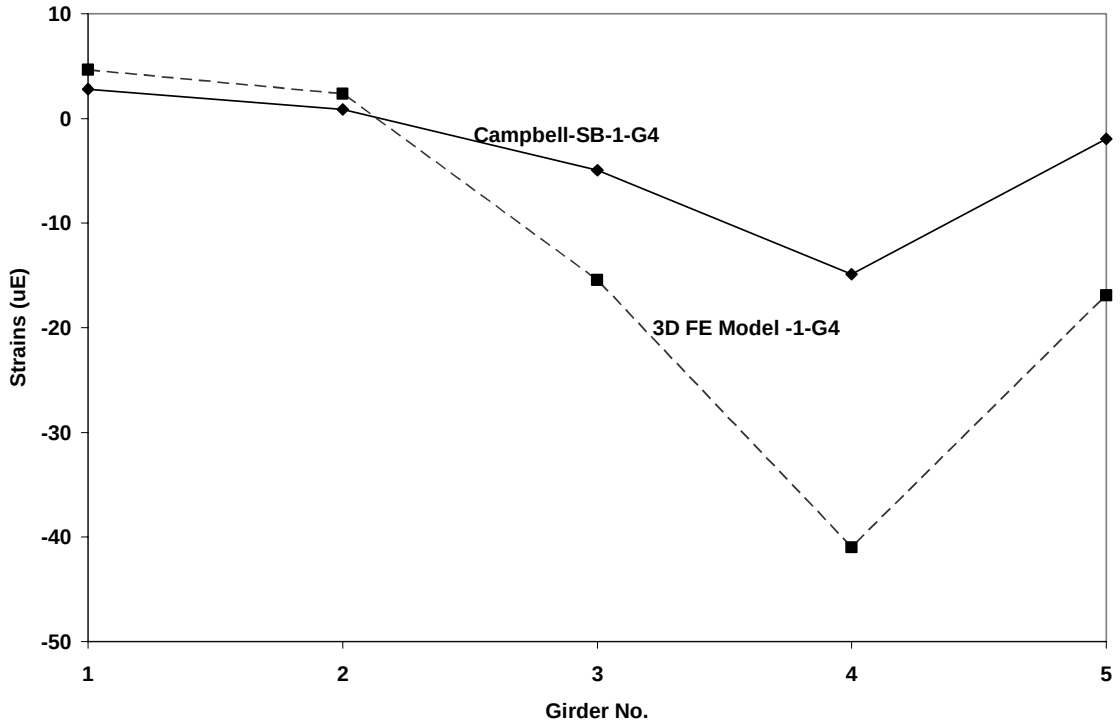


Fig. 3.47 Comparison of Shear Strains (Campbell SB-1-G4_Right)

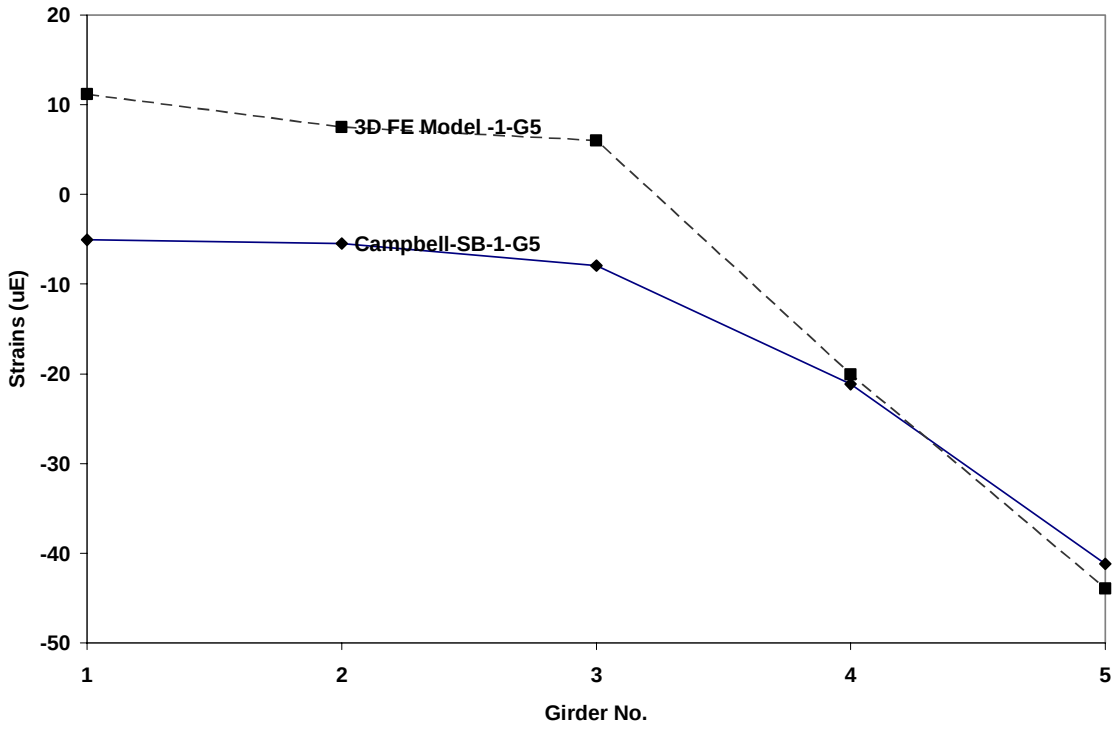


Fig. 3.48 Comparison of Shear Strains (Campbell SB-1-G5_Left)

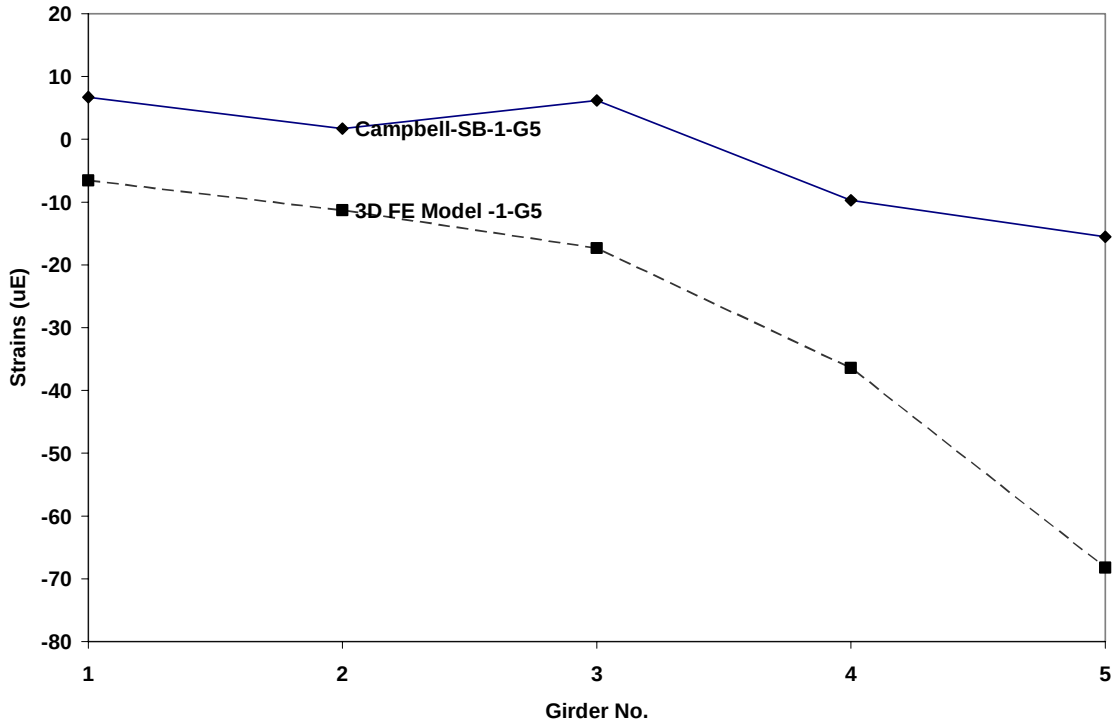


Fig. 3.49 Comparison of Shear Strains (Campbell SB-1-G5_Right)

### 3.2.4 Comparisons with Set 4 Bridges

*Comparison of Flexural Strains:*

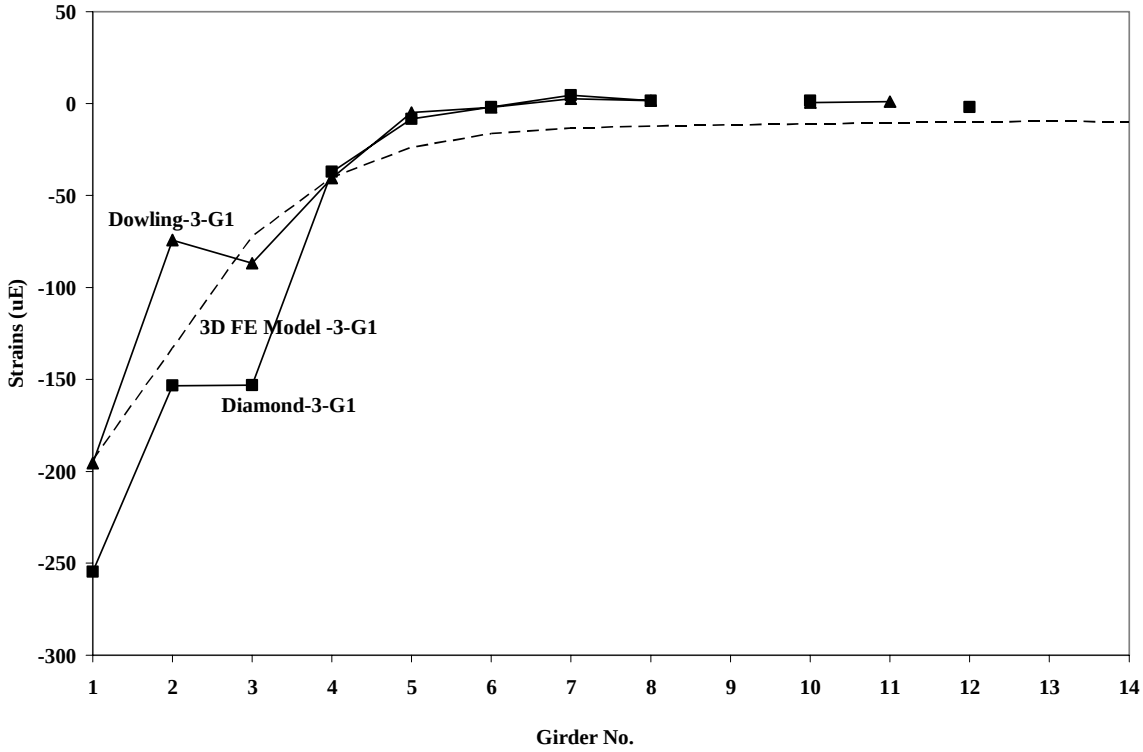


Fig. 3.50 Comparison of Flexural Strains (Diamond & Dowling-3-G1)

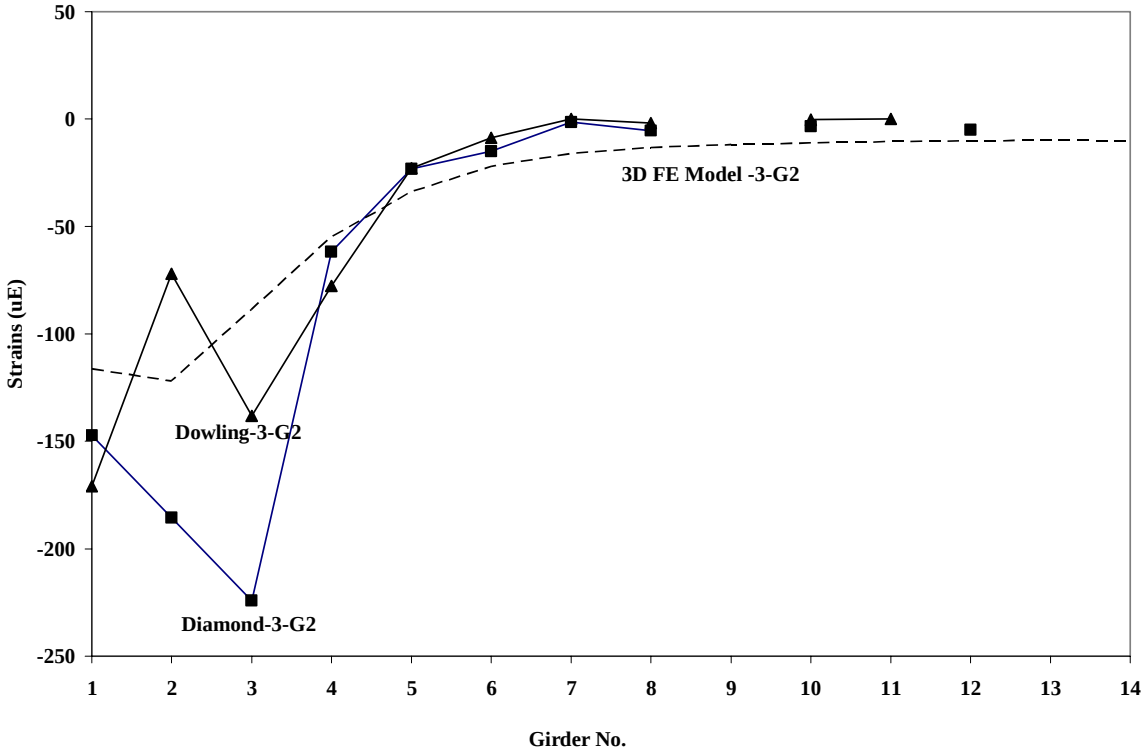


Fig. 3.51 Comparison of Flexural Strains (Diamond & Dowling-3-G2)

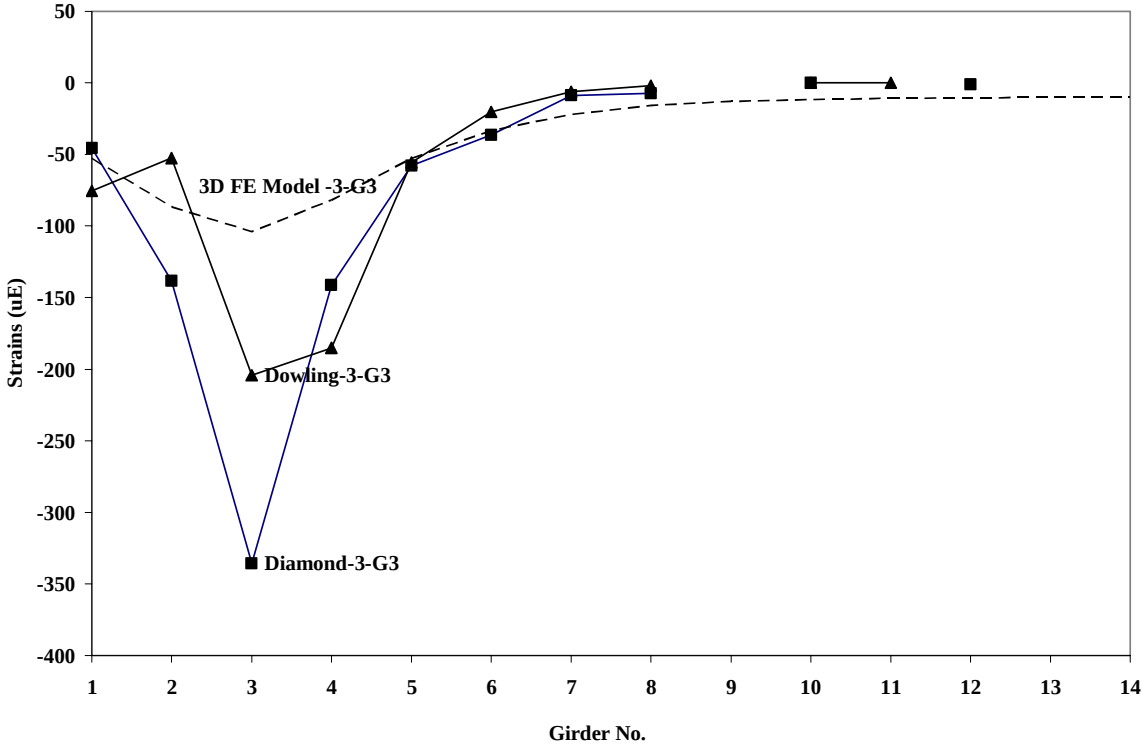


Fig. 3.52 Comparison of Flexural Strains (Diamond & Dowling-3-G3)

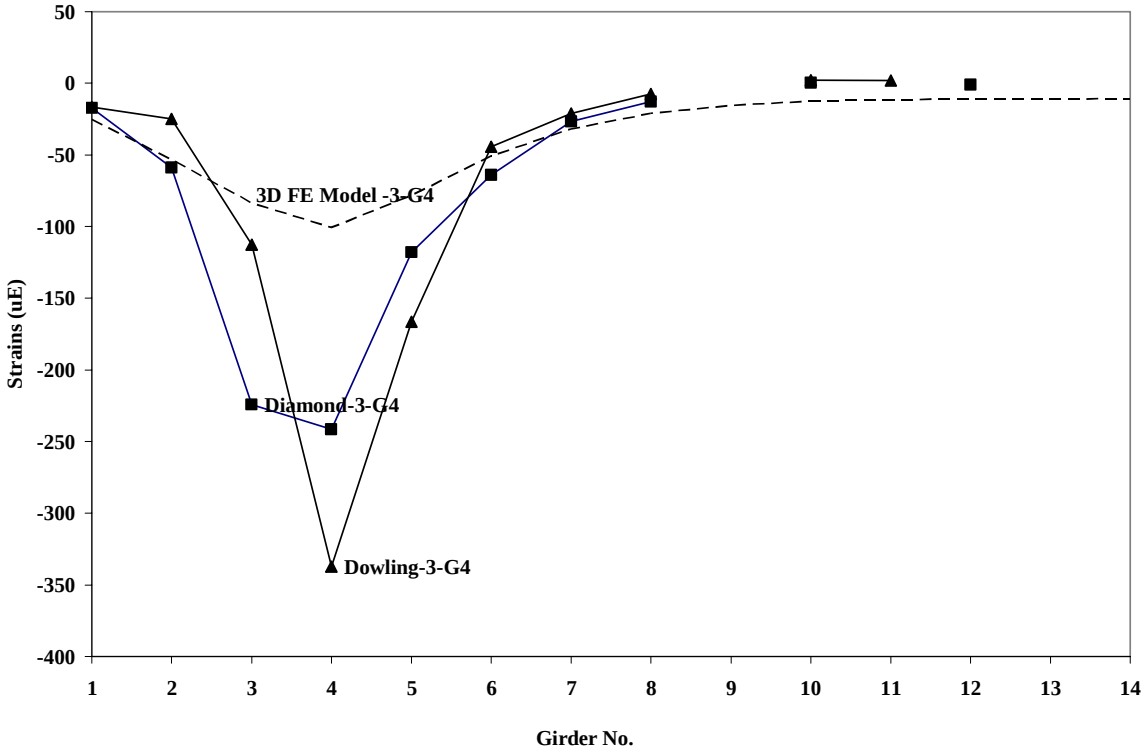


Fig. 3.53 Comparison of Flexural Strains (Diamond & Dowling-3-G4)

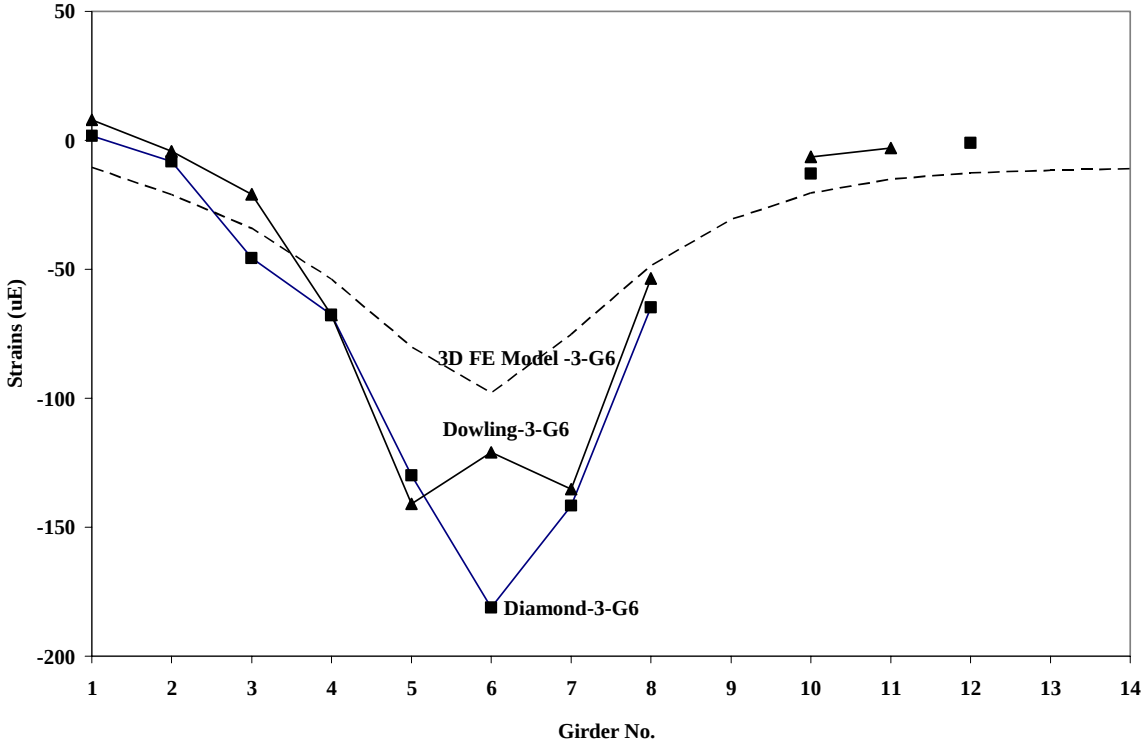


Fig. 3.54 Comparison of Flexural Strains (Diamond & Dowling-3-G6)

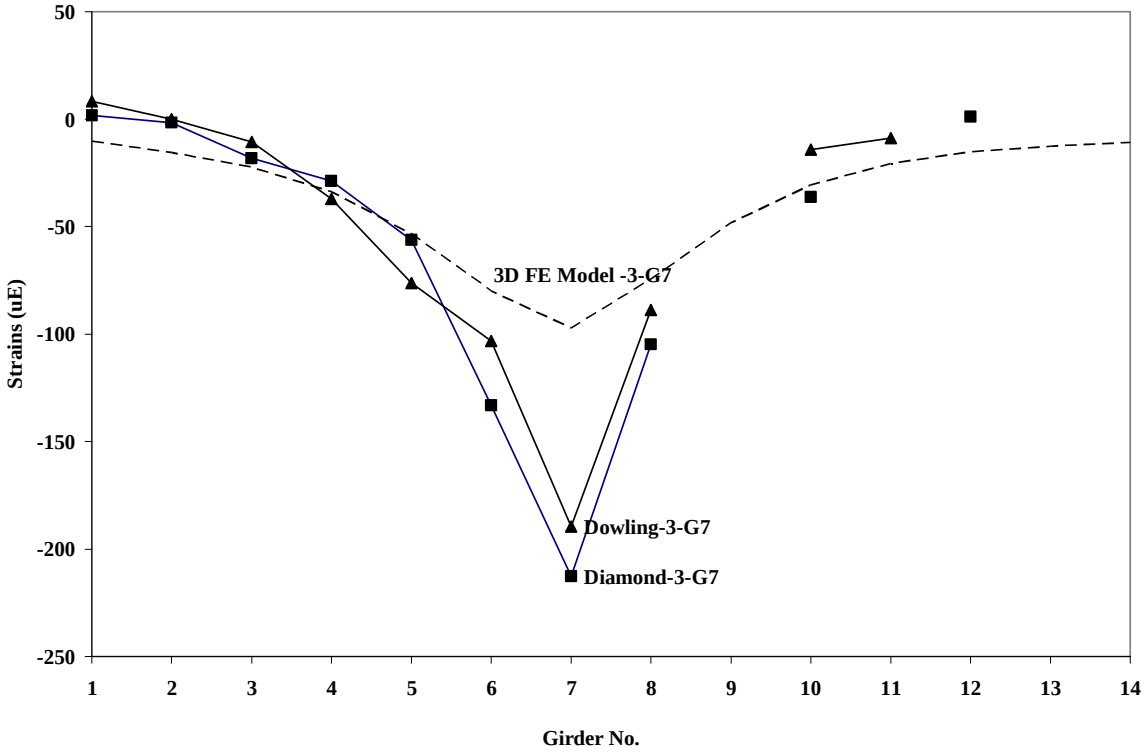


Fig. 3.55 Comparison of Flexural Strains (Diamond & Dowling-3-G7)

*Comparison of Shear Strains:*

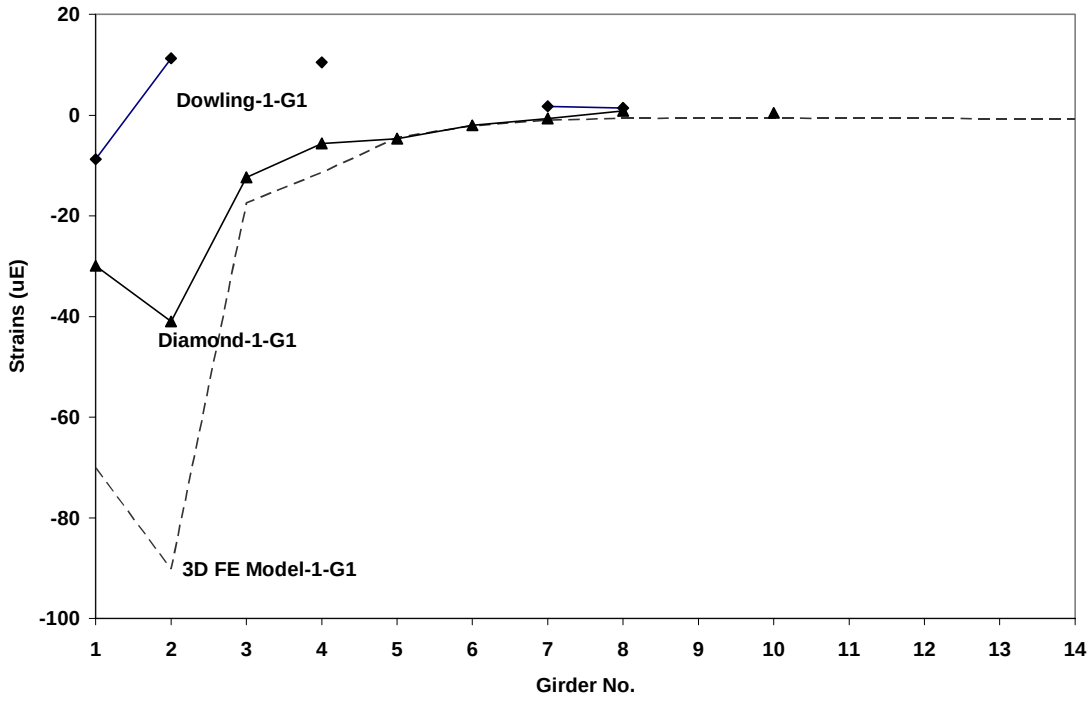


Fig. 3.56 Comparison of Shear Strains (Diamond & Dowling-1-G1_Left)

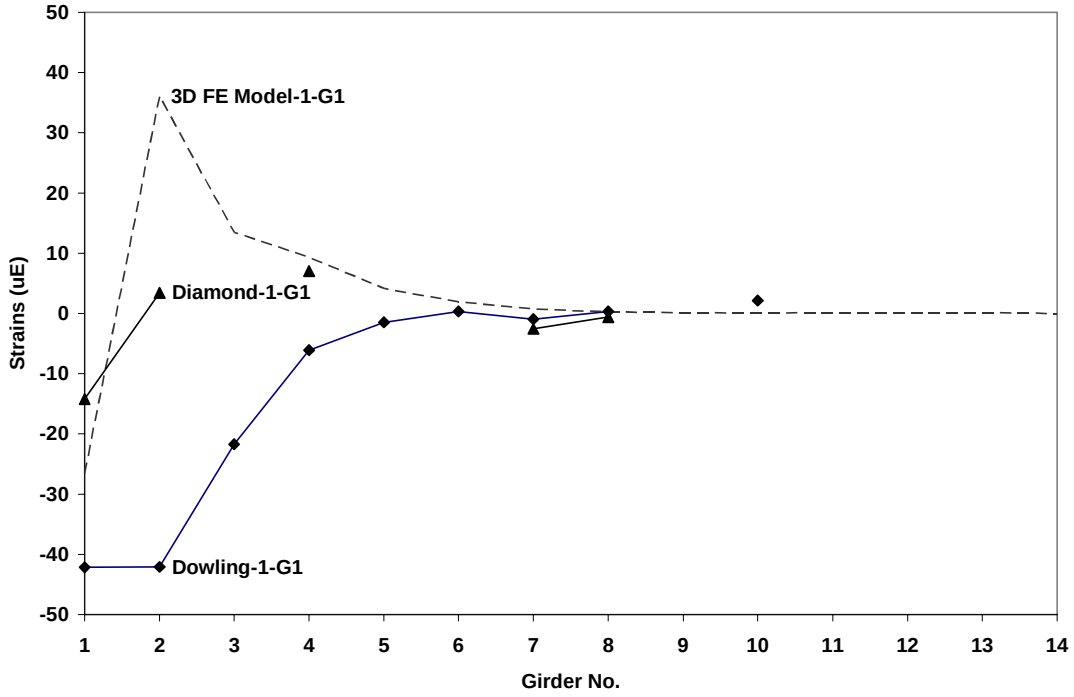


Fig. 3.57 Comparison of Shear Strains (Diamond & Dowling-1-G1_Right)

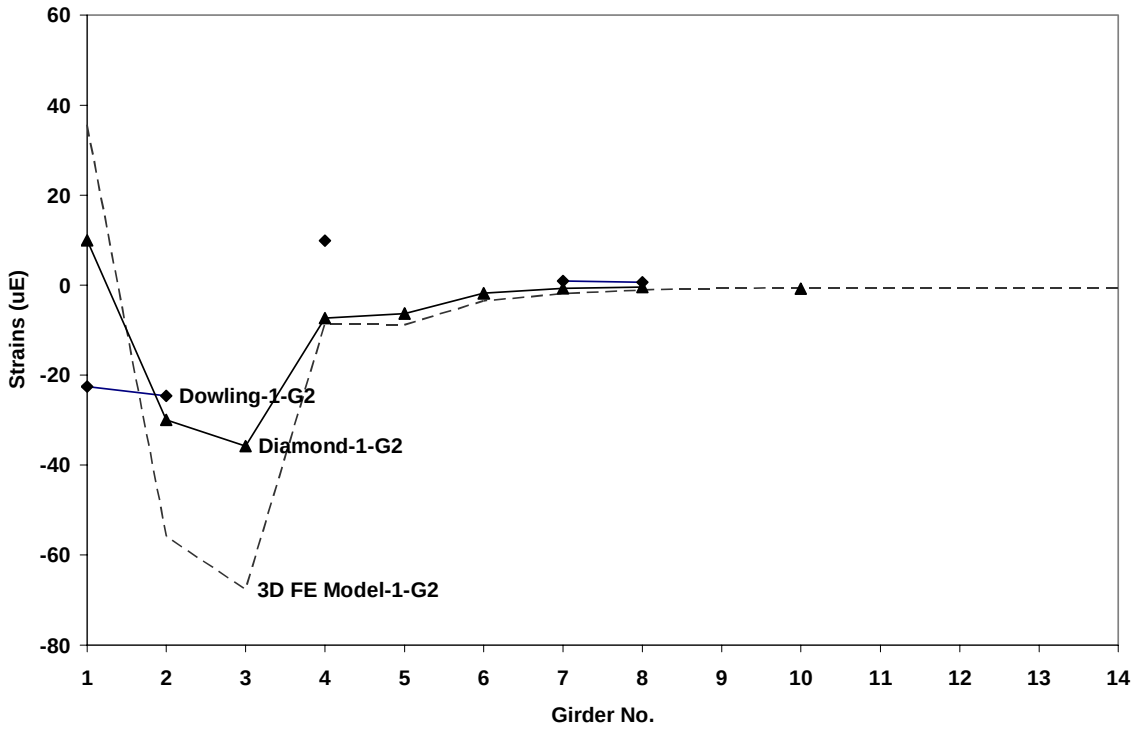


Fig. 3.58 Comparison of Shear Strains (Diamond & Dowling-1-G2_Left)

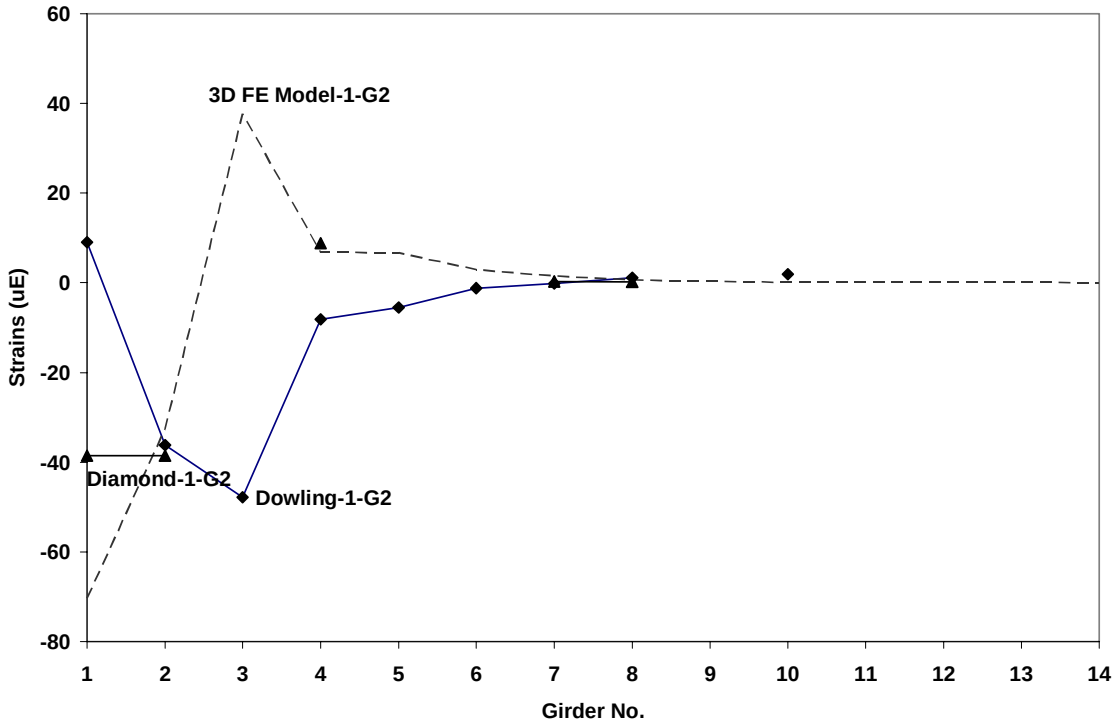


Fig. 3.59 Comparison of Shear Strains (Diamond & Dowling-1-G2_Right)

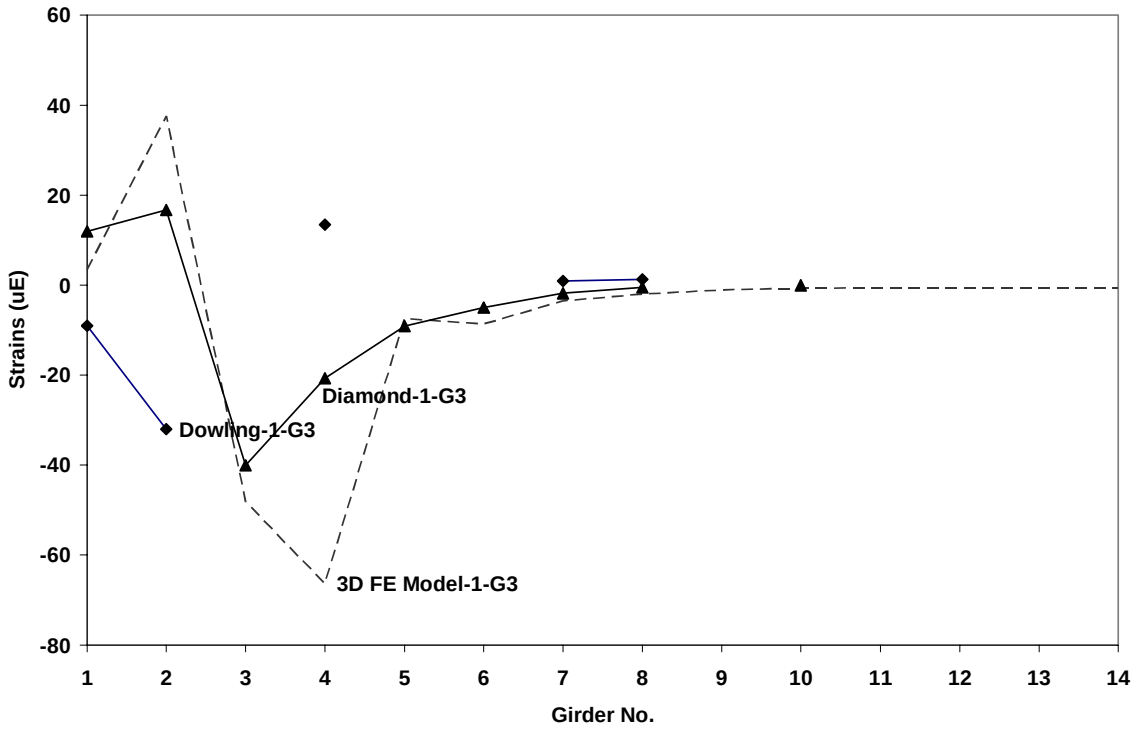


Fig. 3.60 Comparison of Shear Strains (Diamond & Dowling-1-G3_Left)

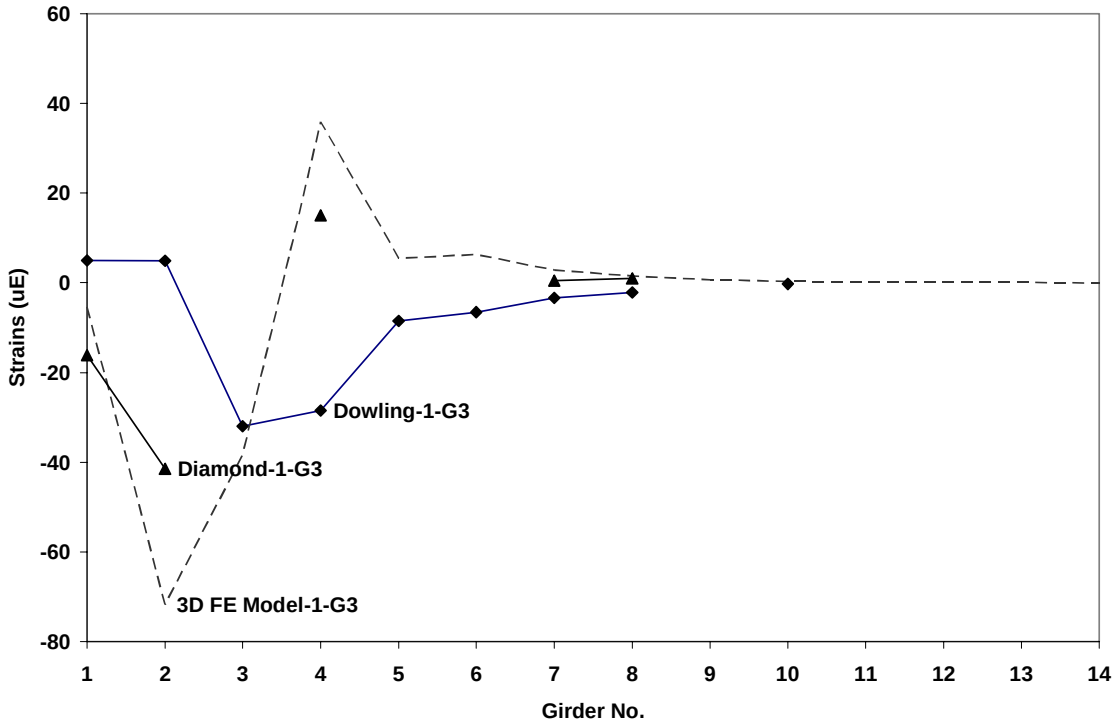


Fig. 3.61 Comparison of Shear Strains (Diamond & Dowling-1-G3_Right)

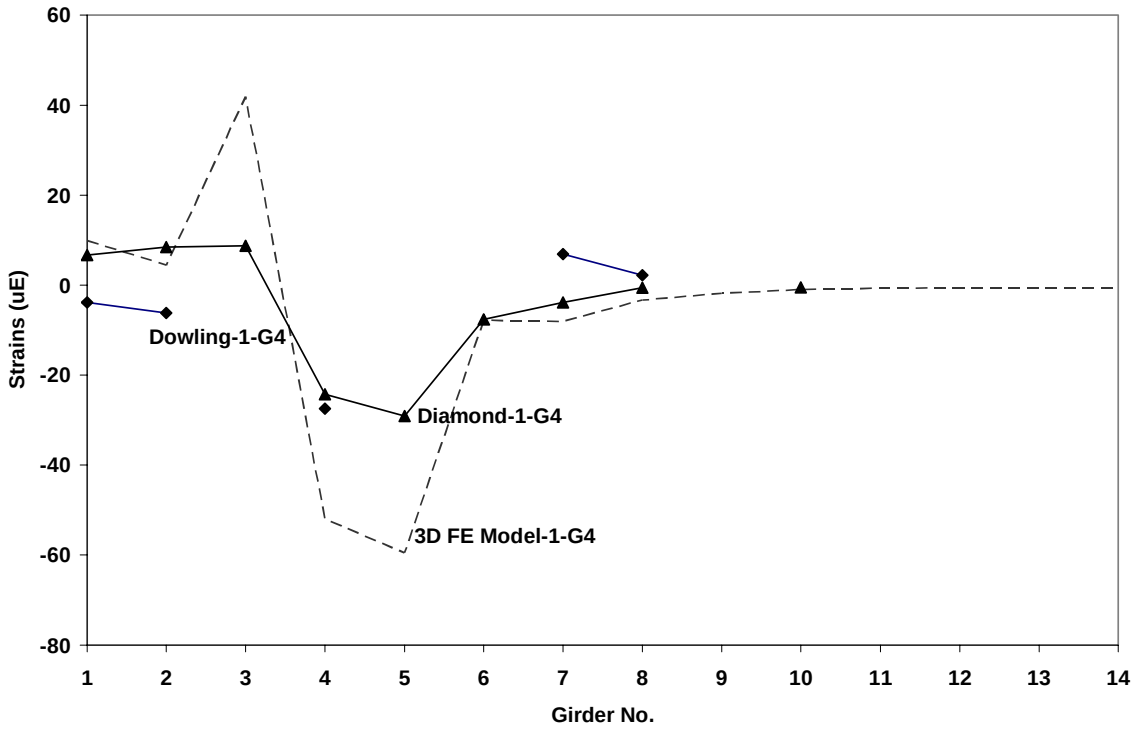


Fig. 3.62 Comparison of Shear Strains (Diamond & Dowling-1-G4_Left)

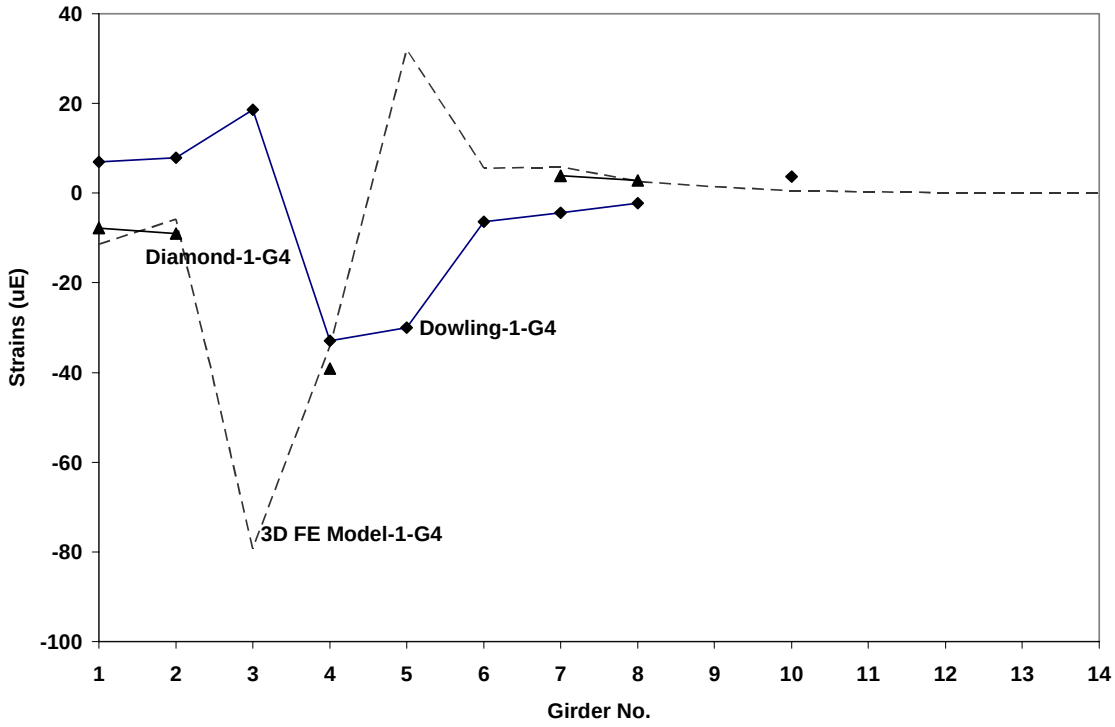


Fig. 3.63 Comparison of Shear Strains (Diamond & Dowling-1-G4_Right)

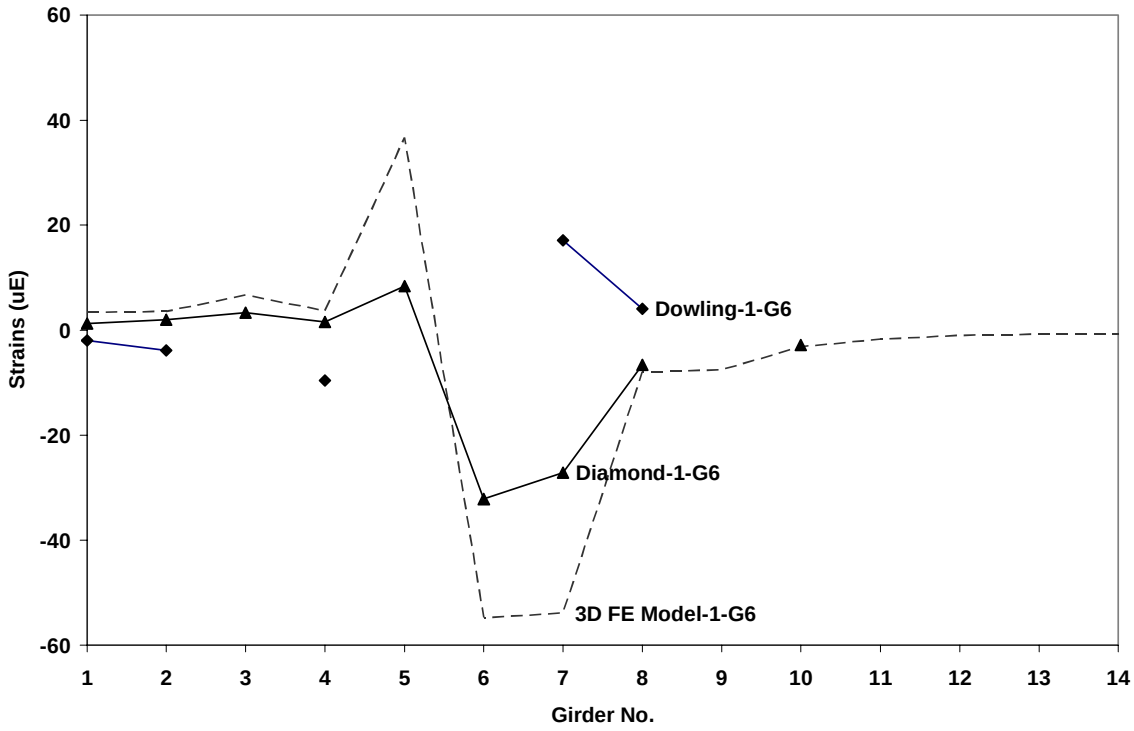


Fig. 3.64 Comparison of Shear Strains (Diamond & Dowling-1-G6_Left)

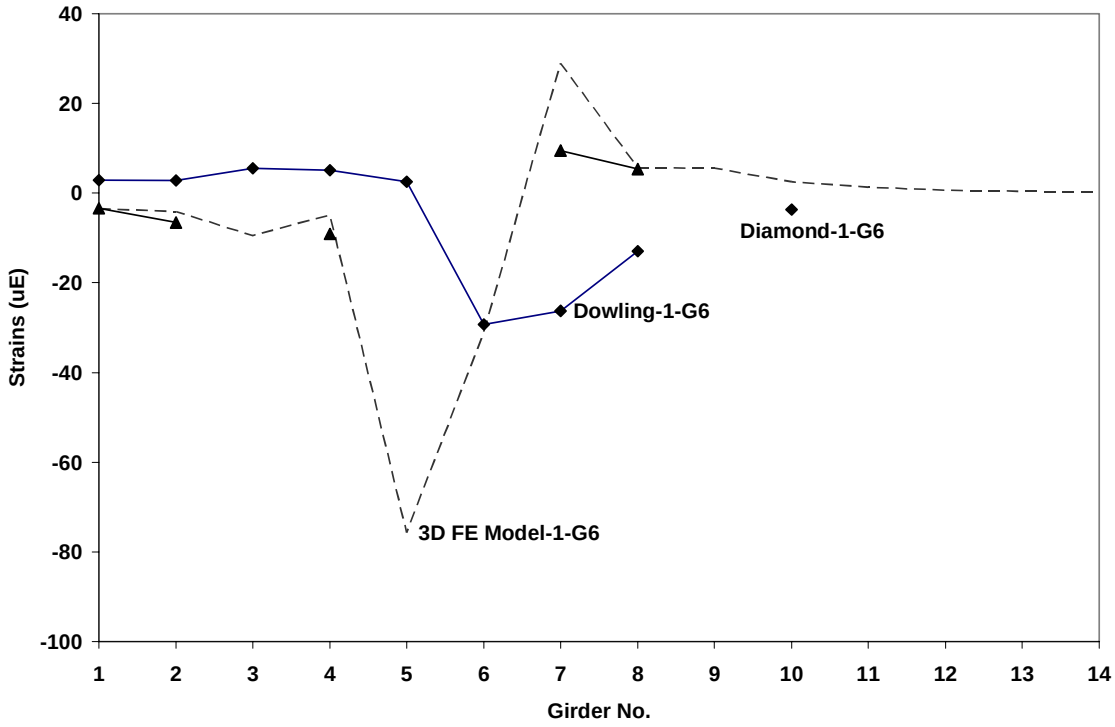


Fig. 3.65 Comparison of Shear Strains (Diamond & Dowling-1-G6_Right)

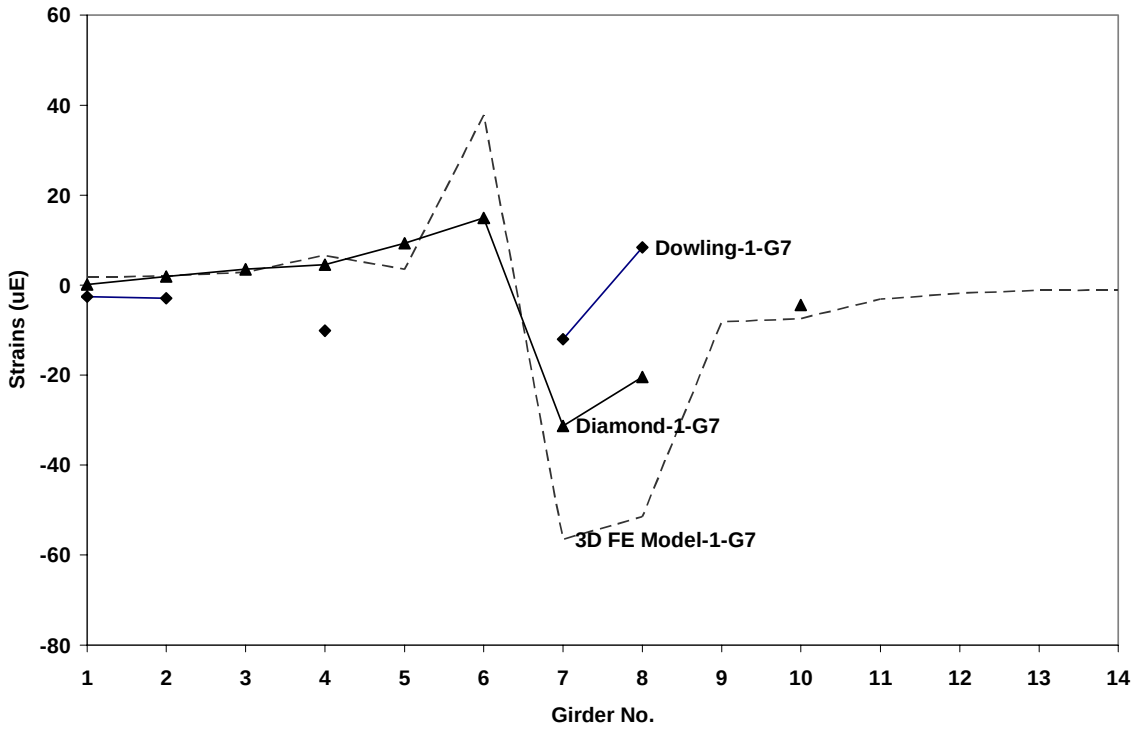


Fig. 3.66 Comparison of Shear Strains (Diamond & Dowling-1-G7_Left)

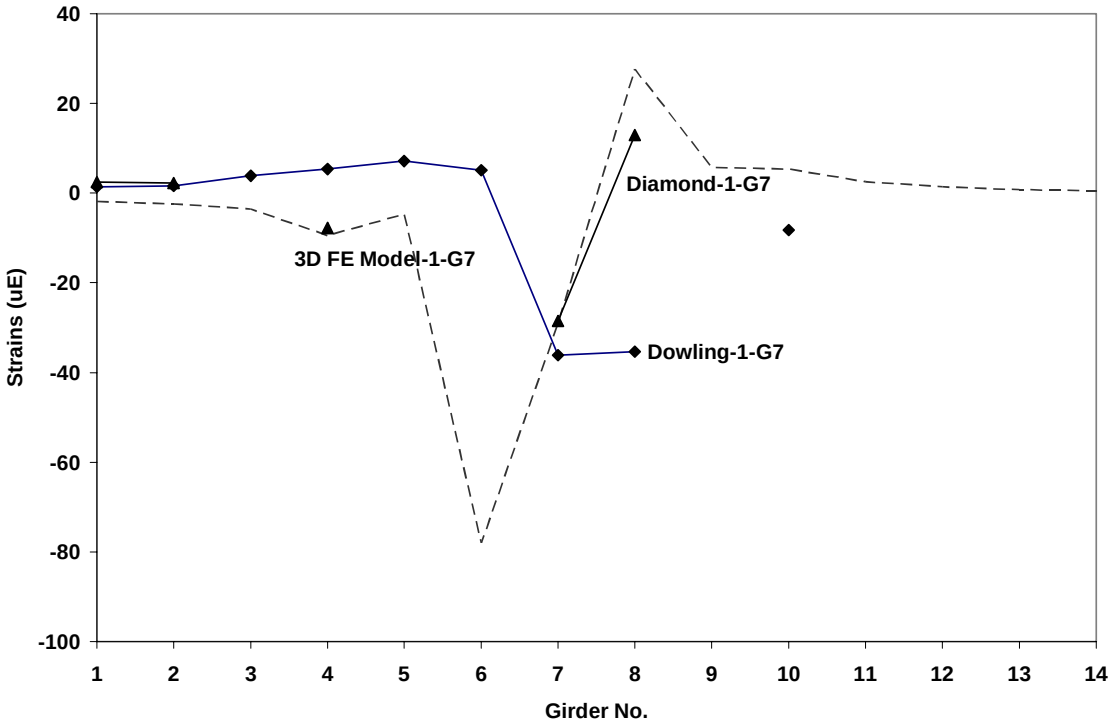


Fig. 3.67 Comparison of Shear Strains (Diamond & Dowling-1-G7_Right)

### 3.3 Discussions

In general, it can be concluded that from the comparisons of strains there is a close match of the modeling results with the experimental ones. It was found that the range of strain variation between field test results and 3D FE modeling results was about the same as the strain variation between field test results for the same set of bridges. Please note that the BDI strain gauges can show a variation of $\pm 10$ micro strains. Of course, the approximation of the modulus of elasticity for concrete can also play a role in causing a difference between modeled strains and field tests.

It was also noted that Diamond and Dowling bridges are the oldest T-girder bridges in the Anchorage area. They were constructed in the early sixties. Over the years, numerous repairs have been done on these bridges. For example, concrete patches are quite noticeable in the bottom flange of the T-girders. In some cases, concrete patches are also observed near the midspan area. Hence the placement of strain gages over the grout becomes inevitable. Owing to excessive patching at the bottom of the third girder of the Dowling Bridge especially at the mid portion of the web, the strain gage had been placed eccentric. Therefore, results depicted from the experiment are not necessarily from the middle of the web. In some cases the results from the experiment vary significantly from the modeled results.

The girders of the Set 3 bridges are post-tensioned. To make up room for the anchorages, the ends of the girders are wider than that at the mid-section. The web narrows abruptly from a width of 13 inches at the support to 6 inches at a distance of 20 inches. The model developed does not take this into consideration to reduce complicacy. It considers an average width of 6 inches throughout the length of the bridge.

When we compare the shear strains, we must keep in mind that the gauges were located at a distance “H” from the end of the concrete diaphragm (H being the height of the superstructure). This region is a very disturbed zone owing to the development of local stresses. Hence it is very difficult to get a clear picture of the stresses originating from shear only.

Moreover, the load position as simulated in the model might not be the exact position as carried out during the testing process. As, all the testing was carried out during the night because of slow traffic, poor visibility due to rain or fog prevented us to place the load in the exact position as desired.

However, as shown in the next chapter we will see that the comparison between live load distribution factors is much better. In summary, we believe that the developed 3D FE models work really well in predicting the load distribution behavior of the decked bulb-tee girder bridges.

# CHAPTER 4 – DISTRIBUTION FACTORS BASED ON FIELD TESTING

In this report, we will present the data as a distribution factor (DF) which we derive from the strain gauges. We will compare these distribution factors to distribution factors derived from the equations presented in the AASHTO LRFD. To determine the moment distribution factors from field testing, we used the following method.

$$DF_{moment} = \frac{\varepsilon_x}{\varepsilon_1 + \varepsilon_2 + \varepsilon_3 + \varepsilon_4 + \varepsilon_5} \tag{4.1}$$

Where $\varepsilon_x$ is the strain measured directly under the loaded girder from the strain gauge at position M1 shown in Figure 2.11, and $\varepsilon_{1to5}$ is the strain measured from all five gauges at position M1 on each respective girder. The single lane distribution factor for shear was calculated in a similar method except each of the girder strains was calculated as an average of the gauges in the S1 position on the left and right side of the girder:

$$\varepsilon_x = \frac{\varepsilon_{S1L} + \varepsilon_{S1R}}{2} \tag{4.2}$$

By determining the shear distribution in this method, the torsional effects on the strain gauges will be averaged out.

## 4.1 DF Analysis of Bridges at 100th Ave and Minnesota (Set 1)

### 4.1.1 Description of the Bridges

Of the eight different bridges tested, the pair located at the intersection of 100th Ave. and Minnesota are the most standard in that they have no skew, have an average span length and width, and are built with typical decked bulb T girders. The bridge is a single span structure. It has a span of 115 ft and no skew. Note, the North Bound and South Bound geometry is the same. Figure 4.1 shows the cross-section of the 100th Ave. bridges.

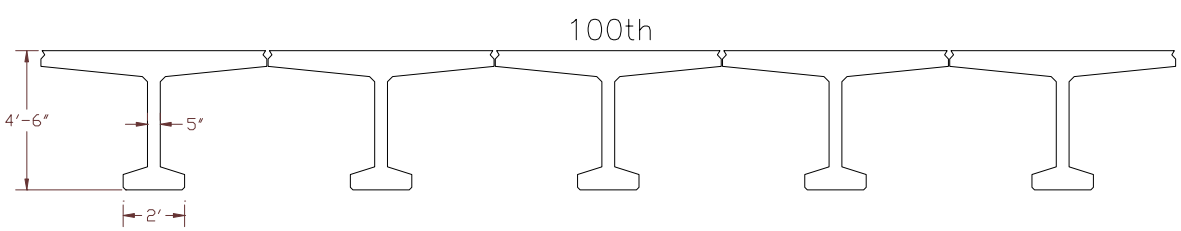


Fig. 4.1 Cross Section of Set 1 Bridges

The deck portion of each girder tapers from a deck thickness of 10.0 in. near the web to a deck thickness of 6.0 in. near the joint. Each longitudinal joint was grouted with a 4.0 in. shear key placed every four feet.

### 4.1.2 Load Distribution Factors for Moment

This section compares the moment distribution factors found from experimental data by using Equation (4.1) to the distribution factors from the AASHTO LRFD equations. Since AASHTO LRFD specifies the same DF equation regardless of number of loaded lanes, it is assumed that the multiple presence factor has been factored out of the AASHTO LRFD equations. According to the AASHTO LRFD Specifications, the load distribution factor, DF, for interior girder moment is calculated by:

$$DF = \frac{S}{D} \tag{4.3}$$

where,

$$\begin{aligned} D &= (11.5 - N_L) + 1.4 N_L (1 - 0.2C)^2 && C \le 5 \\ &= (11.5 - N_L) && C > 5 \end{aligned} \tag{4.4}$$

$$C = K\frac{W}{L} \tag{4.5}$$

$$K = \sqrt{\frac{(1+\mu)I_x}{J}} \tag{4.6}$$

where: S = width of precast member, $\mu$ = Poisson's ratio for girders, $I_x$ = moment of inertia of each girder; J = Saint-Venant's torsional inertia, $N_L$ = number of design lanes, W = edge-to-edge width of bridge, and L = span length of the bridge.

Take the 100th Bridge as an example. The calculation of DF for moments of interior beams ($DF_{IM}$) is shown below using Equations (4.3) to (4.6).

*For Interior Beams:*

$W := 37ft \qquad L := 115ft$

$\theta := 0 \cdot deg \qquad \mu := .2 \qquad A := 1027.25in^2 \qquad N_L := \frac{36}{12}$

$I_x := 358820in^4 \qquad I_y := 360743in^4 \qquad I_p := 727970in^4 \qquad J := \frac{A^4}{40.0 \cdot I_p} \qquad S := 7.40ft$

Thus, distribution factor for moments of interior beams:

$K := \sqrt{\frac{(1+\mu)\cdot I_x}{J}} \qquad K = 3.356 \qquad C := K\cdot\left(\frac{W}{L}\right) \qquad C = 1.08$

Since C is less than 5 $\qquad D := \left[11.5 - N_L + 1.4 \cdot N_L \cdot (1 - 0.2 \cdot C)^2\right] \cdot ft \quad D = 11.082ft$

$$DF_{IM} = \frac{S}{D} = 0.668$$

*For Exterior Beams:*

According to the AASHTO LRFD, the load distribution factor for exterior girder moment is calculated based on the lever rule method, see Figure 4.2.

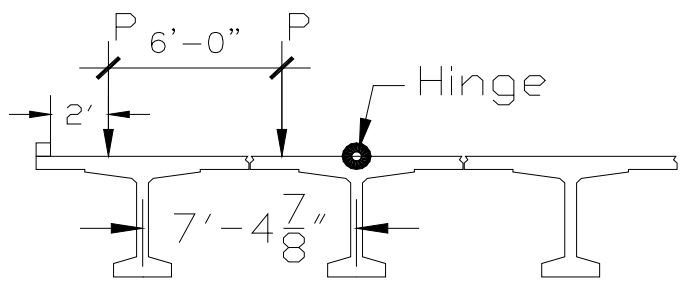


Fig. 4.2 Model for Applying Lever Rule

Distance of left wheel to middle of second girder $d_l$ = 103.0625 in.
Distance of right wheel to middle of second girder $d_r$ = 31.0625 in.
Therefore,

$$DF_{EM} = \frac{d_l + d_r}{2S} = 0.755$$

The moment distribution factors (DFs) from field testing can be calculated using Equation (4.1). For example, we can calculate the moment DF for the Girder 1 of the 100th NB bridge when the load is at the midspan. First, from the figure titled "W100th NB Static Tests over Girder 1 – Strains at Bottom Flange at Midspan" in Section 2.5.1 we find the strains in G1, G2, G3, G4, and G5 are -344, -259, -125.5, -38.4, and 34 micro strains respectively. The distribution factor for the Girder 1 when the load is over the Girder 1 is then found using the following:

$$\frac{-344}{-344 - 259 - 125.5 - 38.4 + 34} = 0.469$$

Similarly, we can find the moment distribution factors for Girder 2, Girder 3, Girder 4, and Girder 5 when the load is over the Girder 1 are 0.353, 0.171, 0.052, and -0.046 respectively. If we repeat the same process to calculate the moment distribution factors for all five girders when the load is moved over to Girder 2, we find the following DF values of 0.230, 0.304, 0.243, 0.140, and 0.083 for Girder 1, Girder 2, Girder 3, Girder 4, and Girder 5 respectively. Figure 4.3 shows the results. The moment distribution factors when the load is at Girder 4 and Girder 5 are shown in Figure 4.4. The distribution factor for girder number two in Figure 4.3 is largest when the load vehicle drives closest to the edge of the bridge in the G1 position. The same trend is apparent on the other side of the bridge where girder number four in Figure 4.4 is largest when the load vehicle drives in the G5 position. This shows that for this particular bridge, the worst loading condition for an interior girder is when the vehicle drives closest to the edge of the bridge not when the vehicle is centered over the top of the girder.

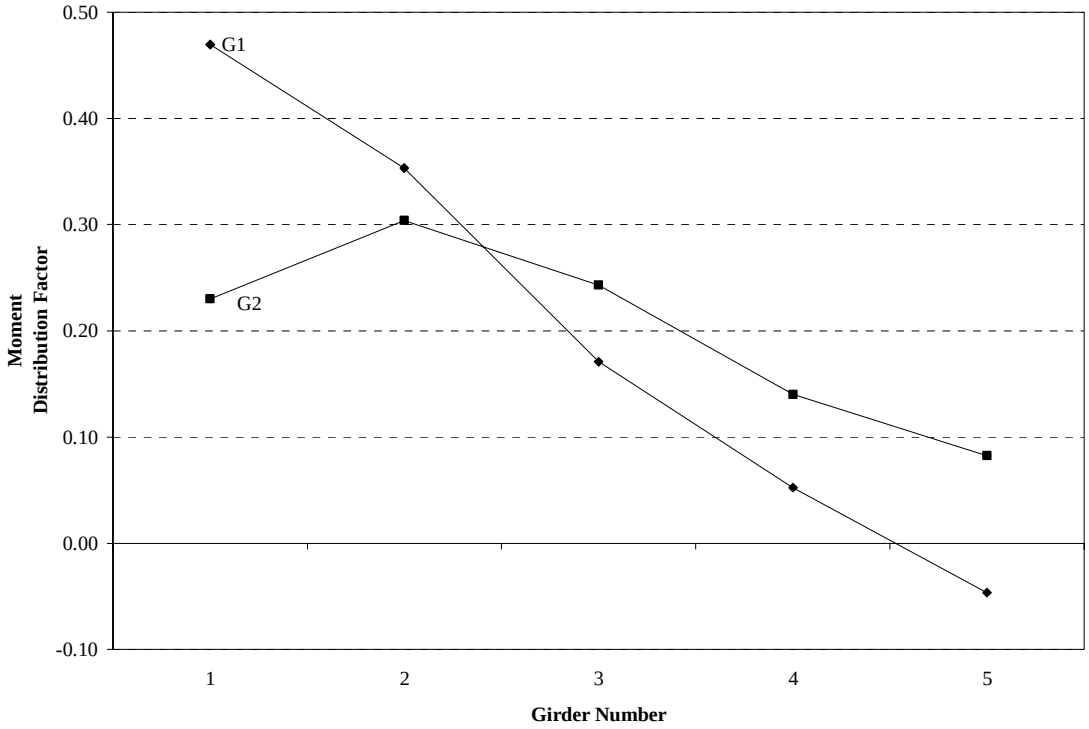


Fig. 4.3 Moment Distribution Factors (100th NB – 3 – G1&G2)

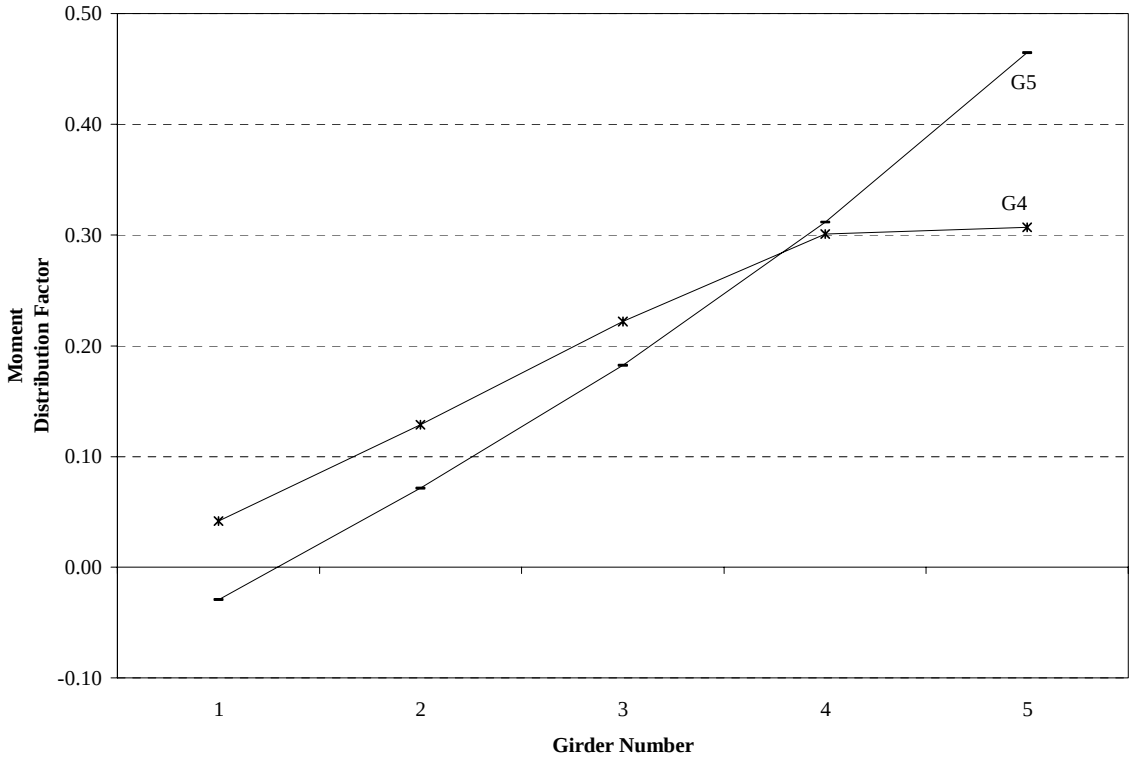


Fig. 4.4 Moment Distribution Factors (100th NB – 3 – G4&G5)

Figures 4.5 and 4.6 show distribution factors for girder moment at 100th Ave. bridges (Set 1). Hereafter, the load distribution for determining girder moment will be referred to as "moment distribution." The maximum moment distribution factors of the interior girders are 0.353 for the 100th NB and 0.365 for the 100th SB. These values are based on field tests. This same moment distribution was predicted to be 0.668 by the AASHTO LRFD. Moment distribution factors for exterior girders are 0.470 for the 100th NB and 0.438 for the 100th SB. These compare with the AASHTO LRFD prediction of 0.755.

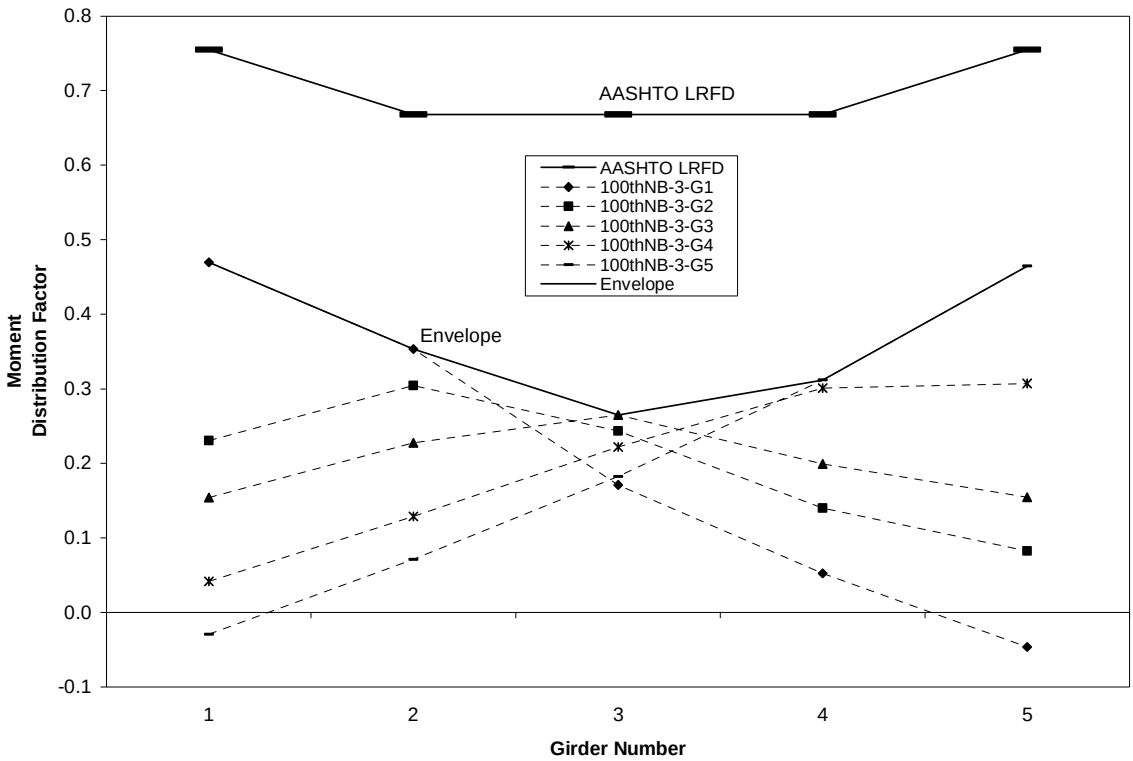


Fig. 4.5 Load Distribution Factors for Moment (100th NB Bridge)

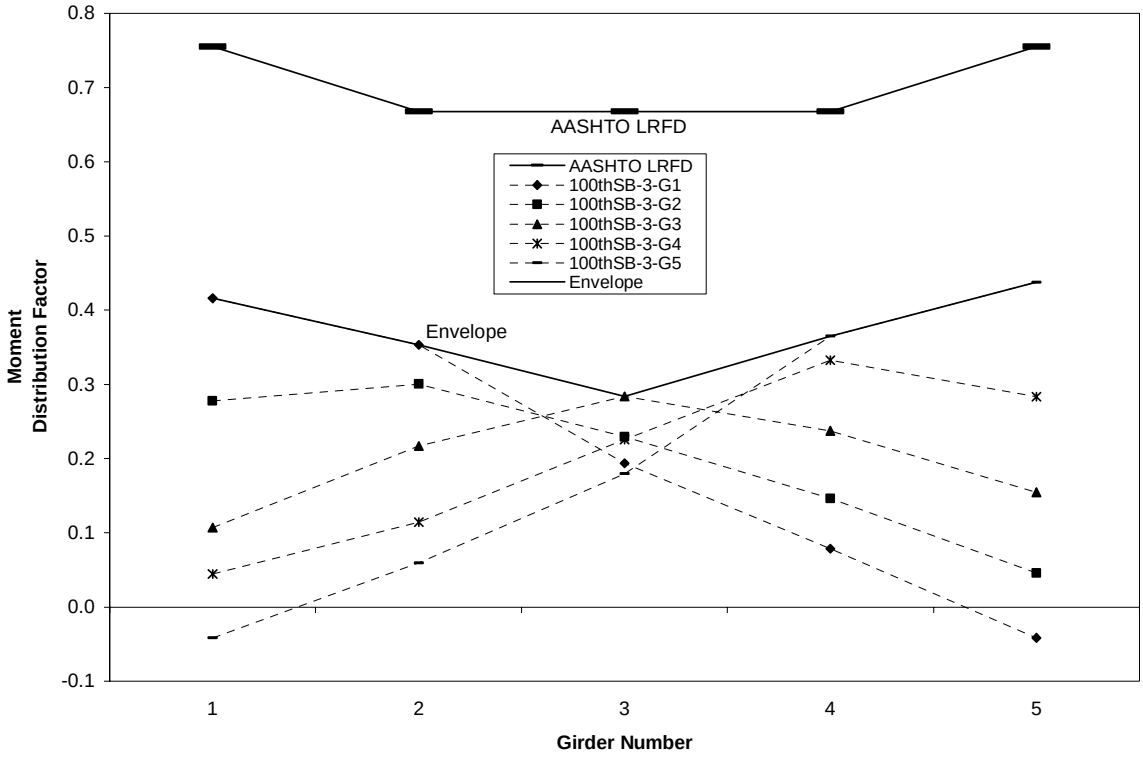


Fig. 4.6 Load Distribution Factors for Moment (100th SB Bridge)

Please note that the G1 and G5 loading on this bridge produce the greatest distribution factors for both the exterior and interior girders. Table 4.1 shows a summary of the moment distribution factors found from 100th NB and SB bridges based on field testing results.

Table 4.1 Distribution Factor for Moment for Set 1 Bridges

| Bridges | Interior Girders | | Exterior Girders | |
|---|---|---|---|---|
| | G2 | G4 | G1 | G5 |
| 100th NB | .35 | .31 | .47 | .46 |
| 100th SB | .35 | .37 | .42 | .44 |
| Average | .35 | | .45 | |

### 4.1.3 Load Distribution Factors for Shear

Shear distribution factors found from experimental data using Equations (4.1) and (4.2) were compared with factors calculated by the lever rule method as specified in AASHTO LRFD Specifications.

Again, take the 100th Bridge as an example. The DF for shear of interior beams ($DF_{IS}$) is shown below.

*For Interior Beams:*
Figure 4.7 shows the lever rule model.

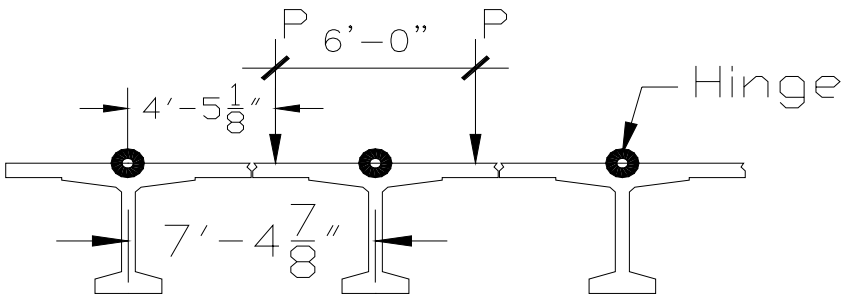


Fig. 4.7 Model for Applying Lever Rule

Distance of left wheel to middle of outside girder $d_0$ = 4'-5 1/8" = 53.125 in.

$$DF_{IS} = \frac{d_0}{S} = 0.598$$

*For Exterior Beams:*
The distribution factor for shear of the exterior beams is the same as the factor for moment of the exterior beams, i.e.,

$$DF_{ES} = DF_{EM} = \frac{d_l + d_r}{2S} = 0.755$$

The shear distribution factor based on field testing results can be found in a similar manner as for moment distribution factors. The only difference is that the strain values from the left and right side of each girder must be averaged.

Figures 4.8 and 4.9 show the shear distribution factor for 100th North Bound, and Figures 4.10 and 4.11 show the shear distribution factor for 100th South Bound. The shear distribution factors of the 100th ave bridges were larger than the moment distribution factors. The worst loading condition for shear distribution always occurred when the load vehicle drove directly over the top of the girder regardless whether or not the girder was an interior or exterior girder.

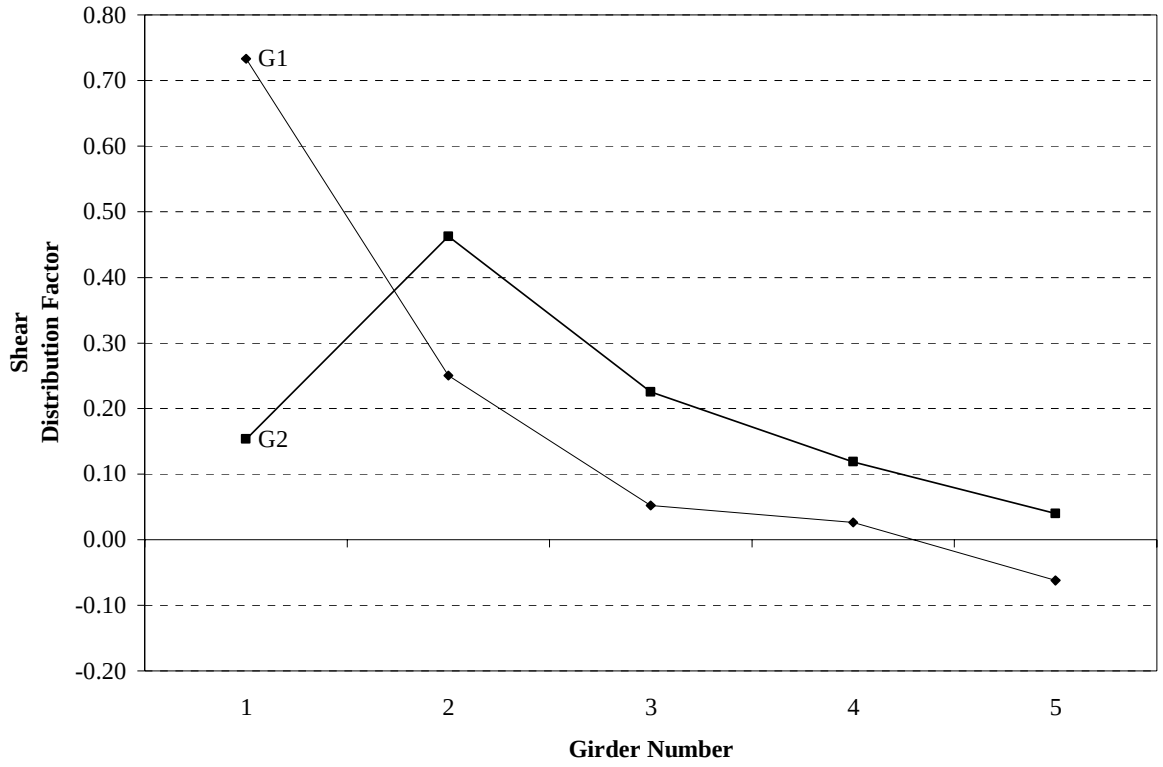


Fig. 4.8 Shear Distribution Factor (100th NB – 1 – G1&G2)

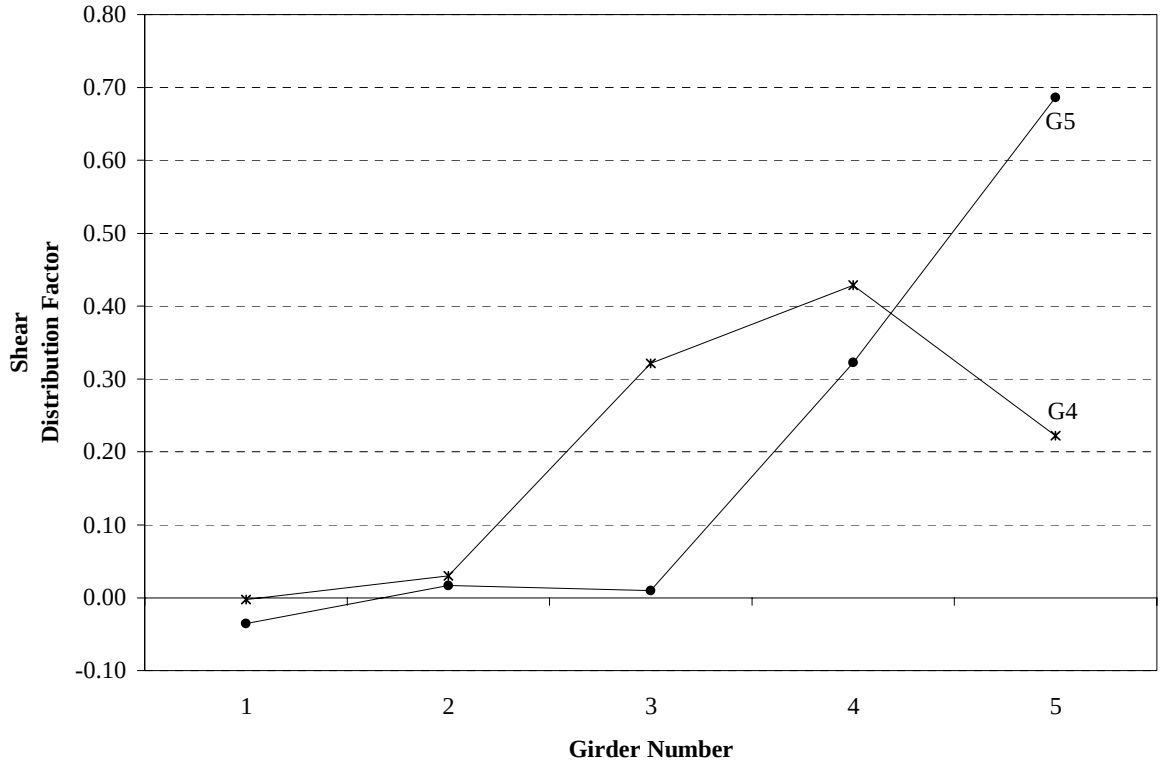


Fig. 4.9 Shear Distribution Factor (100th NB – 1 – G4&G5)

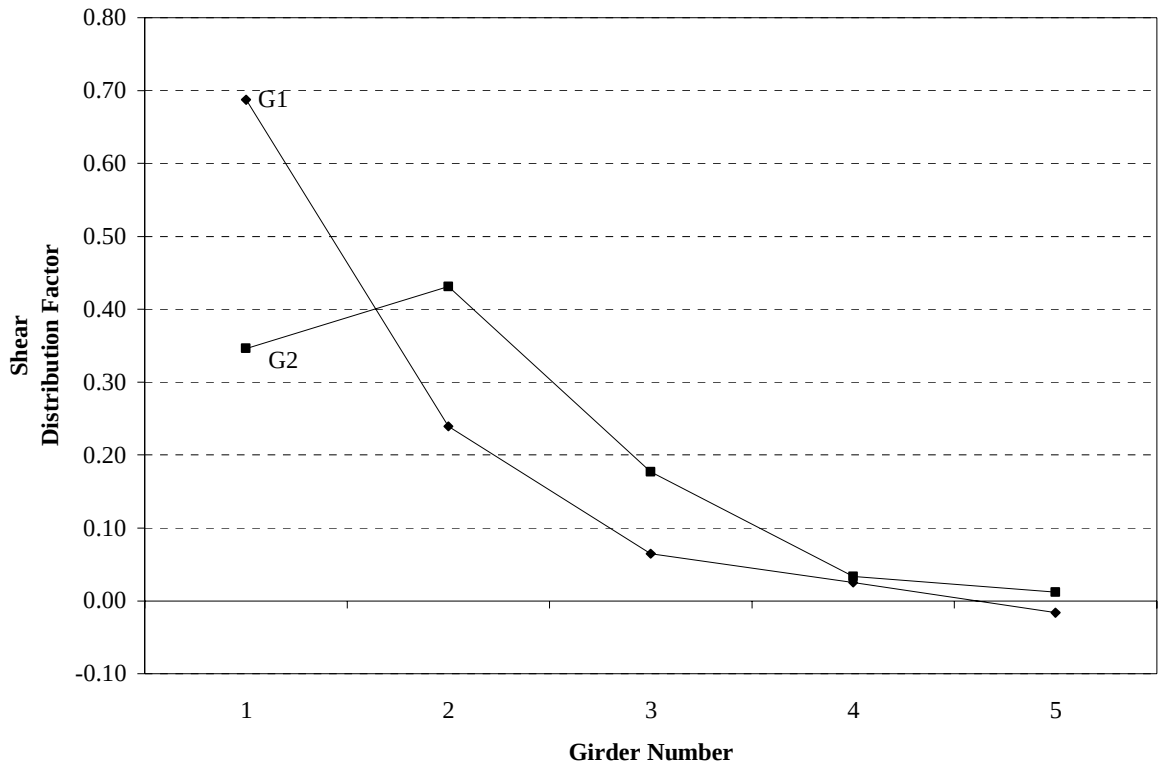


Fig. 4.10 Shear Distribution Factor (100th SB – 1 – G1&G2)

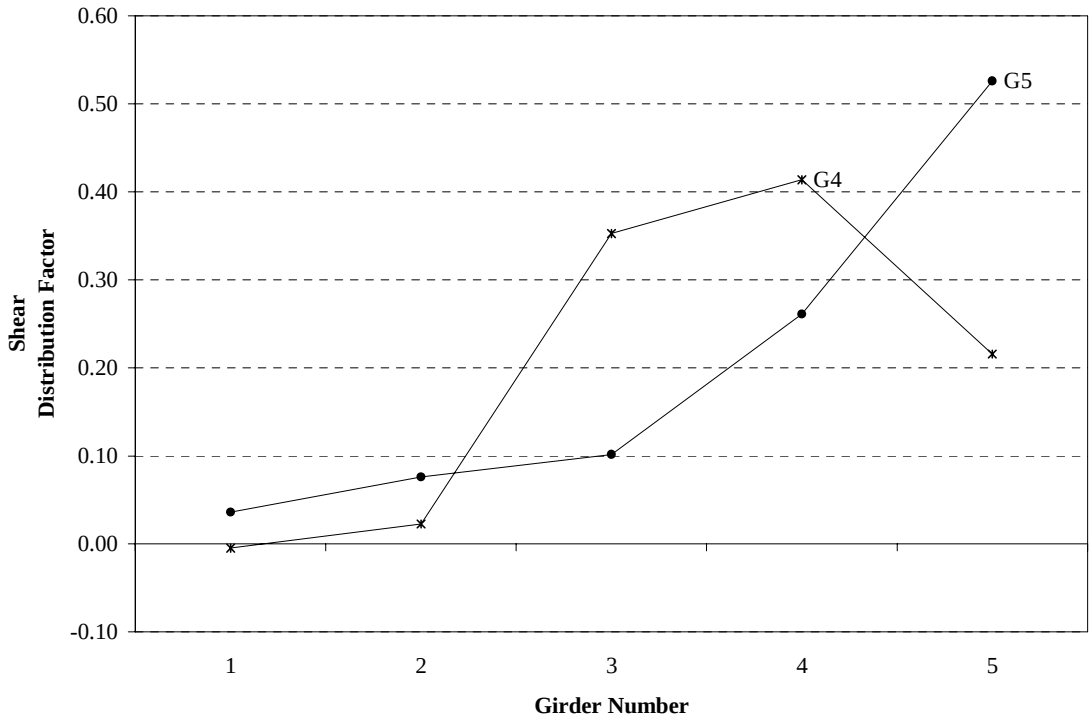


Fig. 4.11 Shear Distribution Factor (100th SB – 1 – G4&G5)

Figures 4.12 and 4.13 show the shear distribution factors for the 100th Street bridges. Based on test results, maximum shear distribution factors of the interior girders are 0.463 for 100th NB and 0.431 for 100th SB. Compare these values with 0.598 which is predicted by the AASHTO LRFD. The shear distribution factors for exterior girders are 0.733 for the 100th NB and 0.688 for the 100th SB. This compares with AASHTO LRFD prediction of 0.755.

Table 4.2 shows a summary of the shear distribution factors found from 100th NB and SB bridges.

Table 4.2 Distribution Factor for Shear for Set 1 Bridges

| Bridges | Interior Girders | | Exterior Girders | |
|---|---|---|---|---|
| | G2 | G4 | G1 | G5 |
| 100th NB | .46 | .43 | .73 | .69 |
| 100th SB | .43 | .41 | .69 | .53 |
| Average | .43 | | .66 | |

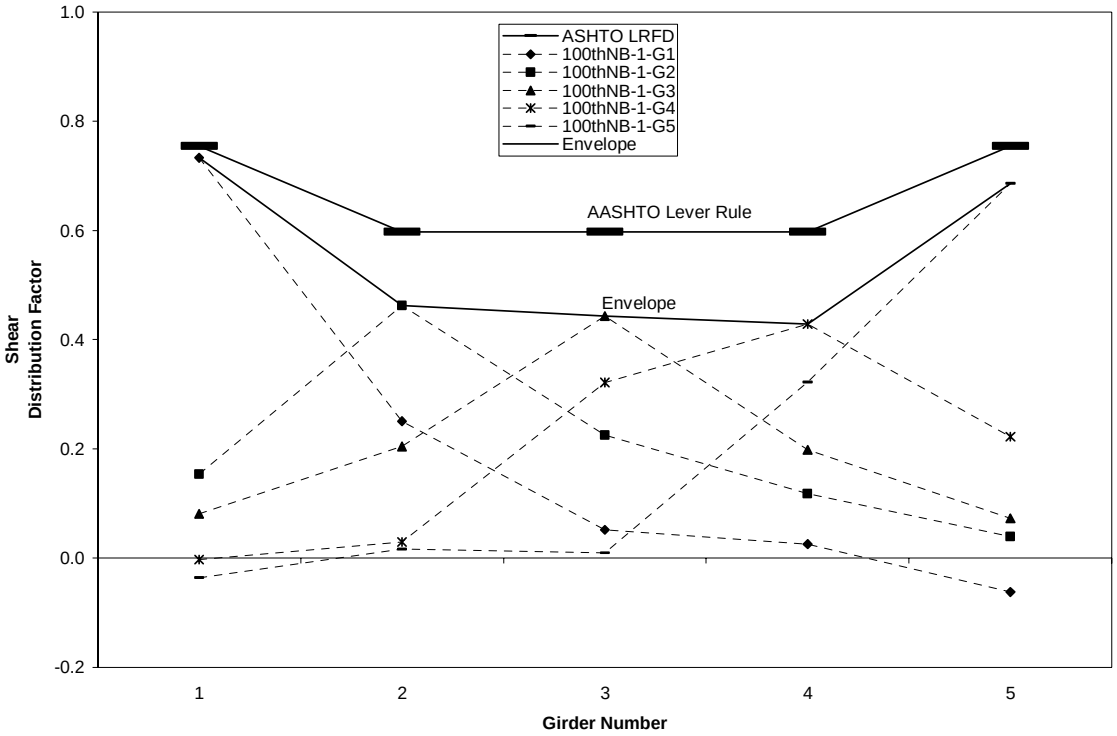


Fig. 4.12 Load Distribution Factors for Shear (100th NB Bridge)

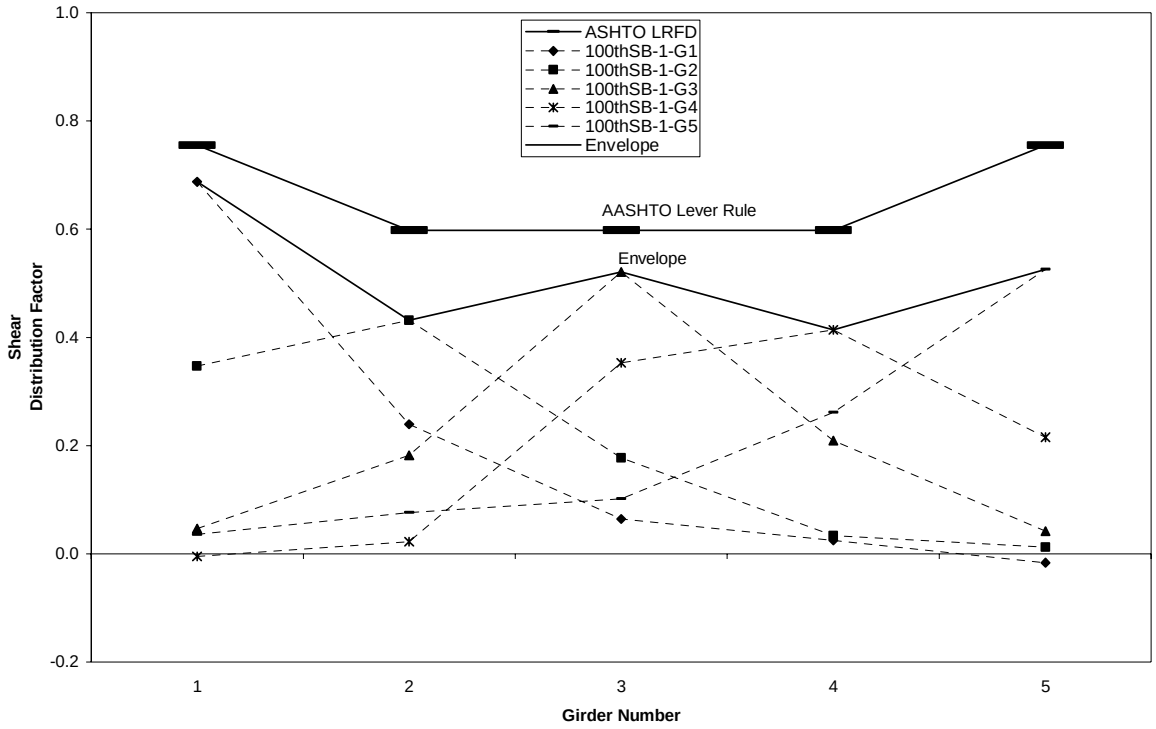


Fig. 4.13 Load Distribution Factors for Shear (100th SB Bridge)

## 4.2 DF Analysis of Bridges at Huffman Intersection (Set 2)

### 4.2.1 Description of the Bridges

The Huffman bridge is an even numbered girder bridge. As shown in Figure 4.14, instead of positioning the vehicle directly over each interior girder, the vehicle was positioned with its driver side wheels on the center line of the bridge (Joint Right), with its wheels centered over the center line of the bridge (Center), and with its passenger side wheels on the center line of the bridge (Joint Left).

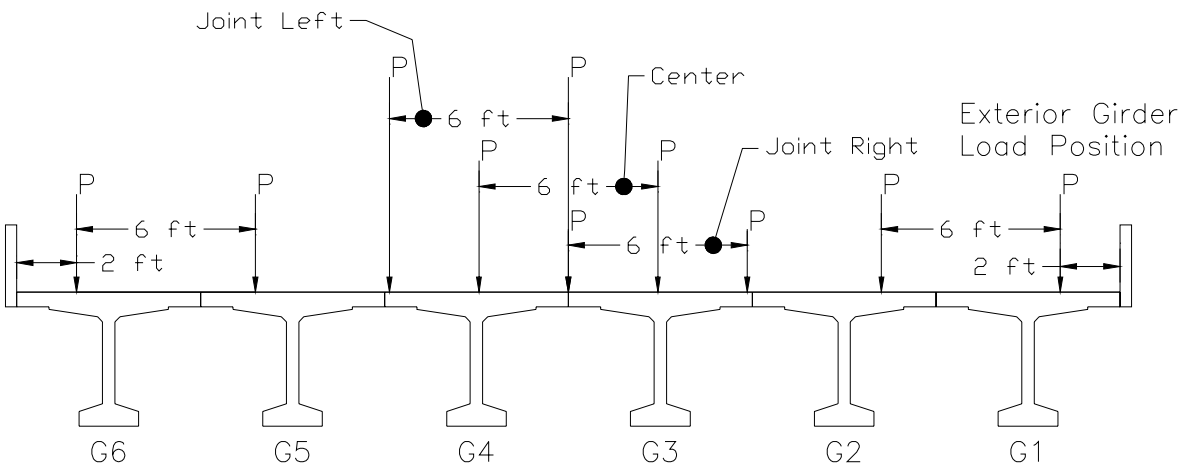


Fig. 4.14 Cross Section of the Bridge

### 4.2.2 Load Distribution Factors for Moment

Similar to Set 1 bridges, the calculation of DF for moments of interior beams ($DF_{IM}$) is shown below using Equations (4.3) to (4.6).

*For Interior Beams:*

$W := 37ft \quad L := 125ft \quad \theta := 28 \cdot deg \quad \mu := .2 \quad A := 903.25 in^2$

$N_L := \frac{36}{12}$

$I_x := 329617 \cdot in^4 \quad I_y := 207971 \cdot in^4 \quad I_p := I_x + I_y$

$J := \frac{A^4}{40.0 \cdot I_p}$

$J = 30954.395254 in^4 \quad S := 6.167ft$

Thus, distribution factor for moments of interior beams:

$$K := \sqrt{\frac{(1+\mu)\cdot I_x}{J}}$$

$K = 3.574656$

$$C := K\cdot\left(\frac{W}{L}\right)$$

$C = 1.058098$

since C is less than 5, therefore:

$$D := \left[11.5 - N_L + 1.4\cdot N_L\cdot(1 - 0.2\cdot C)^2\right]\cdot ft$$

$D = 11.110483\,ft$

$$DF_{IM} = \frac{S}{D} = 0.555$$

*For Exterior Beams:*

According to the AASHTO LRFD, the load distribution factor for exterior girder moment is calculated based on the lever rule method.

Distance of left wheel to middle of second girder $d_l$ = 80.75 in.

Distance of right wheel to middle of second girder $d_r$ = 8.75 in.

Therefore,

$$DF_{EM} = \frac{d_l + d_r}{2S} = 0.605$$

*Skew Adjustment:*

When decked bulb tee girders are sufficiently connected to act as a single unit, the LRFD Specifications recommend that DF for moment be reduced in accordance with Table 4.6.2.2.2e-1. Since the skew angle θ (= $28^0$) is less than $30^0$, the reduction factor is one.

Figures 4.15 and 4.16 show the moment distribution factor for Huffman North Bound, and Figures 4.17 and 4.18 show the moment distribution factor for Huffman South Bound. The twin bridges at Huffman were not loaded directly over the first interior girder (G2 or G4) during the field testing. The following graphs show the distribution from the exterior girders and from loads placed over either of the center girders (G3 or G4). Huffman NB was not tested with a load placed directly over G4, therefore Figure 4.16 only shows the distribution from the load placed over the exterior girder G6. The reported distribution factor for interior girders is the greater of either the distribution factor of the second girder (G2, G5) when the load was placed on the exterior girder, or the distribution from one of the interior girders (G3,G4) when the load was placed directly over the top of that girder.

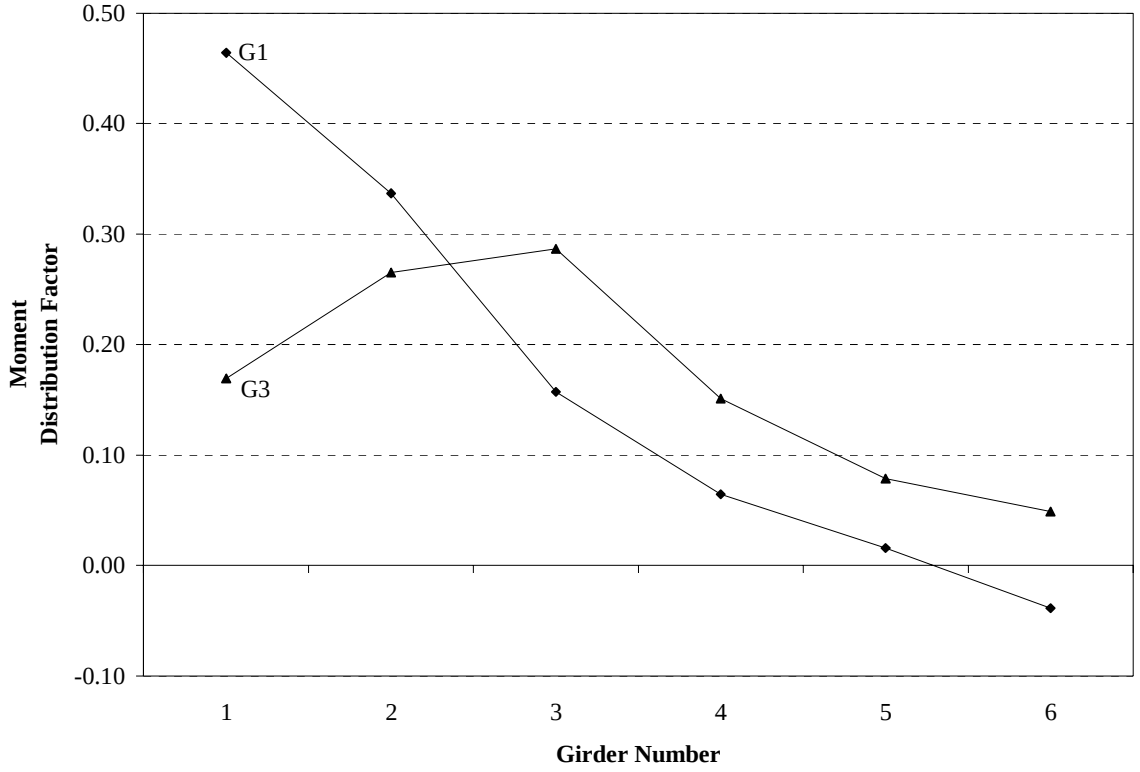


Fig. 4.15 Moment Distribution Factor (Huffman NB – 3 – G1&G3)

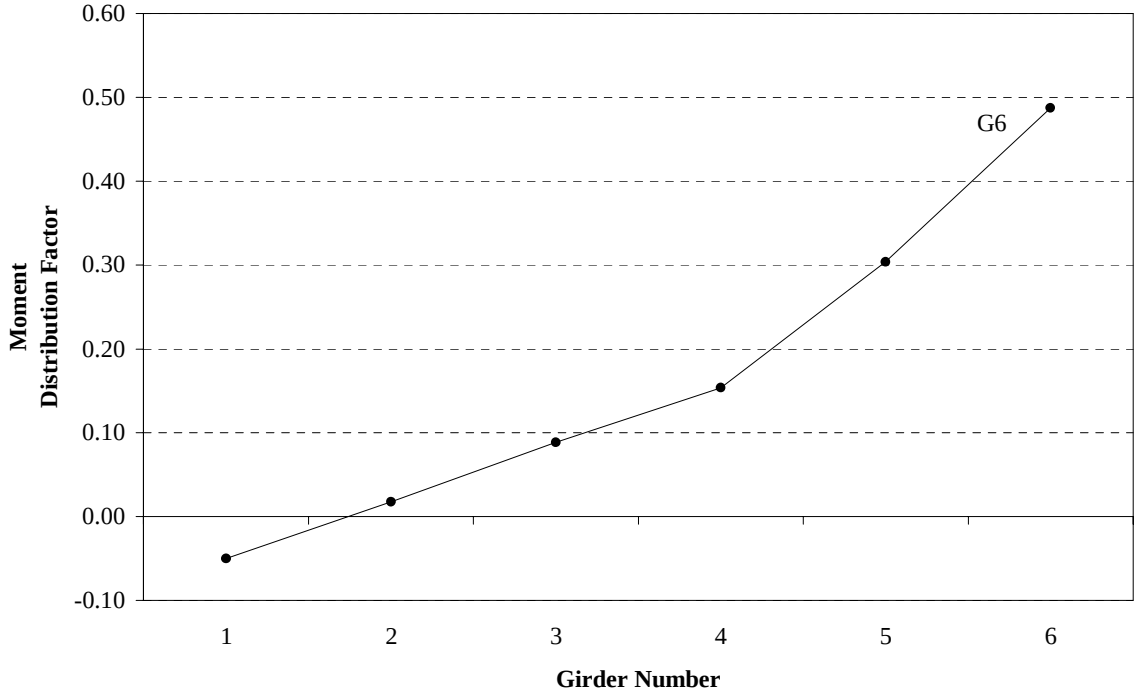


Fig. 4.16 Moment Distribution Factor (Huffman NB – 3 – G6)

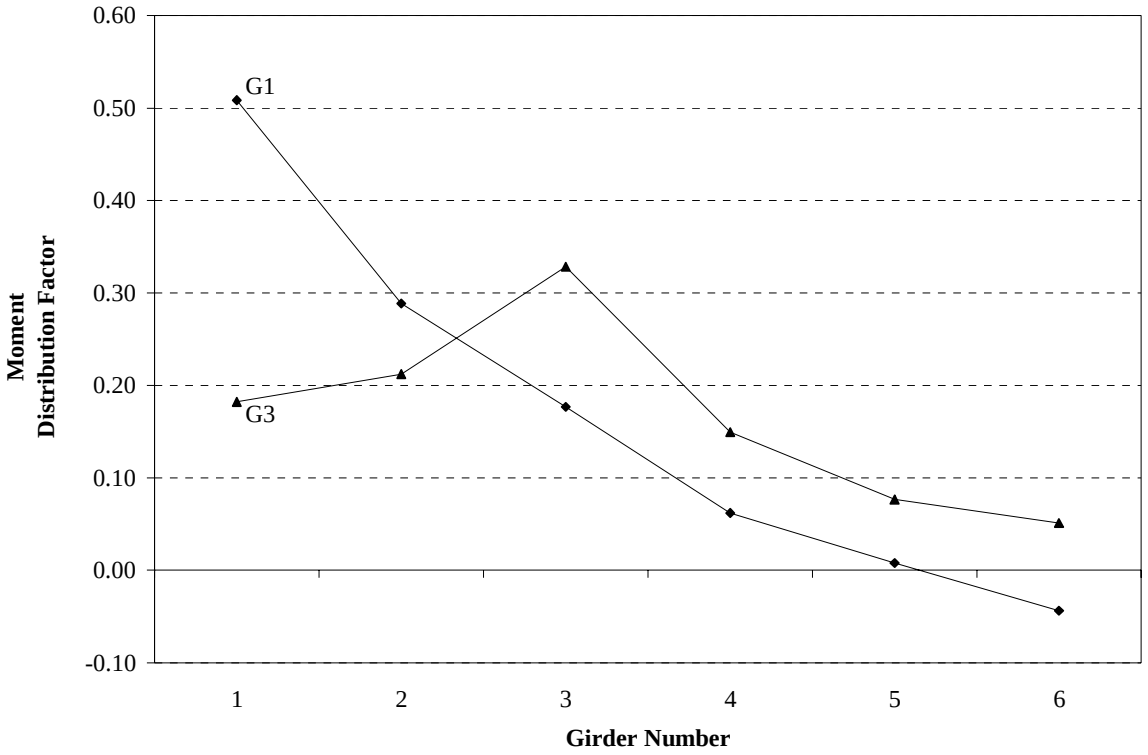


Fig. 4.17 Moment Distribution Factor (Huffman SB – 3 – G1&G3)

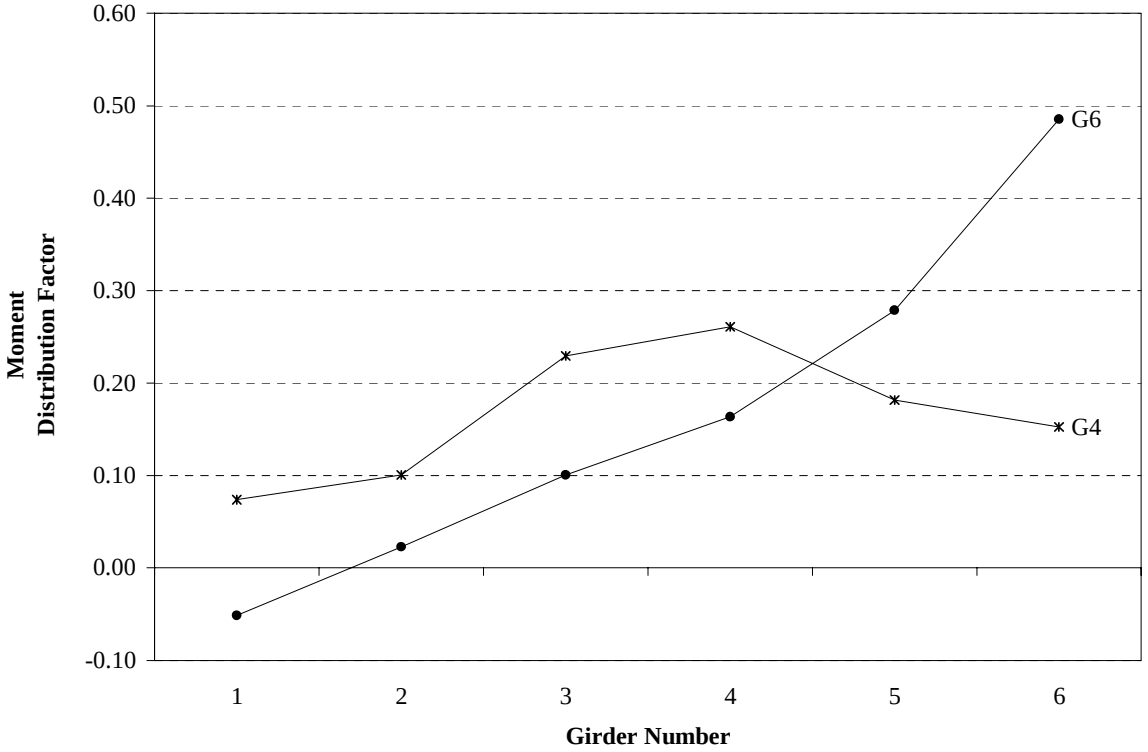


Fig. 4.18 Moment Distribution Factor (Huffman SB – 3 – G4&G6)

Figures 4.19 and 4.20 show the moment distribution factors for the Huffman Street bridges. Based on experimental strains, the maximum moment distribution factors of the interior girders are 0.337 for the Huffman NB and 0.328 for the Huffman SB. This compares with the moment distribution factor of 0.555 based on AASHTO LRFD. The moment distribution factors for exterior girders are 0.487 for the Huffman NB and 0.508 for the Huffman SB, which compare with AASHTO LRFD prediction of 0.605. Table 4.3 shows a summary of the distribution factors for moment of the twin bridges located at Huffman ave.

Table 4.3 Distribution Factor for Moment for Set 2 Bridges

| | Interior Girders | | Exterior Girders | |
|---|---|---|---|---|
| | G2 | G5 | G1 | G6 |
| Huffman NB | .34 | .30 | .46 | .49 |
| Huffman SB | .33† | .28 | .51 | .49 |
| Average | .31 | | .49 | |

† Distribution Factor Found from Girder Number 3 when the load was placed directly over the girder.

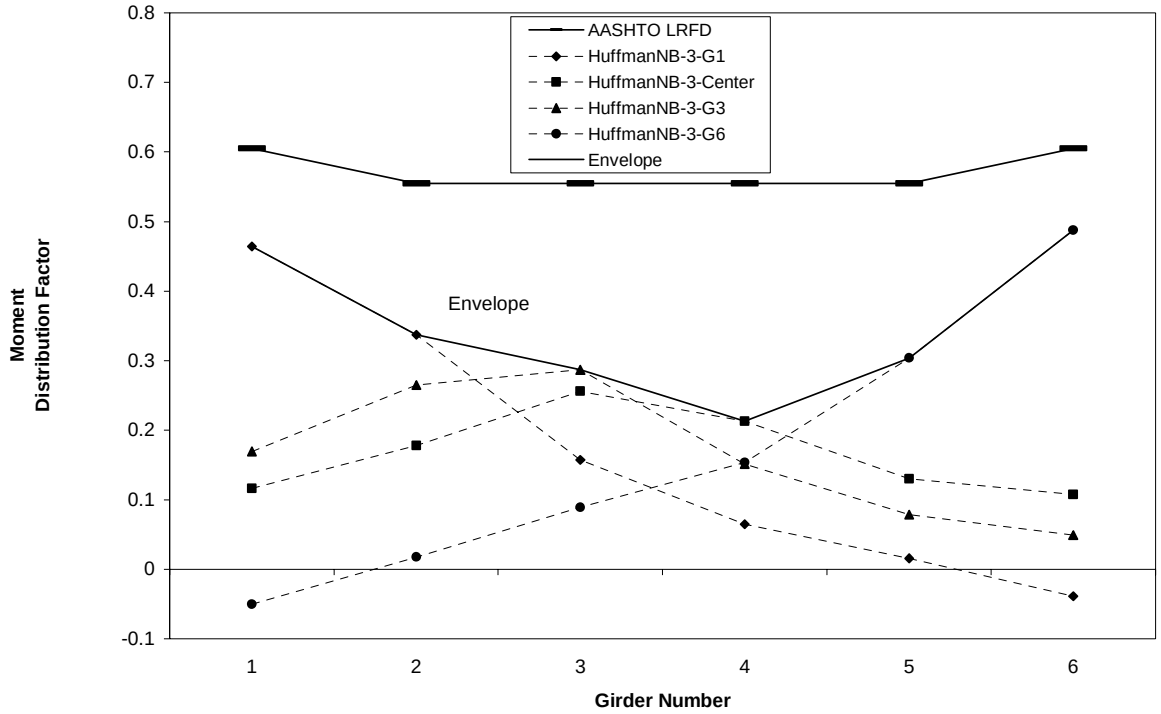


Fig. 4.19 Moment Distribution Factors (Huffman NB Bridge)

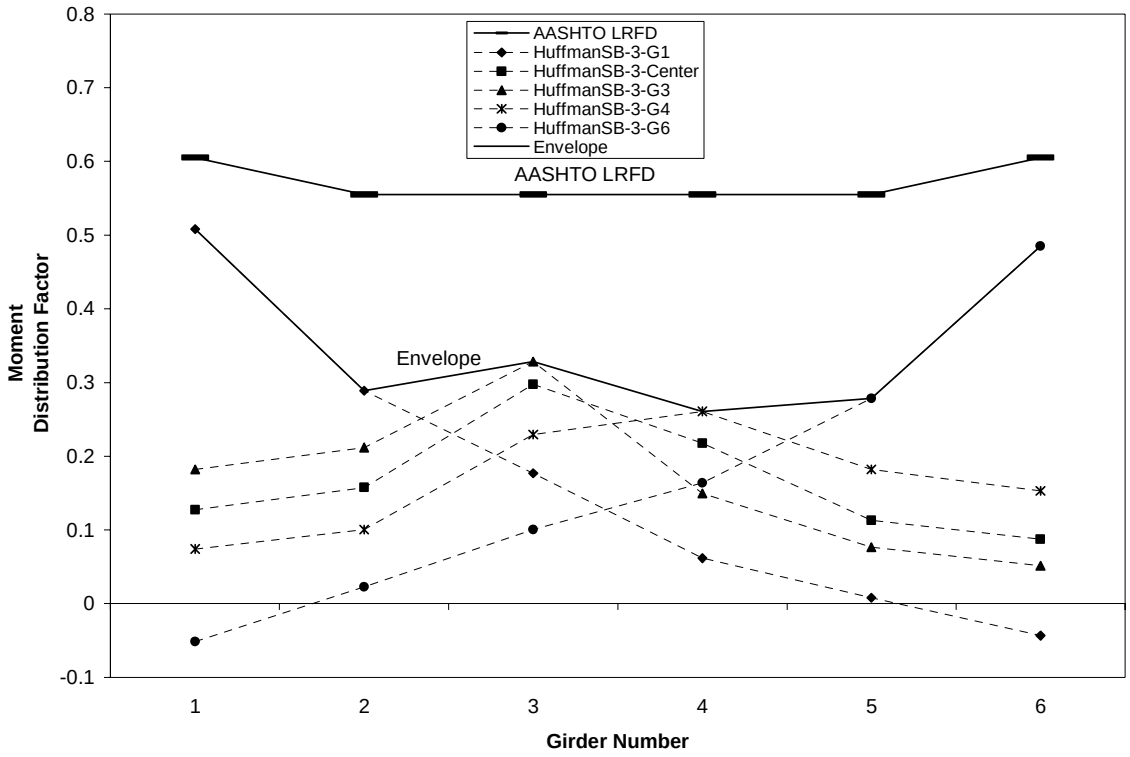


Fig. 4.20 Moment Distribution Factors (HuffmanSB Bridge)

### 4.2.3 Load Distribution Factors for Shear

Shear distribution factors found from experimental data using Equations (4.1) and (4.2) are compared to the shear distribution factor predicted by the AASHTO LRFD lever rule method. Similar to Set 1 bridges, the DF for shear is shown below.

*For Interior Beams:*
Similarly, use the lever rule model.
Distance of left wheel to middle of outside girder $d_0$ = S – 3 = 6.167' – 3' = 3.167 ft

$$DF_{IS} = \frac{d_0}{S} = 0.514$$

*For Exterior Beams:*
The distribution factor for shear of the exterior beams is the same as the factor for moment of the exterior beams, i.e.,

$$DF_{ES} = DF_{EM} = \frac{d_l + d_r}{2S} = 0.605$$

*Skew Adjustment:*
According to LRFD Specifications, shear in the exterior beam at the obtuse corner of the bridge shall be adjusted when the line of support is skewed. When decked bulb tee girders are sufficiently connected act as a unit, a correct factor, CF, should be applied to the load distribution factors for shear. As a preliminary step and lacking any better estimate, the factor, CF, from Table 4.6.2.2.3c-1 in the LRFD Specifications are used here even if it is not specifically for decked bulb tee girders. Another consideration is that the girder ends are embedded in concrete diaphragms. The concrete diaphragms are sufficiently rigid so that near the girder ends, the girders act "sufficiently connected to act as a single unit."

$$CF = 1.0 + 0.2\left(\frac{12Lt_s^3}{K_g}\right)^{0.3} \tan(\theta)$$

in which L = 125 ft; $t_s$ = 6.0 in.; $\theta = 28^0$

If the "deck" and the "basic beam" for decked bulb tee girders are considered to be one unit, then the longitudinal stiffness parameter, $K_g$, can be taken as "$I_x$" of the deck bulb tee girder, i.e. $K_g$ = 367797 in.$^4$ As a result, the skew correction factor CF is calculated to be **1.102**.

However, if the decked bulb tee girder is treated as a "deck" plus a "basic beam", then the longitudinal stiffness parameter, $K_g$, shall be taken as:

$$K_g = n\,(I + A\,e_g^2)$$

where,

n = ratio of modulus of elasticity of beam material and deck material = 1.0;

I = moment of inertia of beam = 177711 in.$^4$;
A = area of beam = 551 in.$^2$;
$e_g$ = distance between the centers of gravity of the basic beam and deck = 54.5 – 3.0 – 23.79 = 27.71 in.

then,
$K_g$ = 600793 in.$^4$; therefore, the skew correction factor CF is calculated to be **1.088**.

The skew corrected distribution factors for shear are as follows:
$DF_{IS}$ = 0.514 CF = 0.514 x 1.102 (or 1.088) = 0.566 (or 0.559);
$DF_{ES}$ = 0.605 CF = 0.605 x 1.102 (or 1.088) = 0.667 (or 0.658).

Figures 4.21 and 4.22 show the shear distribution factor for Huffman North Bound, and Figures 4.23 and 4.24 show the shear distribution factor for Huffman South Bound. In the previous sets of bridges tested, the worst loading condition for shear distribution typically occurred when the load vehicle drove directly over the top of the girder regardless whether or not the girder was an interior or exterior girder. Since the second girder of Huffman was not loaded, the reported distribution factor for interior girders for shear is either from girder three or girder four when the load was placed directly over the respective girder.

The twin bridges at Huffman, have a skew angle of 27.5°. The shear distribution of exterior girders on a skew bridge is affected by whether the girder is located on the obtuse or acute corner of the bridge. The girder numbering system is not symmetric for the Huffman north bound and south bound bridges. For Huffman NB, the shear loading position over the G1 girder is in the acute corner, and the shear loading position over the G6 girder is in the obtuse corner. For Huffman SB, the shear loading position over the G1 girder is in the obtuse corner, and the shear loading position over the G6 girder is in the acute corner.

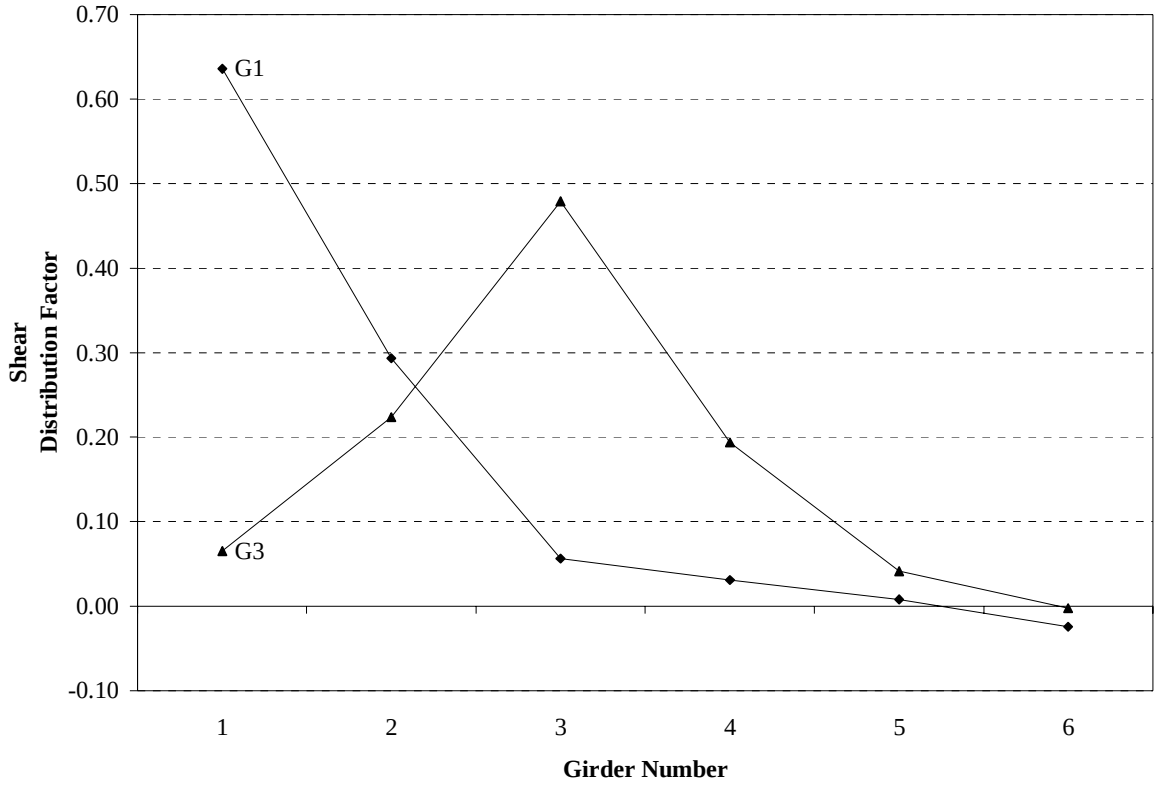


Fig. 4.21 Shear Distribution Factor (Huffman NB – 1 – G1&G3)

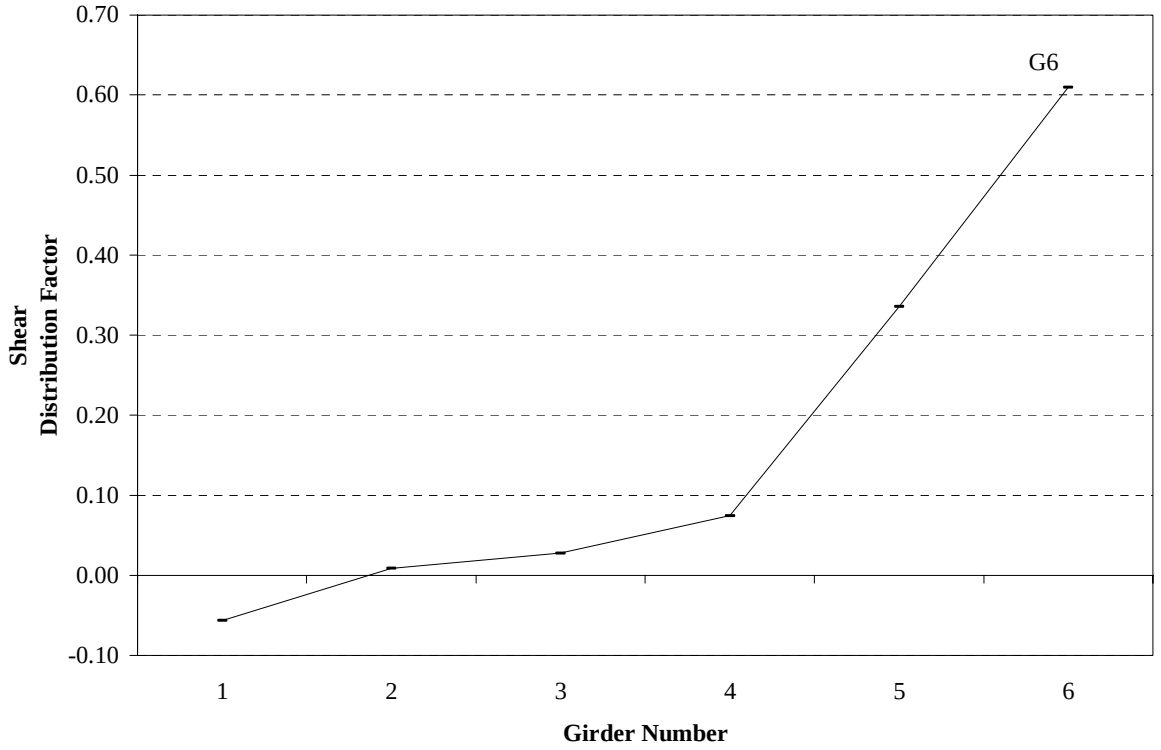


Fig. 4.22 Shear Distribution Factor (Huffman NB – 1 – G6)

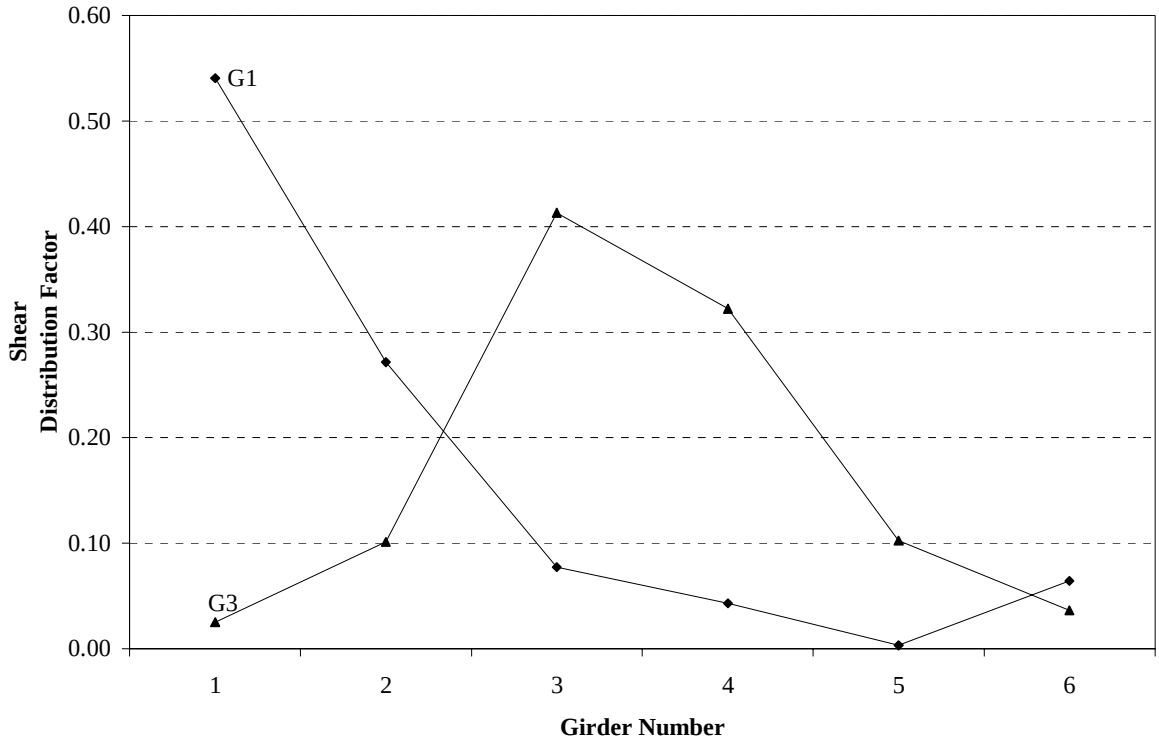


Fig. 4.23 Shear Distribution Factor (Huffman SB – 1 – G1&G3)

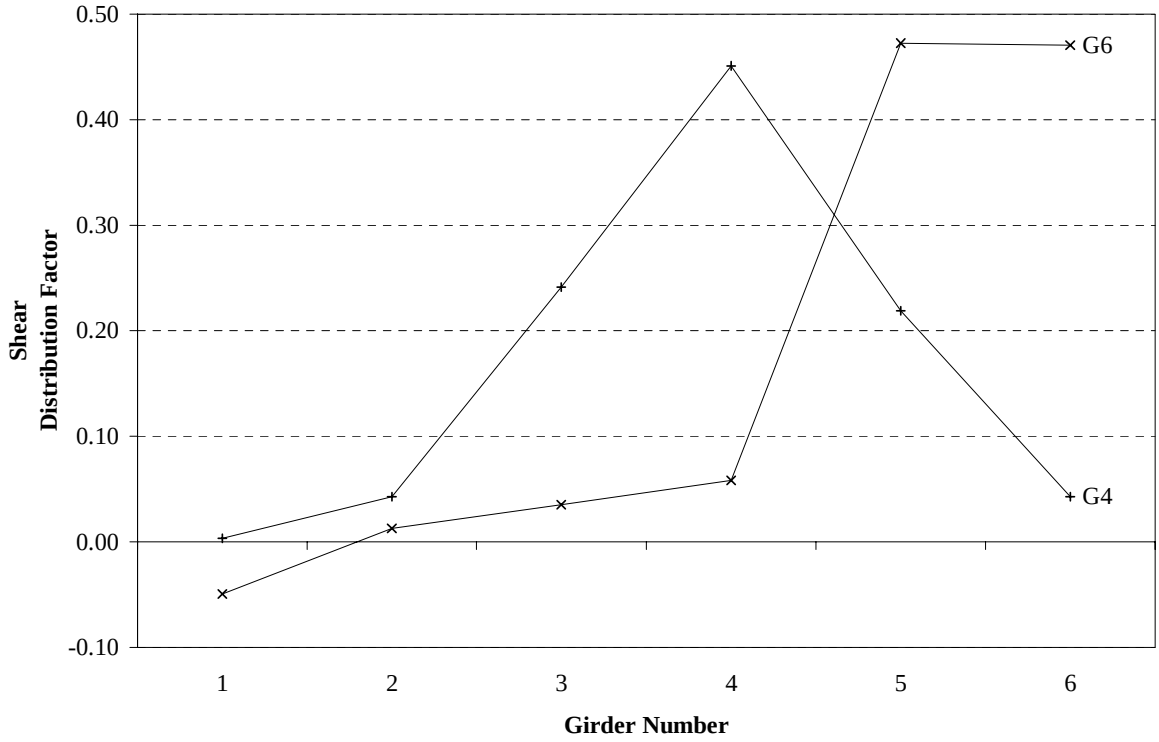


Fig. 4.24 Shear Distribution Factor (Huffman SB – 1 – G4&G6)

Figures 4.25 and 4.26 show the shear distribution factors for the Huffman Street bridges. The maximum shear distribution factors of the interior girders are 0.479 for Huffman NB and 0.472 for Huffman SB based on field testing results. These values are compared to the shear distribution factor of 0.566 (or 0.559) based on AASHTO LRFD. The shear distribution factors for exterior girders are 0.636 for the Huffman NB and 0.541 for the Huffman SB, which compares with AASHTO LRFD prediction of 0.667 (or 0.658). Table 4.4 shows a summary of the shear distribution factors found from Huffman NB and SB bridges. The distribution factors for the exterior girders are separated based off the obtuse and acute corner.

Table 4.4 Distribution Factor for Shear for Set 2 Bridges

| | Interior Girders | | Exterior Girders | |
|---|---|---|---|---|
| | G3 | G4 | Acute | Obtuse |
| Huffman NB | .48 | | .64 | .61 |
| Huffman SB | .45 | .45 | .47 | .54 |
| Average | .46 | | .55 | .58 |

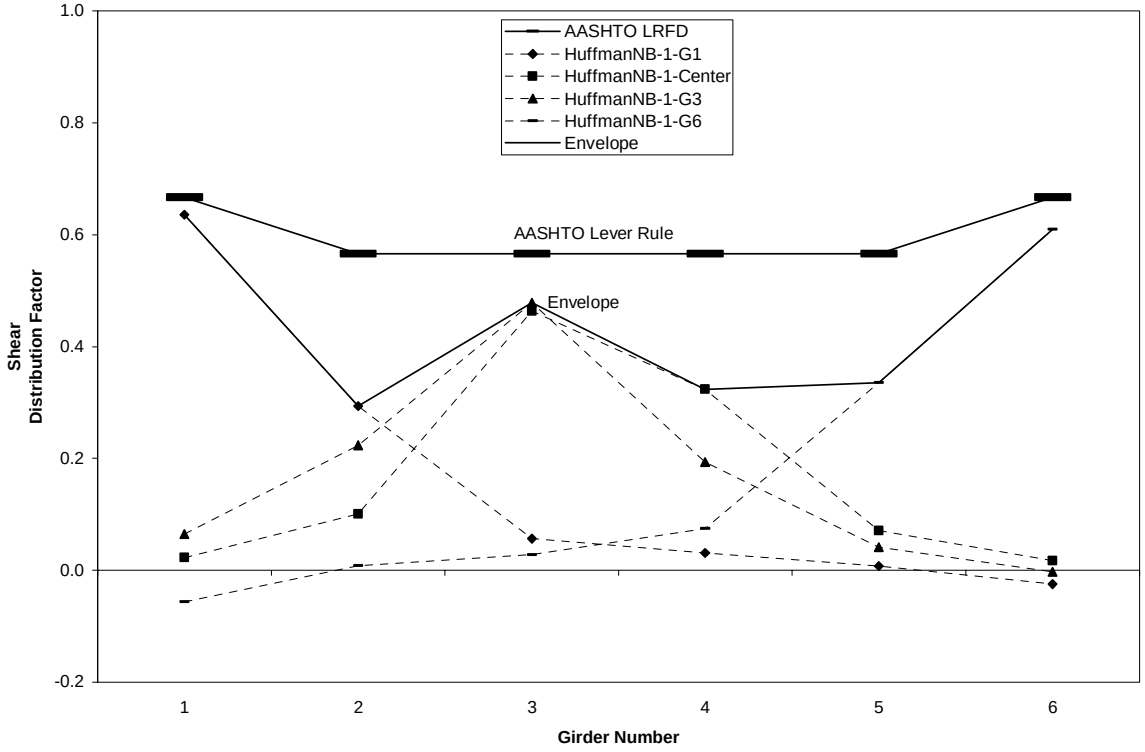


Fig. 4.25 Shear Distribution Factors (Huffman NB Bridge)

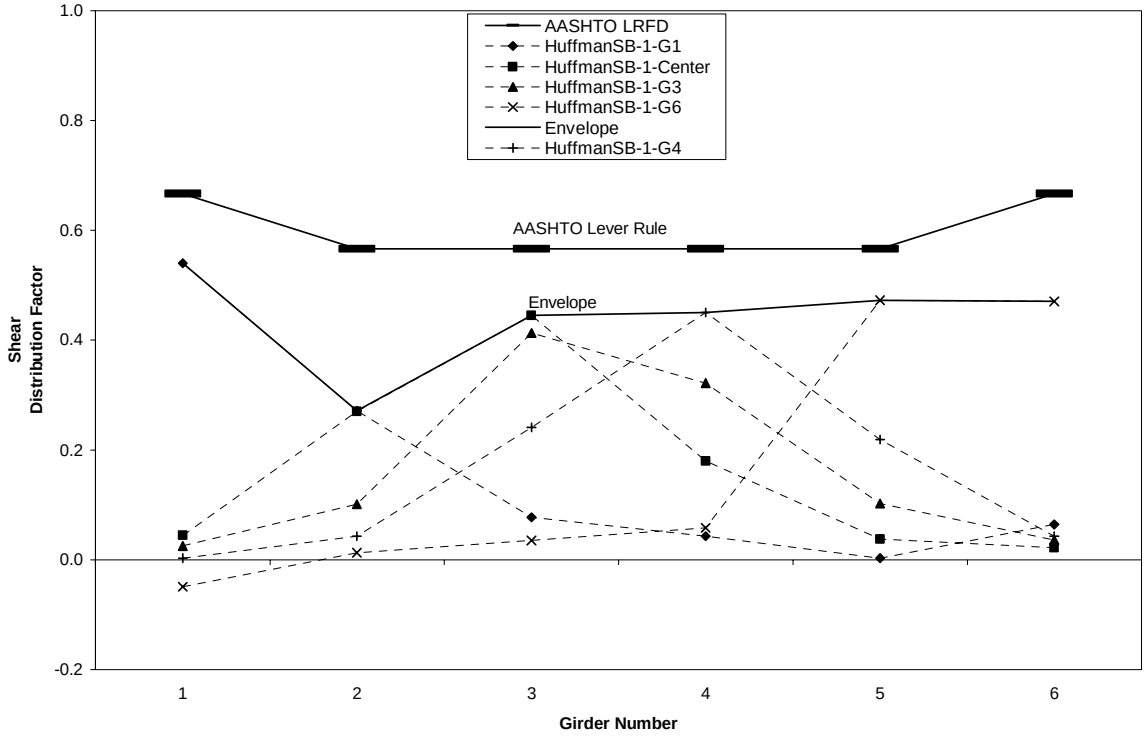


Fig. 4.26 Shear Distribution Factors (Huffman SB Bridge)

## 4.3 DF Analysis of Bridges at Campbell Creek (Set 3)

### 4.3.1 Description of the Bridges

The Campbell Creek Bridge is a single span bridge with a span of 137 ft. It has five bulb tee girders interconnected with shear connectors and with seven intermediate steel diaphragms. Both ends of the bridge are connected to concrete diaphragms of 1.5 ft wide. The bridge has a 4.3 degree skew. Figure 4.27 shows the cross section.

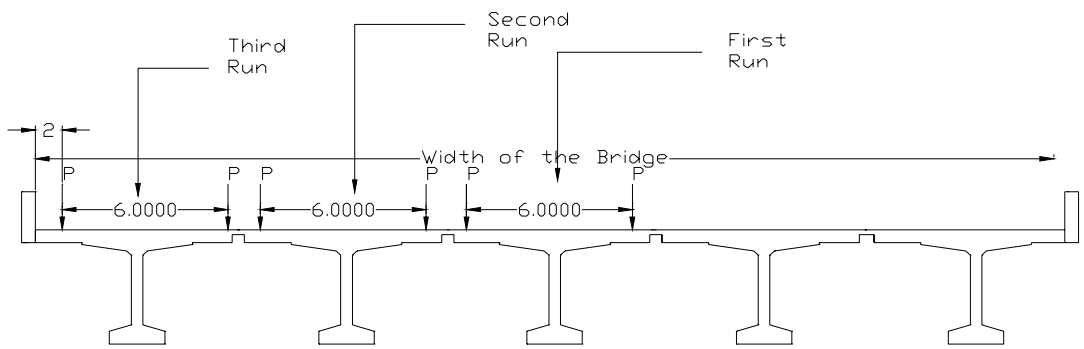


Fig. 4.27 Cross section of the bridge

### 4.3.2 Load Distribution Factors for Moment

Figures 4.28 and 4.29 show the moment distribution factor for Campbell North Bound, and Figures 4.30 and 4.31 show the moment distribution factor for Campbell South Bound. Both the load on the exterior girder and load directly over the first interior girder appear to make the same distribution factor on the second girder. Figure 4.31 shows the moment distribution on the girders for Campbell SB when the load vehicle is positioned over girder number 4 and 5. The data shown in this graph does not follow the same trend as in the other moment distribution graphs. The moment strain gauge placed on girder number 5 for this bridge had not adhered properly to the concrete during testing. Therefore, the strains found from this gauge are suspect. This suspect strain gauge is probably the cause for the abnormal behavior in the graph of Figure 4.31.

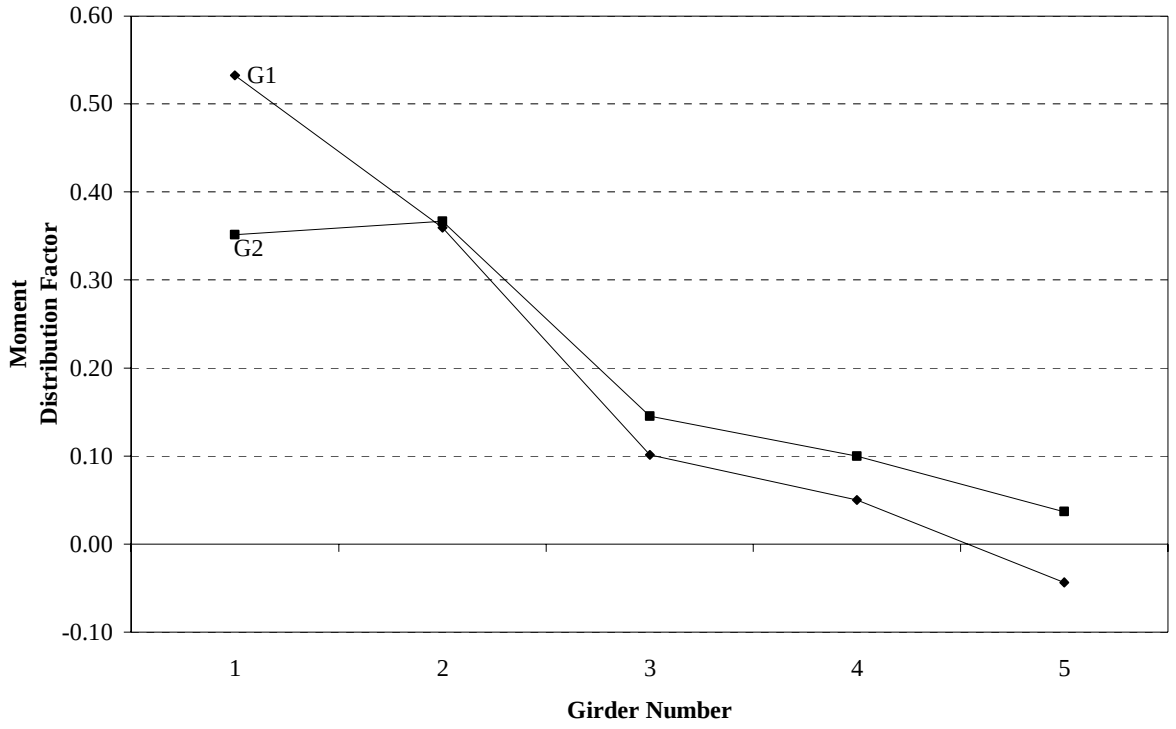


Fig. 4.28 Moment Distribution Factor (Campbell NB – 3 – G1&G2)

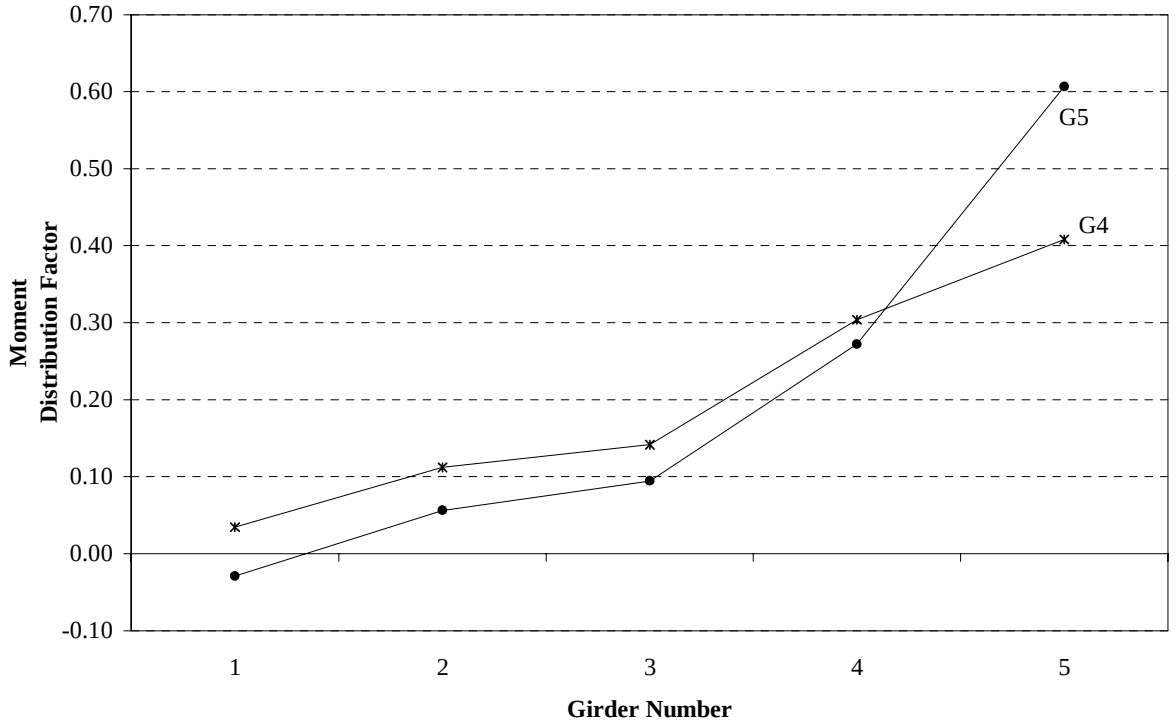


Fig. 4.29 Moment Distribution Factor (Campbell NB – 3 – G4&G5)

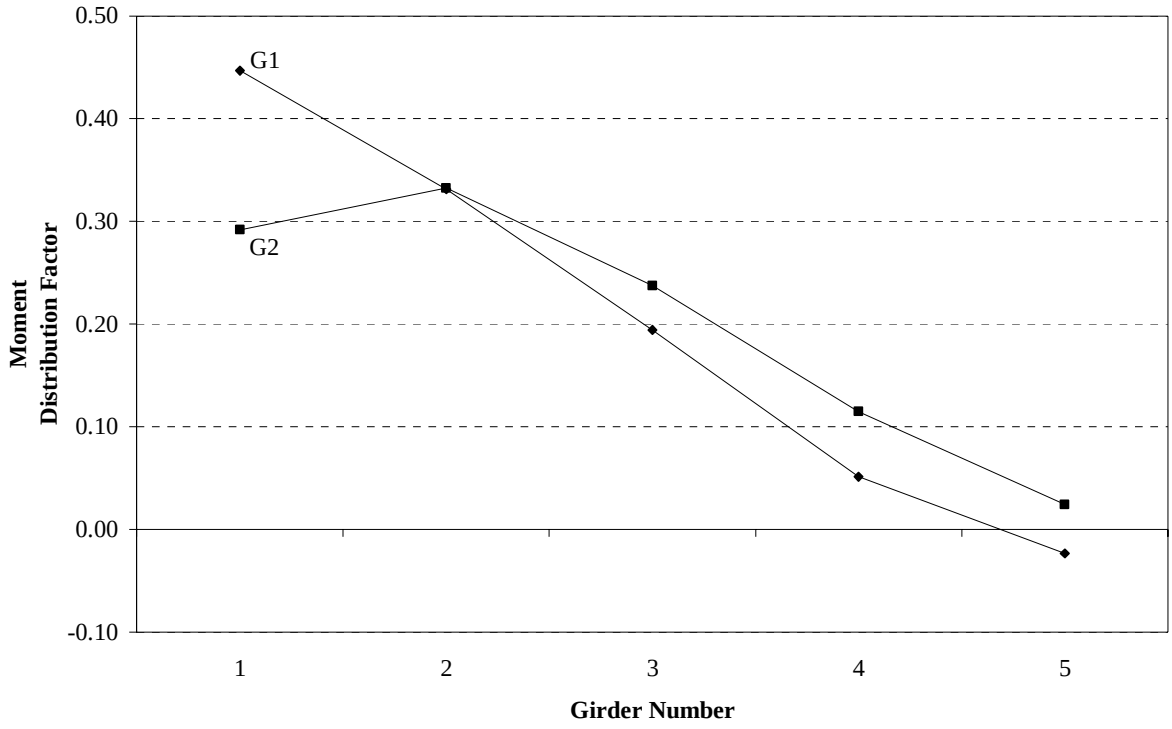


Fig. 4.30 Moment Distribution Factor (Campbell SB – 3 – G1&G2)

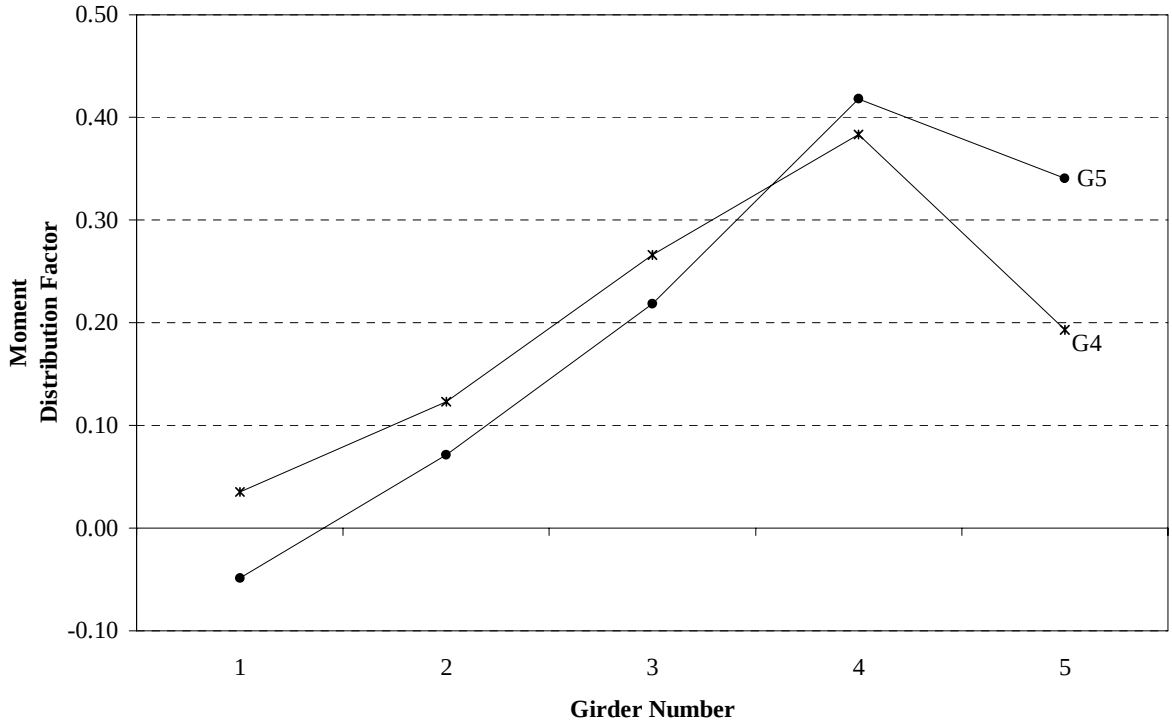


Fig. 4.31 Moment Distribution Factor (Campbell SB – 3 – G4&G5)

Similar to Set 2 bridges, the moment distribution factors can be calculated based on the LRFD Specifications. Figures 4.32 and 4.33 show the moment distribution factors for the Campbell Street bridges. Based on field tests, the maximum moment distribution factors of the interior girders are 0.376 for the Campbell NB and 0.418 for the Campbell SB. This compares with the moment distribution factor of 0.660 based on AASHTO LRFD. The moment distribution factors for exterior girders are 0.607 for the Campbell NB and 0.447 for the Campbell SB. This compares with AASHTO LRFD prediction of 0.758. Table 4.5 shows a summary of the moment distribution factor values found from the twin bridges at Campbell Creek. The average DF value at the bottom of the table does not incorporate the values found Figure 4.31.

Table 4.5 Distribution Factor for Moment for Set 3 Bridges

| | Interior Girders | | Exterior Girders | |
|---|---|---|---|---|
| | G2 | G4 | G1 | G5 |
| Campbell NB | .38 | .30 | .53 | .61 |
| Campbell SB | .33 | .42† | .45 | .34† |
| Average | .34 | | .53 | |

† Suspect Data not Included in the Reported Average

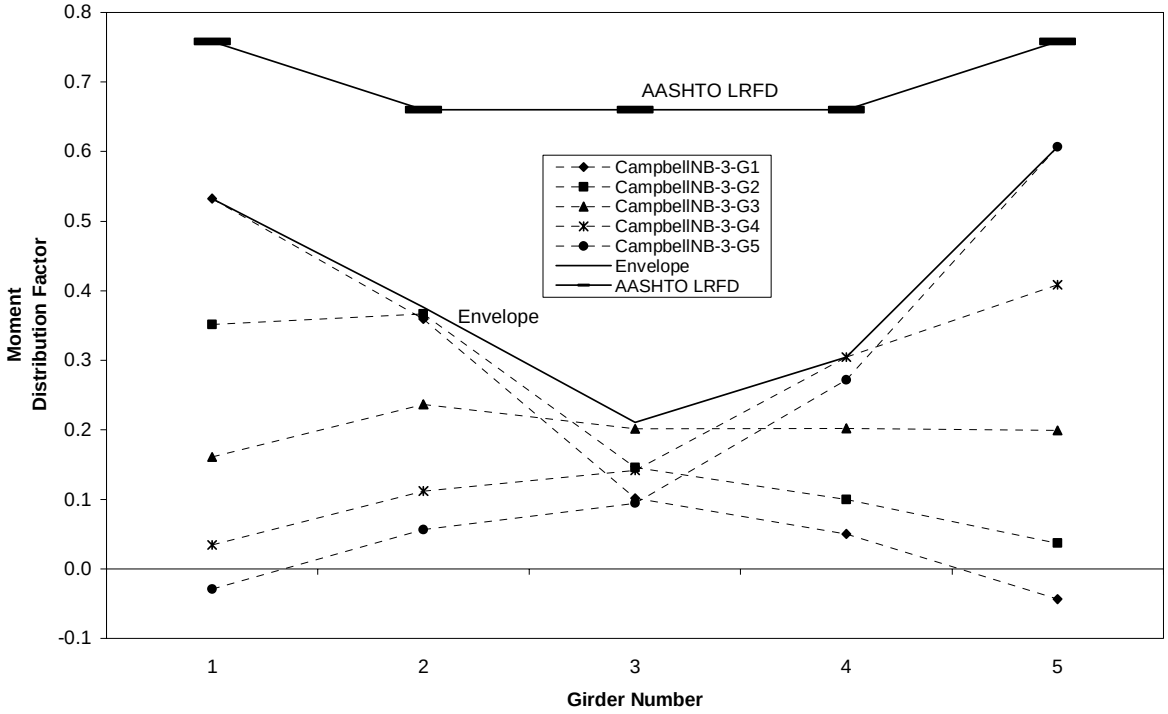


Fig. 4.32 Moment Distribution Factors (Campbell NB Bridge)

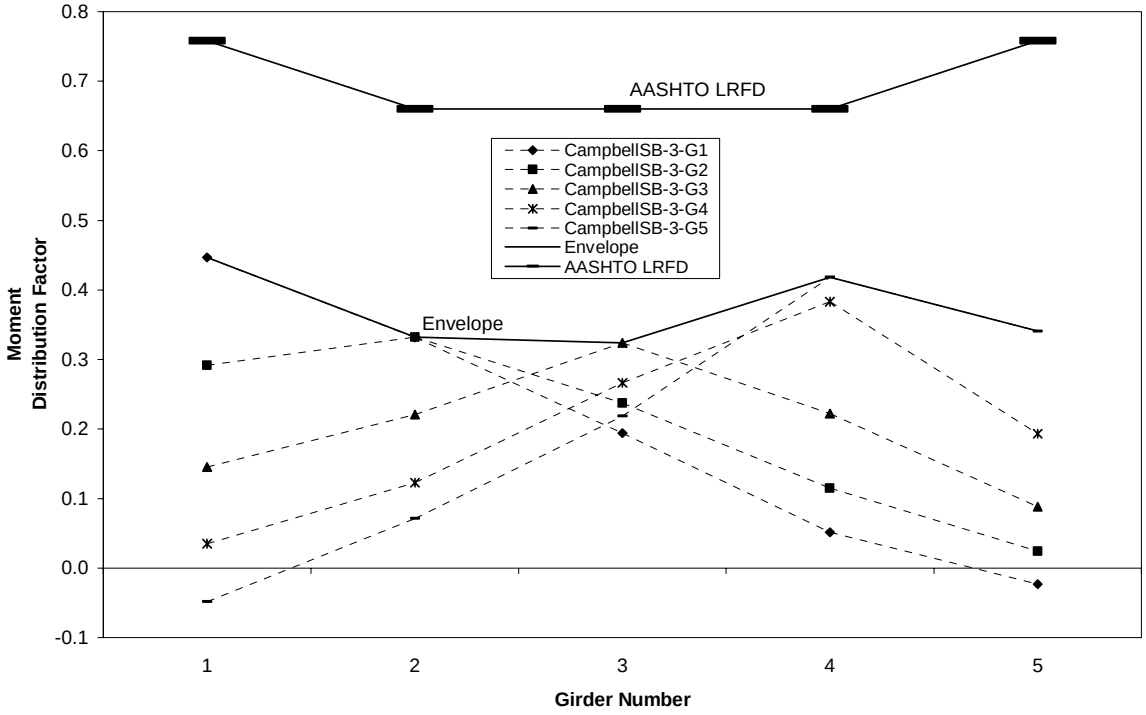


Fig. 4.33 Moment Distribution Factors (Campbell SB Bridge)

### 4.3.3 Load Distribution Factors for Shear

This section provides a comparison for the shear distribution. Shear distribution factors found from experimental data were calculated using Equations (4.1) and (4.2). The AASHTO LRFD approach is based on the lever rule method.

Figures 4.34 and 4.35 show the shear distribution factor for Campbell North Bound, and Figures 4.36 and 4.37 show the shear distribution factor for Campbell South Bound. The worst loading condition for shear distribution always occurred when the load vehicle drove directly over the top of the girder regardless whether or not the girder was an interior or exterior girder.

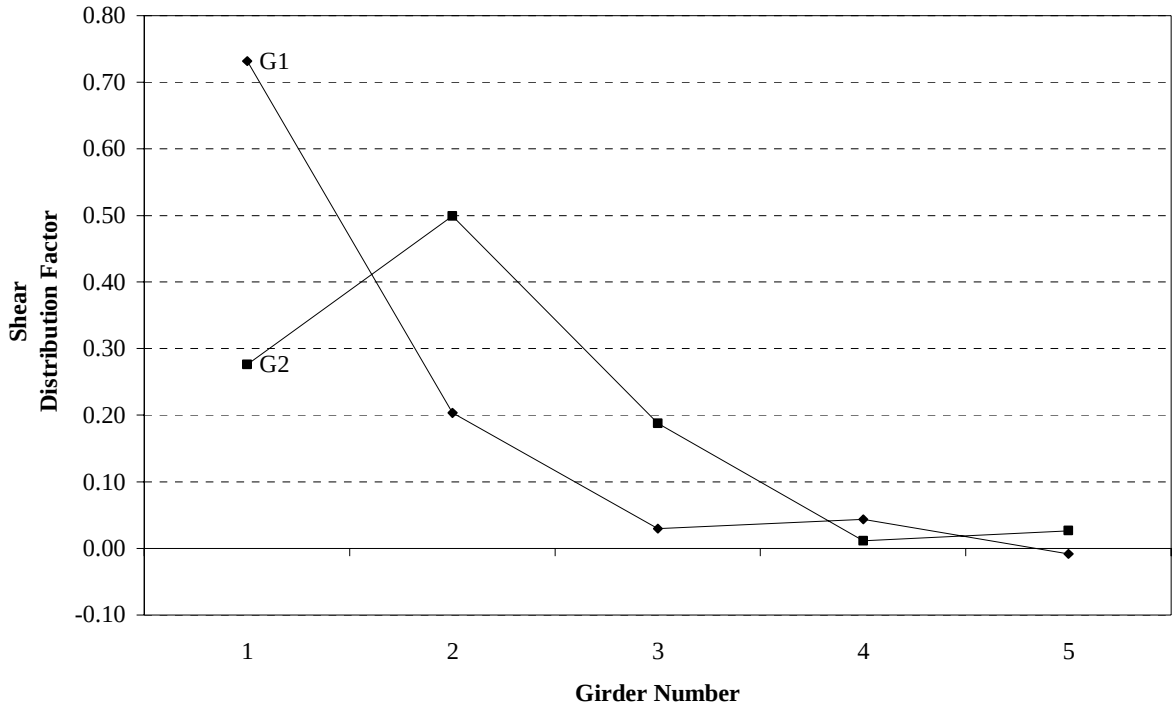


Fig. 4.34 Shear Distribution Factor (Campbell NB – 1 – G1&G2)

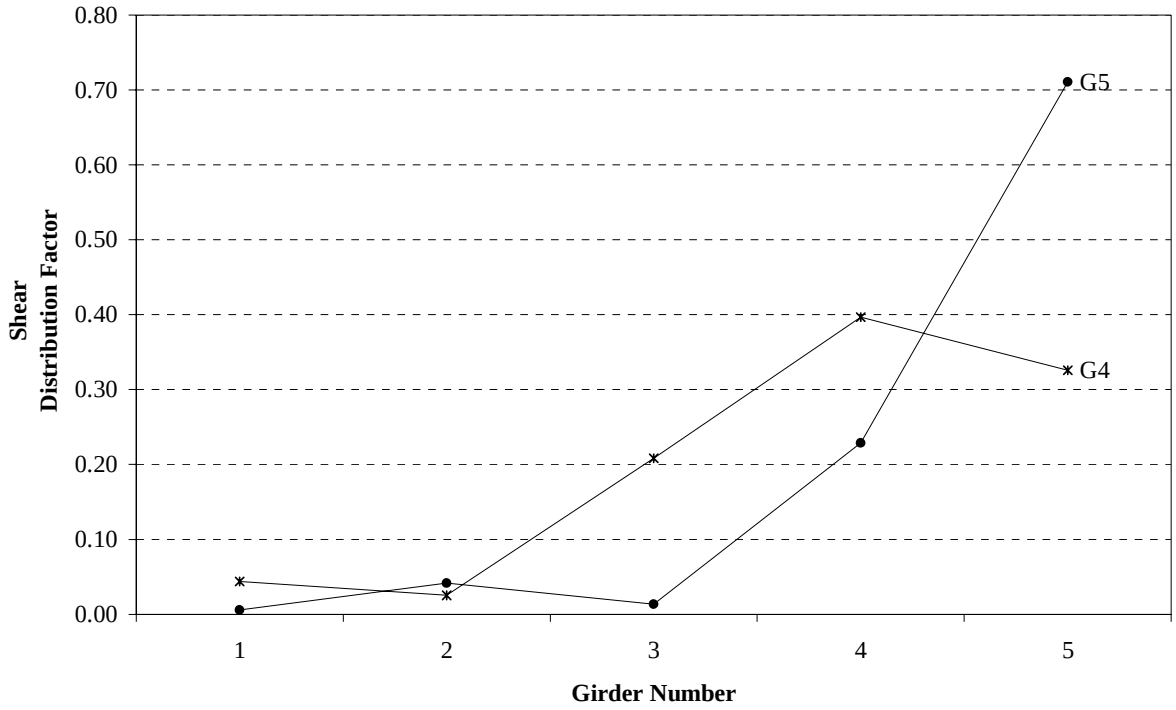


Fig. 4.35 Shear Distribution Factor (Campbell NB – 1 – G4&G5)

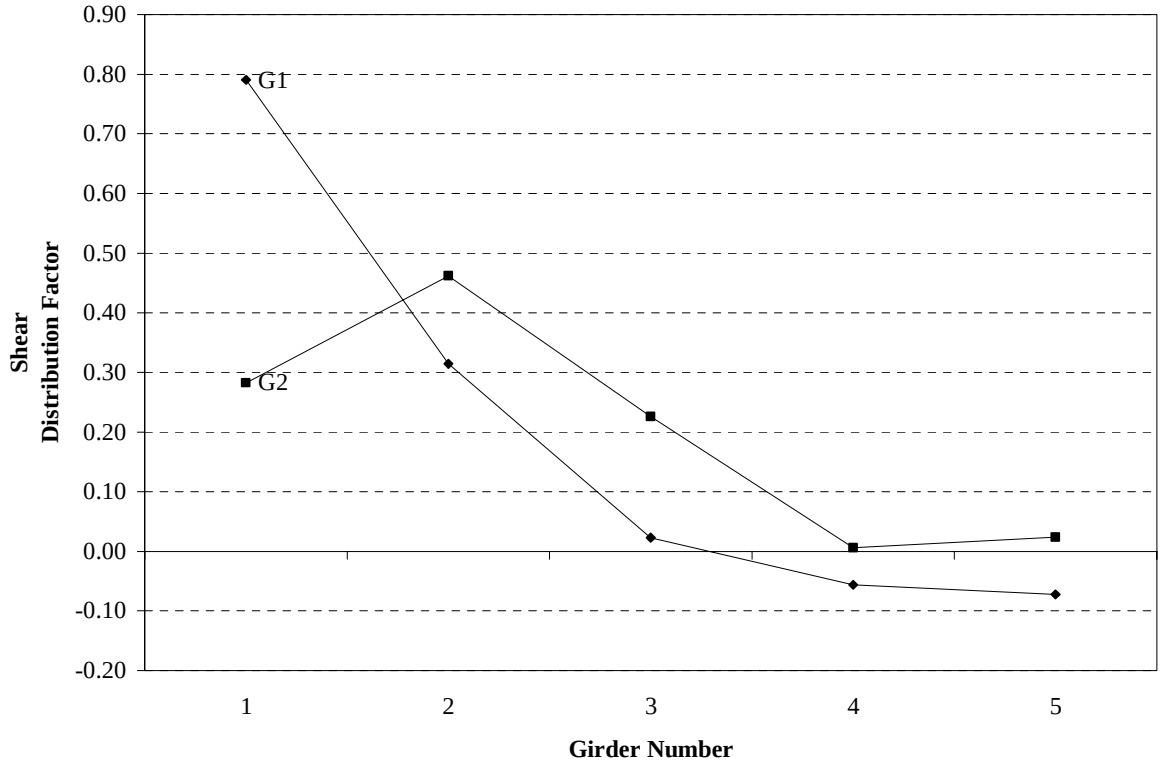


Fig. 4.36 Shear Distribution Factor (Campbell SB – 1 – G1&G2)

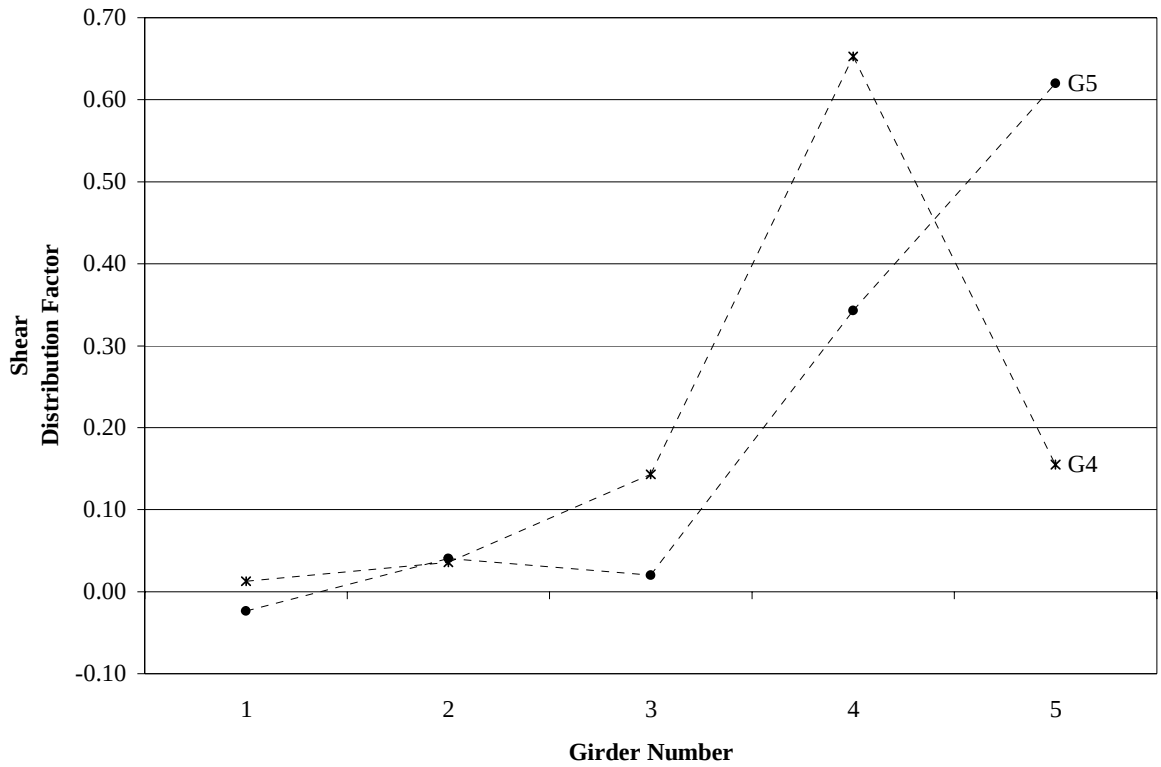


Fig. 4.37 Shear Distribution Factor (Campbell SB – 1 – G4&G5)

Figures 4.38 and 4.39 show the shear distribution factors for Campbell Street NB and SB bridges. Based on experimental strain data, the maximum shear distribution factors of the interior girders are 0.499 for Campbell NB and 0.653 for Campbell SB. The predicted shear distribution factor using AASHTO LRFD is 0.601. The shear distribution factors for exterior girders are 0.732 for the Campbell NB and 0.791 for the Campbell SB, which compare with AASHTO LRFD prediction of 0.759. Table 4.6 shows a summary of the shear distribution factors found from Campbell NB and SB bridges.

Table 4.6 Distribution Factor for Shear for Set 3 Bridges

| | Interior Girders | | Exterior Girders | |
|---|---|---|---|---|
| | G2 | G4 | G1 | G5 |
| Campbell NB | .50 | .40 | .73 | .71 |
| Campbell SB | .46 | .65 | .79 | .62 |
| Average | .50 | | .71 | |

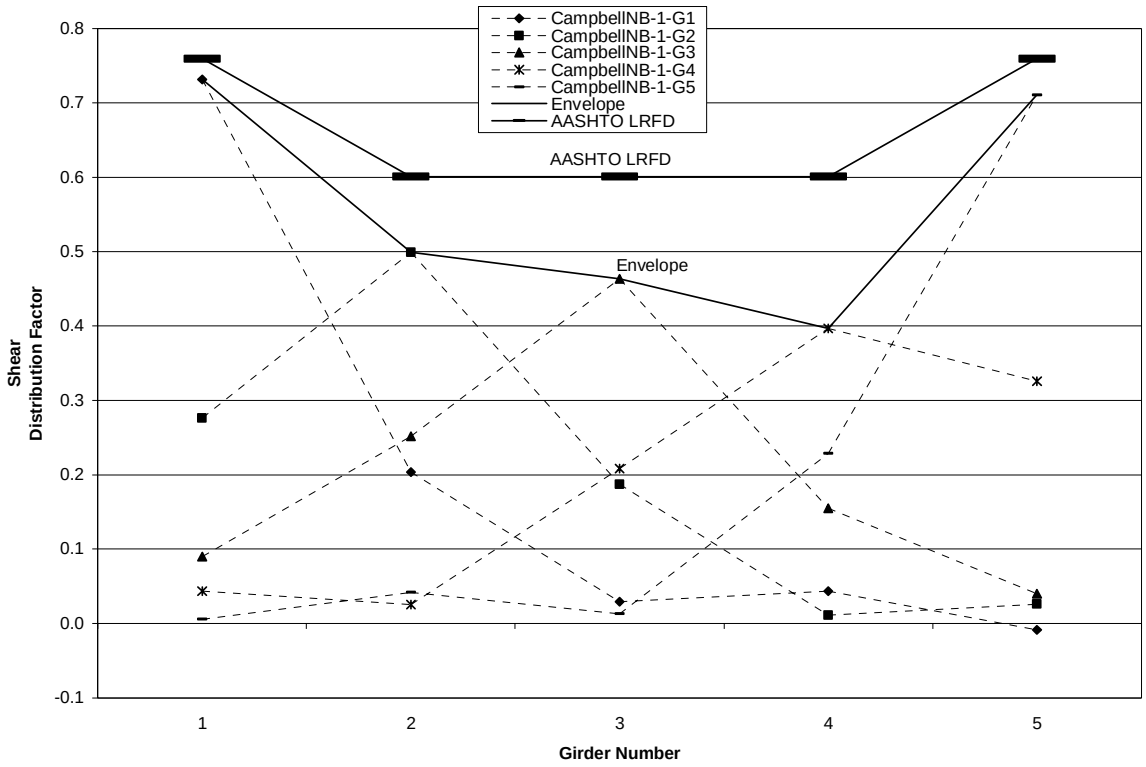


Fig. 4.38 Shear Distribution Factors (Campbell NB Bridge)

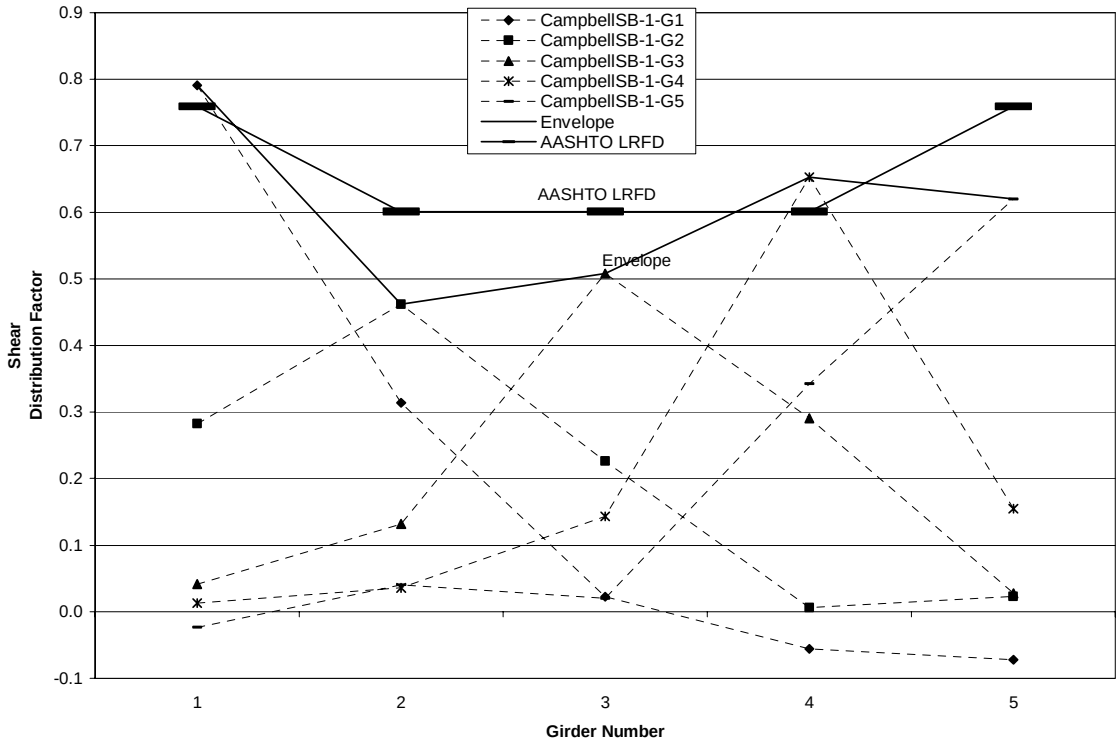


Fig. 4.39 Shear Distribution Factors (Campbell SB Bridge)

## 4.4 DF Analysis of Bridges at Diamond and Dowling (Set 4)

### 4.4.1 Description of the Bridges

The girder shape at Diamond and Dowling intersections is different from other three sets of bridges, see Figure 4.40. Girders are tees instead of bulb tees. Also, these bridges have a width of 106 ft and a span of 109 ft. As a result, they have the highest aspect ratio.

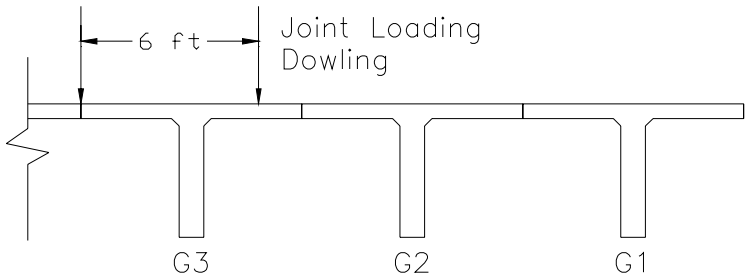


Fig. 4.40 Cross section of the bridge

### 4.4.2 Load Distribution Factors for Moment

Similar to Set 1 bridges, the calculation of DF for moments of interior beams ($DF_{IM}$) is shown below using Equations (4.3) to (4.6).

*For Interior Beams:*

$W := 106ft \quad L := 109ft \quad \theta := 0 \cdot deg \quad \mu := .2 \quad A := 1026 \cdot in^2$

$N_L := \frac{108}{12} \qquad N_L = 9$

$I_x := 279223.5 in^4 \qquad I_y := 362787.1875 in^4 \qquad I_p := I_x + I_y \qquad J := \frac{A^4}{40.0 \cdot I_p} \qquad S := 7.567ft$

**Distribution Factor for moments of Interior Beams** :

$K := \sqrt{\frac{(1+\mu) \cdot I_x}{J}} \qquad K = 2.78659 \qquad C := K \cdot \left(\frac{W}{L}\right) \qquad C = 2.709894$

Since C is less than 5,

$D := \left[11.5 - N_L + 1.4 \cdot N_L \cdot (1 - 0.2 \cdot C)^2\right] \cdot ft$

$D = 5.14327ft$

Distribution Factor for Interior moment is: $DF_{IM} := \frac{S}{D}$

$DF_{IM} = 1.471243$

*For Exterior Beams:*

According to the AASHTO LRFD, the load distribution factor for exterior girder moment is calculated based on the lever rule method.

Distance of left wheel to middle of second girder $d_l$ = (1.5 S – 2.5) ft = 8.851 ft
Distance of right wheel to middle of second girder $d_r$ = ($d_1$ – 6.0) ft = 2.851 ft
Therefore,

$$DF_{EM} = \frac{d_l + d_r}{2S} = 0.773$$

Figures 4.41 and 4.42 show the moment distribution factors for Dowling, and Figures 4.43 and 4.44 show the moment distribution factors for Diamond. Both of the bridges at Diamond and Dowling intersections were wide bridges consisting of 14 girders. Only one side of each bridge was tested and moment gauges were only placed on girders 1 to 8, 10, and 11 on Dowling and 1 to 8, 10, and 12 on Diamond. To determine the distribution factor based off the method as discussed above, the strains on girder number 9 for both bridges and girder 11 for Diamond was found by interpolating between the two surrounding girders. Girders 13 and 14 were assumed to have no strain. The moment gauge placed on G3 for diamond was not located in the center of bottom of girder due to excessive cracking. The gauge was offset from the center by one inch to an area where it could adhere to uncracked concrete. This offset could have caused the strains to be larger than if the gauge were centered on the girder due to the torsional forces in the girder. Both of these bridges are older than the other tested bridges and have been damaged due to over sized vehicles colliding into the exterior girders. While the bridges are both still serviceable, the strains recorded from the testing of these bridges are more sporadic than the other tested bridges. The moment on interior girders for these two bridges is an average of all the distribution factors found on loaded interior girders.

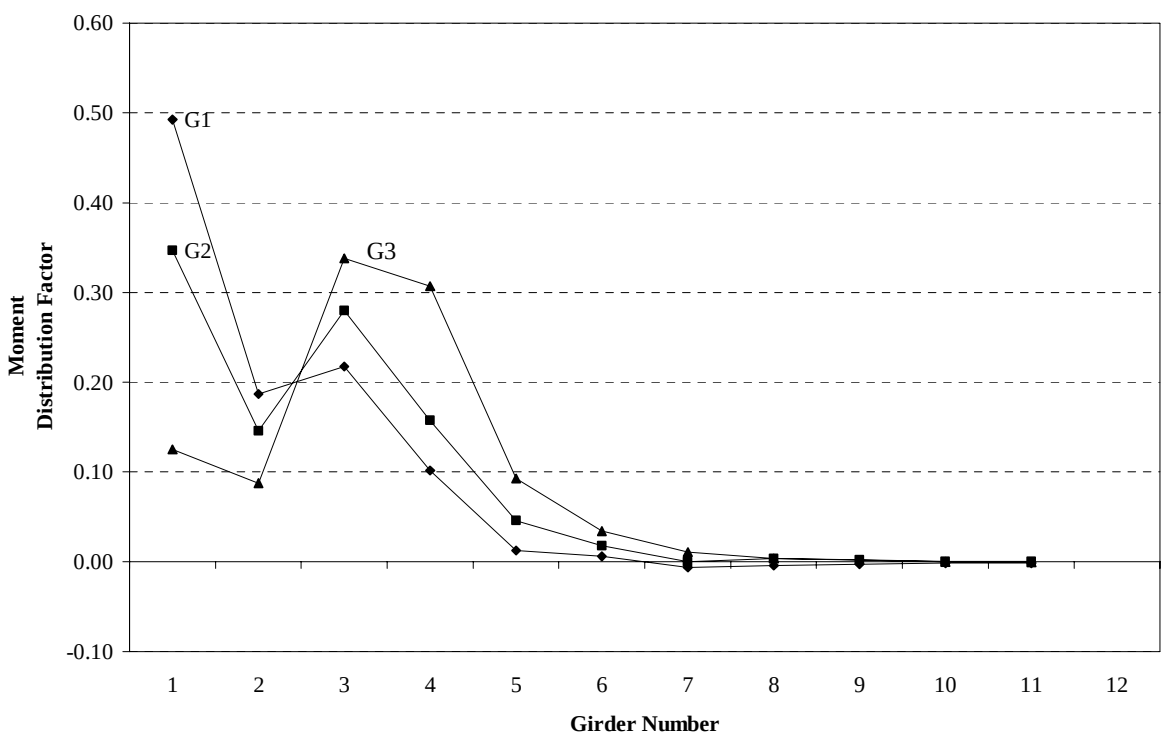


Fig. 4.41 Moment Distribution Factor (Dowling – 3 – G1, G2, G3)

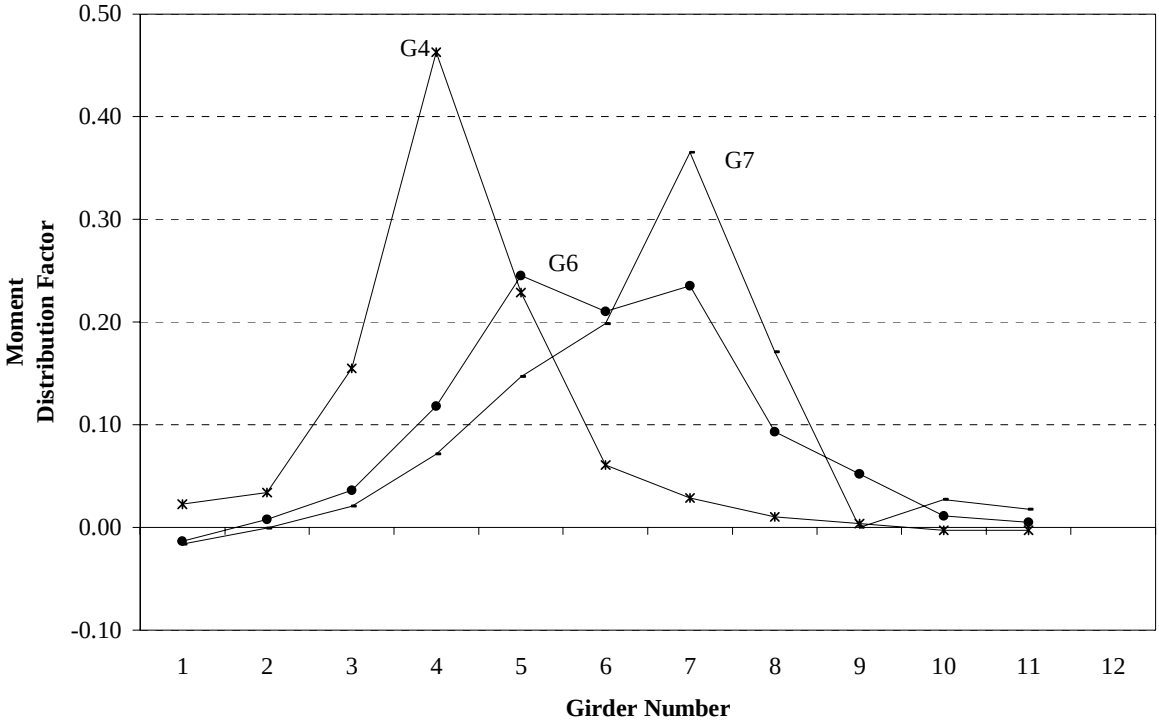


Fig. 4.42 Moment Distribution Factor (Dowling – 3 – G4, G6, G7)

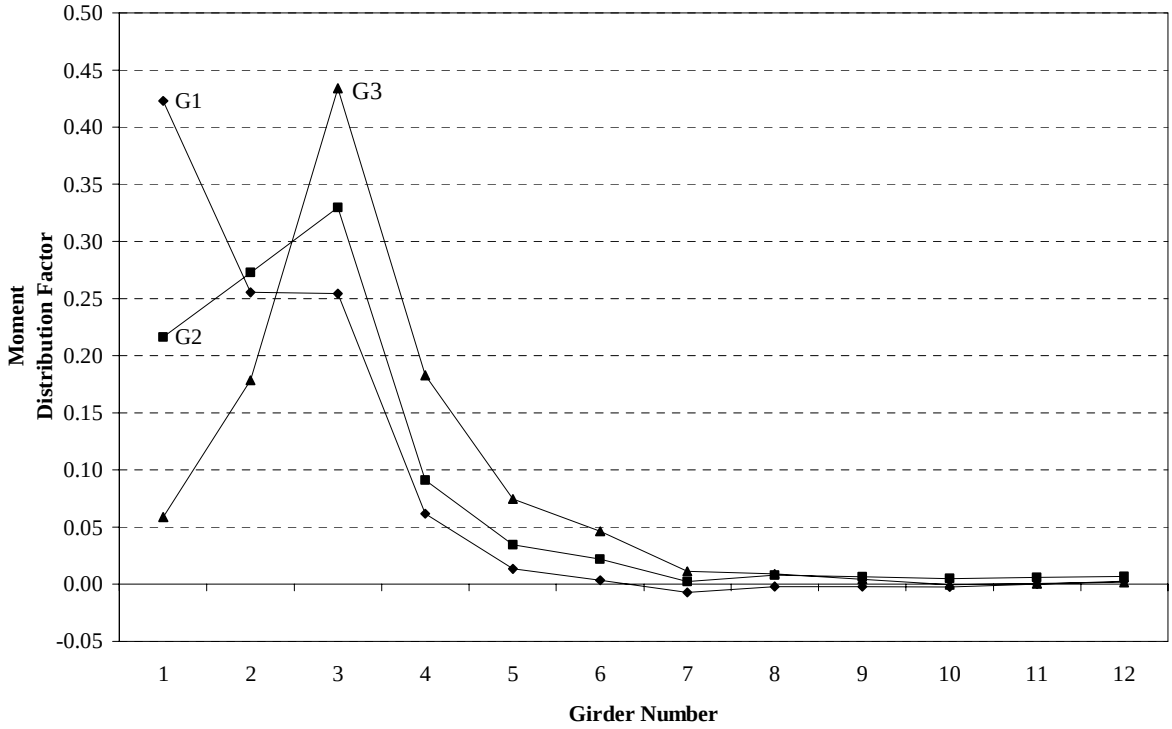


Fig. 4.43 Moment Distribution Factor (Diamond – 3 – G1, G2, G3)

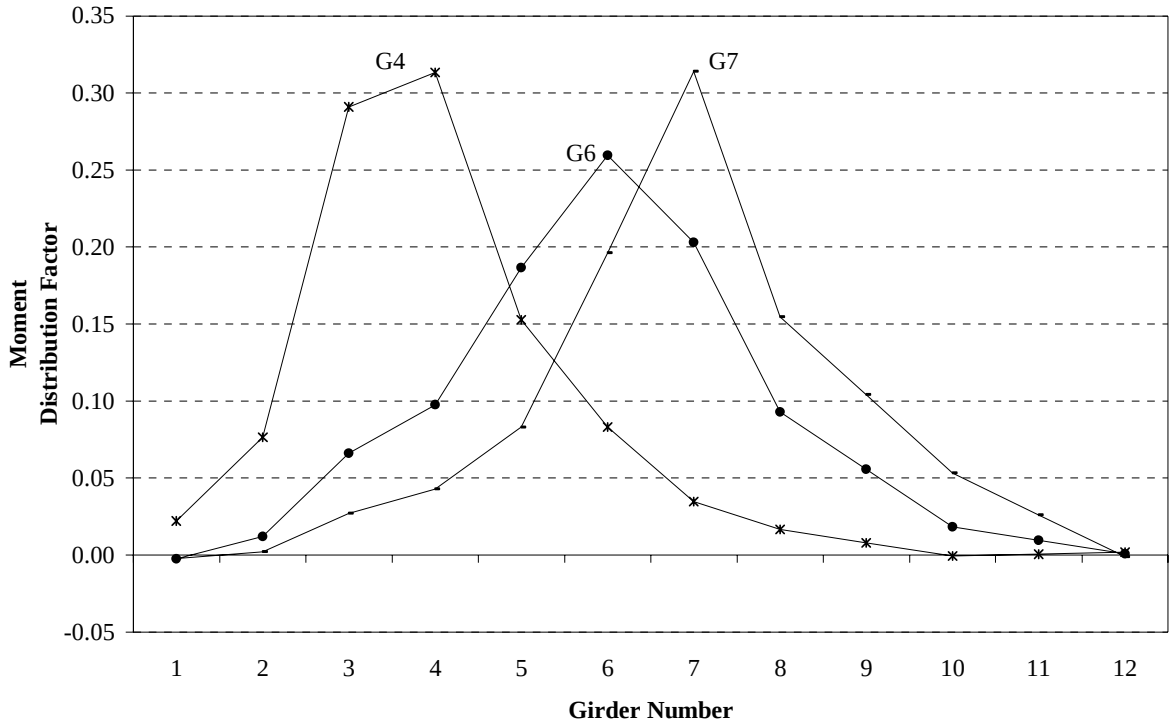


Fig. 4.44 Moment Distribution Factor (Diamond – 3 – G4, G6, G7)

Figures 4.45 and 4.46 show the moment distribution factors for the Diamond and Dowling bridges. Based on field tests, the maximum moment distribution factors for the interior girders are 0.434 for the Diamond bridge and 0.463 for the Dowling bridge, which compare with the moment distribution factor prediction of 1.471 based on AASHTO LRFD. The moment distribution factors for exterior girders are 0.423 for the Diamond bridge and 0.493 for the Dowling bridge, which compare with AASHTO LRFD prediction of 0.773. The LRFD equations give a distribution factor for the interior girder greater than one. While this kind of distribution factor may be possible for a multi lane loaded condition, it is not possible in a single lane loaded condition. Table 4.7 summarizes the moment distribution factors from Diamond and Dowling Bridges.

Table 4.7 Distribution Factor for Moment for Diamond and Dowling

| | Interior Girders | | | | | | Exterior Girders | |
|---|---|---|---|---|---|---|---|---|
| | G2 | G3 | G4 | G6 | G7 | Ave. | G1 | Ave. |
| Dowling | .19 | .34 | .46 | .21 | .37 | .32 | .49 | .46 |
| Diamond | .27 | .43 | .31 | .26 | .31 | | .42 | |

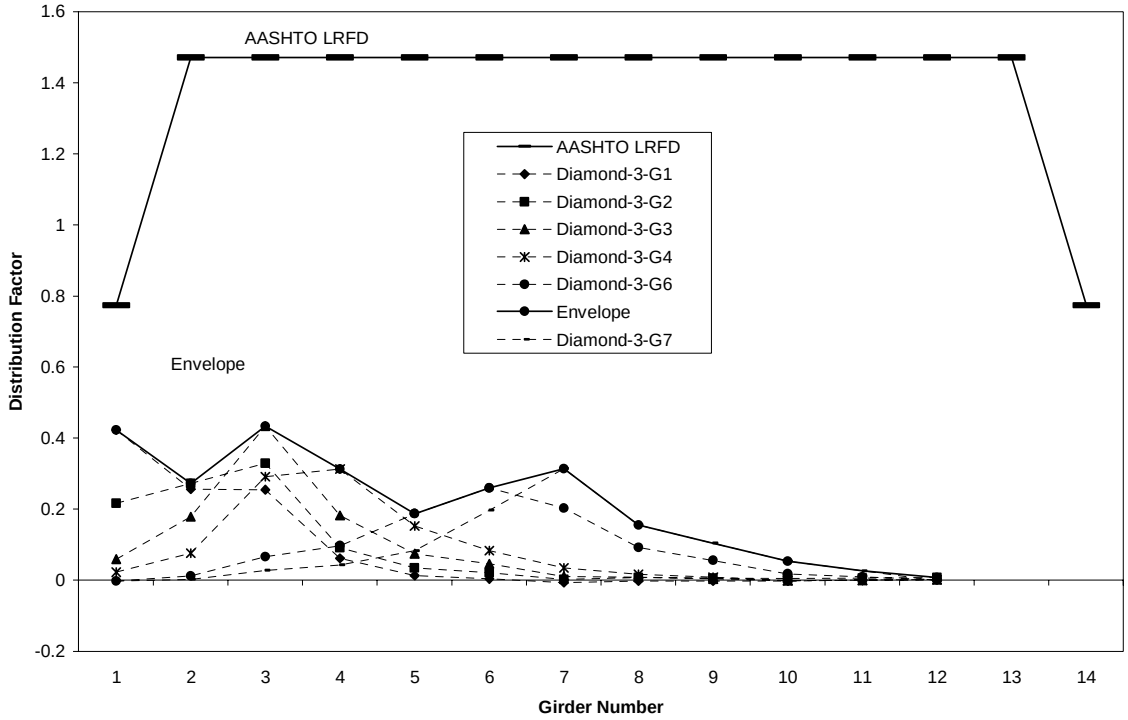


Fig. 4.45 Moment Distribution Factors (Diamond Bridge)

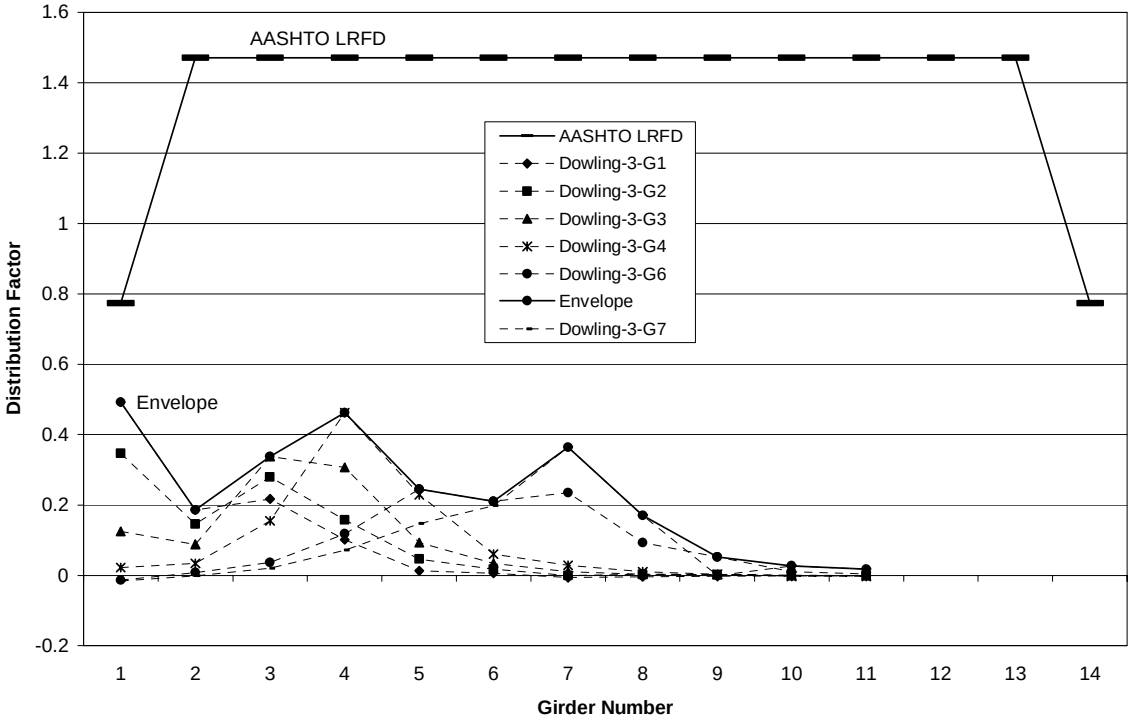


Fig. 4.46 Moment Distribution Factors (Dowling Bridge)

### 4.4.3 Load Distribution Factors for Shear

Shear distribution factors found from experimental data using Equations (4.1) and (4.2) were compared with factors calculated by the lever rule method as specified in AASHTO LRFD Specifications. Similar to Set 1 bridges, the DF for shear is shown below.

*For Interior Beams:*
Again, use the lever rule model.
Distance of left wheel to middle of outside girder $d_0$ = S – 3 = 7.567’ – 3’ = 4.567 ft

$$DF_{IS} = \frac{d_0}{S} = 0.604$$

*For Exterior Beams:*
The distribution factor for shear of the exterior beams is the same as the factor for moment of the exterior beams, i.e.,

$$DF_{ES} = DF_{EM} = \frac{d_l + d_r}{2S} = 0.773$$

Due to the limited number of gauges, we were only able to place shear gauges on one side of girder for the Dowling and Diamond Bridges. As a result, the distribution factors for shear cannot be derived directly. The shear strain data for these two bridges were used to calibrate the 3D Finite Element model developed in Chapter 3. In Chapter 5, we will use our calibrated 3D FE models to re-analyze the shear distribution factors from Diamond and Dowling bridges.

## 4.5 Summary of Findings from Field Testing

The distribution factors calculated from the data obtained by testing the four sets of twin bridges in the Anchorage area are significantly less than the distribution factors found by using the AASHTO LRFD Equations (4.3) to (4.6). Tables 4.8 and 4.9 show this disparity for the four sets of twin bridges tested. The "% Greater" column shows how much greater the LRFD distribution factor is greater than the distribution factor found from experimental data found by method shown in equation below:

$$\%\text{Greater} = \left( \frac{DF_{LRFD} - DF_{exp}}{DF_{exp}} \right)$$

Table 4.8 Distribution Factor for Moment

| Bridges Tested | Interior Girders | | | Exterior Girders | | |
|---|---|---|---|---|---|---|
| | Data | LRFD | % Greater | Data | LRFD | % Greater |
| 100th | 0.35 | 0.66 | 89% | 0.45 | 0.76 | 69% |
| Huffman | 0.31 | 0.55 | 77% | 0.49 | 0.61 | 24% |
| Campbell | 0.34 | 0.66 | 94% | 0.53 | 0.76 | 43% |
| Diamond/Dowling | 0.32 | 1.48 | 363% | 0.46 | 0.77 | 67% |
| | Average % | | 156% | Average % | | 51% |

Table 4.9 Distribution Factor for Shear

| Bridges Tested | Interior Girders | | | Exterior Girders | | |
|---|---|---|---|---|---|---|
| | Data | LRFD | % Greater | Data | LRFD | % Greater |
| 100th | 0.43 | 0.60 | 40% | 0.66 | 0.76 | 15% |
| Huffman | 0.46 | 0.57* | 24% | 0.58 | 0.67* | 16% |
| Campbell | 0.50 | 0.60 | 20% | 0.71 | 0.76 | 7% |
| Diamond/Dowling | 0.55† | 0.60 | 9% | 0.60† | 0.77 | 28% |
| | Average % | | 23% | Average % | | 17% |

** Indicates adjusted with skew adjustment factor.*
*† Indicates value not found directly from data but from a FE model that closely approximates the data.*

When comparing the LRFD equations to the experimental data from the eight tested bridges, the distribution factors found from the LRFD equation proved to be an average of 156% greater for moment on interior girders, 51% greater for moment on exterior girders, 23% greater for shear on interior girders, and 17% greater for shear on exterior girders.

Equations (4.3 – 4.6) describe the moment distribution on interior girders while the equation governing the rest of the distribution factors is the lever rule. The reason the LRFD equation for moment on interior girders is so much higher than the experimental data is due to comparison of the LRFD equations to the data found from the twin bridges located at Diamond and Dowling. The LRFD equation for these bridges is 363% larger than the

experimental values. One of the reasons the LRFD equations are so much larger than the experimental values is that the equations are affected by the overall width of the bridge. Diamond and Dowling bridges are both very wide bridges and the results of the parametric study in chapter 6 show that the distribution factor is not as affected by the overall width of the bridge as the LRFD equations predict. The lever rule which governs the rest of the equation is not based on research of the bulb-tee bridge system, but is a default method for determining the live load distribution of girders. The lever rule is the simple distribution of the vehicle wheel load onto the girders. The lever rule assumes the girders are infinitely stiff and the distribution is only affected by the girder spacing. Since the bridge girders are much stiffer when loaded to produce the maximum shear forces than when loaded for moment, the lever rule predicts the shear distribution better than the moment distribution on exterior girders.

# CHAPTER 5 – DEVELOPMENT OF 2D GRILLAGE MODELS

The decked bulb tee bridges are unique in that they have a longitudinal joint between girders. As part of this research, the question rose as to how the longitudinal joint behaves during load distribution and how it should be modeled. Based on the field testing results and the developed 3D FE models discussed above, a 2D grillage model will be developed here for its calculation efficiency comparing with the 3D FE models.

## 5.1 2D Grillage Model Development

Of the four sets of bridges tested, the set located at the intersection of 100$^{th}$ Ave. and Minnesota is the most standard in that they have no skew, have an average span length and width, and are built with typical decked bulb-tee girders. The data from these two bridges will be used to evaluate the different modeling techniques of the Grillage model. These bridges are 115 ft long with no skew and have the cross-section shown in Figure 5.1.

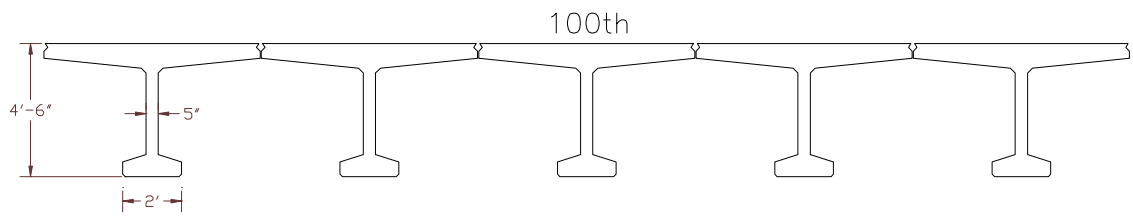


Fig. 5.1 Cross-section of 100$^{th}$ Ave Bridge

The deck portion of each girder tapers from 10.0 in. near the web to 6.0 in. near the joint. Each longitudinal joint has been grouted with 4.0 in. shear keys placed every four feet. The first modeling method used to evaluate the bridge behavior is the grillage model. The grillage model assumes the bridge is a mesh of frame elements. The mesh consists of longitudinal beams and transverse beams. The longitudinal beams represent the stiffness of the bridge in the longitudinal direction. The stiffness of the longitudinal beams is governed by the spacing of the beams and the width of the bridge they represent. The transverse beams are perpendicular to the longitudinal beams and rigidly connected to the longitudinal beams. The stiffness of the transverse beams is governed by the width of the bridge deck they represent. By reducing the bridge system from a three dimensional monolithic structure into a mesh of interlocking perpendicular two-dimensional frame elements, the bridge behavior can be analyzed using simple frame analysis. The grillage analogy has proven to be an accurate method for describing bridge behavior.

### 5.1.1 Longitudinal Joint

The transverse beams (deck thickness) are represented by a solid rectangular section that varies in depth from 10" at the web to 6" at the joint and is 3.8 ft wide. To Approximate the longitudinal joint, we experimented with different connections between the transverse beams. The first condition is called the "rigid" condition in which the connection between beam elements is fully fixed and has full transverse continuity. The other condition is called the

“hinged” condition in which the joint is flexuraly released in transverse direction. The longitudinal joints between bridge girders behave somewhere between these two extreme conditions.

In this section, we look at two other methods which may approximate the behavior of the joint. The first method models the joint as if it were a small rectangular grout section. We modeled this grout section by connecting the transverse beams with a small rectangular member with a depth of three inches and width of 3.8ft. The modulus of elasticity of this grout section is approximated at 2500ksi which is roughly half of the modulus of elasticity used to model the girder section. We found the distribution factor from this reduced section to be almost identical to the purely rigid connection. From the model we found the maximum tensile stress in this small 3 inch grouted section to be 2600psi.

Since the forces generated in the grouted section could easily crack the grout, the second method for approximating the joint uses a one inch long beam that has the same properties of a cracked grout section. The moment of inertia of the cracked grout section was determined by using cracked section analysis methods. The cracked section was assumed to have a width of 3.8ft and a 4” x ¼” shear plate at the bottom of the cracked section providing the tensile strength. Even the reduced stiffness of the cracked grouted section shows distribution factors very close to the purely rigid connection. Figure 5.2 is a graph which compares all of these models to the experimental data.

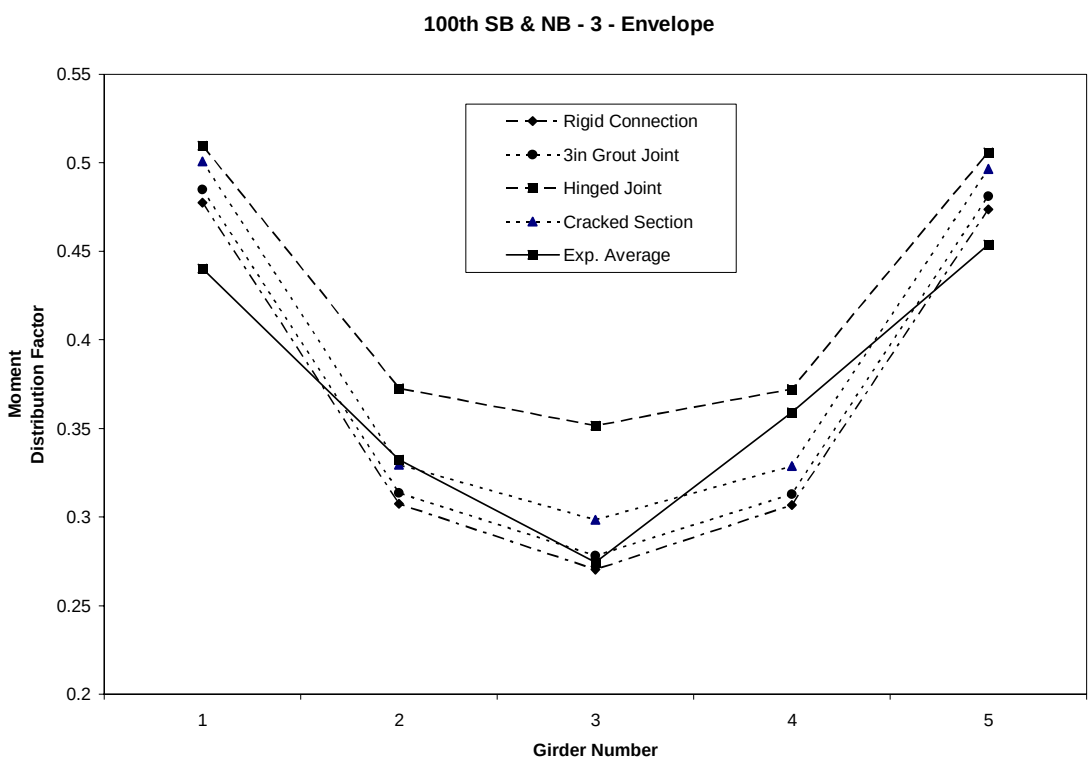


Fig. 5.2 Impact of the Longitudinal Joint on Moment DF

### 5.1.2 Torsional Constant

The grillage model used to model the twin bridges at 100th ave. has 5 longitudinal beams representing the 5 girders of the bridge. Each beam has the same moment of inertia as the decked bulb-tee girders they represent. Saint-Venant's torsional stiffness constant of the longitudinal beams was approximated using the current method described in the AASHTO LRFD for stocky open sections:

$$J = \frac{A^4}{40 \cdot I_p} \tag{5.1}$$

Where "A" is the area of the girder and $I_p$ is the polar moment of inertia. Other methods of determining "J" such as the standard grillage approximation of adding the horizontal and vertical moments of inertia together were compared to Equation (5.1), yet Equation (5.1) produced results that most closely matched the data. Figures 5.3 and 5.4 show a comparison of different torsional rigidity constants for the moment distribution factors for both the hinged and rigid conditions.

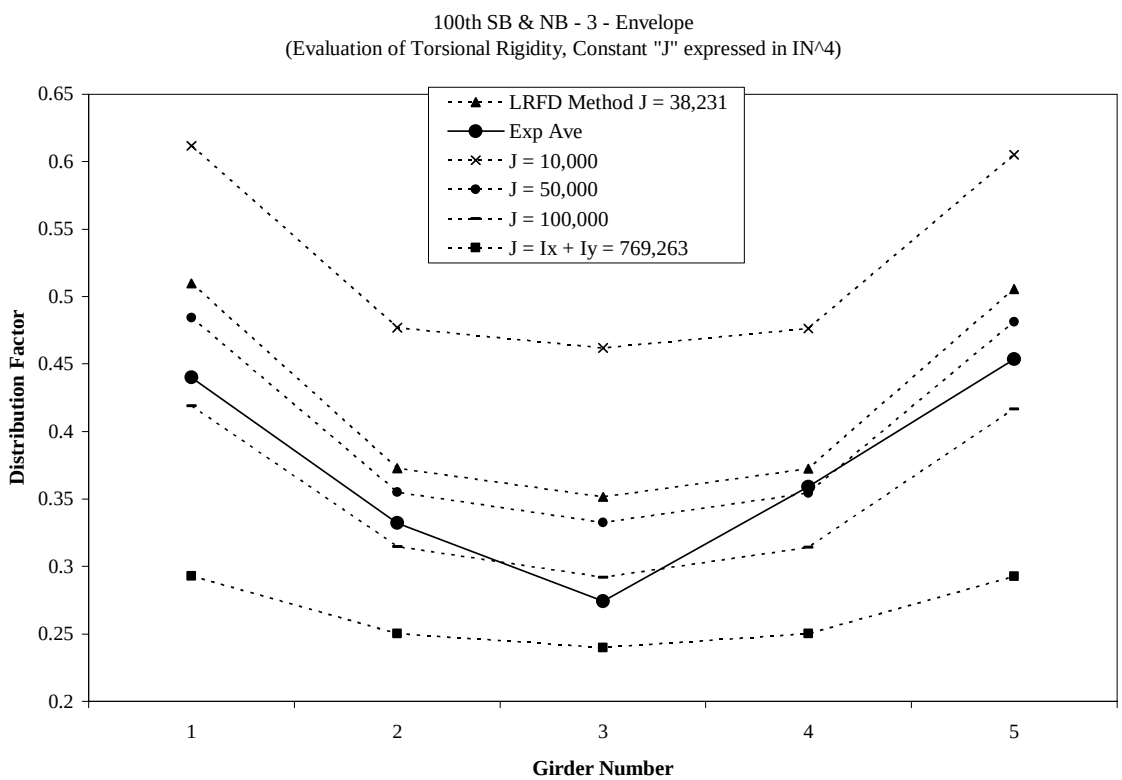


Fig. 5.3 Evaluation of Torsional Constant in Hinged Grillage Models

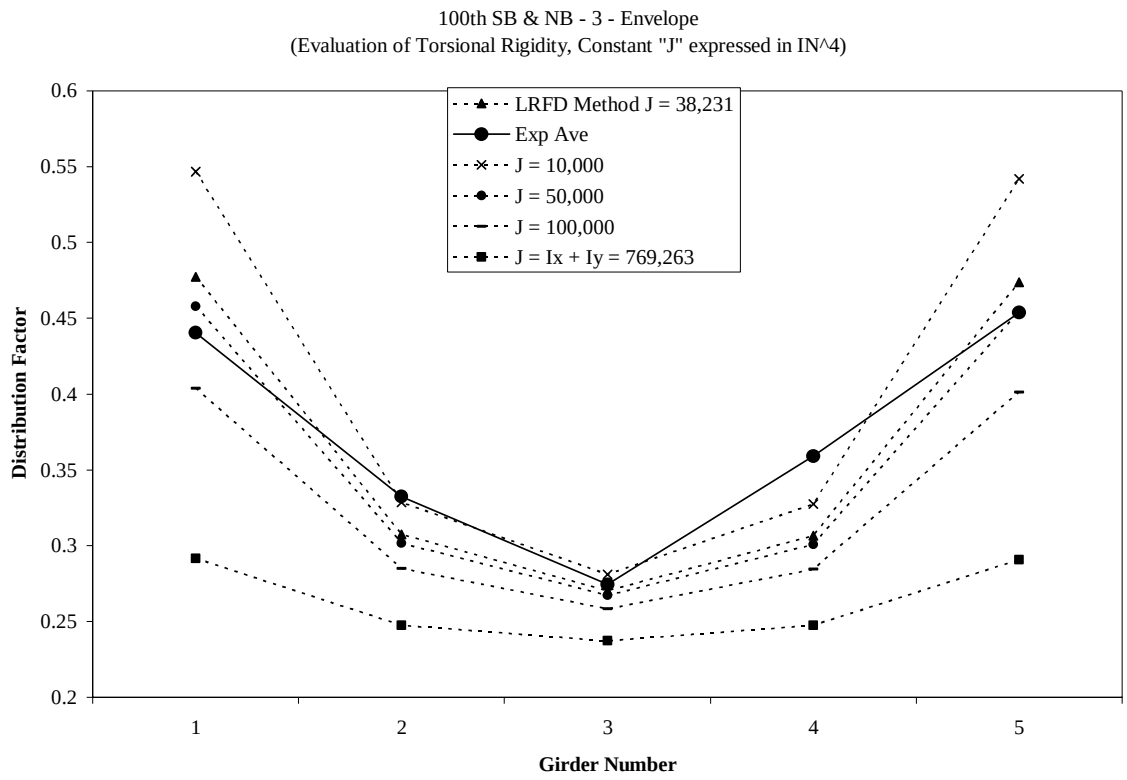


Fig. 5.4 Evaluation of Torsional Constant in Rigid Grillage Models

### 5.1.3 Mesh Density

The transverse stiffness of the bridge deck is approximated by 30 beam lines each separated by 3.8 ft. Different mesh densities were compared, and it was found that increasing the density had little impact on the distribution factor. Figure 5.5 compares the moment distribution factor found from three different mesh densities. The first density is 5 longitudinal frame elements and 30 transverse frame elements (5-30). The second density is 15 longitudinal frame elements with 60 transverse frame elements (15-60). The third mesh density is 30 longitudinal frame elements with 60 transverse frame elements (30-60). To increase the mesh in the transverse direction, the frame elements had the same properties as in the coarser mesh except with half the width. To increase the mesh density in the longitudinal direction, the cross-section of the bridge girders were subdivided into 3 elements for the 15-60 model and into 6 elements for the 30-60. The elements which subdivided the bridge girder had different properties. The middle element had stiffness of the middle portion of the bridge girder and the torsional stiffness found from Equation (5.1). The other longitudinal frame elements were modeled as a rectangular section with a height equal to the average height of the tapered flange across the section. The comparison shows that there is little variation in the distribution factor found from the three different models therefore it is sufficient to use the simplest model of 5 longitudinal girders and 30 transverse girders. This density provides slightly more conservative results than the other two finer densities.

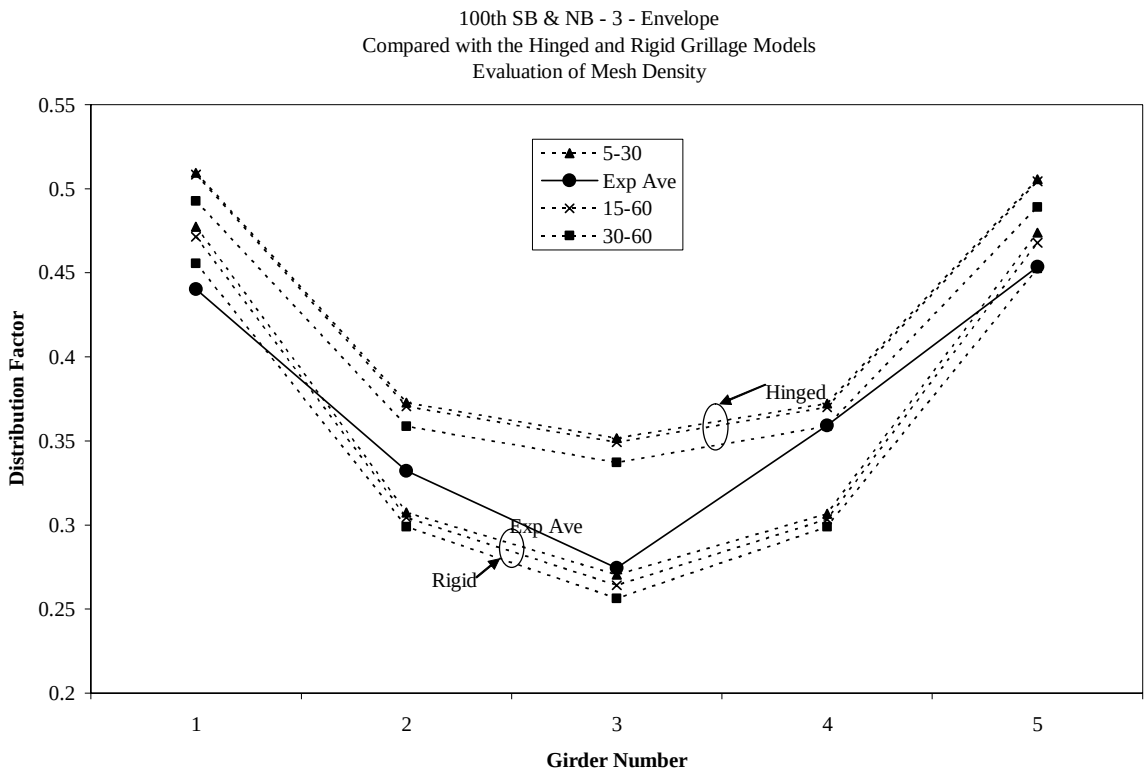


Fig. 5.5 Evaluation of Mesh Density in Grillage Models

### 5.1.4 Effect of the Intermediate Steel Diaphragms (ISD)

Another factor that will affect the behavior of the longitudinal joint is the intermediate steel diaphragms. The exaggerated deflection of the hinged model is shown in Figure 5.6 where each girder rotates slightly at each hinged joint. It appears that any connection between two girders at the bottom flange would help to resist this rotation about the longitudinal joint as shown in Figure 5.7.

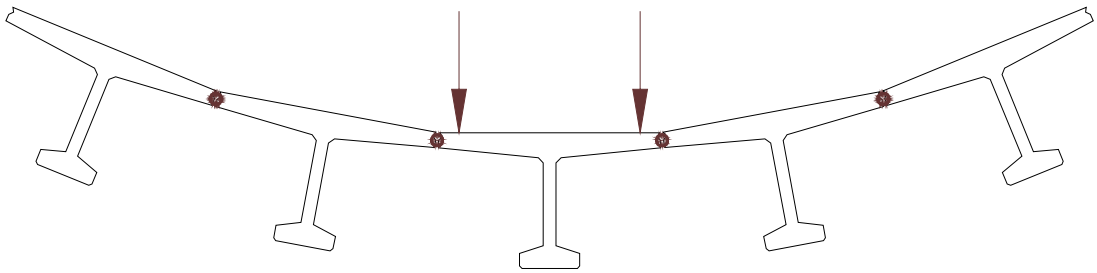

Fig. 5.6 Exaggerated Deflection of the Hinged Model

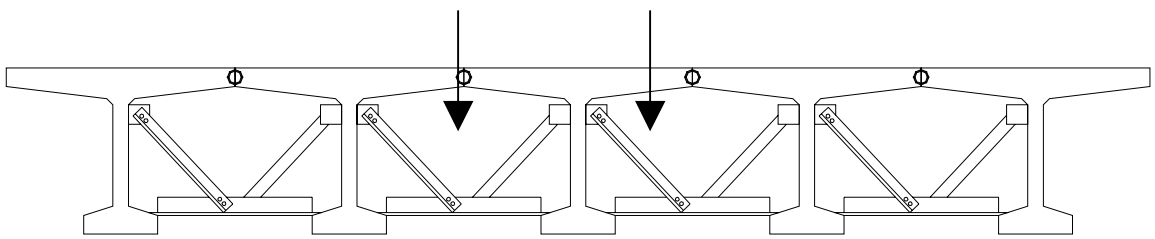

Fig. 5.7 Intermediate Steel Diaphragms help to resist rotation

In the grillage model, the only restraint the girder has to rotating about the hinge joint is the torsional rigidity of the girder. If the joint behaves as a perfect hinge, the grillage model cannot approximate the effects of intermediate steel diaphragms on preventing the girder from rotating about the hinged joint. The 3D Finite Element (FE) models developed in Chapter 3 for the bridge located at 100$^{th}$ ave. and Minnesota better approximate the affects of the intermediate steel diaphragms. Four different 3D models were developed. One model approximates the longitudinal joint as a hinged joint with perfect transverse flexural release across the longitudinal joint and no elements representing the steel diaphragms in the bridge. The other condition is exactly the same except truss elements were placed between the girders at the same location as the steel diaphragms on the tested bridge. These truss elements have the same stiffness and orientation as the K type diaphragms used on the bridge. Another two models have the same properties as the two models previously described except the longitudinal joint is modeled as having full transverse flexural rigidity. The results from these models show that the hinged FE model without the intermediate steel diaphragms has very close distribution factors as the hinged grillage model. The introduction of the steel diaphragms into the hinged model significantly reduces the distribution factor of

the bridge and it has almost the same distribution factors as the FE models with full transverse flexural rigidity and the grillage model that has full transverse flexural rigidity. For all of the bridges, this later set of models better approximates the experimental data both for shear forces and for moment forces.

Figures 5.8 and 5.9 compare the envelope of experimentally found distribution factors for the bridge located at 100th ave to the grillage and FE models. These graphs show that the grillage and FE hinged models do not compare well with the data and have a distinctly different behavior than do the models that are rigidly connected along the longitudinal joint and/or have intermediate steel diaphragms.

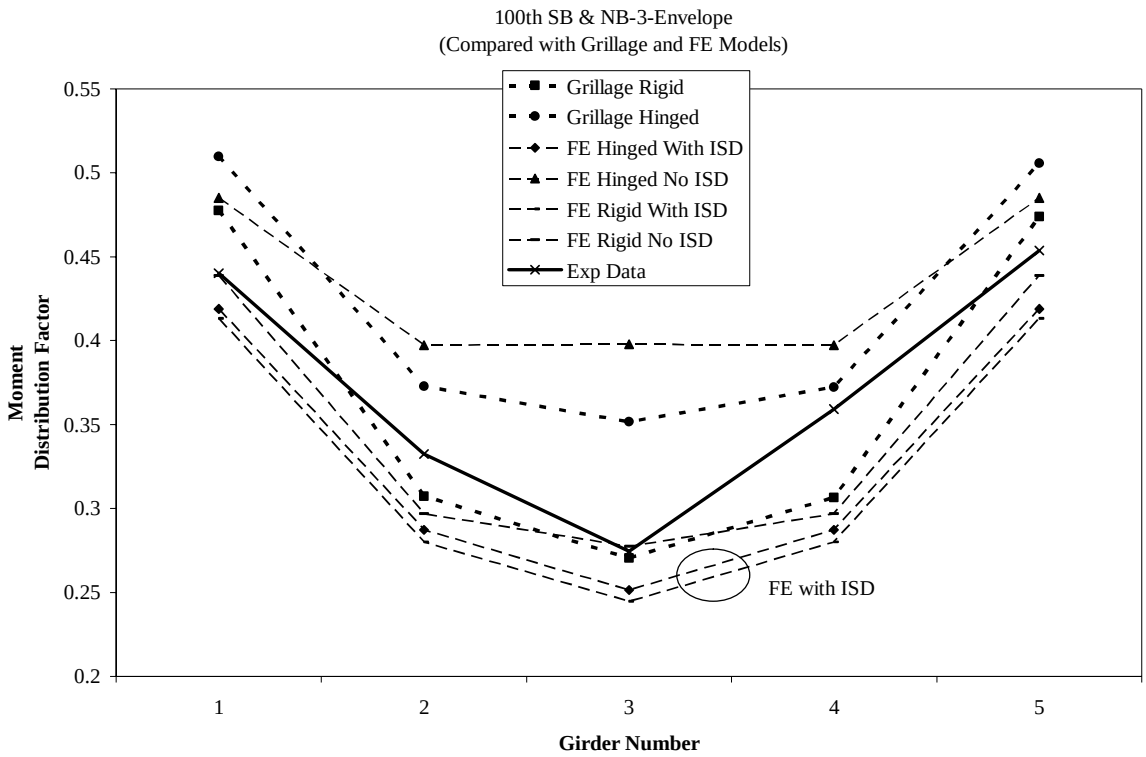


Fig. 5.8 Moment DF comparison With/Without ISD

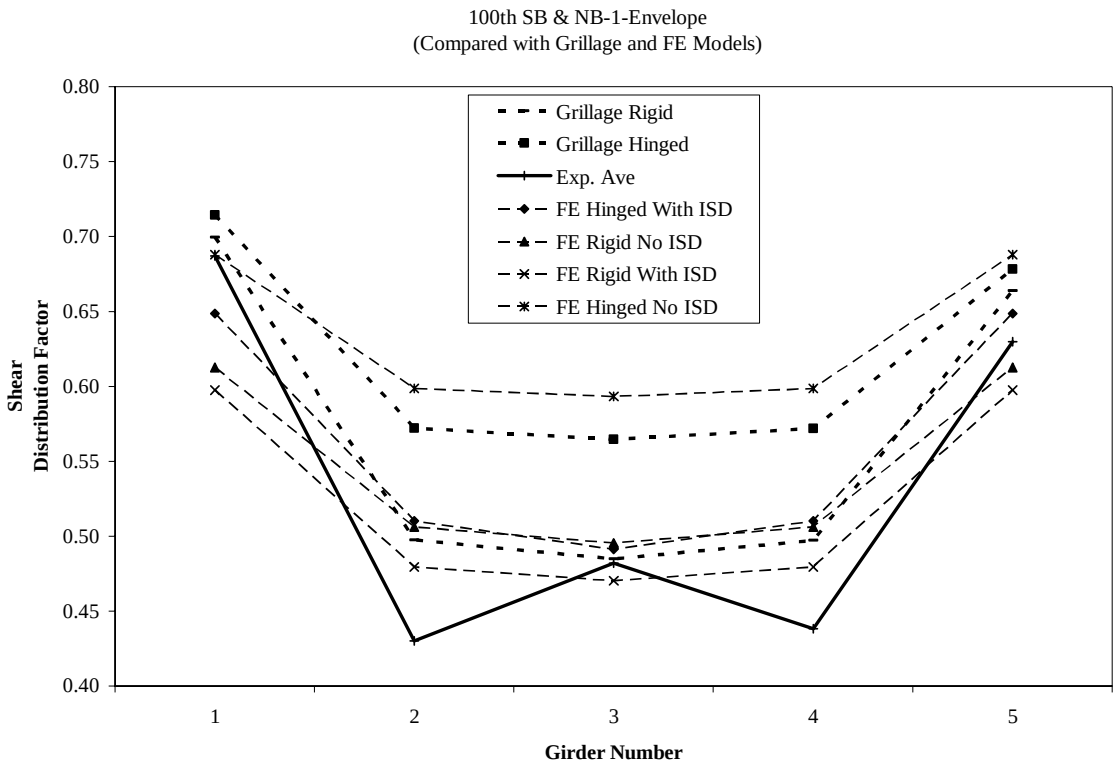


Fig. 5.9 Shear DF comparison With/Without ISD

Another method used to compare the experimental data to the grillage and 3D FE models is to estimate the midspan moments of the girders from the strains measured at the bridge's midspan and from strains in the 3D finite element model to the moments found from the grillage model. Since the grillage model is comprised of one dimensional beam elements, only member forces can be found from the model. To relate these forces to the experimentally measured strains, and the strains from the 3D finite element model, simple mechanics of materials must be used to estimate the moments the bridge experiences from the measured strains. The following equation is used to make this relationship.

$$M = \frac{E \cdot \varepsilon \cdot I}{c} \tag{5.2}$$

Where "M" is the midspan moment, "E" is Young's Modulus for the concrete, "I" is the moment of inertia of the girder, "c" is the distance from the bottom surface of the girder to the neutral axis, and "ε" is the measured strain. While there are many methods for determining the values of E, I, and c, these are only approximate methods and there is a margin of error for determining each of these values. When calculating E using the method described in the ACI Code, the actual value can vary from 80% to 120% of the calculated value [ACI 2002]. Another source of error in determining these values could come from the wearing surface contributing to the stiffness of the girder and varying the location of the neutral axis. Small variations in these three variables have a significant affect when trying to compare the measured strains to the output of the grillage models and the FE Models. The

theoretical values of these three variables based off the simple geometry of the girder and the design strength of the concrete are as follows: E = 4645 ksi, I = 3623345 in^4, and c = 38.13 in. When solving for the forces in the girders using these values, the sum of the moments in all the girders is 2320 ft-kip. This moment could only be produced if the vehicle weighed 89.3 kips. Since the total weight of our load vehicle was 72.6 kips, it is clear that the true modulus of elasticity and moment of inertia must be less than approximated, or the neutral axis higher than approximated. It is also likely that the weight of the load vehicle was greater than 72.6 kips which is the measured weight of the vehicle at the beginning of the bridge testing. To better evaluate the data so that it would compare with our models, the modulus of elasticity was determined by holding the other variables constant and setting M of equation (5.2) equal to the total moment of all the girders across the midspan of the bridge (1882 ft-kips). This is the total moment the bridge would experience if it were subjected to a load of 72.6 kips. The new modulus of elasticity was found to be 3769 ksi. This value is 81% of the value obtained using the equation in the ACI code and is within the acceptable range of deviation. While the true modulus of elasticity may not be this exact value, by using this value of E to compute the midspan moments, the experimental data can be compared to the math models.

Figure 5.10 shows the midspan moments of each of the five bridge girders when the load is positioned directly over the middle girder. The experimental moments are derived from the average of four different strain values taken from two different loading runs over two different twin bridges (100$^{th}$ NB & 100$^{th}$ SB). For all of the following graphs, the dotted lines represent the grillage models, the dashed lines represent the 3D FE models, and the solid lines represent values found from experimental data.

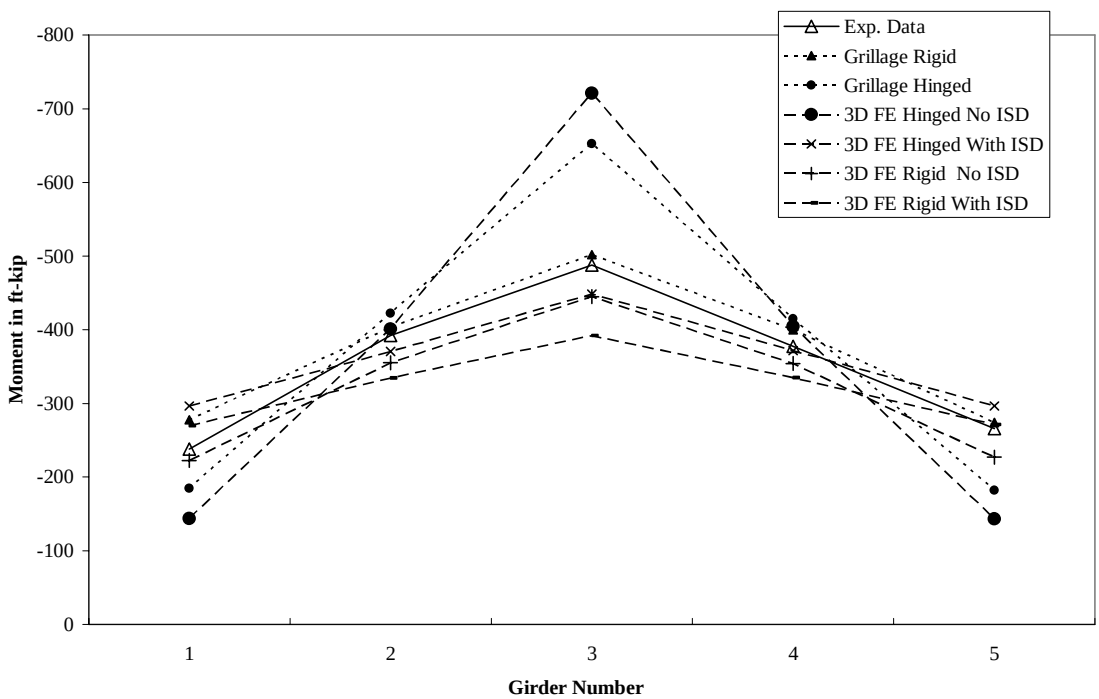


Fig. 5.10 Midspan Moments from Different Models (100$^{th}$ – 3 – G3)

In Figure 5.10, the Grillage Hinged Model and the 3D FE Hinged model without any intermediate steel diaphragms show a much higher midspan moment under girder three than all the other models and the average from the experimental data. This same trend can be seen in Figure 5.11 when the load is placed over the second girder.

When the Load is placed on the exterior girder as shown in Figure 5.12, all the models appear to behave the same and there is no obvious affect of releasing the transverse flexural rigidity. The bridge system also shows little variation between the transverse hinged and rigid conditions when deriving the distribution factor for the exterior girders.

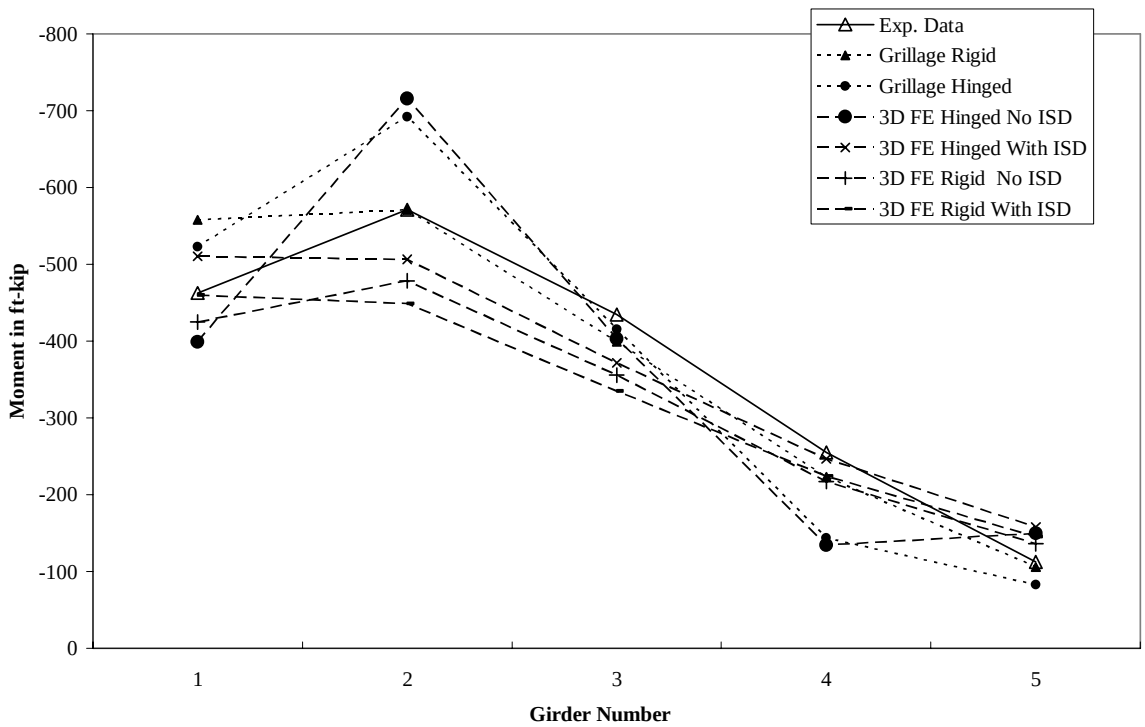


Fig. 5.11 Midspan Moments from Different Models ($100^{th}$ – 3 – G2)

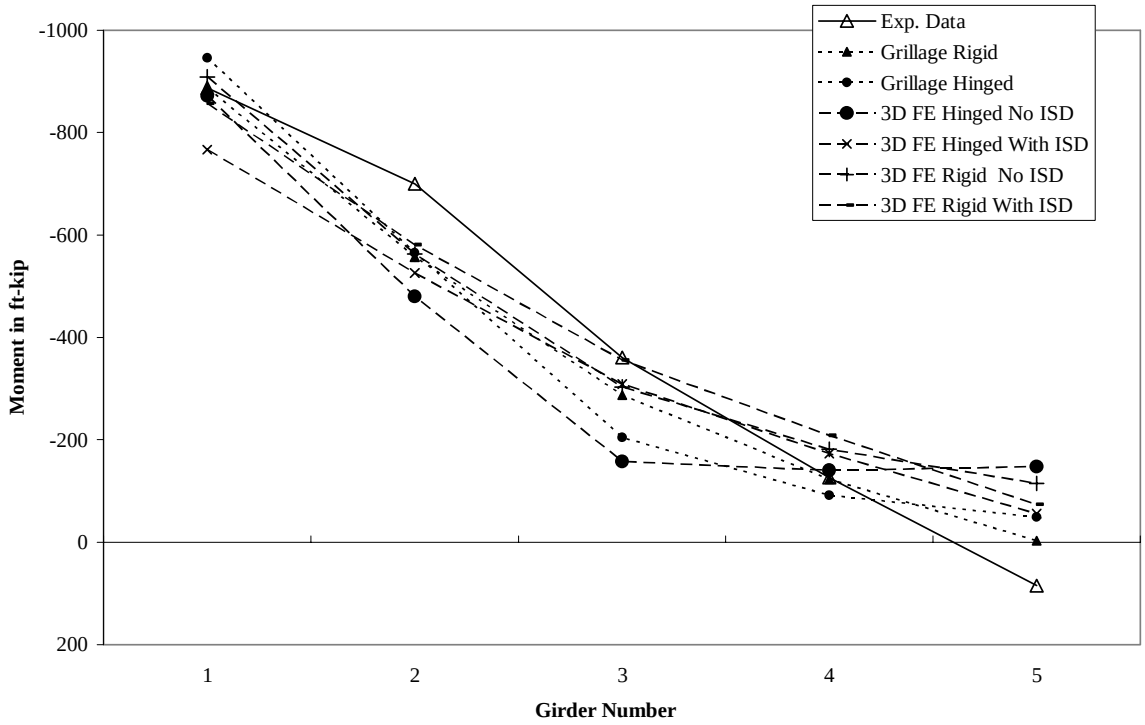


Fig. 5.12 Midspan Moments from Different Models ($100^{th}$ – 3 – G1)

Later in this Chapter, the two methods shown in this section will be used to compare the hinged and rigid models to data from other bridges. The data from the Huffman and Campbell bridges also compare better to a rigid grillage model or a FE hinged model that has intermediate steel diaphragms.

### 5.1.5 Boundary Conditions

Figure 5.13 shows the beam layout of the grillage model. Due to the concrete diaphragms at the ends of the bridge and the eccentricity of the rollers, the actual support conditions will be somewhere between a fixed and pinned condition. The actual support conditions are impossible to measure so Figure 5.14 compares the distribution factor from models with both pinned and fixed supports to the data. The data is much closer to the pinned conditions than the fixed condition. The total moment across all of the girders was calculated to get an idea of the behavior of the support conditions, yet this showed the total moments to be greater than that of a pinned condition. This is due to other unknown variable such as the modulus of elasticity and depth of the neutral axis which will affect the calculation of moments in the girders from the measured strains. Since the distribution of the data more closely matches the pinned support condition, the pinned support conditions are used in the remainder of the models. To approximate the concrete end diaphragms, the support conditions are pinned yet torsionally fixed.

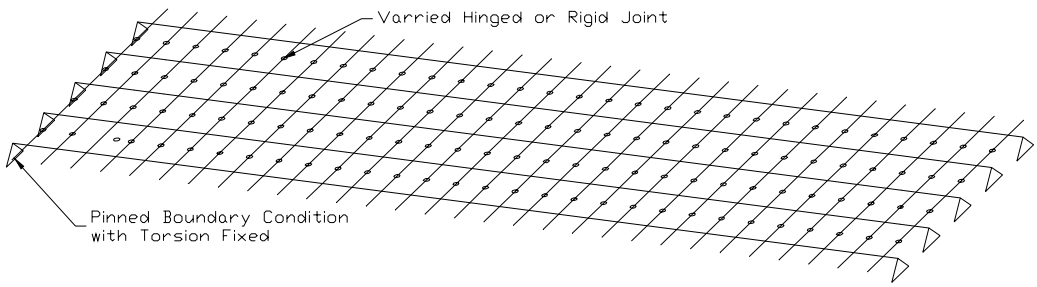


Fig. 5.13 Schematic of Diagram of Grillage Model

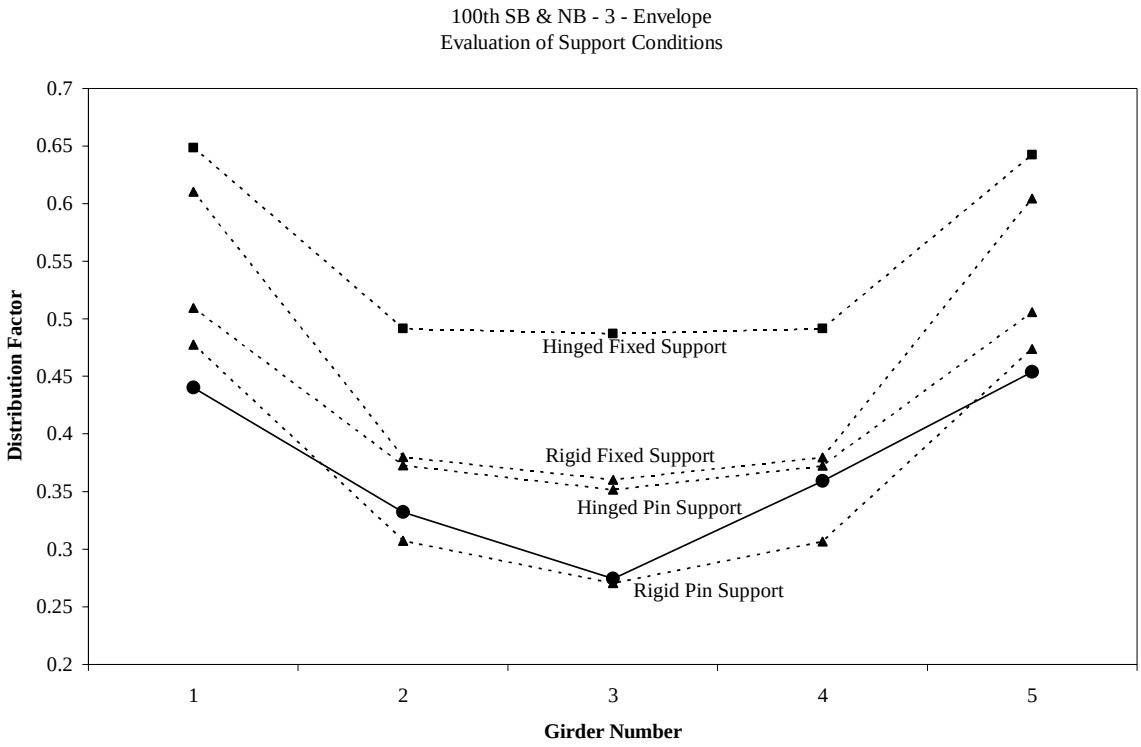


Fig. 5.14 Impact of Model Support Conditions

## 5.2 2D Grillage Model Verification

This section compares the distribution factors found from experimental data to the DF factors found from the grillage model and the AASHTO LRFD equations. The multiple presence factor has been factored out of the AASHTO LRFD results to compare them with the grillage model and experimental data.

### 5.2.1 Comparisons with Set 1 Bridges

The method of calculating the AASHTO LRFD distribution factors for the twin bridges located at 100th Ave and Minnesota was presented in Chapter 4. Figure 5.15 shows the average distribution factors of both 100th SB & NB and compares it to the hinged and rigid grillage models. Figure 5.16 shows the average shear distribution factors of both 100th SB & NB and compares it to the hinged and rigid grillage models.

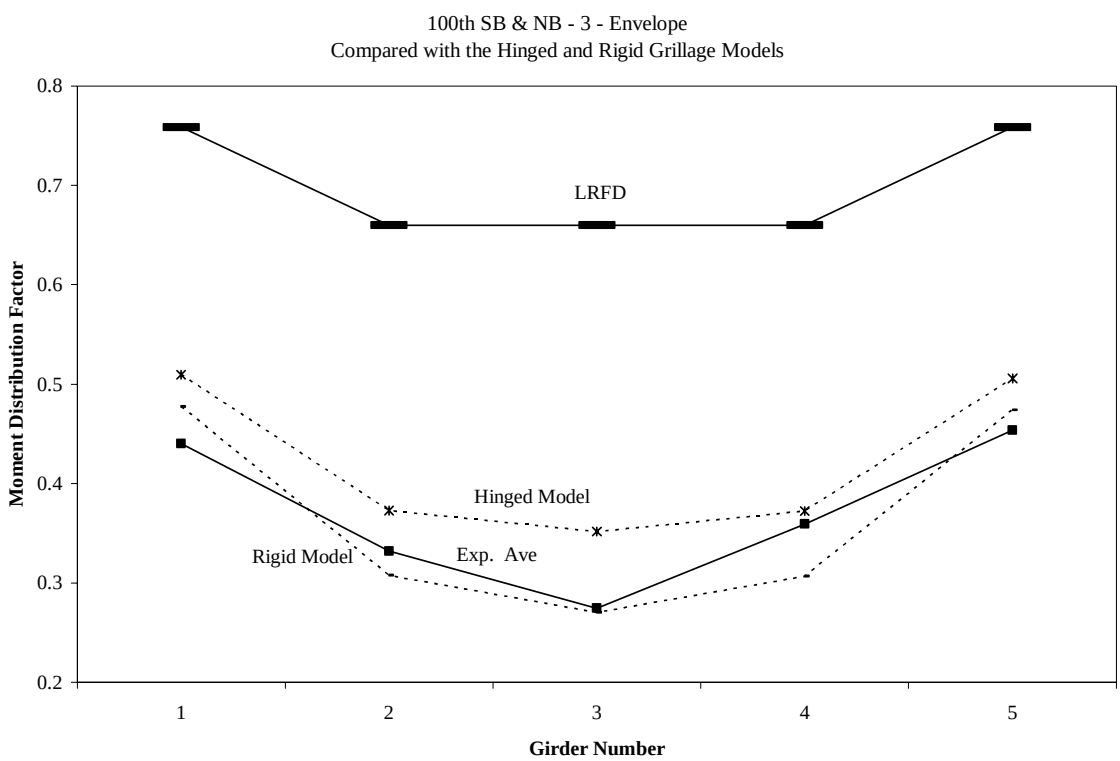


Fig. 5.15 Moment Distribution Factor Comparison (100th NB&SB Bridge)

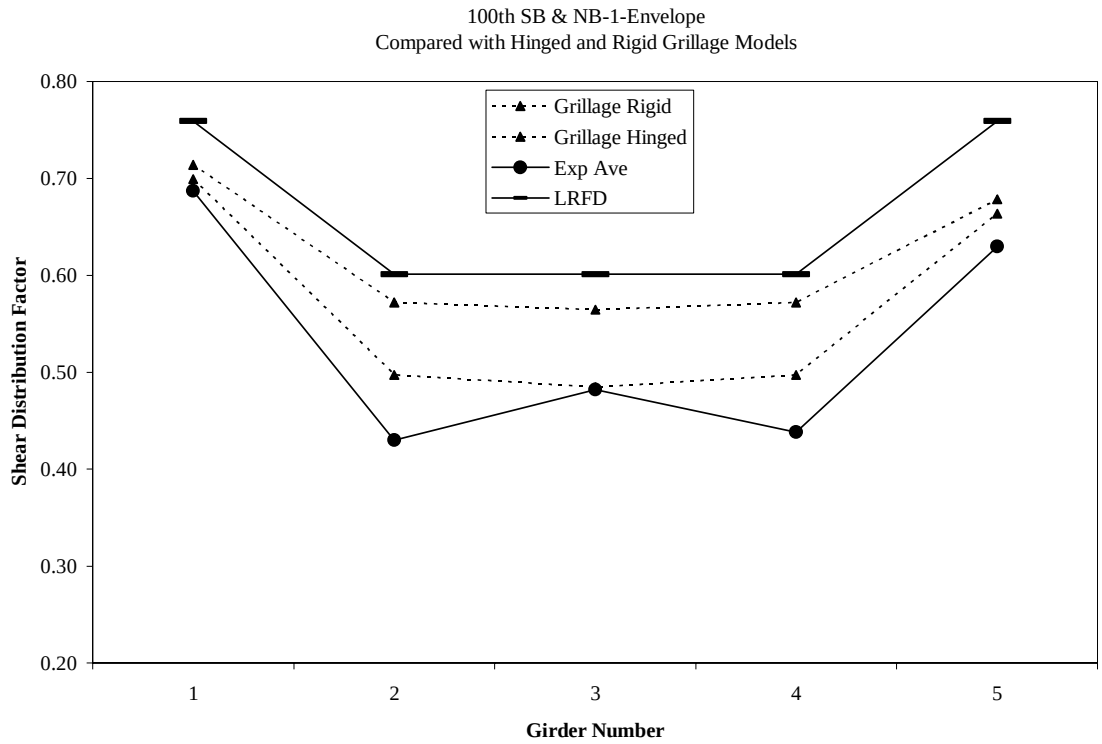


Fig. 5.16 Shear Distribution Factor Comparison (100th NB&SB Bridge)

### 5.2.2 Comparisons with Set 3 Bridges and 3D FE Models

We did not get as consistent of data from the Campbell Creek Bridges as we did from the Set 1 bridges crossing 100th ave. The Campbell Creek Bridges are long with deep girders. They have a 4 degree skew angle which is small enough that it hardly affects the bridge behavior. Since these bridges were the first pair of bridges tested of the eight, we had many errors attributed to developing a procedure for setting up the bridges for testing. For these twin bridges and all subsequent sets of bridges, there is only one 3D FE model per bridge. The FE model has intermediate steel diaphragms and models the longitudinal joint as a pure hinge.

We will compare the data to the grillage and FE models using the same two methods used to evaluate the data in the 100th Ave. Bridge. The first method compares the derived moments from the strains to the forces found in the beam elements of the grillage model. The second method compares the distribution factors from the data to the models and to LRFD equations.

The theoretical values of the mechanical properties of the girders are as follows: E = 4645 ksi, I = 633162 $in^4$, and c = 45.5 in. When these values are used with the experimental data, the total moment of all girders averages to 1736 ft-kips. This value is less than 1876 ft-kips which is the theoretical moment of placing the load vehicle at midspan on a simply supported beam 139ft long. To standardize the moments found from experimental strains, we found an E value of 5020 ksi which is 108% of the theoretical E value.

The Figure 5.17 shows the midspan moments of each of the five bridge girders when the load is positioned directly over the middle girder. The experimental moments are derived from the average of four different strain values taken from two different loading runs over two different twin bridges (Campbell NB & Campbell SB). Figure 5.18 shows the distribution factor average envelope between the two bridges and compares it to both the grillage and FE models. The experimental data used in generating Figure 5.18 does not include the data from the suspect gauge on Campbell SB – M1G5. Figure 5.19 shows the shear distribution factor average envelope between the two bridges comparing it to both the grillage and FE models.

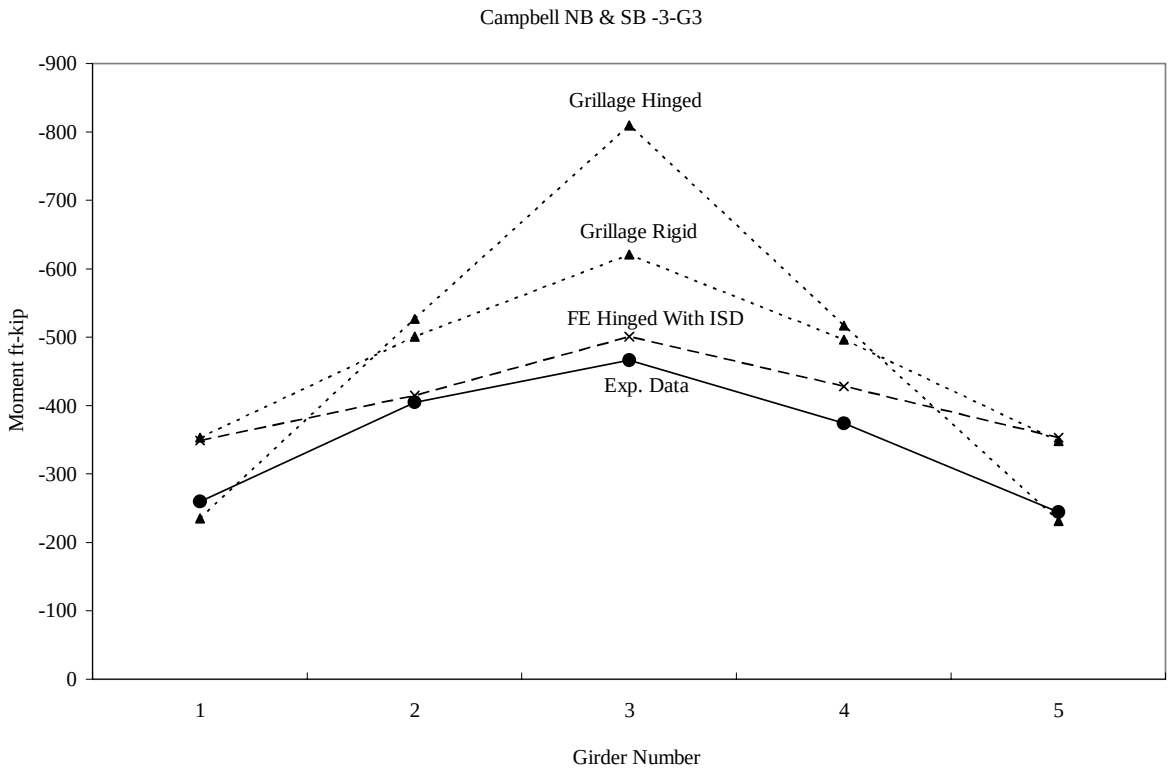


Fig. 5.17 Midspan Moment from Different Models (Campbell NB&SB)

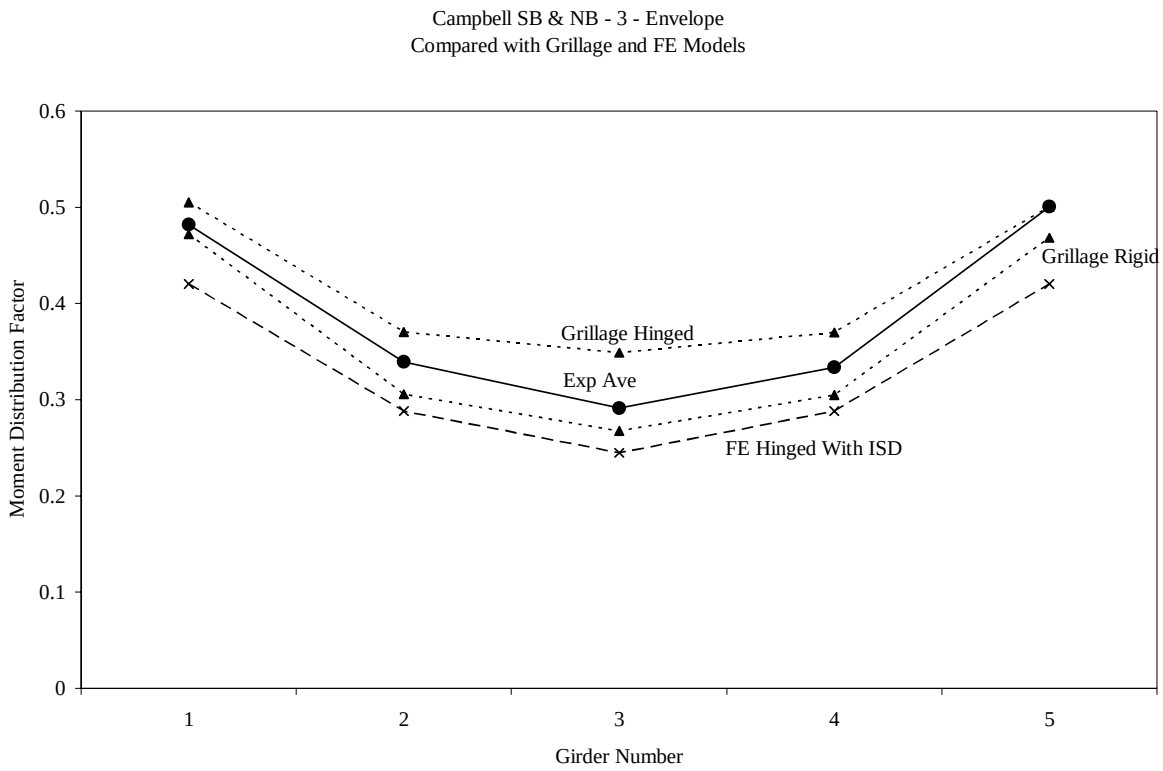


Fig. 5.18 Moment Distribution Factor Comparisons (Campbell NB&SB Bridge)

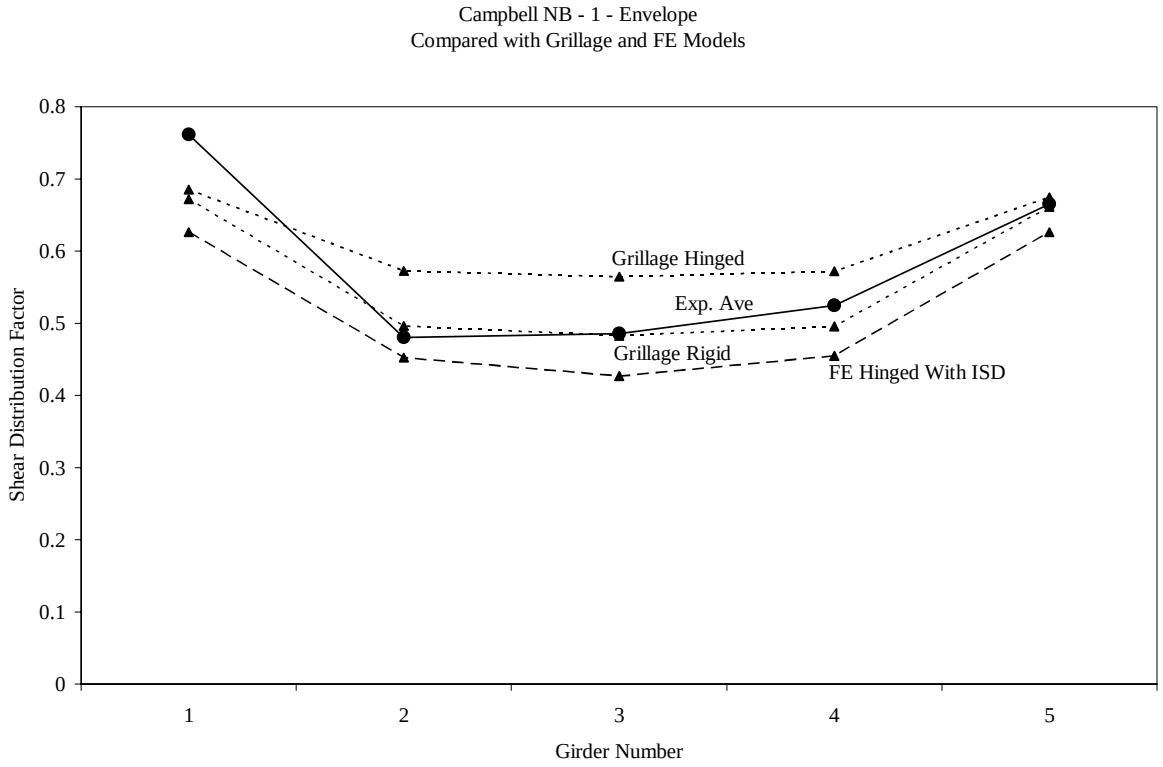


Fig. 5.19 Shear Distribution Factor Comparisons (Campbell NB&SB Bridge)

### 5.2.3 Comparisons with Set 2 Bridges and 3D FE Models

The Huffman twin bridges differ from the Set 3 bridges in that they have a 27.5º skew. We will use the same two methods to compare the models of this bridge to the experimental data as was done on the Campbell bridges and 100th ave bridges. When comparing the deriving the moments for the Huffman twin bridges, we found the approximate modulus of elasticity to be 3800 ksi. This is 82% of 4645 ksi which is the approximation of the modulus of the concrete using the ACI equation. Figure 5.20 shows the midspan moments of each of the six bridge girders when the load is positioned over the third girder. The experimental moments are derived from the average of four different strain values taken from two different loading runs over two different twin bridges (Huffman NB & Huffman SB). Figure 5.20 shows that the experimental data behaves similarly to either the rigid grillage model or the FE hinged model with intermediate steel diaphragms.

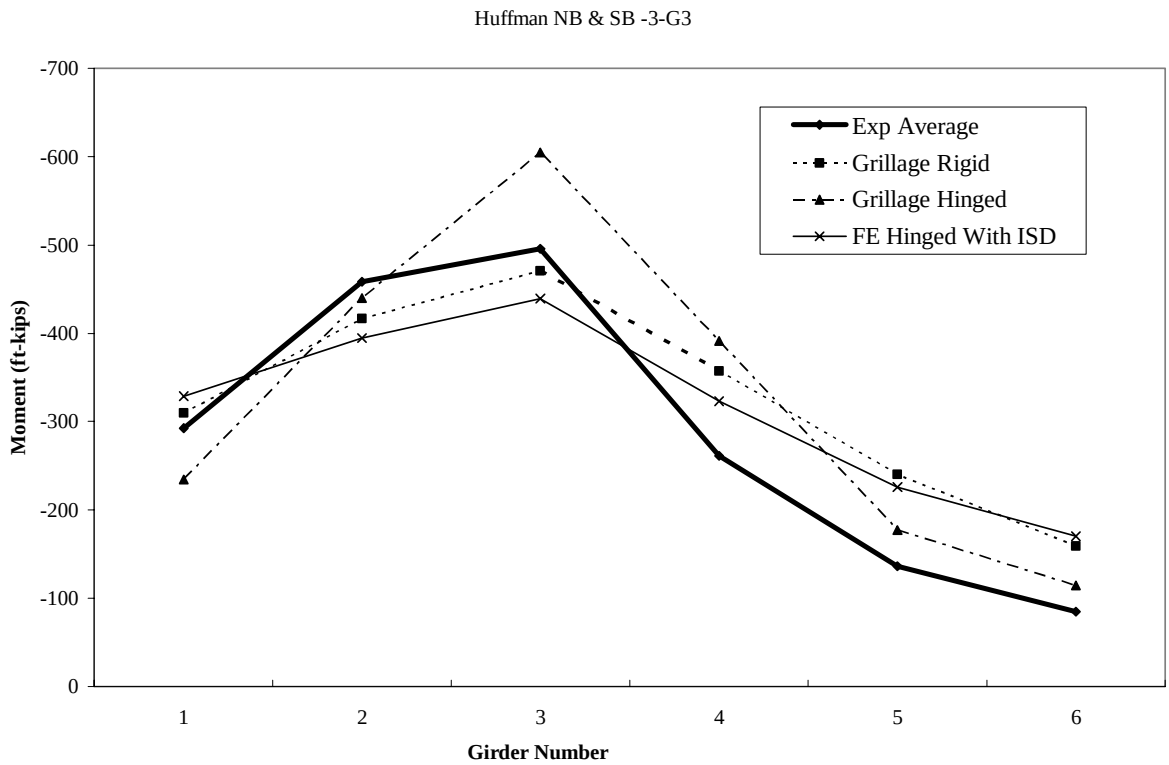


Fig. 5.20 Midspan Moment from Different Models (Huffman NB&SB)

Figure 5.21 shows the distribution factor average envelope between the two bridges and compares it to both the grillage and FE models. Both the grillage and the FE models show a lower distribution factor for the exterior girders than found from testing data. Currently, we do not know why this inconsistency exists. The data from the loads placed on the exterior girders of the twin Huffman bridges appears to be very consistent, yet it does not match the values from the models. However, the distribution on interior girders is consistent.

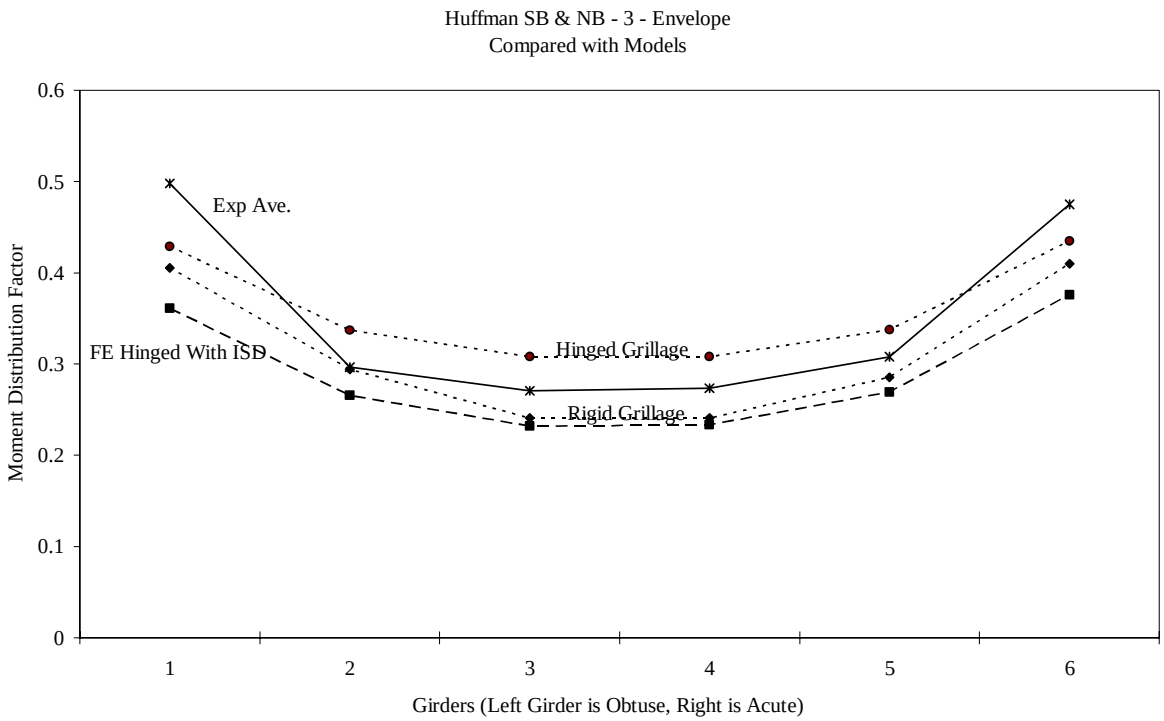


Fig. 5.21 Moment Distribution Factor Comparisons (Huffman NB&SB Bridge)

Figure 5.22 shows the distribution factor average envelope between the two bridges and compares it to both the grillage and FE models. For the case of modeling shear distribution on skew bridges, the three dimensional finite element model is a much better model than the grillage models. When the load vehicle is placed into the acute corner of the bridge, the rear inside wheel load in a grillage model is very close to the supports of the neighboring girder. Because the supports in the grillage model are infinitely stiff, and the shear distribution in the grillage model is found from the reactions of the supports, the grillage model does not distribute the inside rear wheel load realistically. This can be seen in Figure 5.22. Therefore, we mainly use the 3D FE model for the load distribution prediction of skew bridges.

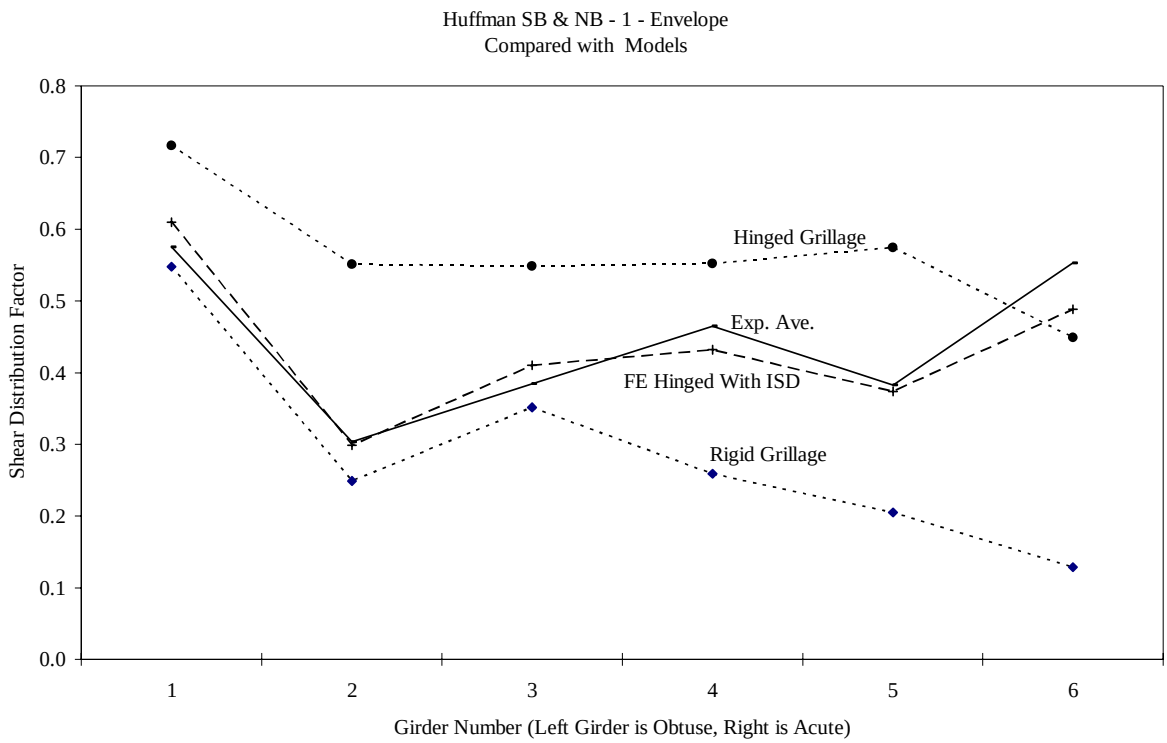


Fig. 5.22 Shear Distribution Factor Comparisons (Huffman NB&SB Bridge)

### 5.2.4 Comparisons with Set 4 Bridges and 3D FE Models

Figure 5.23 only shows the distribution factor of a loaded girder compared with the grillage and FE models. These values have been averaged between Dowling and Diamond. Due to the limited number of gauges, the research team during field testing was only able to place shear gauges on one side of girder for the Dowling and Diamond Bridges. Figures 5.24 through 5.29 show the shear distribution factors based on strain data of just one side of each girder and their comparisons with the 3D FE model predictions. Please note that this distribution include the torsional effects. However, we can conclude that the 3D FE models work really well when the aspect ratio of the bridge is large. Therefore we can assume that the shear distribution factor derived from the FE model is comparable to that of the two twin bridges. Figure 5.30 is a graph which shows how the shear distribution from the FE model compares to the LRFD predictions.

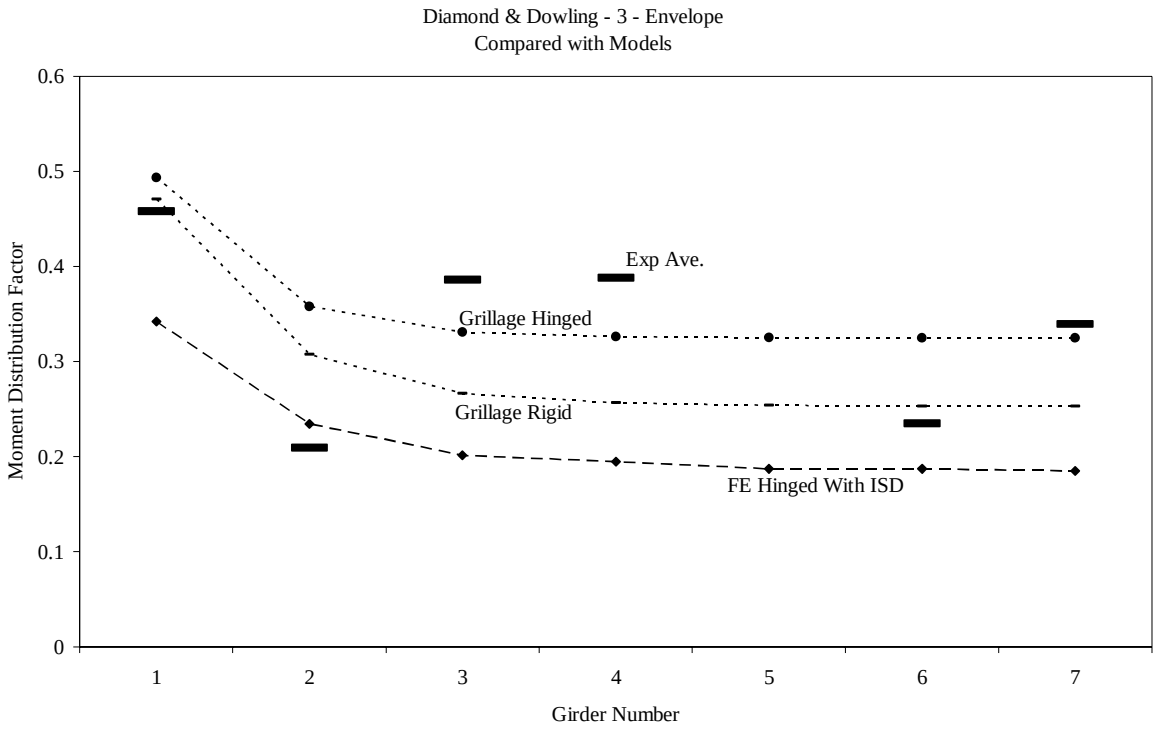


Fig. 5.23 Moment Distribution Factor Comparisons (Diamond & Dowling Bridges)

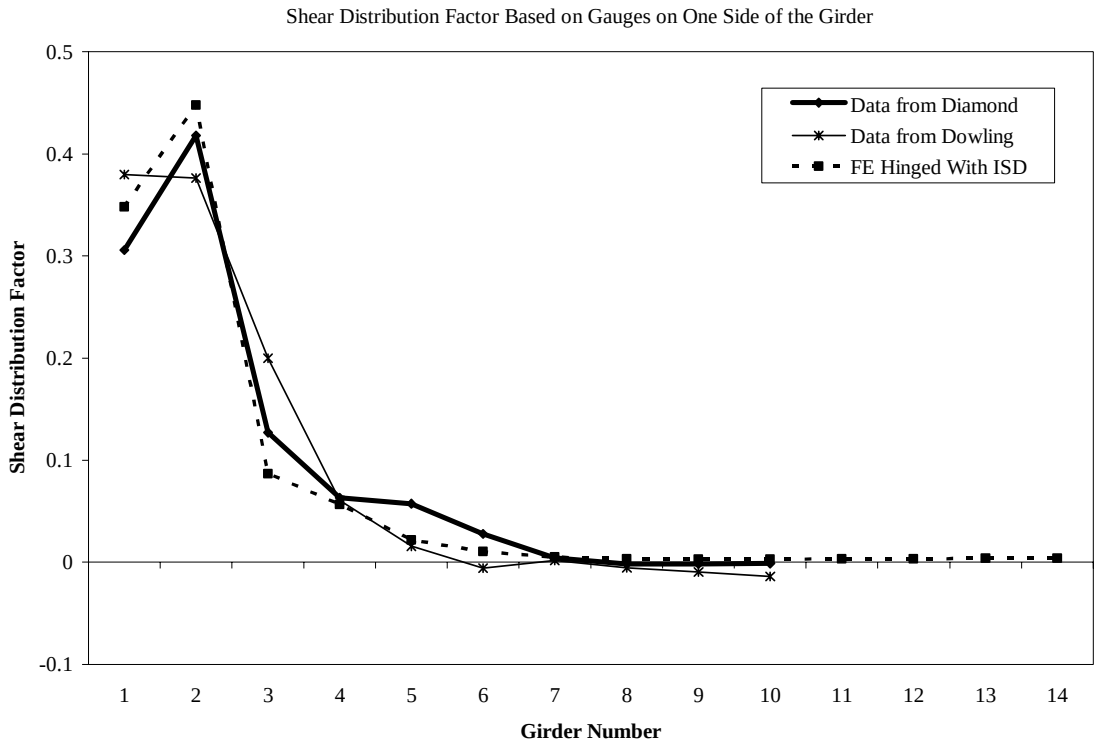


Fig. 5.24 Shear Distribution Factor Comparisons (Diamond & Dowling – 1 – G1)

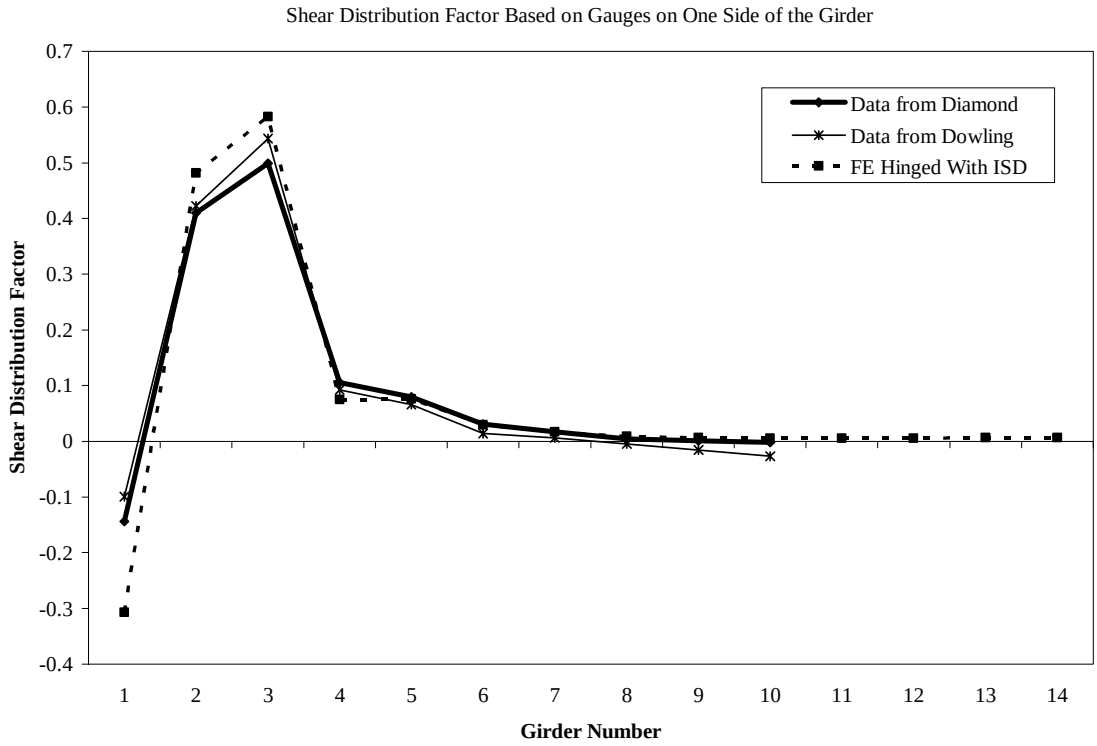


Fig. 5.25 Shear Distribution Factor Comparisons (Diamond & Dowling – 1 – G2)

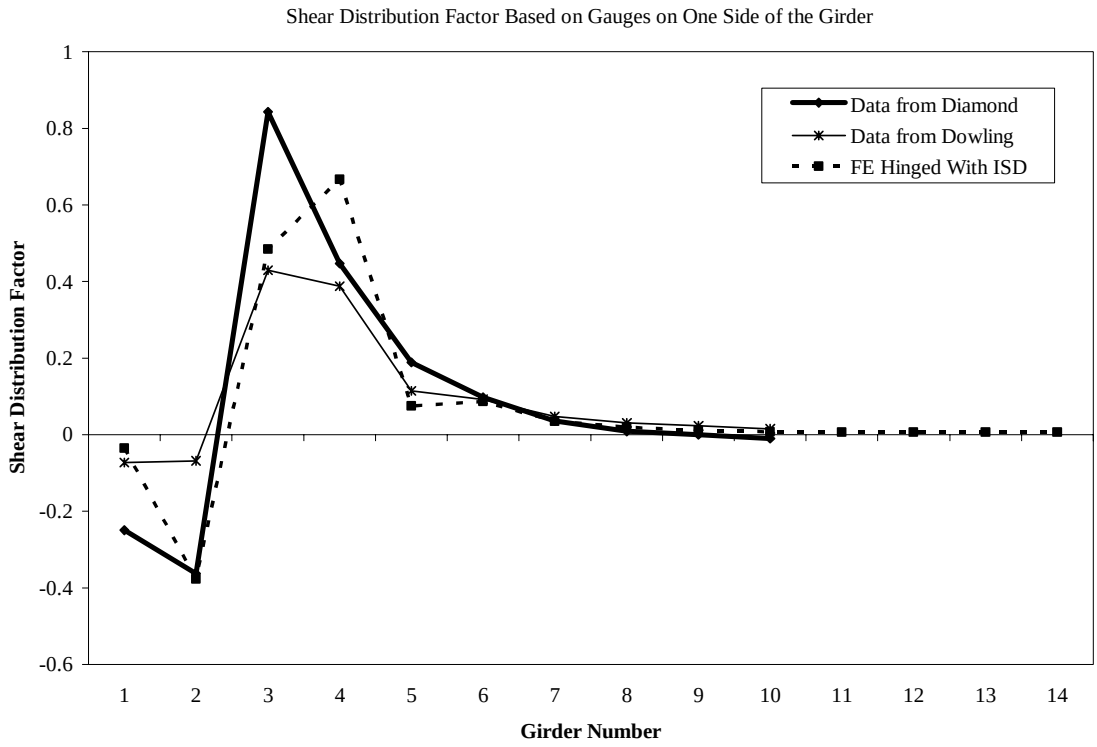


Fig. 5.26 Shear Distribution Factor Comparisons (Diamond & Dowling – 1 – G3)

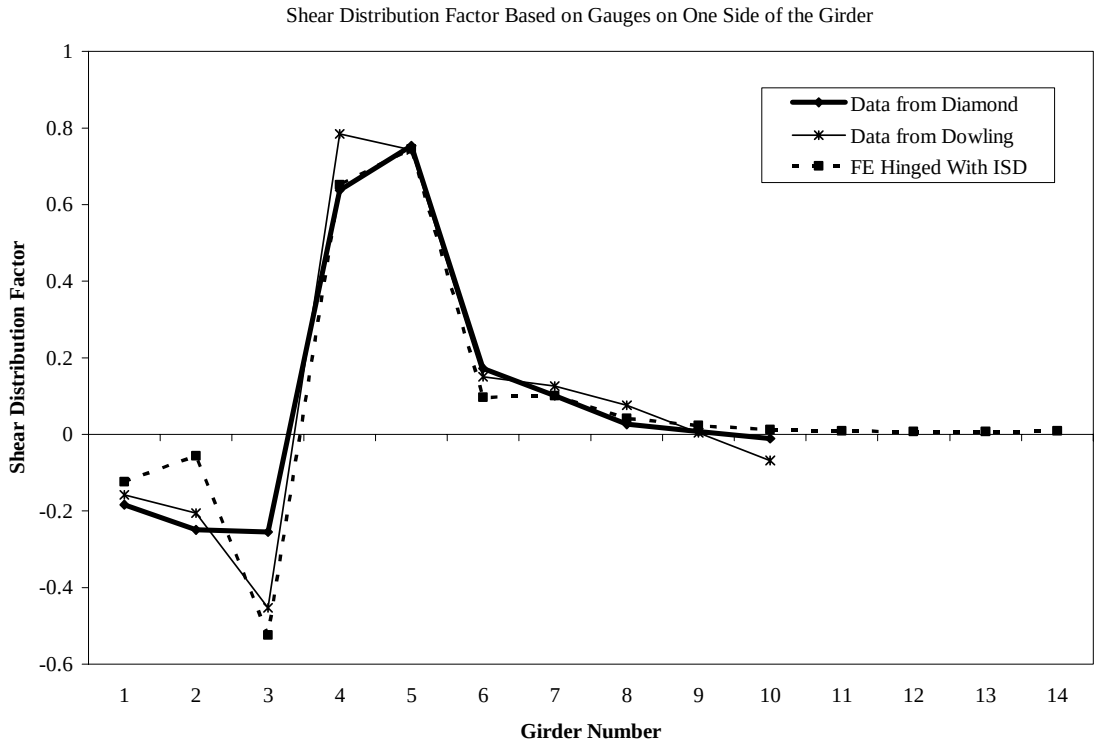


Fig. 5.27 Shear Distribution Factor Comparisons (Diamond & Dowling – 1 – G4)

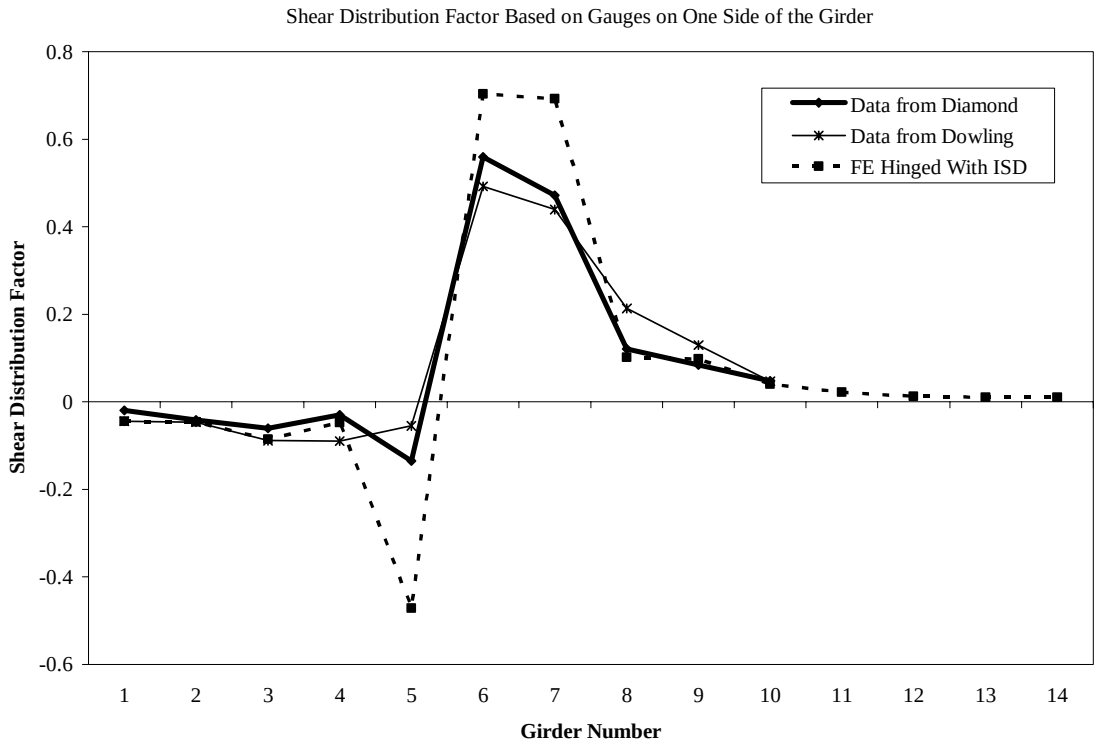


Fig. 5.28 Shear Distribution Factor Comparisons (Diamond & Dowling – 1 – G6)

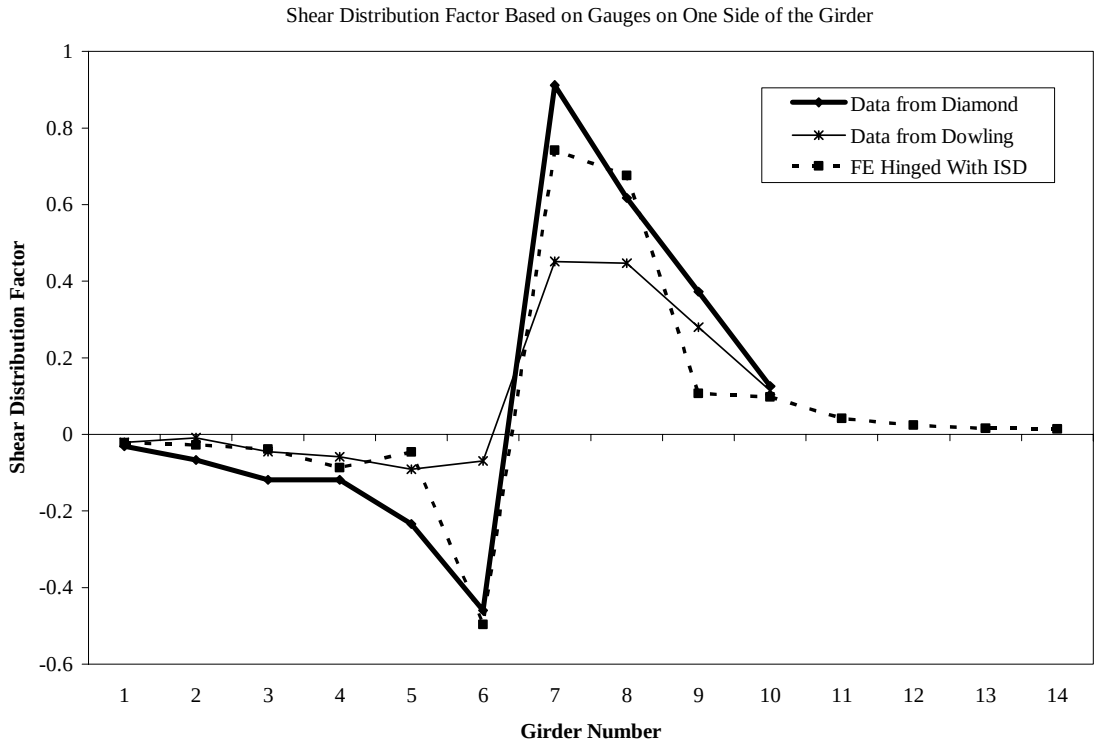


Fig. 5.29 Shear Distribution Factor Comparisons (Diamond & Dowling – 1 – G7)

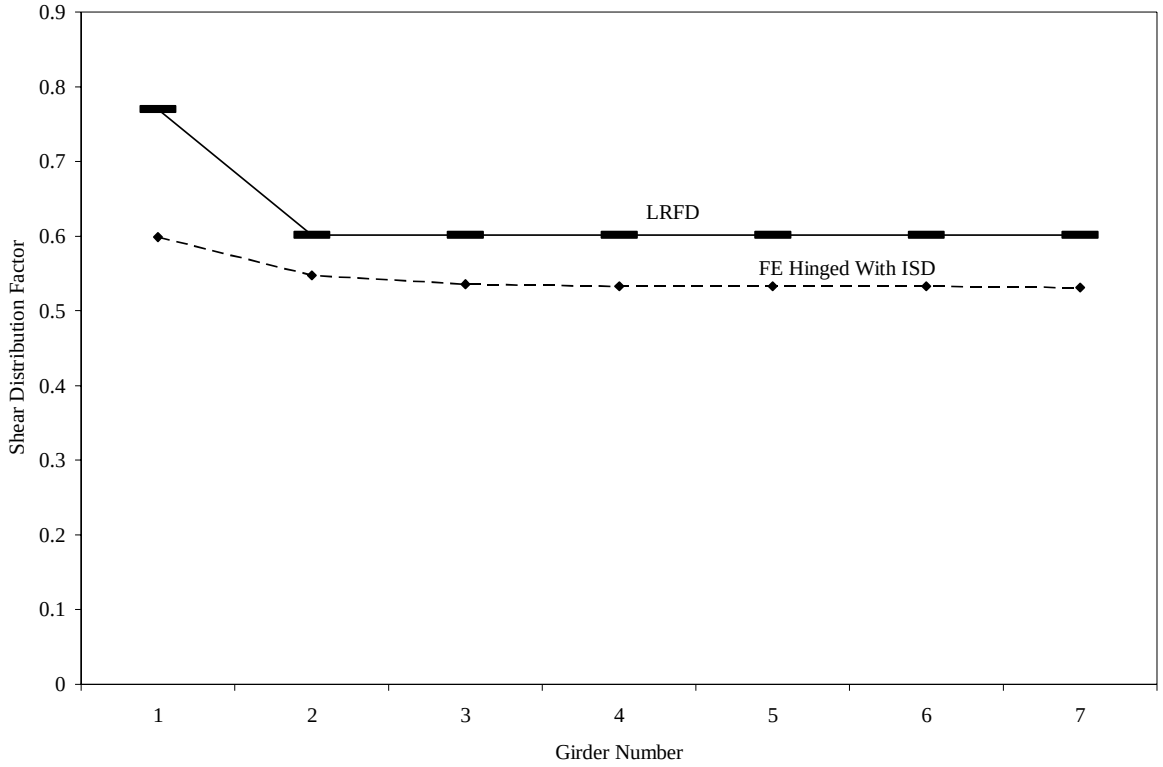


Fig. 5.30 Shear Distribution Factor Comparisons (Diamond and Dowling Bridges)

## 5.3 Summary

In summary, the developed 2D grillage models can accurately predict live load distribution factors of straight bridges while the developed 3D FE models work well in all cases. Although 3D FE model predicts experimental data well, it takes time to run the analysis. Considering the need to run parametric studies, the developed 2D grillage models will be used in developing distribution factor equations of straight bridges. For the effect of skews, the developed 3D FE models will be used to calibrate the results by introducing adjustment factors.

# CHAPTER 6 – PARAMETRIC STUDY

As discussed in Chapter 5, a grillage model was developed. We used the developed 2D grillage model to conduct a parametric study of the decked bulb-tee bridge system. The objective of this parametric study was not to understand general bridge behavior but to develop simplified live-load DF equations that accurately relate to realistic bridges. Two sets of data bases of different grillage models were constructed which vary different bridge parameters. The scope of these data bases were reduced so that they would only include models of spans, girder heights, and girder spacing which are typical of practical decked bulb-tee girder bridges. The current LRFD equations were also evaluated using the data base of typical models.

The programs used to run the grillage models were RISA 3D and SAP 2000 Version 8. The mesh density consisted of one frame element per girder representing the longitudinal stiffness of the bridge and the transverse stiffness was modeled with a frame element positioned every 2.5ft. The end restraints were fixed in all translational degrees of freedom except for one to simulate the roller support. The bending rotation was released yet the torsion and out of plane rotation were fixed to simulate the end diaphragms. The transverse beam sections were modeled as a non-prismatic section which was rectangular with a constant width of 30 inches. The Saint-Venant's torsional stiffness constant of the longitudinal beams was approximated using Equation (5.1).

## 6.1 Selection of Bridge Parameters

### 6.1.1 Two Sets of Bridges

Two different sets of bridges in the parametric study were used. The first set (Set I) comprised of girder cross-sections similar to the Washington style decked bulb-tee girder except the depth of the girder was increased by one inch to have the same depth as the Alaskan style girder. The flange of each girder varies uniformly from the web to the edge of the girder to simplify the modeling of the non-prismatic transverse beam element.

In the first set of models, the girder height (which is related to the stiffness and torsional rigidity), girder spacing, bridge length, and number of girders were all varied. This set modeled three different girder heights: 42", 54", and 66". It varied 4 different girder spacings: 48.5", 68.5", 88.5", and 108.5". It varied the bridge length from 60 to 160 feet at 20 foot increments. Finally the number of girders was changed from 4 to 7. Figure 6.1 shows the different girder cross-sections used in this study. Set I consists of a total of 288 models.

All of the properties for the longitudinal elements for Set I were derived from the cross-sections shown in Figure 6.1.

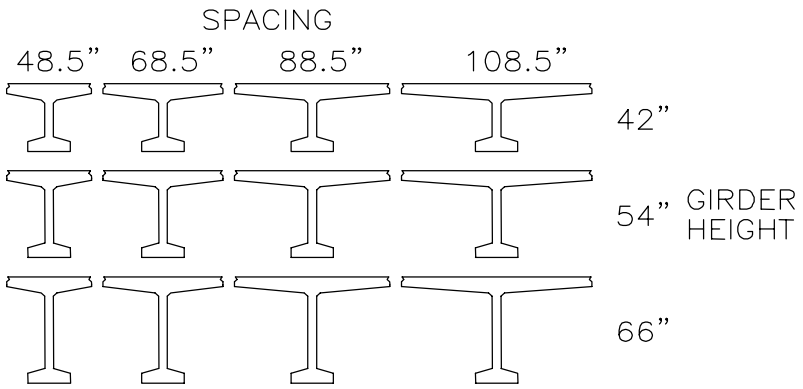


Fig. 6.1 Typical Cross-sections of the girders in Set I.

The second set of bridge models (Set II) is similar to the first set except for a few refinements. The number of girders was not varied in Set II because the data from Set I showed that the number of girders had little impact on the exterior and interior girders' load distribution. All the models in set II have only four longitudinal girders. The girder cross-section used in Set II was modeled after the Alaskan Style Decked Bulb-Tee girder cross section. This girder cross-section has a tapered flange which tapers 2 feet from the center of the girder then decreases by one inch to the standard deck thickness for the remaining width of the girder. The transverse beam elements have the same non prismatic rectangular properties in that for a 6” deck the beams height decreases from 11” to 7” over a two foot section then changes to a uniform 6” deep section to the longitudinal joint between girders.

Set II consists of models with four different girder heights: 36”, 42”, 54”, and 66” all relative to a 6” deck. Set II has five different girder spacings of 48.5”, 60.5”, 72.5”, 84.5”, and 96.5”. The deck thickness was varied in set II as well which in turn affected the overall height of the girder. The three different deck thicknesses modeled in set II were 4”, 6”, and 8”. The span length of the models varied from 40 feet to 180 feet at 20 foot increments. Finally, the rigidity of the longitudinal joint was varied in the second set of models. One condition modeled the longitudinal joint as a perfect hinge while the other condition modeled the joint between the girders as a rigid connection. Figure 6.2 shows a typical cross-section of a girder from which all the beam properties used in the grillage model were derived. Set II consists of a total of 960 models.

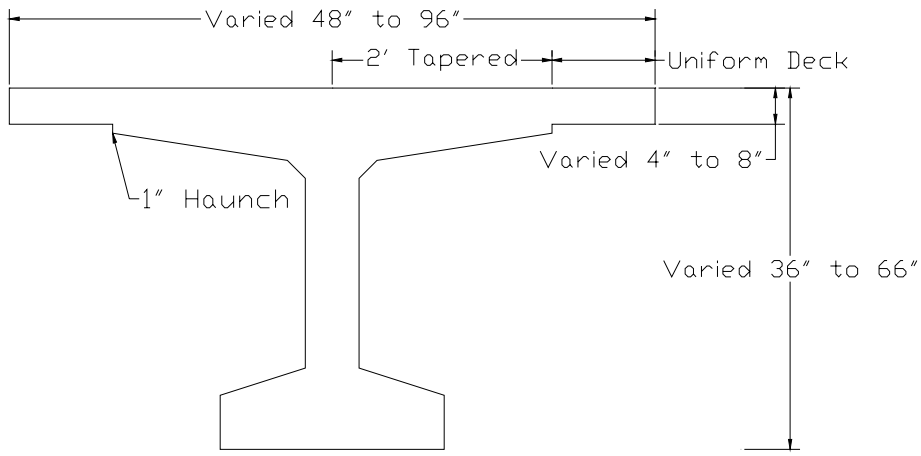


Fig. 6.2 Typical Cross-section used in Set II

### 6.1.2 Loadings

The bridges in the parametric study were all loaded with typical HS20 Truck Loading with axle spacing at 14 feet apart. For moment distribution, the HS20 was positioned on the bridge with the centerline of the bridge halfway between the center of gravity of the truck and the middle axle. For shear distribution, the load vehicle was placed with the rear axle 42 inches from the end of the bridge irrespective of the girder depth in set I, and a distance H equal to the girder depth away from the end of the bridge in set II. In the transverse direction, the exterior girder was loaded with the vehicle's outside wheels placed two feet from the edge of the bridge. The models assume there is no curb on the bridge. The interior girders were loaded with the vehicle centered over the centerline of the girder. Figure 6.3 shows the typical transverse loading of the models in the parametric study.

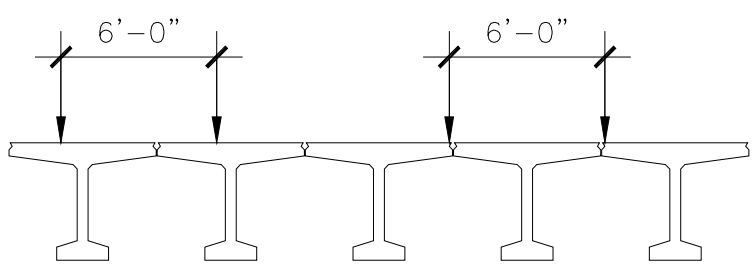


Fig. 6.3 Typical Transverse Loading used in Parametric Study

In some cases, the worst loading condition for the shear distribution factor of the interior girder was not always with the vehicle loaded directly centered over the top of the girder, especially for small girder spacings. For these conditions, the load placed two feet away from the edge of the bridge the same as the worst loading condition for the exterior girder was the worst loading condition for the second girder.

### 6.1.3 Practical Bridge Database

Using the selection scheme described above, both Set I and Set II would include bridges that are unrealistic such as a bridge that has 42” deep girders with a spacing of 108.5” and a length of 160’. Such a bridge could not be designed to carry any kind of truck load. To refine the parametric study so that it consists of only practical bridges, the “Standard Decked Bulb Tee Charts” design aids developed by Concrete Technology Corporation in Tacoma Washington were used to reduce the number of bridges in the parametric study data base [CTC 1995]. Table 6.1 lists the span lengths of realistic bridges in set I and Table 6.2 lists the span lengths of realistic bridges in set II.

Table 6.1 Span Lengths (in feet) of Realistic Bridges in Set I

| Girder Spacing (inches) | Girder Height (inches) | | |
|---|---|---|---|
| | 42 | 54 | 66 |
| 48.5 | 40-120 | 60-140 | 100-180 |
| 68.5 | 40-120 | 60-140 | 80-180 |
| 88.5 | 40-100 | 40-140 | 80-160 |
| 108.5 | 40-100 | 40-120 | 80-140 |

Table 6.2 Span Lengths (in feet) of Realistic Bridges in Set II

| Girder Spacing (inches) | Girder Height (inches) | | | |
|---|---|---|---|---|
| | 36 | 42 | 54 | 66 |
| 48.5 | 40-100 | 40-120 | 60-140 | 100-180 |
| 60.5 | 40-100 | 40-120 | 60-140 | 80-180 |
| 72.5 | 40-80 | 40-100 | 40-140 | 80-160 |
| 84.5 | 40-80 | 40-100 | 40-120 | 80-140 |
| 96.5 | 40-60 | 40-80 | 40-120 | 60-140 |

## 6.2 Comparison with LRFD Equations

Using the practical bridge database of realistic bridges, the results of the two sets of models were compared to the DF equations presented in the ASHTO LRFD. The models were compared to the results of both the equations provided for bridges which are connected sufficiently to act as a unit, and for bridges which are connected only enough to prevent relative vertical displacement at the girder interface.

Figures 6.4 and 6.5 summarize the comparison between the rigid-grillage model predictions from Set I and the LRFD DF equations. In these figures, the abbreviations SE, SI, ME, and MI stand for Shear DF on Exterior Girder, Shear DF on Interior Girder, Moment DF on Exterior Girder, and Moment DF on Interior girder respectively.

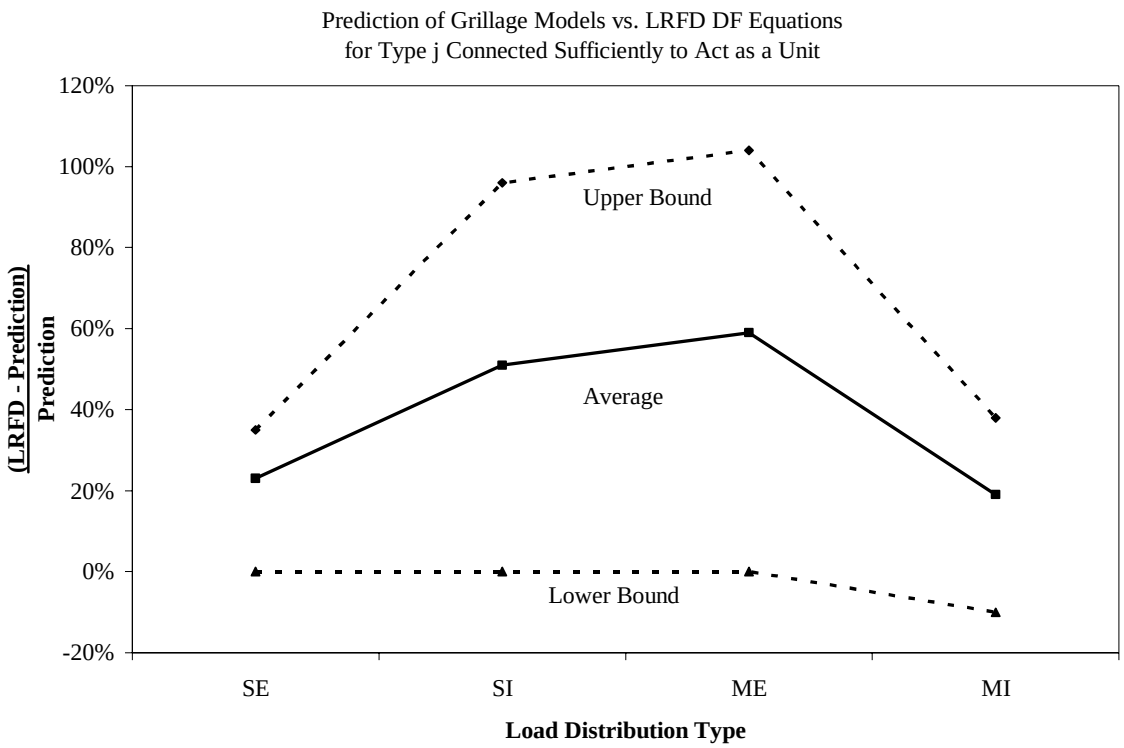


Fig. 6.4 Comparison of LRFD DF Equations to Rigid-Grillage Models from Set I

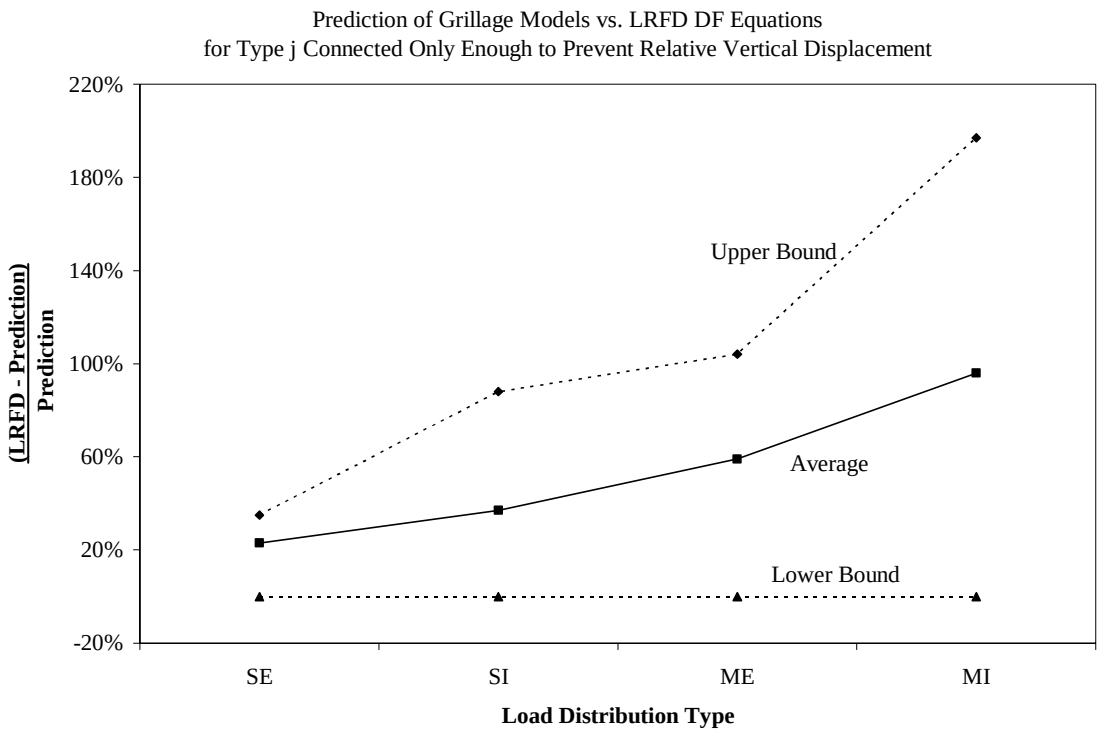


Fig. 6.5 Comparison of LRFD DF Equations to Rigid-Grillage Models from Set I

Figure 6.6 compares the error between the results of LRFD DF equations set aside for bridges sufficiently connected to act as a unit and the predictions of rigid-grillage models of Set II. Figure 6.7 compares the results of LRFD DF equations for bridges connected only enough to prevent relative vertical displacement to the predictions of hinged-grillage models of Set II.

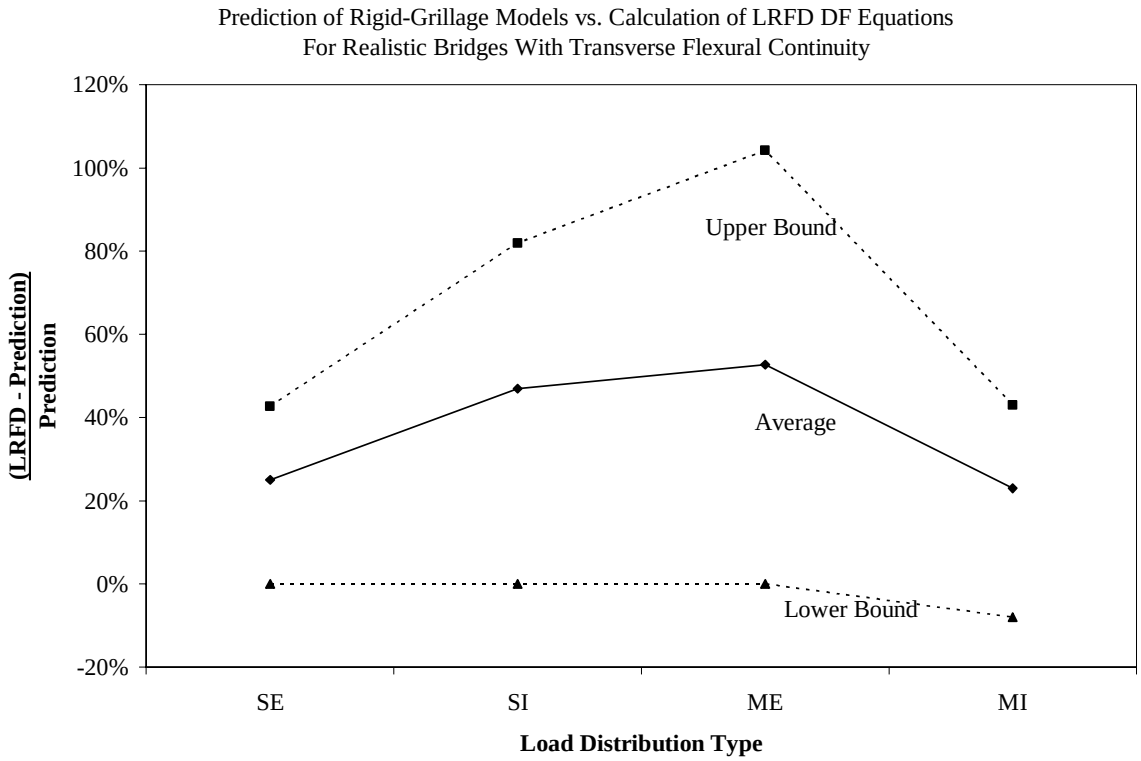


Fig. 6.6 LRFD DF Equations vs. Rigid-Grillage Models from Set II

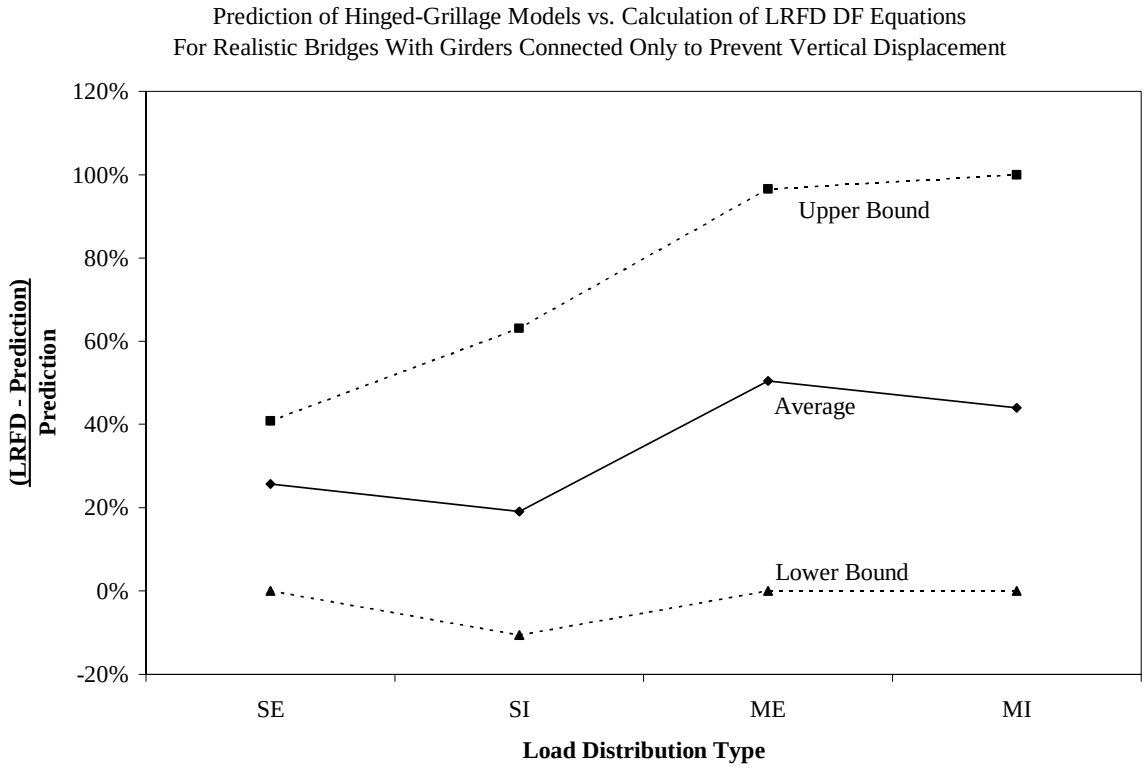


Fig. 6.7 LRFD DF Equations vs. Hinged-Grillage Models from Set II

As shown in Figures 6.4 and 6.6, the LRFD DF equations provided unconservative values when compared to the results from the grillage models in the case of the DF equation for bridges sufficiently connected to act as a unit for moment on interior girders. The maximum unconservative error for the LRFD DF equation was 10% from the data base in Set I (Figure 6.4) and 8% from the rigid models of Set II (Figure 6.6). The bridges where this equation is unconservative relative to the rigid-grillage model is when the girder is very stiff (girder height 66in) and the spacing is very close (48.5 & 68.5).

The S/D formula as specified in the LRFD for moment on the interior girder of bridges with girders connected only enough to prevent relative vertical translation is an average of 96% conservative when compared to the data from Set I (Figure 6.5) and 44% conservative when compared to the data from the hinged models of Set II (Figure 6.7). The reason this S/D equation relates to data from Set II better than the data from Set I is not because the grillage models were modeled with flexural release between girders, but instead it is due largely to the data set only being limited to 4 girders which restricts the aspect ratio of bridges in Set II. Another equation that yields unconservative results is the Lever Rule when compared to the shear DF on interior girders of the hinged models from data Set II. These unconservative values occur when the bridge has a very thin deck (4”) and a very short span (40 ft).

## 6.3 Sensitivity Study of Parameters

This section summarizes the contribution of each of the different parameters to the distribution factors for both moment and shear and for the interior and exterior girders. This was done by showing the average and maximum percent change caused by a given parameter when all other parameters are held constant. The average and maximum are over the set of "practical bridges" described earlier. Table 6.3 shows an example of how the percent change is determined for a given set of bridges.

Table 6.3 Example of Sensitivity Study Calculations

| Girder Spacing (in) | Moment of Inertia ($in^4$) | No. of Girders | Bridge Length (ft) | Moment DF on Interior Girder |
|---|---|---|---|---|
| 48.5 | 191349.1 | 4 | 60 | 0.276 |
| 48.5 | 191349.1 | 5 | 60 | 0.259 |
| 48.5 | 191349.1 | 6 | 60 | 0.254 |
| 48.5 | 191349.1 | 7 | 60 | 0.252 |

Table 6.3 shows all of the bridge parameters held constant except for the number of girders which change from 4 to 7. The percent change of the moment DF due to the change in the number of girders for this particular bridge type could be found by subtracting the smallest DF value (0.252) from the largest DF value (0.276), then dividing by the smallest value (0.252). The result would then be 9.5% for this data set. This process is then repeated for each different bridge set in the data base. The average of all of these values from Set I is shown in figure 6.8.

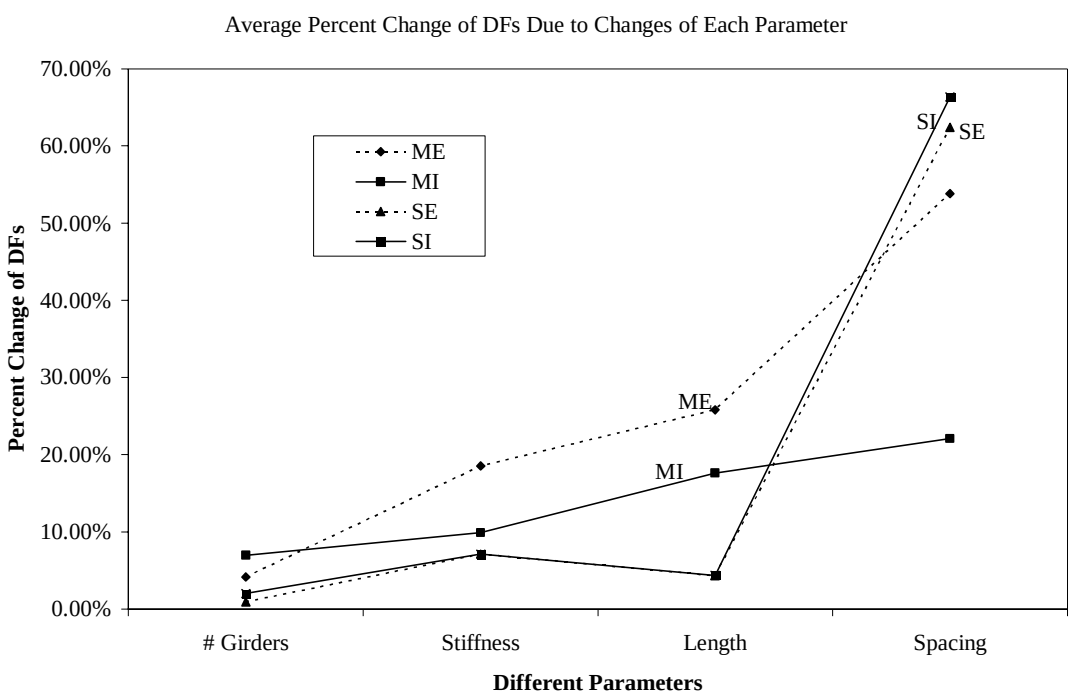


Fig. 6.8 Sensitivity Study (Models from Set I)

Figures 6.9 and 6.10 show the impact of different parameters on the distribution factor for the models of data Set II. The parameter entitled Hinged vs Rigid refers to the comparison of the models with transverse flexural continuity and discontinuity. These values are the same for both Figures 6.9 and 6.10 as they compare the two sets of bridges to each other.

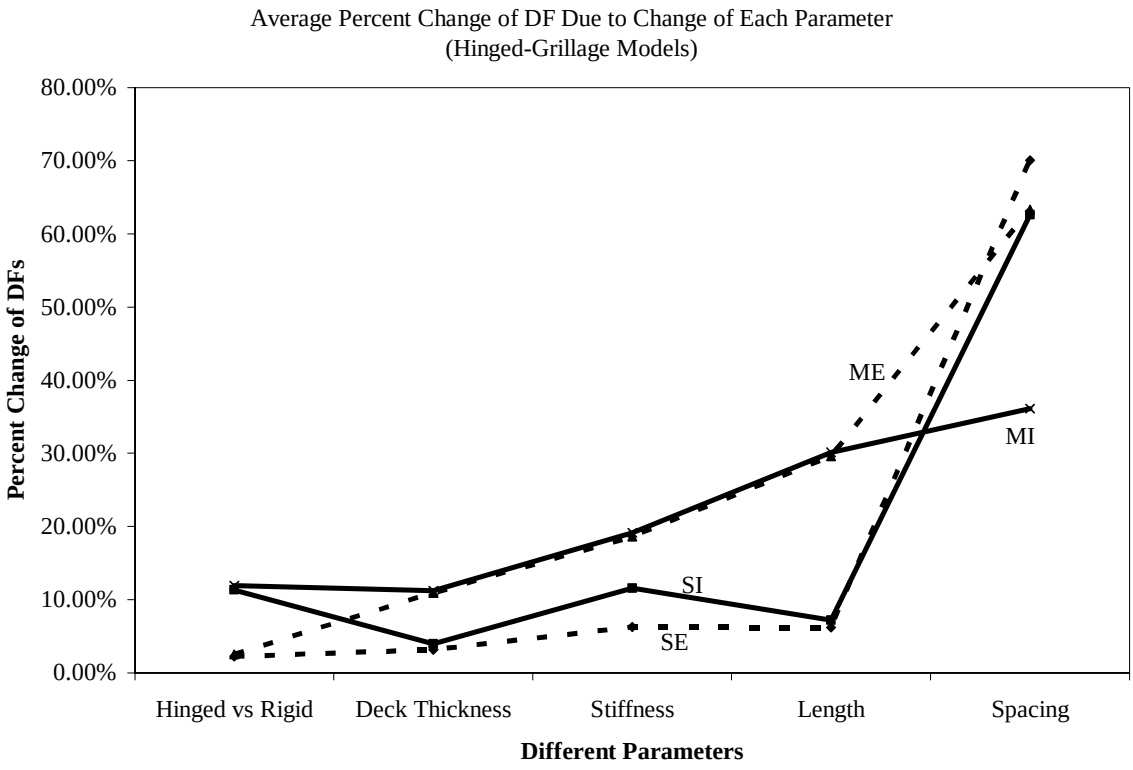


Fig. 6.9 Sensitivity Study of Hinged Models from Set II

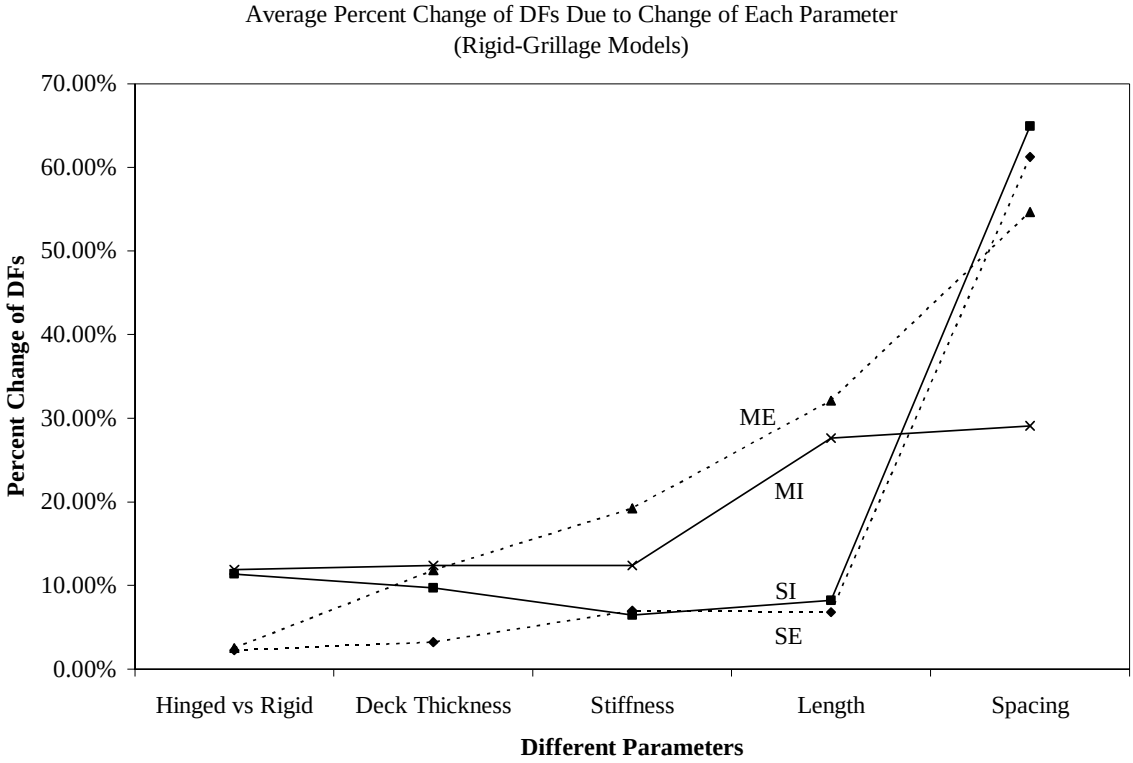


Fig. 6.10 Sensitivity Study of Rigid Models from Set II

When evaluating the effects the different parameters on the load distribution, the magnitude of the effects differs between the shear distribution and the moment distribution. For the moment DF of both interior and exterior girders, spacing has the greatest effect followed by span length, and then by girder stiffness. For the shear DF, spacing had the greatest effect followed by girder stiffness followed by span length.

In both cases, the number of girders, the deck thickness, and varied hinged or rigid condition had relatively smaller effect on the distribution factor. This conflicts with the LRFD equation for moment on interior girders without transverse flexural continuity which gives the distribution factor as a function of the aspect ratio. For the single lane loaded condition, this parametric study shows that the aspect ratio has very little effect on the moment distribution factor for this kind of bridges. When the aspect ratio is increased due to increasing the number of girders, the LRFD equations give an incorrect prediction of DFs. Most of the change due to increasing the number of girders occurs when the number of girders is increased from 4 to 5. The addition of subsequent girders has little to no affect on any of the distribution factors.

When comparing the effects of the different parameters between bridges with transverse flexural continuity and discontinuity, the effects are virtually identical in all cases except for the distribution of moment on interior girders. The DF of moment on interior girders for bridges with transverse discontinuity are effected by the stiffness, length, and spacing

parameters by an average of 5% more than for transverse continuous bridges. When comparing the effect of a bridge having transverse flexural continuity or discontinuity for distribution of shear and moment on exterior girders, there is little to no affect. For the shear and moment distribution on interior girders, the distribution factor is only affected by an average of 12% by the transverse continuity. The deck thickness has very little effect as well by changing the distribution factor by an average 12% or less depending on the case.

## 6.4 Summary of Findings

Based on the two parametric studies and their comparisons with the existing LRFD equations, we conclude the following findings for single lane loaded decked bulb-tee bridges:

- For shear distributions on exterior and interior girders, the LRFD equations are an average of 32% conservative for both the flexural transverse continuous and discontinuous cases.
- For moment distribution on exterior girders the Lever Rule is an average of 50% conservative for both the flexural transverse continuous and discontinuous cases.
- The LRFD equation for distribution of moment on interior girders for bridges with girders only connected enough to prevent relative vertical translation, is an average of 44% to 96% conservative depending on the aspect ratio of the bridge.
- The single lane distribution factor of decked bulb-tee bridges is only dependant on the aspect ratio of the bridge when the aspect ratio changes due to change in girder spacing not when the aspect ratio changes due to changing the total number of girders.
- The LRFD equation for distribution of moment on interior girders for bridges with girders sufficiently connected to act as a unit is an average of 21% conservative and could possibly be up to 10% unconservative for bridges with a girder spacing of less than 60” and a span length of greater than 100ft.
- For the moment DF of both interior and exterior girders, spacing has the greatest effect followed by span length, and then by girder stiffness. For the shear DF, spacing has the greatest effect followed by girder stiffness and then by span length.

# CHAPTER 7 – SINGLE LANE LIVE LOAD DF EQUATIONS

## 7.1 Understanding the Behavior of Load Distribution

Before developing simplified DF equations which approximate the single lane loaded distribution factors for decked bulb-tee bridges, we first worked to better understand the behavior of the bridge and to identify variables affecting the load distribution by using a simple beam on elastic foundation model (BEFM), as shown in Figure 7.1.

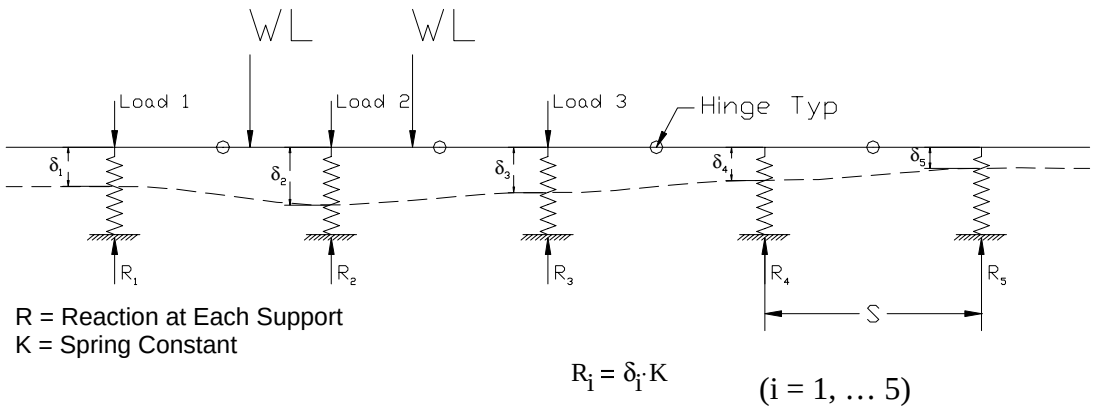


Fig. 7.1 Simple Beam on Elastic Foundation Model (BEFM)

Figure 7.1 shows a simple BEFM which simulates the worst loading condition over an interior girder of a five girder bridge. This model assumes that each girder is a spring support system and is torsionally fixed. When the girder is assumed torsionally fixed, the nodes at each of the spring reaction locations are assumed not to rotate at all but only to deflect vertically. The reaction at each of the girders is simply the displacement of the girder times its spring constant. The force of the load is distributed to the other springs by a one dimensional beam. By resolving unit wheel loads (WL) via the lever rule into respective loads over each neighboring girder, we can solve for the reaction of the girder directly under the loads and determine the distribution factor of that girder. To determine the spring constant of each girder, we assume that the displacement of the girder as a function of force can be determined as a point force loaded on a beam supported by two hinge joints shown in Figure 7.2.

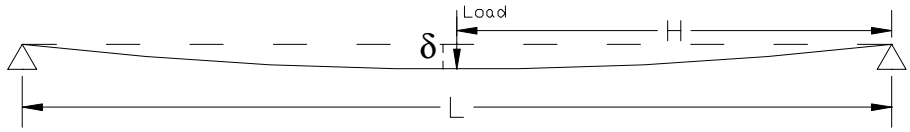


Fig. 7.2 Simply Supported Beam

From the basic mechanics, the governing equation which relates deflection of a uniform cross-section beam to the moment induced on the beam is given by the following expression:

$$\frac{d^2}{dx^2}y = \frac{M(x)}{E \cdot I} \tag{7.1}$$

where E is the modulus of elasticity and I is the area moment of inertia of a cross-section of the beam. From this equation, we can solve for the deflection of the midpoint of the beam as a function of force imposed onto the beam and a function of the unit loads location along the beam.

The vertical displacement at a point located a distance H along the beam with an area moment of inertia $I_1$ is given by the following:

$$\delta = \text{Load}\,\frac{1}{3}\cdot\frac{H^2}{L}\cdot\frac{L^2 - 2\cdot H\cdot L + H^2}{E\cdot I_1} \tag{7.2}$$

By setting our load to be a unit load, we can find an expression for our longitudinal spring constant $K_1$:

$$K_1 = \frac{3}{H^2}\cdot\frac{L\cdot E\cdot I_1}{\left(L^2 - 2\cdot H\cdot L + H^2\right)} \tag{7.3}$$

Next we solve for a relationship of the distribution of force along the transverse direction of the BEFM. By looking at the relationship between two adjacent girders, we solve for the deflection given a load at one of the girders.

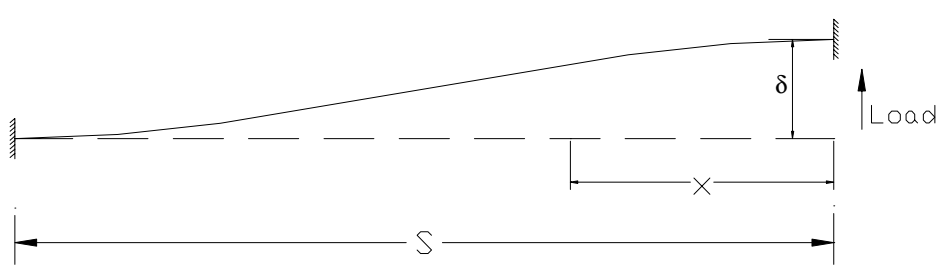


Fig. 7.3 Rigid Supported Beam With Induced Deflection at One Support

From our assumption that the girders are torsionally fixed and the transverse beam does not rotate at the girder locations we get the following moment distribution relationship:

$$M(x) = Load \cdot x - Load \cdot \frac{S}{2} \tag{7.4}$$

At half the distance between the two girders, when x in the above equation = S/2, the moment goes to zero. This shows that if there is a hinge located between the two girders and the girders are torsionaly fixed, the transverse stiffness is unaffected by the presence of a longitudinal joint between the girders. Assuming the transverse moment of inertia of the beam is given by $I_2$, the deflection at the end of the beam can be found by:

$$\delta = \frac{-Load \cdot S^3}{12 \cdot E \cdot I_2} \tag{7.5}$$

For a unit load, the transverse stiffness can be represented by the following relationship:

$$K_t = \frac{E \cdot I_2 \cdot 12}{S^3} \tag{7.6}$$

Now that we have relationships for both the longitudinal and transverse stiffness, we can determine the distribution factor of the bridge system. By examining the vertical force acting on each girder, we can determine the following relationship for the reaction on each girder:

$$\begin{aligned}
Load_1 &= R_1 + (\delta_1 - \delta_2) \cdot K_t \\
Load_2 &= -(\delta_1 - \delta_2) \cdot K_t + R_2 + (\delta_2 - \delta_3) \cdot K_t \\
Load_3 &= -(\delta_2 - \delta_3) \cdot K_t + R_3 + (\delta_3 - \delta_4) \cdot K_t \\
0 &= -(\delta_3 - \delta_4) \cdot K_t + R_4 + (\delta_4 - \delta_5) \cdot K_t \\
0 &= -(\delta_4 - \delta_5) \cdot K_t + R_5
\end{aligned} \tag{7.7}$$

By using the relationship: $\delta = \frac{R}{K_1}$ we can simplify the above equations into the following system of linear equations:

$$\begin{pmatrix} R_1 \\ R_2 \\ R_3 \\ R_4 \\ R_5 \end{pmatrix} \cdot \begin{pmatrix} \frac{K_T}{K_L} + 1 & \frac{-K_T}{K_L} & 0 & 0 & 0 \\ \frac{-K_T}{K_L} & 2\frac{K_T}{K_L} + 1 & \frac{-K_T}{K_L} & 0 & 0 \\ 0 & \frac{-K_T}{K_L} & 2\frac{K_T}{K_L} + 1 & \frac{-K_T}{K_L} & 0 \\ 0 & 0 & \frac{-K_T}{K_L} & 2\frac{K_T}{K_L} + 1 & \frac{-K_T}{K_L} \\ 0 & 0 & 0 & \frac{-K_T}{K_L} & \frac{K_T}{K_L} + 1 \end{pmatrix} = \begin{pmatrix} Load_1 \\ Load_2 \\ Load_3 \\ 0 \\ 0 \end{pmatrix} \tag{7.8}$$

We can further simplify this expression by defining an arbitrary variable C such that:

$$C = \frac{K_L}{K_T} + 2 \tag{7.9}$$

By inputting this relationship into the above expression and solving for the reactions, we get.

$$(C-2) \cdot \begin{pmatrix} C-1 & -1 & 0 & 0 & 0 \\ -1 & C & -1 & 0 & 0 \\ 0 & -1 & C & -1 & 0 \\ 0 & 0 & -1 & C & -1 \\ 0 & 0 & 0 & -1 & C-1 \end{pmatrix}^{-1} \cdot \begin{pmatrix} Load_1 \\ Load_2 \\ Load_3 \\ 0 \\ 0 \end{pmatrix} = \begin{pmatrix} R_1 \\ R_2 \\ R_3 \\ R_4 \\ R_5 \end{pmatrix} \tag{7.10}$$

When we solve this system of linear equations, the value of $R_2$ shows us the percent of $Load_1 - Load_3$ that the second girder in the bridge system resists. This is the distribution factor for that girder. The number of girder in the bridge system governs the size of the matrix, yet the matrix maintains the same basic appearance. The matrix will always be an N x N sized matrix with the N being the number of girders. It is a tridiagonal matrix with the first cell and last cell in the matrix always being C-1. The intermediate diagonal members will always be C with the cells to the left and right of the diagonal always being -1.

While this matrix method is too complex to be used effectively in design, we can use the equation to understand how different parameters of the bridge affect the way it distributes loads. The main component of this method is the $\frac{K_L}{K_T}$ term which represent the ratio of the longitudinal stiffness to the transverse stiffness. This term is directly related to the distribution of the bridge.

This relationship shows the transverse modulus of elasticity divided by the modulus of elasticity in the longitudinal direction. Since the decked bulb Tee bridge girder is made with the same material in the deck and in the girder, and since concrete is an isotropic material, the transverse modulus is equal to the longitudinal modulus and these terms factor out. This helps to explain why the modulus of elasticity does not affect the distribution factor of the bridge.

For the shear distribution, the $K_L$ term (Eq. 7.3) is larger because the center of gravity of the vehicle is much closer to the bridge support and the girder is much stiffer. While the transverse stiffness $K_T$ (Eq. 7.6) remains constant for both the moment distribution and the shear distribution. By comparing the two stiffness ratios, we can see that for a given bridge, the shear distribution factors are higher than moment distribution factors. This also confirms the conclusions we made in Chapter 6 about the most influencing parameters of girder spacing, stiffness, and span on load distributions.

## 7.2 Distribution Factor Equations

While the BEFM theory provided the insight about load distributions and has some value in understanding the behavior of decked bulb-tee bridge systems, the theory is too complex to be used effectively in design or bridge rating. Based on conclusions from Chapter 6 and the BEF model, we develop simplified DF equations for the single lane distribution factor of the decked bulb tee bridge system by considering only three parameters: Spacing, Length, and Girder Stiffness.

The bridge data base from which the following simplified equations were developed is the realistic bridges of Set II in the parametric study. For most cases the transverse hinged condition gave a higher distribution factor, however for the distribution of shear on exterior girders, the rigid condition gave a higher distribution factor when the girder spacing was 48.5 inches. The simplified equations were developed from which ever condition (hinged or rigid) gave the larger distribution factor.

All of the bridges in the data base only have four girders which for the single lane loaded condition tend to have a higher distribution factor than a greater number of girders. We developed two sets of simplified equations for moment and shear distribution on the exterior and interior girders. The first set of equation is very simple and only a function of the girder spacing and conforms to the traditional S/D method of determining the DF. The second set of equation is a function of spacing (S), length (L), and the girder's area moment of inertia (I). Please note that none of these equations includes the multiple presence factor. These simplified DF equations are accurate only when the bridge being modeled is within the following parameters:

- The girders are typical decked bulb tee girders with the deck poured together with the girder as a single unit.
- The girder height is between 36 inches and 66 inches.
- The deck thickness is between 4 and 8 inches.
- The number of girders of the bridge is greater than or equal to four.
- The bridge has no skew. For skew bridges, an adjustment factor will be used.
- The span length of the bridge is between 40ft and 180ft.
- The girder spacing is between 4ft and 9ft.
- The bridge is only loaded by a single lane of traffic.

The variables used in the following simplified equations are defined as follows.

S = Girder Spacing, the distance between the centerlines of two consecutive girders in units of ft.

L = Span Length of the bridge measured from the centers of each support in units of ft.

I = The area moment of inertia about the horizontal axis of one girder in the bridge system. The moment of inertia used should be calculated from the

whole girder including the whole width of the top flange deck portion. The units of this term are in $ft^4$.

Following is a list of recommended equations for the Distribution Factor of the Decked Bulb-Tee bridge girder system when it is subjected to the single lane loaded condition:

Moment over Interior Girder (MI):

$$DF(S) = \frac{S}{13} \tag{7.11}$$

$$DF(S,L,I) = \frac{S}{12.5} + \frac{I}{300} - \frac{L}{10} \cdot \left( \frac{S-3}{200} \right) \tag{7.12}$$

Moment over Exterior Girder (ME):

$$DF(S) = \frac{S}{11} \tag{7.13}$$

$$DF(S,L,I) = \frac{S}{10} + \frac{I}{300} - \frac{L}{10} \cdot \left( \frac{S-1}{300} \right) \tag{7.14}$$

Shear over Interior Girder (SI):

$$DF(S) = \frac{S}{11} \tag{7.15}$$

$$DF(S,L,I) = \frac{S}{12.5} + \frac{I}{250} - \frac{L}{100} \cdot \left( \frac{S}{100} \right) \tag{7.16}$$

Shear over Exterior Girder (SE):

$$DF(S) = \frac{S}{10} \tag{7.17}$$

$$DF(S,L,I) = \frac{S}{12} + \frac{I}{400} - \frac{L}{100} \cdot \left( \frac{S-3}{100} \right) + 0.07 \tag{7.18}$$

## 7.3 Evaluation of Proposed DF Equations

Figures 7.4 through 7.11 compare the two set of simplified equations (Sets of DF(S) and DF(S,L,I), Eq. 7.11 to 7.18) to database from parametric study II. The values shown are the ratio of the DF values found from the simplified equation divided by the values found from the parametric study. Values less than one are unconservative. These values are plotted against the span length to show how they vary for different lengths. The data points are also divided into three different series based on deck thickness. Most of the unconservative values occur with a 4" deck thickness and 40' length. The simplified equations tend to give overly conservative values for bridges with an 8" deck. In general, the set of DF(S,L,I) equations is better than the set of DF(S) in terms of the scatter of data points.

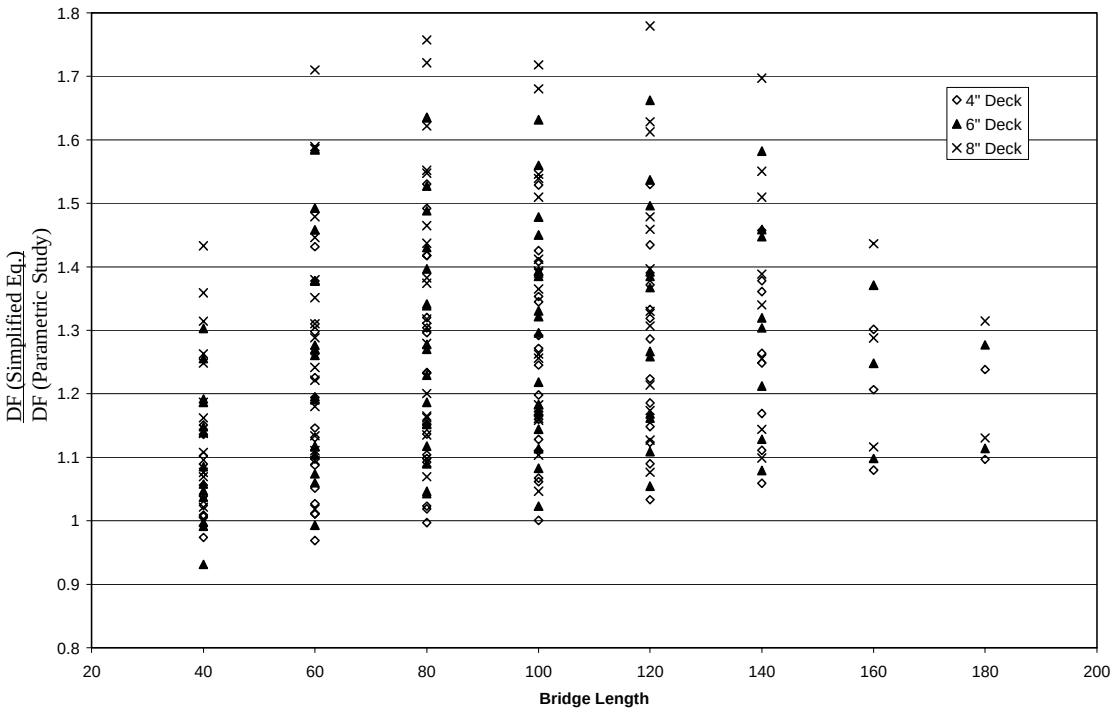


Fig. 7.4 Moment DF for Interior Girders [Set of DF(S)]

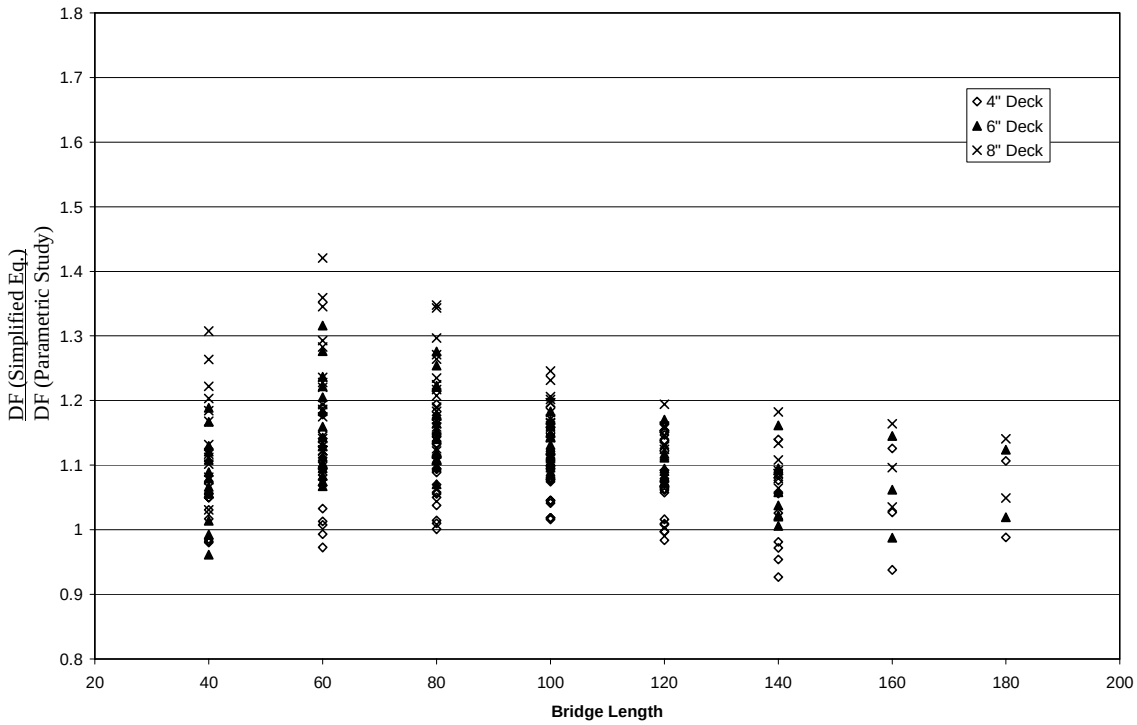


Fig. 7.5 Moment DF for Interior Girders [Set of DF(S,L,I)]

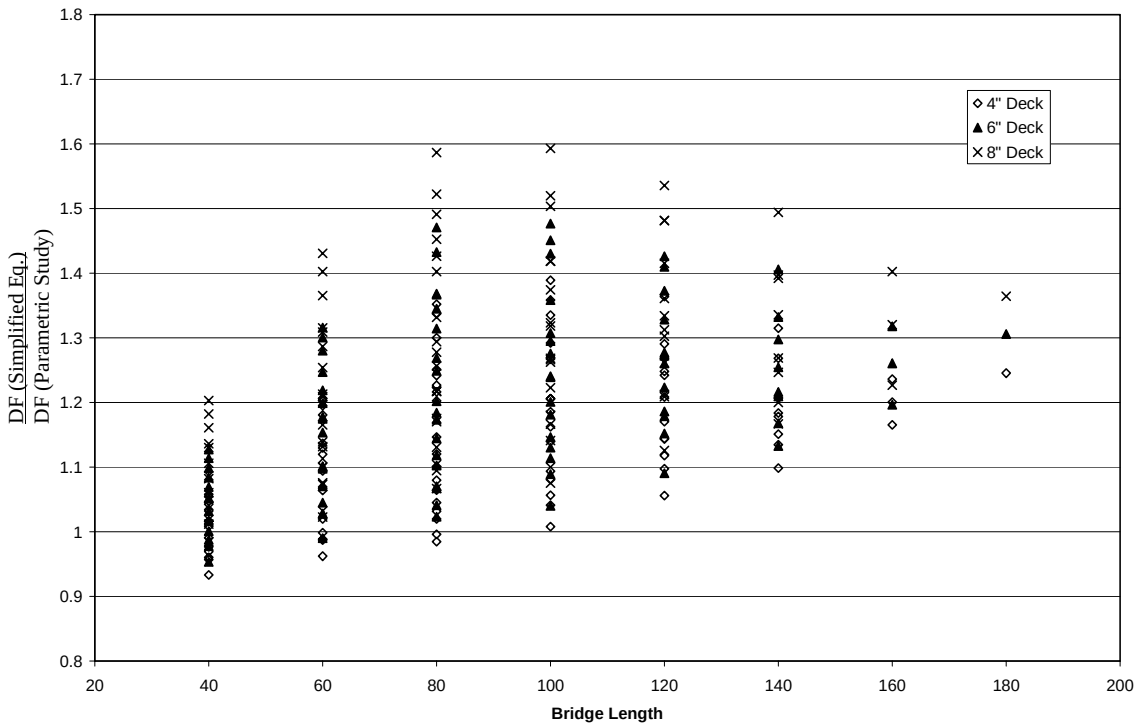


Fig. 7.6 Moment DF for Exterior Girders [Set of DF(S)]

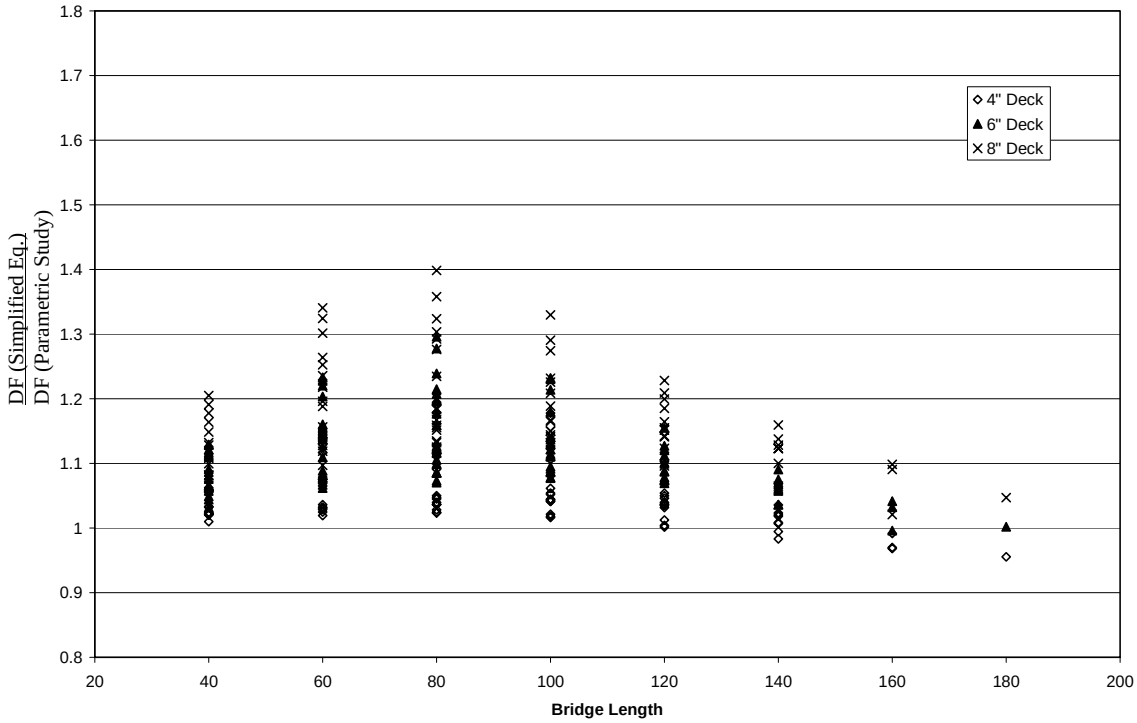


Fig. 7.7 Moment DF for Exterior Girders [Set of DF(S,L,I)]

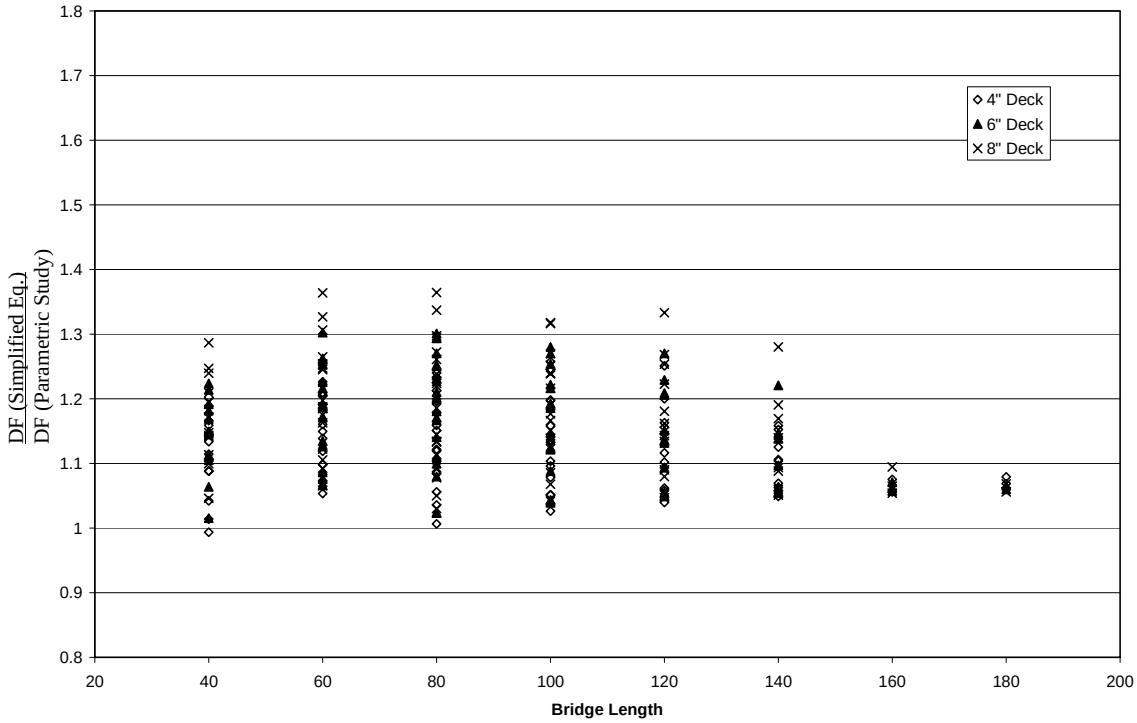


Fig. 7.8 Shear DF for Interior Girders [Set of DF(S)]

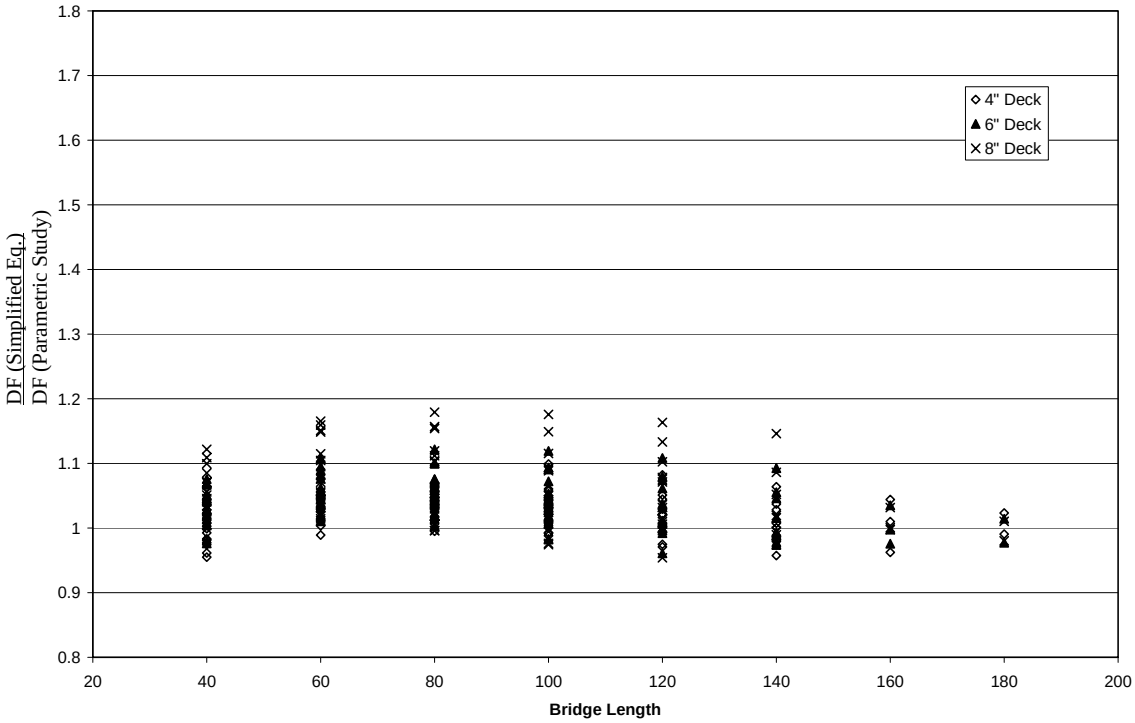


Fig. 7.9 Shear DF for Interior Girders [Set of DF(S,L,I)]

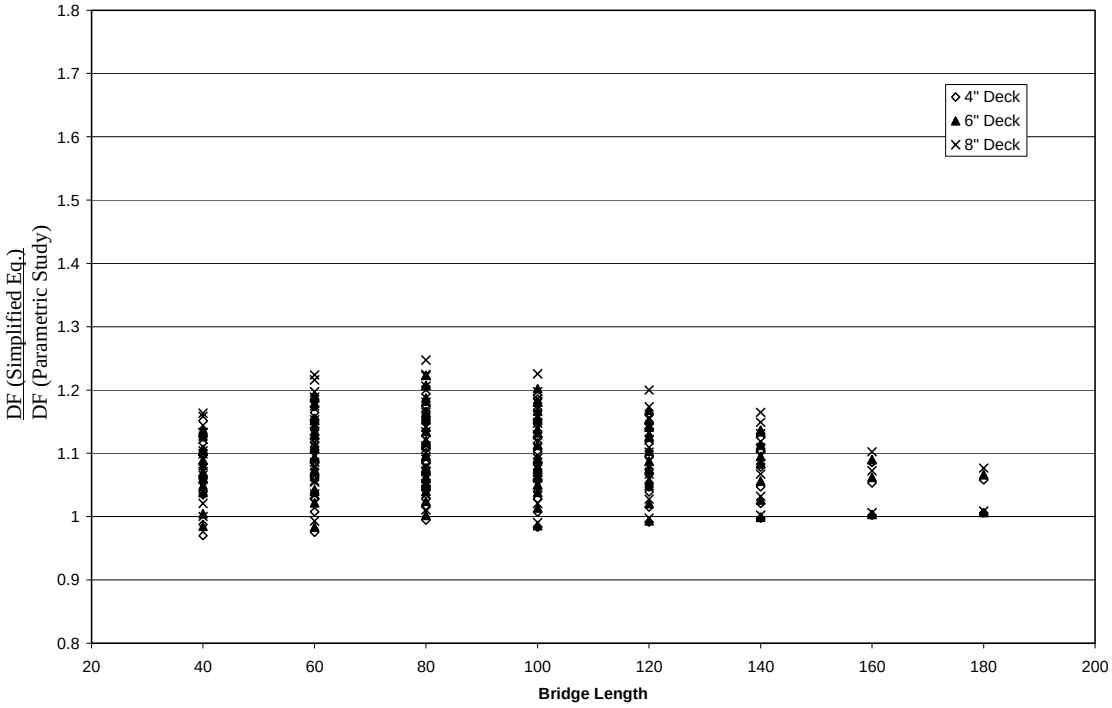


Fig. 7.10 Shear DF for Exterior Girders [Set of DF(S)]

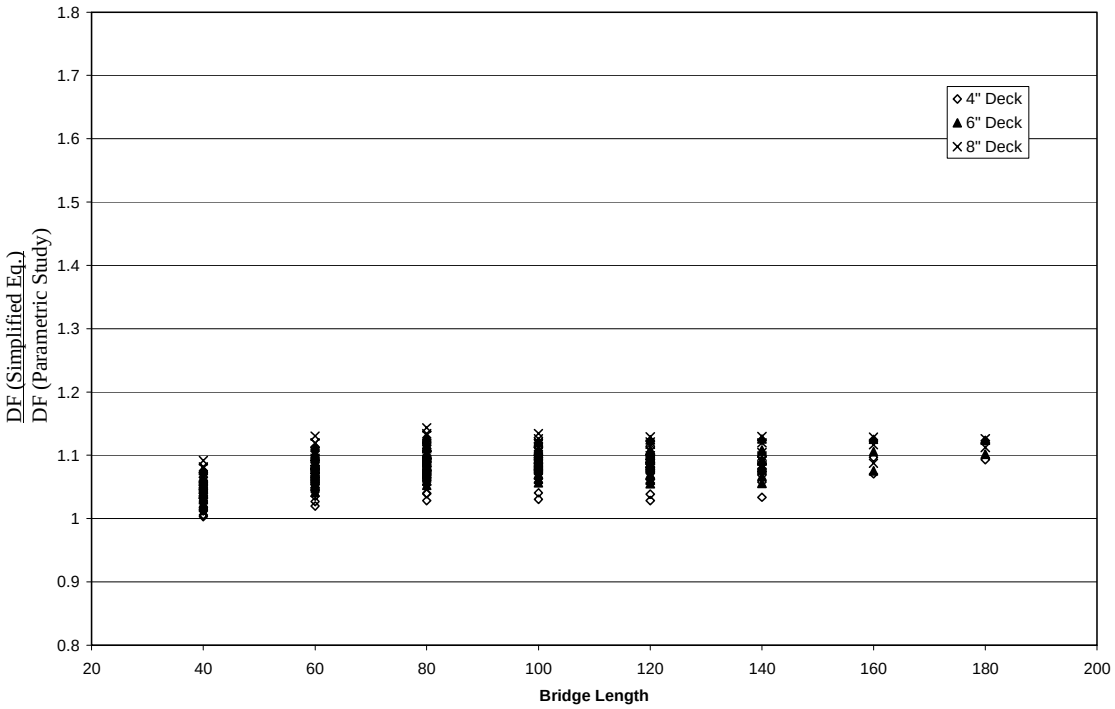


Fig. 7.11 Shear DF for Exterior Girders [Set of DF(S,L,I)]

Figures 7.12 through 7.15 show a summary plot of all of the data for bridges with 6" deck thickness from the second set of models of the parametric study. Each of the following graphs is of the data from the parametric study set II. Only the data points for the bridge models of six inch decks are shown. The graphs do not show the data for the 8" or 4" decks. There is no x-axis scale to the graphs; the vertical axis of each of the graphs is the distribution factor. The data is sorted in three nested groups. The top group is of bridges with the same girder spacing. There are five different sets of bridges with the same girder spacing which increase from 48" on the left hand side of the graph to 96" on the right side of the graph. Nested within each set of bridges with equal girder spacing are four sets with the same girder heights. The bridges with girder heights increase from 36" on the left to 66" on the right. Within each set of bridges with equal girder heights, the span lengths of the bridges increase from left to right. The limits of the span lengths for set of bridges with a given girder height and spacing is defined in Tables 6.1 and 6.2. These tables define the set of "practical bridges" used to develop the simplified equations shown in the following graphs.

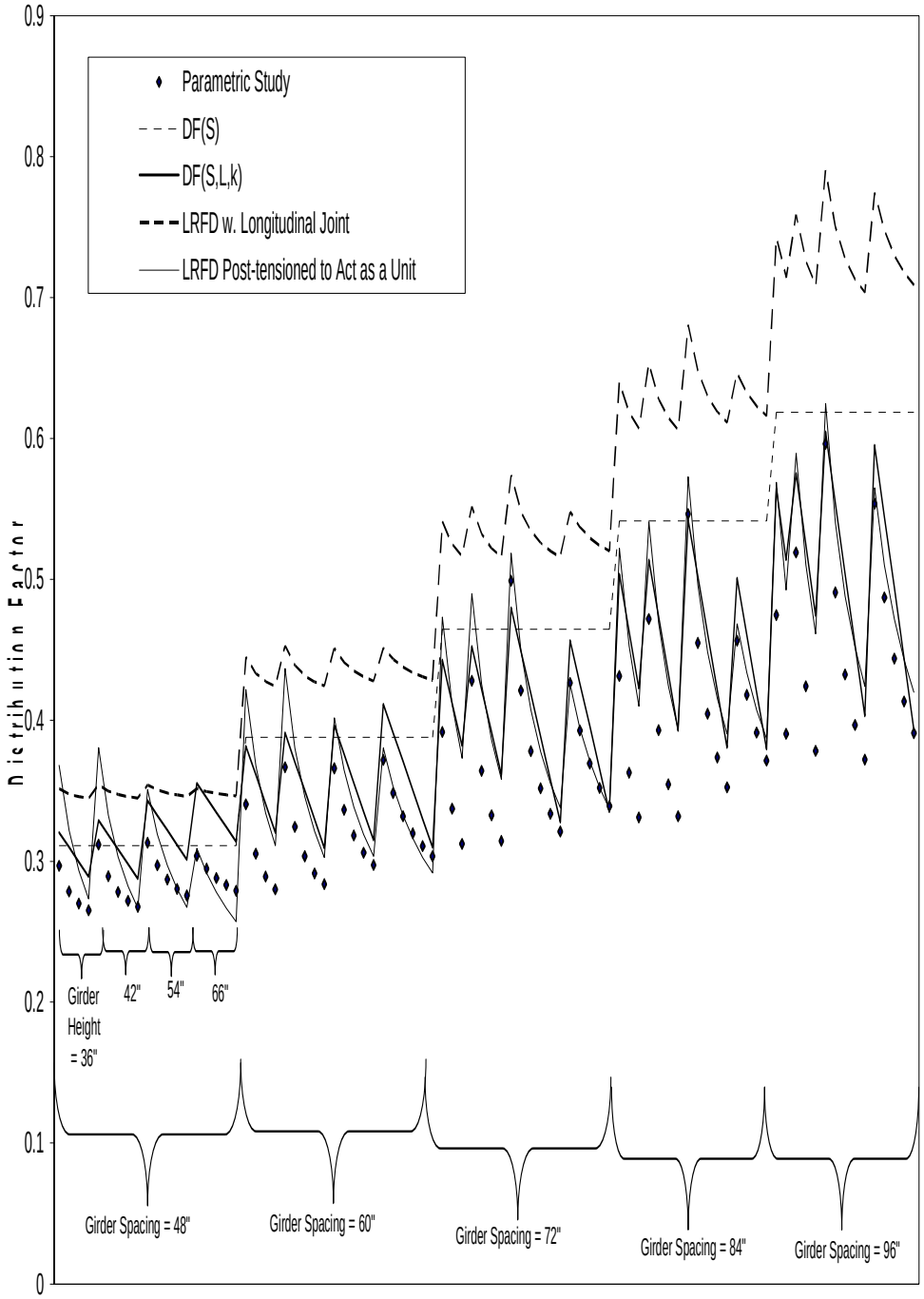


Fig. 7.12 Evaluation of **Moment** Distribution Factors on **Interior** Girders

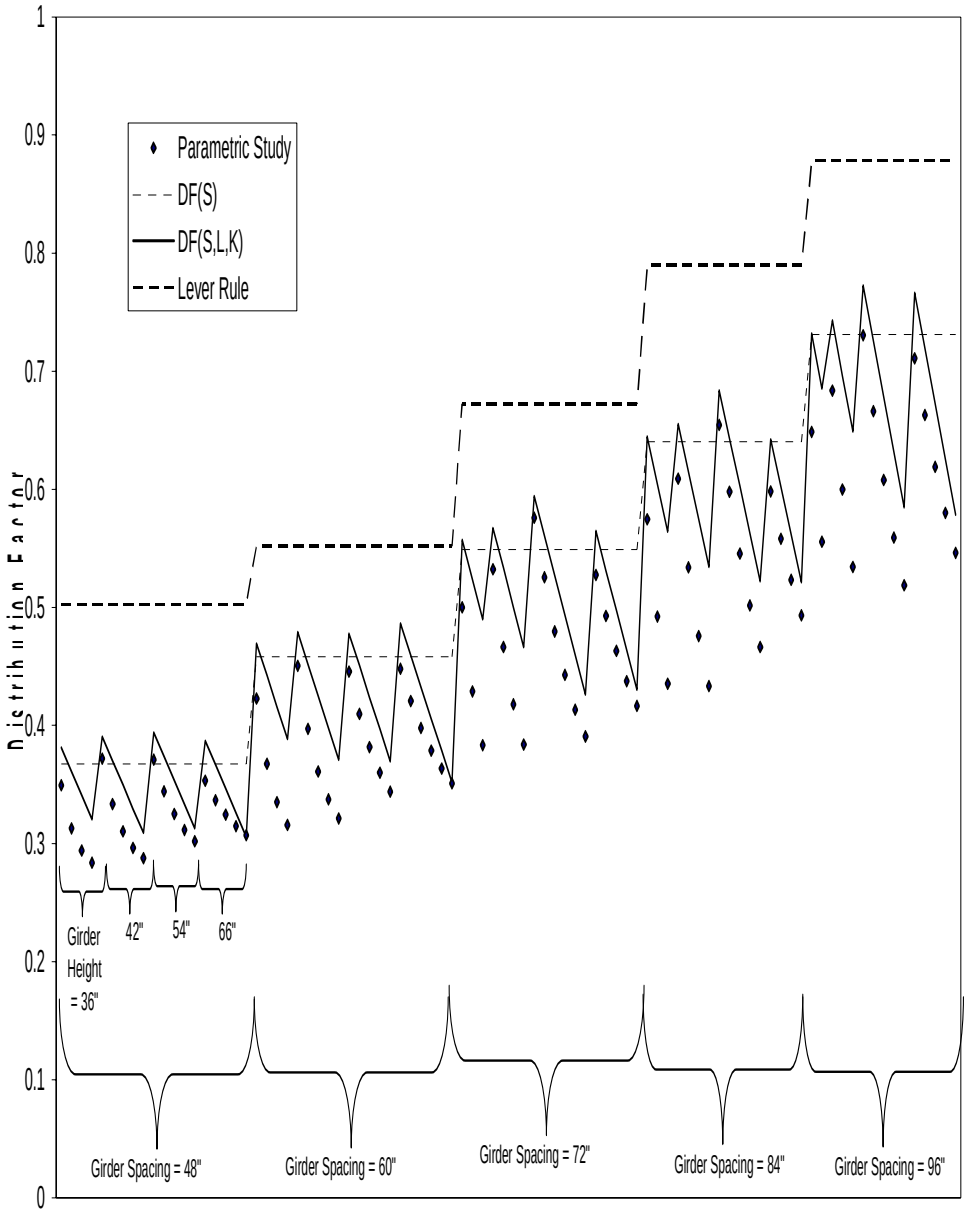


Fig. 7.13 Evaluation of **Moment** Distribution Factors on **Exterior** Girders

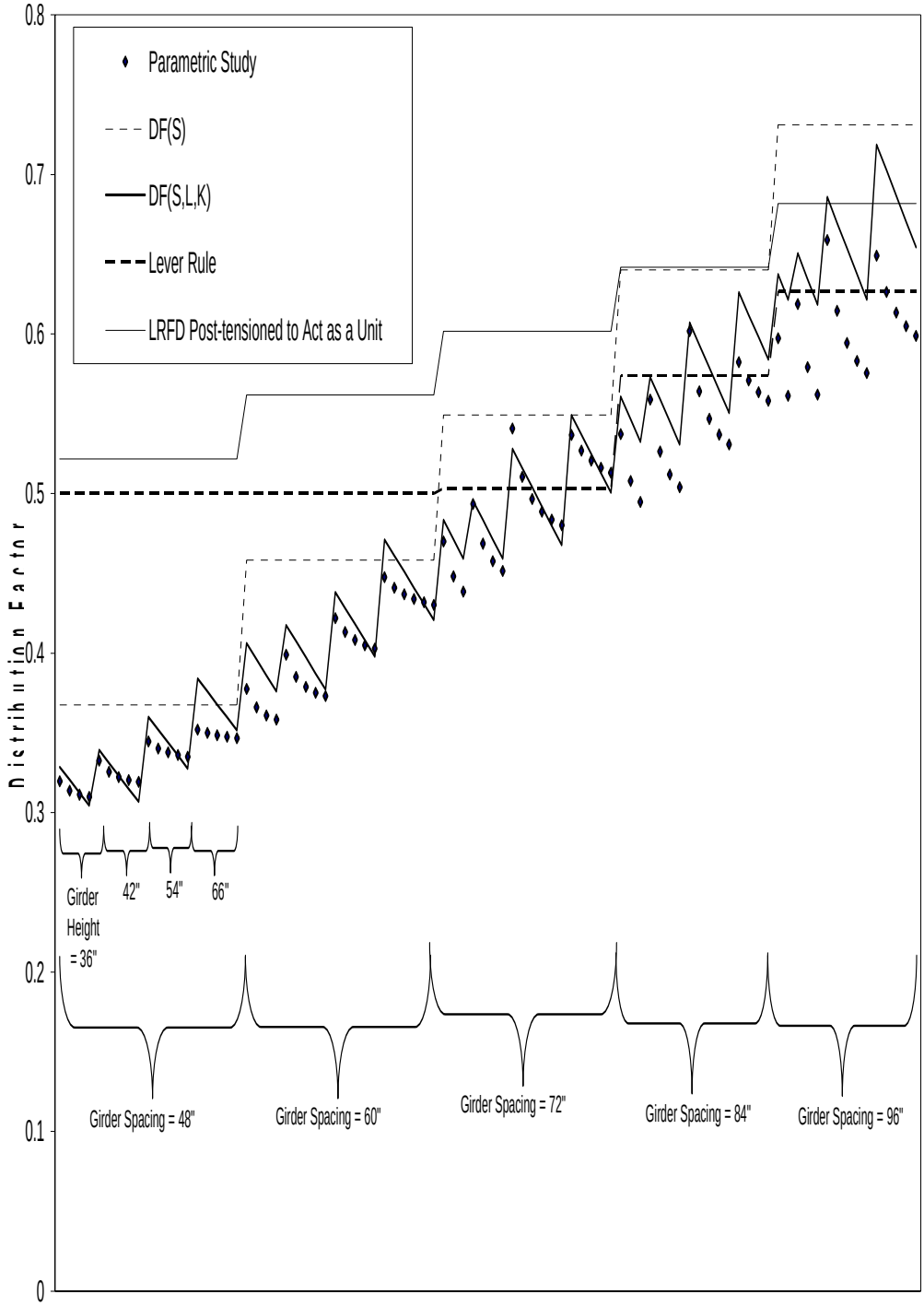


Fig. 7.14 Evaluation of **Shear** Distribution Factors on **Interior** Girders

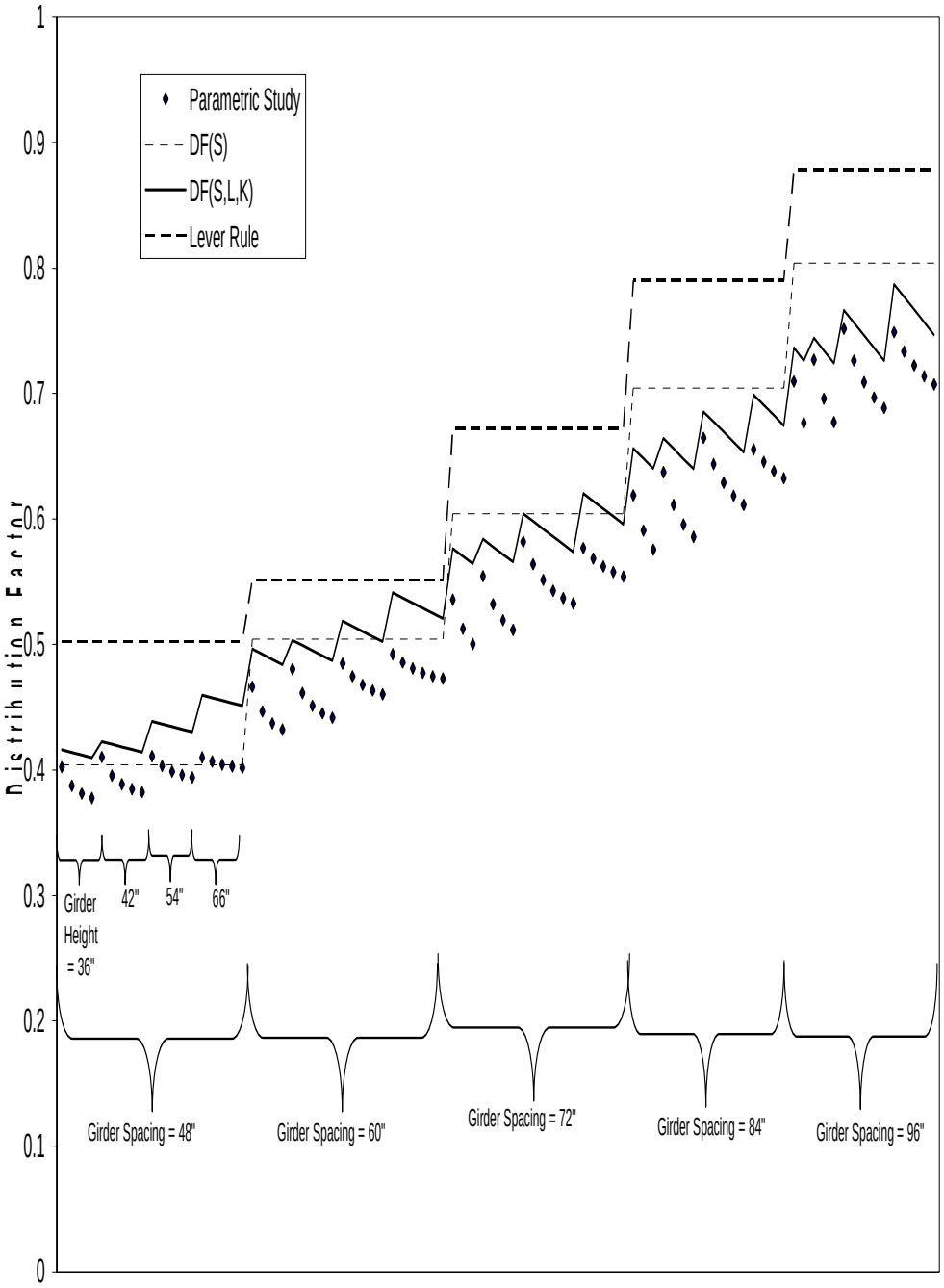


Fig. 7.15 Evaluation of **Shear** Distribution Factors on **Exterior** Girders

Tables 7.1 and 7.2 give a summary of the distribution factor values for the four sets of tested bridges. The proposed DF equations give a higher distribution factor for all of the tested bridges when comparing with field testing results (shown as "Data" in the Tables) and a lower distribution factor when comparing with the LRFD predictions. Please note that for skew bridges (such as Huffman Bridges), the skew adjustment factor specified in the LRFD is proposed to be used at this time before a further research is done in this area.

Table 7.1 Moment Distribution Factors Based on Different Methods

a) Interior Girders

| Tested Bridges | Data | LRFD | DF(S) | DF(S,L,I) |
|---|---|---|---|---|
| 100th | 0.35 | 0.66 | 0.57 | 0.40 |
| Huffman | 0.31 | 0.55 | 0.46 | 0.34 |
| Campbell | 0.34 | 0.66 | 0.57 | 0.39 |
| Diamond/Dowling | 0.32 | 1.48 | 0.58 | 0.40 |

b) Exterior Girders

| Tested Bridges | Data | LRFD | DF(S) | DF(S,L,I) |
|---|---|---|---|---|
| 100th | 0.45 | 0.76 | 0.67 | 0.55 |
| Huffman | 0.49 | 0.61 | 0.61* | 0.48* |
| Campbell | 0.53 | 0.76 | 0.67 | 0.54 |
| Diamond/Dowling | 0.46 | 0.77 | 0.69 | 0.56 |

* Indicates adjusted with skew adjustment factor.

Table 7.2 Shear Distribution Factors Based on Different Methods

a) Interior Girders

| Tested Bridges | Data | LRFD | DF(S) | DF(S,L,I) |
|---|---|---|---|---|
| 100th | 0.43 | 0.60 | 0.67 | 0.58 |
| Huffman | 0.46 | 0.57* | 0.61* | 0.52* |
| Campbell | 0.50 | 0.60 | 0.67 | 0.61 |
| Diamond/Dowling | 0.55† | 0.60 | 0.69 | 0.57 |

b) Exterior Girders

| Tested Bridges | Data | LRFD | DF(S) | DF(S,L,I) |
|---|---|---|---|---|
| 100th | 0.66 | 0.76 | 0.74 | 0.68 |
| Huffman | 0.58 | 0.67* | 0.66* | 0.63* |
| Campbell | 0.71 | 0.76 | 0.74 | 0.70 |
| Diamond/Dowling | 0.60† | 0.77 | 0.76 | 0.68 |

* Indicates adjusted with skew adjustment factor.

† Indicates value not found directly from data but from a FE model that closely approximates the data.

# CHAPTER 8 – CONCLUSIONS

It is the objective of this study to develop a simple load distribution formula that will describe how a single lane highway load is distributed to the Alaska Style bulb tee girder bridge superstructure.

During the research period, the research team successfully completed the following tasks: (1) reviewed all relevant literature on this subject, especially the historical development of AASHTO Specifications on load distribution of this bridge system; (2) tested eight (4 Sets of Twin Bridges) decked bulb-tee bridges in Anchorage, Alaska using one truck to simulate the single lane loading condition; (3) developed three-dimensional finite element models using ABAQUS software available on Arctic Region Supercomputer at UAF to simulate tested bridges and to study the impact of intermediate diaphragms. The number of degrees of freedom of the 3D models varies from 150,000 for Set 1 bridges to 900,000 for Set 2 bridges; (4) calibrated a two-dimensional grillage model based on field testing and 3D FE model results; (5) built a total of 1248 computer models using the developed 2D Grillage modeling technique to study the impact of parameters such as girder spacing, girder stiffness, bridge span, deck thickness, stiffness of the longitudinal joint, and number of girders on the load distribution characteristics; and (6) developed two sets of load distribution factor equations and compared the proposed equations with the LRFD equations.

Based on this 2.5-year research, the research team concluded the following findings for single lane loaded decked bulb-tee bridges:

(1) The following two sets of single-lane live load DF equations are proposed:

Moment over Interior Girder (MI):

$$DF(S) = \frac{S}{13}$$

$$DF(S, L, I) = \frac{S}{12.5} + \frac{I}{300} - \frac{L}{10} \cdot \left( \frac{S-3}{200} \right)$$

Moment over Exterior Girder (ME):

$$DF(S) = \frac{S}{11}$$

$$DF(S, L, I) = \frac{S}{10} + \frac{I}{300} - \frac{L}{10} \cdot \left( \frac{S-1}{300} \right)$$

Shear over Interior Girder (SI):

$$DF(S) = \frac{S}{11}$$

$$DF(S, L, I) = \frac{S}{12.5} + \frac{I}{250} - \frac{L}{100} \cdot \left( \frac{S}{100} \right)$$

Shear over Exterior Girder (SE):

$$DF(S) = \frac{S}{10}$$

$$DF(S, L, I) = \frac{S}{12} + \frac{I}{400} - \frac{L}{100} \cdot \left( \frac{S-3}{100} \right) + 0.07$$

(2) The current LRFD equation for the distribution factor of moment on interior girders includes the aspect ratio as one of its parameters. According to this study, the number of girders and overall width of the bridge has little effect on the load distribution. On the other hand, parameters such as girder spacing, girder stiffness and span length are the most factors which should be considered in the DF equations.

(3) The proposed two sets of DF equations are easy to use and are still more accurate for the single lane loaded condition than the existing LRFD equations provided for this bridge system.

(4) The LRFD equation for distribution of moment on interior girders for bridges with girders only connected enough to prevent relative vertical translation, is an average of 44% to 96% conservative depending on the aspect ratio of the bridge.

(5) For the moment DF of both interior and exterior girders, spacing has the greatest effect followed by span length, and then by girder stiffness. For the shear DF, spacing has the greatest effect followed by girder stiffness and then by span length.

(6) For shear distributions on exterior and interior girders, the LRFD equations are an average of 32% conservative for both the flexural transverse continuous and discontinuous cases.

(7) The research team investigated the effects of the longitudinal joint on the load distribution of decked bulb-tee bridges. Based on field testing and modeling results, it appears that the bridges, although they did not have any transverse post-tensioning, behaved as if they had full transverse flexural continuity. The 3D finite element modeling of these bridges shows that this behavior could be caused by the intermediate steel diaphragms. By varying the stiffness of the hinge joint in the grillage model, these models show that this behavior could also be caused by the stiffness of the grouted joint and shear keys. Further study in this area is needed and recommended.

(8) The skew adjustment factor specified in the LRFD Specs is recommended to be used at this time pending further parametric studies on this topic.

## REFERENCES


1. AASHTO LRFD (1998), "LRFD Bridge Design Specifications," American Association of State Highway and Transportation Officials, Inc., Second Edition.
2. AASHTO STD (1996), "Standard Specifications for Highway Bridges," American Association of State Highway and Transportation Officials, Inc., 16th Edition.
3. ACI Committee 318 (2002), "Building Code Requirements for Structural Concrete and Commentary," American Concrete Institute, Detroit, Mich.
4. Barr, P., Stanton, J., and Eberhard, M. (2000), "Live Load Distribution Factors for Washington State SR 18/SR 516 Overcrossing", Research Report, WA-RD 477.1, Washington State Department of Transportation, Washington State Transportation Center (TRAC), University of Washington, Seattle, WA, Feb.
5. Bishara, A. G. (1984). "Analysis for Design of Bearings at Skew Bridge Support." Report ODOT 14346, Ohio Department of Transportation, Columbus, Ohio.
6. Concrete Technology Corporation (CTC) (1995), "Standard Decked Bulb Tee Charts," Manufacturers of Prestressed Concrete, Tacoma, Washington.
7. Hambly, E. C. (1991), "Bridge Deck Behavior," Second Edition, E & FN Spon.
8. Hays, C. O., Sessions, L. M., and Berry, A. J. (1986). "Further Studies on Lateral Load Distribution Using Finite Element Methods." Transportation Research Record, (1072). Transportation Research Board, Washington, D. C., 6-14.
9. Imbsen, R. A. and Nutt, R. V. (1978), "Load Distribution Study on Highway Bridges Using STRUDL Finite Element Analysis Capabilities," First Conference on Computing in Civil Engineering, Atlanta, Ga., June.
10. Newmark, N. M. (1948), "Design of I-Beam Bridges," Journal of the Structural Division, ASCE, V. 74, No. 1, pp. 305 – 330.
11. Pama, R. P. and Cusens, A. R. (1967), "Edge Stiffening of Multibeam Bridges," Proc. ASCE, Vol. 93, No. ST2, pp. 141 – 161.
12. Reilly, R. J. (1972), "Stiffness Analysis of Grids Including Warping," Proc. ASCE, Journal of Structural Div., ST7, pp. 1511 – 1523.
13. Rowe, R. E. (1955), "A Load Distribution Theory for Bridge Slabs Allowing for the Effect of Poisson's Ratio," Concrete Research, Vol. 7, No. 20, pp. 69 – 78.
14. Sanders, W. W. and Elleby, H. A. (1970), "Distribution of Wheel Loads on Highway Bridges," NCHRP Report 83, Highway Research Board.
15. Spindel, J. E. (1961), "A Study of Bridge Slabs Having no Transverse Stiffness," Ph.D. thesis, London University, London.
16. Stanton, J. and Mattock, A. H. (1986), "Load Distribution and Connection Design for Precast Stemmed Multibeam Bridge Superstructures," NCHRP Report 287, Nov..
17. Watanabe, E. (1968), "Study of Load Distribution in Multi-Beam Highway Bridges," Unpublished M.S. thesis, Iowa State University.
18. Yettram, A. L. and Husain, H. M. (1965), "Grid-Framework Method for Plates in Flexure," Proc. ASCE, Journal of the Engineering Mechanics Div., EM3, pp. 53 – 64.
19. Zokaie, T., Osterkamp, T. A., and Imbsen, R. A. (1991), "Distribution of Wheel Loads on Highway Bridges," Final Report, V. 1 and 2, prepared for NCHRP, Transportation Research Board, National Research Council, Washington D. C..